Radiographic and Pathologic Studies of Feline Appendicular Osteoarthritis

Siti Mariam Zainal Ariffin

DVM

Submitted in fulfilment of the requirements for the degree of
Doctor of Philosophy

School of Veterinary Medicine

College of Medical, Veterinary and Life Sciences

University of Glasgow

November 2014

Abstract

Feline Osteoarthritis (OA) is a pathological change of a diarthrodial articulation which primarily occurs in older cats. The aims of this study were:- 1) to define the radiographic features of OA in the cat for each individual appendicular joint; 2) to relate the radiographic features to the gross pathologic and histopathologic features; 3) to explore underlying causes of OA in cats, 4) to identify the presence of Protease Activated Receptor-2 (PAR-2) and matriptase in feline articular cartilage and synovial membrane and to determine their role in OA pathogenesis.

The present study has defined five radiographic features of OA for each appendicular joint:- presence of osteophytes, enthesiophytes, areas of abnormal mineralisation, synovial effusion and joint remodelling. The study furthermore suggested that increases in radio-opacity beneath the semilunar notch, along the femoral trochlea, beneath the tibial plateau and on the femoral head/neck are also important radiographic features. The radiographic prevalence was highest in the elbow (23.9%, 93/389) and stifle (23.9%, 93/389) joints, followed by the hip (21.1%, 82/389), tarsal (17.7%, 69/389), shoulder (6.7%, 27/389) and carpal (6.4%, 25/389) joints. The results from this study demonstrate that the presence of a radiographically apparent supinator sesamoid bone (SSB), meniscal mineralisation (MM) and two fabellae are related to cartilage pathology and can be indicators of OA.

Prevalence rates for gross pathology changes were highest in the elbow (20.2%, 102/506) joint, followed by the stifle (19.6%, 99/506), hip (18.4%, 93/506), shoulder (17.8%, 90/506), tarsal (15.0%, 76/506), and carpal (9.1%, 46/506) joints. Eight key gross pathologic features were identified- cartilage discolouration, cartilage fibrillation, cartilage ulceration, cartilage erosion, osteophytes, thickening of joint capsule, synovium discolouration and joint remodelling. The radiographic and gross pathologic total scores were positively correlated in each appendicular joint and the joint most likely to have cartilage damage without radiographic evidence of OA is the shoulder (71.1%, 64/90) followed by the elbow (39.1%, 9/23), hip (32.4%, 11/34), stifle (26.1%, 6/23), carpal (23.1%, 21/91) and tarsal (14.9%, 7/47) joints. Four possible underlying conditions that lead to secondary OA were identified:- radioulnar incongruity, hip dysplasia (HD), cranial cruciate ligament (CCL) disease and primary meniscal mineralisation.

The identification of PAR-2 and matriptase proteins and gene expression in feline articular tissues is a novel and important finding supporting the hypothesis that serine proteases are involved in the articular cartilage degradation seen in feline OA.

Table of content

List of Tables

Chapter 1

Chapter 2

Chapter 3

Chapter 4

Chapter 5

Chapter 6

Chapter 7

List of Figures

Chapter 1

Chapter 2

Chapter 3

Chapter 4

Chapter 5

Chapter 6

Chapter 7

Chapter 8

Chapter 9

Chapter 10

Acknowledgements

All praises and gratitude are due to Allah for granting me the strength in completing this PhD thesis.

Pursuing a PhD has been a truly life-changing experience and it would not have been possible to complete it without the support and guidance that I received from many people. I gratefully acknowledge the Ministry of Education Malaysia and Universiti Sultan Zainal Abidin for providing the financial support that allowed this journey to become a reality.

I offer my utmost gratitude to Professor David Bennett, my principal supervisor for the opportunity and support during the whole period of the study. It has been my privilege to work closely with him and learn from his fabulous knowledge and experience. I believed I learnt from the best. His frequent insights, guidance and patience during the writing process are much appreciated. I am also wanted to express my deep thanks to my second supervisor, Dr. Pamela Elizabeth Johnston for her excellent advice on pathological interpretation and taking the time to go through the histopathology data with me.

My sincere gratitude also goes to Professor William Ferrell and Professor John Lockhart for giving me the opportunity to work at their laboratory and offering their advice and expertise in the PAR-2 and matriptase studies. Special thanks to Dr. Dylan Clements from the Royal (Dick) School of Veterinary Studies, University of Edinburgh for providing some of the feline articular cartilage RNA and cDNA for PAR-2 and matriptase studies. I am also deeply thankful to Dr. Caline Koh-Tan for helping and teaching me how to design primers for qPCR study. I owe gratitude to Mrs. Lynette Dunning who taught me the laboratory skills needed for the qPCR and immunohistochemical studies.

Special thanks to Mr. Gawain Hammond and Professor Martin Sullivan for taking the time to become involved in the inter- and intra- observer studies. Thank you, Dr. Mark McLaughlin for your help and knowledge in DAPI staining. I also would like to thank Dr. Timothy Parkin for his expertise in helping me with the statistical analyses.

Thank you, Mrs. Lynn Stevenson and all the staff of the Histopathology Unit, Veterinary Diagnostic Service, University of Glasgow for your professional help during the whole process of the preparation of the histology sections. I also wish to express my gratitude to Mr. Richard Irvine and Mr. Michael Mcguigan for all your amazing help and guidance, you have made the *Post-mortem* room a wonderful place to work.

I would also like to extend my deepest gratitude to my father Mr. Zainal Ariffin, my mother Mrs. Zulliah Alwee and family in Malaysia. Thank you for always supporting me from a distance and encouraging me to do my best. I am extremely fortunate for having been blessed with such an incredible family. Very special thanks are due to my good friend, Dr. Aizan Sofia and office mates, Dr. Intan Nur Fatiha Shafie, Dr. Aseel Karim and Yao Qi. You all gave me the things I did not get from my education including determination, motivation and inspiration. My time at Glasgow was made enjoyable in large part due to the friends that became a part of my life.

Finally, I was very lucky to be able to share this experience with you Mohd Faizal Ghazali, being in the same position, doing our PhD study at the same time and at the same university. Thank you for all your help, support and care towards me.

I would like to express my apology that I could not mention personally every one of those who were important to the production of this piece of work.

Author's Declaration

I declare that, except where explicit reference is made to the contribution of others, this dissertation is the result of my own work and has not been submitted for any other degree at the University of Glasgow or any other institution.

S.M.Z. Ariffin, November 2014

Dedication

This thesis is dedicated to all cat lovers and feline practitioners everywhere

List of abbreviations

Abbreviation	Meaning
%	Percentage
ΔΔCT	Delta delta CT
°C	Degree celcius
µg	Microgram
µl	Microlitre
µm	Micrometre
α	Alpha
Κ	Kappa
ACTB	Beta-actin
ACTH	Adrenocorticotropic hormone
ADAMTS	A disintegrin and metalloproteinase with thromboSpondin motifs
B2M	Beta-2-microglobulin
BCS	Body condition score
BML	Bone marrow edema-like
BMP	Bone morphogenetic protein
bp	Basepair
BSA	Bovine serum albumin
Carp-path OA	Carpal-pathologic OA
Carp-rOA	Carpal-radiographic OA
CCL	Cranial cruciate ligament
CCLT	Cranial cruciate ligament transection
cDNA	Complementary DNA
CKD	Chronic kidney disease
COX	Cyclooxygenase
CR	Computed radiography
dH_2O	Distilled Water
DAB	3, 3'-Diaminobenzidine
DAPI	4',6-Diamidino-2-Phenylindole
DI	Distraction index
DICOM	Digital imaging and communications in medicine
DJD	Degenerative joint disease
DNA	Deoxyribonucleic acid
DPX	Distrene, plasticiser, xylene
dsDNA	Double-stranded deoxyribonucleic acid
e.g.	Example
ECM	Extracellular matrix
EDTA	Ethylenediaminetetracetic acid
El-path OA	Elbow-pathologic OA
El-rOA	Elbow-radiographic OA
FGF	Fibroblast growth factor
FSE	Fast spin-echo
FSH	Follicle stimulating hormone
g	Gram
g	Gravity
GAG	Glycosaminoglycan
GAPDH	Glyceraldehyde 3-phosphate dehydrogenase
GH	Growth hormone
GUSB	Beta-glucuronidase
H&E	Haematoxylin and eosin
HCL	Hydrochloric Acid
HD	Hip dysplasia

Abbreviation	Meaning
Hip-path OA	Hip-pathologic OA
Hip-rOA	Hip-radiographic OA
HPRT	Hypoxanthine guanine phosphoribosyl transferase
i.e.	That is
IGF	Insulin growth factor
IHC	Immunohistochemistry
IL	Interleukin
kV	Kilovolts
L	Litre
LH	Luteinizing hormone
M	Molar
M	Stability value
mA	Milliampere
mAs	Milliampere second
mg	Milligram
minus-RT	Minus-reverse transcriptase
ml	Millilitre
mm	Millimetre
mM	Millimolar
MM	Meniscal mineralisation
MMP	Metalloproteinases
MRI	Magnetic resonance imaging
mRNA	Messenger ribonucleic acid
NaCl	Sodium chloride
NA	Norberg angle
NFPA	Non-functioning pituitary adenoma
nM	Nanomolar
nm	Nanometre
NO	Nitric oxide
NSAID	Non-steroidal anti-inflammatory drug
OA	Osteoarthritis
OST	Osteochondroma
PACS	Picture archiving and communications system
PAR-2	Protease activated receptor-2
PBS	Phosphate buffered saline
PD	Proton density
PGE2	Prostaglandin E2
*PM*E	*Post-mortem* examination
qPCR	Quantitative real-time polymerase chain reaction
RCVS	Royal College of Veterinary Surgeon
RNA	Ribonucleic acid
RPL13a	Ribosomal Protein L13a
RPL-18	60S ribosomal protein L18
RPM	Revolutions per minute
r_s	Spearman's rank correlation coefficient
Sec	Second
SDHA	Succinate dehydrogenase complex, subunit A, flavoprotein
Sh-path OA	Shoulder-pathologic OA
Sh-rOA	Shoulder-radiographic OA
SSB	Supinator sesamoid bone
St-path OA	Stifle-pathologic OA

Abbreviation	Meaning
St-rOA	Stifle-radiographic OA
Tar-path OA	Tarsal-pathologic OA
Tar-rOA	Tarsal-radiographic OA
TBP	TATA-binding protein
TBS	Tris-buffered saline
TGF-β	Transforming growth factor-β
TIMP	Tissue inhibitors of metalloproteinase
TNF	Tumor necrosis factor
Tris-HCL	Tris-hydrochloric acid
TSH	Thyroid-stimulating hormone
VD	Ventro-dorsal
VEGF	Vascular endothelial growth factor

Chapter 1 Introduction

1.1 Preface

Feline Osteoarthritis (OA) is a chronic degenerative disease of feline appendicular joints that causes pain and can affect the quality of life for both the cat and the owner. It has been assumed that although feline OA occurs as a pathological entity, it rarely causes a clinical problem and this is the main reason that the disease has been ignored for so many years. Previous research into feline OA has been relatively limited and focused on the prevalence of radiographic findings of disease. However, there are no published comprehensive accounts of the pathological features of this disease. To fully understand feline OA there is a need to study the radiographic and pathologic features together and to try and identify the relationship between them. This study was based on this approach. Radiography was used in the evaluation of OA affecting all the appendicular joints. The gross and histopathological characteristics were studied and documented. The underlying causes of feline OA were determined and the pathological role of Protease activated receptor-2 (PAR-2) and matriptase in feline OA was investigated by determining their protein and gene expression.

1.2 Normal morphology of a diarthrodial joint

Diarthrodial joints are freely movable articulations. The articulating bones are separated by an articular cavity which contains synovial fluid (Figure 1.1). The articular surface is covered with articular cartilage and enclosed in a fibrous capsule. The fibrous capsule is lined with synovial membrane.

1.2.1 Articular cartilage

The articular cartilage is a flexible connective tissue which serves to minimize friction and allow a gliding motion without causing pain. It is normally white to blue-white, smooth, shiny, elastic and firm in appearance (Bennett, 1990; Dyce et al., 2002). Histologically, the cartilage consists primarily of cells (chondrocytes) and extracellular matrix (ECM).

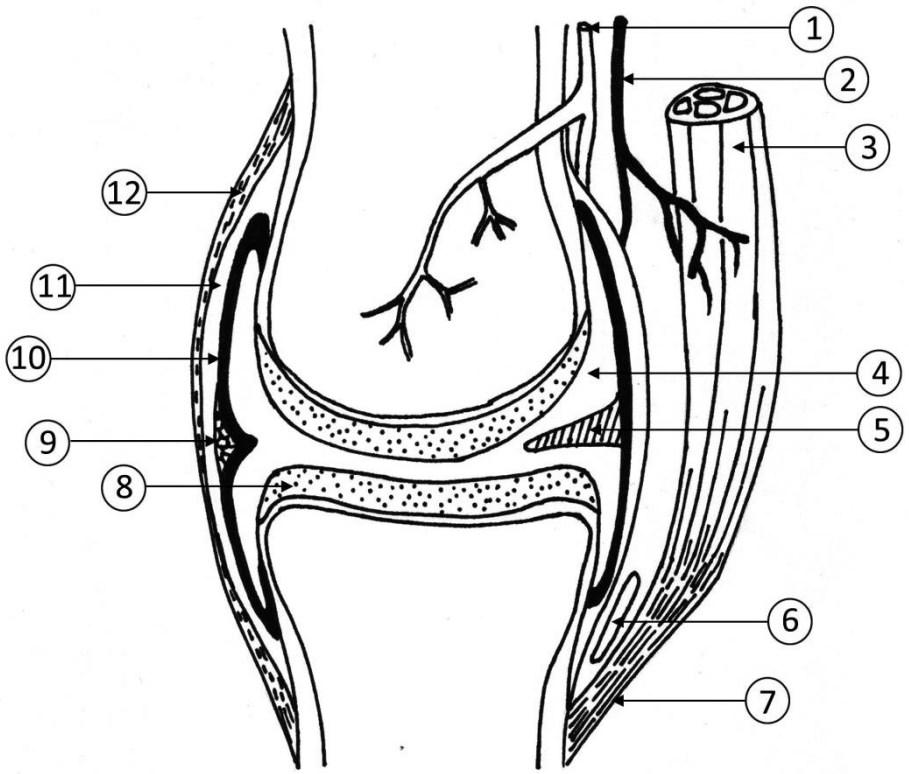

Figure 1.1: Diagrammatic representation of a diarthrodial joint. 1-Blood vessel; 2-Nerve; 3-Muscle; 4-Articular cavity containing synovial fluid; 5-Meniscus; 6-Bursa; 7-Tendon; 8-Articular cartilage; 9-Fat pads; 10-Synovial membrane; 11-Fibrous capsule; 12-Ligament.

The chondrocytes and matrix are organized into 4 layers: superficial, middle, deep and calcified (Pearle et al., 2005). Those chondrocytes near the surface of the articular cartilage are flattened and elongated; in the middle layer, the chondrocytes are larger and more rounded; in the deep layer, the chondrocytes are arranged in columns. The deep layer is separated from the calcified layer by the tidemark, seen as irregular lines of basophilic staining with haematoxylin and eosin (H&E). The calcified cartilage serves to anchor articular cartilage to subchondral bone. Articular cartilage is aneural, avascular and alymphatic. Above the tidemark on the joint side, all the cartilage is nourished by diffusion from the synovial fluid and from vessels in the tissue at the periphery of the cartilage (Dyce et al., 2002). Below the tidemark, the calcified cartilage is nourished by epiphyseal blood vessels (Hoch et al., 2008).

The ECM is composed of water (70-80% of wet weight), collagen (50-60% of dry weight), proteoglycans (25-35% of dry weight) and a variety of noncollagenous proteins and glycoproteins (15-20% of dry weight) (Buckwalter et al., 2005). The amount of water present in the cartilage depends on the proteoglycan and the collagen components of the matrix.

Type II collagen makes up 90% of the total collagen in normal articular cartilage. Type I, III, V, VI, IX, X and XI collagen may also be present (Mankin, 1985; Sandell, 1995). Collagen fibrils run parallel to the joint surface in the superficial layer, are arranged obliquely in the middle layer and run perpendicularly to the tidemark and subchondral bone (Zambrano et al., 1982; Mankin, 1985; Hunziker et al., 2007). The organization of these fibrils into a tight meshwork provides tensile strength to the articular cartilage and helps to immobilize the proteoglycans within the tissue (Buckwalter et al., 2005).

Proteoglycan is produced in the Golgi apparatus of chondrocytes, mainly found in the middle and deep layer of the articular cartilage (Renberg, 2005). It consists of a core protein to which glycosaminoglycan (GAG) chains are attached (proteoglycan subunit) (Teitelbaum and Bullough, 1979; Adams and Billingham, 1982). The GAGs that are commonly found in the articular cartilage include chondroitin-4- sulphate, chondroitin-6- sulphate, keratan sulphate and dermatan sulphate (Buckwalter et al., 2005). These sulphate groups are found at the free end of the GAGs, giving them a distinct negative charge and hydrophilic properties which help to maintain the articular cartilage elasticity and stiffness under compressive loading (Mankin, 1985; Renberg, 2005). The proteoglycan subunit is bound by a link protein to hyaluronan. Hyaluronan forms the backbone of a large aggregating proteoglycan called aggrecan (Mankin, 1985). Proteoglycans are normally located within a meshwork formed by collagen fibrils and

are increased in areas of articular cartilage subject to high stress (Kiviranta et al., 1987).

1.2.2 Subchondral bone

Subchondral bone is the layer of bone just below the articular cartilage. It consists of the subchondral plate and trabecular bone. The subchondral plate is a layer of lamellar bone lying immediately deep to the calcified layer of the articular cartilage (Madry et al., 2010). The subchondral region contains blood vessels and marrow spaces. Subchondral bone thickness is influenced by the anatomical structure of the joint. In joints where the bones have a concave and convex component, the dome-shaped convex subarticular bony structures are thinner and more uniformly shaped than those of the complementary component; the central parts of the joint have a thicker subchondral plate than is found peripherally (Simkin et al., 1991; Dewire and Simkin, 1996). Functions of the subchondral bone include absorbing stress and providing support for the overlying articular cartilage (Radin et al., 1970; Duncan et al., 1987).

1.2.3 Synovial membrane

The synovial membrane covers the inner surface of the fibrous capsule and the intra-articular ligaments and tendons. It forms an opal white, smooth, semitranslucent, glistening layer with few villi and fringe-like folds, and a fine vascular network can clearly be seen (Bennett, 1990; Dyce et al., 2002; Cook et al., 2010). Histologically it consists of a thin lining layer and a thicker supporting layer. The lining layer is composed of two cell types: type A and type B synoviocytes. Type A synoviocytes are bone marrow derived cells of the macrophage lineage which have migrated to the synovial surface from the local blood vessels (Edwards and Willoughby, 1982). They have phagocytic functions and can migrate through the synovium into the synovial cavity and express major histocompatibility complex class II molecules and Ia antigen, which play key roles in antigen presentation in the initial stages of the immune response (Blom and van den Berg, 2007). These cells can produce protective mediators and growth factors such as transforming growth factor-ß (TGF-ß), bone morphogenetic proteins-2 and 4 (BMP-2 and BMP-4), tissue inhibitors of metalloproteinase (TIMP) and interleukin-10 (IL-10). Type B synoviocytes are fibroblast-like cells which are locally derived and are involved in synovial fluid production (Vigorita, 2008). It has been reported that type B synoviocytes are the predominant cells, accounting for 75% and 80% of all synoviocytes in the rabbit and mouse respectively (Krey and Cohen, 1973; Okada et al., 1981). The lining layer varies from one to two cells in thickness (Cook et al., 2010; Smith, 2011).

The supporting layer consists of areolar, fibrous or adipose tissue. The areolar type is the most common of these tissues (Castor, 1960; Knight and Levick, 1983) and the connective tissue matrix is made up of fine fibrillar matrix with Type I collagen (Smith, 2011).

Normal synovium is highly vascular. It contains fenestrated arterioles, capillaries and venules (Dyce et al., 2002). Most of the vessels are located within the supporting layer. The fenestration of capillaries and venules predominantly occurs beneath the synovial lining cell layer (Schumacher, 1969). The dense and highly fenestrated synovial capillary network may have developed to fulfil the metabolic demands of the articular cartilage (Suter and Majno, 1964; Veihelmann et al., 1998). Lymphatic vessels and nerve fibres are present in all types of synovial tissue.

1.2.4 Synovial fluid

Synovial fluid is normally viscous and its colour ranges from pale-straw to medium brown (Dyce et al., 2002). It is produced by type B synoviocytes. Pacchiana et al. (2004) characterised normal shoulder and stifle joint fluid in cats. The total volume of synovial fluid obtained from normal joints by arthrocentesis ranged from one drop to 0.25 ml. Cell counts of normal synovial fluid ranged from two to approximately 1,134 cells/µl (median; 91 cells/µl). Mononuclear cells are predominantly seen. Neutrophils may also be present but in low numbers. Total erythrocyte counts ranged from 0 to 4,535 cells/µl (median; 48 cells/µl). Normal synovial fluid has a high proteoglycan content. The molecules adhere to the surface of the articular cartilage, synovial membrane and any intra-articular structures, to provide lubrication and nourishment of the joint (Bennett, 1990; Dyce et al., 2002).

1.2.5 Joint capsule and ligaments

The joint capsule consists of two parts: the outer layer (stratum fibrosum-also called the fibrous capsule) and the inner layer (stratum synoviale-also called the synovial membrane) (Konig and Liebich, 2007). The outer layer is made up of dense connective tissue, mainly consisting of collagen fibres. The inner layer consists of the synovium (Konig and Liebich, 2007). The joint capsule forms a sleeve which securely joins the bones forming the articulation helping to maintain joint stability and restricting and guiding movements (Bennett, 1990). The fibre orientation and capsule thickness depends on the mechanical load placed on its different regions (Ralphs and Benjamin, 1994). Localised thickening of the capsule may be referred to as ligaments. Other

ligaments are usually present, intra- (for example, the cruciate ligaments of the stifle and the teres ligament of the hip) or extra-articular and can be separate from the capsule (Bennett, 1990). Ligaments help to support and stabilize the joint and may be involved in supporting soft tissue structures within the joint such as the menisci and in providing "overload" protection to the capsule (Hoffmann and Grigg, 1989). Both capsule and ligaments have a poor blood supply, but a rich nerve supply, which is possibly an important source of pain in many joint diseases (Bennett, 1990).

1.2.6 Intra- articular structures

Meniscus

Intra-articular menisci are fibrocartilaginous semilunar structures interposed between the femoral and tibial condyles of the stifle joint and temporomandibular joint. Each stifle joint possess medial and lateral menisci (Dyce et al., 2002; Konig and Liebich, 2007). The menisci are shaped concave proximally to accommodate the convexity of the femoral condyles and flattened distally for articulation with the tibial plateaus (Allen et al., 1995). Normal menisci have a smooth, white and glistening surface (Sun et al., 2010; Pauli et al., 2011). In general, each meniscus consists of a cranial horn, a caudal horn and a "body" (O'Connor and McConnaughey, 1978). The menisci are secured to the tibia and the femur by the cranial and caudal ligaments of the lateral and medial meniscus and by the femoral ligament of the lateral meniscus. The medial and lateral menisci are connected to one another by the intermeniscal ligament. The peripheral border of each meniscus attaches to the joint capsule and the medial meniscus also has an attachment to the medial collateral ligament so it is less mobile than the lateral meniscus (Denny and Butterworth, 2000). Abundant blood and nerve vessels originate from the peripheral part of the joint capsule and supply the meniscal horns. The body of the meniscus, however, has a poor blood and nerve supply (O'Connor and McConnaughey, 1978).

Histologically, the menisci consist primarily of cells (fibrochondrocytes or a mixture of fibroblasts and chondrocytes) and ECM. The cells synthesize and maintain the ECM which predominantly consists of collagens, water and noncollagenous proteins (Allen et al., 1995). Type I collagen makes up 90% of the total collagen found in normal menisci. Type II, III, V and VI are also present (Ingman et al., 1974). The predominance of type I collagen distinguishes the fibrocartilage of the menisci from the hyaline articular cartilage, where type II collagen predominates (Allen et al., 1995). Proteoglycans are present in the ECM of the menisci but the amount is significantly less than that of

hyaline articular cartilage (McNicol and Roughley, 1980). Their exact role is not certain but they may play an important role in shock absorption, joint lubrication and stability, improving tibio-femoral congruence and assisting in weight distribution across the joint (Walker and Erkman, 1975; Bennett, 1990).

Pearson and Davin (1921) described ossicles in the medial meniscus of people and interpreted them as a sesamoid bone or lunula. The lunula is often observed in rodents such as rats, mice, hamsters, guinea pigs and paccas (Pedersen, 1949; Greene, 1955; Shaw and Martin, 1962; Cooper and Schiller, 1975; Hebel and Stromberg, 1976; Araujo et al., 2010). Lunulae have also has been reported in domestic cats (Whiting and Pool, 1985), small non-domestic cats (Rahal et al., 2013) and in large non-domestic cats such as tigers, pumas, leopards, lions, cougars and pumas (Ganey et al., 1994; Cerveny and Paral, 1995; Walker et al., 2002). The craniomedial lunula is most commonly observed, but the presence of the craniolateral lunula is also reported in pigs (Jorgensen and Jensen, 2002). Histologically, the lunula consists of trabecular bone filled with bone marrow, bordered by a thin layer of lamellar bone. The surfaces which articulate with the femur and tibia are covered with articular cartilage (Whiting and Pool, 1985).

Fat pads

Intra-articular fat pads are composed of adipose cells and elastic tissue. The most obvious example is the infra- patellar fat pads within the stifle joint. The fat pad has a rich blood and nerve supply. The functions of fat pad include the filling of dead space that occurs during joint motion, cushioning of bony processes and ligaments or tendons, assisting the flow of synovia across joint surfaces and forming storage deposits of body fat (Bennett, 1990).

Supinator sesamoid bone

The supinator sesamoid bone (SSB) is seen in the elbow joint of cats (Wood et al., 1995) and larger breed dogs (Wood et al., 1985). The SSB, if present, is located on the deep aspect of the tendon of origin of the supinator muscle and articulates with the craniolateral aspect of the head of the radius, and is tightly connected to the joint capsule and synovium (Wood et al., 1995). It has a distinct border and its shape varies from circular to irregular oval. The SSB is generally present in all cat elbow joints, but it is radiographically visible in only about 40% of normal joints (Wood et al., 1995). Sesamoid bones often develop within a soft tissue structure such as a tendon where it contacts a bony structure, the patella being the most obvious example. It is

hypothesized that the function of the SSB might include maintaining anatomical function of the humeroradial articulations especially during flexion, extension, supination and pronotion (Wood et al., 1995).

1.3 Definition and classification of Feline OA

1.3.1 Nomenclature

Feline OA is a common and complex progressive disease. Pathological OA can be defined as "an inherently noninflammatory disorder of movable (synovial) joints characterized by deterioration of articular cartilage and by the formation of new bone at the joint surfaces and margins". From the aetiopathogenesis context, it has been defined as "a complex of interactive degradative and reparative processes in cartilage, bone and synovium, with secondary components of inflammation" and clinically, it may be defined as "a slowly evolving articular disease characterized by the gradual development of joint pain, stiffness, and limitation of motion" (Bennett, 2010). Several names are given to describe the condition of OA. The term osteoarthritis is frequently used in the literature and it is synonymous with osteoarthrosis and degenerative disease of synovial joints (Kellgren and Lawrence, 1957; Hough, 1993). The term degenerative joint disease (DJD) is often, incorrectly used to mean the same as OA. DJD refer to any degenerative process that occurs in any type of joint. It is important to appreciate that OA is a disease only of synovial joints and thus the term cannot be applied to a degenerative arthropathy of the intervertebral disc joints for example, where the term spondylosis deformans is most appropriate (Bennett, 2010). OA is the term that is most commonly used in the recent feline literature to describe the disease in the appendicular joint and is used throughout this thesis.

1.3.2 Types of OA

In human OA, the theory of primary (idiopathic) and secondary OA is well recognised (Kellgren and Moore, 1952). The theory has been applied to canine OA also (Tirgari and Vaughan, 1973; Bennett and May, 1995). Basically, primary OA refers to a condition when there is no specific cause for the joint breakdown, while secondary OA occurs as a result of other diseases which affect the joint and supportive tissues (Rychel, 2010). Most cases of feline OA appear to be primary i.e. there is no obvious underlying cause for the development of the disease (Hardie et al., 2002; Bennett and Clarke, 2004; Clarke et al., 2005; Godfrey, 2005; Clarke and Bennett, 2006; Lascelles et al., 2010).

Primary OA commonly occurs as a late-onset disease without an obvious predisposing factor such as joint injury or developmental abnormalities.

Secondary OA resulting from joint trauma is well reported (Morgan, 1999; Clarke et al., 2005; Godfrey, 2005; Clarke and Bennett, 2006). Clarke et al. (2005) suggested that approximately 25.0% of OA cases resulted from trauma, and Godfrey (2005) reported approximately 13.0% were trauma related. However, it is very difficult to confirm or rule out the occurrence of joint trauma during the lifetime of an individual animal. Many cases of joint trauma may go unnoticed by owners and it may be repetitive low-grade trauma over a period of time that is the important factor.

An association between secondary OA and hip dysplasia (HD) in cats has been described in the literature (Holt, 1978; Schrader and Sherding, 1994; Langenbach et al., 1998; Patsikas et al., 1998; Godfrey, 2005; Clarke et al., 2005; Clarke and Bennett, 2006). HD causes subluxation of the femoral heads and results in abnormal movement and forces across the joint. Over time, this leads to chronic changes in the shape of the bones, cartilage damage, microfractures and secondary OA. Certain breeds are prone to HD (e.g., Siamese and the Maine Coon) (Riser, 1964; Peiffer et al., 1974; Hayes et al., 1979). HD has been incidentally found when cats were radiographed for other reasons (Hayes et al., 1979; Schrader and Sherding, 1994).

Konde et al. (1987) demonstrated the presence of secondary OA in the coxofemoral joints of Siamese cats with mucopolysaccharidosis VI. Severe OA was observed in cats older than 2 years as a result of joint laxity and epiphyseal dysplasia. Scottish Fold osteochondrodysplasia is a well-recognized genetic disorder that affects cartilage throughout the body. The development of OA is rapidly progressive in cats which are homozygous for the abnormal gene compared to heterozygous cats (Malik et al., 1999).

Osteoarthritis associated with acromegaly has been documented in humans (Killinger et al., 2010) and cats (Petersen et al., 1990). In humans, articular changes are frequently severe and can lead to disability. It is believed that elevation of growth hormone (GH) and insulin-like growth factor 1 (IGF-I) levels promote growth of the articular cartilage and periarticular ligaments, subsequently leading to mechanical changes (Lugo et al., 2012).

Other underlying causes of secondary feline OA are developmental luxation of the radial head (Bennett and May, 1995; Bennett et al., 2012a), medial patellar luxation (Loughin et al., 2006), bacterial osteomyelitis (Godfrey, 2005), osteosarcoma (Godfrey, 2005)

and other arthropathies (Lascelles, 2010). In addition to traumatic rupture, cranial cruciate ligament (CCL) failure in the cat may also occur as a gradual 'non-traumatic' event and lead to secondary OA (Harasen, 2005; Schrader and Sherding, 1994).

1.3.3 Prevalence

Several studies have reported on the prevalence of feline OA in the appendicular skeleton. Hardie et al. (2002) conducted a retrospective study from 1994 until 1997 in 100 cats which were more than 12 years of age. The authors also studied the prevalence of DJD affecting the intervertebral joints. The total prevalence of DJD was 90.0% and the total prevalence of appendicular joint OA was 64.0% with the elbow joint most severely affected. However, there was no information on the prevalence of OA in different joints. Kamishina (2003) examined radiographs, pathological changes and the *in vitro* effects of carprofen on the hip joints from a total of 181 cats of unknown age. The prevalence of OA in the hip joint was 14.1% (22 cats), of which 7.1% (11 cats) also had HD. Pacchiana et al. (2004) reported that 16 of 52 cats had radiographic evidence of OA in at least one joint with the elbow joint (21.0%) being most frequently affected.

Clarke et al. (2005) conducted a retrospective study on 218 cats of all ages (median age 10.2 years, range 0.6-16.4 years); they examined archived radiographs at the University of Glasgow Veterinary School between July 1998 and October 2003. They reported that 33.9% (74 cats) of the population had DJD affecting the appendicular and axial skeletons. The total prevalence of appendicular joint OA was 16.5% (36 cats) and 49 joints were affected. The authors also stated that the hip joint (51.0%) was the most commonly affected followed by the elbow joint (26.5%). Most joints (65.3%) only showed mild osteophyte development.

A retrospective radiological study of 292 cats carried out by Godfrey (2005) showed 22.0% (63 cats) had radiographic signs of OA. According to his study, the elbow joint was the most frequently affected and the pathology was bilaterally symmetrical in 41 cats (73.0%).

Clarke and Bennett (2006) investigated a population of 28 cats (median aged 11 years) with clinical OA. They prospectively reported details of affected joints and were interested to study the clinical signs and response to analgesic therapy. 71.0% (20 cats) were considered to have primary OA, 7.0% (2 cats) had secondary OA and 22.0% (6 cats) had a combination of primary and secondary OA. In this study, the elbow (45.0%) and hip (38.0%) joints were the most frequently affected.

Another recent prospective study reported the prevalence of OA in 100 randomly selected cats (Lascelles et al. 2010). The cats were grouped according to age (6 months to 5 years; >5-10 years; >10-15 years; and >15-20 years). OA was graded according to its severity; grade 0 (normal joint); grade 1 (trivial); grade 2 (mild); grade 3 (moderate); and grade 4 (severe). The authors evaluated the entire appendicular skeleton of each cat and again showed that OA increased with age and found that 91.0% of the cats showed OA in at least one appendicular joint (80.0% for the 6 months to 5 years; 84.0% for the >5-10 years; 100.0% for both 10-15 years and >15-20 years respectively); the most commonly affected joints were the hip (65.0%), followed by stifle (50.0%), tarsus (40.0%) and elbow (35.0%) joints. They also found a high percentage of cats affected with bilateral OA which is consistent with previous findings. The authors suggested that geographical differences in the prevalence of OA may exist because of environmental and genetic influences.

In a recent cross-sectional study, Slingerland et al. (2010) reported the prevalence and the clinical features of OA in the appendicular skeleton of 100 cats, all older than 6 years. Sixty-one per cent of cats were diagnosed with OA in at least one joint and 48% in more than one joint. They also found that radiographic OA was mostly observed in the shoulders, elbows, hips and tarsal joints and the prevalence of OA increased with age but was not correlated with body score.

1.4 Radiography and feline OA

Radiography of appendicular joints provides a very important assessment of joint pathology (Morgan, 1972; Houlton, 1994). The radiographic assessment of OA has three main purposes: (1) to establish the diagnosis or severity of OA; (2) to monitor disease activity, progression and possible therapeutic responses; and (3) to look for complications of the disease or treatment (Buckland-Wright, 2003).

Plain radiography is regarded as the gold standard for the diagnosis, assessment and monitoring of OA in humans (Kellgren and Moore, 1952), dogs (Morgan, 1969; Tirgari and Vaughan, 1975; Guthrie, 1989; Innes et al., 2004; Rayward et al., 2004), cats (Langenbach et al., 1998; Godfrey, 2000; Godfrey, 2002; Hardie et al., 2002; Godfrey, 2003; Godfrey, 2005; Clarke et al., 2005; Clarke and Bennett, 2006; Freire et al., 2011) and experimental animals (Boulocher et al., 2010; Nikahva et al., 2011).

Proper joint positioning is important for radiographic interpretation and diagnosis. Houlton (1994) suggested at least two radiographs are needed to evaluate the joint

fully. The mediolateral view is one of the standard radiographic views for the elbow, stifle, shoulder, carpal and the tarsal joints (Slingerland et al., 2010; Freire et al., 2011). Supplementary radiographic views for the elbow, stifle, tarsal and carpal joints includes a caudo-cranial, cranio-caudal, dorso-plantar and a dorso-palmar view respectively (Slingerland et al., 2010; Freire et al., 2011). A ventro-dorsal (VD) radiograph with the hindlimbs extended is the standard view for evaluation of the hip joints (Langenbach et al., 1998; Slingerland et al., 2010; Freire et al., 2011). Stress views of the hip joint have been recommended as providing more precise information with respect to joint laxity and its association with HD (Smith et al., 1990; Langenbach et al., 1998). Stress radiographic positioning often requires the animal to be held by an assistant during the radiographic exposure. The practice is controversial and not recommended in some countries including the U.K. due to health and safety issues.

1.4.1 Radiographic features

Osteophytes are considered to be the hallmark of OA. They usually develop around the periphery of the joint and appear as bony outgrowths. Osteophytes may also develop in the central areas of a joint, around remnants of cartilage and at the site of ligament attachment (Carrig, 1997). Osteophyte formation is a mechanism by which the joint alters its shape (remodelling), in an attempt to improve joint function. Clarke et al. (2005) suggested that osteophyte formation in the cat often tends to be less advanced compared to the dog. The development and size of the osteophyte tends to increase with time as the disease progresses (Marshall, 1969). Freire et al. (2011) stated that radiographic appearance of osteophytes in cats differs from dogs but did not specify the difference.

Damage to (i.e. loss of) the articular cartilage is usually seen as a narrowing of the joint space between opposing articular bony surfaces (Owens, 1982). Narrowing of the joint space can be more reliably demonstrated with weight-bearing radiographs (Morgan, 1969; Leach et al., 1970), but these are not routinely performed in small animal patients and are almost impossible to achieve in the cat. The sensitivity and specificity of this feature in detecting early articular cartilage loss has been questioned (Brandt et al., 1991; Fife et al., 1991). Brandt et al. (1991) believe that the assessment of joint space narrowing does not provide information on the severity of articular cartilage damage in OA.

Subchondral bone sclerosis is a term that has been used to describe increased bone opacity in OA joints (Morgan, 1999). It usually occurs in areas of the joint that are

subject to stress (Marshall, 1969). Sclerosis is reported more often in joints with severe osteophytosis (Clarke et al., 2005) but it has been speculated that this may due to superimposed osteophytes being interpreted as sclerosis (Jewell et al., 1998). The term subchondral sclerosis is often used to refer to an increased thickening of bony trabeculae beneath the articular surface leading to increased bone density and stiffness (Burr and Schaffler, 1997). The terms sclerosis, increased radio-density and increased radio-opacity are often used interchangeably when describing radiographic features of joints. However this should be challenged. Sclerosis is a pathologic feature which means a hardening of tissues. Thrall (2005) recommended that the term radio-opacity should be used to describe bony radiographic changes rather than radio-density. The word opacity is more accurate when describing an area of a radiograph that is more nearly white than its surrounding, i.e where more mineral is present to absorb or deflect the X-ray beam. Moreover, The Nomenclature Committee of the Fleischner Society (Tuddenham, 1984) has recommended that the word opacity be used in place of density when describing an absorber in the path of the x-ray beam. In this study, the term sclerosis is not used and changes in bony mineralisation are described as changes in radio-opacity rather than radio-density.

Enthesiophytes form on non-weight bearing surfaces and are incorporated into adjacent ligamentous or capsular attachments (Marshall and Olsson, 1971; Sokoloff, 1980; Carrig, 1997; Morgan, 1999). They often occur at the attachment of the patellar ligament on the tibial tuberosity in the cat stifle joint (Bennett, 2010).

Freire et al. (2010) reported a prospective study to determine the prevalence of meniscal mineralisation and its correlation with articular damage in 30 cats. Of 57 stifle joints, 34 (60.0%) had radiographic mineralisation within the cranial horn of the medial meniscus. This study showed a relationship between meniscal mineralisation and articular cartilage damage on the medial femoral condyle and medial tibial plateau. They suggested that meniscal mineralization was a response to other degenerative changes within the joint. Bennett (2010) concluded that meniscal mineralisation is commonly seen in the cranial pole of the medial meniscus of the cat and suggested it might represent degenerative meniscal calcification as reported by Freire et al. (2010) or possibly the presence of a sesamoid bone representing a normal feature of the feline meniscus.

Soft tissue swelling and synovial effusion may be present but are less commonly seen in the cat than the dog (Morgan, 1972; Thrall, 2007). Joint effusion can be seen radiographically as a soft tissue opacity and in the stifle joint may compress the

infrapatellar fat pad and displace fascial planes caudal to the joint (Dennis et al., 2001).

The absence of radiographic signs of OA does not rule out the presence of this disease since early pathological changes can occur before radiographic changes are evident.

1.4.2 Radiographic scoring

Several scoring systems have been derived to assess the radiographic changes associated with OA. With human OA, the first and most commonly used system was developed by Kellgren and Lawrence (1957). Later in 2007, a comprehensive atlas was developed which grade individual features of OA (Altman and Gold, 2007). Guthrie (1989) published a grading system for scoring radiographic features of the canine elbow related to elbow dysplasia and secondary OA. Innes et al. (2004) have published radiographic scoring schemes for canine OA. Very little has been published on assessing feline radiographic OA (Hardie et al., 2002; Clarke et al., 2005; Godfrey, 2007; Lascelles et al., 2010; Freire et al., 2011). Scoring systems used in recent studies of feline OA/DJD are shown in Table 1.1.

The studies of Hardie et al. (2002) and Clarke et al. (2005) relied predominantly on assessing osteophyte and enthesiophyte formation and size. There are limitations because of their location and size; the presence of osteophyte and enthesiophyte formation is often underestimated on plain radiography particularly in the early stages of OA. Godfrey (2007) considered joints with an osteophyte score more than zero as having OA and a total osteoarthritis score was calculated by adding the osteophyte, enthesiophyte, soft tissue mineralisation and sclerosis scores together. Joints without osteophyte formation but with other radiographic lesions present were considered as having DJD rather than OA.

Lascelles et al. (2010) and Freire et al. (2011) scored the severity of each radiographic change (Table 1.1). They included a subjective radiographic score, termed an “overall DJD score” from 0 to 10 (0-no radiographic abnormalities identified; 10-ankylosis). This was an “overall impression” score without detailed analysis of each different radiographic feature.

Radiographic scoring	Score	Description
Hardie et al. (2002)	0	Normal
	1	Small enthesiophytes or osteophytes
	2	Obvious enthesiophytes and osteophytes but minimal change to joint structure
	3	Extensive peri and intra-articular mineralisation, severe subchondral sclerosis, and joint remodelling
Clarke et al. (2005)	Mild	Enthesiophytes and osteophytes (slight roughening of the articular margins)
	Moderate	Enthesiophytes and osteophytes (moderate roughening of the articular margins)
	Severe	Obvious osteophytes/enthesiophyte deposition
Godfrey (2005)	Present or absent	Periarticular new bone
		Increased subchondral bone density
Godfrey (2007)		Osteophytes:
	0	Absent
	1	An osteophyte less than 2mm
	2	Osteophytes 2-5mm
	3	Osteophytes more than 5mm
		Enthesiophytes:
	0	Absent
	1	Slight roughening
	2	Moderate bone deposition
	3	Marked bone deposition
		Soft tissue mineralisation:
	0	Absent
	1	Present
		Subchondral sclerosis:
	0	Absent
	1	Present

Table 1.1: A selection of radiographic scoring systems used in recent studies of feline OA

Radiographic scoring	Score	Description
Lascelles et al. (2010)	0	Normal
	1	Trivial
	2	Mild
	3	Moderate
	4	Severe
		Osteophytes, enthesiophytes, joint-associated mineralisation, joint effusion, sclerosis, subluxation, subchondral bone erosions and cysts, presence of intra-articular mineralisation (including suspected meniscal mineralisations within the stifle joints) and new bone formation on the dorsal surface of intertarsal and tarsometatarsal joints.
Freire et al. (2011)	0	Normal
	1	Trivial
	2	Mild
	3	Moderate
	4	Severe
		Osteophytes, enthesiophytes, joint-associated mineralisation,joint effusion, sclerosis, subchondral bone erosions and cysts, coxofemoral subluxation, intra-articular mineralisation (including meniscal mineralisation within the stifle joints) and new bone formation on the dorsal surface of intertarsal and tarsometatarsal joints.

Table 1.1 continued.

1.4.3 Association between radiographic OA and clinical features

Godfrey (2003) conducted a prospective study of 40 cats with clinical OA. Of these, 35 (87.0%) had primary OA and the main radiographic features were osteophytes and increased radiopacity of the bone. He described thickening of joints, reduced mobility and resentment of palpation as the most common physical findings. Owners of cats with OA had reported lameness and inactivity as clinical features.

Clarke and Bennett (2005) reported on the clinical findings in 29 cats with OA. Seventy-two per cent of cats had difficulty or unwillingness to jump, 59.0% showed a changed demeanour, 24.0% had a limp, 38.0% had a stiff gait and 38.0% resented handling.

Clarke and Bennett (2006) conducted a further prospective study to identify a cohort of cats with clinical signs together with radiographic evidence of OA. They recorded abnormalities or changes in food intake, demeanour, activity and behaviour. The physical examination revealed joint pain in 86 joints of 25 cats although 13 of these showed no evidence of radiographic OA. Sixty-four per cent of joints with advanced radiographic features had periarticular thickening detected by palpation and only 4.0% of the joints had a reduced range of motion and crepitus was not detected. They reported that unwillingness to jump, reduced height of jumping, stiff gait, reduced activity level and lameness or limping all improved after treatment with a non-steroidal anti-inflammatory drug (NSAID) concluding that changes in the cats's behaviour and lifestyle were the most important indicators of feline OA. They considered vocalising on handling, resenting handling, aggression on handling and changes in food intake were not specifically associated with clinical OA.

Lascelles et al. (2007) evaluated the used of owner-based questionnaires and a collar mounted activity monitor to detect changes in behaviour before and after NSAID treatment in 13 senior cats with OA. Of 208 appendicular joints assessed 55 (26.4%) had radiographic OA and 18 of them had joint pain. The mobility and quality of life of cats with OA following analgesic administration were improved.

Bennett and Morton (2009) described the use of an owner questionnaire to gather information on mobility, activity, grooming and temperament, before and after a 28-day course of meloxicam treatment in 23 cats with chronic musculoskeletal pain. Owners were asked to score their cat's current lifestyle or behaviour compared with how it was when it was a young adult, and then to make the same comparison after the course of treatment. Owners reported changes in their cat's behaviour and lifestyle

over time and a reverse in these behavioural patterns when pain relief was administered. The greatest changes were prominent in the activity and mobility domains particularly in jumping behaviour.

A more recent study by Slingerland et al. (2011) of one hundred client-owned cats found that 61.0% of the cats had radiographic evidence of OA in at least one appendicular joint. Of the 100 cats, 13 were lame. They reported decreased mobility, reduced grooming and inappropriate use of the litter tray as features of OA.

1.4.4 Other diagnostic modalities

1.4.4.1 Computed tomography (CT) scanning

CT scanning is able to define soft tissue as well as bony changes because of excellent contrast resolution, cross-sectional display and its ability to quantify specific attenuation values (Carrig, 1997). CT can detect the early stages of canine OA and is also capable of identifying the presence and source of intra-articular bodies and calcification (Carrig, 1997).

The development of micro-CT has revolutionised the use of animal models in musculoskeletal research. X-ray attenuation data acquired at multiple viewing angles can be used to reconstruct 3D images and this has proved valuable in examining the morphological changes occurring in OA joints (Barck et al., 2004; Piscaer et al., 2008a; Piscaer et al., 2008b). Boyd et al. (2005) investigated the subchondral bone changes in a CCL-transected cat for OA using a micro-CT technique. They reported the quantitative 3D assessments of osteoarthritic joints including subchondral bone morphology, bone volume and surface density and trabecular bone thickness. Furthermore, Botter et al. (2006) quantified the subchondral bone changes in a murine OA model using a micro-CT technique. They reported the quantitative and qualitative 2D and 3D assessments of osteoarthritic joints including subchondral bone morphology and bone mineral density, trabecular bone patterns, meniscus morphology, heterotropic ossification and subchondral cyst formation. However, the ability of micro-CT to visualise the degenerative changes in articular cartilage is disputed due to its low sensitivity for soft tissue (Tremoleda et al., 2011).

1.4.4.2 Magnetic resonance imaging (MRI)

Magnetic resonance imaging (MRI) is widely used in human rheumatology as a diagnostic tool for OA. This technique provides multiplanar tomographic imaging, which eliminates

the problem of superimposition of overlapping structures; it also enables assessment of the whole joint since it provides bone and soft tissue detail, including direct visualization of articular cartilage (Peterfy, 2002).

MRI is a sensitive and specific tool for detecting articular cartilage damage in the human knee (Disler, 1997; Rech et al. 1996; Bredella et al., 1999). Cartilage defects are described as focal areas of hypointensity, irregularities of the surface, loss of the sharp interface on the surface of the cartilage or as frank defects in the articular cartilage (Hayes and Conray, 1992). Sowers et al. (2003) evaluated the association of knee pain with the radiographic and MRI features in a cohort of middle-aged women with OA. Of 58 patients who were radiographically normal on the Kellgren-Lawrence grading but had knee pain, 26.0% had full thickness cartilage defects detailed by MRI and another 10.0% had moderately severe cartilage defects of >50.0% of its thickness. MRI has also demonstrated bony changes (Nolte-Ernsting et al., 1996).

Kamishina et al. (2006) evaluated the hip joint of 12 cats using MRI with T2-weighted fast spin-echo (FSE) and proton density (PD)-weighted images. The technique was used to detect abnormalities in the signal intensity of articular cartilage and subchondral bone rather than to detect morphological changes. They also compared MR images with high-detail radiographs and with the gross and histopathological features of feline hip joints. MR images of 18 normal femoral heads demonstrated that the articular cartilage appears as an intermediate signal intensity compared to the low signal intensity of subchondral bone and the high signal intensity of synovial fluid. Due to the latter the cartilage appeared to be obscured particularly at the caudal aspects. However, subchondral bone was detectable as a band of low signal intensity beneath the articular cartilage. MRI examination of 6 hip joints with radiographic OA revealed a thickened band with low signal intensity corresponding to a thickened subchondral bone which was also visible on the high-detail radiograph. Femoral head cartilage was partially visible on the cranial and caudal aspects using PD-weighted imaging. They failed to recognized abnormalities on the T2-weighted FSE in 3 cats with OA. The thickness of the feline hip articular cartilage is less than 200 μm, and this is a major reason why it is difficult to see cartilage lesions with routine MRI machines. van Bree et al. (2011) also reported that canine articular cartilage visualisation by MRI is difficult because the articular cartilage is so thin and there is insufficient contrast between joint fluid and articular cartilage.

A more recent study by Guillot et al. (2012) reported OA related lesions in 6 cats using MRI. They included physical examination and radiography as part of the study.

Osteophytes and increased bone opacity were detected on both MRI and radiography. In one cat that was radiographically normal, mild osteophyte formation, articular effusion and thinning of the articular cartilage were seen on the MR images. They also reported bone marrow edema-like (BML) lesions within the subchondral bone in 2 cats with OA. BML have been reported in the subchondral bone of human OA joints (Kwan Tat et al., 2010) and have been associated with pain and disease progression (Taljanovic et al., 2008; Wenham and Conaghan, 2009).

1.4.4.3 Arthroscopy

Arthroscopy provides for the direct observation and assessment of articular cartilage (Bennett, 1990; van Bree and Van Ryssen, 1998; Staiger and Beale, 2005). Its ability to permit a thorough evaluation of the anatomic structures within the joint, allows the clinician to grade the severity of cartilage disease and to measure outcomes in OA therapeutic trials (Franssen et al., 1989; Raatikainen et al., 1990). The use of arthroscopy in dogs was first reported in 1978 (Siemering, 1978). It has been used to diagnose medial compartment disease of the elbow (Vermote et al., 2010) and has become the preferred method for removal of osteochondral fragments associated with elbow dysplasia (Beale et al., 2003).

Staiger and Beale (2005) conducted an arthroscopic assessment of the cat elbow joint with a suspected fragmented medial coronoid process. They used arthroscopy to evaluate the elbow joint, remove the loose osteochondral fragments and to debride the articular surface.

1.4.4.4 Ultrasonography

The use of ultrasonography has been reported in the diagnosis of cartilage abnormalities, tendon and ligament abnormalities, meniscal tears, arthropathies and neoplasia in dog (Reed et al., 1995; Soler et al., 2007). Normal articular cartilage appears as a smooth echo band at the tissue surface with a hypoechoic matrix (Chhem et al., 1994; Myers et al., 1995). In OA, articular cartilage is visible as a hyperechoic and inhomogenous band (Kramer et al., 1997). However, it may not be visualized in the presence of excessive anechoic joint effusion (Samii and Long, 2002). Osteophytes appear as irregularly circumscribed protuberances on the bony surfaces (Michele et al., 1998; Samii and Long, 2002). Joint capsule thickening appears as a hyperechoic, thick line between the synovium and the surrounding musculature (Samii and Long, 2002).

Assessment of cartilage thickness of normal and osteoarthritic joints using high frequency ultrasonography is reported in humans (Myers et al., 1995).

1.5 Pathologic changes associated with OA

1.5.1 Articular cartilage

1.5.1.1 Gross findings

In the early stages the surface appears rough, soft, dull and fibrillated (Mankin, 1985; Poole, 1999). Yellow-brown discolouration, shallow furrows or streaking, superficial fraying, splitting and pitting of the articular cartilage are also reported as early gross pathological features (Bennett et al., 1942; Bennett, 1990; Gahunia et al., 1995; Weisbrode and Doige, 2001). As the disease progresses, focal loss of cartilage with extensive erosion is seen (Gahunia et al., 1995; MacPhail, 2000; Weisbrode and Doige, 2001). The cartilage can be completely lost (ulceration) exposing the subchondral bone. In some OA joints, mineralised bodies can be seen lying free or adhered to the synovium. It is believed that these represent fragments of articular cartilage released into the articular cavity (Weisbrode and Doige, 2001).

1.5.1.2 Histopathological findings

Changes to the articular cartilage are first seen at the superficial layer (Mankin et al. 1971). Superficial fibrillation with an uneven articular surface was described as an early microscopic feature of OA (Weisbrode and Doige, 2001; Pritzker et al., 2006; Cook et al., 2010). An initial loss of proteoglycan is seen as a reduced staining with cationic stains such as Safranin O or Toluidine Blue (Gahunia et al., 1995; Pritzker et al., 2006; Cook et al., 2010). As OA progresses, vertical fissures and fibrillation will extend into the middle zone. In advanced OA, the fissures may extend into the deep and calcified layers. Erosion and ulceration with marked reduction of Safranin O or Toluidine Blue staining throughout the entire cartilage can occur (Pritzker et al. 2006; Cook et al., 2010). Necrosis of individual chondrocytes occurs in the deep layer, making the cartilage hypocellular (Ryan et al., 2013). The remaining chondrocytes can undergo regenerative hyperplasia and form “clusters” (Weisbrode and Doige, 2001).

The calcified articular cartilage layer shows important changes during OA. Multiplication of the tidemark is often seen and an increase of the calcified cartilage thickness is reported (Henrotin et al., 2012). It is claimed that the articular cartilage undergoes continuous calcification and endochondral ossification and this may cause the layer of

calcified cartilage to thicken and subsequently alter the load distribution within the joint (Bullough and Jagannath, 1983). Invasion of blood vessels from the subchondral bone beyond the tidemark is observed in osteoarthritic cartilage.

1.5.2 Bone

Bony changes occur mainly in the subchondral bone plate, the trabecular portion of the medullary canal and at the attachment of the joint capsule (Dedrick et al., 1993; Renberg, 2005).

Subchondral bone changes are thought to be an important feature of OA even though the question of whether these bony changes occur before cartilage degeneration or subsequent to it remains controversial (Neogi, 2012). Weisbrode and Doige (2001) suggest that thinning or absence of the articular cartilage increases the stresses on the subchondral bone causing it to become more dense and thicker eventually having a smooth "ivory-like" surface (eburnation). However, other studies have reported that changes in the subchondral bone may occur at an early stage even prior to the onset of cartilage degeneration (Radin and Rose, 1986; Carlson et al., 1994; Hayami et al., 2006; Quasnichka et al., 2006).

In a feline cranial cruciate ligament transection (CCLT) model, decreases in bone volume and subchondral bone plate thickness have been observed (Boyd et al., 2005). A similar finding was found in a canine CCLT model (Sniekers et al., 2008). However, another study found no changes in the thickness of the canine subchondral bone plate (Boyd et al., 2002). In human OA, an increase in bone volume and thickening of the subchondral plate and trabecular bone was reported (Grynpas et al., 1991; Bobinac et al., 2003). Variation of the bone parameter may be due to the method used in measuring the subchondral bone plate thickness. Development of digital microscopic image analysis and micro-CT has facilitated detailed evaluation of subchondral bone (Sniekers et al., 2008). Moreover, a change in the subchondral bone varies between disease stages. In early-stage OA, thinning of the subchondral bone plate and trabecular occur as a result of an increased remodelling rate and turn over. In late-stage OA, thickening of the subchondral bone plate is evident (Burr and Gallant, 2012). Subchondral bone "cysts" are occasionally seen in osteoarthritic joints of humans and dogs (Baird et al., 1998) but have not been reported in the cat. A subchondral "cyst" arises from the replacement of bone trabeculae and marrow by mixed connective tissue (Bennett, 1990).

Osteophyte formation is an important feature of OA (Weisbrode and Doige, 2001). They develop at the point of joint capsule attachment and along the articular margin (Dedrick et al., 1993). Histologically, an osteophyte is first identified as an area of proliferating cells in the periosteum covering the bone at the cartilage and bone junction. The cells undergo chondrogenesis and osteogenesis to form woven bone. Later, endochondral ossification becomes a prominent feature of osteophytic growth. As the osteophyte grows, it develops a trabecular structure and the epiphyseal cortex becomes resorbed, such that the marrow spaces of the osteophytes become contiguous with those of the epiphysis. The osteophyte remains covered by fibrocartilage or fibrous periosteum (Bennett, 1990). In an experimental study, it was reported that osteophytes can develop as early as 3 days after induction of the disease process in dogs long before any morphological or biochemical changes in the articular cartilage (Gilbertson, 1975).

Changes of the subchondral bone, osteophyte production and cyst formation are all part of a pathologic process referred to as remodelling which occurs in any osteoarthritic joint. Remodelling of the internal structure of the epiphyses is also seen, making the bone a completely different shape. Wolff's law states that the internal architecture of a bone changes shape to accommodate the stresses placed upon it. Secondary OA due to ligament damage and instability for example can lead to altered joint kinematics and stress distribution (Bennett, 1990).

1.5.3 Synovium

The gross changes that occur in the OA synovium include hyperaemia and thickening (Myers et al., 1990; Cook et al., 2010). Hyperplasia and hypertrophy of the synovial lining layer are seen in early OA. Villous hyperplasia is also present characterised by short to "finger-like" projections (Bennett, 1990; Cook et al., 2010). Fibrin deposition at the synovial surface and fibrosis of the supporting layer may occur in advanced OA (Loeuille et al., 2005). These changes are often accompanied by infiltration of the synovial supporting layer with lymphocytes and plasma cells, either diffusely or as perivascular aggregates (Smith et al., 1997; Oehler et al., 2002; Smith, 2002). Accumulation of macrophages is also reported (Haywood et al., 2003). It has been claimed that such changes possibly represent a response to cartilage and other joint debris (Alsalameh et al., 1990). However, Oehler et al. (2002) reported that the inflammatory pattern observed in the synovial membrane is not dependent on the presence of cartilage-breakdown products. Increased vascularity is commonly seen in OA synovial tissue.

1.5.4 Intra-articular structures

Changes in menisci are reported in human and animal OA (Hellio Le Graverand et al., 2001; Pauli et al., 2011; Sun et al., 2012). Gross changes include discolouration from white to a dark yellow to light brown or reddish colour. Fibrillation and tears are also reported. Histologically, there may be hypo- or hyper-cellularity along with hypertrophy and abnormal cell clusters (Pauli et al., 2011). Decreased collagen content has also been demonstrated (Pauli et al., 2011). However, studies of proteoglycan content have given conflicting results. Sun et al. (2012) reported that the proteoglycan content increased in human menisci with OA. A similar finding was reported in experimental rabbit menisci (Videman et al., 1979). However, Djurasovic et al. (1998) reported that the proteoglycan content decreased in the menisci of experimental OA dogs. Another study reported that the proteoglycan content decreased in menisci during the first three months after the experimental induction of OA but increased gradually thereafter (Adams et al., 1983). Neither collagen nor proteoglycan studies have been reported in the cat.

Mineralisation within the medial meniscus of the stifle joint is commonly seen in cats. It can be seen in very young cats and where there is no other evidence of OA. Although the exact significance of this meniscal mineralisation is uncertain, Freire et al. (2010) concluded that it is invariably associated with cartilage damage, particularly on the medial femoral and tibial condyles and as such it is a feature of OA.

1.6 Molecular pathology and pathobiology of OA

1.6.1 Alteration in the extracellular matrix

The aetiology of idiopathic OA remains unknown. It has been hypothesized that OA begins with a disruption of the superficial layer of the articular cartilage resulting in biochemical changes that lead to degradation of the articular tissue (Teitelbaum and Bullough, 1979; Radin et al., 1995). Other workers reported that the inciting event of OA is attributed to damage to the collagen network (Maroudas et al., 1973; Mow, 1990).

Regardless of the inciting event, degeneration of the articular surface initiates several changes. Fibrillation disrupts collagen fibres parallel to the articular surface. As OA progresses, the disruption becomes perpendicular to the deeper layers and causes further damage to the articular cartilage. Collagen cross- linkages breakdown and this is thought to occur due to degradative proteases produced by the chondrocytes. Instead of forming an interlocking meshwork, the collagen fibrils become radially aligned which in

turn decreases their ability to retain proteoglycans (Burr and Radin, 1990). Proteoglycans are lost from the superficial layer of the articular cartilage into the synovial fluid. This occurs prior to the hypertrophic response of chondrocytes (Muir, 1986). Damage to the collagen fibrils will increase the cartilage water content, resulting in abnormal hydration of the remaining proteoglycans (Mankin and Brandt, 1997). All these changes will decrease the stiffness of the matrix which results in loss of mechanical articular function.

1.6.2 Chondrocyte response to tissue damage

The cellular responses begin when chondrocytes release biochemical mediators (cytokines), following detection of tissue damage, changes in osmolality, charge density or strain (Buckwalter et al., 2005). In normal joints, the biosynthesis of the cartilage matrix is stimulated by various anabolic cytokines and growth factors including IGF-1, TGF-ß, BMPs and fibroblast growth factor-2 (FGF-2). Most of the catabolic cytokines are not expressed or are maintained at low levels during homeostasis and are only produced in response to tissue injury (Lotz, 1997). In OA, both anabolic and catabolic cytokine production is enhanced. OA chondrocytes produce increased levels of the inflammatory cytokines such as IL-1ß, IL-6, and Tumour Necrosis Factor-α (TNF-α) (Pujol et al., 1991; Martel-Pelletier et al., 1999; Maccoux et al., 2007).

Chondrocyte "cluster formation" seen in OA can be induced by several growth factors and FGF-2 appears the most important (Quintavalla et al., 2005). The clustered chondrocytes attempt to repair the damaged matrix by increasing synthesis of ECM components (Sandell and Aigner, 2001; Buckwalter et al., 2005). Proliferation and differentiation of chondrocytes results in the synthesis of high levels of vascular endothelial growth factor (VEGF) and bone sialoprotein (Pesesse et al., 2011), which promote endothelial cell proliferation and migration (Henrotin et al., 2012). These changes cause blood vessel invasion from the subchondral bone to beyond the tidemark.

It is assumed that the chondrocytes begin to synthesize abnormal collagen and proteoglycan when their ability to maintain the balance of anabolic and catabolic activities associated with normal matrix turnover is compromised (Renberg, 2005). The abnormal chondrocytes may produce Type I collagen, which is less biomechanically effective than type II collagen in weight distribution, and proteoglycans with less aggregated and shorter GAG sidechains (von der Mark et al., 1977; Buschmann et al., 1992; Bonaventure et al., 1994*). In situ* analyses by Aigner and Dudhia (1997) showed that chondrocytes at the superficial layer reduced their expression of matrix

components particularly aggrecan, while chondrocytes in the middle and deep layers were actively synthesizing matrix components. McDevitt and Muir (1976) suggested that proteoglycan content and quality changes can occur before there is any grossly visible damage to the articular cartilage surface.

Chondrocyte death by apoptosis has been reported in human (Blanco et al., 1998; Kim et al., 2000) and animal OA (Adams and Horton 1998; Thomas et al., 2007; Mistry et al., 2004; Zamli et al., 2013). It is claimed that chondrocyte apoptosis is responsible for the hypocellularity seen in OA cartilage mainly in the regions close to the fibrillated areas (Kim et al., 2000; Mistry et al., 2004). IL-1 and TNF-α have been reported as directly promoting chondrocyte apoptosis (Goggs et al., 2003; Afonso et al., 2007). However, other studies of chondrocyte apoptosis have given contradictory results. Zamli et al. (2013) reported that the chondrocyte apoptosis level increased with advancing stages of OA, suggesting that apoptosis plays an important role in cartilage loss. Sandel and Aigner (2001) however claimed that apoptosis occurs only at a very low rate and the death of chondrocytes has only a minor impact on the pathogenesis of OA.

1.6.3 Metabolic disruption of cartilage homeostasis

Chondrocytes perform a continuous synthetic activity and remove the existing ECM by degradative enzymes in a delicate balance. In OA, however, this balance is disturbed with both synthesis and degradation enhanced, but with an overall shift towards catabolism over anabolism. Chondrocytes synthesize degradative enzymes which include various proteases. The primary categories include metalloproteinases (MMP), serine and cysteine. The MMP family plays a major role in the articular cartilage breakdown, especially those specific enzymes known as collagenase and stromelysin (Renberg, 2005). The collagenases, particularly collagenase-1 (MMP-1) and collagenase-3 (MMP-13) are mainly involved in type II collagen degradation (Reboul et al., 1996; Martel-Pelletier, 2004), whereas stromelysin-1 (MMP-3) is involved in proteoglycan degradation (Pelletier et al., 1991). *In vitro* studies of cartilage degradation in cats demonstrated that MMP-13 activity was increased in response to catabolic cytokines such as IL-1 and oncostatin M (Gabriel et al., 2010). Other MMPs that have been reported to be involved in OA include MMPs 2, 7, 8, 9 and 14 (Coughlan et al., 1998; Chubinskaya et al., 1999; Yoshihara et al., 2000; Zrimsek et al., 2007; Wu et al., 2008). The activity of these enzymes is normally controlled by the tissue inhibitor of the metallproteinases (TIMPs) of which there are 4 (TIMP-1, 2, 3, and 4). However, in OA cartilage, the cytokines such as IL-1β and TNF-α are able to modulate chondrocyte metabolism to increase MMP synthesis and inhibit the synthesis of TIMPs (Todhunter, 1992; Martel-Pelletier, 2004).

The unbalanced activity between TIMP and MMP results in progressive articular cartilage degradation.

Aggrecanases are a relatively new family of degradative enzymes that have been identified in the articular cartilage. The aggrecanases are members of the 'A Disintegrin and Metalloproteinase with ThromboSpondin motifs' (ADAMTS). Aggrecanase-1 (ADAMTS-4) and aggrecanase-2 (ADAMTS-5) are the most potent aggrecanases responsible for aggrecan degradation in OA articular cartilage (Tortorella et al., 2001).

Involvement of the serine proteases such as matriptase has been reported in human OA (Milner et al., 2010). Matriptase is able to activate MMP-1, MMP-13 and inflammatory mediators thus making it an important contributor to cartilage degradation.

1.6.4 Synovium

Synovitis in OA is likely to contribute to disease progression. Cartilage-breakdown products can activate synoviocytes, mainly the Type A synoviocyte to produce inflammatory cytokines including IL-1 and TNF- α that may accelerate destruction of the articular cartilage (Benito et al., 2005). The cytokines have a direct effect on the chondrocytes and synoviocytes to stimulate MMP production. The chondrocytes and synoviocytes then produce further IL-1 and TNF-α, which then further stimulates the MMP production. IL-1 also stimulates the Type B synoviocyte to produce collagen types I and III that may contribute to fibrosis of the joint capsule in the osteoarthritic joint (Lotz, 1997; Pelletier et al., 1997).

The Type A synoviocyte is also involved in the formation of osteophytes (Blom et al., 2004; van Lent et al., 2004). Together with chondrocytes, the activated synovial macrophages can produce several growth factors such as TGF-β and BMP-2 in high quantities (Cutolo et al., 1993; Champagne et al., 2002; Rader et al., 2002). Production of these factors by synoviocytes is strongly diminished when macrophages are removed from the synovial lining, thus reducing the osteophyte formation in an experimental OA model (Blom et al., 2004). Osteophytes often develop at the cartilage and bone junction and are thought to originate from mesenchymal cells in the periosteum, and start as chondrogenic outgrowths with subsequent transformation to bony structures. These chondro- and osteogenesis processes are induced by TGF-β and BMP-2 (van Beuningen et al., 1998).

The synovial macrophages of OA joints also secrete VEGF (Bonnett and Walsh, 2005). It has been hypothesized that production of VEGF is a possible molecular mechanism which exacerbates synovial angiogenesis and inflammation in OA (Haywood et al., 2003), although the exact regulation of angiogenesis in an OA joint is not completely understood (Ashraf and Walsh, 2008).

1.6.5 Role of other inflammatory mediators

In addition to cytokines, other inflammatory mediators also play a major role in the OA pathological process. Chondrocytes, as well as synoviocytes of OA joints produce nitric oxide (NO), prostaglandin E2 (PGE2) and a newly identified cell membrane receptor family, the protease-activated receptor-2 (PAR-2) (Abe et al., 2006; Xiang et al., 2006; Boileau et al., 2007). NO promotes cellular injury and chondrocyte apoptosis (Hashimoto et al., 1998), whereas PGE2 exerts anabolic and catabolic activities on chondrocytes leading to a decrease in proteoglycan synthesis and an increase in the degradation of both aggrecan and type II collagen (Attur et al., 2008). PGE2 also plays an important role to induce pain by directly exciting nociceptive primary sensory neurons and indirectly stimulating the release of pain related peptide such as substance P and calcitonin gene-related peptide (Ma, 2010).

Several studies in humans and animal models have demonstrated a key role of PAR-2 in mediating arthritic inflammation (Ferrell et al., 2003; Xiang et al., 2006; Boileau et al., 2007; Boileau et al., 2009; Ferrell et al., 2010; Amiable et al., 2011). PAR-2 messenger ribonucleic acid (mRNA) and protein levels in OA chondrocytes, synoviocytes and osteoblasts are significantly elevated compared to normal cells, suggesting that PAR-2 plays a pathological role in OA (Xiang et al., 2006; Boileau et al., 2007; Amiable et al., 2009; Tindell et al., 2012). Matriptase has been recognised as an endogenous activator of PAR-2 (Milner et al., 2010). The expression level of PAR-2 in these cells is upregulated by IL-1β and TNF-α (Xiang et al., 2006; Boileau et al., 2007). PGE2 may also be involved in the upregulation of PAR-2 in the osteoblast (Amiable et al., 2009). PAR-2 activation increases the production of MMP-1, MMP-13, cyclooxygenase-2 (COX-2) and bone resorption (Boileau et al., 2007; Amiable et al., 2009). Boileau et al., (2009) reported that PAR-2 production is significantly reduced in a canine CCLT model treated with Brachystemma calycinum D don plant extract. This decreased the cartilage severity and reduced several inflammatory and catabolic factors such as MMP-13 and inducible NO synthase. These findings suggest that PAR-2 is an important mediator of OA. There are no published reports of PAR-2 in feline OA.

1.7 Study objectives

The objectives and aims of the study were as follows:

1. To define the radiographic features of osteoarthritis in the cat for each individual appendicular joint.

2. To relate the radiographic features to the gross pathologic and histopathologic features.

3. Explore underlying causes of OA in cats.

4. To identify the presence of PAR-2 and matriptase in feline articular cartilage and synovial membrane and to determine their role in OA pathogenesis.

Chapter 2 Materials and Methods

2.1 Cat cadavers

Fifty-eight cats submitted to the *post-mortem* examination (*PM*E) service at the school of Veterinary Medicine, University of Glasgow were enrolled into this study (Appendices (ia)). The cats were euthanatised for reasons unrelated to the study. Consent was provided by the owners of the cats (Appendices (v)) and ethical approval was granted by the local Ethics and Welfare Committee.

2.2 Determination of OA population

The derivation of the OA population is shown in Figure 2.1. Each cat was evaluated for radiographic changes associated with OA. Cats with radiographic changes, either unilaterally or bilaterally affected, were designated as "shoulder (Sh)/elbow (El)/stifle (St)/hip (Hip)/carpal (Carp)/tarsal (Tar)-radiographic OA (rOA)" population. Cats without radiographic changes were categorised as "no Sh/El/St/Hip/Carp/Tar-rOA" All joints were subject to a gross pathological examination and those joints with articular cartilage changes and osteophytes were designated as "Sh/El/St/Hip/Carp/Tar - pathological (path) OA" while those without were grouped as a "no Sh/El/St/Hip/Carp/Tar-path/normal" population.

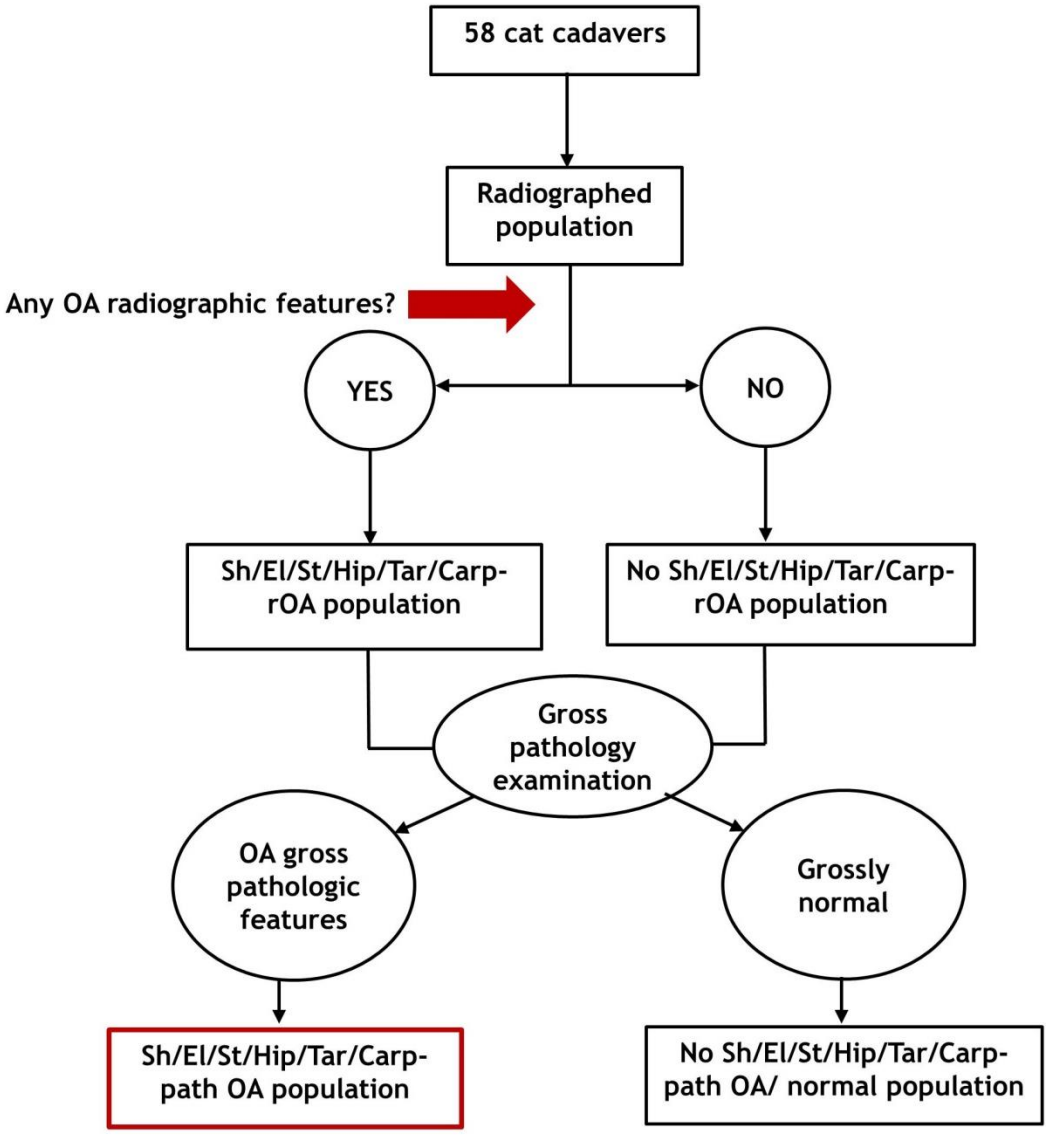

Figure 2.1: A flow chart defining the Shoulder/Elbow/Stifle/Hip/Tarsal/Carpal radiographic OA (Sh/El/St/Hip/Tar/Carp-rOA), the no radiographic OA (No Sh/El/St/Hip/Tar/Carp-rOA), the pathological OA (Sh/El/St/Hip/Tar/Carp-path OA) and the no pathology/normal (No Sh/El/St/Hip/Tar/Carp -path OA/normal) populations.

2.3 Radiography

2.3.1 Computed radiography (CR)

Radiographs of each cadaveric shoulder, elbow, stifle, carpal, tarsal (medio-lateral view) and hip joint (ventro-dorsal view) were taken on a pre-set programme (Appendices (iia)) using a veterinary digital radiographic system (ZooMax HF Generators, Budapest, Hungary) and CR cassettes (CR MM3.0 Extremities Cassette, Agfa Healthcare, Mortsel, Belgium). The cassette containing the joint image was given an identification number and loaded into an image digitizer (CR 35-X Digitizer, Agfa Healthcare, Mortsel, Belgium). The digital image produced was transferred to a personal computer workstation running Windows XP using NX software (Agfa Healthcare, Mortsel, Belgium) for display.

2.3.2 Software

2.3.2.1 Image storage

All images were saved as a Digital Imaging and Communications in Medicine (DICOM) file format. From the workstation, the DICOM files were exported to a Picture Archiving and Communications System (PACS). PACS is a computer system which allows for digital storage, viewing, transmission and retrieval of radiographs. Selected images were chosen and saved as a tagged image file format for use in the thesis.

2.3.2.2 ClearCanvas Workstation 2.0 SP1

ClearCanvas Workstation 2.0 SP1 is a PACS viewer. All radiographs were viewed using ClearCanvas and a 24" LCD Ultra-sharp™ U2410 colour monitor (Dell, UK). Measurements were done where appropriate.

2.3.2.3 Adobe Photoshop CS6

Selected images were imported into a photo editing software (Adobe Photoshop CS6, San Jose, USA) for further cropping, editing, rotating and labelling.

2.3.3 Scoring of radiographic changes

The radiographs were examined without knowledge of the age, breed, and gender of the cat and without knowledge of the gross pathological findings of the joints. The severity of radiographic OA in each radiograph was scored according to changes in the

periarticular bone and soft tissue. The scoring scheme used was based on that described by Innes et al. (2004), Godfrey (2007), Lascelles et al. (2010) and Freire et al. (2011) (Table 2.1).

The size of osteophytes, enthesiophytes, areas of abnormal mineralisation, SSB of the elbow joint and meniscal mineralisation within the stifle joint were all measured using the digital ruler in millimetres. The measurement was made at the greatest dimension. Osteophytes appeared protruding from the surface of the bone, generally at defined areas of the joint. Enthesiophytes appeared as a new bone growth within a tendon or ligament insertion. Areas of abnormal mineralisation were identified as discrete areas which appeared separate from the bone, more than 80% of the border of the mineralised area could be seen or at least partly free from superimposition on the bones of the joint. SSB was identified at the cranial aspect of the humero-radial articulation. Meniscal mineralisation appeared as mineralised areas between the femoral condyle and tibial plateau.

Increased bone-opacity was only assessed beneath the semilunar notch of the ulna in the elbow, femoral condyle and tibial plateau of the stifle and femoral head/neck of the hip. Synovial effusion was determined by assessing the presence of distension of the joint capsule with fluid. A change in joint space was only assessed in the humero-radial, humero-ulnar and hip joints. Joint remodelling, defined as a change in the shape of the bone was scored as absent or present. New bone formation on the fabellae of the stifle joint was scored. The presence of 1 or 2 fabellae were also recorded but was not part of the scoring scheme. All these features were subjectively assessed. Elbow incongruity was determined as described by Wind and Packard (1986). The incongruity was characterised by a relative “overgrowth” (Type 1) or “undergrowth” (Type 2) of the radial head or by an elliptical shape of the semilunar notch (Type 3). All these features were subjectively scored (Table 2.1).

The total radiographic score was determined by summing the individual scores. A global score was determined based on an overall assessment of the severity of the radiographic changes.

Radiographic feature	Score	Description
Osteophytes	0	Absent : No abnormality
	1	Mild* : < 2 mm
	2	Moderate* : 2-5 mm at one or more locations
	3	Severe* : > 5 mm at one or more locations
Enthesiophytes	0	Absent : No abnormality
	1	Mild* : < 1 mm
	2	Moderate* : 1-3 mm
	3	Severe* : > 3 mm
Areas of abnormal mineralisation	0	Absent : No abnormality
	1	Mild : Single area
	2	Moderate* : Several areas but none greater than 10 mm
	3	Severe* : Several areas and including at least one greater than 10 mm
Supinator sesamoid bone (SSB)	0	Absent : No abnormality
	1	Present* : < 3 mm
	2	Present* : ≥ 3 mm (with additional mineralisation on the surface of the SSB
	3	Present* : ≥ 3 mm (with additional area(s) of mineralisation in the region of the SSB
Meniscal mineralisation	0	Absent : No abnormality
	1	Mild* : < 2 mm
	2	Moderate* : 2-3 mm
	3	Severe* : > 3 mm
Increase radio-opacity	0	Absent
	1	Present
Synovial effusion	0	Absent
	1	Present
Joint space	0	Even joint space
	1	Increase joint space
	2	Decrease joint space
Joint remodelling	0	Absent
	1	Present
New bone formation on the fabellae	0	Absent
	1	Present
Elbow incongruity	0	Absent
	1	Present
Global Score	0	No abnormality
	1	Mild changes
	2	Moderate changes
	3	Severe changes

Table 2.1: OA radiographic scoring for feline appendicular joints. *Measurement made at greatest dimension.

2.3.4 Inter- and Intra- observer variability and sensitivity of radiographic assessment of increased radio-opacity beneath the semilunar notch

Fifty-paired sets of elbow radiographs were randomly selected for analysis. The radiographs were numbered, randomly arranged and subjected to assessment by four observers: two diagnostic imaging Royal College of Veterinary Surgeon (RCVS)/European College Diplomates, one orthopaedic surgeon RCVS Diplomate and one postgraduate student (Table 2.2). Each observer was blinded to the cat's details and scored increased radio-opacity for each elbow joint as either "Absent (Score 0)" or "Present (Score 1)". To assess inter- observer variability, four observers scored the radiographs once. To assess intra- observer variability, two observers repeated the assessment with a minimum interval of 2 weeks.

Observers	Descriptions
1	Senior lecturer in Veterinary Diagnostic Imaging, RCVS/European College Diplomate in Diagnostic Imaging.
2	Professor of Veterinary Diagnostic Imaging, RCVS/European College Diplomate in Diagnostic Imaging.
3	Postgraduate student, DVM
4	Professor of Small Animal Orthopaedic Surgery, RCVS Diplomate in Small Animal Orthopaedic Surgery.

Table 2.2: Details of each observer involved in the inter- and intra- observer studies.

Sensitivity was defined as the proportion of elbow joints that were positive for marginal osteophytes on the surface of the bone and/or, areas of mineralised joint capsule superimposed on the articular bone and/or osteochondromas at gross pathologic examination that showed presence of increased radio-opacity based on radiography.

Specificity was defined as the proportion of elbow joints that were free of any abnormality at gross pathologic examination that were negative for the presence of increased radio-opacity based on radiography.

2.3.5 Norberg angle measurement and HD assessment

Ventro-dorsal radiographs of each hip (right and left) were assessed for the presence of HD. Only radiographs showing ideal positioning where the femora were parallel to each other and the pelvis was not significantly tilted were selected. Only the Norberg angle (NA) and the percentage coverage of the femoral head by the dorsal acetabular edge were used to assess HD, both evaluating the degree of femoral head subluxation. HD was defined as less than 50.0% coverage of the femoral head by the dorsal edge of the acetabulum (Clarke et al., 2005).

NA of Hip-rOA and no Hip-rOA was measured on printed radiographs. Briefly, the centre of each femoral head was identified and marked with a small dot by finding the best fitting of several concentric circles marked on a transparent plastic sheet. The two femoral head centres were joined by a line, and the angle between each centre and the cranial effective acetabular rim was measured and recorded (Figure 2.2.A).

The area coverage of the femoral head by the dorsal acetabular edge was measured in square centimetres with a digital polygonal ruler (Digimizer Version 4.2.4.0). The percentage coverage was determined by dividing the area of femoral head covered by the total area of a femoral head (Figure 2.2.B).

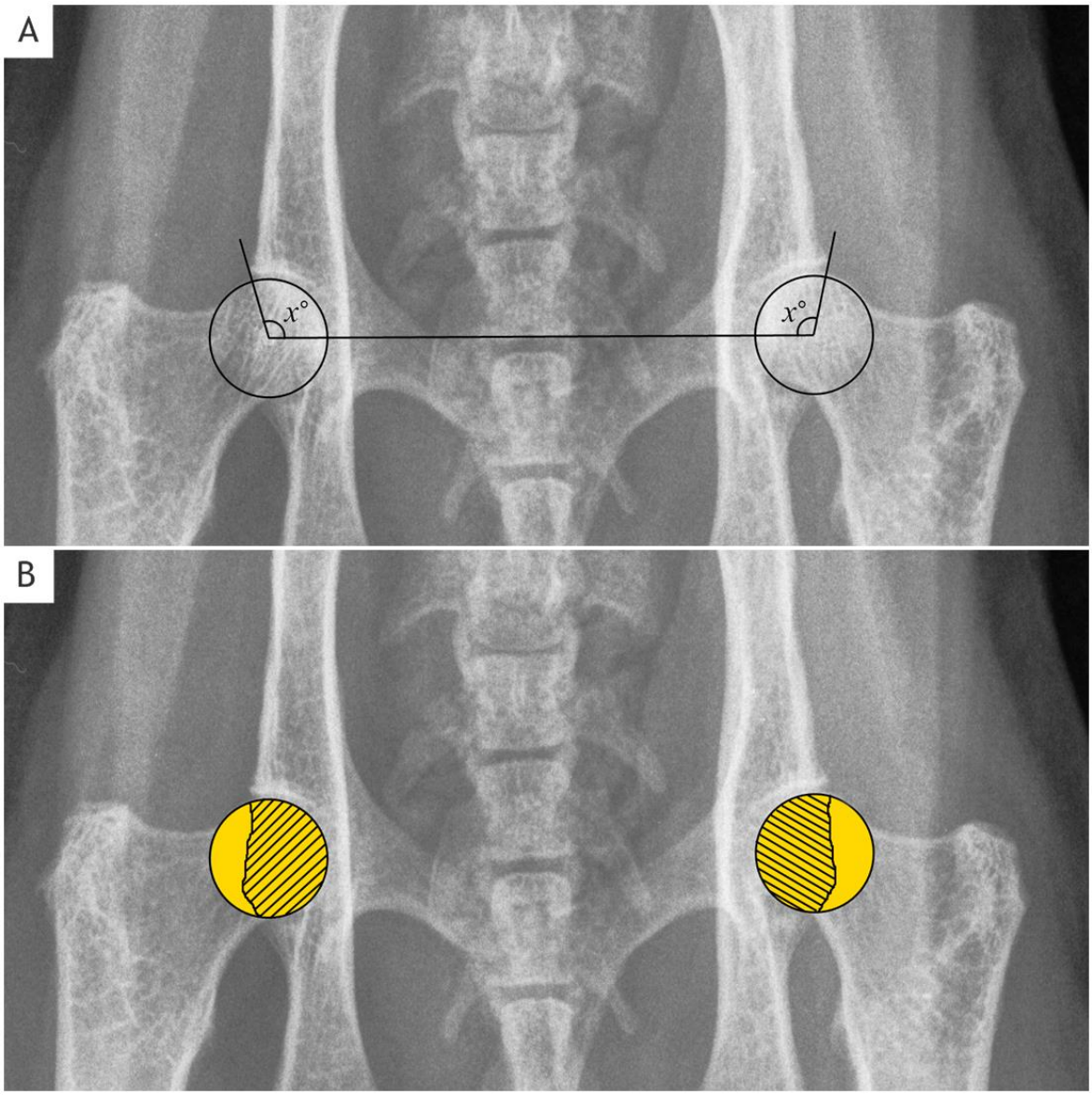

Figure 2.2: Showing measurement of the Norberg angle ($X°$) (A) and area of the femoral head covered by the dorsal acetabular edge (B). The percentage coverage is determined by dividing the area of femoral head covered (shaded area) by the total area of a femoral head (yellow area).

2.4 *Post-mortem* examination

The weight (kg), age (years), breed, sex and the body condition score (BCS) (based on Laflamme (1997)) of each cat were recorded. Each appendicular joint was examined using the routine *PM*E procedure followed by Glasgow University Veterinary School (GUVS) Pathology Department. Each joint was digitally photographed and the images stored.

2.4.1 Scoring for gross pathologic changes

The gross pathologic changes were scored according to a modified version of that used by Cook et al. (2010) (Table 2.3). The joint capsule was assessed for either focal or diffuse areas of visible thickening. Synovium discolouration was determined by assessing the change of synovial vascularity and appearance from opal white to yellow-brown. Cartilage surface discolouration was determined by assessing the change of cartilage appearance from white or blue-white to yellow-brown. Cartilage fibrillation was assessed as indicator of OA pathology by determining the surface structure of articular cartilage from smooth and shiny to dull and roughening. Cartilage erosion was assessed as focal or diffuse areas of cartilage loss. Cartilage ulceration, defined as a full thickness cartilage loss with exposure of the subchondral bone was scored as focal, multifocal or diffuse. All cartilage changes of the medial and lateral parts of the distal humeral and femoral condyles and tibial plateaus were assessed independently to determine which part was most severely affected. Osteophytes were identified as new bone formations around the periphery of the joint and scored based on their size and the extent of margin involvement. Joint remodelling was determined by assessing only change in the bone shape.

The presence of areas of mineralisation within the joint capsule and osteochondromas was noted. Osteochondromas were defined as white to pink, oval to round calcified bodies which were clearly delineated, totally free or partly attached to the synovium. If attached, it had a degree of mobility.

The total gross pathologic score was determined by summing the individual scores. A global score was determined based on an overall assessment of the severity of the gross pathologic changes.

Gross pathologic features	Score	Description
Thickening of joint capsule	0	Normal : No abnormality
	1	Mild : Focal areas of visible thickening
	2	Moderate : Diffuse involvement with marked thickening
	3	Severe : Diffuse involvement with thickening to the point of fibrosis
Synovium discolouration	0	Normal : Opal white with sparse well defined blood vessels
	1	Mild : Slight yellowish with notable increase in vascularity
	2	Moderate : Moderate yellowish with diffuse hypervascularity
	3	Severe : Severe yellow to brown discolouration with diffuse hypervascularity
Cartilage surface discolouration	0	Absent : White to blue-white
	1	Present : Yellow brown discolouration
Cartilage fibrillation	0	Absent : Smooth and shiny
	1	Mild : Dull and visible surface roughening
	2	Moderate : Dull with marked surface roughening
	3	Severe : Dull with severe surface roughening
Cartilage erosion	0	Absent : No visible loss of cartilage
	1	Mild : Focal area of cartilage loss
	2	Moderate : Multifocal areas of cartilage loss
	3	Severe : Diffuse areas of cartilage loss
Cartilage ulceration	0	Absent : No total loss of cartilage
	1	Mild : Focal area of full thickness cartilage loss
	2	Moderate : Multifocal areas of full thickness cartilage loss
	3	Severe : Diffuse areas of full thickness cartilage loss
Osteophytes	0	Absent : No osteophyte visible
	1	Mild : Small and focal osteophytes
	2	Moderate : Multiple and moderate osteophytes
	3	Severe : Multiple and large osteophytes
Joint remodelling	0	Absent
	1	Mild
	2	Moderate
	3	Severe
Global score	0	No abnormality
	1	Mild changes
	2	Moderate changes
	3	Severe changes

Table 2.3: OA gross pathologic scoring for feline appendicular joints.

2.4.2 Collection of samples for histologic examination

Representative samples were collected from each cat to reflect the different severities of pathological change. Selected epiphyses consisting of articular cartilage and bone were collected from several OA and normal joints. Additional samples were collected from some joints and included joint capsule (synovium) and intra-articular structures including menisci, SSB, tendon of origin of supinator muscle, cranial cruciate ligaments and osteochondromas. Pituitary glands and the left or right kidney of each cat were randomly collected. All samples were fixed in 10.0% buffered neutral formaldehyde (Appendices (iiia)) for at least 3 days to ensure adequate fixation.

2.5 Histopathology

2.5.1 Tissue preparation and processing

Following fixation in formalin, the calcified tissues including the cartilage, SSB, mineralized menisci and the osteochondromas were decalcified in 14.0% ethylenediaminetetracetic acid (EDTA) solution pH 8.0 (Appendices (iiia)) at room temperature until the tissues were soft enough to allow cutting with the microtome knife. The decalcified and soft tissues were processed using the Shandon Excelsior™ (Thermo Scientific, UK) tissue processor on a pre-set programme (Appendices (iiib)) for 17 hours. The processed tissues were embedded in paraffin wax (TCS Biosciences Ltd, Buckingham, UK). The paraffin-embedded tissues were cut at 2.5 to 3.0 µm with a microtome (Shandon™ Finesse, Thermo Scientific, UK) and mounted onto glass slides (Superfrost™, Thermo Scientific, UK). The slides were dried at 60.0 °C for one hour and were heated at 37.0 °C overnight. The slides were used for both histopathological and immunohistochemical examination.

2.5.2 Histological stains

2.5.2.1 Haematoxylin and eosin (H&E)

All sections were routinely stained with H&E for assessment of tissue morphology. Sections were deparaffinised by immersion in histo-clear (National Diagnostics, New Jersey, USA) and then rehydrated with 70.0% absolute alcohol and 70.0% methylated spirit before rinsing in water (Appendices (iiic)). The sections were immersed in Gill's haematoxylin for five minutes and rinsed in water for 30 seconds. Sections were dipped in 1.0% acid alcohol (Appendices (iiia)) for 10 seconds to eliminate excess haematoxylin and to enhance cellular differentiation, followed by washing in running tap water.

Sections were blued in Scott's tap water substitute (Appendices (iiie)) and counterstained in eosin for five minutes. Sections were dehydrated with 70.0% methylated and 70.0% alcohol spirit before being cleared in histo-clear and mounted with DPX (Cellpath, UK) (Appendices (iiic)).

2.5.2.2 Safranin O fast green

Safranin O is a cationic dye that stains acidic proteoglycan present in cartilaginous tissues. All articular tissue samples were stained with Safranin O. Sections were deparaffinised and rehydrated (Appendices (iiic)). The sections were immersed in Weigert's iron haematoxylin for ten minutes. Sections were washed in water for ten minutes. Following washing, sections were stained in 0.001% Fast Green (Appendices (iiia)) for five minutes. Sections were rinsed in 1.0% acetic acid (Appendices (iiia)) for 10 seconds followed by staining in 0.1% Safranin O solution (Appendices (iiia)) for seven minutes. Sections were washed in water and dipped in 1.0% acetic acid to remove excess Safranin O. Sections were dehydrated, cleared in histo-clear and mounted with DPX (Appendices (iiic)).

2.5.2.3 von Kossa stain

von Kossa stain was used to demonstrate calcium deposition in the synovium and kidney. Sections were deparaffinised and rehydrated (Appendices (iiic)). The sections were placed in 1.0% silver nitrate solution (Appendices (iiia)) for one hour with a light source directed on the solution. Sections were washed in water and placed in 5.0% sodium thiosulphate (Appendices (iiia)) for five minutes. Sections were washed in water and counterstained in 1.0% neutral red (Appendices (iiia)) for one minute. Sections were dehydrated, cleared in histo-clear and mounted with DPX (Appendices (iiic)).

2.5.2.4 4',6-Diamidino-2-Phenylindole (DAPI) stain

DAPI is a blue fluorescent nucleic acid stain that strongly binds to double-stranded deoxyribonucleic acid (dsDNA). It was used to demonstrate DNA deposition in the tidemark of the articular cartilage sections. The sections were deparaffinised in xylene for five minutes and dehydrated in serial alcohol dilution (100, 90, 80, and 70%) (Appendices (iiid)) for two minutes. 1X PBS (Appendices (iiia)) was added onto the sections to keep them moist. Sections were incubated with 300 nM DAPI (Invitrogen, Paisley, UK) (Appendices (iiif)) diluted in 1X PBS for five minutes. The sections were washed three times with 1X PBS for two minutes and rinsed with tap water for 30

seconds. One drop of SlowFade®Gold Antifade (Invitrogen, Paisley, UK) liquid mountant was applied to the section and a cover glass placed.

2.5.2.5 Immunohistochemistry (IHC)

Collagen Type I and Type II

Localisation of collagen types I and II (Table 2.4) was performed for the articular cartilage, osteochondromas, SSB and menisci. Sections were deparaffinised, rehydrated and subsequently rinsed in water (Appendices (iiid)). Antigen retrieval was done by placing the sections in 0.01 M heated sodium citrate buffer pH 6.0 (Appendices (iiia)) for 1 minute 40 seconds. Endogenous peroxidase was blocked by adding 150 µl peroxidase blocking solution (Dako Cytomotion, Cambridgeshire, UK) onto the sections for five minutes and followed by washing with 1X TBS pH 7.5 (Appendices (iiia)). Sections were then incubated with the primary antibody (Table 2.4) diluted in universal diluent containing 0.05 M Tris-HCL buffer with 1.0% BSA for one hour. The sections were washed twice with TBS buffer followed by the addition of the secondary antibody (horse anti-mouse) diluted in universal diluent buffer. After two washes, peroxidase-conjugated avidin (Vector Laboratories, Peterborough, UK) was added to the sections and incubated for thirty minutes. The sections were incubated twice for five minutes with 3,3'-Diaminobenzidine (DAB) (Vector Laboratories, Peterborough, UK), which produces a brown coloured deposit within positive staining. Sections were washed in running water and counterstained in Gill's haematoxylin. The sections were blued in Scott's tap water (Appendices (iiie)) followed by dehydration, cleared in xylene and mounted with DPX (Appendices (iiid)).

Growth hormone (GH) and Prolactin

Any pituitary gland with histological evidence of an adenoma was stained with GH and prolactin antibodies. The optimal GH and prolactin antibodies concentration was 0.1 µg/ml (1:10000) and 0.2 µg/ml (1:6400) respectively (Table 2.4). Sections were deparaffinised, rehydrated and subsequently rinsed in water (Appendices (iiid)). Antigen retrieval was performed by placing the sections in 0.01 M heated sodium citrate buffer pH 6.0 (Appendices (iiia)) for 1 minute 40 seconds. Endogenous peroxidase was blocked by adding 150 µl peroxidase blocking solution (Dako Cytomotion, Cambridgeshire, UK) onto the sections for five minutes, followed by washing with 1X TBS pH 7.5 (Appendices (iiia)). Sections were then incubated with the primary antibody diluted in universal diluent containing 0.05 M Tris-HCL buffer with 1.0% BSA for one hour. The sections were washed twice with TBS buffer followed by the addition of the secondary antibody (horse

anti-rabbit) diluted in universal diluent buffer. After two washes, peroxidase-conjugated avidin was added to the sections and incubated for thirty minutes. The sections were incubated twice for five minutes with DAB, which produces a brown coloured deposit within positive staining. Sections were washed in running water and counterstained in Gill's haematoxylin. The sections were blued in Scott's tap water (Appendices (iiie)) followed by dehydration, cleared in xylene and mounted with DPX (Appendices (iiid)).

Antibody	Description	Company
Collagen Type I	1000 µg/ml mouse monoclonal IgG1	Abcam, Cambridge, UK.
Collagen Type II	1000 µg/ml mouse monoclonal IgG_{2a}	Abcam, Cambridge, UK.
Secondary antibody for Collagen Types I and II	Anti-mouse biotinylated IgG raised in horse	Vector Laboratories, Peterborough, UK
Growth hormone	1000 µg/ml rabbit polyclonal IgG	ThermoFisher Scientific, UK.
Prolactin	1000 µg/ml Rabbit polyclonal IgG	Novus Biologicals, USA.
Secondary antibody for growth hormone and prolactin	Anti-rabbit biotinylated IgG raised in horse	Vector Laboratories, Peterborough, UK
PAR-2 (SAM-11)	200 µg/ml mouse monoclonal IgG_{2a}	Santa Cruz Biotechnology, California, USA.
Isotype PAR-2	200 µg/ml mouse monoclonal IgG_{2a}	eBioscience, Hatfield, UK.
Matriptase (ST-14)	200 µg/ml rabbit polyclonal IgG	Sigma-Aldrich, Irvine, UK.
Isotype matriptase	200 µg/ml rabbit polyclonal IgG	Abcam, Cambridge, UK.
Secondary antibody for PAR-2 and matriptase	Anti-mouse/anti-rabbit biotinylated IgG raised in horse	Vector Laboratories, Peterborough, UK.

Table 2.4: List of antibodies used for immunohistochemical staining for light microscopy.

Protease activated receptor-2 (PAR-2) and matriptase

PAR-2 and matriptase immunohistochemical staining of articular cartilage and synovium was performed according to the protocol of Tindell et al. (2012). Details of the OA and healthy samples included in the study are given in Appendices (ib). One section from the elbow joint of each cat was stained. The optimal PAR-2 and matriptase antibodies concentration was 2 µg/ml (1:100) and 4 µg/ml (1:50) respectively (Table 2.4). The sections were deparaffinised and rehydrated (Appendices (iiid)). Sections were washed in 1X PBS (Appendices (iiia)) for five minutes. Subsequent antigen retrieval was done by placing the sections in 0.01 M heated sodium citrate buffer pH 6.0 (Appendices (iiia)) for five minutes. Endogenous peroxidase was blocked by immersing the sections in 1.0%

hydrogen peroxide in methanol for thirty minutes. Sections were washed twice with 1X PBS for five minutes and blocked with supplemented blocking serum (Appendices (iiig)) for thirty minutes followed by incubation with the primary antibody diluted in primary antibody diluent (Appendices (iiig)) for 2 hours. The sections were washed twice in 1X PBS followed by incubation with the secondary antibody (horse anti-mouse/rabbit) diluted in secondary antibody diluent (Appendices (iiig)) for thirty minutes. After two washes with 1X PBS for five minutes, the sections were incubated with peroxidase-conjugated avidin for thirty minutes. Sections were washed twice with 1X PBS for five minutes. The antigen-antibody complex was visualized using DAB. Sections were counterstained with haematoxylin and washed in running tap water. The sections were dehydrated, cleared in xylene and mounted with DPX (Appendices (iiid)). To determine non-specific staining, replicate sections were incubated with non-specific antibody (isotype) (Table 2.4).

2.5.3 Evaluation of histopathologic and immunohistochemical changes

2.5.3.1 Evaluation of articular cartilage, bone and intra-articular structures

The histopathologic features were assessed according to changes in the articular cartilage, bone and intra-articular structures. The articular cartilage changes included structural and chondrocyte alterations, tidemark integrity and changes in Safranin O staining intensity. Bone changes included thickening of the subchondral bone plate and trabeculae, osteophyte formation, presence of subchondral bone "cysts" and subchondral bone fibrosis. Menisci were evaluated for the presence of mineralisation, ossicles and for evidence of degenerative changes including tissue surface and cellular alterations, changes in orientation of collagen fibres and changes in Safranin O staining intensity. The tendon of origin of the supinator muscle was assessed for the presence of SSB. Cranial cruciate ligaments were evaluated for the presence of degenerative changes including alterations in the cellularity, orientation of collagen fibres and changes in Safranin O staining intensity. Histopathologic features of osteochondromas were also evaluated. Two serial sections of each sample were evaluated. A scoring scheme was not used for these tissues.

2.5.3.2 Evaluation of synovial tissues

The synovium changes included lining layer hyperplasia, villous hypertrophy, inflammatory cell infiltration and calcification indicated by von Kossa staining. The severity of the inflammatory cell infiltration was scored according to a modified version

of Cook et al. (2010) (Table 2.5). A note was made of whether the whole section or only part of it was affected. Two serial sections of each sample were evaluated.

Synovium	Score	Description
Inflammatory cells infiltration	0	No cellular infiltration
	1	Mild inflammatory cell infiltrate
	2	Moderate inflammatory cell infiltrate including small lymphoid follicles
	3	Severe, diffuse inflammatory cell infiltrate including large lymphoid follicles

Table 2.5: Microscopic scoring of inflammatory cell infiltration of OA synovial tissue.

2.5.3.3 Evaluation of pituitary glands

Haematoxylin and eosin stained sections of pituitary glands were examined for the presence of an adenoma. The evidence of adenoma was scored as absent or present. Samples with the presence of an adenoma were stained with GH and Prolactin antibodies. The GH and Prolactin staining was subjectively scored using four staining categories: 0 = negative staining; 1 = 25% positivity; 2 = 50% positivity; 3 = 75% positivity; 4 = 100% positivity. One section per pituitary gland was evaluated.

2.5.3.4 Evaluation of kidney sections

Changes in the cortex were assessed and scored according to a modified version of Chakrabarti et al. (2012) (Table 2.6). Cortical interstitial changes included fibrosis and inflammation. The interstitial fibrosis and inflammation were scored on a scale of 0 to 3 with 0.5 intervals. Glomerular changes included thickening of the basement membrane and mesangial matrix. Thickening of the mesangial matrix was evaluated by scoring the degree of its expansion. Glomerular changes were scored on a scale of 0 to 3. The presence of protein and mineralisation in the tubule and undulating capsule were also recorded but was not part of the scoring. The total score was calculated by summing the individual scores and a global score was determined based on an overall assessment of the severity of the histopathologic changes. Cats were grouped into 3 categories based on the total and global scores. Cats with a total and global score of 0 were grouped as “normal kidney”, cats with a total score less than 4 and global score of 1 were grouped as “mild” and cats with a total score of 4 and above and global scores of 2 and 3 were grouped as “chronic kidney disease”. One section per kidney was evaluated.

Histopathologic features of the cortex		Score	Descriptions
Interstitium	Fibrosis	0	No fibrosis
		0.5-1.5	Mild (Scattered multifocal areas of fibrosis)
		2.0-2.5	Moderate fibrosis
		3	Severe (Diffuse and coalescing fibrosis)
	Inflammation	0	No inflammation
		0.5-1.5	Mild (Inflammation affecting <5% of the section)
		2.0-2.5	Moderate (Inflammation affecting 25% to 50% of the section)
		3	Severe (Diffuse inflammation)
Glomerulus	Thickening of basement membrane	0	No abnormality
		1	Mild
		2	Moderate
		3	Severe
	Thickening of the mesangial matrix	0	Matrix could encircle no more than 1 nucleus
		1	Matrix could surround several nuclei but not extend to peripheral capillary loops
		2	Matrix expansion involving peripheral capillary loops, affecting <50% of the glomerulus
		3	Matrix expansion affecting >50% of the glomerulus
Tubule	Leaking of protein	-	Present or absent
	Mineralisation	-	Present or absent
Capsule	Undulating capsule	-	Present or absent
Global score	0: No abnormality (Total score 0) 1: Mild 2: Moderate 3: Severe		

Table 2.6: Chronic kidney disease histopathologic scoring for cats.

2.5.3.5 Evaluation of PAR-2 and matriptase sections

Positive chondrocytes were subjectively assessed. One section per joint was evaluated. Six randomly selected photomicrographs of each section stained for PAR-2 and matriptase were taken (400x magnification). The photomicrographs included the superficial, middle and deep layers of the articular cartilage and it was ensured before evaluation that an intact cartilage surface was present. Positive synovial cells were subjectively assessed. Six randomly selected photomicrographs of each section stained for PAR-2 and matriptase were taken (400x magnification).

2.5.4 Image viewing and capture

All H&E, Safranin O fast green, von Kossa, and IHC stained sections were examined under a light microscope (Olympus BX51M, Southend-on-Sea, UK). DAPI stained sections were examined using an inverted fluorescence microscope (Olympus IX71, Southend-on-Sea, UK). Images of the sections were captured by using cellSens Entry imaging system (Olympus Soft Imaging Solutions, Germany).

2.6 PAR-2 and matriptase gene expression

2.6.1 Articular cartilage and synovial samples

Articular cartilage and synovial tissues were collected from 10 cats and 3 foetuses (Appendices (ib)) within 24 hours of euthanasia. The articular cartilage and synovium of the elbow joints were identified as OA or healthy based on the gross pathologic assessment as previously described (see section 2.4.1, page 66 and Table 2.3, page 67). The samples were placed into RNA*later* (Ambion, Darmstadt, Germany) and were stored at 4 ºC until required for ribonucleic acid (RNA) extraction.

Eight-teen total RNA samples from the articular cartilage of feline elbow joints were received from the Royal (Dick) School of Veterinary Studies, University of Edinburgh and were also included in the study (Appendices (ib)).

2.6.2 Tissue homogenisation

Tissue samples were disrupted using a mortar and pestle in liquid nitrogen. The disrupted samples were weighed using digital electronic scales. Samples of approximately 30 mg were placed into RNase-free microcentrifuge tubes and 350 µl of RLT buffer with 3.5 µl B-mercaptoethanol were added. The lysate was homogenised by

repeated passage through a clean syringe and 21-gauge needle (ten times). The homogenised lysate was centrifuge at 12,000 RPM for three minutes at 20 °C.

2.6.3 RNA isolation

Following centrifugation, the supernatant was transferred to a new RNase-free microcentrifuge tube and 350 µl of 70.0% ethanol (Appendices (iva)) was added. The supernatant was then applied to RNeasy® mini column (Qiagen, Crawley, UK) and centrifuged at 8000 g for 15 seconds. The flow through was discarded and the column was placed into a new tube. The RNeasy® mini column was washed by adding 350 µl RW1 buffer and centrifuged at 8000 g for 15 seconds. Possible genomic DNA contamination was eliminated by including DNase treatments. A DNase I incubation mixture (Appendices (ivb)) was added onto the RNeasy® mini column and incubated for fifteen minutes. Afterwards, the column was spun at 8000 g for 15 seconds. The column was washed again by adding 350 µl RW1 buffer and centrifuged at 8000 g for 15 seconds. The column was washed twice by adding 500 µl of RPE buffer and centrifuged at 12,000 RPM for two minutes. To elute the RNA, the column was transferred to a new RNase-free microcentrifuge tube. 30 µl of RNase-free water was added directly onto the centre of the silica gel membrane and centrifuged at 12,000 RPM for one minute. All steps were carried out at 20 to 25 °C.The RNA samples were stored at -80 °C until further analysis.

2.6.4 Estimation of the quantity and integrity of total RNA

The isolated RNA was spectophotometrically quantified by using the NanoDrop ND-1000 Spectrophotometer (Thermo Scientific, Epsom, UK) at an absorption of 260 nm. The RNA purity was assessed by measuring the ratio of the absorbance at 260 and 280 nm. A typical ratio of 1.8 to 2.0 was obtained for most of the samples which is acceptable. The RNA concentration in µg per µl was recorded.

2.6.5 cDNA synthesis from total RNA

Complementary DNA (cDNA) was synthesised from total RNA by using the Precision™ Reverse Transcription Premix (PrimerDesign Ltd., Southampton, UK) according to the manufacturer's recommendations. cDNA synthesis was carried out on 1 ng RNA, at 55 °C for 20 minutes. The cDNA was stored at -20 °C until further use. The absence of contamination of RNA with genomic DNA was verified with minus-reverse transcriptase (minus-RT) controls. The cDNAs were used for both the selection of reference genes for normalisation and comparative assessment of PAR-2 and matriptase mRNA levels in normal and OA cases.

2.6.6 Selection of reference genes for normalisation in articular tissue

2.6.6.1 Reference gene primers

The selection of reference genes was carried out using Cat geNorm™ Housekeeping Gene Selection Kit (PrimerDesign Ltd., Southampton, UK) (Table 2.7).

Gene symbol	Description
GAPDH	Glyceraldehyde 3-phosphate dehydrogenase
RPL-18	60S ribosomal protein L18
ACTB	Beta-actin
SDHA	Succinate dehydrogenase complex, subunit A, flavoprotein
GUSB	Beta-glucuronidase
HPRT	Hypoxanthine guanine phosphoribosyl transferase

Table 2.7: Six candidate reference genes for normalisation in different feline articular tissues (OA and healthy).

2.6.6.2 Quantitative real-time polymerase chain reaction (qPCR)

qPCR was performed using 2X *Precision™* MasterMix with SYBR green (PrimerDesign Ltd., Southampton, UK) following the manufacturer's instructions. The reaction mix was prepared as follows (volumes listed are for a single sample):

Mastermix	10 µl
Primer	1 µl
RNase free Water	4 µl
Total Volume	15 µl

Each sample was measured in duplicate; therefore two reaction mixes were prepared for each cDNA sample. 15 µl reaction mixtures were pipetted into each well of a BrightWhite fast optical 96 well plate (PrimerDesign Ltd., Southampton, UK). 5 µl of cDNA at 1 ng/µl was then added giving a final volume in each well of 20 µl. A working concentration of primers is 300 nM. A non-template control was added to the plate where 5 µl of water was mixed with the 15 µl reaction mix and a minus-RT was also included in the plate using the minus-RT control cDNA.

The plate was covered using an adhesive optical seal (PrimerDesign Ltd., Southampton, UK) and spun at 200 g for 2 minutes. The plate was then transferred to a *StepOnePlus*™ Real-Time PCR System (Applied Biosystems, California, US) where it was read on the following cycle:

- Enzyme activation at 95 °C for 10 minutes

- 40 cycles of template denaturation at 95 °C for 15 seconds and data collection at 60 °C for 1 minute

A dissociation curve was subsequently measured on the following cycle:

- Incubation at 95 °C for 15 seconds
- Incubation at 60 °C for 15 seconds
- Incubation at 95 °C for 15 seconds

A melting curve was created at the end of the assay. The data was rejected when a peak at the wrong melt temperature or a double peak was found.

2.6.6.3 Expression stability analysis

Using the results of the qPCR, the expression stability of the reference genes was then quantified using geNorm qbasePLUS software (PrimerDesign Ltd., Southampton, UK). A stability value (*M*) is generated by geometric averaging of multiple target genes and mean pairwise variation of a gene from all other target genes in a given sample (Vandesompele et al., 2002). It is based on the principle that the expression ratio between two ideal reference genes is observed in all samples independent of tissue type or experimental conditions. Reference genes with the lowest *M* values are deemed the most stable. Three most stable genes were selected as a reference gene for the PAR-2 and matriptase qPCR experiment.

2.6.7 The comparative assessment of PAR-2 and matriptase mRNA levels in cats with and without OA

2.6.7.1 Primer design

Primers were designed using the online primer design tool at the National Centre for Biotechnology Information website (http://www.ncbi.nlm.gov/tools/primer-blast) and were commercially synthesised (Eurofins, Germany). Feline mRNA sequences of PAR-2 (XM_003991699.1) and matriptase (XM_003992587.1) were used and primers were selected on the basis of similarity in length and melting temperature and low self-3´complementarity. Primer details are shown in Table 2.8.

Primer name	Forward primer sequence 5´-3´	Reverse primer sequence 5´-3´	Product length
PAR-2	CTC TTT TCT CCC CAG ACC GC	GGG TAG CAA AGG GGT GTA TGT C	228 bp
Matriptase	AGG ATT GTG ACT GTG GGC TG	GAG AGA TGA TCG AAG CCC CG	144 bp

Table 2.8: Primer sequences used for amplification of PAR-2 and matriptase.

2.6.7.2 Primer optimisation

Melt curve analysis of each primer was included. To ensure a single product the experiment needed to yield a single peak. Annealing temperatures were standardised for each primer when a single peak was observed.

2.6.7.3 qPCR

Reaction mixture, plate preparation and amplification were prepared as described in section 2.6.6.2, page 77. Each sample was measured in triplicate. A primer mixture was created with both reverse and forward primers at 100 nM per primer.

2.6.7.4 Data analysis

Analysis of data was performed using Microsoft Excel. All samples were normalised to the copy numbers of pre-determined reference genes as described previously (section 2.6.6.3, page 78). The normalised values, which reflect the PAR-2 and matriptase mRNA levels, were analysed using 2-sample t-test to determine if there were any difference in PAR-2 and matriptase mRNA expression levels between the OA and healthy groups. The delta delta CT (ΔΔCT) method was used to calculate the fold change in PAR-2 and matriptase mRNA expression between the OA and healthy groups (Yuan et al., 2006).

2.7 Statistical analysis

Throughout the thesis statistical analyses and graphs were performed using GraphPad Prism for Windows, version 5 (GraphPad Software Incorporation, California, USA). The normality of the data was examined using the D'Agostino and Pearson Omnibus normality test. For the comparison of two paired samples that data did not follow a normal distribution, a non-parametric test Wilcoxon signed rank was used. For the comparison of two unpaired samples, continuous data with a normal distribution was analysed with a 2-sample t –test, the Mann–Whitney U test was used as a non-parametric test for non-normal distributed data with a significance level (α) set at 0.05. Prevalence was calculated where appropriate and correlation analysis was determined using Spearman's Rank Correlation. Correlation coefficient (r_s) results were interpreted

according to a modified categorisation of that used by Dancey and Reidy (2004) (Table 2.9). Correlation was significant at the 0.05 level.

Spearman's correlation coefficient (r_s)	Descriptions
0.0	No correlation
0.10 – 0.20	Slight correlation
0.21 – 0.40	Fair correlation
0.41 – 0.70	Moderate correlation
0.71 – 0.80	Good correlation
0.81 – 0.99	Almost perfect
1.0	Perfect correlation

Table 2.9: Interpretation of Spearman's correlation coefficient.

Cohen's Kappa (K) analysis for the inter- and intra- observer study was performed using Minitab®17 (Minitab Incorporation, Pennsylvania, USA). Interpretation of the Cohen's Kappa (K) value was performed as described by Landis et al. (1977) (Table 2.10).

Cohen's Kappa (K) statistic value	Strength of agreement
<0.00	Poor
0.00-0.20	Slight
0.20-0.40	Fair
0.41-0.60	Moderate
0.61-0.80	Substantial
0.81-1.00	Almost perfect

Table 2.10: Interpretation of Cohen's Kappa (K) statistic for strength of agreement.

Chapter 3 Radiographic and pathologic features of osteoarthritis of the feline shoulder joint

3.1 Introduction and aims

The shoulder is a ball and socket joint, also called the glenohumeral or scapulohumeral joint. The joint comprises the distal end of the scapula and the head of humerus. The glenoid cavity is the concave part of the distal scapula. It is covered with hyaline articular cartilage. The cranial part of the glenoid forms the supraglenoid tubercle from which projects the coracoid process. The articular surface of the glenoid cavity extends onto the ventral surface of the supraglenoid tubercle. The edge of the glenoid is surrounded by a fibrocartilagenous rim called the labrum. The scapula has a prominent ridge or spine along the centre of its lateral surface. The distal end of the spine forms the acromion and part of the acromion is enlarged to form the suprahamate process. The humeral head has a convex articular surface, covered by articular cartilage and is about twice as extensive as the glenoid cavity of the scapula. The joint has a loose fibrous capsule which attaches to the periphery of the articular surfaces. The fibrous capsule is thickened medially and laterally to form glenohumeral ligaments (Bardet, 1998). The medial glenohumeral ligament appears as a transverse band and extends downward from the medial surface of the supraglenoid tubercle across the shoulder articulation to attach to the joint capsule at the junction of the humerus (Craig et al., 1980). In contrast, the medial glenohumeral ligament appears more often as a Y shape in dog (Bardet, 1998). The lateral glenohumeral ligament is usually a single large band that extends downward from the lateral rim of the glenoid cavity and tapers slightly as it inserts on the humerus (Bardet 1998; Rochat, 2012). The clavicle is a “free-floating” bone and is an obvious feature of the feline shoulder. It can be identified on lateral radiographic projections, sometimes superimposed on the proximal humerus or distal scapula and should be recognised as a normal anatomical structure.

Osteoarthritis of the shoulder joint occurs more commonly in older cats (Godfrey, 2007). Radiographic signs include osteophyte formation on the caudal rim of the glenoid and on the caudal edge of the humeral head (Bennett et al., 2012a). Reduced joint space on the caudal aspect of the joint is possible to appreciate although assessing joint space in non-weight bearing views is difficult.

The purpose of this study was to define the radiographic features of shoulder OA and to relate the radiographic findings to the gross pathologic features. In particular this chapter will address the following questions:

a) Can the radiographic features be a good indicator of the severity of cartilage pathology?

b) Is shoulder OA mainly idiopathic (primary) in nature?

3.2 Materials and methods

3.2.1 Determination of shoulder OA population

Determination of the shoulder OA population was done as described in Section 2.2, page 58 and Figure 2.1, page 59.

3.2.2 Comparative analyses of signalment, body weight and body condition score between Sh-path OA and no Sh-path OA/normal cats

Median of age, BW and BCS of Sh-path OA and no Sh-path OA/normal cats were illustrated with a scatter plot graph and statistically analysed by using Mann-Whitney *U* test. The distribution of breed and gender of Sh-path OA and no Sh-path OA/normal cats was visualised using stacked bar graph. The distribution of BCS of Sh-path OA and no Sh-path OA/normal cats was graphed.

3.2.3 Radiographic assessment of shoulder joint

Radiographic changes associated with shoulder OA were assessed and scored using a radiographic scoring system (see Section 2.3.3, page 60 and Table 2.1, page 62). The radiographic features assessed were osteophytes, enthesiophytes, areas of abnormal mineralisation, synovial effusion and joint remodelling. The total radiographic score was calculated by summing the individual scores. A global score was determined based on an overall assessment of the severity of the radiographic changes. The prevalence of Sh-rOA and no Sh-rOA was calculated as the percentage of cats which had and had no radiographic changes. The prevalence of each radiographic feature was determined as the percentage of affected shoulder joints which had the feature. The mean and SD of osteophyte size were calculated.

3.2.4 Gross pathologic assessment of shoulder joint

Gross pathologic changes associated with OA were assessed and scored using a gross pathologic scoring system (see Section 2.4.1, page 66 and Table 2.3, page 67). The total gross pathologic score was calculated by summing the individual scores. A global score

was determined based on an overall assessment of the severity of the gross pathologic changes. The prevalence of Sh-path OA and no Sh-path OA/normal were determined as the percentage of cats which had or had no changes in the articular cartilage. The prevalence of each gross pathologic feature was calculated as the percentage of affected shoulder joints which had the feature.

3.2.5 Correlation studies

3.2.5.1 Correlation between radiographic and gross pathologic OA scores

A correlation analysis between radiographic and gross pathologic scores of the left and right shoulder joint was performed using a nonparametric, Spearman's rank correlation. Correlation coefficient results were interpreted as described in Table 2.9, page 80. The correlation was illustrated by scatter plot graphs.

3.2.5.2 Correlation between radiographic OA scores and age, BW and BCS

Correlation analysis between total radiographic OA scores for the left and right shoulder joints and age, BW and BCS was done using Spearman's rank correlation. The coefficient results were interpreted as described in Table 2.9, page 80. The correlation for left and right shoulder joints was illustrated by scatter plot graphs.

3.2.5.3 Correlation between gross pathologic OA score and age, BW and BCS

Correlation analysis between gross pathologic OA score and age, BW and BCS was performed using a nonparametric, Spearman's rank correlation. The coefficient results were interpreted as described in Table 2.9, page 80. The correlation for left and right shoulder joints was illustrated by scatter plot graphs.

3.3 Results

3.3.1 Shoulder OA population

A total of 116 shoulder joints from 58 cats were evaluated for the radiographic signs of OA. Of 58 cats evaluated, 21 had radiographic changes associated with shoulder OA (Sh-rOA). All shoulder joints with radiographic OA had gross cartilage changes. Of 37 cats with radiographically normal shoulders (no Sh-rOA), 27 had cartilage changes, thus giving a total population of cats with shoulder OA (Sh-path OA) of 48 (Table 3.1).

Population	Number of cats	Percentage (%)
Sh-rOA	21	36.2
No Sh-rOA	37	63.8
Sh-path OA	48	82.8
No Sh-path OA/normal	10	17.2

Table 3.1: Showing the number and percentage of cats in the Sh-rOA, no Sh-rOA, Sh-path OA and no path OA/normal populations. Total number of cats is 58.

3.3.2 Comparative analyses of signalment, body weight and body condition score between Sh-path OA and normal cats

3.3.2.1 Signalment

The mean age of the Sh-path OA cats was 7.6 years (SD 4.3) with a minimum age of 2 years and a maximum of 20 years. The median age was 5 years. The mean age of the no Sh-path OA/normal cats was 2.7 years (SD 2.4) with a minimum age of 3 months and a maximum of 8 years. The median age was 2.5 years. The age difference between the Sh-path OA and no Sh-path/normal cats was significant ($P<0.001$) (Figure 3.1.A). Fifteen Sh-path OA cats were castrated males (MC), 7 cats were female (F) and 26 cats were spayed female (FS). One of the no Sh-path OA/normal cats was M, 2 cats were MC, 6 cats were F and 1 was FS. In the OA group 79.2% were domestic short hair (DSH), 14.6% were domestic long hair (DLH) and 8.3% were pedigree cats. In the normal group 90.0% were DSH and 10.0% were pedigree cats (Figure 3.2.A and 3.2.B).

3.3.2.2 Body weight

The mean BW of the Sh-path OA cats was 3.4 kg (SD 1.1) with a minimum weight of 1.9 kg and a maximum of 7.0 kg. The median BW was 3.1 kg. The mean BW of the no Sh-path OA/normal cats was 3.6 kg (SD 1.3) with a minimum weight of 0.8 kg and a

maximum of 5.6 kg. The median was 3.6 kg. The difference between the Sh-path OA and no Sh-path OA/normal cats for BW was not significant (P=0.37) (Figure 3.1.B).

3.3.2.3 Body condition score

The Sh-path OA cats had a median body condition score (BCS) of 3with a minimum BCS of 1 and a maximum of 5. The no Sh-path OA/normal cats had a median BCS of 3 with a minimum BCS of 2 and a maximum of 5 (Figure 3.3). There was no significant difference between BCS of Sh-path OA and no Sh- path OA/normal cats (P=0.43) (Figure 3.1.C).

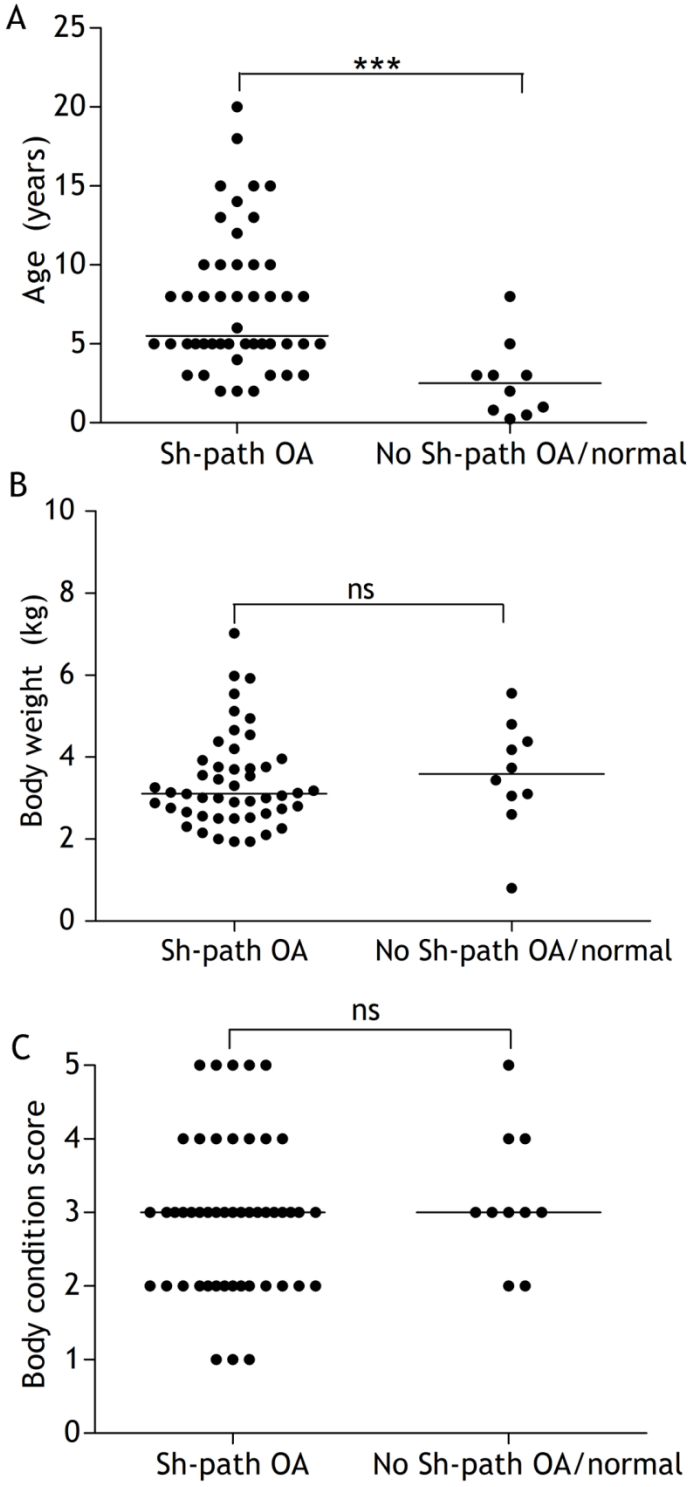

Figure 3.1: The comparative analysis of age, BW and BCS between Sh-path OA (*N*=48) and no Sh-path OA/normal (*N*=10) cats.

(A) The age difference between the OA and normal cats is significant. There is no significant difference in BW (B) and BCS (C) of cats with and without OA. Data presented as median and plotted in vertical scatter plot. (Mann Whitney *U* test, *** represents P<0.001; ns: not significant P>0.05).

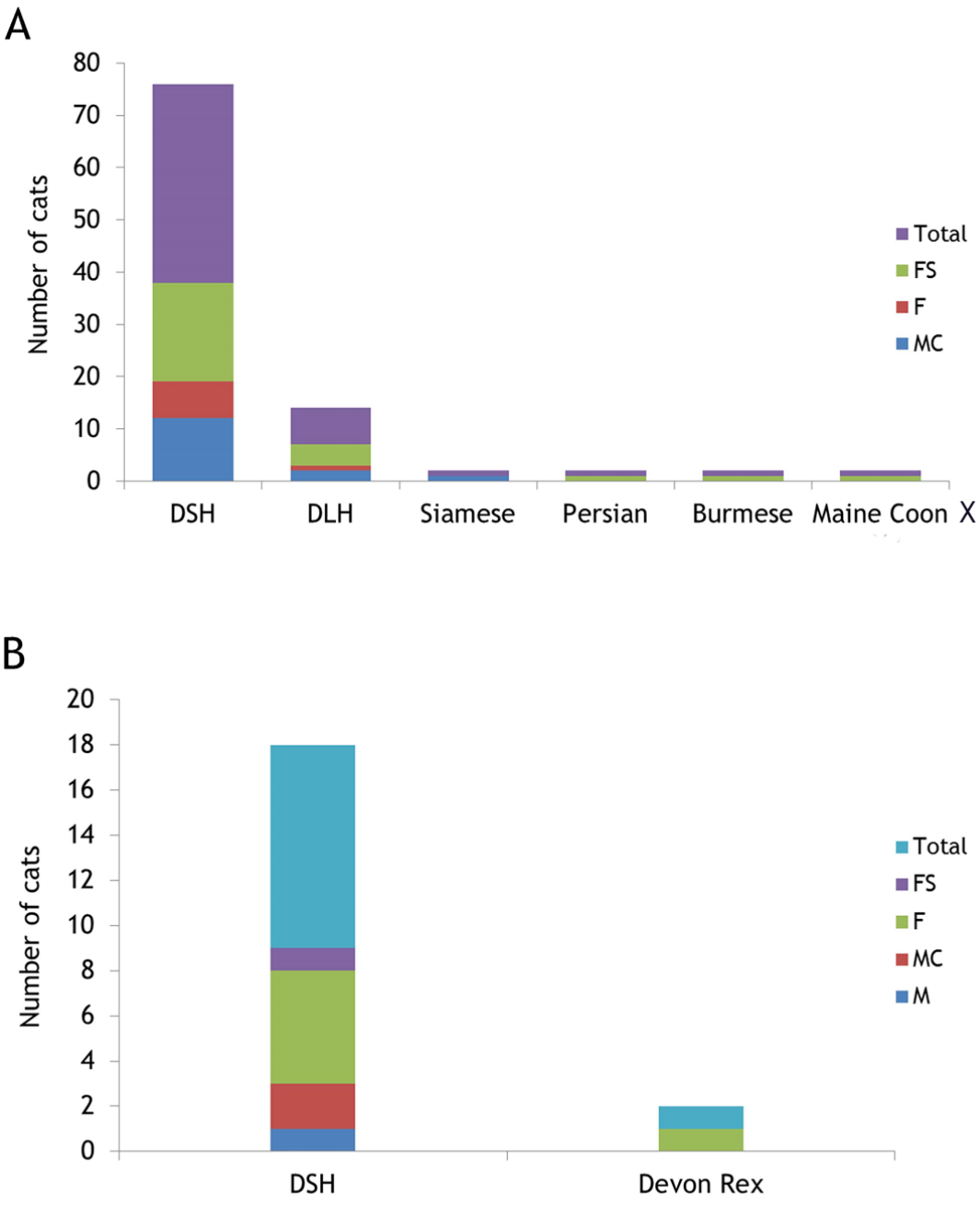

Figure 3.2: Breed and gender distribution of Sh-path OA (A) and no Sh-path OA/normal (B) cats.

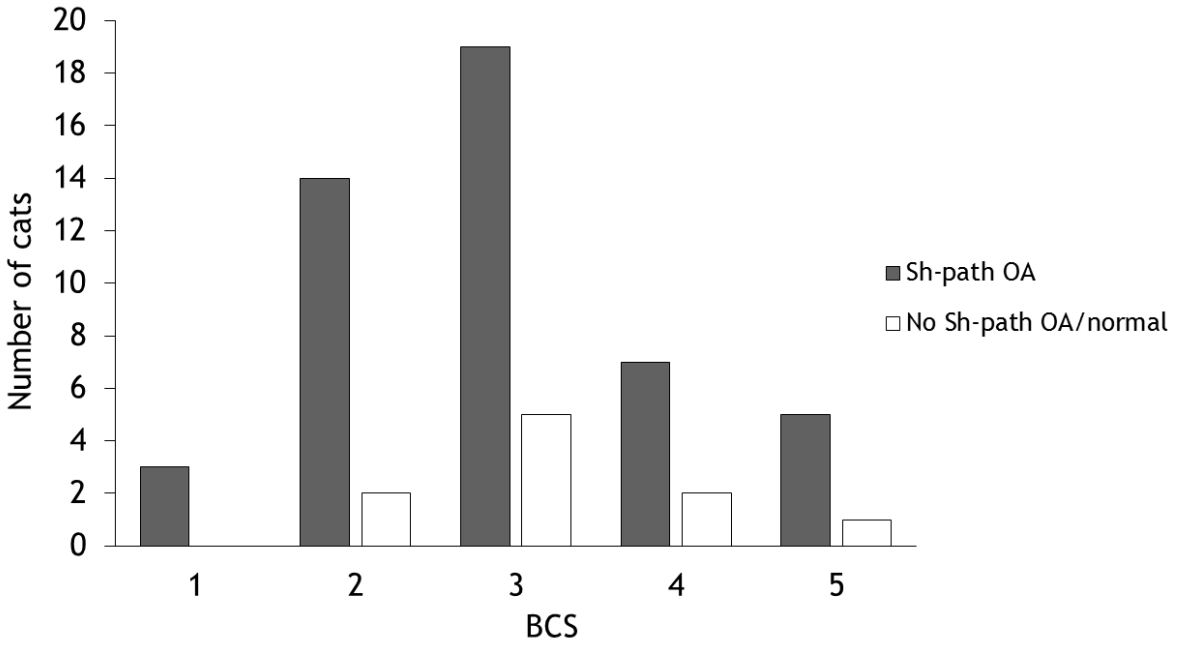

Figure 3.3: Distribution of body condition scores (BCS) of Sh-path OA and no Sh-path OA/normal cats.

3.3.3 Radiographic findings

The overall incidence of Sh-rOA was 36.2% (21 of 58 cats). Of 21 cats with radiographic changes, 6 cats had bilateral and 15 had unilateral shoulder involvement (11 on the left and 4 on the right) giving a total number of 27 Sh-rOA (Table 3.2). The mean and median total radiographic score for the left and right shoulder joint were 1 with a minimum total score of 1 and a maximum of 2 for both shoulder joints. The total radiographic scores were not significantly different between left and right shoulder joints (P=0.12). All joints with radiographic changes were given a Global score of 1 (Tables 3.3 and 3.4).

Twenty-six (96.3%) joints with radiographic changes had osteophytes. In 6 cats this was bilateral and in 14 cats unilateral. Osteophytes were seen on the caudal aspect of the humeral head and at the caudal edge of the glenoid (Figures 3.4.B and 3.4.D). Severity was graded mild in 23/26 joints (88.5%) (15 on the left and 8 on the right) and moderate in 3/26 joints (11.5%) (1 on the left and 2 on the right). The mean osteophyte size in mm ± SD for mild affected joints was 0.9 ± 0.2 and for moderate affected joint was 2.8 ± 0.1 (Table 3.5).

Areas of abnormal mineralisation was seen in 1/27 joints (3.7%). The mineralisation was scored as mild and located at the caudal edge of the glenoid (Figure 3.4.C).

Enthesiophytes, synovial effusion and joint remodelling were not seen in any joint.

	Radiographic findings			
	No Sh-rOA		Sh-rOA	
	Number of Joints	Percentage (%)	Number of joints	Percentage (%)
Left shoulder	41	70.1	17	29.3
Right shoulder	48	82.8	10	17.2
Total	89	76.7	27	22.4

Table 3.2: Showing numbers of shoulder joints with normal and abnormal radiographic findings. Total number of joints 116.

	Radiographic OA Global score			
	Score 0	Score 1	Score 2	Score 3
Left shoulder	41	17	0	0
Right shoulder	48	10	0	0
Total	89	27	0	0

Table 3.3: Showing the number of shoulder joints with different radiographic OA Global Scores.

Cat ID	Osteophytes		Enthesiophytes		Area of abnormal mineralisation		Synovial effusion		Joint remodelling		Total score		Global score	
	L	R	L	R	L	R	L	R	L	R	L	R	L	R
X1	0	0	0	0	0	0	0	0	0	0	0	0	0	0
X2	0	0	0	0	0	0	0	0	0	0	0	0	0	0
X3	0	0	0	0	0	0	0	0	0	0	0	0	0	0
X4	0	0	0	0	0	0	0	0	0	0	0	0	0	0
X5	0	0	0	0	0	0	0	0	0	0	0	0	0	0
X6	0	0	0	0	0	0	0	0	0	0	0	0	0	0
X7	1	0	0	0	0	0	0	0	0	0	1	0	1	0
X8	0	0	0	0	0	0	0	0	0	0	0	0	0	0
X9	0	0	0	0	0	0	0	0	0	0	0	0	0	0
X10	0	0	0	0	0	0	0	0	0	0	0	0	0	0
X11	0	0	0	0	0	0	0	0	0	0	0	0	0	0
X12	0	0	0	0	0	0	0	0	0	0	0	0	0	0
X13	0	0	0	0	0	0	0	0	0	0	0	0	0	0
X14	0	0	0	0	0	0	0	0	0	0	0	0	0	0
X15	1	0	0	0	0	0	0	0	0	0	1	0	1	0
X16	2	0	0	0	0	0	0	0	0	0	2	0	1	0
X17	0	0	0	0	0	0	0	0	0	0	0	0	0	0
X18	1	0	0	0	0	0	0	0	0	0	1	0	1	0
X19	0	0	0	0	0	0	0	0	0	0	0	0	0	0

Table 3.4: Radiographic features and Global scores of the left (L) and right (R) shoulder joints in 58 cats. Scoring: 0: normal, 1: mild, 2: moderate, 3: severe. Global score: 0: normal, 1: mild, 2: moderate, 3: severe.

Cat ID	Osteophytes		Enthesiophytes		Area of abnormal mineralisation		Synovial effusion		Joint remodelling		Total score		Global score	
	L	R	L	R	L	R	L	R	L	R	L	R	L	R
X20	0	0	0	0	0	0	0	0	0	0	0	0	0	0
X21	1	0	0	0	0	0	0	0	0	0	1	0	1	0
X22	0	0	0	0	0	1	0	0	0	0	0	1	0	1
X23	0	0	0	0	0	0	0	0	0	0	0	0	0	0
X24	1	0	0	0	0	0	0	0	0	0	1	0	1	0
X25	0	0	0	0	0	0	0	0	0	0	0	0	0	0
X26	0	0	0	0	0	0	0	0	0	0	0	0	0	0
X27	0	0	0	0	0	0	0	0	0	0	0	0	0	0
X28	2	1	0	0	0	0	0	0	0	0	2	1	1	1
X29	1	1	0	0	0	0	0	0	0	0	1	1	1	1
X30	0	0	0	0	0	0	0	0	0	0	0	0	0	0
X31	2	0	0	0	0	0	0	0	0	0	2	0	1	0
X32	1	1	0	0	0	0	0	0	0	0	1	1	1	1
X33	1	0	0	0	0	0	0	0	0	0	1	0	1	0
X34	0	0	0	0	0	0	0	0	0	0	0	0	0	0
X35	1	0	0	0	0	0	0	0	0	0	1	0	1	0
X36	0	0	0	0	0	0	0	0	0	0	0	0	0	0
X37	0	0	0	0	0	0	0	0	0	0	0	0	0	0
X38	0	0	0	0	0	0	0	0	0	0	0	0	0	0
X39	0	0	0	0	0	0	0	0	0	0	0	0	0	0
X40	1	0	0	0	0	0	0	0	0	0	1	0	1	0

Table 3.4 continued

Cat ID	Osteophytes		Enthesiophytes		Area of abnormal mineralisation		Synovial effusion		Joint remodelling		Total score		Global score	
	L	R	L	R	L	R	L	R	L	R	L	R	L	R
X41	0	0	0	0	0	0	0	0	0	0	0	0	0	0
X42	1	0	0	0	0	0	0	0	0	0	1	0	1	0
X43	0	0	0	0	0	0	0	0	0	0	0	0	0	0
X44	0	0	0	0	0	0	0	0	0	0	0	0	0	0
X45	1	1	0	0	0	0	0	0	0	0	1	1	1	1
X46	0	0	0	0	0	0	0	0	0	0	0	0	0	0
X47	0	0	0	0	0	0	0	0	0	0	0	0	0	0
X48	0	0	0	0	0	0	0	0	0	0	0	0	0	0
X49	1	1	0	0	0	0	0	0	0	0	1	1	1	1
X50	1	2	0	0	0	0	0	0	0	0	1	2	1	1
X51	0	0	0	0	0	0	0	0	0	0	0	0	0	0
X52	0	0	0	0	0	0	0	0	0	0	0	0	0	0
X53	0	0	0	0	0	0	0	0	0	0	0	0	0	0
X54	0	1	0	0	0	0	0	0	0	0	0	1	0	1
X55	0	0	0	0	0	0	0	0	0	0	0	0	0	0
X56	0	0	0	0	0	0	0	0	0	0	0	0	0	0
X57	0	1	0	0	0	0	0	0	0	0	0	1	0	1
X58	0	1	0	0	0	0	0	0	0	0	0	1	0	1

Table 3.4 continued.

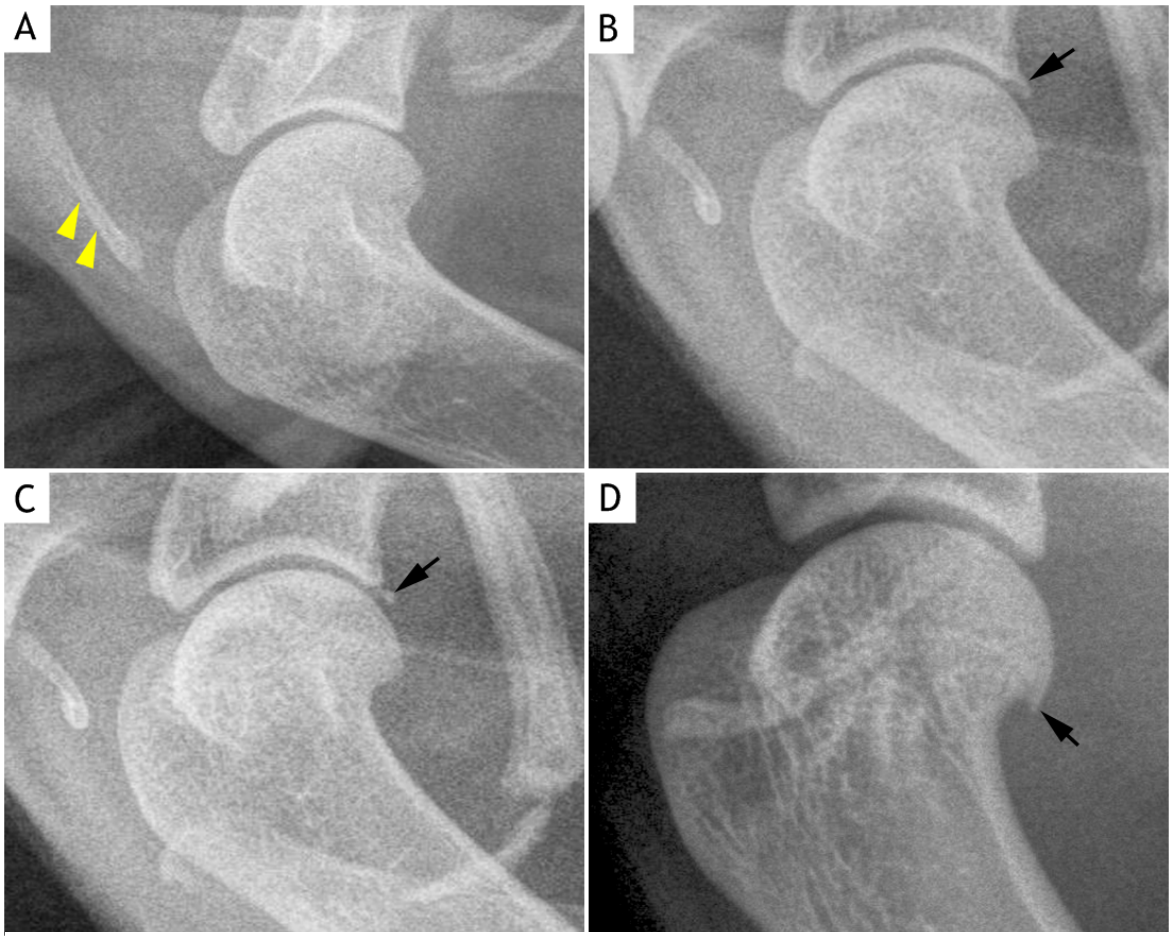

Figure 3.4: Mediolateral radiographs of the shoulder joint.

(A) A normal shoulder joint. Note the clavicle (yellow arrowheads). Cat ID: X19, left shoulder. (B) A shoulder joint with moderate osteophyte formation on the caudal aspect of the glenoid (black arrow). Cat ID: X50, right shoulder. (C) A shoulder joint with separate mineralised body (ossicle) (black arrow) at the caudal edge of the glenoid. Cat ID: X22, right shoulder (see Figure 3.7.C for gross pathology). (D) A shoulder joint with moderate osteophyte formation on the caudal aspect of the humeral head. Cat ID: X28, left shoulder.

	Left shoulder		Right shoulder	
Cat ID	Score	Osteophyte size (mm)	Score	Osteophyte size (mm)
X7	1	0.9	0	-
X15	1	1.2	0	-
X16	2	2.7	0	-
X18	1	0.8	0	-
X21	1	1.3	0	-
X24	1	1.1	0	-
X28	1	0.9	1	1.2
X29	1	0.8	1	0.8
X31	2	2.9	0	-
X32	1	1.2	1	1.4
X33	1	0.9	0	-
X35	1	0.6	0	-
X40	1	0.9	0	-
X42	1	0.7	0	-
X45	1	1	1	1.2
X49	1	1.1	1	0.9
X50	1	0.9	2	2.7
X54	0	-	1	0.7
X57	0	-	1	0.6
X58	0	-	1	0.4

Table 3.5: All shoulder joints with osteophytes were graded according to their size (mm) and whether a single site or multiple sites were involved.

3.3.4 Gross pathologic findings

Gross pathologic examinations were performed on 116 joints from 58 cats. Ten cats (17.2%) had grossly normal articular cartilage on both left and right humeral heads and glenoids. Six cats had unilateral grossly normal articular cartilage (1 on the left and 5 on the right side); thus giving a total of 26 no Sh-path OA/normal joints. Cartilage abnormalities were identified in 90 of 116 (77.6%) shoulder joints (Table 3.6), bilaterally in 42 cats and unilaterally in 6 cats (5 on the left and 1 on the right) thus giving a prevalence of Sh-path OA cat of 82.8%. The possible total gross pathologic score was 22; the highest score recorded was 8. The median of gross pathologic total score for left and right Sh-path OA joints was 3. Of 90 shoulder joints, 88 were given a Global score of 1 and two were given a Global score of 2 (Table 3.7 and Table 3.8). The total gross pathologic feature scores were not significantly different between left and right shoulder joints (P=0.74).

Normal humeral heads and glenoids had a white, smooth and glistening articular surface (Figures 3.5.A and 3.6.A). Of 90 affected shoulders, 56 (62.2%) had cartilage changes on both humeral head and glenoid, 24 (26.7%) had cartilage changes on the humeral head only and 10 (11.1%) had cartilage changes on the glenoid only. Degenerative cartilage often had a diffuse yellow discolouration (Figures 3.5.C and 3.6.D). Discolouration was present in 73 of the 90 shoulder joints (81.1%) (33 on the left and 40 on the right).

The articular cartilage showed fibrillation or roughening in all 90 affected shoulders; 74 (82.2%) had mild, 11 (12.2%) moderate and 5 (5.6%) severe fibrillation. Five shoulder joints (5.6%) had cartilage erosion (3 on the left and 2 on the right side). The erosion was seen at either the caudomedial periphery or caudal aspect of the humeral head and glenoid in 2 and 3 joints respectively (Figures 3.5.C and 3.6.B). Four shoulder joints (4.4%) had cartilage ulceration (2 on the left and 2 on the right side) (Figures 3.5.D and 3.6.D).

Of the 90 shoulder joints, 78 (86.7%) had osteophyte formation. In 74 joints (94.9%) osteophyte development was mild, in 4 (5.1%) it was moderate and no severe grade was observed. Osteophyte formation on the humeral head and glenoid occurred circumferentially and appeared as a raised bony projection (Figures 3.5.C and 3.5.D). No gross joint remodelling was seen. Thickening of the joint capsule and discolouration of the synovium were observed in 9 (10.0%) and 10 (11.2%) of the 90 joints respectively. Osteochondromas were seen in one joint (Figure 3.6.C). In all shoulder joints, the

medial or lateral glenohumeral ligaments were intact and no pathologic changes of the ligament were evident.

	Gross pathologic findings			
	No Sh-path OA		Sh-path OA	
	Number of Joints	Percentage (%)	Number of joints	Percentage (%)
Left shoulder	11	19.0	47	81.0
Right shoulder	15	25.9	43	74.1
Total	26	22.4	90	77.6

Table 3.6: Showing numbers of shoulder joints with normal and abnormal gross pathologic findings. Total number of joints 116.

	Gross pathologic OA Global scores			
	Score 0	Score 1	Score 2	Score 3
Left shoulder	11	47	0	0
Right shoulder	15	41	2	0
Total	26	88	2	0

Table 3.7: Showing the number of shoulder joints with different gross pathologic OA Global Scores.

Cat ID	Cartilage surface discolouration		Cartilage fibrillation		Cartilage erosion		Cartilage ulceration		Osteophytes		Joint remodelling		Thickening of joint capsule		Synovium discolouration		Total score		Global Score		Sample for histopathologic examination
	L	R	L	R	L	R	L	R	L	R	L	R	L	R	L	R	L	R	L	R	
X1	0	0	0	0	0	0	0	0	0	0	0	0	0	0	0	0	0	0	0	0	CBS-L
X2	0	0	0	0	0	0	0	0	0	0	0	0	0	0	0	0	0	0	0	0	CBS-L
X3	0	0	0	0	0	0	0	0	0	0	0	0	0	0	0	0	0	0	0	0	CBS-R
X4	1	1	1	1	0	0	0	0	0	0	0	0	0	0	0	0	2	2	1	1	
X5	1	1	1	1	0	0	0	0	0	0	0	0	0	0	0	0	2	2	1	1	
X6	1	1	2	1	0	0	0	0	1	0	0	0	0	0	0	0	4	2	1	1	CBS-L
X7	0	1	1	1	0	0	0	0	1	1	1	0	0	0	0	0	3	3	1	1	
X8	1	1	1	1	0	0	0	0	1	0	0	0	0	0	0	0	3	2	1	1	CBS-L
X9	0	0	1	0	0	0	0	0	0	0	0	0	0	0	0	0	1	0	1	0	CBS-R
X10	0	0	1	0	0	0	0	0	1	1	0	0	0	0	0	0	2	1	1	1	
X11	0	0	1	0	0	0	0	0	0	0	0	0	0	0	0	0	1	0	1	0	CBS-R
X12	0	1	1	1	0	0	0	0	1	1	0	0	0	0	0	0	2	3	1	1	
X13	0	0	0	0	0	0	0	0	0	0	0	0	0	0	0	0	0	0	0	0	CBS-R
X14	0	0	0	0	0	0	0	0	0	0	0	0	0	0	0	0	0	0	0	0	
X15	1	1	1	1	0	0	0	0	1	1	0	0	0	0	0	0	0	0	1	1	
X16	1	0	1	0	0	0	0	0	1	0	0	0	0	0	0	0	3	0	1	0	CBS-L
X17	1	0	1	0	0	0	0	0	0	0	0	0	0	0	0	0	2	0	1	0	CBS-L
X18	0	1	1	1	1	0	0	0	1	1	0	0	0	0	0	0	3	3	1	1	
X19	0	0	0	0	0	0	0	0	0	0	0	0	0	0	0	0	0	0	0	0	CBS-R

Table 3.8: Gross pathologic features and Global scores of the left (L) and right (R) shoulder joints in 58 cats. Global score: 0: normal, 1: mild, 2: moderate, 3: severe. Samples selected for histopathologic examination: CBS-L: Cartilage Bone Synovium-Left; CBS-R: Cartilage Bone Synovium-Right, OST-R: Osteochondromas.

Cat ID	Cartilage discolouration		Cartilage fibrillation		Cartilage erosion		Cartilage ulceration		Osteophytes		Joint remodelling		Thickening of joint capsule		Synovium discolouration		Total score		Global Score		Sample for histopathologic examination
	L	R	L	R	L	R	L	R	L	R	L	R	L	R	L	R	L	R	L	R	
X20	0	0	0	0	0	0	0	0	0	0	0	0	0	0	0	0	0	0	0	0	CBS-R
X21	1	1	1	2	1	1	0	1	1	1	0	0	0	1	0	1	4	8	1	2	CBS-R
X22	1	1	1	2	0	0	0	0	1	1	0	0	0	0	0	0	3	4	1	1	CBS-R, OST
X23	0	0	1	1	0	0	0	0	1	1	0	0	0	0	0	0	2	2	1	1	
X24	1	1	2	2	1	0	0	2	1	2	0	0	0	0	0	1	5	8	1	2	CBS-R
X25	0	1	1	1	0	0	0	0	1	1	0	0	0	0	0	0	2	3	1	1	
X26	1	1	2	2	0	0	0	0	1	1	0	0	0	0	0	0	4	4	1	1	
X27	1	1	2	2	0	0	0	0	1	1	0	0	0	0	1	1	5	5	1	1	
X28	1	1	3	3	0	0	1	0	2	1	0	0	2	1	0	0	9	6	1	1	CBS-L
X29	1	1	1	1	0	0	0	0	1	1	0	0	0	0	0	0	3	3	1	1	
X30	1	1	1	1	0	0	0	0	1	1	0	0	0	0	0	0	3	3	1	1	
X31	1	1	1	1	0	0	0	0	1	1	0	0	0	0	1	0	4	3	1	1	CBS-L
X32	1	1	1	1	0	0	0	0	1	1	0	0	0	0	0	0	3	3	1	1	
X33	0	1	1	1	0	0	0	0	1	0	0	0	0	0	0	0	2	2	1	1	
X34	0	0	1	1	0	0	0	0	1	1	0	0	0	0	0	0	2	2	1	1	
X35	1	1	1	1	0	0	0	0	1	1	0	0	0	0	0	0	3	3	1	1	
X36	1	1	1	1	0	0	0	0	1	1	0	0	0	0	0	0	3	3	1	1	
X37	1	1	2	1	0	0	0	0	1	1	0	0	0	0	0	0	4	3	1	1	
X38	1	1	1	1	0	0	0	0	1	1	0	0	0	0	0	0	3	3	1	1	
X39	1	1	1	3	0	0	0	1	1	2	0	0	0	0	0	0	3	7	1	1	CBS-R
X40	1	1	2	1	1	1	0	0	1	2	0	0	0	0	0	0	5	5	1	1	CBS-L
X41	1	1	1	1	0	0	0	0	1	1	0	0	1	1	1	1	5	5	1	1	

Table 3.8 continued.

Cat ID	Cartilage discolouration		Cartilage fibrillation		Cartilage erosion		Cartilage ulceration		Osteophytes		Joint remodelling		Thickening of joint capsule		Synovium discolouration		Total score		Global Score		Sample for histopathologic examination
	L	R	L	R	L	R	L	R	L	R	L	R	L	R	L	R	L	R	L	R	
X42	1	1	3	1	0	0	0	0	1	1	0	0	0	0	0	0	5	3	1	1	CBS-L
X43	1	1	1	1	0	0	0	0	1	1	0	0	0	0	0	0	3	3	1	1	
X44	1	1	3	1	0	0	1	0	1	1	0	0	0	0	0	0	6	3	1	1	CBS-L
X45	1	1	1	1	0	0	0	0	1	1	0	0	1	0	0	0	4	3	1	1	
X46	0	1	1	1	0	0	0	0	1	1	0	0	1	1	0	0	3	4	1	1	CBS-L
X47	0	0	1	1	0	0	0	0	1	1	0	0	0	0	0	0	2	2	1	1	
X48	1	1	1	1	0	0	0	0	1	1	0	0	1	0	0	0	4	3	1	1	
X49	1	1	1	1	0	0	0	0	1	1	0	0	0	0	1	1	4	4	1	1	CBS-R
X50	1	1	1	1	0	0	0	0	1	1	0	0	0	0	1	0	4	3	1	1	
X51	0	0	0	0	0	0	0	0	0	0	0	0	0	0	0	0	0	0	0	0	CBS-R
X52	0	0	0	0	0	0	0	0	0	0	0	0	0	0	0	0	0	0	0	0	
X53	0	0	0	0	0	0	0	0	0	0	0	0	0	0	0	0	0	0	0	0	
X54	0	1	1	1	0	0	0	0	1	1	0	0	0	0	0	0	2	3	1	1	
X55	1	1	1	0	0	0	0	0	0	0	0	0	0	0	0	0	2	1	1	0	
X56	1	1	1	1	0	0	0	0	1	1	0	0	0	0	0	0	3	3	1	1	
X57	0	1	0	1	0	0	0	0	0	1	0	0	0	0	0	0	0	3	0	1	
X58	0	1	1	1	0	0	0	0	1	1	0	0	0	0	0	0	2	3	1	1	CBS-L

Table 3.8 continued.

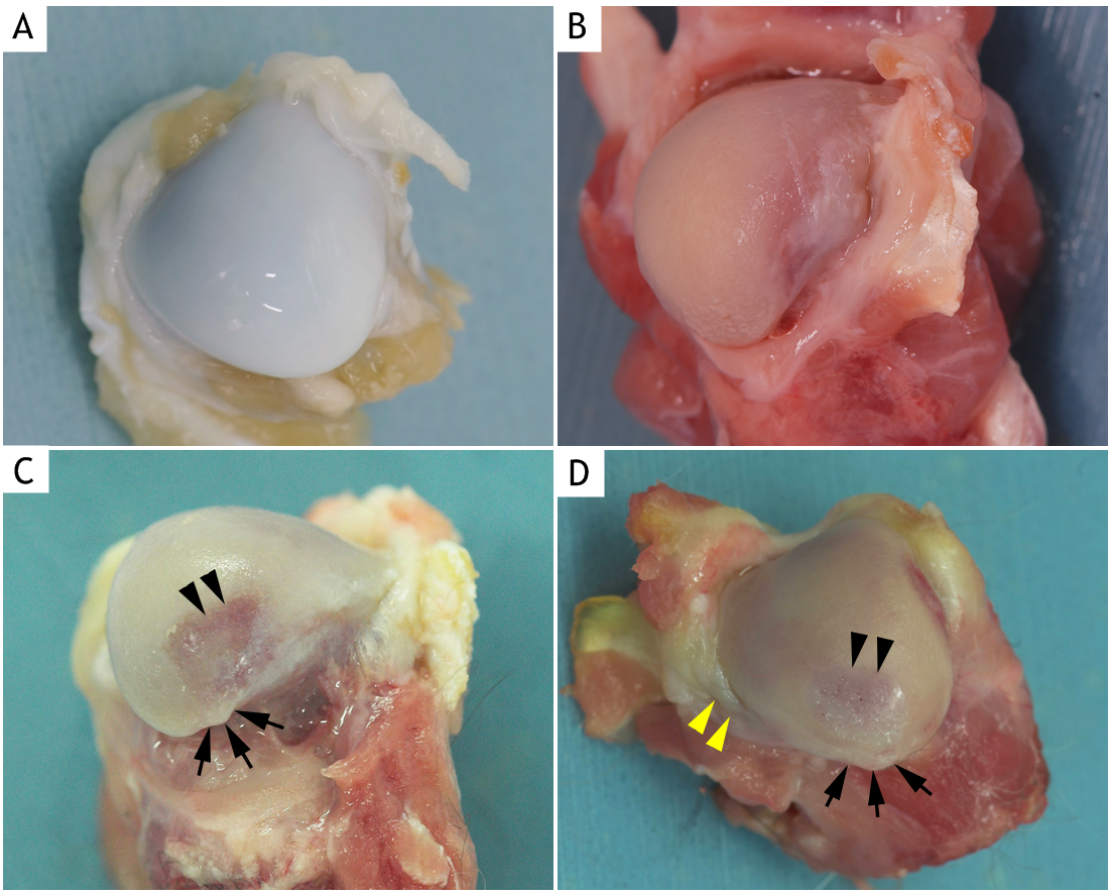

Figure 3.5: Photographs of humeral articular surface showing gross pathologic features.

(A) Normal humeral cartilage has a smooth and glistening appearance. Cat ID: X19, left shoulder. (B) Generalised surface dullness and fibrillation is observed. Cat ID: X6, left shoulder. (C) Close to the periphery of the humeral head (caudomedial aspect), a localised cartilage erosion is seen (arrowheads). There is also diffuse yellow discolouration of the articular cartilage. Osteophyte formation also can be identified (black arrows). Cat ID: X24, right shoulder. (D) There is an obvious area of cartilage damage where there is a total loss of cartilage (arrowheads) and osteophyte formation (black arrows) is noted on the caudal humeral head. A mildly thickened synovial membrane is also present (yellow arrowheads). Cat ID: X28, left shoulder.

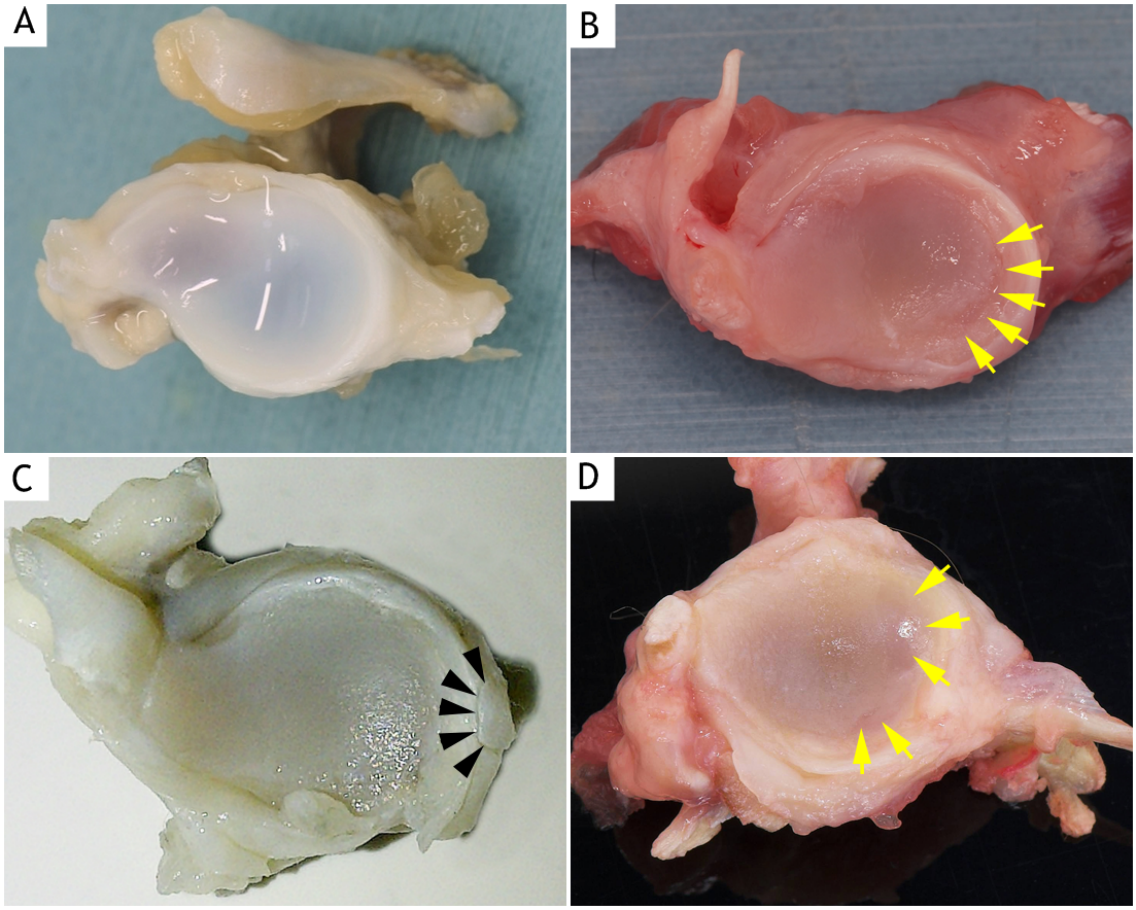

Figure 3.6: Photographs of glenoid articular surface showing gross pathologic features.

(A) Note a smooth and glistening appearance of normal glenoid cartilage. Cat ID: X19, left shoulder. (B) Cartilage fibrillation and dullness is seen. Localised cartilage erosion can be identified at the caudomedial glenoid rim (yellow arrows). Cat ID: X40, left shoulder. (C) Generalised surface dullness with fibrillation is observed. A discrete osseocartilagenous body is seen at the caudal edge of the glenoid (black arrowheads); it is adherent to the labrum and synovium. Cat ID: X22, right shoulder (see Figure 3.4.C for radiograph). (D) Cartilage fibrillation and ulceration (yellow arrows) is present. A moderately thickened joint capsule and osteophytes are also present. Cat ID: X24, right shoulder.

3.3.5 Correlation studies

3.3.5.1 Correlation between radiographic and gross pathologic OA scores

All shoulders with radiographic changes had gross lesions. Of 90 radiographically normal joints, 64 (71.1%) had gross lesions. There was a significant moderate and fair positive correlation between the radiographic and gross pathologic scores in the left (r_s=0.46, P<0.001) and right (r_s=0.31, P<0.05) shoulder joints respectively (Figures 3.7.A and 3.7.B).

3.3.5.2 Correlation between radiographic OA total scores and age, BW and BCS

There was a significant fair positive correlation between the radiographic total score of the left (r_s=0.28, P<0.05) and right (r_s =0.27, P<0.05) shoulder joints and age (Figures 3.8.A and 3.8.B). There was a slight, negative relationship between the radiographic total score of the left (r_s=-0.12, P=0.35) and right (r_s=-0.21, P=0.10) shoulder joints and BW, which was not statistically significant (Figures 3.8.C and 3.8.D). A similar finding was also observed between the radiographic total score of the left (r_s=-0.14, P=0.29) and right (r_s=-0.14, P=0.29) shoulder joints and BCS (Figures 3.8.E and 3.8.F).

3.3.5.3 Correlation between gross pathologic OA score and age, BW and BCS

Correlation analysis revealed a significant moderate positive relationship between the gross pathologic score of the left (r_s =0.49, P<0.001) and right (r_s =0.49, P<0.001) shoulder joints and age (Figures 3.9.A and 3.9.B). Correlation analysis revealed a slight negative relationship between the gross pathologic score of the left (r_s=-0.19, P=0.14) and right (r_s=-0.14, P=0.29) shoulder joints and BW. The relationship however was not statistically significant (Figures 3.9.C and 3.9.D). A similar finding was also observed between the gross pathologic total score of the left (r_s=-0.20, P=0.14) and right (r_s=-0.22, P=0.10) shoulder joints and BCS (Figures 3.9.E and 3.9.F).

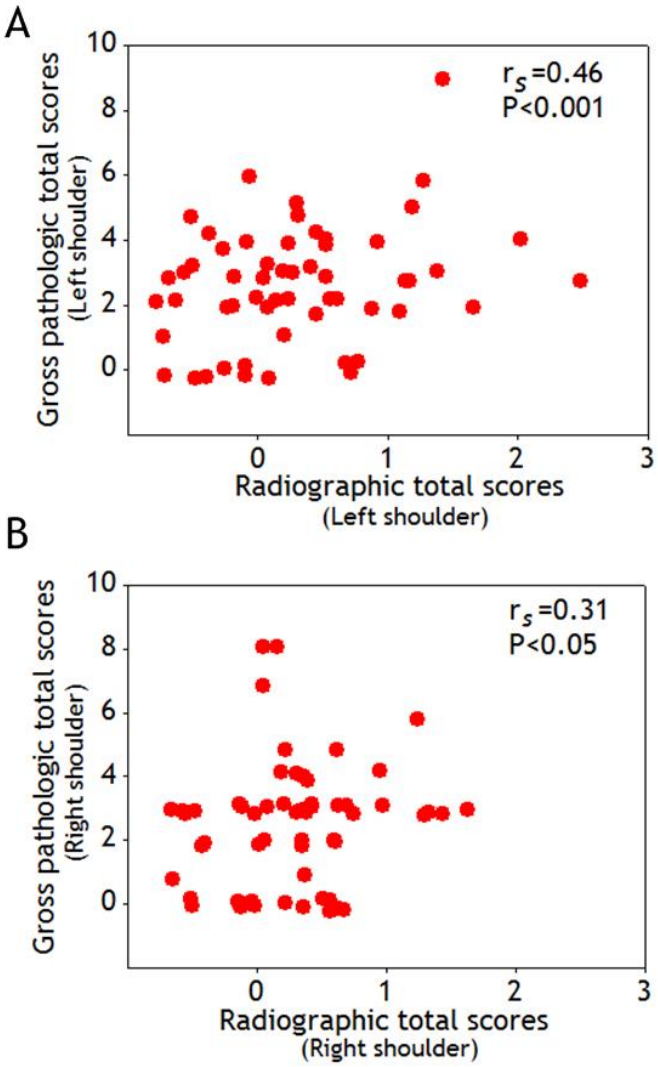

Figure 3.7: Graph demonstrating correlation between radiographic and gross pathologic OA scores in left (A) and right (B) shoulder joints. There is a significant moderate and fair relationship between the radiographic and gross pathologic scores in the left and right shoulder joints respectively.

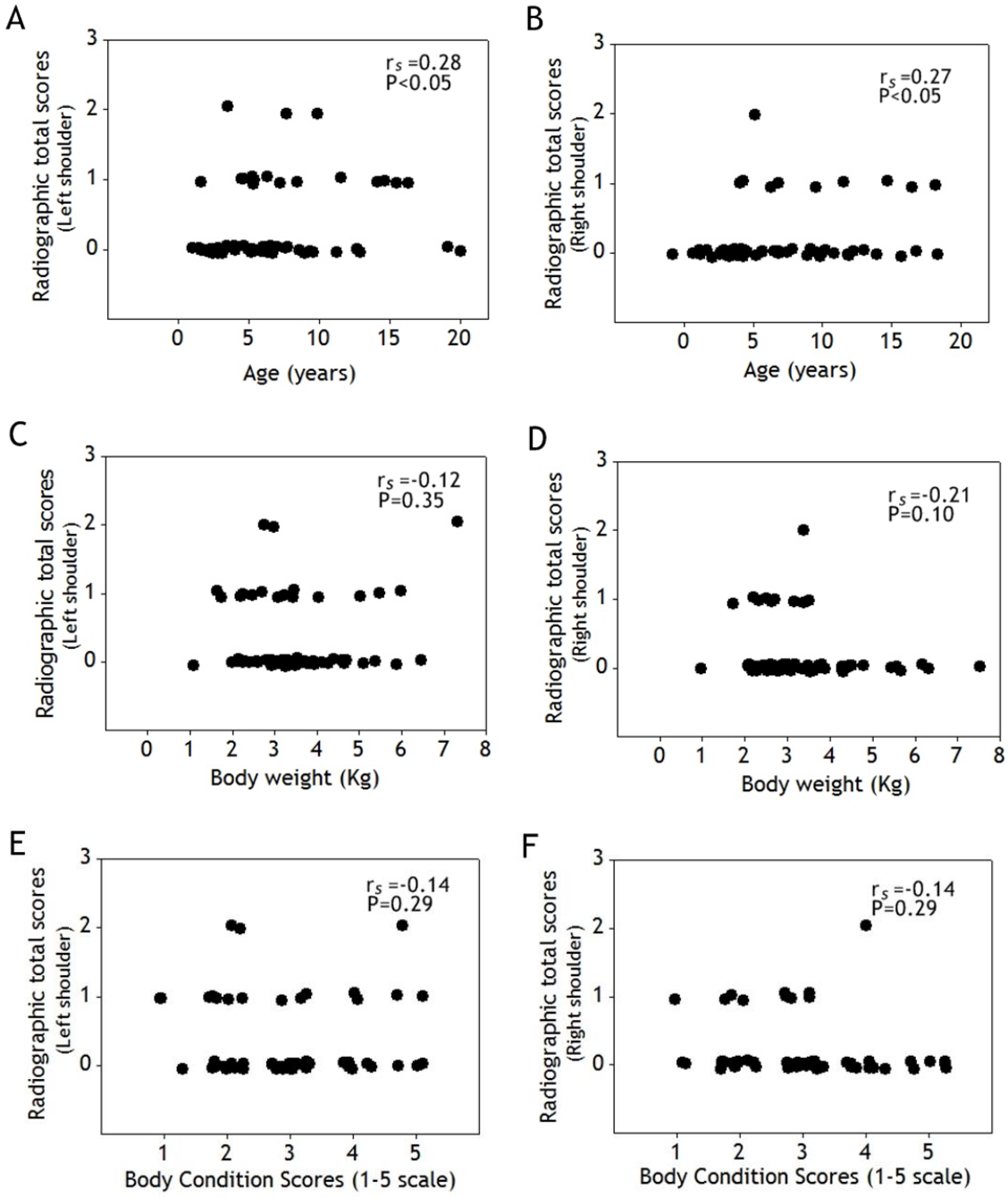

Figure 3.8: Correlation analysis of radiographic total scores of the left (A, C, and E) and right (B, D, and F) shoulder joints and age, BW and BCS. (A & B) A significant fair positive relationship between gross pathologic score of the left and right shoulder joints and age. (C & D) Correlation analysis of radiographic total score of the left and right shoulder joints and BW. (E & F) Correlation analysis of radiographic total score of the left and right shoulder joints and BCS. There are no significant relationships between the radiographic total score of the left and right shoulder joints and the BW and BCS.

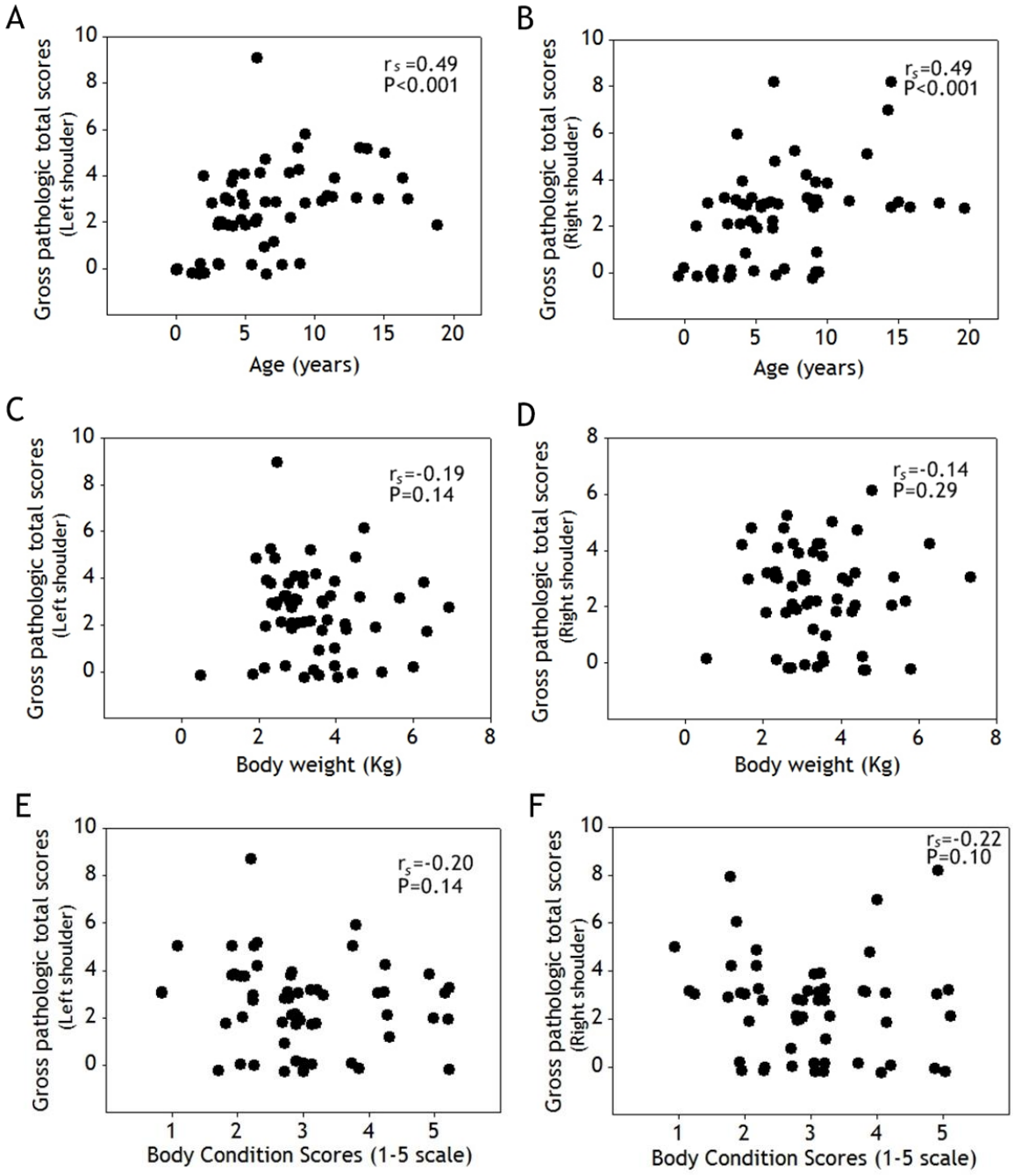

Figure 3.9: Correlation analysis of gross pathologic scores of the left (A, C, and E) and right (B, D, and F) shoulder joints and age, BW and BCS. (A & B) A significant moderate positive relationship between gross pathologic score of the left and right shoulder jointss and age. (C & D) Correlation analysis of gross pathologic score of the left and right shoulder joints and BW. (E & F) Correlation analysis of gross pathologic score of the left and right shoulder joints and BCS. There are no significant relationships between the gross pathologic score of the left and right shoulder joints and the BW and BCS.

3.4 Discussion

The overall prevalence of Sh-rOA and Sh-path OA was 36.2 % (21 of 58 cats) and 82.8% (48 of 58 cats) respectively. The radiographic prevalence was much higher than that reported in a previous study by Godfrey (2005) (5%, 1 of 18 cats) and slightly lower than in the study reported by Clarke and Bennett (2006) (39.3%, 11 of 28 cats). The present study demonstrated that a large number of cats had shoulder OA, particularly when assessed by gross pathologic examination. The marked difference between the prevalence as assessed by radiography and by gross pathologic examination reflects the difficulty in identifying radiographic changes which in many cases are minimal or absent. Even though the left shoulder was more often affected than the right, the radiographic and gross pathologic total score showed no difference which suggests that the severity of disease in the left and right shoulders was similar.

The presence of radiographic osteophytes was an important feature in diagnosing shoulder OA. The osteophytes were seen protruding from the surface of the bone, at the caudal edge of the glenoid and the caudal aspect of the humeral head. The location of the radiographic osteophytes was similar to those reported in previous studies (Godfrey, 2007 and Bennett et al., 2012a). Shoulder joints which were radiographically normal had a high incidence (71.1%) of gross cartilage lesions on the humeral head or glenoid or both. This suggests that radiography has a low sensitivity in detecting OA (cartilage) pathology in the shoulder joint. In addition, because osteophytes on the medial and lateral aspects of the humeral head and glenoid are difficult to see radiographically, the extent of joint pathology may be underestimated (Carrig, 1997).

Most cats with shoulder OA were domestic shorthaired spayed females. The mean age of cats with Sh-path OA was higher (7.6 years), than those without (2.7 years). Other studies have reported that cats with shoulder OA have a higher mean age than cats without OA (Clarke et al., 2005; Godfrey, 2005). The correlation of cartilage lesions with increasing age indicates that they are age-acquired OA lesions. The mean values of BW and the BCS of affected cats were 3.4 kg and 3.0 respectively, which are generally ideal for adult cats. The BW and BCS were found to be negatively correlated with the gross pathologic severity, but this was not statistically significant. No correlation has been reported so far between body weight and gross pathologic findings in the cat. The studies of Clarke et al. (2005) and Lascelles et al. (2010) demonstrated no significant association between body weight and/or BCS and radiographic signs of OA.

Cartilage abnormalities were more often found on the humeral head (88.9%; 80/90 shoulder joints) than the glenoid (73.3%; 66/90 shoulder joints). A similar finding has been reported in canine shoulder OA where cartilage pathology was typically observed on the caudal humeral head more than the glenoid (Bardet, 1998; Craig and Reed, 2013). The reason why the humeral head is more commonly affected than the glenoid is not clear. However, the structural difference between the humeral head and glenoid may be a factor; the humeral head has a convex structure, whereas the glenoid a concave structure. Convex surfaces are subjected to compression and maybe more susceptible to mechanical loading and trauma. This interpretation is supported by an anatomical study by Simkin et al. (1980) which found subchondral bone plate underlying convex articular surfaces is significantly thinner than that under the corresponding concave sides. The study further suggested that the thin layer of the subchondral bone underlying the convex articular surfaces makes that side less stiff and more susceptible to mechanical loading. The gross and histopathologic features of fibrillation, erosion and ulceration seen in this study are similar to those previously reported in OA of the cat shoulder joint (Bennett et al., 2012a). Cartilage erosion at the medial periphery of the glenoid rim and humeral head was seen in two joints suggesting that shoulder subluxation may be a causative factor. Bardet (1998) reported that recurrent instability episodes can erode the articular cartilage of the canine medial glenoid rim and further reduce its concavity. However no gross damage of the medial or lateral glenohumeral ligaments consistent with instability was seen in this study. Cartilage erosion and ulceration found at the caudal humeral head were consistent with canine shoulder OA (Craig and Reed, 2012).

This study did not provide any conclusive evidence for an underlying cause of feline shoulder OA. The medially located cartilage damage in two cases might suggest a medial joint laxity or subluxation but no soft tissue changes were identified to support this. It thus appears that shoulder OA is mainly idiopathic (primary).

Chapter 4 Radiographic and pathologic features of osteoarthritis of the feline elbow joint

4.1 Introduction and aims

The elbow joint is primarily a hinge joint, allowing movement in one plane only; flexion and extension. It also allows rotation of the antebrachium to a pronated or supinated position. The joint forms by the distal humeral condyle, with the radial head and the trochlear notch of the ulna. The distal humeral condyle comprises of medial and lateral parts which is covered with a layer or articular cartilage. The distal humeral condyle widens distally forming lateral and medial epicondyles. The radial head has a concave articular surface, covered by articular cartilage and articulates with the lateral part of the distal humeral condyle. The trochlear notch of the ulna forms congruent surfaces with the medial part of the distal humerus. The humeroulnar, humeroradial and the radioulnar joints share a common fibrous capsule which attaches along the articular margin of the elbow. The joint is stabilised and support by three major ligaments, the lateral collateral ligament, the medial collateral ligament and the annular ligament. The lateral collateral ligament has a superficial and deep part, both attach proximally to the lateral epicondyle and distally to a long antebrachial portion on the radius (Engelke et al., 2011). The medial collateral ligament originates from the medial humeral epicondyle and divisible into cranial and caudal parts. The cranial part attaches to the caudal aspect of the radius, while the caudal part inserts medioproximally on the ulna (Engelke et al., 2011).

Osteoarthritis of the elbow is common in the cat. The incidence of elbow OA in cats ranges from 21.0 to 54.5% (Pacchiana et al., 2004; Clarke et al., 2005; Godfrey, 2005; Clarke and Bennett, 2006; Lascelles et al., 2010; Freire et al., 2011). Many studies have reported the radiographic features associated with elbow OA, however only Freire et al. (2011) correlate their findings with gross pathologic disease. Little is known about the usefulness of radiographic features of elbow OA as indicator of articular cartilage damage in cats. Disease of the articular cartilage is mainly reported in the medial compartment of the elbow joint, specifically the medial part of the humeral condyle and the medial coronoid process of the ulna (Bennett et al., 2012a; Ryan et al., 2013; Freire et al., 2014). Most cases of elbow OA in the cat appear to be of a primary or idiopathic nature, which is very different to the dog where most cases are secondary to some other disease problem, such as elbow dysplasia.

The purpose of this study was to define the radiographic features of elbow OA and relate the radiographic findings to the gross pathologic features. In particular the following questions were to be addressed:

a) Can the radiographic features be a good indicator of the severity of cartilage pathology?

b) Is the increased radio-opacity beneath the semilunar notch an important and reliable feature of radiographic OA?

c) Is the radiographic visualisation of the supinator sesamoid bone always an indicator of OA in the feline elbow joint?

d) Is elbow OA mainly idiopathic (primary) in nature?

4.2 Materials and methods

4.2.1 Determination of elbow OA population

Determination of the elbow OA population was done as described in Section 2.2, page 58 and Figure 2.1, page 59.

4.2.2 Comparative analyses of signalment, body weight and body condition score between El-path OA and no El-path OA/normal cats

Median of age, BW and BCS of El-path OA and no El-path OA/normal cats were illustrated with a scatter plot graph and statistically analysed by using the Mann-Whitney *U* test. The distribution of breed and gender of El-path OA and no El-path OA/normal cats was visualised using a stacked bar graph. The distribution of BCS of El-path OA and no El-path OA/normal cats was shown by a column bar graph.

4.2.3 Radiographic assessment of the elbow joint

Radiographic changes associated with elbow OA were assessed using a radiographic scoring system (see Section 2.3.3, page 60 and Table 2.1, page 62). The radiographic features assessed were osteophytes, enthesiophytes, areas of abnormal mineralisation, supinator sesamoid bone (SSB), increase radio-opacity beneath the trochlear notch of the ulna, synovial effusion, joint space, joint remodelling and elbow incongruity. The total radiographic and the global scores were recorded. The prevalence of El-rOA and no El-rOA was calculated as the percentage of cats which had or had no radiographic

changes. The prevalence of each radiographic feature was determined as the percentage of affected elbow joints which had the feature. The mean and SD of osteophyte and SSB size were calculated. The age of cats with and without radiographic SSB was statistically analysed by using the Mann-Whitney *U* test and was illustrated with a scatter plot graph.

4.2.4 Gross pathologic assessment of the elbow joint

Gross pathologic changes associated with OA were assessed and scored using a gross pathologic scoring system (see Section 2.4.1, page 66 and Table 2.3, page 67). The gross cartilage changes (cartilage discolouration, fibrillation, ulceration and erosion) on the medial and lateral parts of the distal humeral condyle and radius/ulna were scored independently. The total gross pathologic score was calculated by summing the individual scores. A global score was determined based on an overall assessment of the severity of the gross pathologic changes. The prevalence of El-path OA and no El-path OA/normal were determined as the percentage of cats which did have or did not have changes in the articular cartilage. The prevalence of each gross pathologic feature was calculated as the percentage of affected elbow joints which had the feature. The Wilcoxon Signed Rank test was used to analyse the difference between gross cartilage damage scores of the medial and lateral parts of the humeral condyle. The Mann Whitney *U* test was used to analyse the difference between gross cartilage damage scores between elbow joints with or without SSB and age difference between cats with and without SSB. The same test was used to analyse the difference between gross pathologic scores of the left and right elbow joint. The results were illustrated with a scatter plot graph.

4.2.5 Inter- and Intra- observer variability and sensitivity of radiographic assessment of increase radio-opacity beneath the semilunar notch

The inter- and intra-observer study was done as described in Section 2.3.4, page 63. The Cohen's Kappa (K) results were interpreted as described in Table 2.10, page 80.

4.2.6 Correlation studies

4.2.6.1 Correlation between radiographic and gross pathologic OA scores

A correlation analysis between total radiographic and total gross pathologic scores for the left and right elbow joints was performed using a nonparametric, Spearman's rank

correlation. Correlation coefficient results were interpreted as described in Table 2.9, page 80. The correlation was illustrated by scatter plot graphs.

4.2.6.2 Correlation between radiographic OA scores and age, BW and BCS

Correlation analysis between total radiographic OA scores for the left and right elbow joints and age, BW and BCS was done using Spearman's rank correlation coefficient. The coefficient results were interpreted as described in Table 2.9, page 80. The correlation for left and right elbow joints was illustrated by scatter plot graphs.

4.2.6.3 Correlation between gross pathologic OA scores and age, BW and BCS

Correlation analysis between total gross pathologic OA scores for the left and right elbow joints and age, BW and BCS was performed using Spearman's rank correlation coefficient. The coefficient results were interpreted as described in Table 2.9, page 80. The correlation for left and right elbow joints was illustrated by scatter plot graphs.

4.3 Results

4.3.1 Elbow OA population

A total of 116 elbow joints from 58 cats were evaluated for the radiographic signs of OA. Of 58 cats evaluated, 50 had radiographic changes associated with elbow OA (El-rOA). All El-rOA cats had cartilage changes. Of 8 cats with radiographically normal elbows (no El-rOA), two had cartilage changes, thus giving a total population of 52 cats with elbow OA (El-path OA) (Table 4.1).

Population	Number of cats	Percentage (%)
El-rOA	50	86.2
No El-rOA	8	13.8
El-path OA	52	89.7
No El-path OA/normal	6	10.3

Table 4.1: Showing the number and percentage of the El-rOA, no El-rOA, El-path OA and no El-path OA/normal populations. Total number of cats is 58.

4.3.2 Comparative analyses of signalment, body weight and body condition score between El-path OA and no El-path OA/normal cats

4.3.2.1 Signalment

The mean age of the El-path OA was 7.3 years (SD 4.3) with a minimum age of 2 years and a maximum of 20 years. The median age was 5 years. The mean age of the no El-path OA/normal cats with normal elbow joints was 1.9 years (SD 1.6) with a minimum age of 3 months and a maximum of 5 years. The median age was 1.5 years. The age difference between the El-path OA and no El-path OA/normal cats was significant ($P<0.001$) (Figure 4.1.A). Sixteen El-path OA cats were MC, 10 cats were F and 26 cats were FS. One of the no El-path OA/normal cats was M, 2 cats were MC and 3 cats were F. In the El-path OA group 78.8% were DSH, 13.5% were DLH and 7.7% were pedigree cats. In the no El-path OA/normal group 83.3% were DSH and 16.7% were pedigree cats (Figures 4.2.A and 4.2.B).

4.3.2.2 Body weight

The mean BW of the El-path OA cats was 3.5 kg (SD 1.1) with a minimum weight of 1.9 kg and a maximum of 7.0 kg. The median BW was 3.1 kg. The mean BW of the no El-path OA/normal cats was 3.2 kg (SD 1.3) with a minimum weight of 0.8 kg and a

maximum of 4.8 kg. The median was 3.4 kg. The difference between the El-path OA and no El-path OA/normal cats for BW was not significant (P=0.97) (Figure 4.1.B).

4.3.2.3 Body condition score

The El-path OA cats had a median BCS of 3with a minimum BCS of 1 and a maximum of 5. The no El-path OA/normal cats had a median BCS of 3with a minimum BCS of 2 and a maximum of 4. There was no significant difference between BCS of the El-path OA and no El-path OA/normal cats (P=0.83) (Figure 4.1.C). The distribution of BCS of the El-path OA and no El-path OA/normal cats is shown in Figure 4.3.

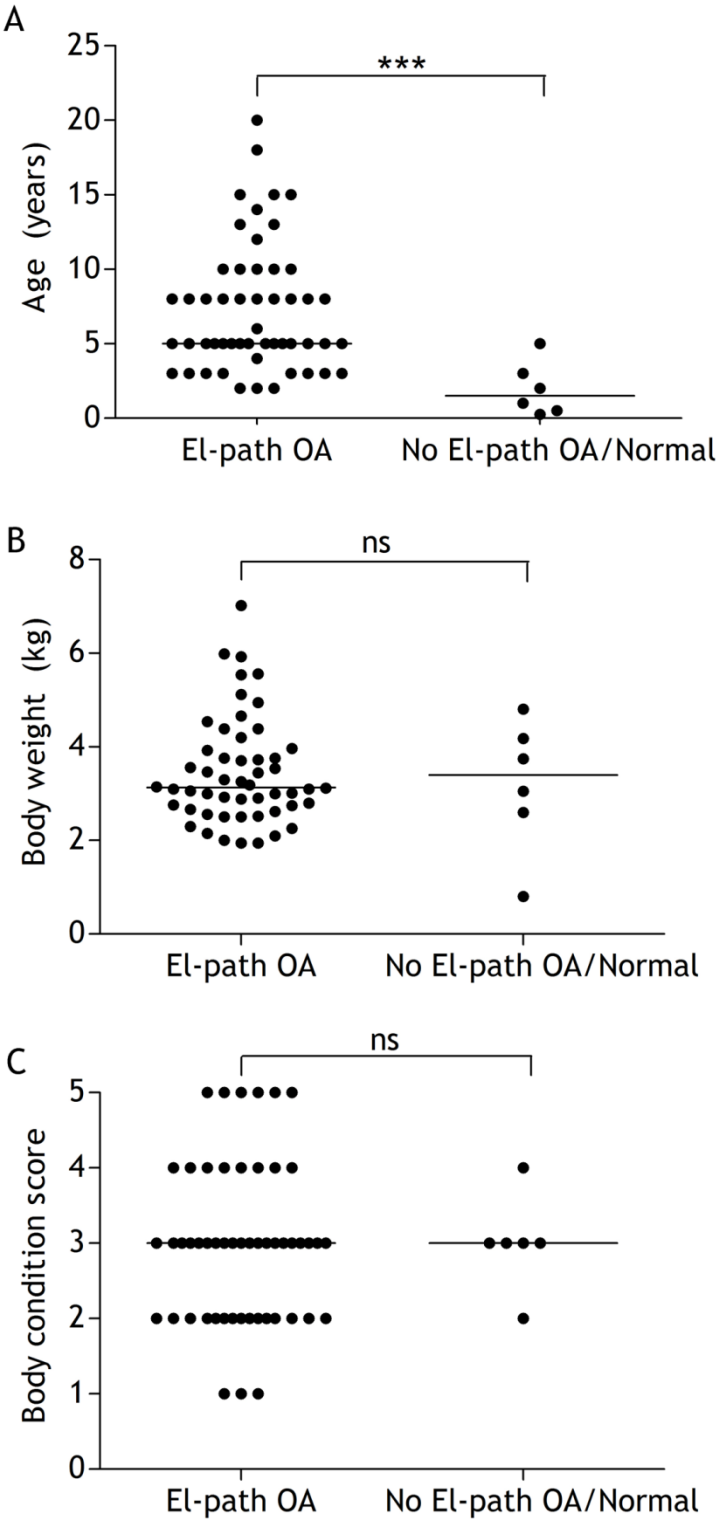

Figure 4.1: The comparative analysis of age, BW and BCS between El-path OA (*N*=52) and no El-path OA/normal (*N*=6) cats.

(A) The age difference between the OA and normal cats is significant. There is no significant difference in BW (B) and BCS (C) of cats with and without OA. Data presented as median and plotted in vertical scatter plot. (Mann Whitney *U* test, *** represents P<0.001; ns: not significant P>0.05).

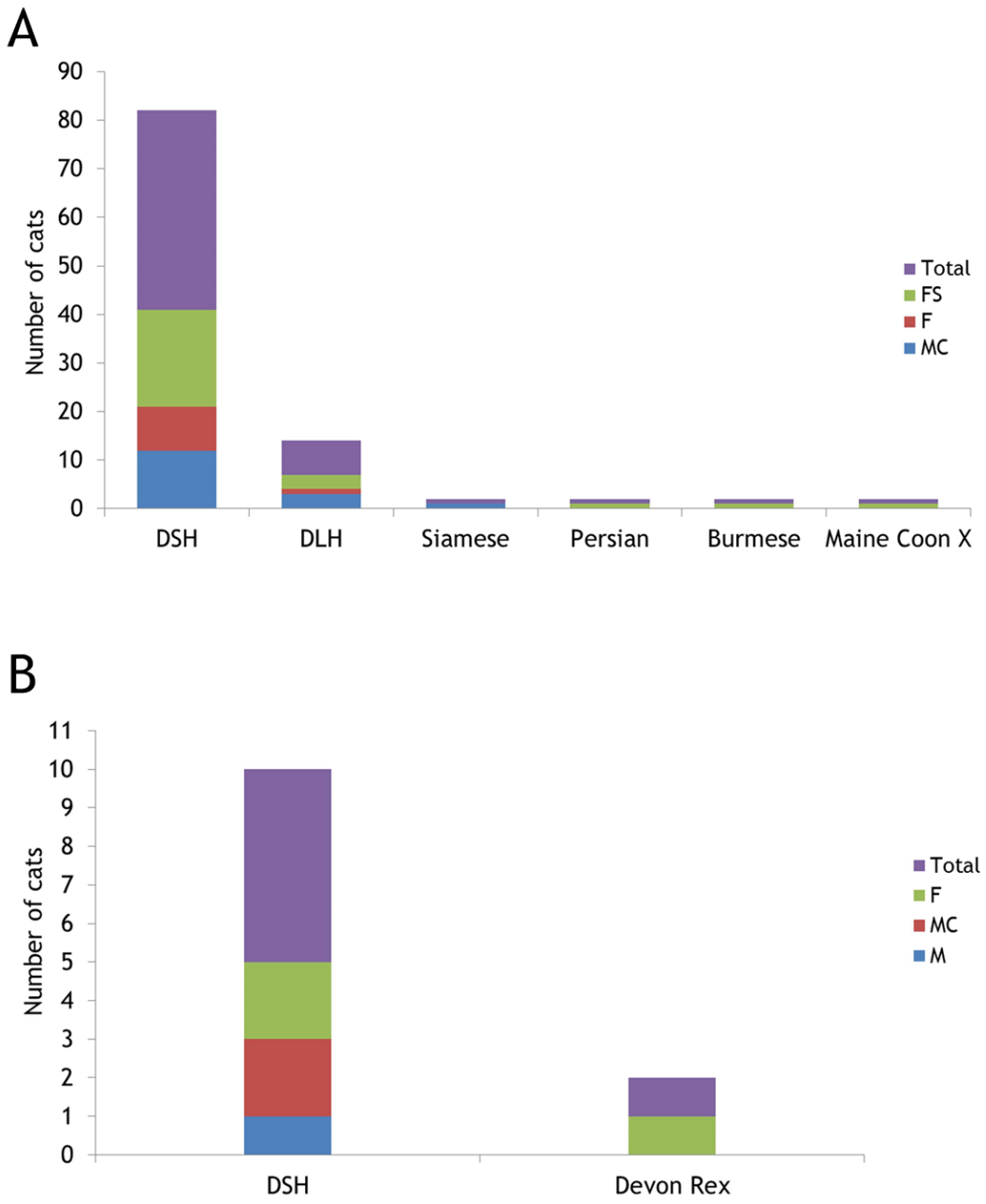

Figure 4.2: Breed and gender distribution of El-path OA (A) and no El-path OA/normal (B) cats.

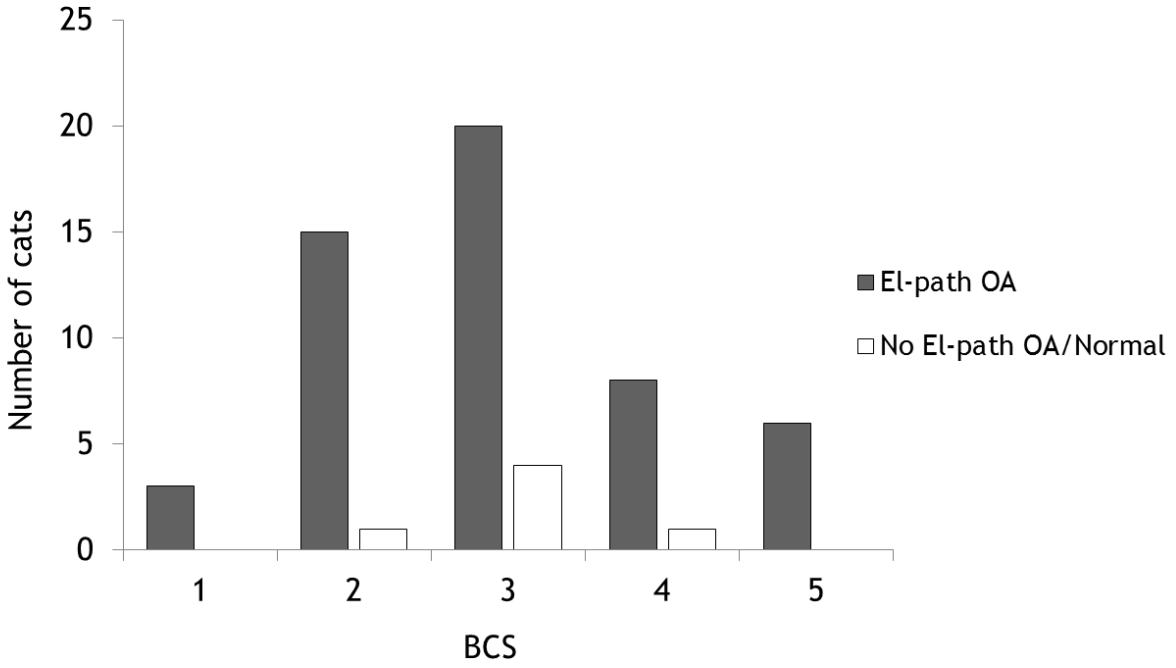

Figure 4.3: Distribution of body condition scores (BCS) of El-path OA and no El-path OA/normal cats.

4.3.3 Radiographic findings

The overall prevalence of El-rOA was 86.2% (50 of 58 cats). Of 50 cats with radiographic changes, 43 cats had bilateral and 7 had unilateral elbow involvement (4 on the left and 3 on the right) giving a total number of 93 El-rOA joints (Table 4.2). The mean total radiographic score of left and right elbow joints was 4.6 and 4.7 respectively. The median total radiographic score of left and right elbows was 3.5 and 4 respectively. The minimum score recorded for the left and right elbow joints was 1. The maximum score recorded for the left and right elbow joints was 12 and 13 respectively. The total radiographic scores were not significantly different between left and right elbow joints (P=0.61). Of 93 elbow joints, 68 were given a Global score of 1, 21 a Global score of 2 and 4 a Global score of 3 (Tables 4.3 and 4.4).

Seventy-eight (83.9%) of the 93 elbow joints had osteophytes. Thirty-one cats had bilateral and 16 cats unilateral elbow involvement. Osteophytes were seen at the distal humeral condyle (Figures 4.4.B, 4.4.C and 4.4.D) and head of radius (Figure 4.4.D). Severity was graded mild in 42/93 joints (45.1%) (20 on the left and 22 on the right), moderate in 24/93 joints (25.8%) (13 on the left and 11 on the right) and severe in 12/93 joints (12.9%) (6 left and 6 right). The mean osteophyte size in mm ± SD for mildly affected joints was 1.3 ± 0.4, for moderately affected joints was 2.8 ± 0.7 and for severely affected joints was 5.4 ± 0.7 (Table 4.5).

Extra-articular enthesiophytes were present in 9/93 joints (9.7%), bilaterally in two cats and unilaterally in five cats (2 on the left and 3 on the right). They were graded mild in 6 joints and moderate in the other 3. Enthesiophytes at the attachment of the extensor carpi radialis muscle were identified in 7 joints (Figure 4.5.A). Two joints had enthesiophytes at the attachment of the triceps brachii tendon (Figure 4.5.B).

Areas of abnormal mineralisation were present in 24/93 joints (25.8%), bilaterally in 9 cats and unilaterally in 6 cats (5 on the left and 1 on the right). In thirteen elbow joints this was graded mild, moderate in 10 and severe in one (Figure 4.6).

Eighty-six (92.5%) of the 93 elbows were scored as having an increased radio-opacity beneath the semilunar notch (Figures 4.4.D, 4.6.A-B, 4.7.B-E). The feature was not seen in 7 elbow joints (Figure 4.7.A). Thirty-nine cats had bilateral and 8 cats had unilateral changes (3 on the left and 5 on the right).

The SSB was present in 55 (59.1%) of 93 elbow joints, bilaterally in 23 cats and unilaterally in 9 cats (4 on the left and 5 on the right) (Figures 4.8.B-D). In all cases there were also osteophytes and an increased radio-opacity beneath the semilunar notch. In 34 joints the sesamoid bone was less than 3 mm in size, in 10 it was 3 mm or greater with additional mineralisation on the surface of the sesamoid bone and in 11 joints there were additional areas of mineralisation in the region of the sesamoid bone. The mean SSB size in mm ± SD for Score 1 was 1.9 ± 0.6, for Score 2 was 3.6 ± 0.7 and for Score 3 was 3.6 ± 0.5 (Table 4.6). The mean age of the cats with and without SSB were 8.1 (SD 4.5) and 5.1 (SD 3.8) respectively. The age difference was significant ($P<0.01$) (Figure 4.9).

	Radiographic findings			
	No El-rOA		El-rOA	
	Number of Joints	Percentage (%)	Number of joints	Percentage (%)
Left elbow	11	19.0	47	81.0
Right elbow	12	20.7	46	79.3
Total	23	19.8	93	80.2

Table 4.2: Showing numbers of joints with normal and abnormal radiographic findings. Total number of joints 116.

	Radiographic OA Global score			
	Score 0	Score 1	Score 2	Score 3
Left elbow	11	32	13	2
Right elbow	12	36	8	2
Total	23	68	21	4
Percentage (%)	19.8	58.6	18.1	3.4

Table 4.3: Showing the number of joints with different radiographic OA Global Scores.

Cat ID	Osteophytes		Enthesiophytes		Area of abnormal mineralisation		Supinator sesamoid bone		Increase radio-opacity		Synovial effusion		Joint space		Joint remodelling		Elbow incongruity		Total score		Global score	
	L	R	L	R	L	R	L	R	L	R	L	R	L	R	L	R	L	R	L	R	L	R
X1	2	2	0	0	0	0	0	0	1	1	0	0	0	0	0	0	0	0	3	3	1	1
X2	0	0	0	0	0	0	0	0	0	0	0	0	0	0	0	0	0	0	0	0	0	0
X3	2	3	0	0	1	1	2	1	1	1	0	0	2	0	0	0	0	0	8	6	2	1
X4	0	2	1	0	0	0	0	0	0	1	0	0	0	0	0	0	0	0	1	3	1	1
X5	0	0	0	0	0	0	0	0	0	0	0	0	0	0	0	0	0	0	0	0	0	0
X6	0	1	0	0	0	0	0	0	1	1	0	0	1	0	0	0	0	0	2	2	1	2
X7	1	0	0	0	0	0	1	0	1	0	0	0	0	0	0	0	0	0	3	0	1	0
X8	0	1	0	0	0	0	0	0	0	1	0	0	0	0	0	0	0	0	0	2	0	1
X9	2	1	0	0	0	0	0	0	0	0	0	0	0	0	0	0	0	0	2	1	1	1
X10	2	0	0	1	0	0	0	0	1	1	0	0	0	1	0	0	0	0	3	3	1	1
X11	2	0	1	0	0	0	1	1	0	1	0	0	0	0	0	0	0	0	3	5	1	1
X12	2	2	0	0	1	1	1	3	1	1	0	0	2	2	0	0	0	0	7	9	2	2
X13	0	0	0	0	0	0	0	0	0	0	0	0	0	0	0	0	0	0	0	0	0	0
X14	1	0	0	0	0	0	1	0	0	0	0	0	2	0	0	0	0	0	4	0	1	0
X15	2	0	0	0	0	0	0	1	1	1	0	0	2	2	0	0	0	0	5	4	1	1
X16	2	0	0	0	0	0	1	1	1	1	0	0	0	0	0	0	0	0	4	4	1	1
X17	1	1	0	0	0	0	0	0	1	1	0	0	0	0	0	0	0	0	2	1	1	1
X18	3	3	1	1	2	2	2	3	1	1	0	0	2	2	0	0	0	0	11	12	2	2

Table 4.4: Radiographic features and Global scores of the left (L) and right (R) elbow joints in 58 cats. Scoring: 0: normal, 1: mild, 2: moderate, 3: severe. Global score: 0: normal, 1: mild, 2: moderate, 3: severe.

Cat ID	Osteophytes		Enthesiophytes		Area of abnormal mineralisation		Supinator sesamoid bone		Increase radio-opacity		Synovial effusion		Joint space		Joint remodelling		Elbow incongruity		Total Score		Global score	
	L	R	L	R	L	R	L	R	L	R	L	R	L	R	L	R	L	R	L	R	L	R
X19	0	0	0	0	0	0	0	0	0	0	0	0	0	0	0	0	0	0	0	0	0	0
X20	0	2	0	0	0	0	3	1	1	1	0	0	0	2	0	0	0	0	4	6	1	1
X21	0	1	0	0	0	0	0	0	1	1	0	0	0	0	0	0	1	0	2	2	1	1
X22	1	0	0	0	0	0	1	1	1	1	0	0	2	0	0	0	1	0	6	2	1	1
X23	1	2	2	2	0	0	1	2	1	1	0	0	2	0	0	0	1	0	8	7	2	2
X24	1	1	0	0	0	0	0	0	1	1	0	0	2	0	0	0	1	0	5	2	1	1
X25	0	0	0	0	0	0	0	0	0	0	0	0	0	0	0	0	0	0	0	0	0	0
X26	3	2	0	0	0	0	1	1	1	1	0	0	2	2	0	0	0	0	7	6	2	1
X27	1	1	0	0	1	1	1	1	1	1	0	0	2	2	1	1	0	1	7	10	2	2
X28	2	2	0	2	2	0	1	3	1	1	0	0	2	1	0	1	0	0	9	10	2	2
X29	2	2	0	0	0	0	2	0	1	1	0	0	1	2	1	1	1	1	8	7	2	2
X30	3	3	0	0	2	1	3	3	1	1	0	0	2	2	1	1	1	1	13	12	3	3
X31	1	1	0	0	0	0	1	1	1	1	0	0	0	0	1	1	0	0	4	4	1	1
X32	1	2	0	0	1	1	3	3	1	1	0	0	2	2	0	0	0	0	8	9	2	2
X33	1	1	0	0	0	0	0	0	1	1	0	0	0	0	0	0	0	0	2	2	1	1
X34	0	0	0	0	0	0	1	1	1	1	0	0	2	2	0	0	0	0	5	4	1	1
X35	0	0	0	0	1	0	0	0	1	0	0	0	2	0	0	0	0	0	4	0	1	0
X36	1	1	0	2	0	0	0	0	1	1	0	0	0	0	0	0	0	0	2	4	1	1
X37	1	1	0	0	0	0	2	1	1	1	0	0	1	0	0	0	0	0	5	3	1	1
X38	3	3	0	0	1	0	1	1	1	1	0	0	0	0	0	0	0	0	6	5	1	1

Table 4.4 continued

Cat ID	Osteophytes		Enthesiophytes		Area of abnormal mineralisation		Supinator sesamoid bone		Increase radio-opacity		Synovial effusion		Joint space		Joint remodelling		Elbow incongruity		Total Score		Global score	
	L	R	L	R	L	R	L	R	L	R	L	R	L	R	L	R	L	R	L	R	L	R
X39	1	3	0	0	0	0	0	0	1	1	0	0	1	0	0	0	0	0	3	4	1	1
X40	3	0	0	0	2	0	0	0	1	0	0	0	2	0	0	0	0	0	8	0	2	0
X41	2	2	0	0	1	0	0	0	1	1	0	0	1	1	0	0	0	0	5	4	1	1
X42	2	2	0	0	2	2	3	3	1	1	1	1	2	2	1	1	1	0	13	12	3	3
X43	1	1	0	0	0	1	0	1	1	1	0	0	0	1	0	0	0	0	2	5	1	1
X44	0	1	0	0	0	0	0	1	0	1	0	0	0	0	0	0	1	0	1	3	1	1
X45	1	1	0	0	0	0	0	1	1	1	0	0	0	0	0	0	0	0	2	3	1	1
X46	0	0	0	0	0	0	0	0	1	1	0	0	0	2	0	0	0	0	1	2	1	1
X47	1	1	0	0	3	2	0	0	1	1	0	0	2	0	1	1	0	0	8	5	2	1
X48	0	1	0	0	0	0	0	0	0	1	0	0	0	1	0	0	0	0	0	3	0	1
X49	3	3	0	0	2	2	2	2	1	1	1	0	1	2	1	1	0	0	11	9	2	2
X50	1	1	0	0	0	0	0	1	1	1	0	0	2	0	0	0	0	0	4	3	1	1
X51	0	0	0	0	0	0	0	0	0	0	0	0	0	0	0	0	0	0	0	0	0	0
X52	0	0	0	0	0	0	0	0	0	0	0	0	0	0	0	0	0	0	0	0	0	0
X53	0	0	0	0	0	0	0	0	0	0	0	0	0	0	0	0	0	0	0	0	0	0
X54	1	1	0	0	0	0	1	1	1	1	0	1	0	0	0	0	0	0	3	4	1	1
X55	1	1	0	0	0	0	1	2	1	1	0	0	0	0	0	0	0	0	3	4	1	1
X56	2	1	0	0	0	0	3	2	1	1	0	0	2	2	0	0	0	0	8	6	2	1
X57	0	1	0	0	0	0	0	0	0	0	0	0	0	0	0	0	0	0	0	1	0	1
X58	1	1	0	0	0	0	1	1	1	1	0	0	0	0	0	0	0	0	3	3	1	1

Table 4.4 continued.

Cat ID	Left elbow		Right elbow	
	Score	Osteophyte size (mm)	Score	Osteophyte size (mm)
X1	2	2.1	2	2.4
X3	2	2.85	3	7.7
X4	0	-	2	2.3
X6	0	-	1	1.9
X7	1	1.8	0	-
X8	0	-	1	1.4
X9	2	4.4	2	2.2
X10	2	3	0	-
X11	2	2	0	-
X12	2	3.9	2	2.1
X14	1	1.2	0	-
X15	2	3.5	0	-
X16	2	2.3	0	-
X17	1	0.8	1	1.2
X18	3	5.2	3	5.1
X20	0	-	2	3.2
X21	0	-	1	0.8
X22	1	1.4	0	-
X23	1	1.8	2	2.5
X24	1	0.5	1	0.8
X26	3	5.4	2	3.5
X27	1	1.6	1	1.6
X28	2	3.5	2	3.8
X29	2	3.4	2	3
X30	3	5.2	3	5.4
X31	1	1.8	1	1.8
X32	1	0.8	2	2.5
X33	1	1.2	1	1.8
X34	0	-	0	-
X35	0	-	0	-
X36	1	1.4	1	1.5
X37	1	1.8	1	1.2
X38	3	5.2	3	5.1
X39	1	1.8	3	5.1
X40	3	5.1	0	-
X41	2	2.3	2	2.1
X42	2	2.8	2	2.3
X43	1	1.4	1	1.8
X44	0	-	1	0.8
X45	1	1.6	1	1.4
X46	0	-	0	-
X47	1	1.04	1	1.8
X48	0	-	1	1.4
X49	3	5.2	3	5.1
X50	1	1.4	1	0.8
X54	1	1.1	1	1.2
X55	1	0.5	1	0.3
X56	2	3	1	0.8
X57	0	-	1	1
X58	1	1.7	1	1.8

Table 4.5: Osteophytes when present were graded according to their size (mm) and whether a single site or multiple sites were involved.

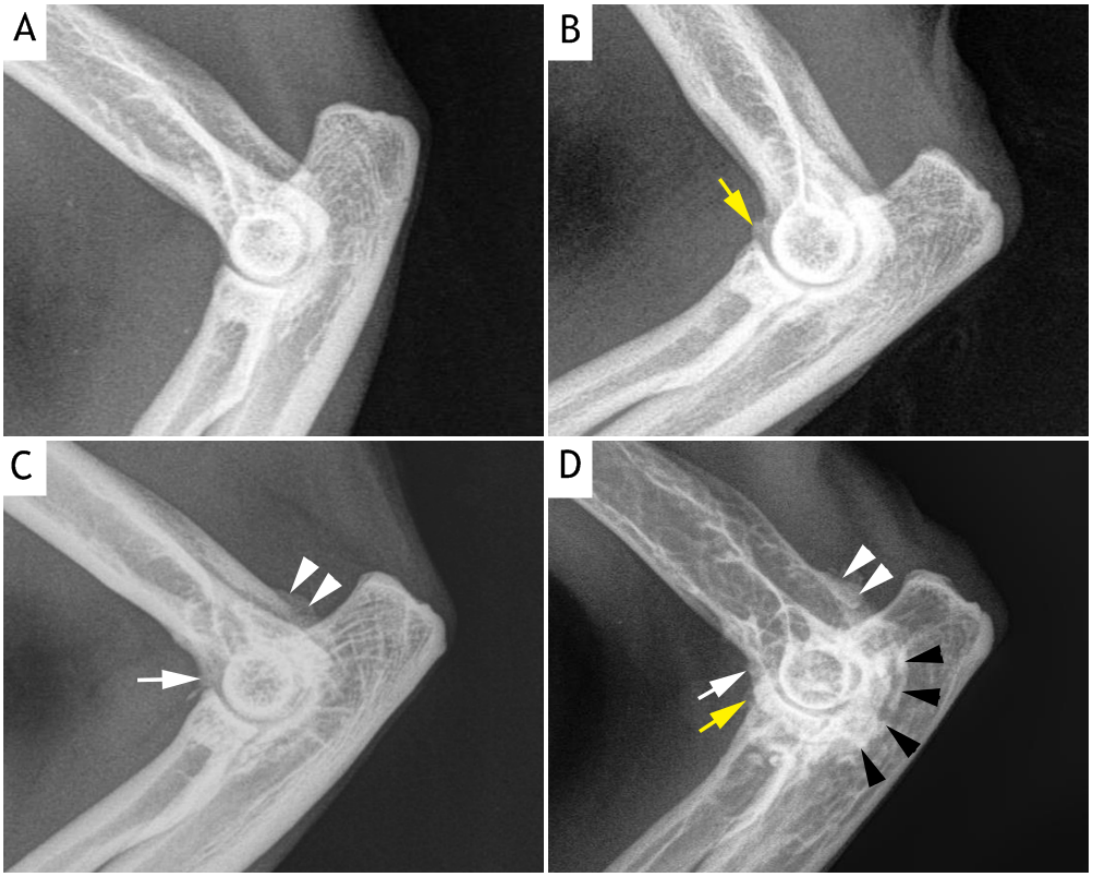

Figure 4.4: Mediolateral radiographs of the right elbow.

(A) A normal elbow joint. Cat ID: X19, left elbow. (B) An elbow joint with mild osteophyte formation on the distal humeral condyle (arrow). Cat ID: X45, left elbow. (C) An elbow joint with moderate osteophyte formation on the caudal (arrowheads) and cranial aspects of distal humeral condyle (arrow). Cat ID: X38, right elbow. (D) Large and severe osteophyte formation is seen on the caudal aspect of the distal humeral condyle (white arrowheads). A small osteophyte is present on the cranial aspect of the distal humeral condyle (white arrow) and on the radial head (yellow arrow). Increased radio-opacity beneath the semilunar notch can also be identified (black arrowheads). Cat ID: X26, left elbow.

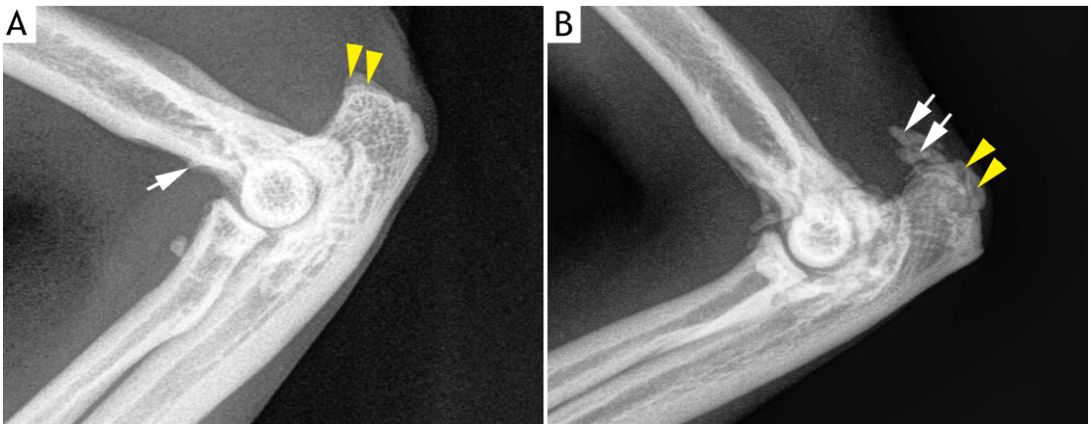

Figure 4.5: Mediolateral radiograph of elbow joints.

(A) An extra-articular enthesiophyte is identified at the extensor carpi radialis (white arrow) and triceps brachii muscle (yellow arrowheads) attachments. Cat ID: X36, right elbow. (B) Showing soft tissue mineralisation (white arrows) and new bone on the olecranon (yellow arrowheads) consistent with enthesiophyte formation at the attachment of the triceps muscle. Cat ID: X28, right elbow.

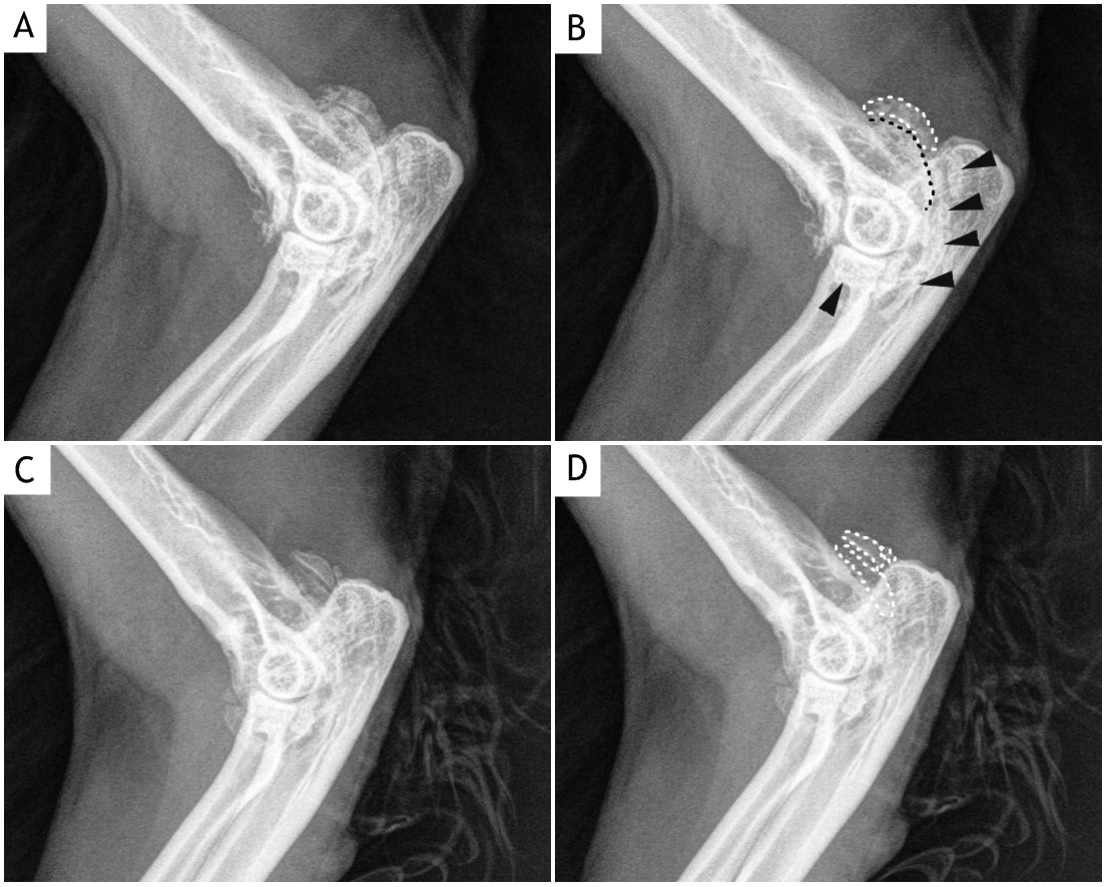

Figure 4.6: Mediolateral radiographs of left elbow joints showing examples of either abnormal mineralisation within the joint capsule or the presence of osteochondromas. Figure B and D are the same as A and C but with specific lesions highlighted.

The border of the mineralised areas highlighted by white dotted line in B and D are clearly delineated and interpreted as an osteochondroma or calcification within the joint capsule. Compare this with the area in B delineated by black dotted line where only approximately 50% of the border can be visualised; this is interpreted as an osteophyte on the caudal aspect of the humerus although it could conceivably be a mineralised body. The discrete areas of increased bone opacity highlighted in B with arrowheads might represent areas of mineralisation but are totally superimposed on the proximal ulna and radius and thus could also represent osteophytes. These ulnar lesions were scored as positive for increased bone opacity and not as abnormal mineralisation. The gross pathological examination of these joints demonstrated the presence of both soft tissue mineralisation within the joint capsule adjacent to the ulna and periarticular osteophytes along the margin of the semilunar notch. A craniocaudal view does not necessarily help to distinguish osteophytes and soft tissue mineralisation. A & B: Cat ID: X18, left elbow, C & D: Cat ID: X18, right elbow.

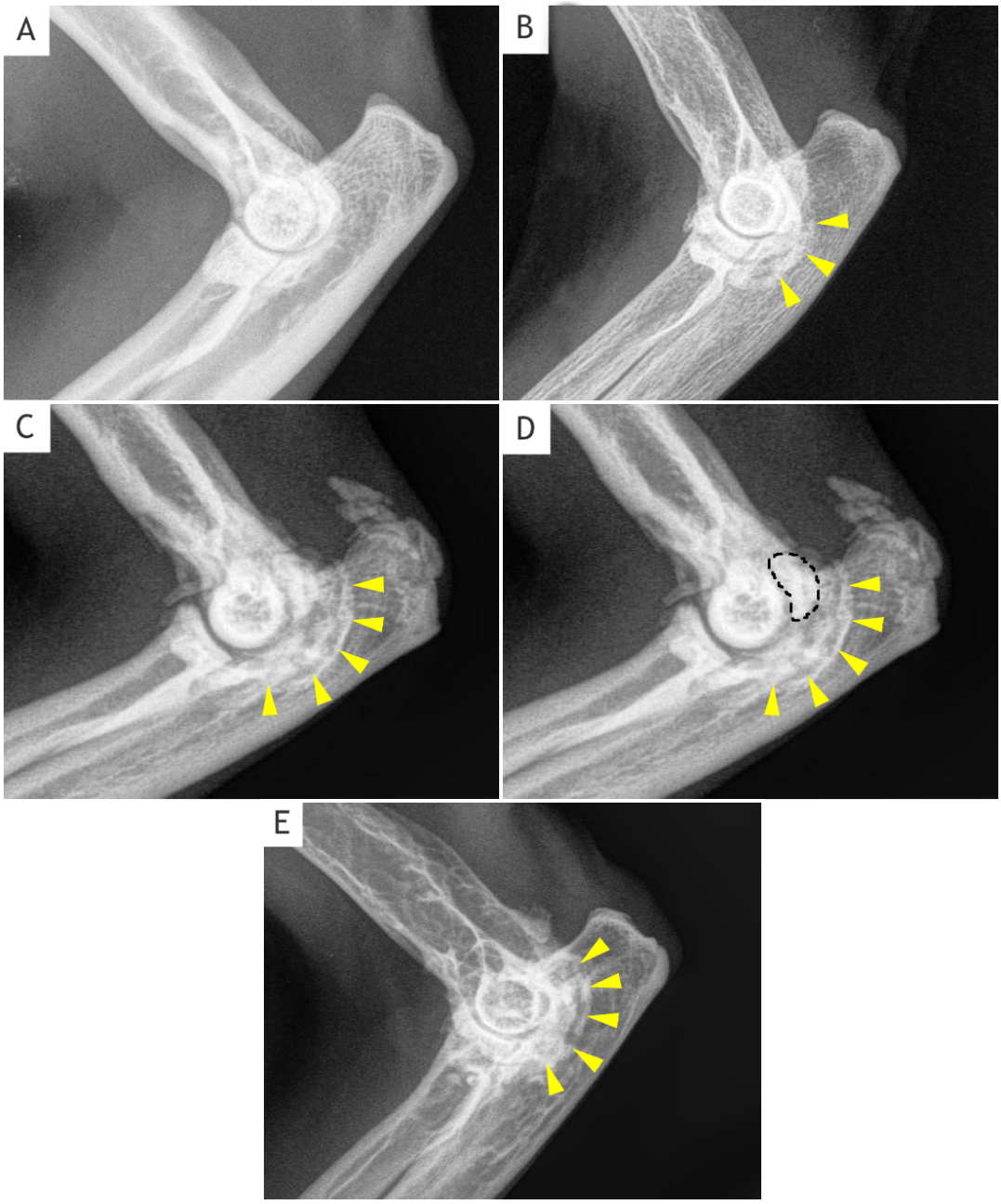

Figure 4.7: Examples of elbow radiographs with and without increased radio-opacity beneath the semilunar notch of the ulna. Figure C is the same as D with specific lesions highlighted.

(A) Normal elbow joint with normal bone opacity beneath semilunar notch. Cat ID: X19, left elbow. (B, C, D & E) Increased radio-opacity beneath the semilunar notch of the ulna is present (yellow arrowheads). (D) Delineated area may represent an osteochondroma (See Figure 4.17.B for gross pathology). B: Cat ID: X56, right elbow, C & D: Cat ID: X28, right elbow, E: Cat X26, right elbow.

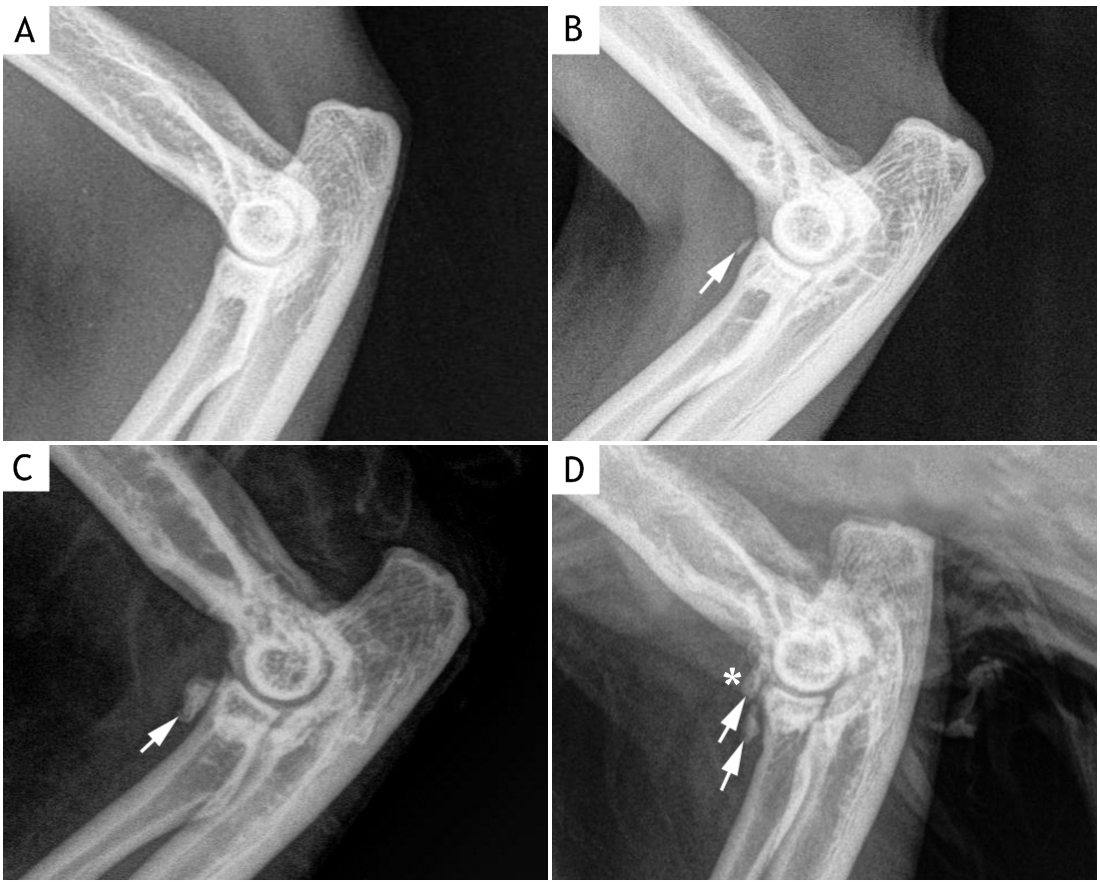

Figure 4.8: Elbow radiographs showing examples of the supinator sesamoid bone.

(A) Normal elbow joint with no supinator sesamoid bone. Cat ID: X19, left elbow. (B) Small, oval shaped supinator sesamoid bone located at the craniolateral aspect of the head of radius (arrow). Cat ID: X38, right elbow. (C) Supinator sesamoid bone is identified with additional mineralisation present on its surface (white arrow). Cat ID: X37, left elbow. (D) Two areas of mineralisation are seen in the region of the sesamoid bone (white arrows). It is difficult to know which represents the true sesamoid bone, but it was always assumed to be the body closer to the radial head (asterisk). This was confirmed at gross pathologic examination. Cat ID: X12, right elbow.

Cat ID	Left elbow		Right elbow	
	Score	SSB size (mm)	Score	SSB size (mm)
X3	2	3.2	1	2.3
X5	1	0.7	0	-
X7	1	2.6	0	-
X11	1	1.5	1	0.6
X12	1	1.5	3	3.5
X14	1	1.7	0	-
X15	0	-	1	1.1
X16	1	2.4	1	2.3
X18	2	3.5	3	3.1
X20	3	4.1	1	1.8
X22	1	1.9	1	1.3
X23	1	2.3	2	5
X26	1	2.1	1	2.2
X27	1	1.9	3	3.3
X28	1	2.6	3	4.6
X29	2	3.0	0	-
X30	3	3.9	3	4
X31	1	2.3	1	2.8
X32	3	3.1	3	3.1
X34	1	1.1	1	1.4
X37	2	3.2	1	1.2
X38	1	2.8	1	2
X42	3	3.4	3	3.6
X43	0	-	1	2.8
X44	0	-	1	0.6
X45	0	-	1	1.6
X49	2	3	2	3
X50	0	-	1	1.8
X54	1	2.3	1	2.4
X55	1	2.8	2	4.4
X56	3	3.5	2	4.6
X58	1	1.8	1	2.8

Table 4.6: A visible supinator sesamoid bone was graded according to its size (mm) and whether additional mineralisation was present either on its surface or as a discrete deposit close-by.

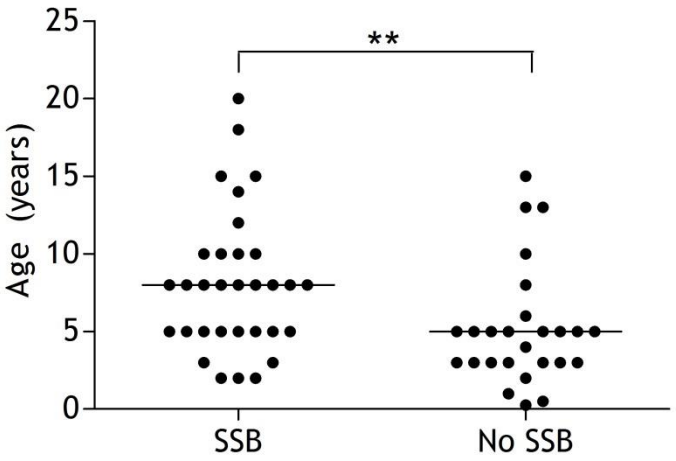

Figure 4.9: Showing age differences between cats with and without supinator sesamoid bone (SSB). Data presented as median. (Mann Whitney *U* test, represents P<0.01).**

The numbers of cases showing different combinations of increased bone opacity beneath the semilunar notch, osteophytes, discrete areas of mineralisation and supinator sesamoid bones are shown in Table 4.7 and Table 4.8.

Features	Increase radio-opacity	Osteophytes	Areas of abnormal mineralisation	Supinator sesamoid bone
Increase radio-opacity		35	13	24
Osteophytes	35		13	24
Areas of abnormal mineralisation	13	13		10
Supinator sesamoid bone	24	24	10	

Table 4.7: Showing numbers of left elbow joints with combinations of radiographic features.

Features	Increase radio-opacity	Osteophytes	Areas of abnormal mineralisation	Supinator sesamoid bone
Increase radio-opacity		34	10	21
Osteophytes	34		10	23
Areas of abnormal mineralisation	10	10		9
Supinator sesamoid bone	21	23	9	

Table 4.8: Showing numbers of right elbow joints with combinations of radiographic features.

Synovial effusion was identified in 4/93 joints (4.3%), bilaterally in one cat and unilaterally in two cats (1 on the left and 1 on the right) (Figures 4.10.A-B).

Of 93 elbow joints, 15 (16.1%) had remodelling, bilaterally in seven cats and unilaterally in one cat (on the right). Joint remodelling was defined as a change in anatomical shape and a widening of the distal humeral condyle (Figures 4.10.A-B).

Changes in joint space were observed in 45 (48.4%) of 93 elbow joints; this included those joints which were thought to be incongruent. Eleven elbows had an increase in joint space (two in the humero-ulnar, three in the humero-radial and six in both humero-ulnar and humero-radial joints) and 34 had a decrease in the humero-ulnar joint space particularly the caudal part (Figure 4.10.A).

Joint incongruity were observed in 9/93 (9.7%) joints, bilaterally in two cats and unilaterally in five cats (4 on the left side and 1 on the right) (Table 4.9). Of 9 incongruent elbow joints, 1 had an increase in joint space (Figure 4.11.C), 5 had a decrease in the joint space and 3 had both (Figure 4.11.B).

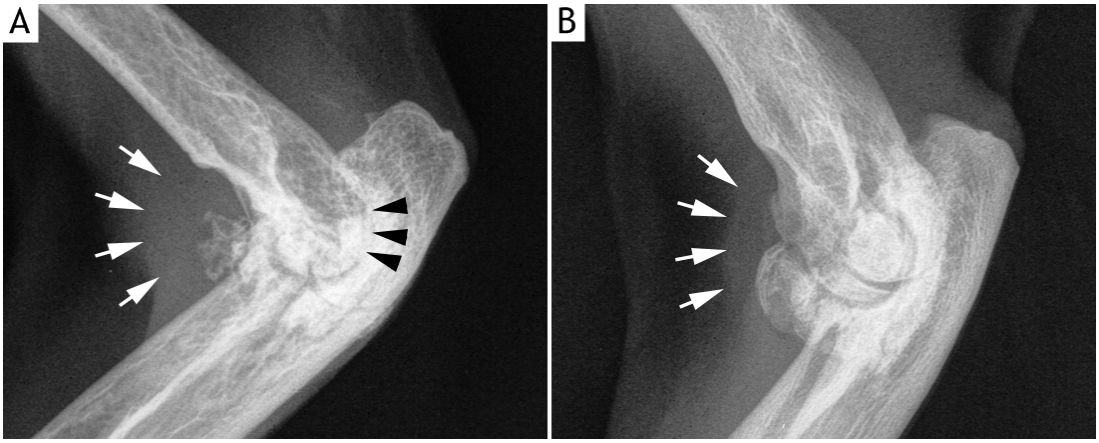

Figure 4.10: Mediolateral radiographs of the right elbow with severe OA.

(A) A change in anatomical shape of the distal humeral condyle is observed. There is a decrease in the humero-ulnar joint space particularly the caudal part (arrowheads) and joint effusion and/or soft tissue thickening is present (white arrows). Cat ID: X42, left elbow. (B) Joint remodelling with enlargement of the distal humeral condyle is present. Soft tissue thickening and/or synovial effusion is also present (white arrows). Cat ID: X30, left elbow.

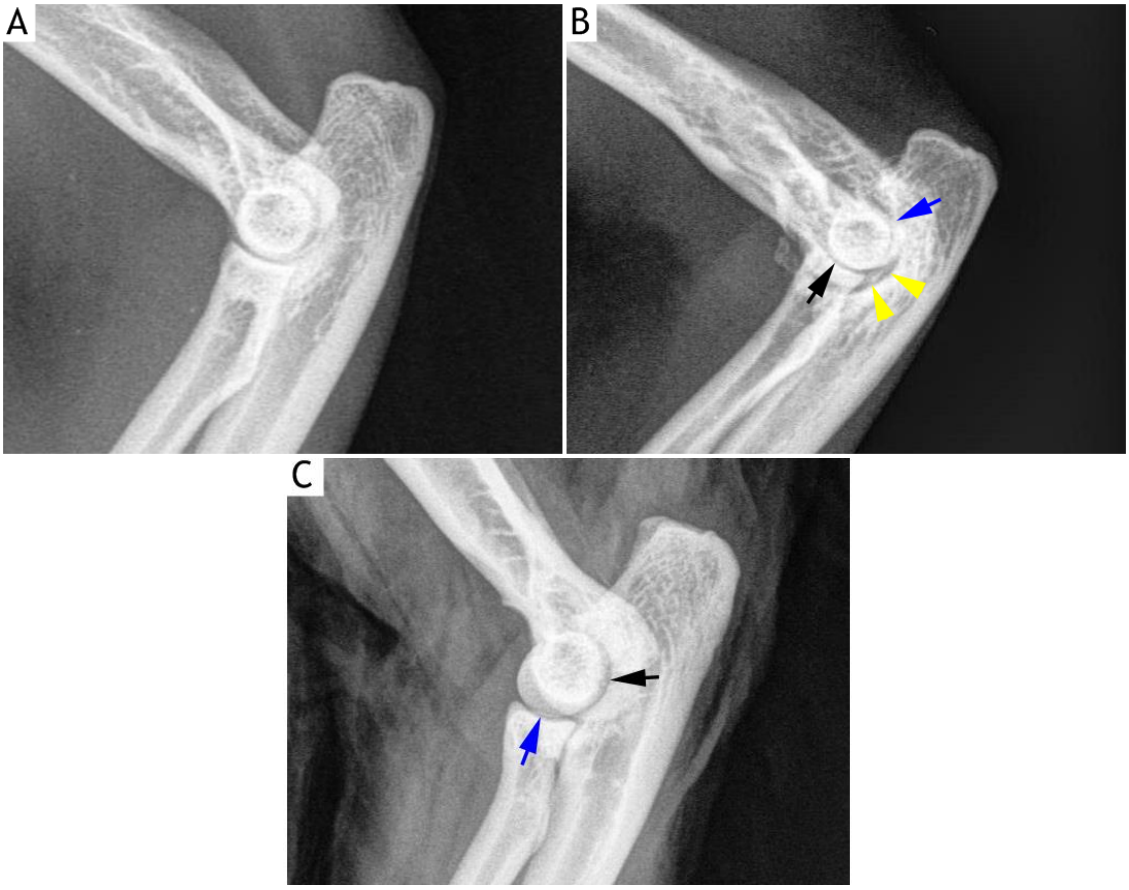

Figure 4.11: Showing congruent and incongruent elbow joints.

(A) Elbow radiograph showing a normal and congruent articulation. Cat ID: X19, left elbow. (B) A severely incongruent joint due to a relative "overgrowth" of the radial head (Type 1). There is a decrease in the joint space at the humero-radial (black arrow) and caudal humero-ulnar (blue arrow) articulations and an increase of the humero-ulnar joint space at its cranial aspect (yellow arrowheads). (Cat ID: X28, left elbow). (C) Incongruent joint resulting from possible "undergrowth" of the radial head (Type 2). There is an increase of the humeroradial joint space (blue arrow) and possibly the humeroulnar joint space (black arrow). (Cat ID: X21, left elbow).

Type of elbow incongruity	Left elbow	Right elbow
Incongruency Type 1 (characterised by a relative "overgrowth" of the radial head)	2	0
Incongruency Type 2 (characterised by a relative "undergrowth" of the radial head)	4	3
Incongruency Type 3 (characterised by an elliptical shape of the semilunar notch)	0	0
Congruent joint	52	55
Total	58	58

Table 4.9: Showing numbers of elbow joints with and without radiographically identifiable incongruity.

4.3.4 Gross pathologic findings

Gross pathologic examinations were performed on 116 joints from 58 cats. Six cats (10.3%) had grossly normal articular cartilage on both left and right humeral condyle, radius and ulna. Two cats (3.4%) had unilateral grossly normal articular cartilage (1 on the left and 1 on the right side), thus giving a total of 14 no El-path OA/normal joints (Global score 0) (Table 4.10). Cartilage abnormalities were identified in 102 (El-path OA) of 116 (87.9%) elbow joints. Fifty-two cats (89.7%) had cartilage lesions, bilaterally in 50 cats and unilaterally in 2 cats (1 on the left and 1 on the right) (Table 4.10). Of 102 El-path OA joints, 58 were given a Global score of 1, 27 were given a Global score of 2 and 17 a Global score of 3 (Table 4.11). The possible total gross pathologic score was 42; the highest score recorded was 40 (Table 4.12). The median gross pathologic total scores for left and right El-path OA joints was 9 and 8 respectively. The total gross pathologic feature scores were not significantly different between left and right elbow joints (P=0.84).

Of 102 El-path OA joints, 99 (97.0%) had cartilage changes on the humeral condyle, radius and ulna, and 3 (3.0%) had cartilage changes on the humeral condyle only. Changes were always seen throughout the joint i.e. there were no cases of just medial compartment disease.

Normal humeral condyle, radius and ulna had a white, smooth and glistening articular surface (Figure 4.12.A). Ninety-seven El-path OA joints (95.1%) had cartilage discolouration, characterised by a dull yellow surface (Figures 4.12.C-D). Cartilage fibrillation was identified in all El-path OA joints. It was scored as mild in 50 joints, moderate in 34 joints and severe in 18 joints. Mild cartilage fibrillation was seen as a focal roughening of the articular surface (Figure 4.12.B), while in the moderate to severely affected joints, diffuse cartilage roughness was always identified. Cartilage erosion was identified in 55/102 (53.9%) elbow joints, it was mild in 31 joints, moderate in 18 joints and severe in 6 joints (Figure 4.12.D). Forty-one (40.2%) elbow joints had cartilage ulceration. Cartilage ulceration with marked “wear-lines” was commonly seen particularly at the medial humeral condyle and the semilunar notch of the ulna (Figures 4.12.C and 4.13.A-B).

Total articular cartilage damage score on the medial part of the humeral condyle was significantly greater (P<0.001) than on the lateral side in both left and right elbow joints (Figures 4.14.A-B). The median score for medial and lateral parts of the humeral condyle was 3 (SD 2.5) and 1.5 (SD 1.6) respectively. All elbows with radiographic

osteophytes, increased radio-opacity beneath the semilunar notch and decreased humero-ulnar joint had cartilage changes.

Of 102 El-path OA joints, 93 (91.1%) had osteophyte formation. In 45 elbow joints osteophyte development was mild, in 31 it was moderate and in 19 elbow joints it was severe. Osteophytes were commonly seen at the medial edge and caudal aspect of the humeral condyle (Figures 4.12.B-D, 4.18.A), on the proximal edge of the anconeal process and around the semilunar notch (Figures 4.13.A-B).

All elbow joints (55) with the presence of a radiographically apparent SSB had gross pathology of the articular cartilage. Of these 55 elbow joints, 53 had gross cartilage changes and osteophytes (Figure 4.15); two had gross cartilage changes only. However, forty-seven joints without a radiographically evident sesamoid bone did have gross cartilage pathology. The cartilage damage scores were significantly higher in left elbow joints with a radiographically visible supinator sesamoid bone than in left elbow joints without a radiographically supinator sesamoid bone ($P<0.001$) (Figure 4.16.A). A similar finding was also observed in the right elbow ($P<0.001$) (Figure 4.16.B).

Areas of mineralisation within the joint capsule appeared as firm plaques embedded within the joint capsule and in some cases an exposed surface was “articulating” with areas of the joint surface (Figures 4.13.B and 4.18). A total of 25 osteochondromas (Figure 4.17) were found in 12 elbow joints (bilateral in two cats and unilateral in 8 cats). The osteochondromas were white oval shaped bodies seen protruding into the articular cavity and all were attached to the synovium. Fragmentation (fracture) of the medial coronoid process was not seen in any of the 102 joints.

Thickening of the joint capsule and discolouration of the synovium were observed in 41/102 (40.2%) and 55/102 (53.9%) elbow joints respectively (Figures 4.13.A and 4.18.B). Joint remodelling was identified in 19/102 (18.6%) elbow joints which also had severe osteophytosis (Figure 4.18). Remodelling was apparent radiographically in 15 of these elbow joints (Figure 4.10).

Radioulnar incongruity whereby the radial head is elevated above the level of the ulnar coronoid was seen in the 2 elbow joints where it was apparent on the radiograph (Figure 4.11.B). This was interpreted as a relative “overgrowth” of the radial head (Type 1 incongruity) (Figures 4.19.B and 4.19.C). It was not possible to identify a Type 2 incongruity (“undergrowth” of the radial head) on gross pathologic examination even in those cats where it was identified on the radiograph (Figure 4.11.C).

	Gross pathologic findings			
	No El-path OA		El-path OA	
	Number of Joints	Percentage (%)	Number of joints	Percentage (%)
Left elbow	7	12.1	51	87.9
Right elbow	7	12.1	51	87.9
Total	14	12.1	102	87.9

Table 4.10: Showing numbers of elbow joints with normal and abnormal gross pathologic findings. Total number of joints 116.

	Gross pathologic OA Global scores			
	Score 0	Score 1	Score 2	Score 3
Left elbow	7	28	14	9
Right elbow	7	30	13	8
Total	14	58	27	17

Table 4.11: Showing the number of elbow joints with different gross pathologic OA Global Scores.

Cat ID	Cartilage surface discolouration		Cartilage fibrillation		Cartilage erosion		Cartilage ulceration		Osteophytes		Joint remodelling		Thickening of joint capsule		Synovium discolouration		Total score		Global Score		Sample for histopathologic examination
	L	R	L	R	L	R	L	R	L	R	L	R	L	R	L	R	L	R	L	R	
X1	2	2	4	2	1	0	0	0	2	0	0	0	0	0	0	0	9	4	1	1	CBS-R, §
X2	0	0	0	0	0	0	0	0	0	0	0	0	0	0	0	0	0	0	0	0	CBS-L&R, §
X3	3	3	7	7	5	6	4	4	3	3	0	0	0	0	0	1	22	24	3	3	CBS-L,OST,§
X4	3	3	5	4	2	3	1	2	2	2	0	0	0	0	0	1	13	15	2	2	CBS-R, §
X5	1	0	2	0	0	0	0	0	0	0	0	0	0	0	0	0	3	0	1	0	§
X6	1	2	2	2	0	0	0	0	0	1	0	0	0	0	0	0	3	5	1	1	CBS-L, §
X7	3	2	3	2	0	0	0	0	2	0	0	0	0	0	0	0	8	4	1	1	CBS-R, §
X8	0	0	0	2	0	0	0	0	0	1	0	0	0	0	0	0	0	3	0	1	CBS-L, §
X9	2	2	2	2	2	2	0	0	2	1	0	0	0	0	0	0	8	7	1	1	§
X10	3	3	5	4	2	1	0	0	1	2	0	0	0	0	0	0	11	10	2	1	CBS-L, §
X11	2	2	2	2	0	0	0	0	1	1	0	0	0	0	0	0	5	5	1	1	§
X12	3	3	5	4	3	3	1	1	2	2	0	1	1	1	1	1	16	16	2	2	CBS-L&R, §
X13	0	0	0	0	0	0	0	0	0	0	0	0	0	0	0	0	0	0	0	0	CBS-L&R, §
X14	2	2	2	2	0	0	0	0	0	0	0	0	0	0	0	0	4	4	1	1	§
X15	3	2	2	2	1	1	0	0	1	2	0	0	0	0	1	1	8	8	1	1	§
X16	3	3	5	6	2	4	1	2	2	3	0	1	0	1	1	1	14	21	2	3	CBS-L&R, §
X17	1	1	2	2	0	0	0	0	1	1	0	0	0	0	0	0	4	4	1	1	CBS-R, §
X18	3	3	5	5	5	4	2	2	3	3	0	0	1	1	1	1	20	19	2	2	CBS-L,OST,§
X19	0	0	0	0	0	0	0	0	0	0	0	0	0	0	0	0	0	0	0	0	CBS-L, §

Table 4.12: Gross pathologic features and Global scores of the left (L) and right (R) elbow joints in 58 cats. Scoring for cartilage changes represents the total cartilage damage score arrived at by summing the individual scores (medial part of humeral condyle, lateral part humeral condyle and the radius/ulna). Global score: 0: normal, 1: mild, 2: moderate, 3: severe. Sample selected for histopathologic examination: CBS-L: Cartilage Bone Synovium-Left; CBS-R: Cartilage Bone Synovium-Right; CBS-L&R: Cartilage Bone Synovium-Left and right; OST: Osteochondromas; §: Tendon of origin of supinator muscle.

Cat ID	Cartilage surface discolouration		Cartilage fibrillation		Cartilage erosion		Cartilage ulceration		osteophytes		Joint remodelling		Thickening of joint capsule		Synovium discolouration		Total score		Global Score		Sample for histopathologic examination
	L	R	L	R	L	R	L	R	L	R	L	R	L	R	L	R	L	R	L	R	
X20	2	2	2	2	0	0	0	0	2	2	1	1	0	0	0	0	7	7	1	1	CBS-R, §
X21	0	0	2	2	0	0	0	0	1	1	0	0	0	0	0	0	3	3	1	1	§
X22	3	3	4	4	1	0	0	0	1	1	0	0	0	0	1	1	10	10	1	1	§
X23	3	3	5	4	1	1	0	0	1	1	0	0	1	1	1	1	12	11	2	2	CBS-L,OST, §
X24	2	2	2	2	0	0	0	0	1	1	0	0	0	0	1	0	6	5	1	1	CBS-R, §
X25	1	1	1	1	0	0	0	0	0	0	0	0	0	0	0	0	2	2	1	1	§
X26	3	3	7	7	4	4	4	4	2	2	1	1	1	1	1	1	23	23	3	3	CBS-L,OST, §
X27	3	3	7	7	6	5	3	2	3	3	0	0	1	1	1	1	24	22	3	3	CBS-R, §
X28	3	3	4	5	2	3	0	0	1	3	0	0	0	1	1	1	11	16	2	2	CBS-L, OST, §
X29	3	3	4	4	2	2	1	0	2	3	0	0	1	1	1	3	14	16	3	2	CBS-L, OST, §
X30	3	3	7	7	4	5	3	4	3	3	1	1	1	1	2	2	24	26	3	3	CBS-L, OST, §
X31	2	2	2	2	0	1	1	0	1	1	0	0	0	1	0	1	6	9	1	1	§
X32	3	3	6	5	4	4	1	1	2	2	0	0	1	1	1	1	18	17	2	2	CBS-R, §
X33	1	2	2	2	0	0	0	0	1	1	0	0	0	0	0	0	4	5	1	1	CBS-L, §
X34	3	2	3	2	0	0	1	0	1	1	0	0	0	0	1	1	9	6	1	1	, §
X35	2	2	2	2	0	0	0	0	1	1	0	0	0	0	0	0	5	5	1	1	§
X36	3	3	3	4	1	2	1	1	2	2	0	0	0	1	1	1	11	14	2	2	CBS-R, OST, §
X37	3	3	5	7	3	4	3	3	2	3	0	1	1	1	1	1	18	23	2	3	CBS-R, OST, §
X38	3	3	4	4	2	1	1	1	2	2	0	0	0	0	0	0	12	11	2	2	CBS-R, §

Table 4.12 continued.

Cat ID	Cartilage surface discolouration		Cartilage fibrillation		Cartilage erosion		Cartilage ulceration		Osteophytes		Joint remodelling		Thickening of joint capsule		Synovium discolouration		Total score		Global Score		Sample for histopathologic examination
	L	R	L	R	L	R	L	R	L	R	L	R	L	R	L	R	L	R	L	R	§
X39	3	3	4	3	1	1	1	1	2	2	0	0	0	0	0	1	11	10	2	1	CBS-R,OST, §
X40	3	3	2	2	0	0	0	0	2	1	0	0	1	1	0	0	9	6	1	1	CBS-L, §
X41	3	2	2	2	1	0	0	0	2	2	0	0	1	1	1	1	10	8	1	1	§
X42	3	3	9	9	9	9	0	9	3	3	3	3	2	2	2	2	40	40	3	3	CBS-L&R,OST,§
X43	3	3	2	3	0	0	0	1	1	1	0	0	0	0	1	1	7	9	1	1	§
X44	3	3	3	2	1	0	0	0	1	1	0	0	0	0	0	0	7	5	1	1	CBS-R, §
X45	2	1	2	1	0	0	0	0	1	1	0	0	0	1	0	1	6	7	1	1	§
X46	2	3	2	2	0	0	0	0	1	1	0	0	0	1	1	0	6	7	1	1	CBS-L, §
X47	3	3	6	6	4	3	3	2	3	3	2	1	2	2	1	2	24	22	3	3	CBS-L,OST, §
X48	2	2	2	2	0	0	0	0	1	1	0	0	1	0	1	0	7	5	1	1	§
X49	3	3	5	5	2	2	1	1	2	2	1	1	2	1	1	1	17	16	2	2	CBS-R,OST, §
X50	3	2	3	2	2	2	0	0	1	1	0	0	0	0	1	0	10	7	1	1	CBS-R, §
X51	0	0	0	0	0	0	0	0	0	0	0	0	0	0	0	0	0	0	0	0	CBS-L&R, §
X52	0	0	0	0	0	0	0	0	0	0	0	0	0	0	0	0	0	0	0	0	CBS-L&R, §
X53	0	0	0	0	0	0	0	0	0	0	0	0	0	0	0	0	0	0	0	0	CBS-R, §
X54	3	3	8	9	3	3	2	2	2	3	1	1	1	1	2	2	22	25	3	3	CBS-L, §
X55	3	3	6	6	2	1	0	1	2	1	0	0	1	2	2	2	16	16	2	2	CBS-L, §

Table 4.12 continued.

Cat ID	Cartilage surface discolouration		Cartilage fibrillation		Cartilage erosion		Cartilage ulceration		Osteophytes		Joint remodelling		Thickening of joint capsule		Synovium discolouration		Total score		Global Score		Sample for histopathologic examination
	L	R	L	R	L	R	L	R	L	R	L	R	L	R	L	R	L	R	L	R	§
X56	3	3	9	9	4	4	2	2	3	3	2	2	2	2	2	2	27	27	3	3	CBS-L&R, §
X57	1	1	1	3	0	0	0	0	1	1	0	0	0	0	0	0	3	7	1	1	CBS-R, §
X58	3	3	5	5	1	0	0	0	1	1	0	0	0	0	0	0	10	9	1	1	§

Table 4.12 continued.

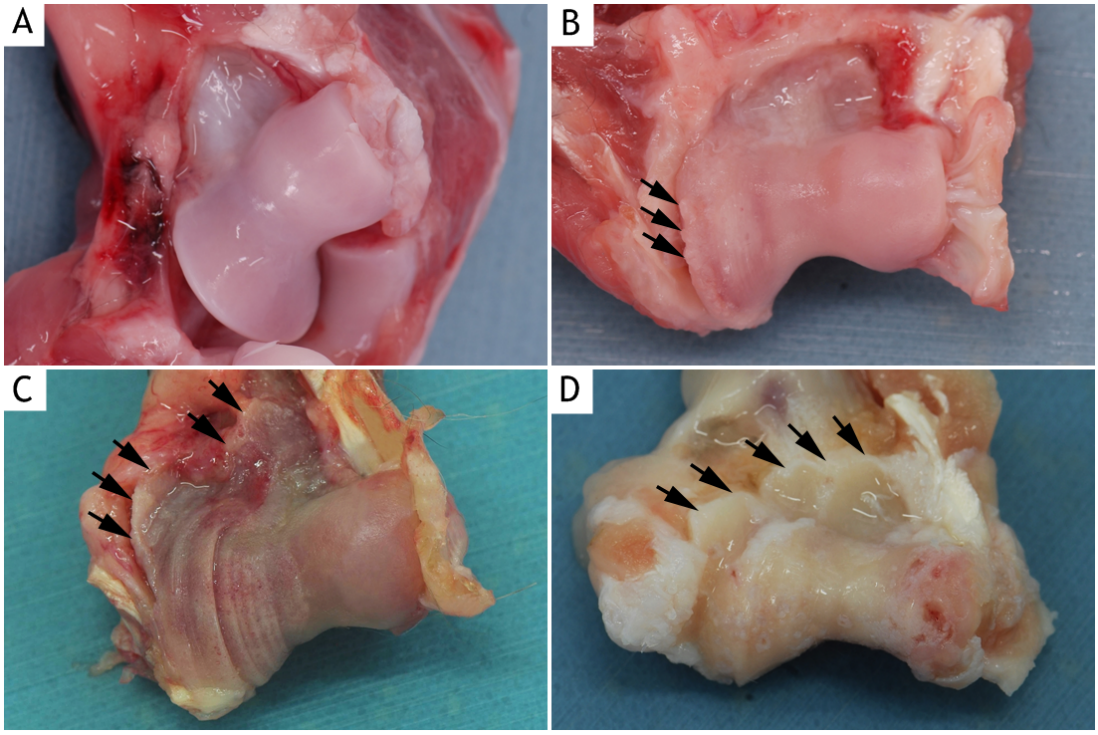

Figure 4.12: Examples of pathological changes of the distal humerus of the elbow joint.

(A) Normal distal humerus. Note the shiny and smooth appearance of the articular cartilage. Cat ID: X19, left elbow. (B) Mild fibrillation with roughening of the articular cartilage of the medial humeral condyle. Osteophytes can be identified at the joint margin (black arrows) (see Figure 4.4.B for radiograph). Cat ID: X45, left elbow. (C) Severe articular changes with marked ridges and grooves mainly on the medial side ("wear lines") although changes on the lateral side are also evident. Large osteophytes are also seen (black arrows) (See Figure 4.4.D for radiograph). Cat ID: X26, left elbow. (D) Marked cartilage erosion and ulceration with osteophytes at the joint margin (arrows) (See Figure 4.10.A for radiograph). Cat ID: X42, left elbow.

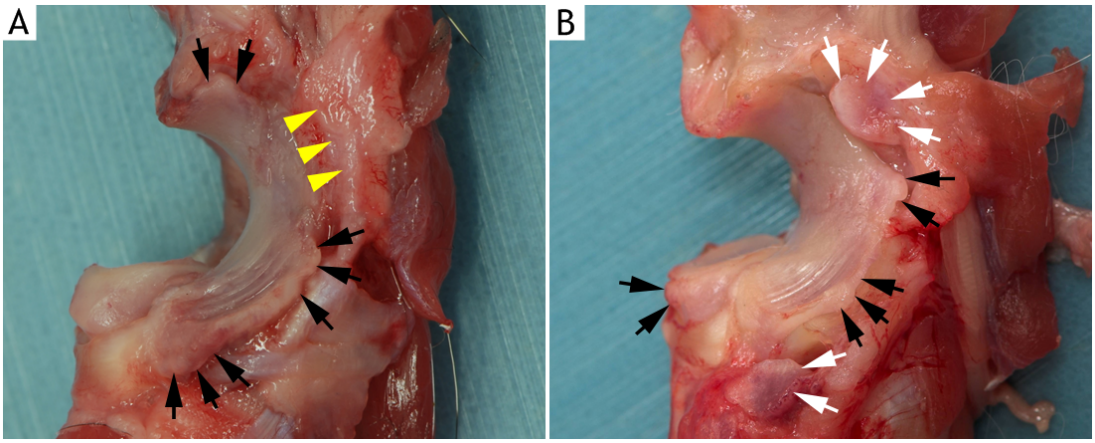

Figure 4.13: Examples of pathological changes of the right radius and ulna.

(A) Cartilage fibrillation, erosion and ulceration with prominent ridges and grooves ("wear lines") are seen on the semilunar notch of the ulna. Osteophyte formation is present on the proximal edge of the anconeal process and at the medial and distal edges of the semilunar notch (black arrows) (See Figure 4.5.A for radiograph). There is thickening of the joint capsule and synovium (yellow arrows). Cat ID: X36, right elbow. (B) Cartilage changes can be seen similar to (A). Osteophyte formation is identified on the cranial surface of the radial head and medial edge of the semilunar notch (black arrows) (See Figure 4.7.E for radiograph). Thickening of the joint capsule with calcified plaques (white arrows) adjacent to the semilunar notch is seen. Cat ID: X26, right elbow.

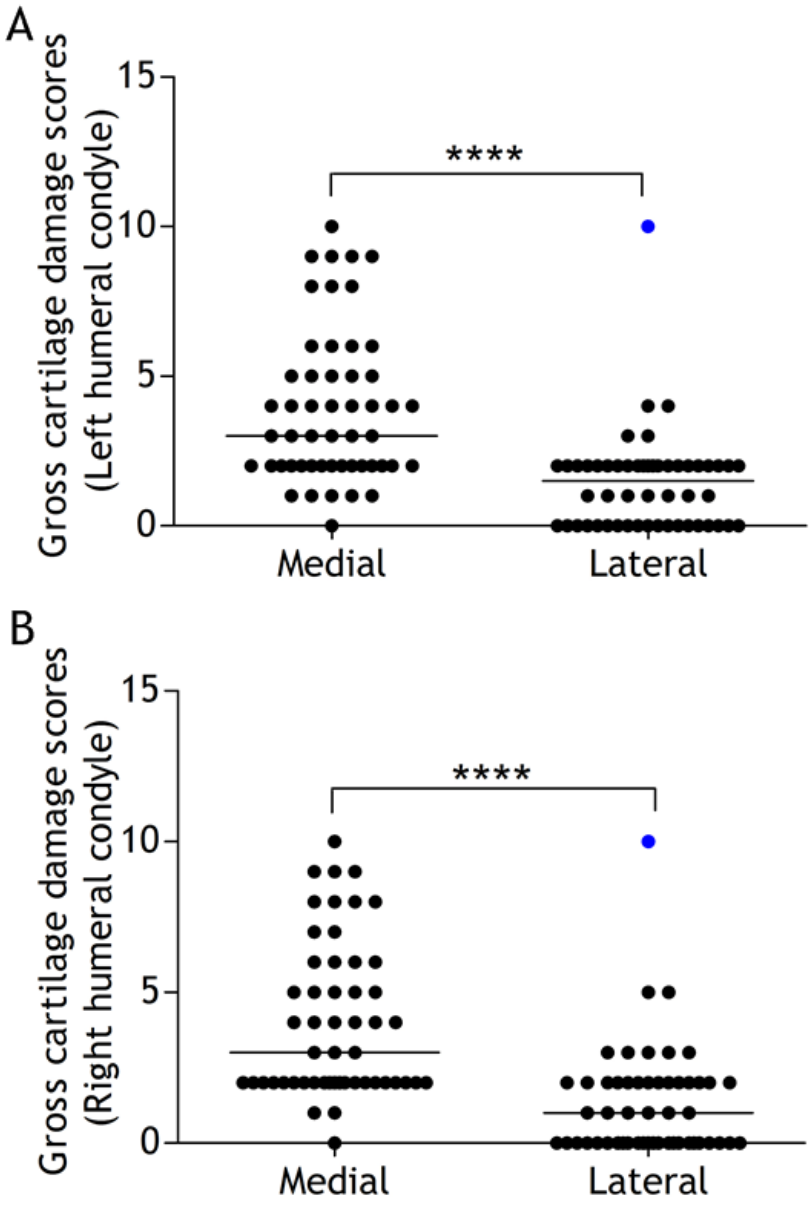

Figure 4.14: The gross cartilage damage scores were significantly different between the medial and lateral parts of the humeral condyle of the left (A) and right (B) elbow joints. Data presented as median. (Wilcoxon signed rank test, ** represents P<0.001). Outliers are represented as blue-coloured dots in the vertical scatter graph.**

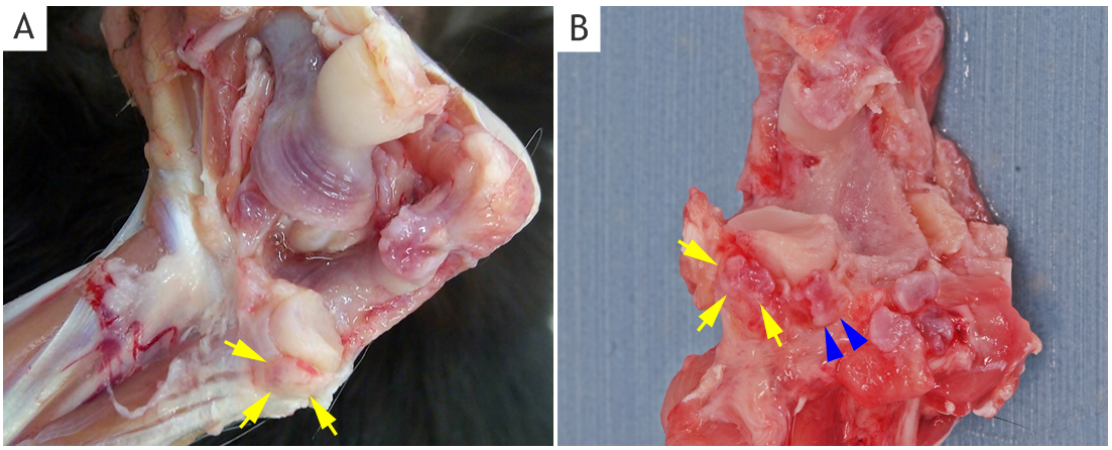

Figure 4.15: Elbow joints showing the supinator sesamoid bone.

(A & B) The supinator sesamoid bone is an ovoid nodular structure, embedded on the deep aspect of the tendon of origin of the supinator muscle (yellow arrows). It articulates with the craniolateral aspect of the head of the radius. Note an additional mineralisation in the region of the sesamoid bone (blue arrowheads) (see Figure 4.8.D for radiograph). Cartilage changes particularly on the medial part of the humeral condyle and the semilunar notch and osteophyte formation are also seen. A: Cat ID: X37, left elbow, B: Cat ID: X12, right elbow.

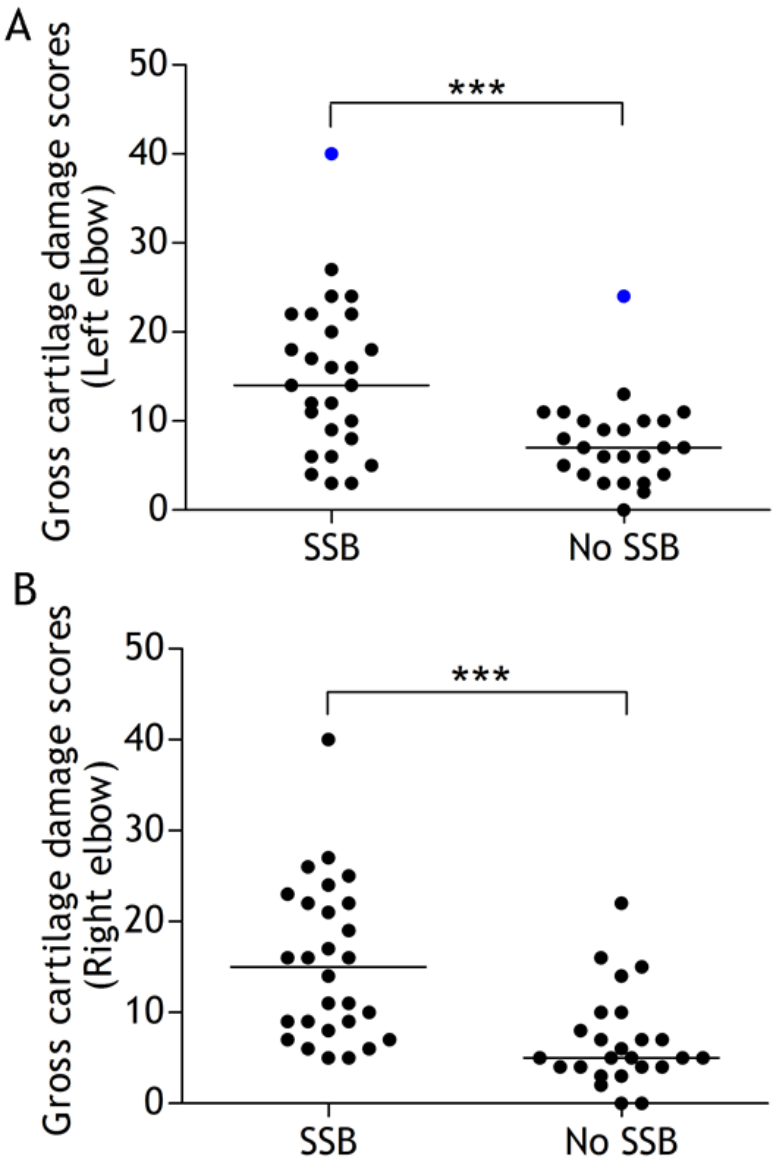

Figure 4.16: Comparison of the gross cartilage damage scores of left (A) and right (B) elbow joints with and without a radiographically evident supinator sesamoid bone (SSB). The gross cartilage damage scores were significantly higher in elbow joints with a visible supinator sesamoid bone than in the elbow joints without. Data presented as median. (Mann Whitney *U* test, * represents P<0.001). Outliers are represented as blue-coloured dots in the vertical scatter graph.**

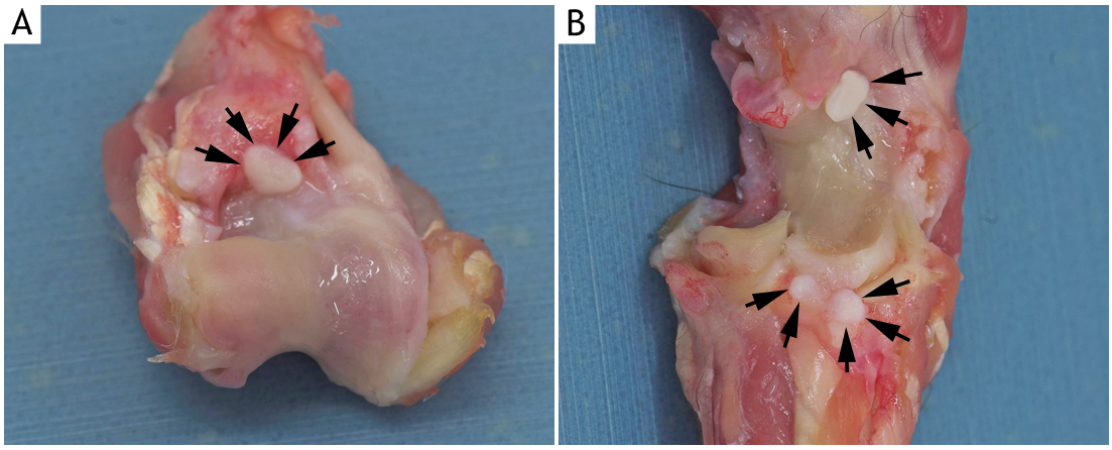

Figure 4.17: Osteochondromas are seen on the surface of the synovium to which they are attached (black arrows) (A & B). In some cases they may detach from the synovium and lie free within the joint cavity forming a "joint mouse". No cases of a totally free ossicle were seen in this study. A & B: Cat ID: X28, right elbow, see Figures 4.7.C-D for radiographs.

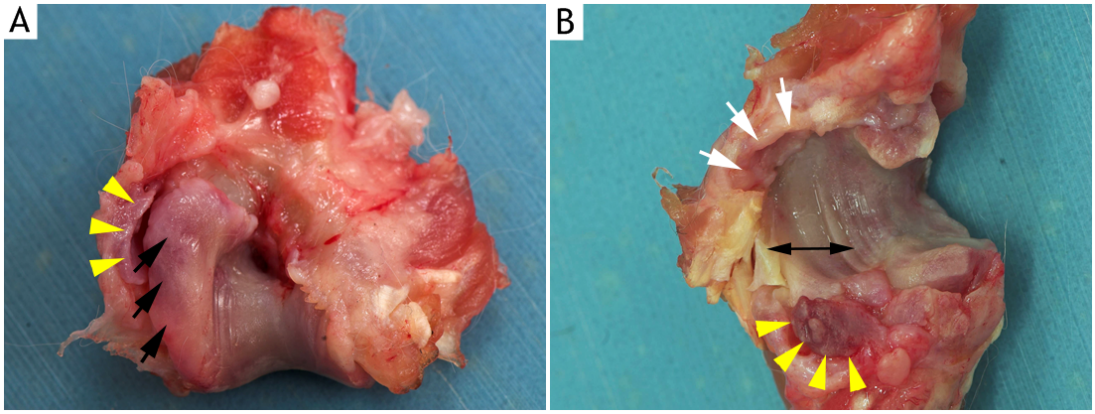

Figure 4.18: Caudal aspect of the distal humerus (A), and radius and ulna (B).

(A) Joint remodelling and severe osteophyte formation (black arrows) at the caudal aspect of the left humeral condyle. There is also a calcified plaque within the joint capsule adjacent to the osteophytes (yellow arrows); its exposed surface is 'articulating' with the medial ridge of the humeral condyle (extensively covered with osteophytes). The medial and lateral part of the humeral condyle has considerably increased in size (see Figures 4.6.A and 4.6.B for radiographs). Cat ID: X18, left elbow. (B) Advanced remodelling of the semilunar notch with a significantly increased articular surface (↔) on the medial side which corresponded to an increased size of the medial part of the humeral condyle (see Figure 4.10.B for radiograph). There is also a calcified plaque with an irregular surface in the region of the supinator sesamoid bone (yellow arrows). Thickening of the joint capsule is obvious (white arrows). Cat ID: X30, left elbow.

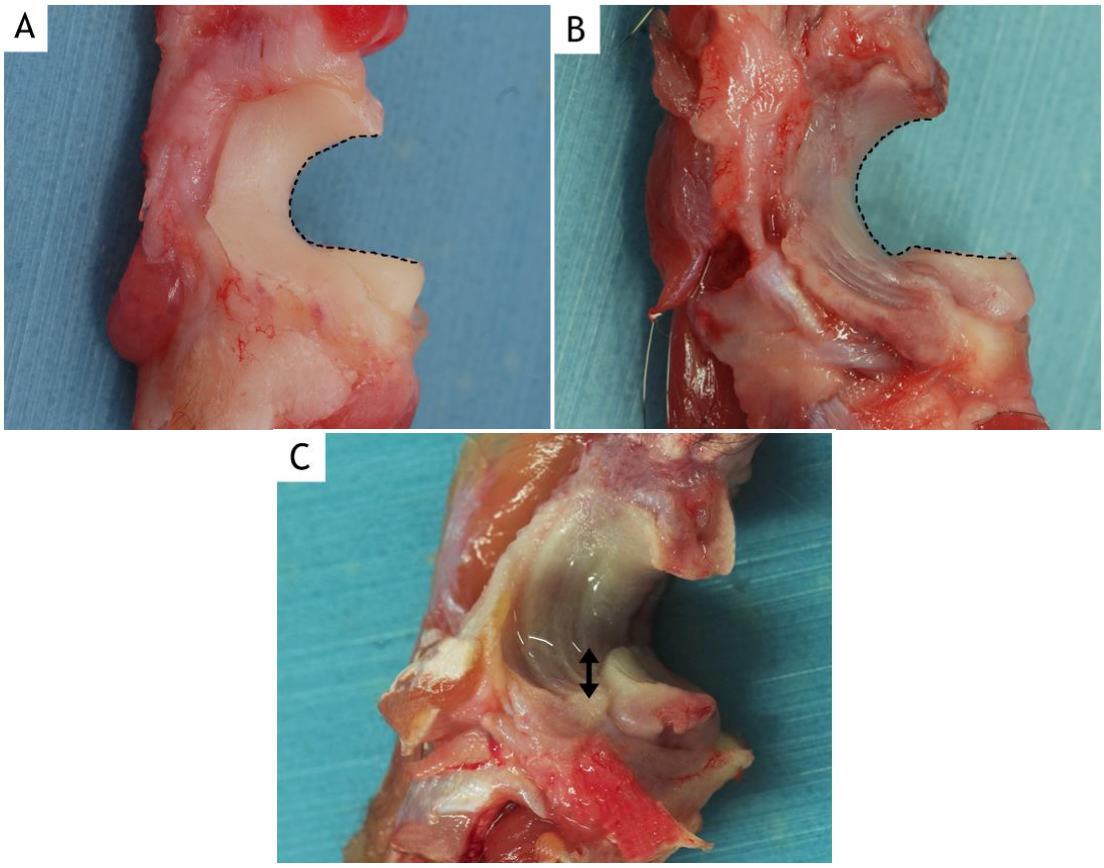

Figure 4.19: Type I incongruity -relative "overgrowth" of the radial head.

(A) The congruent articulation of the semilunar notch of the ulna and radial head is clearly delineated in this normal joint. Cat ID: X19, left elbow. (B) The dotted line indicates an incongruent articulation between the semilunar notch of the ulna and the radial head. The step between the radial head and the coronoid process of the ulna is seen. Cat ID: X37, left elbow. (C) The double arrow indicates the step between the radius and ulna. The incongruity is due to a relative "overgrowth" of the radial head (See Figure 4.11.B for radiograph). Cat ID: X28, left elbow.

4.3.5 Inter- and Intra- observer variability and sensitivity of radiographic assessment of increased radio-opacity beneath the semilunar notch

Of 100 elbow joints selected for this study 83 (83.0%) had marginal osteophytes on the surface of the bone, and/or areas of mineralised joint capsule superimposed on the articular bone and /or osteochondromas at gross pathologic examination, all of which could be expected to produce an increase in radio-opacity beneath the ulnar notch. Seventeen elbow joints (17.0%) were free of any gross abnormalities which could cause an increased radio-opacity. Depending on the degree of experience of the observer in assessing feline radiographs the number of elbow joints with increased radio-opacity beneath the semilunar notch varied between 46 and 91 (Table 4.13).

	Observers				Presence of gross pathology
	1	2	3	4	
Total number of elbow joints scored positive	68	46	86	91	83
Total number of elbow joints scored negative	32	54	14	9	17

Table 4.13: Results of the radiographic assessment by four different observers, compared to the gross pathology (absolute numbers).

4.3.5.1 Sensitivity and specificity

The sensitivity and specificity of the radiographic assessment for increased radio-opacity beneath the semilunar notch compared to the gross pathologic examination ranged between 52.0% to 99.0% and 47% to 71% respectively (Table 4.14).

Assessment of Increased radio-opacity	Observers			
	1	2	3	4
Sensitivity (%), (n/83)	75.0, (62/83)	52.0, (43/83)	98.0, (81/83)	99.0, (82/83)
Specificity (%), (n/17)	65.0, (11/17)	71.0, (12/17)	71.0, (12/17)	47.0, (8/17)

Table 4.14: Sensitivity and specificity of the radiographic assessment of each observer.

4.3.5.2 Inter- and intra- observer agreement of radiographic assessment

Inter-observer agreement for the radiographic assessment using two categories (presence and absence of increased radio-opacity beneath the ulnar notch) showed a "substantial" agreement of $\kappa = 0.80$ between observers 3 and 4, while the inter-

observer agreement for observers 1 and 2 was only "slight to fair" (κ = 0.11 - 0.30) (Figure 4.20.A).

The intra-observer agreement was determined to assess the repeatability and consistency of two observers (observer 3 and 4) in the radiographic interpretation. The two observers showed "almost perfect" intra-observer agreement (κ = 0.88 - 0.87) (Figure 4.20.B).

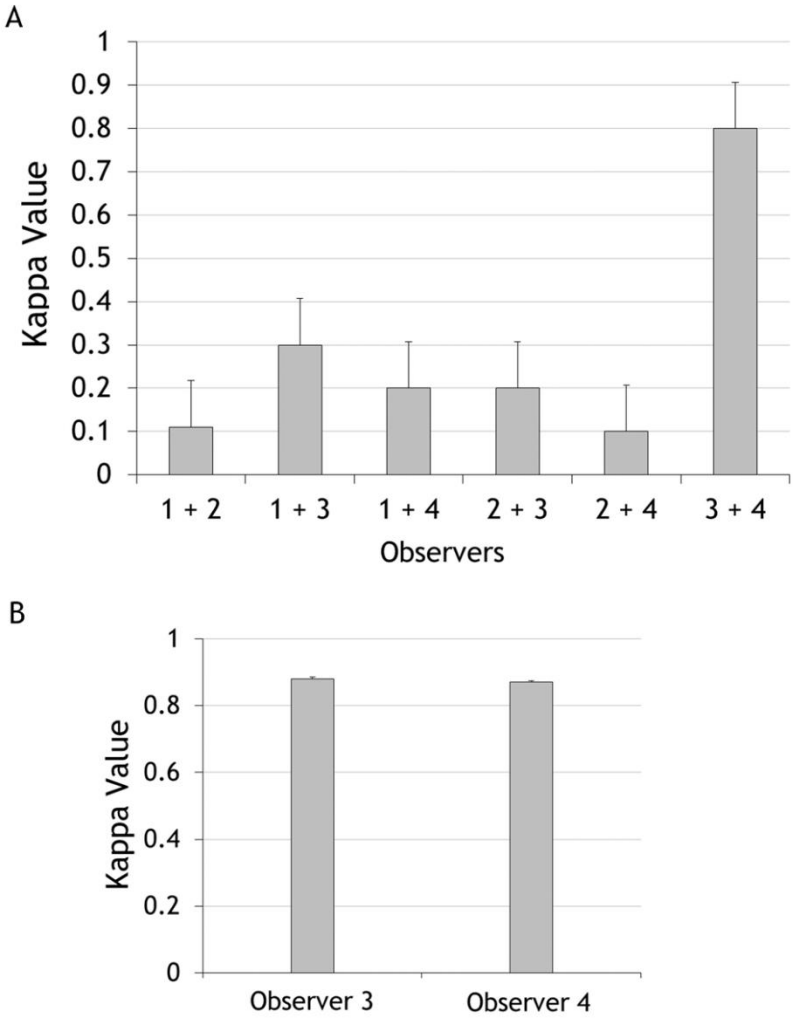

Figure 4.20: Inter-observer agreement for the increased radio-opacity beneath the semilunar notch (A). Inter-observer agreement was best between observers 3 and 4 with substantial agreement, while it was only slight to fair between the other two observers. (B) Intra-observer agreement for the increased radio-opacity beneath the semilunar notch. Both observer 3 and 4 showed "almost perfect" intra-observer agreement.

4.3.6 Correlation studies

4.3.6.1 Correlation between total radiographic and gross pathologic OA scores

All elbow joints with radiographic changes had gross lesions. Of 23 radiographically normal joints, 9 (39.1%) had gross lesions although the pathology was usually mild. There was a significant good positive correlation between the radiographic and gross pathologic total scores in both left (r_s=0.77, P<0.0001) and right (r_s=0.79, P<0.0001) elbow joints (Figures 4.21.A and 4.21.B).

4.3.6.2 Correlation between radiographic OA total scores and age, BW and BCS

There was a significant fair positive correlation between the radiographic total score of the left (r_s=0.30, P<0.05) and right (r_s=0.34, P<0.05) elbow joints and age (Figures 4.22.A and 4.22.B). There was a slight, negative relationship between the radiographic total score of the left (r_s=-0.17, P=0.20) and right (r_s=-0.22, P=0.10) elbow joint and BW, which was not statistically significant (Figures 4.22.C and 4.22.D). A similar finding was also observed between the total radiographic score of the left (r_s=-0.22, P=0.10) and right (r_s=-0.16, P=0.22) elbow joint and BCS (Figures 4.22.E and 4.22.F).

4.3.6.3 Correlation between total gross pathologic OA scores and age, BW and BCS

Correlation analysis revealed a significant moderate positive relationship between the total gross pathologic score of the left (r_s=0.44, P<0.001) and right (r_s=0.49, P<0.001) elbow joints and age (Figures 4.23.A and 4.23.B). Correlation analysis revealed a slight negative relationship between the total gross pathologic score of the left (r_s=-0.20, P=0.14) and right (r_s=-0.25, P=0.06) elbow joints and BW (Figures 4.23.C and 4.23.D). However, the relationships were not statistically significant. A similar finding was also observed between the gross pathologic total score of the left (r_s=-0.20, P=0.15) and right (r_s=-0.18, P=0.18) elbow joints and BCS (Figures 4.23.E and 4.23.F).

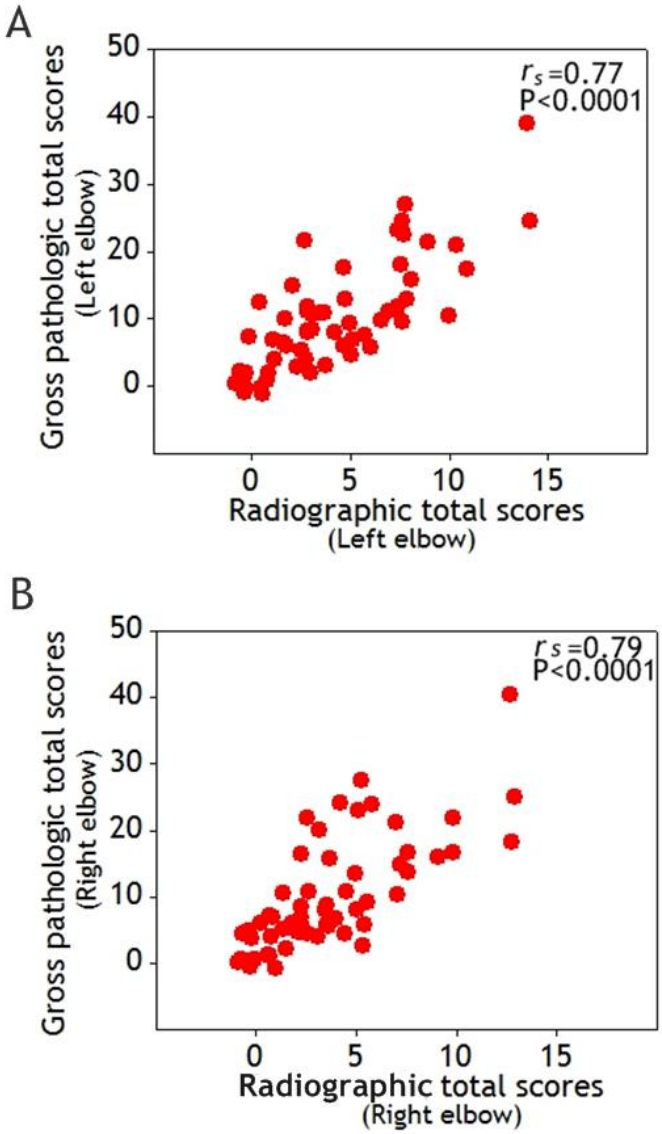

Figure 4.21: Graph demonstrating correlation between radiographic and gross pathologic OA scores in left (A) and right (B) elbow joints. There is a significant good relationship between the radiographic and gross pathologic total scores in both left and right elbow joints.

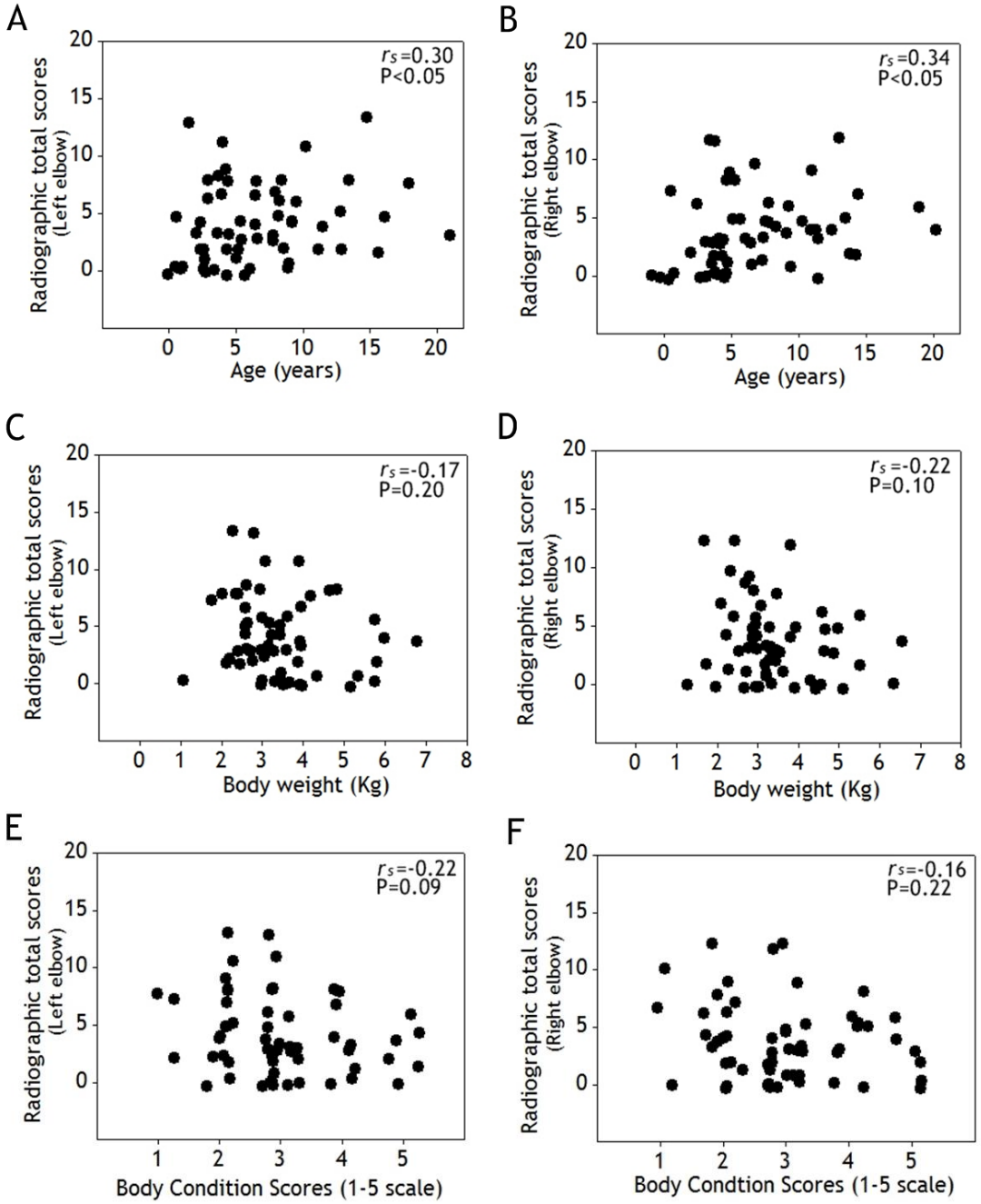

Figure 4.22: Correlation analysis of radiographic total scores of the left (A, C, and E) and right (B, D, and F) elbow joints and age, BW and BCS. (A & B) A significant fair positive relationship between radiographic total scores of the left and right elbow joints and age. (C & D) Correlation analysis of radiographic total scores of the left and right elbow joints and BW. (E & F) Correlation analysis of radiographic total scores of the left and right elbow joints and BCS. There are no significant relationships between the radiographic total scores of the left and right elbow joint and BW and BCS.

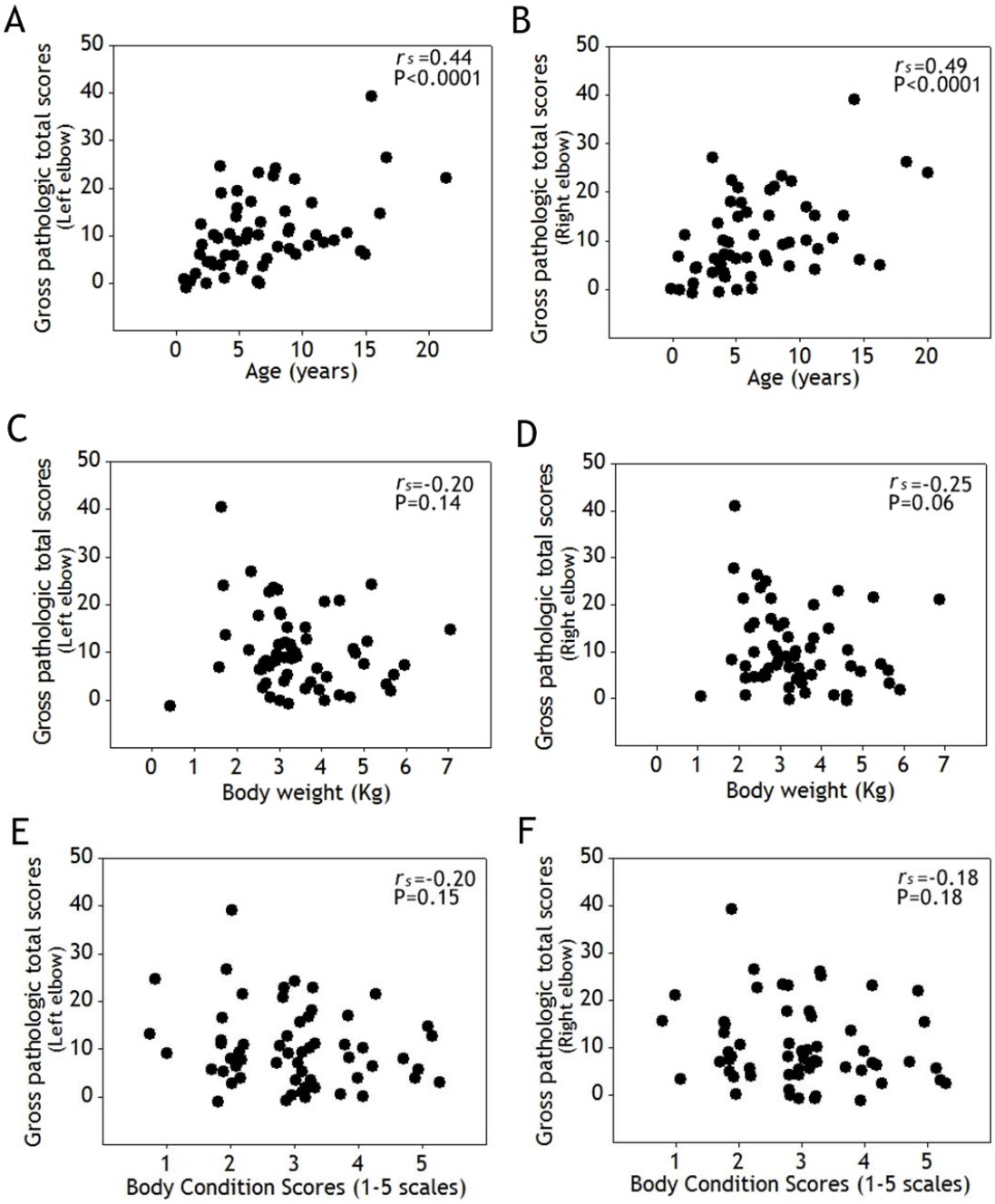

Figure 4.23: Correlation analysis of gross pathologic total scores of the left (A, C, and E) and right (B, D, and F) elbow joints and age, BW and BCS. (A & B) A significant moderate positive relationship between gross pathologic total scores of the left and right elbow joints and age. (C & D) Correlation analysis of gross pathologic total scores of the left and right elbow joints and BW. (E & F) Correlation analysis of gross pathologic total scores of the left and right elbow joints and BCS. There are no significant relationships between the gross pathologic total scores of the left and right elbow and BW and BCS.

4.4 Discussion

The overall prevalence of El-rOA and El-path OA was 86.2 % (50/58 cats) and 89.7% (52/58 cats) respectively. The high prevalence of OA may be due to the older age group seen in this population (mean age 7.3 years). The present study showed a large number of cats had elbow OA when assessed by both radiographic and gross examination. There was no remarkable difference in the radiographic and gross pathologic prevalence reflecting the ease of identifying radiographic changes which in many cases are obvious. The radiographic prevalence was much higher than that reported in previous studies where there was a range of 21.0% to 72.0% (Pacchiana et al., 2004; Clarke et al., 2005; Godfrey et al., 2005; Clarke and Bennett, 2006; Lascelles et al., 2010; Freire et al., 2011).

The main radiographic features of elbow OA were osteophytes, increased radio-opacity beneath the semilunar notch, presence of the supinator sesamoid bone, changes in the joint space and abnormal areas of mineralisation. Extra-articular enthesiophytes, synovial effusion and remodelling were less frequently seen. A combination of osteophytes, increased radio-opacity beneath the ulnar semilunar notch, the presence of the supinator sesamoid bone and abnormal soft tissue mineralisation characterised feline elbow OA.

The presence of radiographic osteophytes is regarded as a hallmark feature for diagnosing elbow OA. All the elbow joints with radiographic evident osteophytes had gross cartilage changes. However, there were 15 elbow joints with undetectable radiographic osteophytes which had cartilage changes and osteophyte formation evident on gross pathologic examination. Failure to identify osteophytes with computed radiography may be explained by the location and the size of the osteophytes. 39.1% of elbow joints which were radiographically normal had gross cartilage lesions on the humeral condyle and radius and ulna. The presence of radiographic changes thus indicates that cartilage changes are present but over a third of radiographically normal joints may have pathological changes indicating OA.

This study also demonstrated that an increased radio-opacity beneath the semilunar notch was a key radiographic feature in evaluating elbow OA. An increased radio-opacity may be caused by marginal osteophytes on the surface of the bone, areas of mineralised joint capsule superimposed on the articular bone or superimposed osteochondromas. Assessing increased radio-opacity is very subjective. The result of the inter- and intra- observer studies showed inconsistency between observers in their

ability to differentiate between elbow joints with increased radio-opacity beneath the semilunar notch and those without. Sensitivity was better between observers (observers 3 and 4) who had an interest in feline musculoskeletal disease and focussed or had considerable experience in evaluating feline radiographs. Sensitivity is thought to be more important than specificity in detecting increased radio-opacity of the trochlear notch in the diagnosis of OA secondary to medial coronoid disease in dogs (Burton et al., 2008; Draffan et al., 2009). There was substantial inter-observer agreement between observers 3 and 4, and intra-observer analysis of both observers found that the repeatability and consistency in the radiographic interpretation was almost perfect. The findings suggest that assessing increased radio-opacity beneath the semilunar notch appears to be a useful feature to assess. The results of the inter- and intra- observer study however reflects that training and experience at assessing feline radiographs are essential to reach high sensitivity, reliability and repeatability since radiographic assessment of increased radio-opacity is mainly based on subjective interpretation.

The radiographic presence of intra-articular and periarticular mineralisation is common in feline OA (Godfrey, 2011). It can sometimes be difficult to distinguish between areas of mineralisation and osteophytes. In this study, areas of mineralisation including osteochondromas were only diagnosed if more than 80% of the border of the mineralised area could be seen and at least part of the mineralised area was free from superimposition on the bones of the joint. Otherwise the changes were described as an increased radio-opacity.

Changes in the joint space were mostly observed in the humero-ulnar joint. A decrease in the joint space usually indicates articular cartilage loss and is usually associated with advanced stages of OA. It is difficult to accurately assess joint space without using weight bearing radiographs and these are seldom possible in veterinary patients because of health and safety issues.

Osteochondromas were found in 12 elbow joints. In all cases they were attached to the synovium. Many theories of osteochondroma pathogenesis in OA have been proposed. The development of osteochondromas is thought to depend on the metaplastic transformation of synovial cells into chondrocytes (Jeffreys, 1967; Allan, 2000). These chondrocytes form cartilaginous nodules which can become ossified. Resnick (1996) suggested that the pathogenesis of osteochondroma in OA may involve destruction of the articular cartilage, leading to the development of osteocartilagenous bodies. They can be completely free within the articular cavity (von Lindern et al., 2002), free but

embedded within the surface of the synovium or actually attached to the synovium (Bennett et al., 2012a). There is further discussion on these structures in Chapter 8.

A number of elbow joints (55/116) in this study had a radiographically detectable SSB. Clarke et al. (2005) retrospectively reported the present of SSB in 7/189 elbow joints, which all seven also had radiographic OA. In the present study, all joints with radiographic detactable SSB had gross cartilage changes. In 47 joints with no radiographically visible SSB, gross cartilage changes were also present. Those cats where the SSB was radiographically visible were older than those without and the joints tended to have more severe changes in the articular cartilage. It appears that the radiographic presence of a SSB is associated with the presence of articular cartilage damage and is an indicator of elbow OA. In an anatomical study by Wood et al. (1995) 40.0% of cats had a radiographically present SSB in the elbow joint. However, this study did not include an investigation of the articular cartilage. There is further discussion on SSB in Chapter 8.

In the present study, there was no gross presence of a SSB in those joints where it was not radiographically apparent. It appears that the SSB develops when the cat ages or has OA. It is reasonable to believe that when the joint becomes arthritic, the bone becomes a focus of new bone deposition and thus the SSB is more likely to be radiographically visible. One study suggested that a sesamoid bone will form in response to excessive mechanical friction occurring in a tendon (Meyer et al., 1964). In contrast, other studies regard the sesamoid bone as a vestigial structure and consider it to be a phylogenetical remnant of a primitive supplementary bone (Le Minor, 1987). Wood et al. (1995) suggested that the ossification of the supinator sesamoid bone in the cat takes place at the site where maximal stress occurs repeatedly. When it is present, this sesamoid bone helps in maintaining movement of the humeroradial articulation during flexion, extension, supination and pronation. Further studies could be done on serial radiography over time to look at the development of SSB.

Gross pathologic studies of the articular cartilage demonstrated significant degenerative changes which predominantly involved the medial compartment of the joint. Severe articular changes with marked ridges and grooves (“wear lines”) were found mainly on the medial side although changes on the lateral side were also evident. This finding supports previous studies reported by Freire et al., 2011, Bennett et al., 2012a; Ariffin et al., 2012; Ryan et al., 2013 and Freire et al., 2014. The more advanced pathology in the medial compartment of the joint probably reflects an increased load bearing of this part of the joint. Boczek-Funcke et al. (2000) reported on forelimb movements during

target reaching and food taking in cats. They found that the elbow moved more towards the medial side than did the paw, due to a marked outward rotation of the humerus. It is thus reasonable to assume that the elbow joint load is more on the medial side during active movements.

A good correlation between total radiographic scores and gross pathologic total scores was found in both left and right elbow joints indicating that high radiographic scores correlated with high gross pathologic scores. Freire et al. (2011) also found that the India ink retention score which represents cartilage damage was significantly correlated with the radiographic score of the elbow joint. A fair to moderate positive correlation was observed between the radiographic and gross pathologic total scores and age in both left and right elbow joints. Other studies have also reported a positive relationship between the presence of radiographic OA and age in the cat (Hardie et al., 2002; Clarke et al., 2005; Godfrey, 2005; Lascelles et al., 2010).

Elbow incongruity is well recognised in the dog (Wind, 1986; Samoy et al., 2006) and can be identified radiographically. The incongruities observed in this study are similar to those reported in the dog although were not commonly seen (only 9 out of 116 elbow joints; 2 and 7 elbow joints had a relative "overgrowth" (Type 1) and "undergrowth" (Type 2) of the radial head respectively). However, the Type 2 incongruity was not confirmed at the gross pathologic examination and these could be a radiographic artefact. Evaluation of elbow joint congruity is influenced by joint positioning and is best assessed on the flexed 90 degrees mediolateral radiographic view with the x-ray beam centred on the joint (Murphy et al., 1998). Only the Type 1 incongruity was confirmed as a possible cause of elbow OA.

Streubel et al. (2012) have described medial humeral "epicondylitis" in 6 cats. "Epicondylitis" could be a feature of feline OA although only 3 of their 6 cases had cartilage changes typical of OA. An alternative explanation is that medial humeral "epicondylitis" is a primary entity characterised by a flexor enthesiopathy mainly involving the flexor carpi ulnaris muscle. Due to the location of the ulnar nerve that lies in close proximity to the medial humeral epicondyle, pathologic changes affecting the epicondyle causing with new bone formation can cause nerve damage and subsequently pain. They further suggest that the lesion could then result in the development of OA; the lesion is likely to be painful and this could lead to altered weight bearing and load distribution within the elbow joint, thus initiating OA. The term "epicondylitis"; implying an inflammation of the epicondyle is probably not a good term to use. Epicondylar or flexor enthesiopathy is preferred (De Bakker et al., 2012). Unfortunately,

the cranio-caudal view was not part of the protocol used in the present study and thus it was not possible to assess the presence or absence of "epicondylitis". However in two cats this view was included and in both cases epicondylitis was present (Figure 4.24). It is very likely that this is a common finding in the feline elbow.

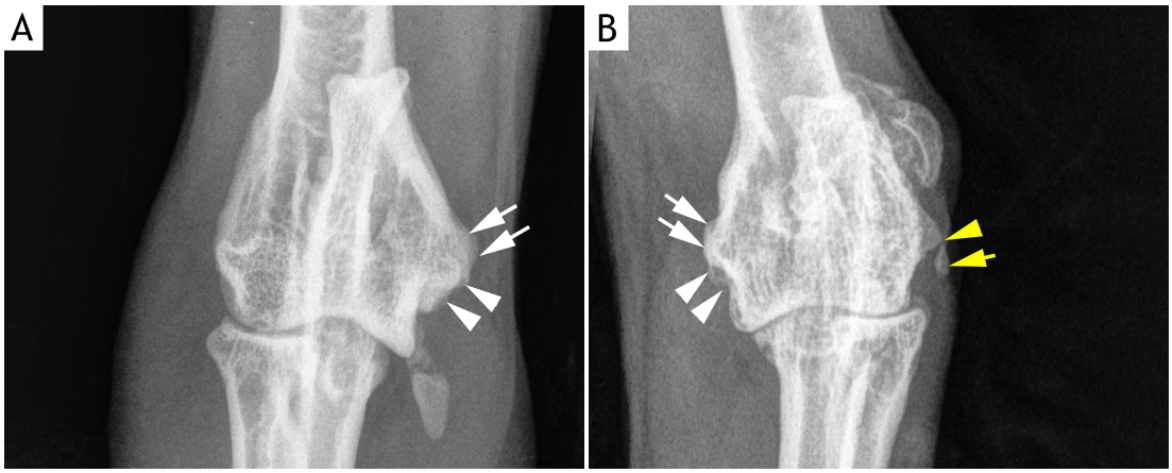

Figure 4.24: Craniocaudal radiographs of two elbow joints.

(A) Enthesiophytes at the attachment of the medial ulnar collateral ligament (white arrowheads) and the common flexor carpi ulnaris tendon (white arrows). Cat ID: X27, right elbow. (B) New bone on the medial epicondyle consistent with enthesiophyte formation at the attachment of the medial ulnar collateral ligament (white arrowheads) and the common flexor ulnaris tendon (white arrows). An enthesiophyte at the lateral collateral ligament is seen (yellow arrowhead). An area of abnormal mineralisation within the lateral joint capsule or collateral ligament is observed (yellow arrow). Cat ID: X18, left elbow.

No fragmentation of the medial part of the coronoid process was seen in this study and this can be excluded as an underlying cause of feline OA, a conclusion also made by Freire et al. (2011). There are reports of fragmented medial coronoid process in the cat (Staiger and Beale, 2005), but this fragmentation was probably explained by osteochondromatosis.

Chapter 5 Radiographic and pathologic features of osteoarthritis of the feline stifle joint

5.1 Introduction and aims

The stifle joint is composed of two major articulations, the femorotibial and femoropatellar joints. The femorotibial joint consists of two condylar joints between corresponding femoral and tibial condyles. The medial and lateral femoral condyles form the articular surfaces of the distal femur. The proximal tibia has two articular cartilage surfaces, the medial and lateral parts which articulate with the condyles of the femur. The articular surfaces of the tibia also referred to as the tibial plateau. The medial tibial plateau is an ellipsoid in shape and has larger articular surface, whereas the lateral tibial plateau has a rounded surface (Prose, 1984). The menisci are interposed between the articular surfaces of the femoral and tibial condyles. Because the medial tibial plateau is larger than the lateral, the medial meniscus has a larger diameter and covers a smaller surface area of the tibia than does the lateral meniscus. The femoropatellar joint consists of the articulation between the trochlea of the femur and the articular surface of the patella. The patella articulates within the trochlear groove, which is formed by the trochlear ridges of the medial and lateral condyles. It is held in contact with the trochlear groove by the tendon of the quadriceps femoris and the patellar ligament which is continued from the patella to the tibial tuberosity. The joint capsule is continuous with the periosteum of both the femur and the tibia. It is in close contact to the joint and separated by the infrapatellar fat body at the distal aspect of the patella. The joint capsule is comprised of the patellar, lateral femorotibial and medial femorotibial sacs.

The main stabilising structures of the stifle joint are the cranial and caudal cruciate ligament and the medial and lateral collateral ligaments (Dyce et al., 2010). The cranial cruciate ligament arises from the caudomedial aspect of the lateral femoral condyle and passes craniodistally to attach on the tibia. The caudal cruciate ligament originates from the lateral surface of the medial femoral condyle and passes caudodistally and attaches on the lateral aspect of the popliteal notch of the tibia. The medial collateral ligament originates from the medial epicondyle of the femur and attaches to the proximal part of the tibia. The lateral collateral ligament originates from the lateral epicondyle of the femur and attaches to the fibular head (Dyce et al., 2010).

The stifle joint has 3 fabellae. The medial fabella is located in the tendon of the medial head of the gastrocnemius and the lateral fabella in the common tendon of the lateral

head of the gastrocnemius and the plantaris. Both fabellae articulate with small articular surfaces on the dorsal aspect of the femoral condyles. The third fabella is located in the popliteal tendon and thus is termed the popliteal fabella.

Previous studies have described osteophytes, enthesiophytes, increased radio-opacity of the subchondral bone, soft tissue mineralisation and joint remodelling as common radiographic signs indicative of stifle OA (Hardie et al., 2002; Clarke et al., 2005; Godfrey, 2007; Slingerland et al., 2011). Other studies have included the presence of meniscal mineralisation as one of the radiographic features of stifle OA (Lascelles et al., 2010; Freire et al., 2011; Ariffin et al., 2013). However, meniscal mineralisation may not only represent degenerative calcification but the presence of a sesamoid bone regarded as a normal feature of the feline meniscus (Whiting and Pool, 1985). To date, no comprehensive study has been published showing whether these mineralisations are always pathological or whether they might represent normal anatomical structures.

Freire et al. (2011) reported that the stifle joint is more likely to have changes in the articular cartilage without showing any signs of radiographic features compared to other joints. Gross cartilage changes are commonly seen on the patella and the medial femoral condyle and tibial plateau (Freire et al., 2011; Bennett et al., 2012a; Ariffin et al., 2013). The radiographic presence of a fabella and its association with primary OA has been reported in humans (Pritchett, 1984). Men with knee OA had a significantly higher incidence of a visible lateral fabella, and it was suggested that the presence of a fabella may predispose the knee to OA. No association between the presence of a fabella and OA has been reported in the cat.

The aim of this study was to define the radiographic features of stifle OA and relate the radiographic findings to the gross pathologic features. In particular the following questions were to be addressed:

a) Can the radiographic features be a good indicator of the severity of cartilage pathology?

b) How does the presence of radiographically apparent meniscal mineralisation relate to cartilage pathology?

c) Does the radiographic presence of 1 or 2 fabellae relate to cartilage pathology?

d) Are there any underlying causes of stifle OA in the cat?

5.2 Materials and methods

5.2.1 Determination of stifle OA population

Identification of the stifle OA population was done as described in Section 2.2, page 58 and Figure 2.1, page 59.

5.2.2 Comparative analyses of signalment, body weight and body condition score between St-path OA and no St-path/normal cats

Median and SD of age, BW and BCS of St-path OA and no St-path OA/normal cats were illustrated with a scatter plot graph and statistically analysed by using Mann-Whitney *U* test. The distribution of breed and gender of St-path OA and no St-path OA/normal cats was visualised using a stacked bar graph. The distribution of BCS of St-path OA and no St-path OA/normal cats was shown by a column bar graph.

5.2.3 Radiographic assessment of the stifle joint

Radiographic changes associated with stifle OA were assessed using a radiographic scoring system (see Section 2.3.3, page 60 and Table 2.1, page 62). The radiographic features assessed were osteophytes, enthesiophytes, areas of abnormal mineralisation, meniscal mineralisation (MM), increased radio-opacity of the femoral condyle and tibial plateau, synovial effusion, joint remodelling and new bone formation on the fabellae. The presence of 1 or 2 fabellae was recorded but was not included in the scoring. The total radiographic score and the global score were determined. The prevalence of St-rOA and no St-rOA was calculated as the percentage of cats which had or had no radiographic changes. The prevalence of each radiographic feature was determined as the percentage of affected stifle joints which had the feature. The mean and SD of osteophyte and MM size were calculated. The age of cats with and without radiographic MM was statistically analysed by using the Mann-Whitney *U* test and was illustrated with a scatter plot graph.

5.2.4 Gross pathologic assessment of the stifle joint

Gross pathologic changes associated with OA were assessed and scored using a gross pathologic scoring system (see Section 2.4.1, page 66 and Table 2.3, page 67). The gross pathologic changes on the patella, medial and lateral femoral condyles and tibial plateau were scored independently. The total gross pathologic score and the global score were determined. The prevalence of St-path OA and no St-path OA/normal were

determined as the percentage of cats which had or had no gross changes in the articular cartilage. The prevalence of each gross pathologic feature was calculated as the percentage of affected stifle joints which had the feature. The Wilcoxon Signed Rank test was used to analyse the difference between the gross cartilage damage scores of the medial and lateral condyles of the femur and tibial plateau. The Mann Whitney *U* test was used to analyse the difference between the gross cartilage damage scores of the femoral condyles, tibial plateau and patella of left and right stifle joints with one and two radiographically visible fabellae and between stifle joints with and without radiographic MM. The same test was used to analyse the difference between total gross pathologic scores of the left and right stifle joints. The results were illustrated with a scatter plot graph.

5.2.5 Correlation studies

5.2.5.1 Correlation between radiographic and gross pathologic OA scores

A correlation analysis between radiographic and gross pathologic scores for the left and right stifle joints was performed using a nonparametric, Spearman's rank correlation. Correlation coefficient results were interpreted as described in Table 2.9, page 80. The correlation was illustrated by scatter plot graphs.

5.2.5.2 Correlation between radiographic size of MM and cartilage damage scores

A correlation analysis between the radiographic size of MM and cartilage damage scores was performed using a nonparametric, Spearman's rank correlation. Correlation coefficient results were interpreted as described in Table 2.9, page 80.

5.2.5.3 Correlation between radiographic OA scores and age, BW and BCS

A correlation analysis between total radiographic OA scores for the left and right stifle joints and age, BW and BCS was carried out using Spearman's rank correlation. The coefficient results were interpreted as described in Table 2.9, page 80. The correlation for left and right stifle joints was illustrated by scatter plot graphs.

5.2.5.4 Correlation between gross pathologic OA scores and age, BW and BCS

A correlation analysis between gross pathologic OA scores for the left and right stifle joints and age, BW and BCS was done using a nonparametric, Spearman's rank correlation. The coefficient results were interpreted as described in Table 2.9, page 80. The correlation for left and right stifle joints was illustrated by scatter plot graphs.

5.3 Results

5.3.1 Stifle OA population

A total of 116 stifle joints from 58 cats were evaluated for the radiographic signs of OA. Of 58 cats, 50 had radiographic changes associated with stifle OA (St-rOA). Of 8 cats with radiographically normal stifle joints (no St-rOA), 2 had cartilage changes, and one cat with radiographically detectable MM had no cartilage changes thus giving a total population of 51 cats with stifle OA (St-path OA) (Table 5.1).

Population	Number of cats	Percentage (%)
St-rOA	50	86.2
No St-rOA	8	13.8
St-path OA	51	87.9
No St-path OA/normal	7	12.1

Table 5.1: Showing the number and percentage of the St-rOA, no St-rOA, St-path OA and no St-path OA/normal populations. Total number of cats is 58.

5.3.2 Comparative analyses of signalment, body weight and body condition score between St-path OA and no St-path OA/normal cats

5.3.2.1 Signalment

The mean age of the St-path OA cats was 7.3 years (SD 4.3) with a minimum age of 2 years and a maximum of 20 years. The median age was 5 years. The mean age of the no St-path OA/normal cats was 2.5 years (SD 1.9) with a minimum age of 3 months and a maximum of 5 years. The median age was 3 years. The age difference between the St-path OA and no St-path OA/normal cats was significant ($P<0.01$) (Figure 5.1.A). Sixteen St-path OA cats were MC, 8 cats were F and 26 cats were FS. One of the no St-path OA/normal cats was M, 1 cat was MC and 5 cats were F. In the St-path OA group 80.0% were DSH, 12.0% were DLH and 8.0% were pedigree cats. In the no St-path OA/normal group 86.0% were DSH and 14.0% were pedigree cats (Figures 5.2.A and 5.2.B).

5.3.2.2 Body weight

The mean BW of the St-path OA cats was 3.5 kg (SD 1.1) with a minimum weight of 1.9 kg and a maximum of 7.0 kg. The median BW was 3.2 kg. The mean BW of the no St-path OA/normal cats was 3.2 kg (SD 1.1) with a minimum weight of 0.8 kg and a maximum of 4.8 kg. The median was 3.0 kg. The difference between the St-path OA and no St-path OA/normal cats for BW was not significant ($P=0.51$) (Figure 5.1.B).

5.3.2.3 Body condition score

The St-path OA cats had a median BCS of 3 with a minimum BCS of 1 and a maximum of 5. The no St-path OA/normal cats had a median BCS of 3 with a minimum BCS of 2 and a maximum of 3. There was no significant difference between BCS of the St-path OA and no St-path OA/normal cats (P=0.52) (Figure 5.1.C). The distribution of BCS of St-path OA and no St-path OA/normal cats is shown in Figure 5.3.

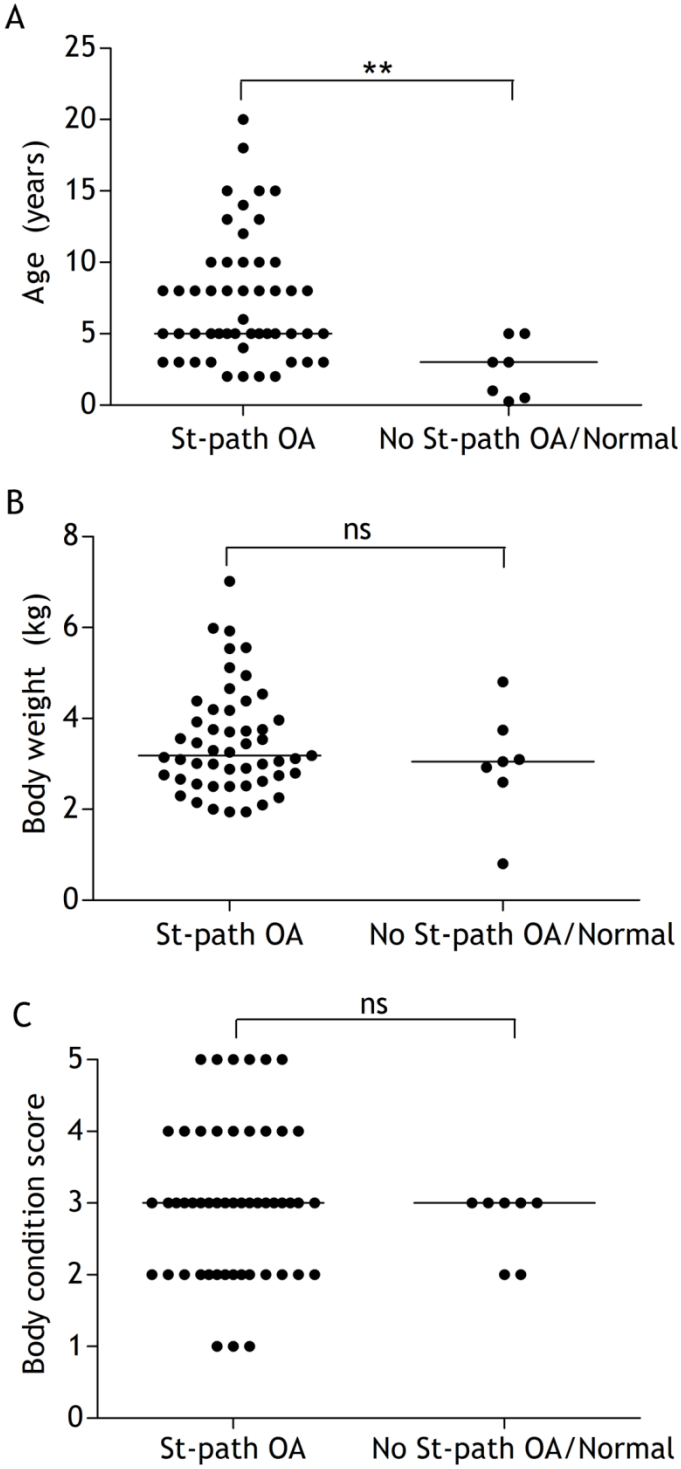

Figure 5.1: The comparative analysis of age, BW and BCS between St-path OA (*N*=51) and no St-path OA/normal (*N*=7) cats.

(A) The age difference between the St-path OA and No St-path/normal cats is significant. There is no significant difference in BW (B) and BCS (C) of cats with and without OA. Data presented as median and plotted in vertical scatter plot. (Mann Whitney *U* test,** represents P<0.01; ns: not significant P>0.05).

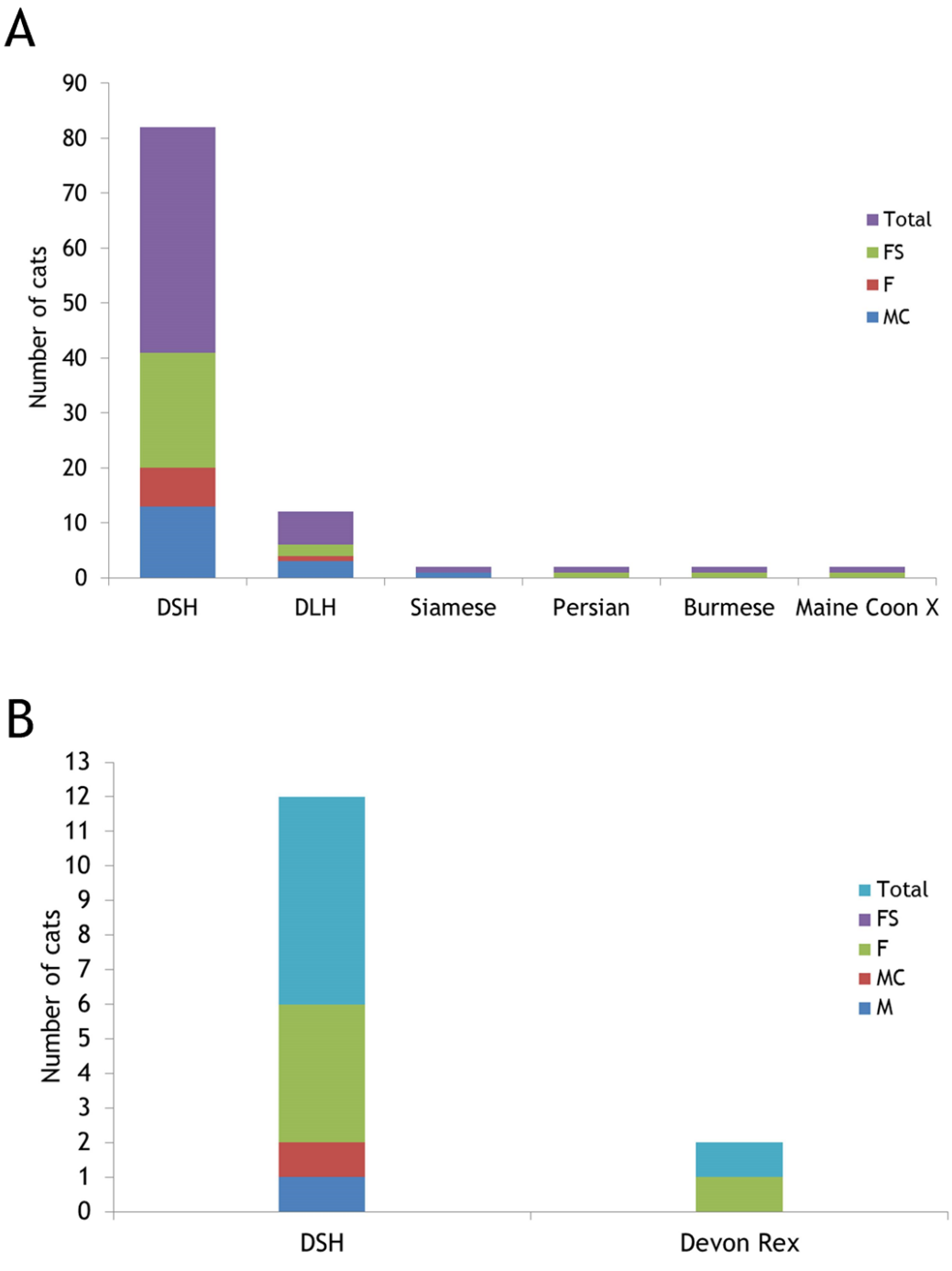

Figure 5.2: Breed and gender distribution of St-path OA (A) and no St-path OA/normal (B) cats.

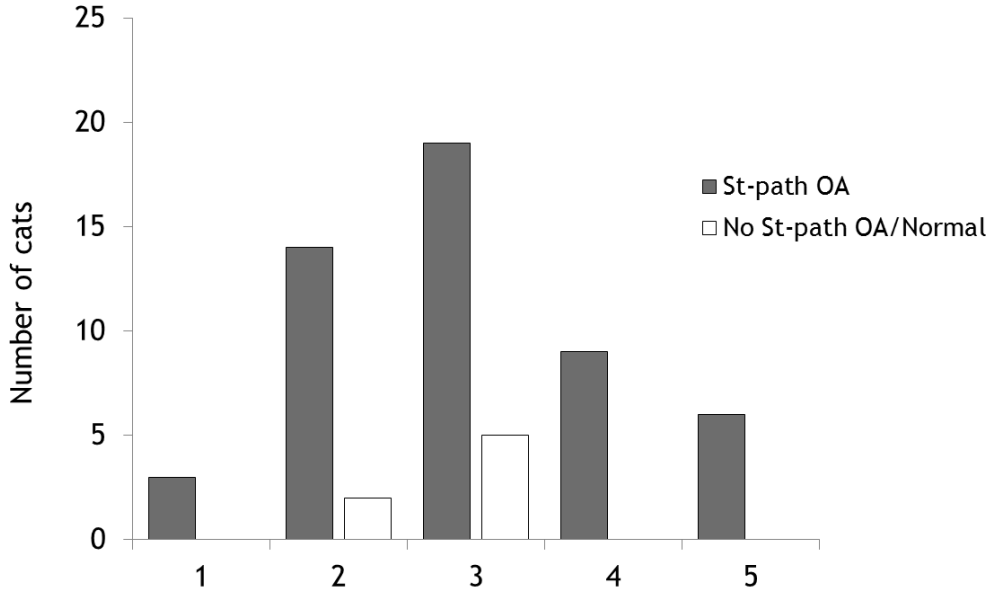

Figure 5.3: Distribution of body condition scores (BCS) of St-path OA and no St-path OA/normal cats.

5.3.3 Radiographic findings

The overall prevalence of St-rOA was 86.2% (50 of 58 cats). Of 50 cats with radiographic changes, 43 cats had bilateral and 7 had unilateral stifle involvement (3 on the left and 4 on the right) giving a total number of 93 (80.2%) St-rOA joints (Table 5.2). Twenty-three stifle joints had no radiographic changes (St-rOA). The mean total radiographic score of left and right stifle joints was 5.4 and 4.8 respectively. The median total radiographic score of left and right stifle joints was 5 and 4 respectively, with a range from 1 to 15. Of 93 stifle joints, 62 were given a Global score of 1, 25 a Global score of 2 and 6 a Global score of 3 (Tables 5.3 and 5.4).

Osteophytes were observed in 57 (61.3%) of 93 St-rOA joints, bilaterally in 21 cats and unilaterally in 15 cats (9 on the left and 6 on the right). Osteophytes were seen at the proximal aspect of the femoral trochlea, cranial and caudal edge of the tibial plateau, proximal and distal pole of the patella and on the fabellae (Figures 5.4.B-D). Severity was graded mild in 37/93 joints (39.8%) (18 on the left and 19 on the right), moderate in 18/93 joints (19.4%) (10 on the left and 8 on the right) and severe in 2/93 joints (2.2%) (both were left). The mean osteophyte size in mm ± SD for mildly affected joints was 1.2 ± 0.4, for moderately affected joints was 2.8 ± 0.4 and for severely affected joints was 5.2 ± 0.1 (Table 5.5).

Extra-articular enthesiophytes were identified in 33/93 joints (35.5%), bilaterally in 10 cats and unilaterally in 13 cats (7 on the left and 6 on the right). They were graded mild in 17 joints, moderate in 10 joints and severe in the other 6. The mean mild enthesiophyte size in mm ± SD was 0.61 ± 0.18, for moderate enthesiophyte size it was 1.8 ± 0.5 and for severe enthesiophyte size it was 5.5 ± 1.2. The enthesiophytes were seen on the cranial surface of the patella, presumably at the attachment of the quadriceps muscle in 9 joints (Figure 5.5.B), at the attachment of the patellar ligament to the tibial tuberosity in 21 joints (Figure 5.5.C) and in three joints were present on both the tibial tuberosity and the patella (Figure 5.5.D).

Areas of abnormal mineralisation (other than meniscal mineralisation) were present in 17/93 joints (18.3%), bilaterally in 4 cats and unilaterally in 9 cats (5 on the left and 4 on the right). In 7 stifle joints this was graded mild, moderate in 9 and severe in 1 (Figure 5.6). Areas of abnormal mineralisation were commonly seen at the cranial and caudal parts of the stifle joint.

Of 93 St-rOA joints, 89 (95.7%) had an increase in radio-opacity, irrespective of the location. Increase in radio-opacity along the femoral trochlea was identified in 84/93 stifle joints (90.3%) (44 on the left and 40 on the right) (Figures 5.7.B-D). Seventy-three (78.5%) of the 93 St-rOA joints were scored as having an increase in radio-opacity beneath the tibial plateau (Figure 5.7.D). The feature was not seen in 4 stifle joints (Figure 5.7.A).

Overall, the prevalence of MM was 42.2% (49/116). Meniscal mineralisation was present in 49 (52.7%) of the 93 St-rOA joints, bilaterally in 20 cats and unilaterally in 9 cats (25 on the left side and 24 on the right side) (Figure 5.8). Of 49 stifle joints, 46 also had osteophytes and/or increased radio-opacity of the femoral condyle and/or the tibial plateau. In 3 of 49 stifle joints, there were no other radiographic signs. In 29 joints the mineralisation was less than 2 mm (Figure 5.8.B), in 7 it was 2-3 mm (Figure 5.8.C), and in 13 it was more than 3 mm (Figure 5.8.D). The mean MM in mm ± SD for Score 1 was 1.5 ± 0.5, for Score 2 it was 2.7 ± 0.3 and for Score 3 it was 4.2 ± 0.9 (Table 5.6). The mean age of the cats with and without MM was 8.4 (SD 4.4) and 5.1 (SD 3.7) respectively. The age difference was significant ($P<0.01$) (Figure 5.9).

	Radiographic findings			
	No St-rOA		St-rOA	
	Number of Joints	Percentage (%)	Number of joints	Percentage (%)
Left stifle	12	20.7	46	79.3
Right stifle	11	19.0	47	81.0
Total	23	19.8	93	80.2

Table 5.2: Showing numbers of stifle joints with normal and abnormal radiographic findings. Total number of joints 116.

	Radiographic OA Global score			
	Score 0	Score 1	Score 2	Score 3
Left stifle	12	29	14	3
Right stifle	11	33	11	3
Total	23	62	25	6
Percentage (%)	19.8	53.4	21.6	5.2

Table 5.3: The number and percentage of stifle joints with different radiographic OA Global scores.

Cat ID	Osteophytes		Enthesiophytes		Area of abnormal mineralisation		Increase radio - opacity of femoral condyle (FC) and tibial plateau (TP)				Meniscal mineralisation		Synovial effusion		Joint remodelling		New bone formation on the fabellae		1 or 2 Fabellae		Total score		Global score	
							L		R															
	L	R	L	R	L	R	FC	TP	FC	TP	L	R	L	R	L	R	L	R	L	R	L	R	L	R
X1	1	1	0	0	0	0	0	1	0	1	0	0	0	0	0	0	1	0	1	1	3	2	1	1
X2	0	0	0	0	0	0	0	0	0	0	0	0	0	0	0	0	0	0	2	2	0	0	0	0
X3	0	0	0	0	0	0	0	0	1	0	0	1	0	0	0	0	0	0	1	1	0	2	0	1
X4	1	0	1	0	0	0	1	1	0	0	1	0	1	0	0	0	0	0	1	1	6	0	1	0
X5	1	0	0	0	0	0	1	1	0	0	1	0	1	0	0	0	0	0	2	2	5	0	1	0
X6	0	1	0	0	0	0	1	1	1	1	0	0	0	0	0	0	0	0	2	2	2	3	1	1
X7	1	2	1	0	0	2	1	1	1	1	0	3	1	1	0	0	1	1	2	2	6	11	2	3
X8	0	0	0	0	0	0	1	1	0	0	0	1	0	0	0	0	0	0	2	1	2	1	1	1
X9	0	0	0	0	0	0	0	0	0	0	0	0	0	0	0	0	0	0	1	1	0	0	0	0
X10	0	0	0	0	0	0	0	0	0	0	0	0	0	0	0	0	0	0	1	1	0	0	0	0
X11	0	1	0	0	1	0	1	0	1	0	0	0	0	0	0	0	0	0	2	1	2	2	1	1
X12	2	0	0	0	2	0	1	1	1	1	3	1	0	0	0	0	1	0	2	2	10	3	2	1
X13	0	0	0	0	0	0	0	0	1	1	0	0	0	0	0	0	0	0	1	1	0	2	0	1
X14	0	0	0	0	0	0	0	0	0	0	0	0	0	0	0	0	0	0	2	2	0	0	0	0
X15	0	1	1	1	0	2	1	1	1	1	0	1	0	1	0	0	1	0	2	2	4	8	1	2
X16	1	2	3	3	0	0	1	1	1	1	0	0	0	1	0	0	0	0	2	2	6	8	2	2
X17	0	0	0	0	0	0	1	0	1	0	1	1	0	0	0	0	0	0	2	2	2	2	1	1
X18	2	2	0	0	1	2	1	1	1	1	3	3	1	0	0	0	1	1	2	2	10	10	2	2
X19	0	0	0	0	0	0	0	0	0	0	0	0	0	0	0	0	0	0	1	1	0	0	0	0
X20	1	1	0	0	0	0	1	1	0	1	0	0	0	1	0	0	0	0	2	2	3	3	1	1

Table 5.4: Radiographic features and Global scores of the left (L) and right (R) stifle joints in 58 cats. Scoring (excluding the presence of 1 or 2 fabellae): 0: absent, 1: mild/present, 2: moderate, 3: severe. Global score: 0: no abnormality, 1: mild, 2: moderate, 3: severe. For fabellae, figure is number visible on radiograph.

Cat ID	Osteophytes		Enthesiophytes		Area of abnormal mineralisation		Increase radio - opacity of femoral condyle (FC) and tibial plateau (TP)				Meniscal mineralisation		Synovial effusion		Joint remodelling		New bone formation on the fabellae		1 or 2 Fabellae		Total score		Global score	
							L		R															
	L	R	L	R	L	R	FC	TP	FC	TP	L	R	L	R	L	R	L	R	L	R	L	R	L	R
X21	0	0	0	0	0	0	1	1	1	1	0	0	1	1	0	0	0	0	2	2	3	3	1	1
X22	0	0	1	0	0	0	1	1	1	1	1	1	0	1	0	0	0	1	2	2	4	5	1	1
X23	0	0	0	0	0	0	0	0	1	1	0	0	0	1	0	0	0	0	2	2	0	3	0	1
X24	0	0	0	1	0	0	1	1	0	1	0	0	0	0	0	0	0	0	2	2	2	2	1	1
X25	0	0	1	0	0	0	1	1	1	1	0	0	0	0	0	0	0	0	1	1	5	2	1	1
X26	2	1	0	0	0	0	1	1	1	1	1	0	1	1	0	0	0	0	2	2	6	4	2	1
X27	1	1	0	0	0	0	1	1	1	1	1	2	1	1	0	0	0	0	2	2	5	7	2	1
X28	2	1	3	3	0	0	1	1	1	1	1	2	1	0	0	0	0	0	1	2	9	8	2	2
X29	0	0	0	0	0	0	1	1	1	1	1	0	0	0	0	0	0	0	1	1	3	2	1	1
X30	2	1	0	3	1	0	1	1	1	1	3	2	1	0	0	0	1	1	2	2	10	9	2	2
X31	2	1	1	0	1	0	1	1	1	1	3	2	0	0	1	1	0	0	2	2	10	6	2	2
X32	2	2	1	0	0	1	1	1	1	1	3	3	1	1	1	0	0	0	1	1	10	9	2	2
X33	0	0	0	0	0	0	0	0	0	0	0	0	0	0	0	0	0	0	1	1	0	0	0	0
X34	0	0	0	0	0	0	1	1	0	0	0	0	0	0	0	0	0	0	2	2	2	0	1	0
X35	2	0	1	0	0	0	1	1	1	1	0	0	1	0	0	0	0	0	2	2	6	2	2	1
X36	3	0	0	0	3	0	1	1	1	1	3	2	1	0	1	0	1	0	2	2	14	4	3	1
X37	1	1	1	0	0	2	1	0	1	1	1	2	0	0	0	0	0	0	2	2	4	7	1	2
X38	1	1	1	0	0	0	1	1	1	0	0	0	1	1	0	0	0	1	2	2	5	4	1	1

Table 5.4 continued.

Cat ID	Osteophytes		Enthesiophytes		Area of abnormal mineralisation		Increase radio - opacity of femoral condyle (FC) and tibial plateau (TP)				Meniscal mineralisation		Synovial effusion		Joint remodelling		New bone formation on the fabellae		1 or 2 Fabellae		Total score		Global score	
							L		R															
	L	R	L	R	L	R	FC	TP	FC	TP	L	R	L	R	L	R	L	R	L	R	L	R	L	R
X39	0	0	0	0	0	0	1	0	1	1	0	0	1	0	0	0	0	0	1	2	2	2	1	1
X40	0	1	2	1	0	0	1	1	1	1	0	0	0	1	0	0	0	0	2	2	4	5	1	1
X41	0	1	2	2	0	0	1	1	1	1	0	0	1	1	0	0	1	1	2	2	6	7	2	2
X42	3	2	2	3	2	2	1	1	1	1	3	3	1	1	1	1	1	1	2	2	15	15	3	3
X43	0	0	0	2	0	0	0	0	1	1	0	0	0	1	0	0	0	0	1	1	0	5	0	1
X44	1	0	0	0	0	0	1	1	1	1	2	0	0	1	0	0	1	1	1	1	6	4	2	1
X45	1	0	2	1	2	1	1	1	1	1	3	3	0	0	0	0	1	1	2	2	11	8	3	2
X46	1	0	0	0	0	0	1	0	1	0	0	0	0	0	0	0	0	0	2	2	2	1	1	1
X47	1	2	0	0	0	0	1	1	1	1	0	0	1	0	0	0	0	0	2	2	4	4	1	1
X48	2	2	0	0	0	0	1	0	1	1	0	0	0	0	1	0	0	0	1	1	4	4	1	1
X49	1	1	0	0	0	0	1	0	1	0	1	1	0	0	0	0	0	0	2	2	3	3	1	1
X50	1	1	2	1	0	0	1	0	1	0	0	0	1	0	0	0	0	0	2	2	5	3	1	1
X51	0	0	0	0	0	0	0	0	0	0	0	0	0	0	0	0	0	0	1	1	0	0	0	0
X52	0	0	0	0	0	0	0	0	0	0	1	1	0	0	0	0	0	0	2	2	1	1	1	1
X53	0	0	0	0	0	0	0	0	0	0	0	0	0	0	0	0	0	0	1	1	0	0	0	0
X54	1	1	0	1	0	0	1	0	0	0	1	1	0	1	0	0	1	1	2	2	4	5	1	1
X55	1	1	0	0	0	0	1	1	0	1	1	1	1	0	0	0	1	1	2	2	6	4	2	1
X56	2	2	2	2	1	2	1	1	1	1	1	1	1	1	0	0	1	1	2	2	10	11	2	3

Table 5.4 continued.

Cat ID	Osteophytes		Enthesiophytes		Area of abnormal mineralisation		Increase radio - opacity of femoral condyle (FC) and tibial plateau (TP)				Meniscal mineralisation		Synovial effusion		Joint remodelling		New bone formation on the fabellae		1 or 2 Fabellae		Total score		Global score	
							L		R															
	L	R	L	R	L	R	FC	TP	FC	TP	L	R	L	R	L	R	L	R	L	R	L	R	L	R
X57	0	1	1	2	0	0	1	1	1	1	1	1	1	0	0	0	0	0	1	1	5	6	1	2
X58	1	0	0	0	0	0	1	1	1	1	1	1	1	1	0	0	0	0	1	1	5	4	1	1

Table 5.4 continued.

	Left stifle		Right stifle	
Cat ID	Score	Osteophyte size (mm)	Score	Osteophyte size (mm)
X1	1	1.6	1	1.6
X4	1	1.4	0	-
X5	1	1.1	0	-
X6	0	-	1	1.2
X7	1	1.8	2	2.5
X11	0	-	1	0.6
X12	2	2.3	0	-
X15	0	-	1	1.7
X16	1	1.5	2	2.8
X17	0	-	0	-
X18	2	2.8	2	3.0
X20	1	1.4	1	0.5
X26	2	2.8	1	0.7
X27	1	1.2	1	1.6
X28	2	2.4	1	1.5
X30	2	2.2	1	1.2
X31	2	2.4	1	1.2
X32	2	2.0	2	2.3
X35	2	2.4	0	-
X36	3	5.2	0	-
X37	1	1.5	1	1.1
X38	1	1.0	1	0.7
X40	0	-	1	1.5
X41	0	-	1	0.7
X42	3	5.1	2	3.5
X44	1	1.4	0	-
X45	1	1.5	0	-
X46	1	1.2	0	-
X47	1	1.3	2	2.3
X48	2	2.5	2	2.7
X49	1	1.1	1	0.5
X50	1	1.2	1	0.7
X54	1	1.5	1	1.1
X55	1	1.4	1	1.4
X56	2	2.5	2	3.0
X57	0	-	1	0.5
X58	1	0.5	0	-

Table 5.5: Osteophytes when present were graded according to their size (mm) and whether a single site or multiple sites were involved.

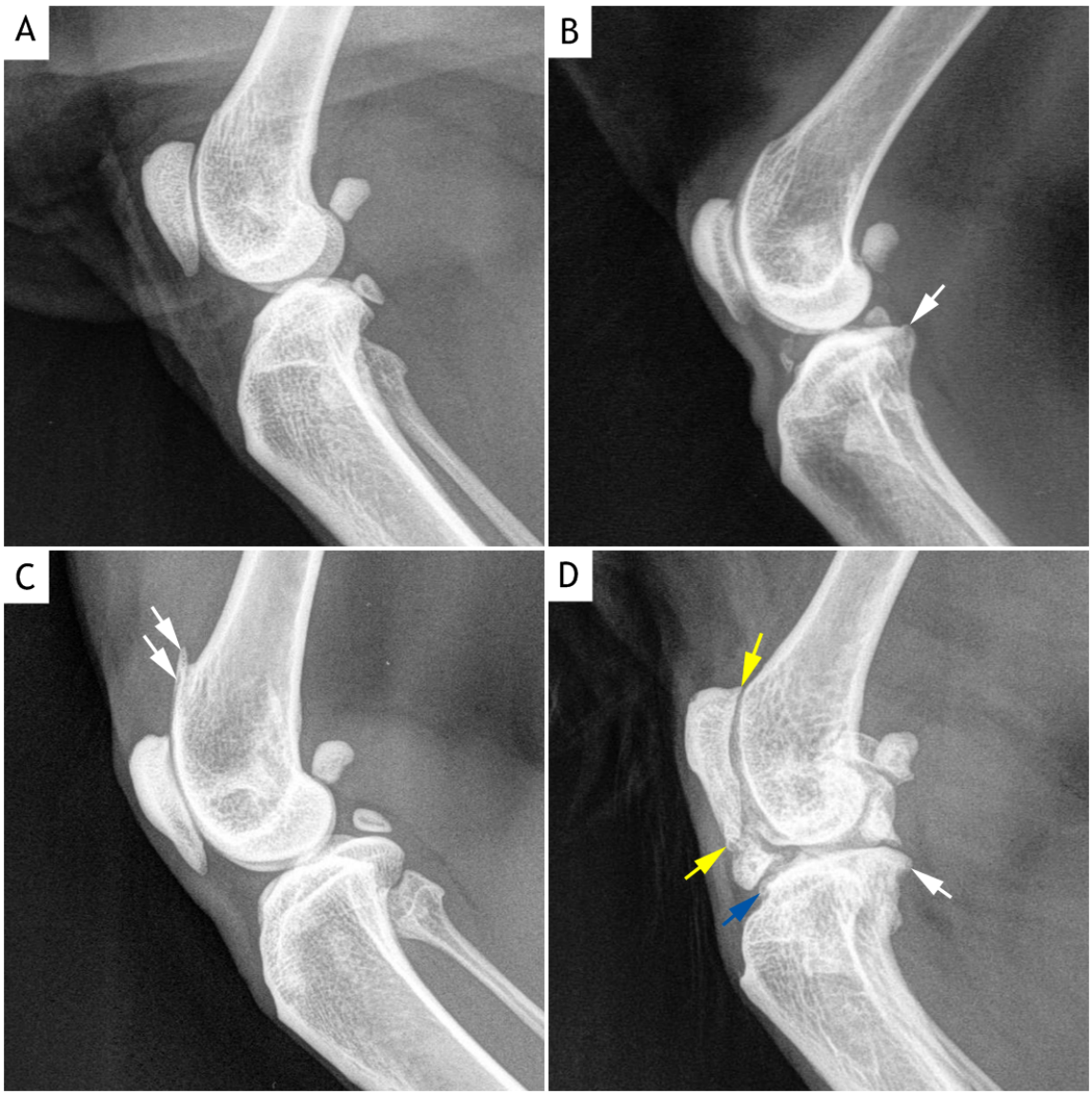

Figure 5.4: Mediolateral radiographs of stifle joints showing osteophytes.

(A) Normal stifle joint. Three sesamoid bones are visible in the stifle joint, the patella, lateral fabella and the popliteal sesamoid bone. Cat ID: X51, right stifle. (B) Note the presence of osteophyte on the tibial plateau (white arrow). Cat ID: X32, right stifle. (C) Large osteophyte is seen on the proximal aspect of the femoral trochlea (white arrows). Cat ID: X48, left stifle. (D) Multiple osteophyte formation is observed at the proximal and distal poles of the patella (yellow arrows), cranial edge (blue arrow) and on the caudal edge (white arrow) of the tibial plateau. Cat ID: X36, left stifle.

Figure 5.5: Mediolateral radiographs of stifle joints showing examples of extra-articular enthesiophytes.

(A) Normal stifle joint with an absence of enthesiophytes. Cat ID: X51, right stifle. (B) A large enthesiophyte is identified at the attachment of the quadriceps muscle/tendon on the patella (white arrows). Cat ID: X50, left stifle. (C) An enthesiophyte is present at the attachment of the patellar ligament on the tibial tuberosity. Cat ID: X42, left stifle. (D) Enthesiophytes can be seen on both the patella and tibial tuberosity. Cat ID: X28, left stifle.

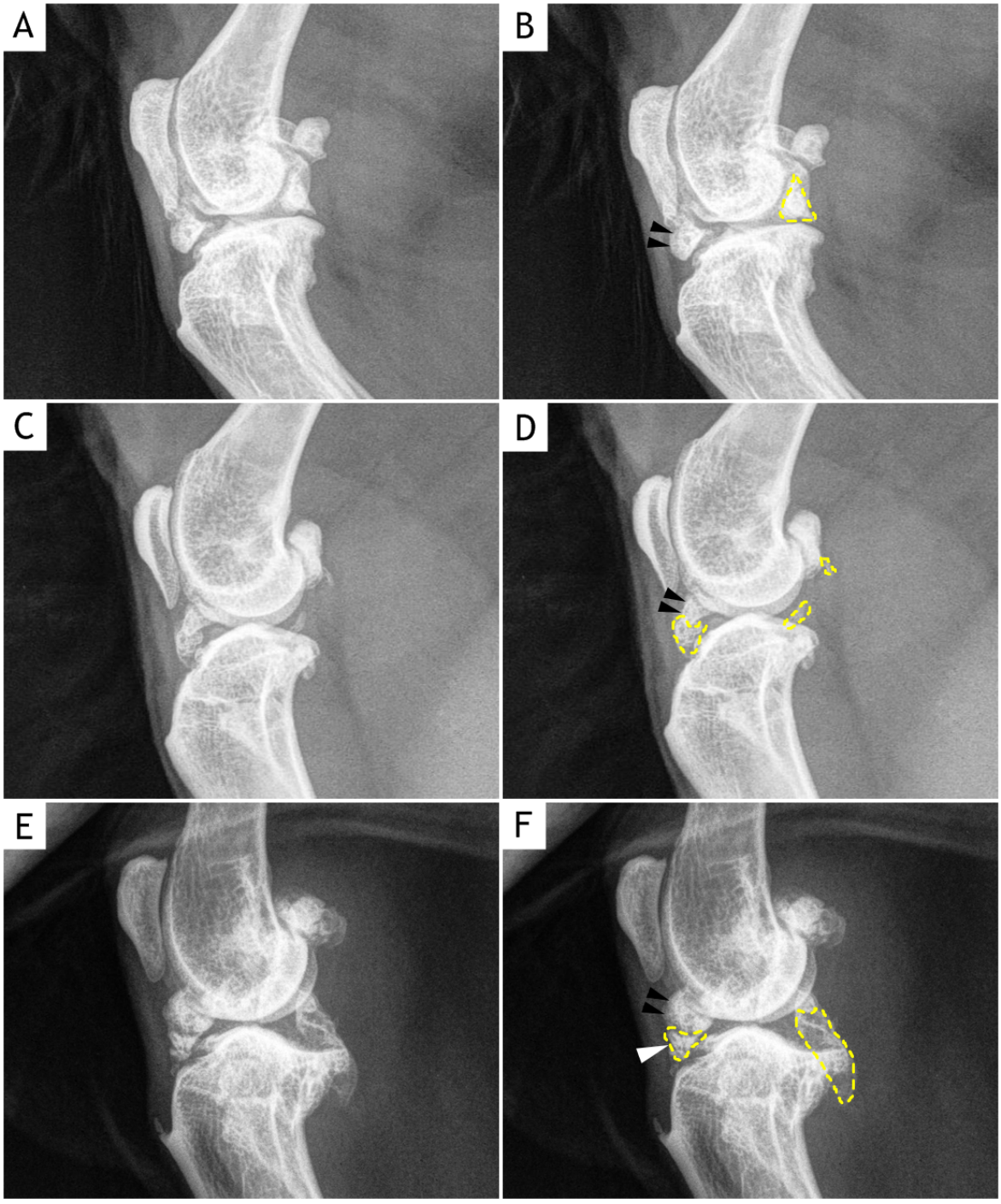

Figure 5.6: Mediolateral radiographs of stifle joints showing abnormal mineralisations.

Figure B, D and F are the same as A, C and E but with specific lesions highlighted. (B, D & F) Note that the borders of the mineralised areas (yellow dotted lines) are clearly delineated. These areas represent either mineralisation within the joint capsule or the presence of intra-articular mineralised bodies referred to as osteochondromas. In B, D and F, gross pathologic examination showed mineralisations to be within the joint capsule and in one case an osteochondroma (white arrowhead) (See Figure 5.20.C for gross pathology). Meniscal mineralisation is present in all 3 radiographs (black arrowheads). A & B: Cat ID: X36, left stifle. C & D: Cat ID: X18, left stifle. E & F: Cat ID: X42, right stifle.

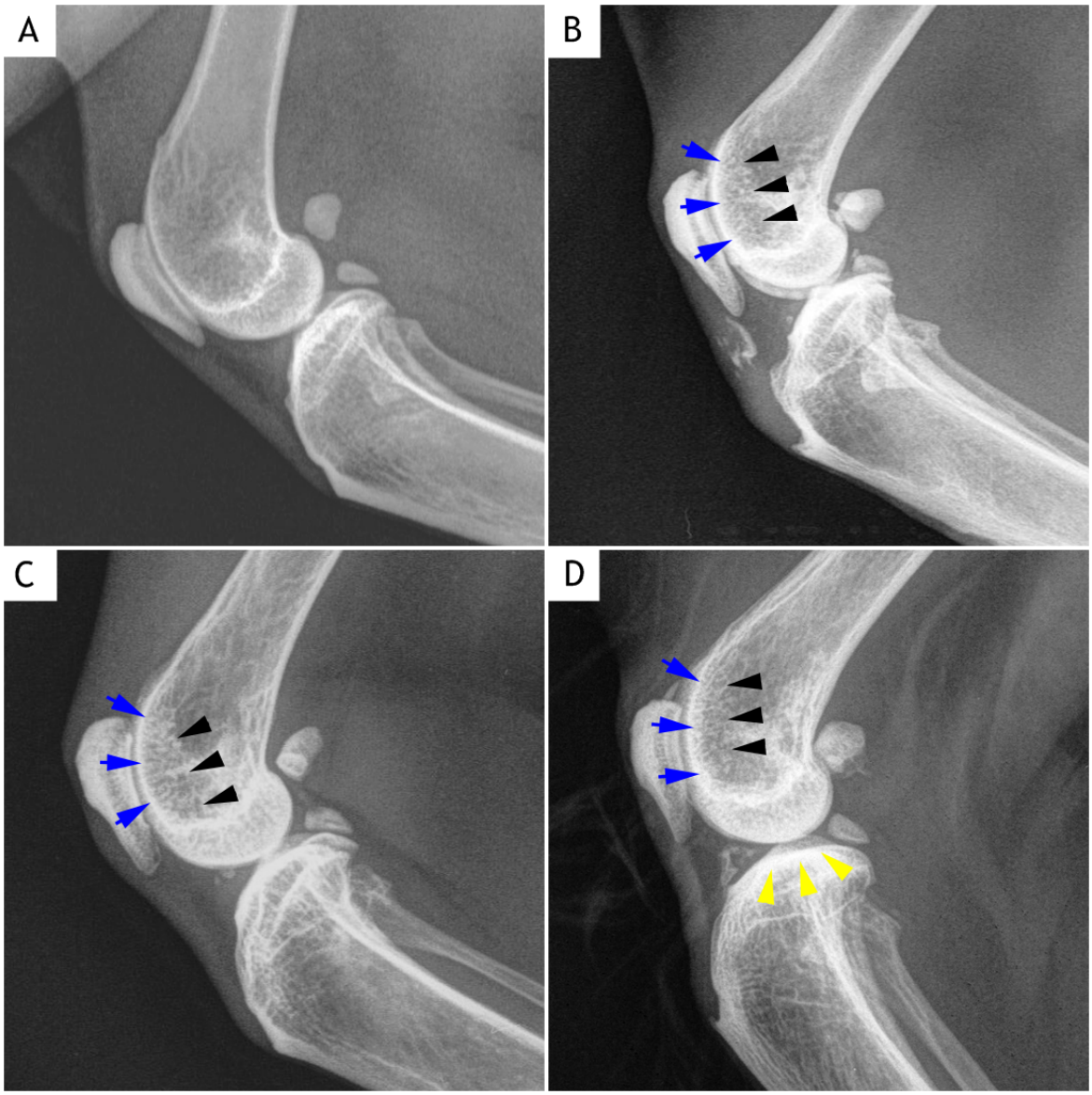

Figure 5.7: Mediolateral stifle radiographs with and without increased radio-opacity of the femoral condyle and beneath the tibial plateau.

(A) Normal stifle joint with normal bone opacity of the femoral condyle and tibial plateau. Cat ID: X51, right stifle. (B, C, D) There is an apparent increased radio-opacity along the margin of the femoral trochlea (black arrowheads) and beneath the tibial plateau (yellow arrowheads). The presence of osteophytes certainly explains some of this opacity. In addition there is increased radio-opacity at the surface of the femoral trochlea (blue arrows); this proved difficult to assess and was not scored in this study. B: Cat ID: X32, right stifle, C: Cat ID: X15, left stifle, D: Cat X26, left stifle.

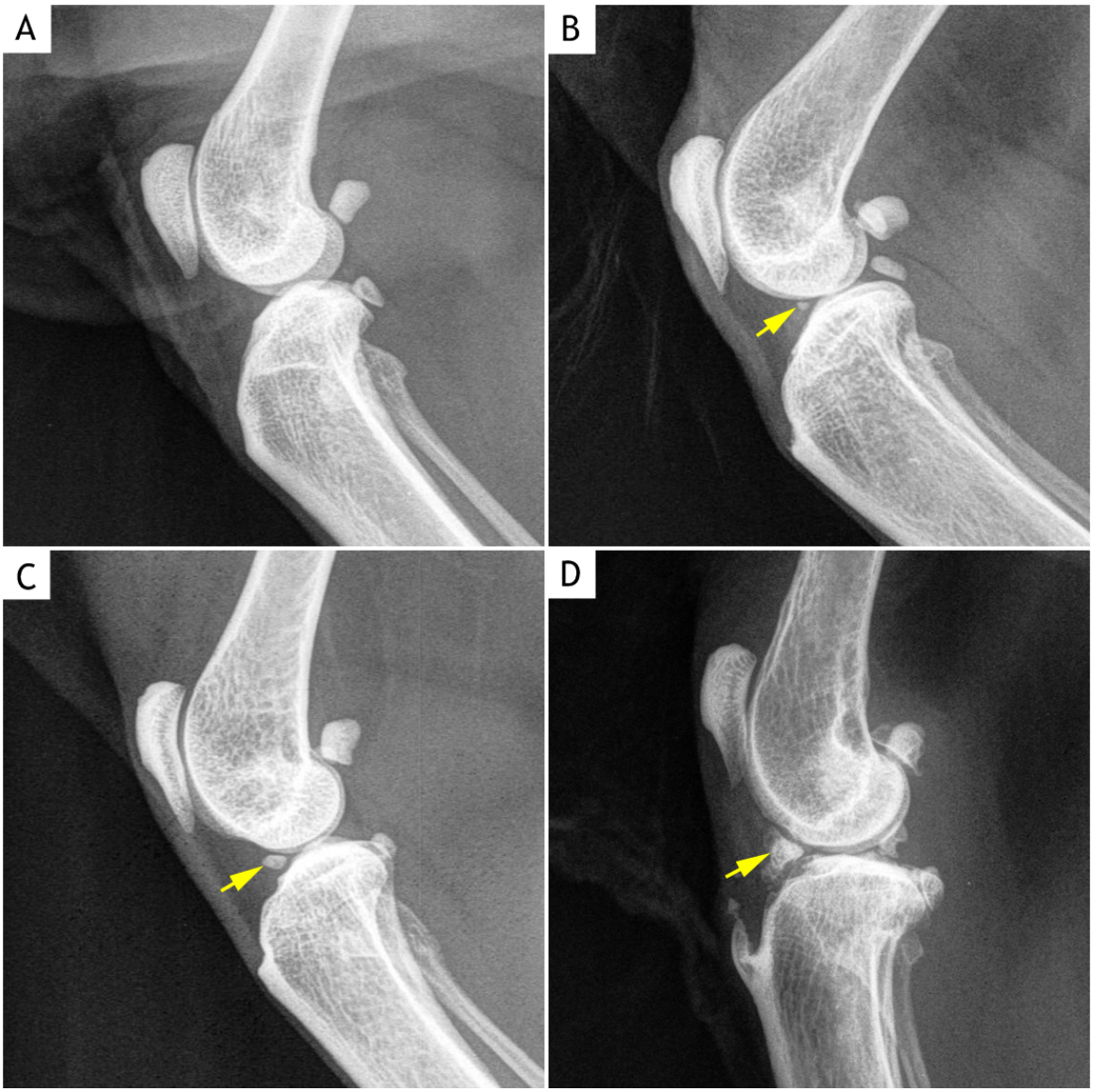

Figure 5.8: Mediolateral stifle radiographs showing examples of meniscal mineralisation.

(A) Normal stifle joint with no meniscal mineralisation. Cat ID: X51, right stifle. (B) Small area of meniscal mineralisation located in the cranial compartment of the stifle joint (yellow arrow). Cat ID: X22, left stifle. (C) Oval shaped area of meniscal mineralisation, 2-3 mm in diameter (yellow arrow). Cat ID: X36, right stifle. (D) Large area of meniscal mineralisation is identified (yellow arrow). Cat ID: X42, left stifle.

Cat ID	Left stifle		Right stifle	
	Score	MM size (mm)	Score	MM size (mm)
X3	0	-	1	1.8
X4	1	1.6	0	-
X5	1	1.4	0	-
X7	0	-	3	5.6
X8	0	-	1	0.9
X12	3	5.0	1	1.5
X15	0	-	1	1.2
X17	1	1.8	1	1.7
X18	3	5.1	3	5.0
X22	1	1.5	1	1.8
X26	1	1.8	0	-
X27	1	1.6	2	3.0
X28	1	1.9	2	2.3
X29	1	1.6	0	-
X30	3	3.5	2	2.4
X31	3	3.7	2	2.9
X32	3	3.5	3	3.2
X36	3	3.4	2	2.6
X37	1	1.7	2	2.6
X42	3	3.4	3	3.3
X44	2	3.0	0	-
X45	3	6.0	3	4.5
X49	1	1.7	1	1.7
X52	1	1.5	1	1.5
X54	1	1.5	1	1.2
X55	1	1.2	1	1.4
X56	1	1.9	1	0.8
X57	1	1.5	1	1.4
X58	1	0.8	1	0.8

Table 5.6: A visible area of meniscal mineralisation was scored according to its size (mm).

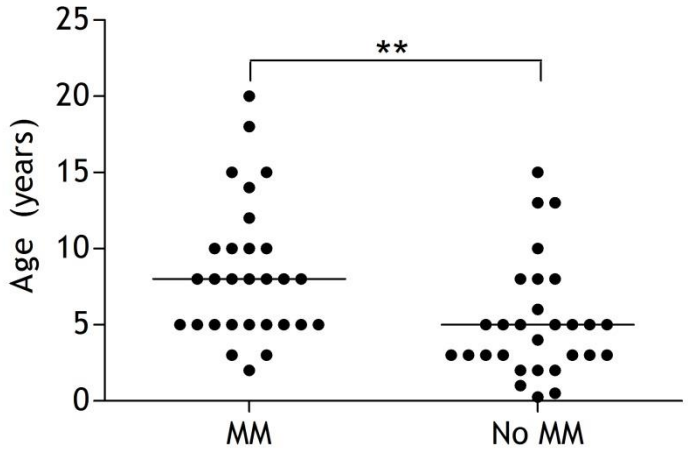

Figure 5.9: Showing age differences between cats with and without meniscal mineralisation. Data presented as median. (Mann Whitney *U* test, ** represents P<0.01).

The number of cases showing different combinations of increased bone opacity, osteophytes, discrete areas of mineralisation and meniscal mineralisation are shown in Tables 5.7 and 5.8.

Features	Increase bone opacity	Osteophytes	Areas of abnormal mineralisation	Meniscal mineralisation
Increase bone opacity		30	8	24
Osteophytes	30		8	20
Areas of abnormal mineralisation	8	8		8
Meniscal mineralisation	24	20	8	

Table 5.7: Showing numbers of left stifle joints with combinations of radiographic features.

Features	Increase bone opacity	Osteophytes	Areas of abnormal mineralisation	Meniscal mineralisation
Increase bone opacity		26	8	21
Osteophytes	26		7	15
Areas of abnormal mineralisation	8	7		8
Meniscal mineralisation	21	15	8	

Table 5.8: Showing numbers of right stifle joints with combinations of radiographic features.

Synovial effusion was identified in 41 (44.1%) of 93 St-rOA joints, bilaterally in 8 cats and unilaterally in 25 cats (11 on the left and 14 on the right). The effusion was identified by loss of the infrapatellar fat pad shadow in the stifle joint, by distension of the joint capsule and by displacement (or loss of clarity) of the gastrocnemius fascial planes caudal to the stifle joint (Figure 5.10.B).

Joint remodelling was observed in 7 (7.5%) of the 93 St-rOA joints (2 cats with bilateral and 3 cats with unilateral involvement) identified as changes in anatomical shape of the femoral and tibial plateau, fabellae and the patella (Figure 5.11).

Of the 93 St-rOA joints, 24 (25.8%) had only one fabella visible and 69 (74.2%) had 2 fabellae visible (bilaterally in 31 cats and unilaterally in 7 cats) (Figure 5.12). Of 69 joints with 2 fabellae visible, 24 (36.4%) had new bone formation on the fabella (Figure 5.11). Of 23 no St-rOA joints, 16 (69.6%) had one fabella and 7 (30.4%) had two fabellae visible.

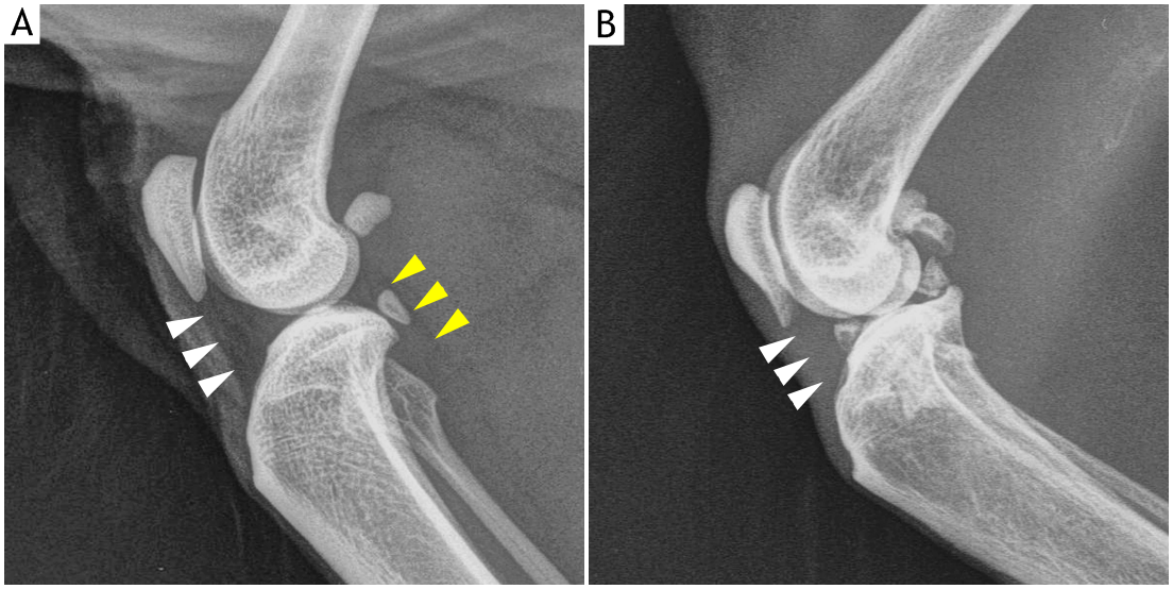

Figure 5.10: Mediolateral radiographs of right stifle joint showing synovial effusion.

(A) Normal stifle joint. The infrapatellar fat pad appears normal (white arrowheads) as does the gastrocnemius fascial plane (yellow arrowheads). Cat ID: X51, left stifle. (B) Joint effusion is present with complete loss of the infrapatellar fat pad shadow (white arrows) and gastrocnemius facial plane. Cat ID: X27, right stifle.

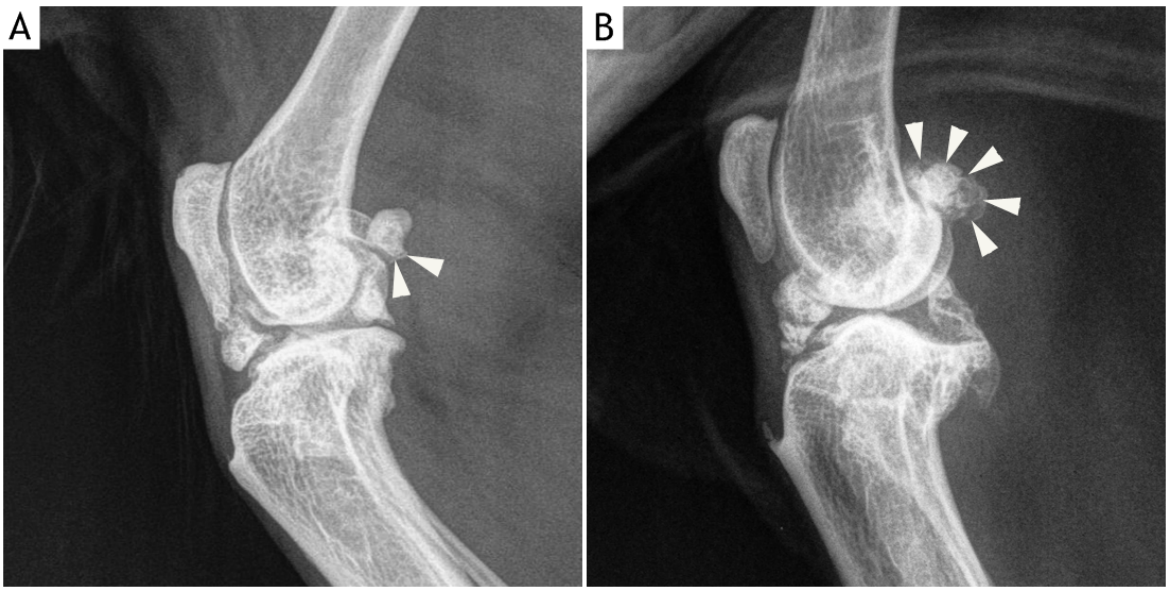

Figure 5.11: Mediolateral radiographs of left stifle joint with severe OA showing marked remodelling.

(A & B) A change in anatomical shape of the distal femoral condyle, tibial plateau, patella and fabellae is observed in both joints. Note the presence of new bone formation on the fabellae (white arrowheads). A: Cat ID: X36, left stifle; B: Cat ID: X42, right stifle.

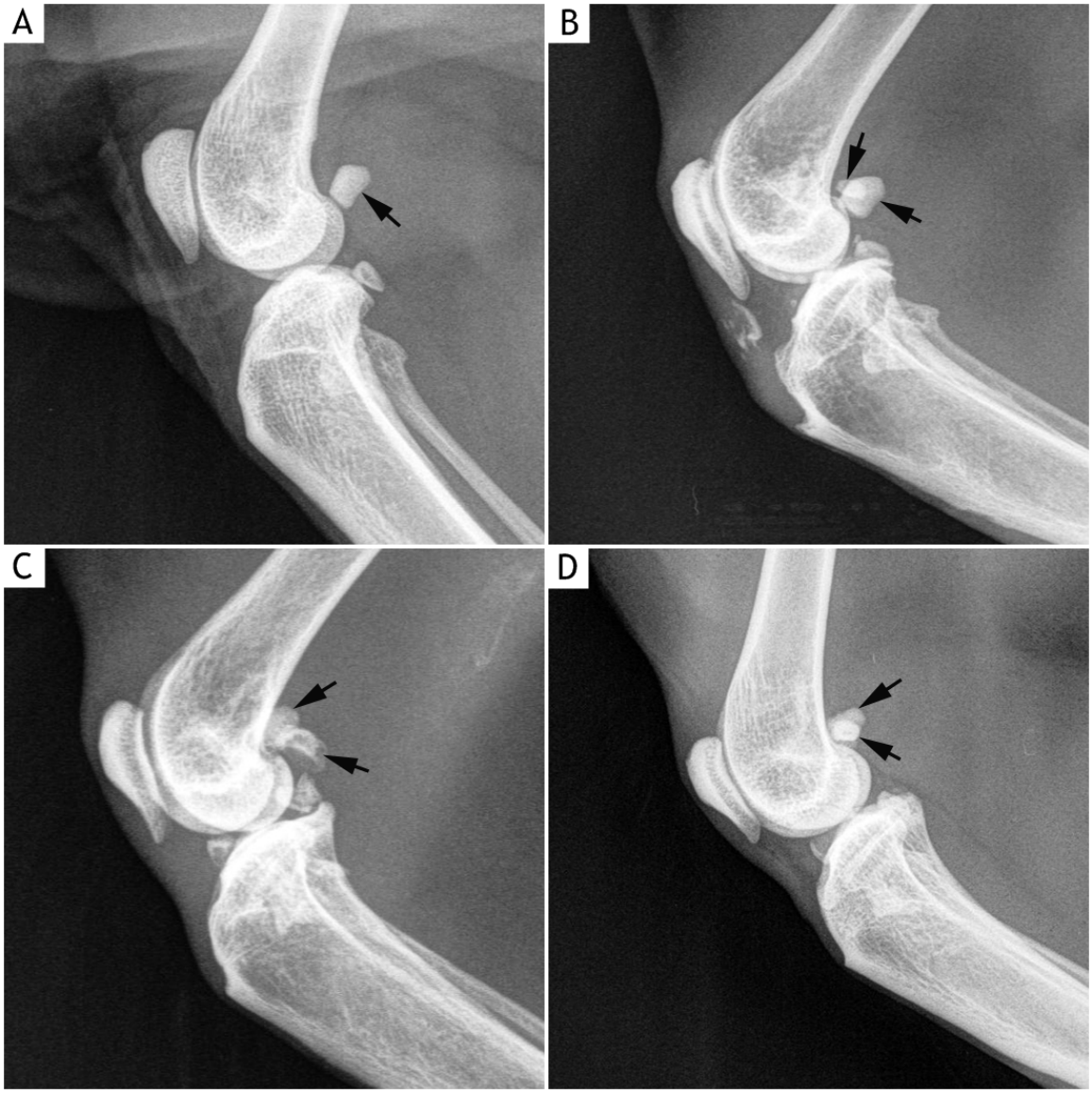

Figure 5.12: Mediolateral radiographs of stifle joints illustrating the presence of 1 or 2 fabellae.

(A) Normal stifle joint with 1 fabella visible (black arrow). (B - D) Examples of OA stifle joints with 2 fabellae visible (black arrows).

5.3.4 Gross pathologic findings

Gross pathologic examinations were performed on 116 stifle joints from 58 cats. The overall prevalence of St-path OA was 87.9% (51 of 58 cats). Of 51 cats with cartilage abnormalities, 48 cats had bilateral and 3 cats had unilateral stifle involvement (2 on the left and 1 on the right giving a total number of 99 (85.3%) St-path OA joints (Table 5.9). Of 99 St-path OA joints, 78 were given a Global score of 1, 18 were given a Global score of 2 and 3 a Global score of 3 (Table 5.10). The total gross pathologic score possible was 62; the highest score recorded was 42 (Table 5.11). The median gross pathologic total scores for left and right St-path OA joints was 9 and 10 respectively. . The total gross pathologic scores were not significantly different between left and right St-path OA joints (P=0.42). Seven cats (12.1%) had grossly normal articular cartilage on both left and right femoral condyles, tibial plateaus and patellae. Three cats (5.2%) had unilateral grossly normal articular cartilage (1 on the left and 2 on the right side), thus giving a total of 17 no St-path OA/normal joints (Global score 0) (Table 5.9).

A healthy femoral condyle, tibial plateau and patella had a glistening white and smooth articular surface (Figures 5.13.A and 5.14.A). Of 99 St-path OA joints, 75 (75.8%) had cartilage changes on the femoral condyle, tibial plateau and patella, 12 (12.1%) had cartilage changes on the femoral condyle and tibial plateau, 2 (2.0%) had cartilage changes on the tibial plateau and patella, 9 (9.1%) had cartilage changes on the tibial plateau only and 1 (1.0%) had cartilage changes on the femoral condyle only. Twelve (12.1%) stifle joints had only the medial femorotibial compartment affected (7 on the left and 5 on the right side).

Dull and yellow cartilage discolouration were seen in 97/99 (98.0%) stifle joints (Figure 5.14.B). Cartilage fibrillation was seen in all St-path OA joints, characterised by focal to diffuse cartilage roughness. Thirty-seven (37.4%) stifle joints had cartilage erosion, seen as a partial loss of articular cartilage (Figures 5.13.C-D and 5.14.C-D). Cartilage ulceration was identified in 14/99 (14.1%) stifle joints (Figure 5.13.D). The articular cartilage damage scores on the medial femoral condyle and tibial plateau were significantly greater (P<0.001) than on the lateral side in both left and right stifle joints (Figure 5.15).

Osteophyte formation was observed in 81/99 (81.8%) St-path OA joints. The osteophytes were commonly seen along the trochlear margin (Figure 5.16), at the lateral and medial margins of the tibial plateau (Figures 5.17.A-C) and at the distal pole of the patella (Figure 5.17.D). In 52 stifle joints osteophyte development was mild, in 25 it was

moderate and in 4 stifle joints it was severe. All St-rOA joints with increased radio-opacity on the distal femoral condyle and tibial plateau had osteophyte formation along the trochlear margin and tibial plateau.

In all 49 joints with radiographically evident MM, the mineralisation was identified grossly at the cranial horn of the medial meniscus. The meniscus was typically enlarged and distorted (Figure 5.18.B), with discolouration of the surface (dull and yellow compared with the normal smooth, white and glistening surface) (Figure 5.18.A). Of the 49 stifle joints with radiographically apparent MM, 47 had gross articular cartilage abnormalities. Of these 47 stifle joints, 42 had gross cartilage changes and osteophytes (Figures 5.18.C-D) and 5 had gross cartilage changes only. Only 2 stifle joints with radiographically visible MM had no gross cartilage changes. Fifty-two joints without radiographically evident MM had gross articular cartilage pathology. Irrespective of the MM status, all the cartilage changes were more pronounced in the medial femorotibial compartment of the joint. The cartilage damage scores of the medial femoral condyle and tibial plateau were significantly higher in joints with a radiographically visible MM (mean FC=3.4; mean TP=3.7) than those joints without a radiographically visible MM (mean FC=1.7; mean TP=2.2) ($P<0.001$) (Figure 5.19).

The areas of abnormal mineralisation (other than meniscal mineralisation) appeared grossly as calcified plaques attached to the infrapatellar fat pad and joint capsule (Figures 5.20.A-B) and in some cases the area of mineralisation had its surface covered by fibrocartilage which was articulating with the medial tibial plateau (Figure 5.20.B). Osteochondromas were seen in 2 stifle joints (of two different cats). These were attached to the synovium and protruded into the articular cavity (Figures 5.20.C-D).

Thickening of the joint capsule and discolouration of the synovium were observed in 9 (9.1%) and 30 (30.3%) joints respectively (Figure 5.18.C). Joint remodelling (changes in shape of the femoral condyle, tibial plateau, fabella and patella) was identified in 13 (13.1%) joints (Figures 5.16.D, 5.16.F, 5.17.C and 5.18.C-D).

A complete rupture of the CCL was not identified in any stifle joint. Degenerative changes were observed in 2/99 CCLs from OA stifle joints. The degenerated CCLs were characterised by a dull, rough and yellow appearance (Figure 5.21.A).

Gross pathologic examinations revealed the presence of one fabella and two fabellae in 34/116 and 82/116 stifle joints respectively. There were 6 St-path OA joints with two fabellae which were not radiographically visible. Of 69 St-rOA joints with two

radiographically visible fabellae, 67 had gross cartilage changes. Of 7 no St-rOA joints with two radiographically visible fabellae, 3 had gross cartilage changes thus giving a total number of 70 (70.1%) St-path OA joints with 2 fabellae (35 on the left and 35 on the right). The mean gross cartilage damage scores (femoral condyle, tibial plateau and patella) for the left joints with two fabellae was significantly higher than those without ($P<0.01$) (Figure 5.22.A). A similar finding was also observed in the right stifle ($P<0.05$) (Figure 5.22.B). Of 17 no St-path OA/normal joints, 11 (64.7%) had only one fabella visible and 6 (35.3%) had 2 fabellae visible radiographically.

	Gross pathologic findings			
	No St-path OA		St-path OA	
	Number of Joints	Percentage (%)	Number of joints	Percentage (%)
Left stifle	8	13.8	50	86.2
Right stifle	9	15.5	49	84.5
Total	17	14.7	99	85.3

Table 5.9: Showing numbers of stifle joints with normal and abnormal gross pathologic findings. Total number of joints 116.

	Gross pathologic OA Global scores			
	Score 0	Score 1	Score 2	Score 3
Left stifle	8	40	8	2
Right stifle	9	38	10	1
Total	17	78	18	3

Table 5.10: Showing the number of stifle joints with different gross pathologic OA Global Scores.

Cat ID	Cartilage surface discolouration		Cartilage fibrillation		Cartilage erosion		Cartilage ulceration		Osteophytes		Joint remodelling		Thickening of joint capsule		Synovium discolouration		Total score		Global Score		Sample for histopathologic examination
	L	R	L	R	L	R	L	R	L	R	L	R	L	R	L	R	L	R	L	R	
X1	4	5	6	6	0	1	0	0	1	1	0	0	0	0	0	0	11	13	1	1	CBS-L, †,
X2	0	0	0	0	0	0	0	0	0	0	0	0	0	0	0	0	0	0	0	0	CBS-L&R, †
X3	3	5	3	10	0	3	0	2	0	1	0	0	0	0	0	1	6	22	1	2	†
X4	1	0	2	0	0	0	0	0	1	0	0	0	0	0	0	0	4	0	1	0	†
X5	1	3	2	5	0	0	0	0	1	1	0	0	0	0	0	0	4	9	1	1	CBS-R, †
X6	0	5	2	4	0	0	0	0	0	1	0	0	0	0	0	0	2	10	1	1	†
X7	5	5	8	9	3	3	1	1	2	2	0	0	0	0	0	0	19	20	2	2	CBS-L&R, †, Δ
X8	4	4	2	4	1	0	0	0	1	0	0	0	0	0	0	0	8	8	1	1	†
X9	0	1	0	1	0	0	0	0	0	1	0	0	0	0	0	0	0	3	0	1	†
X10	0	0	0	0	0	0	0	0	0	0	0	0	0	0	0	0	0	0	0	0	CBS-L, †
X11	2	1	1	1	0	0	0	0	1	1	0	0	0	0	0	0	4	3	1	1	†
X12	5	5	8	7	5	2	0	0	2	1	0	0	0	0	1	0	21	15	2	1	CBS-L, †, Δ
X13	2	2	1	1	0	0	0	0	0	0	0	0	0	0	0	0	3	3	1	1	†
X14	0	0	0	0	0	0	0	0	0	0	0	0	0	0	0	0	0	0	0	0	CBS-L&R, †, Δ
X15	4	4	4	5	2	0	0	0	1	1	0	0	0	0	0	0	11	10	1	1	†
X16	4	3	4	3	0	0	0	0	2	2	0	0	0	0	0	1	10	9	1	1	CBS-L, †
X17	4	4	3	3	0	0	0	0	0	0	0	0	0	0	0	0	7	7	1	1	†
X18	5	5	9	8	4	3	0	0	3	2	0	0	0	0	1	1	22	19	2	2	CBS-L, †, Δ
X19	0	0	0	0	0	0	0	0	0	0	0	0	0	0	0	0	0	0	0	0	CBS-L&R, †, Δ
X20	1	2	3	3	0	0	0	0	0	1	0	0	0	0	0	0	4	6	1	1	CBS-L, †

Table 5.11: Gross pathologic scores and Global scores of the left (L) and right (R) stifle joints in 58 cats. Scoring for cartilage changes represents the total cartilage damage score arrived at by summing the individual scores (medial femoral condyle, lateral femoral condyle, medial tibial plateau, lateral tibial plateau and the patella). Global score: 0: normal, 1: mild, 2: moderate, 3: severe. Samples selected for histopathologic examination: CBS-L: Cartilage Bone Synovium-Left; CBS-R: Cartilage Bone Synovium-Right; CBS-L&R: Cartilage Bone Synovium-Left and right; OST: Osteochondromas; †: Menisci; Δ: Cranial cruciate ligaments from left and right stifle joints.

Cat ID	Cartilage surface discolouration		Cartilage fibrillation		Cartilage erosion		Cartilage ulceration		Osteophytes		Joint remodelling		Thickening of joint capsule		Synovium discolouration		Total score		Global Score		Sample for histopathologic examination
	L	R	L	R	L	R	L	R	L	R	L	R	L	R	L	R	L	R	L	R	†
X21	1	5	2	4	0	0	0	0	0	0	0	0	0	0	0	1	3	10	1	1	†
X22	5	5	6	7	0	0	0	1	1	0	0	0	0	0	0	0	12	13	1	1	†, Δ
X23	4	5	4	5	0	0	0	0	1	1	0	0	0	0	0	0	9	11	1	1	CBS-L, †
X24	3	2	7	3	2	0	0	0	1	0	0	0	0	0	0	0	13	5	1	1	†
X25	0	2	1	1	0	0	0	0	0	0	0	0	0	0	0	0	1	3	1	1	†
X26	5	5	11	3	1	0	3	0	2	1	0	0	0	0	0	0	22	9	2	1	CBS-L, †
X27	5	5	8	11	3	7	0	0	1	2	0	0	0	1	0	1	17	27	1	2	†
X28	4	5	4	10	0	4	0	3	2	2	0	0	0	0	0	1	10	25	1	2	CBS-R,OST, †
X29	4	5	3	3	0	0	0	0	1	0	0	0	0	0	0	0	8	8	1	1	†
X30	5	5	12	8	5	3	4	0	2	2	1	0	0	0	1	0	30	18	2	2	CBS-L&R, †, Δ
X31	5	5	8	7	3	2	0	0	2	2	1	1	0	0	0	0	19	17	2	1	CBS-R, †
X32	5	5	6	7	3	4	0	0	2	2	0	1	0	0	1	1	17	20	1	2	†
X33	3	0	2	0	0	0	0	0	0	0	0	0	0	0	0	0	5	0	1	0	†
X34	5	5	4	4	0	1	0	0	1	1	0	0	0	0	1	1	11	12	1	1	CBS-R, †
X35	3	5	6	6	0	1	0	0	2	2	1	0	0	0	0	0	12	14	1	1	†
X36	5	5	13	4	11	1	5	0	3	2	1	0	2	1	1	1	41	14	3	1	CBS-L, †, Δ
X37	5	5	10	8	3	3	1	1	2	2	1	1	0	1	1	1	23	22	2	2	CBS-L&R, †,
X38	4	4	7	3	2	0	0	0	2	1	0	0	0	0	0	0	15	8	1	1	†
X39	4	5	4	6	0	0	0	0	1	1	0	0	0	0	0	0	9	12	1	1	†
X40	4	4	2	5	0	1	0	0	1	1	0	0	0	0	0	0	7	11	1	1	CBS-R, †
X41	3	5	5	4	0	0	0	0	1	1	0	0	0	0	0	0	9	10	1	1	†

Table 5.11 continued.

Cat ID	Cartilage surface discolouration		Cartilage fibrillation		Cartilage erosion		Cartilage ulceration		Osteophytes		Joint remodelling		Thickening of joint capsule		Synovium discolouration		Total score		Global Score		Sample for histopathologic examination
	L	R	L	R	L	R	L	R	L	R	L	R	L	R	L	R	L	R	L	R	
X42	5	5	12	11	9	8	7	6	3	3	2	3	2	2	2	2	42	40	3	3	CBS-L&R,OST, †, Δ
X43	5	3	3	2	0	0	0	0	1	1	0	0	0	0	0	0	9	6	1	1	†
X44	1	5	1	5	0	0	0	0	1	1	0	0	0	0	0	0	3	11	1	1	†
X45	5	5	9	8	5	5	0	1	2	2	1	1	2	2	1	1	25	25	2	2	CBS-L&R, †, Δ
X46	4	3	4	4	0	0	0	0	1	0	0	0	0	0	0	0	9	7	1	1	†
X47	4	4	4	4	1	0	0	0	1	1	0	0	0	0	1	1	11	10	1	1	CBS-L, †
X48	4	4	4	6	0	1	0	0	2	1	1	0	0	0	1	0	12	12	1	1	†
X49	4	5	4	8	0	5	0	2	1	1	0	0	0	0	0	0	9	21	1	2	CBS-R, †
X50	2	2	3	3	0	0	0	0	1	1	0	0	0	0	0	1	6	7	1	1	†
X51	0	0	0	0	0	0	0	0	0	0	0	0	0	0	0	0	0	0	0	0	CBS-R, †, Δ
X52	0	0	0	0	0	0	0	0	0	0	0	0	0	0	0	0	0	0	0	0	CBS-L, †, Δ
X53	0	0	0	0	0	0	0	0	0	0	0	0	0	0	0	0	0	0	0	0	CBS-L, †, Δ
X54	4	5	5	3	0	0	0	0	1	1	0	0	0	0	1	1	12	9	1	1	†, Δ
X55	4	1	4	2	0	0	0	0	0	1	0	0	0	0	0	0	8	4	1	1	†, Δ
X56	4	5	6	7	0	1	0	0	1	1	0	0	0	1	1	1	12	16	1	1	CBS-R, †
X57	4	3	3	3	0	0	0	0	1	1	0	0	0	0	0	1	8	8	1	1	†
X58	1	2	2	4	0	0	0	0	1	1	0	0	0	0	0	0	4	7	1	1	CBS-L,†

Table 5.11 continued.

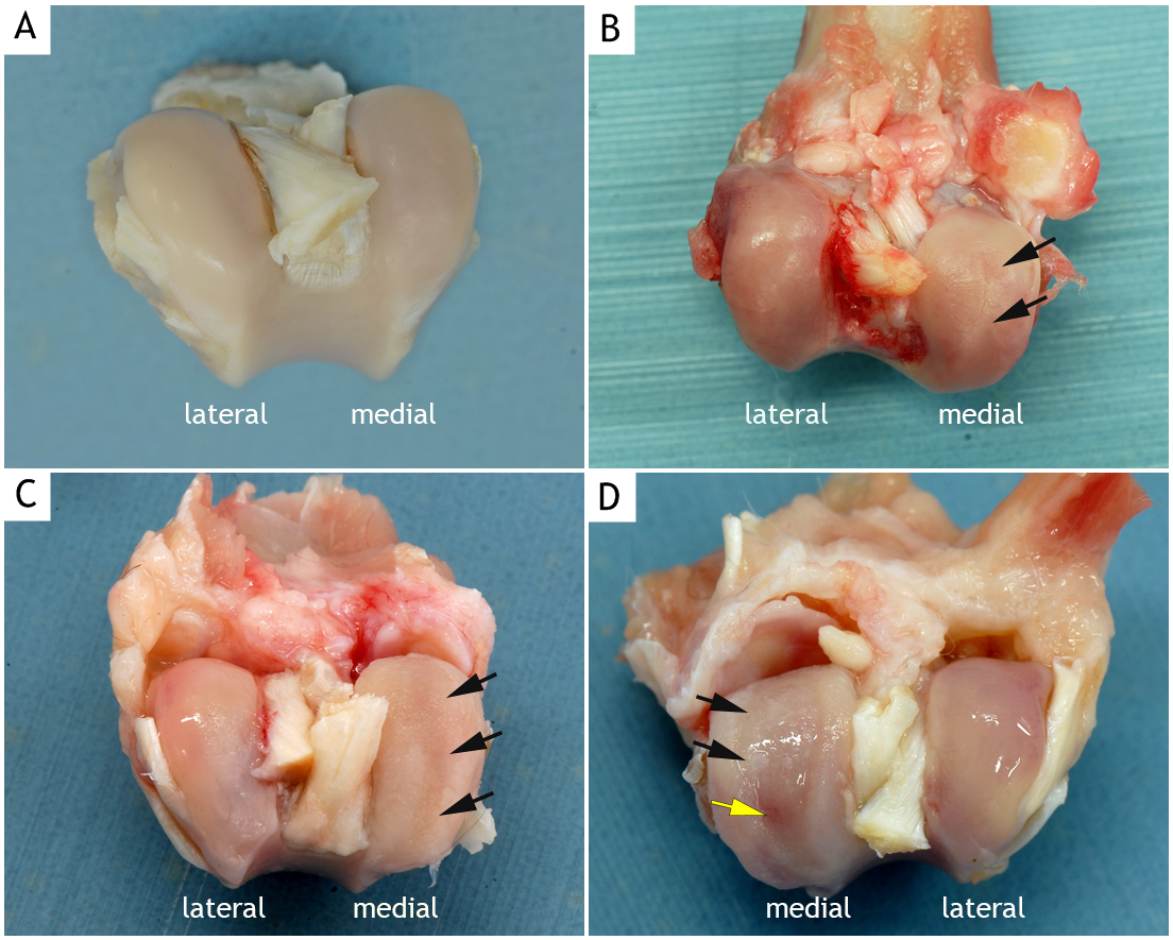

Figure 5.13: Examples of gross cartilage changes of the distal femoral condyles of the stifle joint.

(A) Normal distal femoral condyle. Note the smooth appearance of the articular cartilage. The joint had been fixed in formalin prior to photographing. Cat ID: X51, left stifle. (B) Mild changes with increase in fibrillation or roughening of the articular surface of the medial femoral condyle (arrows). The medial femoral condyle is duller than the lateral (see Figure 5.5.B for radiograph). Cat ID: X50, left stifle. (C) Moderate articular changes with cartilage loss and erosions particularly on the medial femoral condyle (arrows). A yellowish articular discolouration is seen on both medial and lateral femoral condyles which also appear dull (see Figure 5.7.C for radiograph). Cat ID: X15, left stifle. (D) Severe changes with loss of cartilage, erosions (black arrows) and ulceration (yellow arrow) particularly on the medial femoral condyle (see Figures 5.6.E-F for radiographs). Cat ID: X42, right stifle.

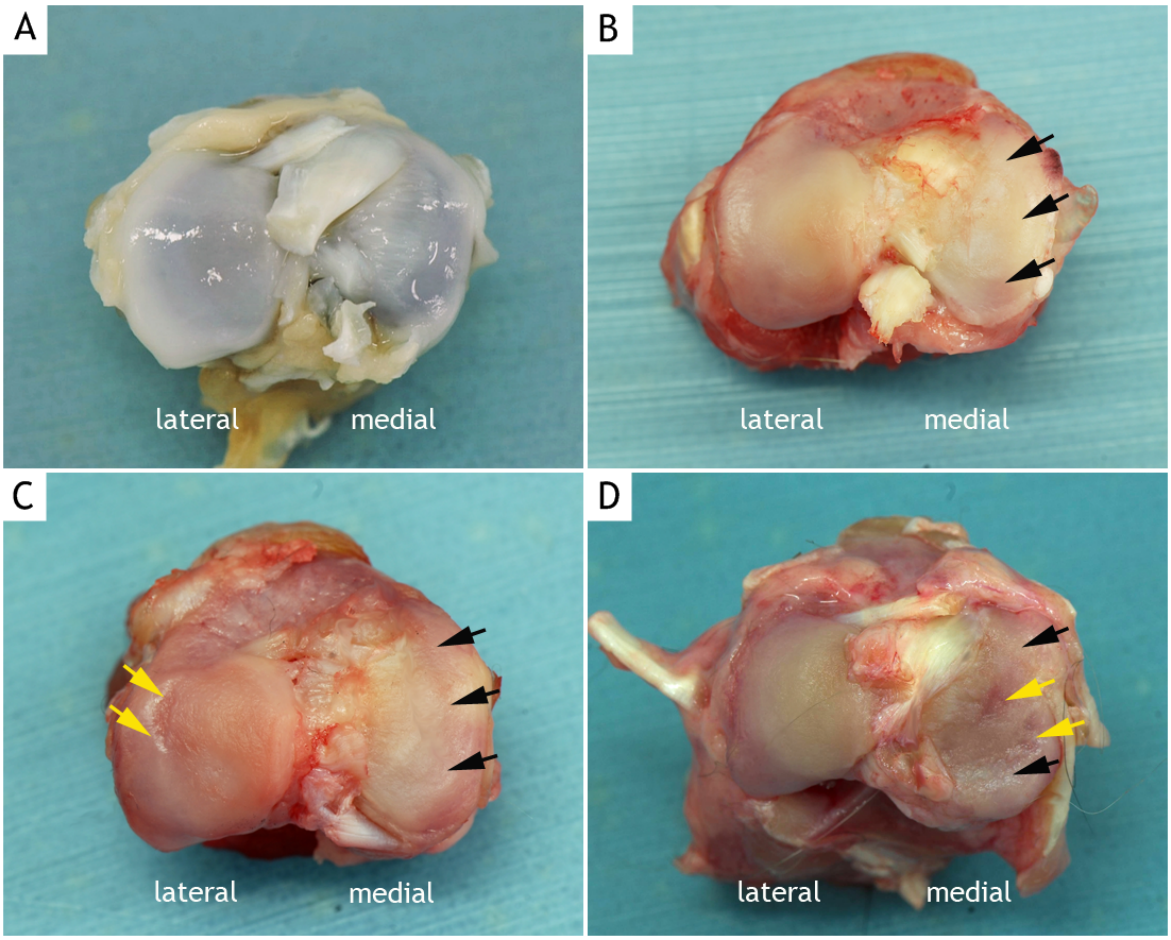

Figure 5.14: Examples of gross cartilage changes of tibial plateau of the stifle joint.

(A) Normal tibial plateau of the stifle joint. The articular surface is white, smooth and shiny. Cat ID: X51, left stifle (B) Mild articular fibrillation (black arrows) is seen on the medial part of the tibial plateau. Cartilage discolouration is also observed. Cat ID: X50, left stilfe. (C) Moderate fibrillation (black arrows) is observed particularly on the medial part of the tibial plateau. Cartilage erosion is seen on the lateral part of the tibial plateau (yellow arrows). (D) Severe cartilage fibrillation (black arrows) and erosion (yellow arrows) is identified on the medial part of the tibial plateau. Mild fibrillation and cartilage discolouration is also observed on the lateral part of the tibial plateau. Cat ID: X30, left stifle.

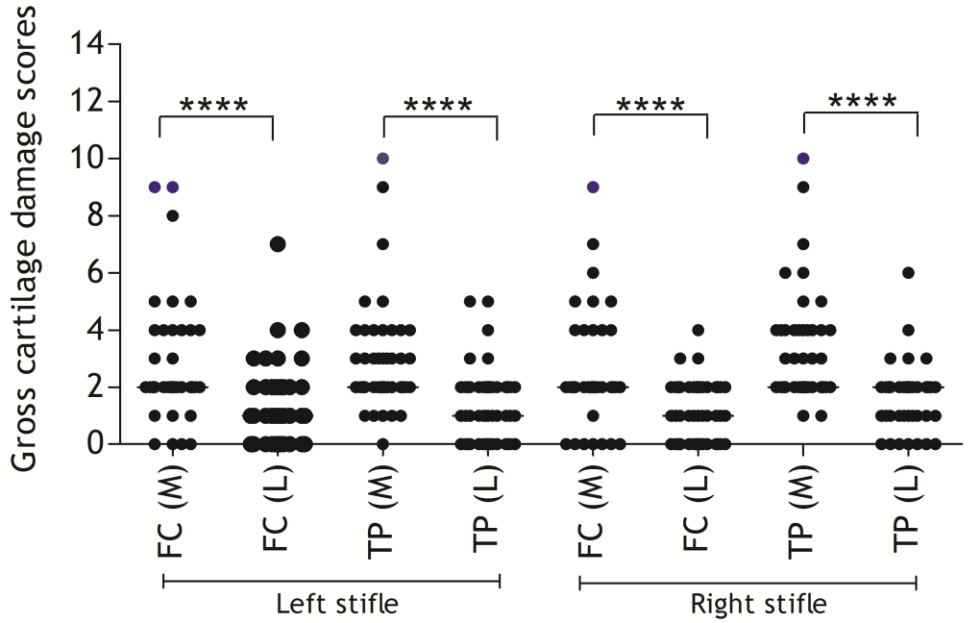

Figure 5.15: Comparison of gross cartilage damage scores of medial (M) and lateral (L) femoral condyles (FC) and medial and lateral part of the tibial plateaus (TP) of left and right stifle joints. The gross cartilage damage scores were significantly different between medial and lateral FC and medial and lateral part of the TP in both stifle joints. Data presented as median. Outliers are represented as blue-coloured dots. (Wilcoxon Signed rank test, ** represents P<0.001).**

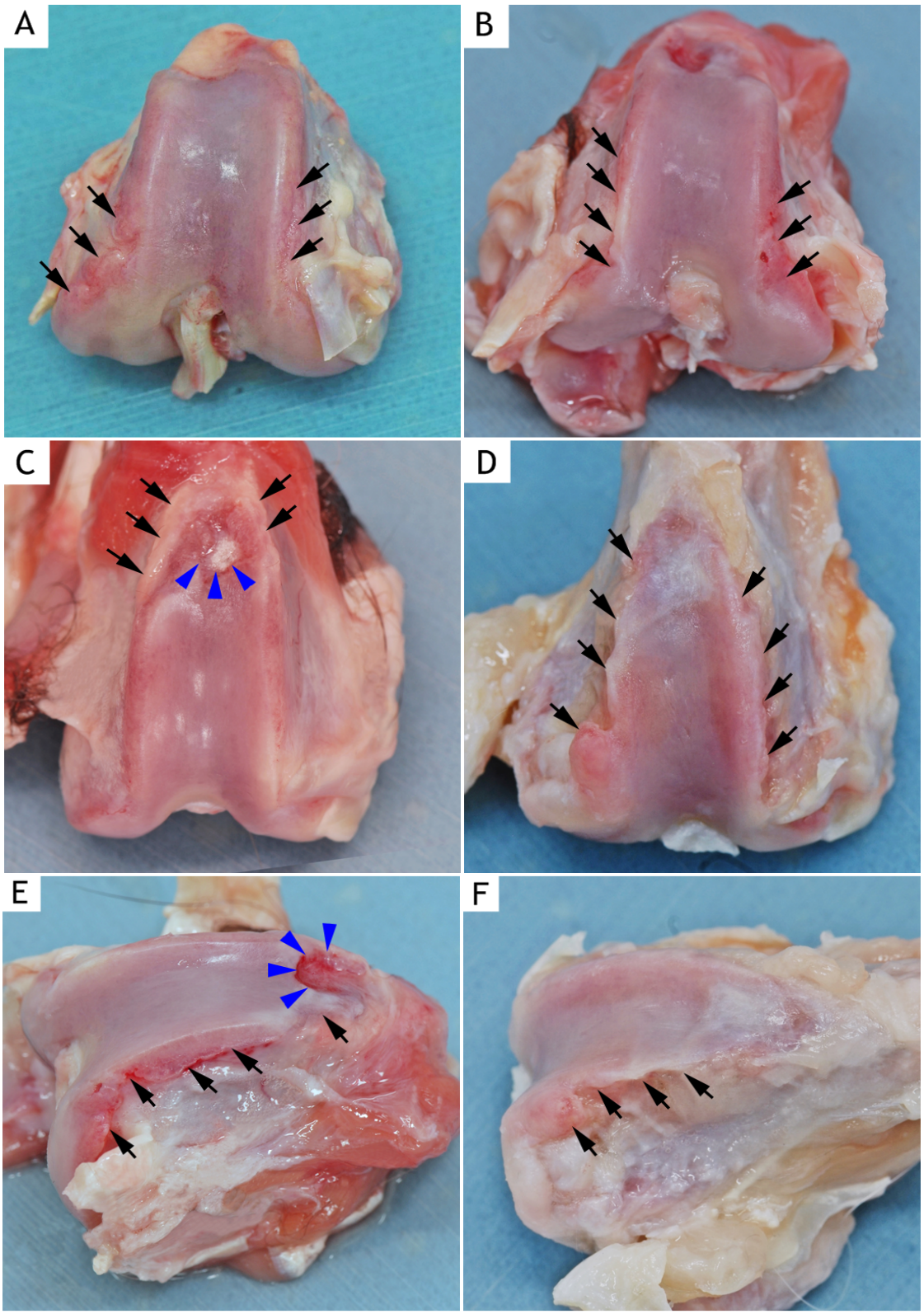

Figure 5.16: Examples of osteophyte formation on the distal femoral condyles of the stifle joint.

(A - F) Osteophytes (black arrows) can be identified along the trochlear margin of the distal femur. Osteophyte formation at these areas is seen as an increased radio-opacity of the femoral condyle (see Figures 5.7.B-D for radiographs). (C & E) Osteophyte formation (blue arrowheads) is seen at the proximal part of the trochlear groove. Joint remodelling is observed in (D) and (F). A: Cat ID: X15, left stifle; B: Cat ID: X32, right stifle; C: Cat ID: X26, left stifle; D: Cat ID: X42, left stifle; E: Cat ID: X7, right stifle; F: Cat ID: X42, right stifle.

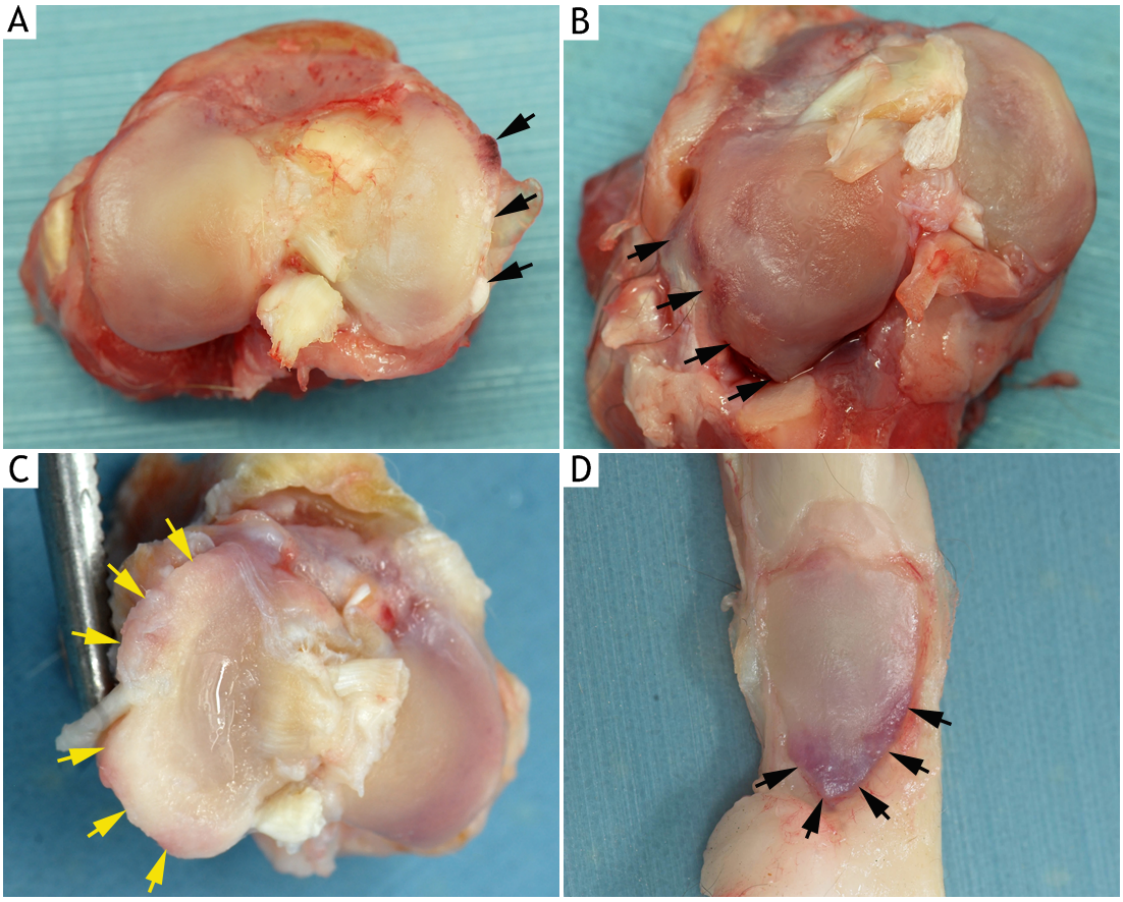

Figure 5.17: Examples of osteophyte formation on the tibial plateau and patella of the stifle joint.

(A) Mild Osteophyte formation is seen at the margin of the medial part of the tibial plateau (black arrows). Cat ID: X50, left stilfe. (B) Moderate osteophyte formation is identified at the margin of the lateral part of the tibial plateau. Osteophyte formation at these areas is seen as an increased radio-opacity of the tibial plateau (see Figure 5.7.D for radiograph). Cartilage fibrillation and erosion are also observed on both the medial and lateral part of the tibial plateau. Cat ID: X26, left stifle. (C) Joint remodelling and extensive osteophyte formation is observed at the margin of the medial part of the tibial plateau (yellow arrows) (see Figure 5.11.B for radiograph). Cat ID: X42, right stifle. (D) Osteophytes are seen on the distal part of the patella (black arrows) (see Figure 5.4.D for radiograph). Cat ID: X36, left stifle.

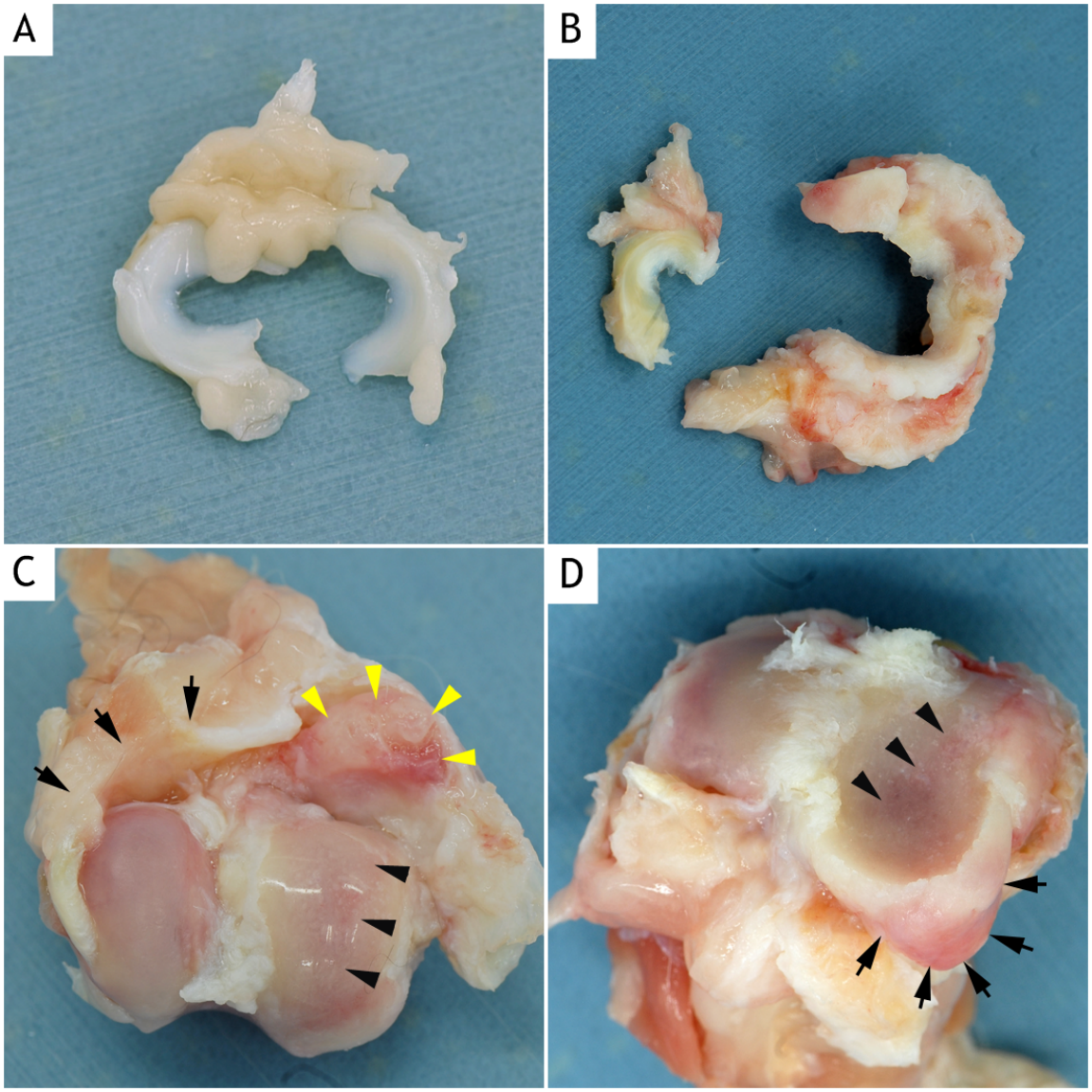

Figure 5.18: Examples of normal and mineralised menisci of the stifle joint.

(A) Photographs of lateral and medial menisci taken from a normal feline stifle joint. Normal menisci are white, smooth and shiny in appearance. Cat ID: X51, left stifle. (B) Menisci from Cat X42 which had radiographic intra-articular mineralisation. The affected medial meniscus is discoloured, enlarged and distorted. (C) Joint from Cat X42 shows severe loss of articular cartilage particularly of the medial femoral condyle (black arrowheads). Remodelling of the medial fabella is also observed (yellow arrowheads). Thickening of the joint capsule is obvious (black arrows). (D) Cartilage changes particularly on the medial part of the tibial plateau is also seen in Cat X42 (black arrowheads). Joint remodelling with obvious osteophyte formation (black arrows) at the caudal aspect of the medial tibial plateau is also observed. B, C and D: Cat ID: X42, left stifle.

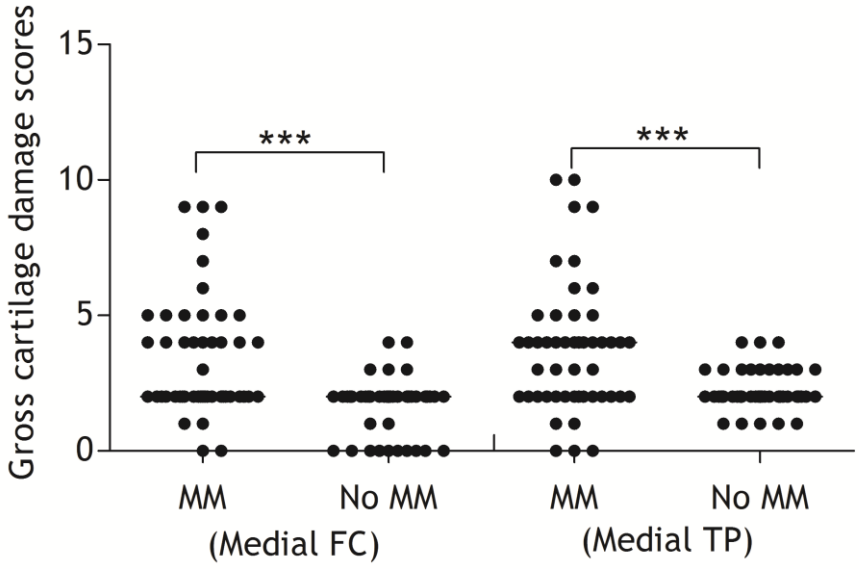

Figure 5.19: Comparison of the gross cartilage damage scores of the medial femoral condyles (FC) and tibia plateau (TP) of joints with and without a radiographically evident meniscal mineralisation (MM). The gross cartilage damage scores were significantly higher in stifle joints with visible MM than in stifle joints without. Data presented as median. (Mann Whitney *U* test, * represents P<0.001).**

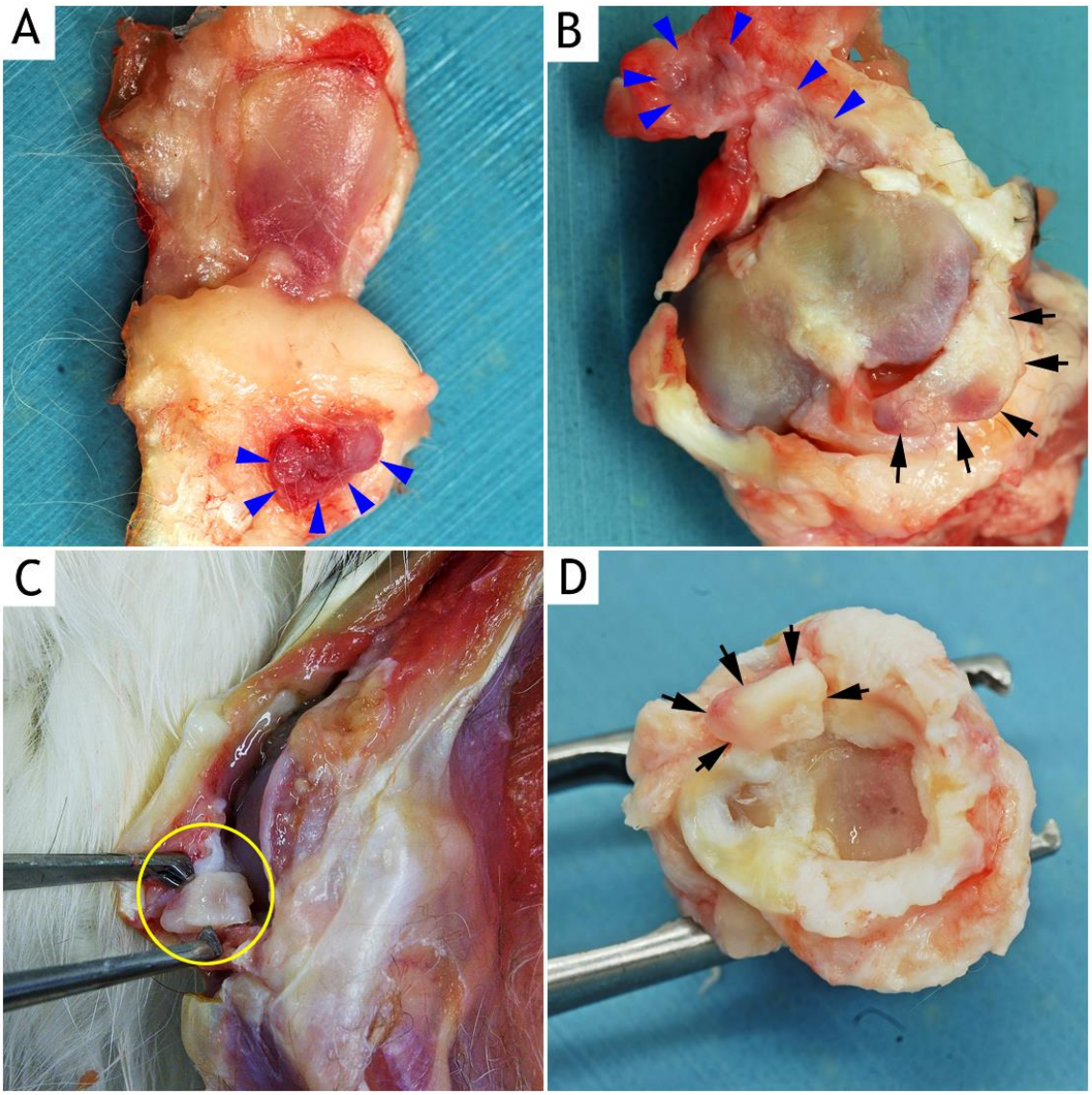

Figure 5.20: Showing examples of abnormal mineralisation within the joint capsule.

(A & B) Areas of mineralisation appear as calcified plaques attached to the infra-patellar fat pad (blue arrowheads). There is also a calcified plaque (black arrows) where its proximal surface is articulating with the medial tibial plateau. A: Cat ID: X18, left stifle; B: Cat ID: X36, left stifle. (C) An osteochondroma (circle) is seen on the surface of the synovium (see Figures 5.6.E-F for radiographs). Cat ID: X42, right stifle. (D) An osteochondroma (black arrows) is attached to the synovial membrane and located at the cranial part of the tibial plateau. Cat ID: X42, left stifle.

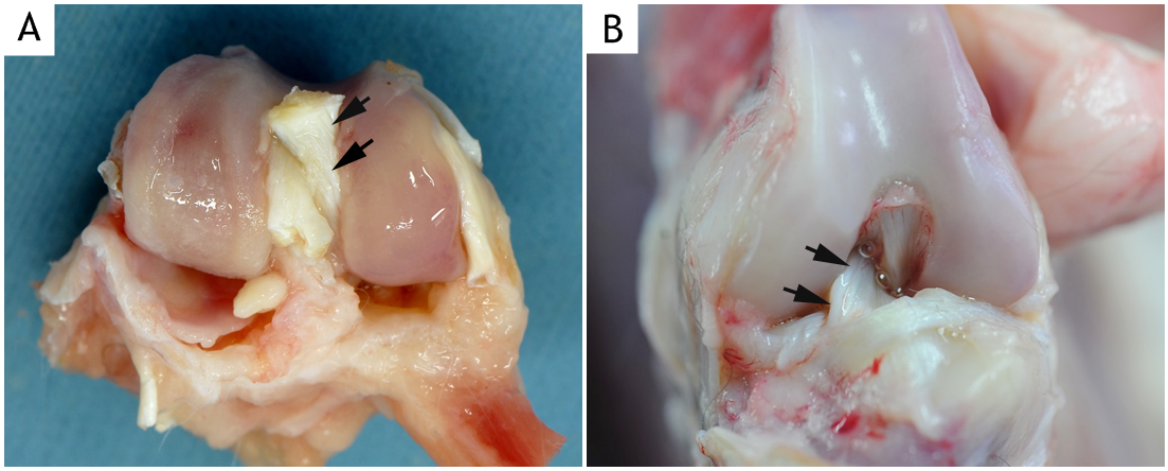

Figure 5.21: Showing example of degenerative changes of cranial cruciate ligament.

(A) The degenerated CCL is discoloured, dull and rough in appearance (black arrows). There is also severe cartilage change on the medial femoral condyle. Cat ID: X42: left stifle. (B) Normal CCL is identified by its shiny white and smooth appearance (black arrows). Cat ID: X53, right stifle.

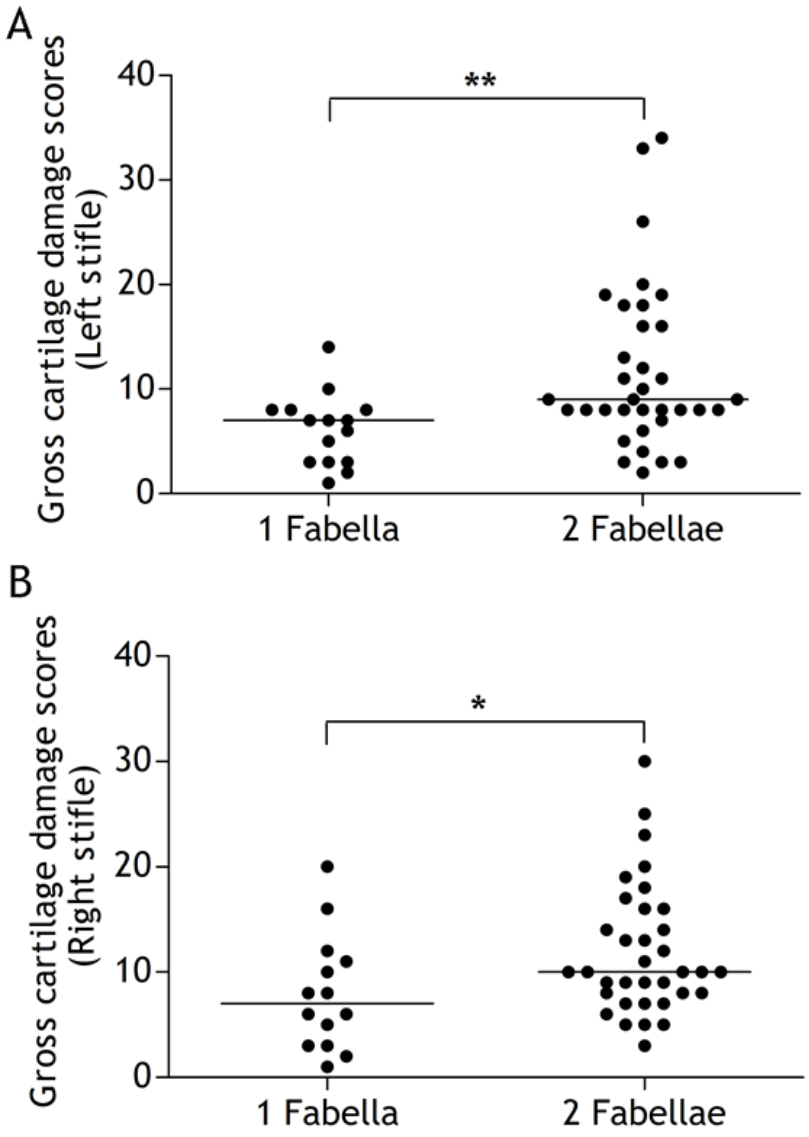

Figure 5.22: Comparison of the gross cartilage damage scores of the femoral condyles, tibial plateau and patella of left (A) and right (B) stifle joints with one and two radiographically visible fabellae. The gross cartilage damage scores were significantly higher in stifle joints with 2 fabellae than in those with just one. Data presented as median. (Mann Whitney *U* test, ** represents P<0.01 and * represents P<0.05).

5.3.5 Correlation studies

5.3.5.1 Correlation between total radiographic and gross pathologic OA scores

Of 23 radiographically normal joints, 6 (26.1%) had gross lesions. There was a significant good positive correlation between the radiographic and gross pathologic total scores in both left (r_s=0.71, P<0.0001) and right (r_s=0.71, P<0.0001) stifle joints (Figures 5.23.A and 5.23.B).

5.3.5.2 Correlation between radiographic size of MM and cartilage damage scores

The radiographic size of the MM was significantly correlated with the cartilage damage scores of medial femoral condyle and medial tibial plateau. This correlation was moderate with both medial femoral (r_s=0.64, P<0.0001) and tibial (r_s=0.65, P<0.0001) plateau.

5.3.5.3 Correlation between total radiographic scores and age, BW and BCS

There was a significant moderate positive correlation between the radiographic total score of the left (r_s=0.44, P<0.001) and right (r_s=0.51, P<0.0001) stifle joints and age (Figures 5.24.A and 5.24.B). There was a slight, negative relationship between the radiographic total score of the left (r_s=-0.13, P=0.33) and right (r_s=-0.24, P=0.10) stifle joints and BW, which was not statistically significant (Figures 5.24.C and 5.24.D). A similar finding was also observed between the total radiographic score of the left (r_s=-0.13, P=0.31) and right (r_s=-0.23, P=0.10) stifle joints and BCS (Figures 5.24.E and 5.24.F).

5.3.5.4 Correlation between total gross pathologic OA score and age, BW and BCS

Correlation analysis revealed a significant moderate positive relationship between the total gross pathologic score of the left (r_s=0.41, P<0.01) and right (r_s=0.41, P<0.01) stifle joints and age (Figures 5.25.A and 4.25.B). Correlation analysis revealed a fair and slight negative relationship between the total gross pathologic score of the left (r_s=-0.24, P=0.10) and right (r_s=-0.17, P=0.20) stifle joints and BW respectively (Figures 5.25.C and 5.25.D). However, the relationships were not statistically significant. A similar finding was also observed between the total gross pathologic score of the left (r_s=-0.23, P=0.10) and right (r_s=-0.17, P=0.21) stifle joints and BCS (Figures 5.25.E and 5.25.F).

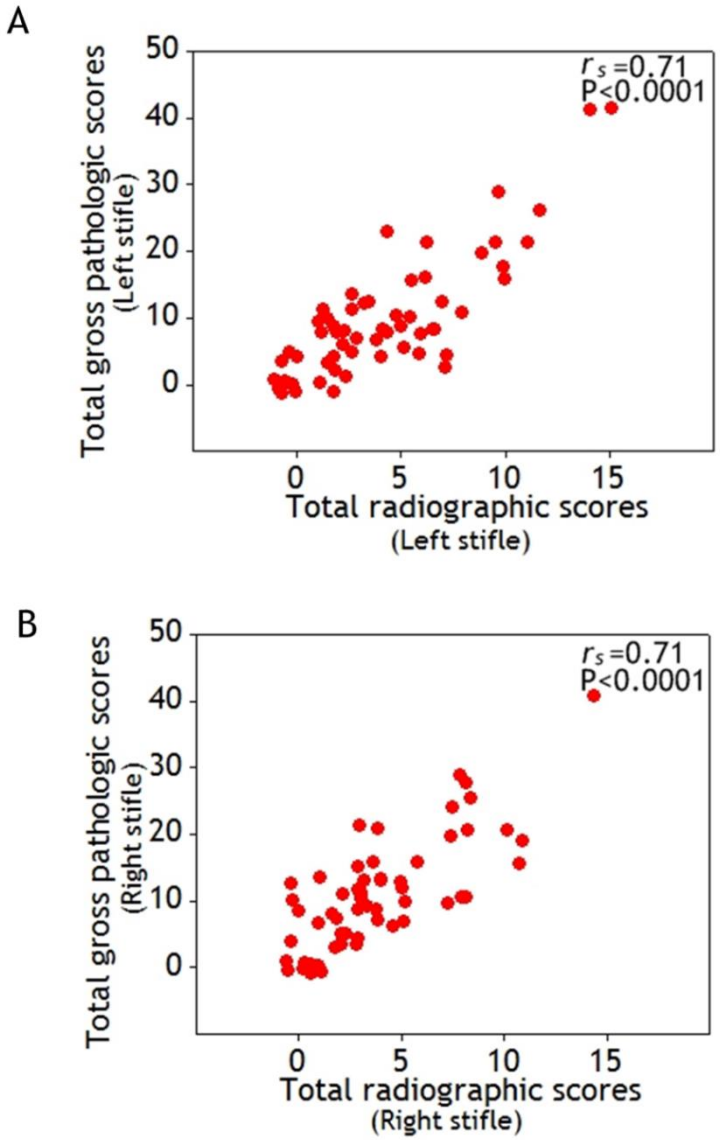

Figure 5.23: Graph demonstrating correlation between radiographic and gross pathologic OA scores in left (A) and right (B) stifle joints. There is a good significant relationship between the radiographic and gross pathologic scores in both left and right stifle joints.

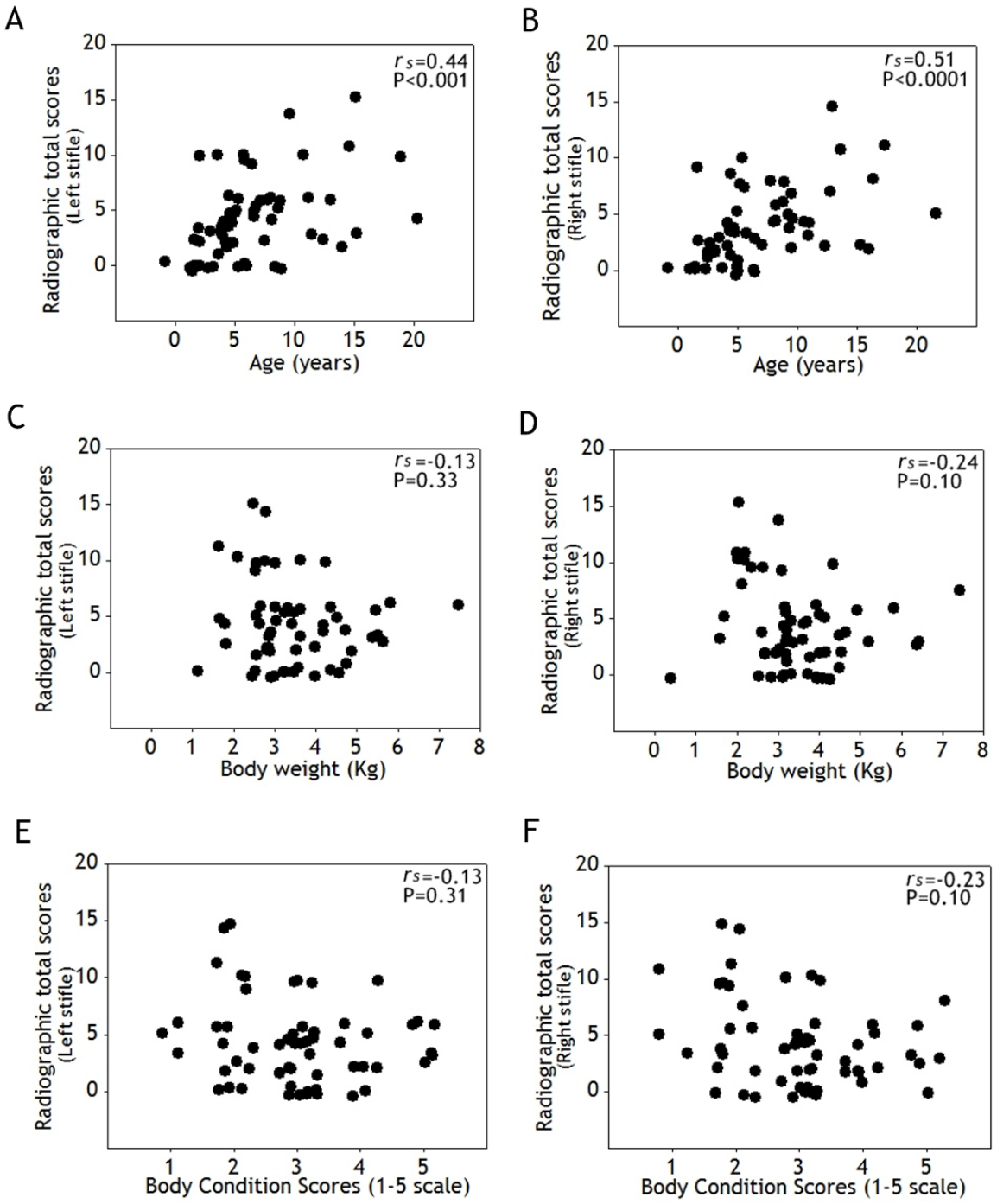

Figure 5.24: Correlation analysis of total radiographic scores of the left (A, C, and E) and right (B, D, and F) stifle joints and age, BW and BCS. (A & B) A significant moderate positive relationship between radiographic total scores of the left and right stifle joints and age. (C & D) Correlation analysis of radiographic total scores of the left and right stifle joints and BW. (E & F) Correlation analysis of radiographic total scores of the left and right stifle joints and BCS. There are no significant relationships between the radiographic total scores of the left and right stifle joint and BW and BCS.

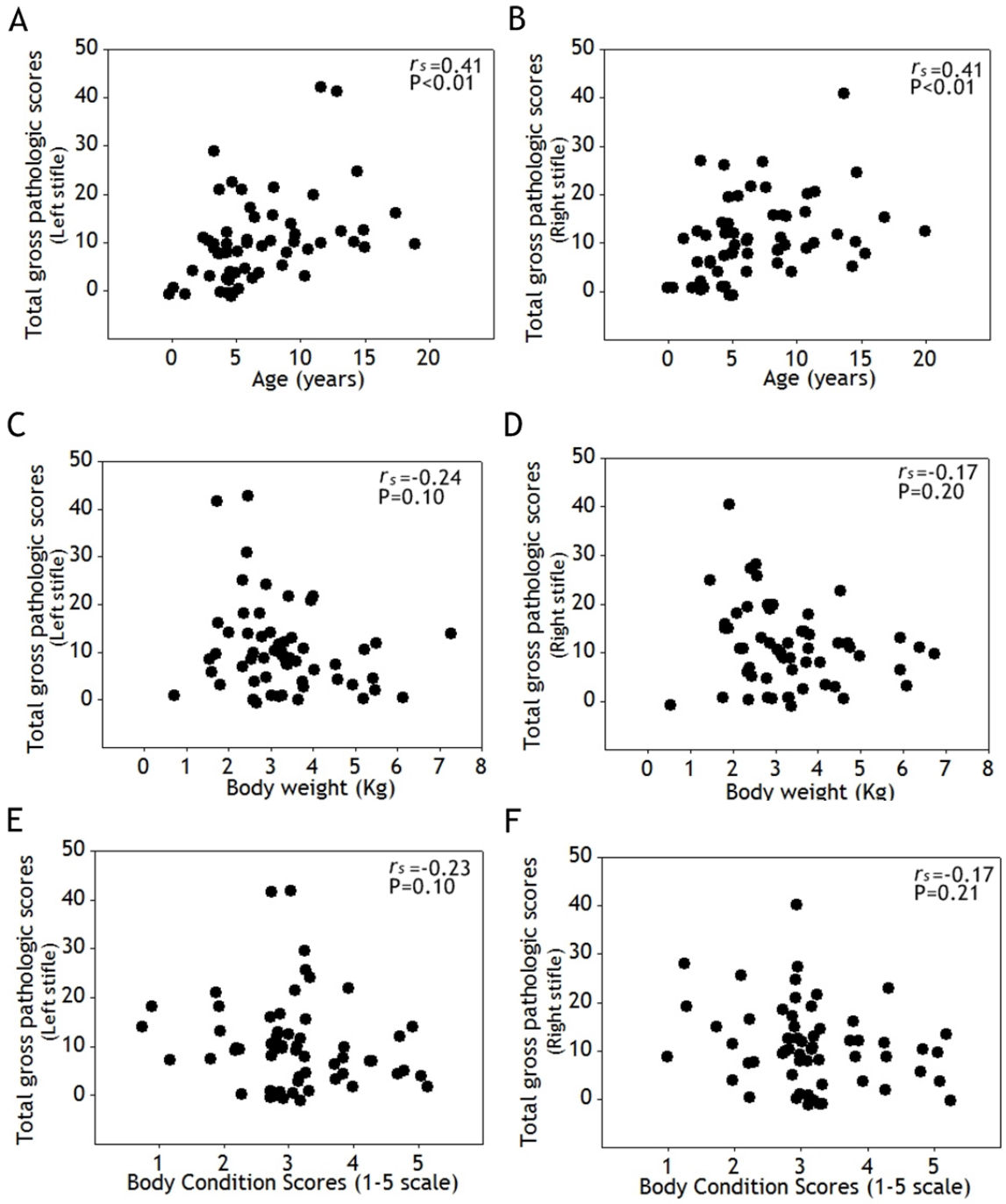

Figure 5.25: Correlation analysis of total gross pathologic scores of the left (A, C, and E) and right (B, D, and F) stifle joints with age, BW and BCS. (A & B) A significant moderate positive relationship between gross pathologic scores of the left and right stifle joints and age. (C & D) Correlation analysis of gross pathologic scores of the left and right stifle joints and BW. (E & F) Correlation analysis of gross pathologic scores of the left and right stifle joints and BCS. There are no significant relationships between the gross pathologic scores of the left and right stifle joint with BW and BCS.

5.4 Discussion

The results of the present study demonstrated a high prevalence of St-rOA (86.2%; 50 of 58 cats) and St-path OA (87.9%; 51 of 58 cats). The overall prevalence of St-rOA and St-path OA joints was 80.2% (93 of 116 joints) and 85.3% (99 of 116 joints) respectively. The radiographic prevalence of the stifle joint reported in the present study was considerably higher than the 63.0% and 65.0% reported by Lascelles et al. (2010) and Freire et al. (2011), probably because of the differences in defining the radiographic features of stifle OA. These groups defined stifle OA by the presence of osteophytes, enthesiophytes, joint-associated mineralisation, joint effusion, sclerosis, subchondral bone erosions and cysts and meniscal mineralisation. In the present study, increased radio-opacity of the femoral condyle and tibial plateau was scored independently and new bone formation on the fabellae was included as an indicator of OA, and this probably contributed to the higher prevalence.

The main radiographic features of stifle OA were osteophytes, increased radio-opacity of the femoral condyle and tibial plateau, presence of meniscal mineralisation, synovial effusion, new bone formation affecting the fabellae and the presence of extra-articular enthesiophytes. Abnormal areas of mineralisation (other than meniscal mineralisation) and joint remodelling were seen but were less frequent.

Osteophytes are a key radiographic feature of stifle OA. In the present study, osteophytes were seen in 57 stifle joints of 36 cats which is similar to that previously reported (Godfrey, 2007). Identification of osteophytes in the stifle joint is easier on a mediolateral view, perhaps because it allows evaluation of both femorotibial and femoropatellar joints thus increasing the sensitivity of the radiographic diagnosis of OA (Chaisson et al., 2000; Godfrey 2007). Most commonly seen was an osteophyte projecting caudally from the caudal edge of the tibial plateau (Figures 5.4.B-D, 5.6, 5.10.B). Osteophytes projecting from the cranial edge of the tibial plateau near the attachment of the cranial cruciate ligament were also seen (Figure 5.4.D). Based on its location there has been an argument that this lesion showed be classified as an enthesiophyte of the cranial cruciate ligament. Morgan (1999) stated this feature could represent both an enthesiophyte and an osteophyte in stifle joints of dogs. In the present study gross pathologic examination has confirmed that the lesion should be described as an osteophyte located at the cranial edge of the tibial plateau (Figure 5.17.C). Osteophytes were commonly seen at the proximal aspect of the femoral trochlea (Figures 5.4.C and 5.16.C). Osteophytes were also seen affecting the femoropatellar joint. Differentiation between enthesiophytes at the attachment of the

quadriceps muscle and osteophytes on the proximal and distal poles of the patella was made based on the location and shape. Increased-radio opacity was common in the stifle joint. It was particularly visible on the distal femoral condyle, along the trochlear margin, but also beneath the tibial plateau. This radio-opacity is, at least in part, a reflection of the marginal osteophytes on the surface of the bone as seen in Figures 5.16 and 5.17. Subchondral bone thickening may also help explain this feature (see Chapter 8).

Extra-articular enthesiophytes were mainly identified at the attachment of the patellar ligament to the tibial tuberosity. This site was also the commonest location recorded in cats by Godfrey (2007). Enthesiophyte formation may occur as a response to repetitive strain or without any clear reason (Rogers et al., 1997).

Areas of abnormal mineralisation (other than meniscal mineralisation) were less common (17/93 joints; 18.3%), and represented mineralisation of the joint capsule or osteochondromas. This feature was recorded in 15/61 (25%) stifle joints by Godfrey (2007). Innes et al. (2004) reported that periarticular mineralisation was an uncommon feature of canine stifle joints with OA secondary to cranial cruciate ligament rupture.

A number of stifle joints (49/93) in this study had radiographically detectable MM. There are several different hypotheses for MM, including primary ossification centres, normal anatomical features of development, and the result of meniscal degeneration as part of OA (Pederson 1949; Jorgensen and Jensen 2002; Walker et al., 2002; Freire et al., 2010). Those cats where the MM was radiographically visible were significantly older (mean 8.4 years) than those without (mean 5.1 years) and the joints tended to have more severe changes in the articular cartilage particularly in the medial compartment of the joint, consistent with the findings of Freire et al. (2010) and Ariffin et al. (2013). Radiographic size of MM was moderately correlated with gross cartilage damage score of the medial femoral condyle and medial tibial plateau, suggesting that the risk of severe cartilage damage increased in a linear fashion with increasing MM size. Meniscal mineralisation was radiographically visible in only two stifle joints (one cat) where the articular cartilage was normal and which could have a represented a primary intrameniscal calcification. Primary ossification of the lateral menisci has been reported in a dog with no other abnormalities observed (Weber, 1998).

Menisci are important for the normal mechanical functions of the stifle joint. Calcification of the meniscus may affect its elasticity and cause stiffness thus altering its biomechanical properties, leading to a gradual loss of function (Sun et al., 2010).

This in turn would affect its "shock absorbing" properties and this could lead to increased mechanical loading of the medial femoral condyle and medial part of the tibial plateau with resultant OA. Even if MM is not a primary aetiological factor in feline stifle OA it could be a contributory factor and help explain the more severe disease of the medial compartment of the stifle joint. Mineralisation of the lateral meniscus was never identified in this study, either radiographically, grossly or histopathologically (See Chapter 8).

Synovial effusion was radiographically observed in 41/93 stifle joints. However, on gross pathologic examination synovial effusion was only confirmed in 20 cases. Computed radiograph (CR) may not be very useful for assessing synovial effusion in the cat stifle joint. It was difficult to assess synovial effusion radiographically in the present study and it is not clear whether part of this was due to the use of cadavers where the exact time of death was not always known. MRI has been reported in dogs with experimentally induced stifle OA (D'Anjou et al., 2008); the authors reported that the distribution of the synovial fluid is more easily assessed with MRI compared to CR.

The presence of two fabellae was radiographically identified in 76/116 (65.5%) stifle joints. Of the 76 joints, 70 had gross cartilage changes. The mean gross cartilage damage scores were significantly higher in left and right stifle joints with two fabellae visible than stifle joint with 1 fabella visible. The finding suggests that radiographic presence of 2 fabellae is associated with severe cartilage damage and is an indicator of stifle OA. In all mammals, the fabellae start as a nodule of hyaline cartilage that undergoes endochondral ossification (Sarin and Carter, 2000). The fabellae begin to ossify by way of multiple ossific nuclei which rapidly develop into a single ossification centre that spreads outward while preserving a layer of hyaline cartilage at the articular surface (Sarin and Carter, 2000). There is a general agreement that all cats have two fabellae, a lateral and medial fabella, located in the lateral and medial heads of the gastrocnemius muscle (Schaefer, 1932). Mineralisation of the lateral fabella can be seen as early as 3 months of age (Schaefer, 1932). The medial fabella is often not sufficiently mineralised and appears on a routine radiograph. Lack of mineralisation of the medial fabella is commonly observed in the domestic short haired and some pedigree cats like the Persian, and this has not been significantly related to sex, size of animal or any pathologic condition (Arnbjerg and Heje, 1993). The medial fabella is more likely to be seen in an arthritic joint where new bone deposition may occur as a result of the arthritic process. Pritchett (1984) retrospectively examined the incidence of fabellae in radiographically healthy and OA knees of 600 men. They found that men with primary OA of the knee had a significantly higher incidence of lateral fabellae than

did age-matched normal controls and suggested that the presence of a fabella predisposed the knee to OA.

In all cases the CCL was intact. However, gross pathologic examination showed that degenerative changes were present in two CCLs from OA stifle joints. Degenerative changes of the CCL ("cruciate disease") have been reported in cats (Harasen, 2005), although is far less common than seen in the dog (Bennett et al., 1988). It is possible that cruciate disease might be a cause of stifle OA in the cat.

A good correlation between total radiographic scores and total gross pathologic scores was observed in both left and right stifle joints showing that more severe radiographic changes are associated with more severe gross pathology. A moderate positive correlation was found between the total radiographic scores and age in both stifle joints. This suggests that the severity of radiographic changes is moderately influenced by age in this study group. A similar finding was observed between the total gross pathologic scores and age in both stifle joints. Body weight and BCS were observed to be negatively associated with the severity of radiographic and gross pathologic OA in both stifle joints. This could be due to the consequence of age on BCS and body weight, where cats tend to have low BCS and lose weight as they become older (Kronfeld et al., 1994; Laflamme, 2005).

Apart from MM and cruciate ligament degeneration, there was no detectable underlying cause identified to explain a secondary OA, suggesting that stifle OA is mainly idiopathic or primary in nature, noticeably influenced by advancing age.

Chapter 6 Radiographic and pathologic features of osteoarthritis of the feline hip joint

6.1 Introduction and aims

The hip joint is a ball and socket articulation consisting of the femoral head and acetabulum. The femoral head has a convex articular surface, covered by articular cartilage except over a round depression, the fovea capitis femoris, which is located at the centre of the head (Dyce et al., 2010). The cavity of the acetabulum comprises of the convex articular lunate surface and the non-articular acetabular fossa. The non-articular acetabular fossa is continuous with the acetabular notch. The notch is converted into a foramen by the transverse acetabular ligament. The femoral head is joined to the acetabular fossa by the intracapsular ligament of the femoral head (Konig and Liebich, 2007). The edge of the acetabulum is surrounded by a fibrocartilagenous rim called the labrum. The joint has a spacious fibrous capsule which attaches proximally to the acetabular margin and distally to the neck of the femur.

Osteoarthritis of the hip joint is a common radiographic abnormality in cats. The most frequent radiographic changes are osteophyte formation on the dorsocranial acetabular rim and on the femoral neck (Kamishina and Miyabayashi, 2002). Increase in radio-opacity of the acetabulum and femoral head and remodelling are also common radiographic features of hip OA (Clarke et al., 2005; Godfrey, 2007).

A positive association between OA and hip dysplasia (HD) is frequently reported. Langenbach et al. (1998) evaluated the feline hip for HD and joint laxity. The hip joints were scored as being excellent, good, fair, borderline or having mild HD, moderate HD and severe HD, based on the criteria for canine HD as defined by the Orthopaedic Foundation for Animals (OFA). Mild HD is diagnosed when there is significant subluxation present and the femoral head is partially outside the acetabulum. In moderately affected joints the femoral head is barely seated into a shallow acetabulum and OA changes are observed. Severe HD is diagnosed when there is significant subluxation present and the femoral head is partly or completely outside the shallow acetabulum; severe OA changes are also evident. Joint laxity was determined by measuring the Norberg angle (NA). In addition, the distraction index (DI) was also used as an assessment for joint laxity using the PennHip method as described for dogs (Smith et al., 1990). HD was identified in 25/78 cats. Of these, 15 had OA and the NA of these cats (84.0 ° ± 10) was significantly lower than that of cats without OA (95.0 ° ± 5). The mean DI in cats with OA (0.6 ± 11) was significantly higher than that of cats with normal

hip joints (0.49 ± 0.14). They also reported that hip joints with a DI of less than 0.4 did not show any radiographic findings associated with OA. Smith et al. (1990) hypothesised that the higher the DI, the greater the hip laxity which increases the risk of developing hip dysplasia with OA.

Clarke et al. (2005) retrospectively reported the incidence of OA secondary to HD in 5/25 (20.0%) hip joints. They defined HD when there was less than 50 per cent of the femoral head covered by the dorsal acetabular rim on a ventrodorsal pelvic radiograph. Clarke and Bennett (2006) used the same method in the diagnosis of HD. They prospectively reported the incidence of HD in 11/56 (19.6%) hip joints. The NA of the hip joint was also measured. The mean NA for dysplastic hips with secondary OA, non-dysplastic hips with OA and normal hips was 87.5 °, 99.2 ° and 100.1 ° respectively. To date, there is no acceptable protocol for grading the severity of feline HD.

The aim of this study was to define the radiographic features of hip OA and to relate the radiographic findings to the gross pathologic features. In particular the following questions were to be addressed:

a) Can the radiographic features be a good indicator of the severity of cartilage pathology?

b) Are there any underlying causes of hip OA in the cat?

6.2 Materials and Methods

6.2.1 Determination of hip OA population

Determination of the hip OA population was done as described in Section 2.2, page 58 and Figure 2.1, page 59.

6.2.2 Comparative analyses of signalment, body weight and body condition score between Hip-path OA and no Hip-path/normal cats

Median of age, BW and BCS of Hip-path OA and no Hip-path OA/normal cats were illustrated with a scatter plot graph and statistically analysed by using Mann-Whitney *U* test. The distribution of breed and gender of Hip-path OA and no Hip-path OA/normal cats was visualised using a stacked bar graph. The distribution of BCS of Hip-path OA and no Hip-path OA/normal cats was shown by a column bar graph.

6.2.3 Radiographic assessment of the hip joint

Radiographic changes associated with hip OA were assessed using a radiographic scoring system (see Section 2.3.3, page 60 and Table 2.1, page 62). The radiographic features assessed were osteophytes, enthesiophytes, areas of abnormal mineralisation, increased radio-opacity of the femoral head/neck, changes in joint space, synovial effusion and joint remodelling. Changes in radio-opacity involving the articular margin of the femoral head and acetabulum were not assessed in this study. Hip dysplasia was assessed using the percentage coverage of the femoral head by the dorsal acetabular edge as described in Section 2.3.5, page 64 and Figure 2.2, page 65. The NA for each joint was determined. The mean percentage of femoral head covered ≥50% and <50% and the NA were calculated in Hip-rOA and no Hip-rOA joints. The 2-Sample t-test was used to compare mean NA of hip joints with ≥50% and <50% coverage and hip joints with or without OA. The total radiographic scores and the global scores were determined. The prevalence of Hip-rOA and no Hip-rOA was calculated as the percentage of cats which had or had no radiographic changes. The prevalence of each radiographic feature was determined as the percentage of affected hip joints which had the feature. The mean and SD of osteophyte size was calculated.

6.2.4 Gross pathologic assessment of the hip joint

Gross pathologic changes associated with OA were assessed and scored using a gross pathologic scoring system (see Section 2.4.1, page 66 and Table 2.3, page 67). The gross pathologic changes of the femoral head and acetabulum were not scored individually but given a single overall score. The total gross pathologic scores and the global scores were determined. The prevalence of Hip-path OA and no Hip-path OA/normal were determined as the percentage of cats which had or had no gross changes in the articular cartilage. The prevalence of each gross pathologic feature was calculated as the percentage of affected hip joints which had the feature. The Wilcoxon signed rank test was used to analyse the difference between total gross pathologic scores of the left and right hip joints. The results were illustrated with a scatter plot graph.

6.2.5 Correlation studies

6.2.5.1 Correlation between total radiographic and gross pathologic OA scores

A correlation analysis between total radiographic and gross pathologic scores for the left and right hip joints was performed using a nonparametric, Spearman's rank

correlation. Correlation coefficient results were interpreted as described in Table 2.9, page 80. The correlation was illustrated by scatter plot graphs.

6.2.5.2 Correlation between total radiographic OA scores and age, BW and BCS

A correlation analysis between total radiographic OA scores for the left and right hip joints and age, BW and BCS was carried out using Spearman's rank correlation. The coefficient results were interpreted as described in Table 2.9, page 80. The correlation for left and right hip joints was illustrated by scatter plot graphs.

6.2.5.3 Correlation between total gross pathologic OA scores and age, BW and BCS

A correlation analysis between total gross pathologic OA scores for the left and right hip joints and age, BW and BCS was done using a nonparametric, Spearman's rank correlation. The coefficient results were interpreted as described in Table 2.9, page 80. The correlation for left and right hip joints was illustrated by scatter plot graphs.

6.3 Results

6.3.1 Hip OA population

A total of 116 hip joints from 58 cats were evaluated for the radiographic signs of OA. Of 58 cats, 46 had radiographic changes associated with hip OA (Hip-rOA). All Hip-rOA cats had cartilage changes. Of 12 cats with radiographically normal hip joints (no Hip-rOA), 2 had cartilage changes, thus giving a total population of 48 cats with hip OA (Hip-path OA) (Table 6.1).

Population	Number of cats	Percentage (%)
Hip-rOA	46	79.3
No Hip-rOA	12	20.7
Hip-path OA	48	82.8
No Hip-path OA/normal	10	17.2

Table 6.1: Showing the number and percentage of the Hip-rOA, no Hip-rOA, Hip-path OA and no Hip-path OA/normal populations. Total number of cats is 58.

6.3.2 Comparative analyses of signalment, body weight and body condition score between Hip-path OA and no Hip-path OA/normal cats

6.3.2.1 Signalment

The mean age of the Hip-path OA cats was 7.5 years (SD 4.4) with a minimum age of 2 years and a maximum of 20 years. The median age was 5.5 years. The mean age of the no Hip-path OA/normal cats was 3.4 years (SD 2.3) with a minimum age of 3 months and a maximum of 8 years. The median age was 3 years. The age difference between the Hip-path OA and no Hip-path OA/normal cats was significant ($P<0.01$) (Figure 6.1.A). Fifteen Hip-path OA cats were MC, 8 cats were F and 25 cats were FS. One of the no Hip-path OA/normal cats was M, 3 cats were MC, 5 cats were F and 1 cat was FS. In the Hip-path OA group 79% were DSH, 13% were DLH and 8% were pedigree cats. In the no Hip-path OA/normal group 80% were DSH, 10% were DLH and 10% were pedigree cats (Figures 6.2.A and 6.2.B).

6.3.2.2 Body weight

The mean BW of the Hip-path OA cats was 3.4 kg (SD 1.1) with a minimum weight of 1.9 kg and a maximum of 7.0 kg. The median BW was 3.1 kg. The mean BW of the no St-path OA/normal cats was 3.5 kg (SD 1.1) with a minimum weight of 0.8 kg and a

maximum of 4.8 kg. The median was 3.6 kg. The BW difference between the Hip-path OA and no Hip-path OA/normal cats was not significant (P=0.42) (Figure 6.1.B).

6.3.2.3 Body condition score

The Hip-path OA cats had a median BCS of 3 with a minimum BCS of 1 and a maximum of 5. The no Hip-path OA/normal cats had a median 3 with a minimum BCS of 2 and a maximum of 5. There was no significant difference between BCS of the Hip-path OA and no Hip-path OA/normal cats (P=0.66) (Figure 6.1.C). The distribution of BCS of Hip-path OA and no Hip-path OA/normal cats is shown in Figure 6.3.

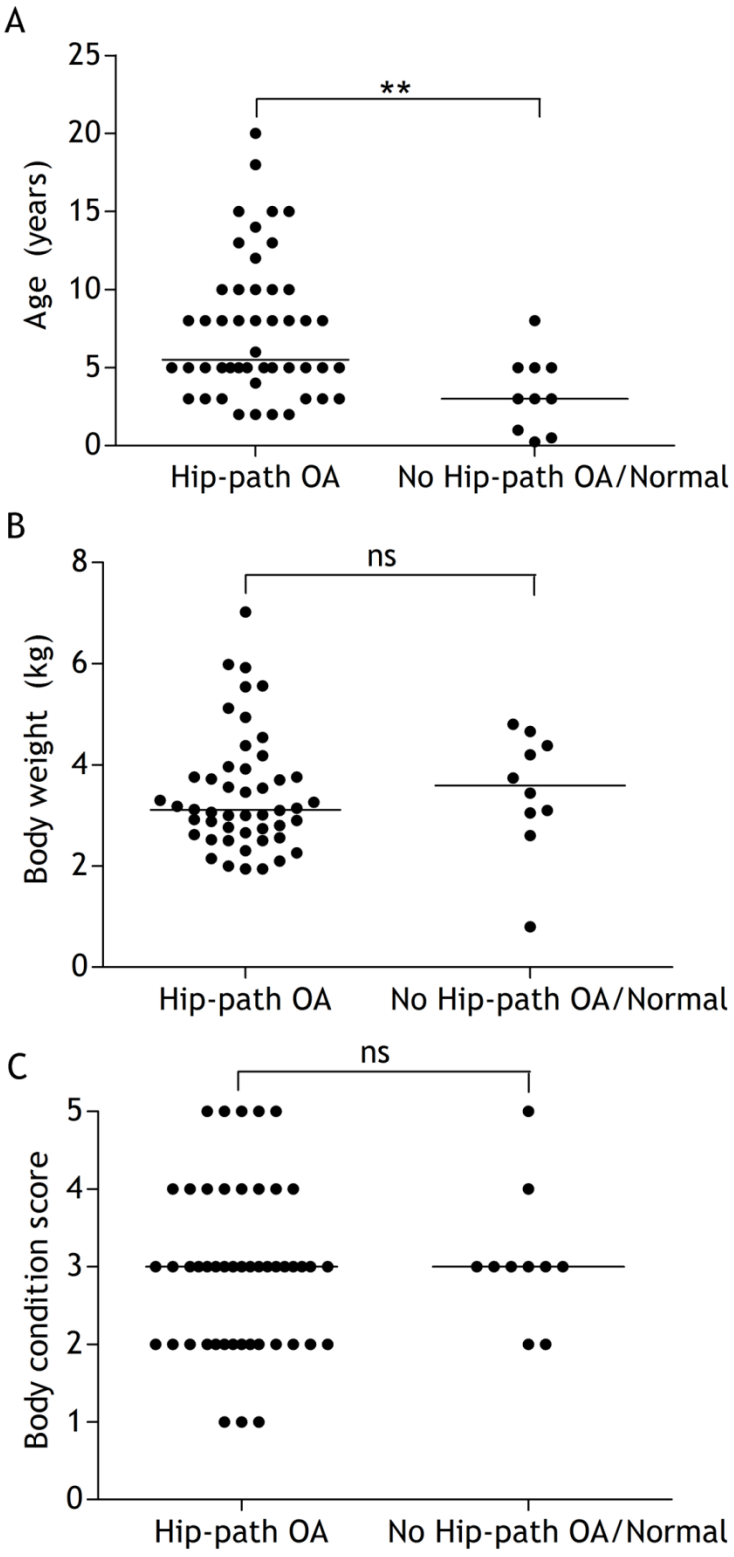

Figure 6.1: The comparative analysis of age, BW and BCS between Hip-path OA (*N*=48) and no Hip-path OA/normal (*N*=10) cats.

(A) The age difference between the Hip-path OA and No Hip-path/normal cats is significant. There is no significant difference in BW (B) and BCS (C) of cats with and without hip OA. Data presented as median and plotted in vertical scatter plot. (Mann Whitney *U* test, ** represents P<0.01; ns: not significant P>0.05).

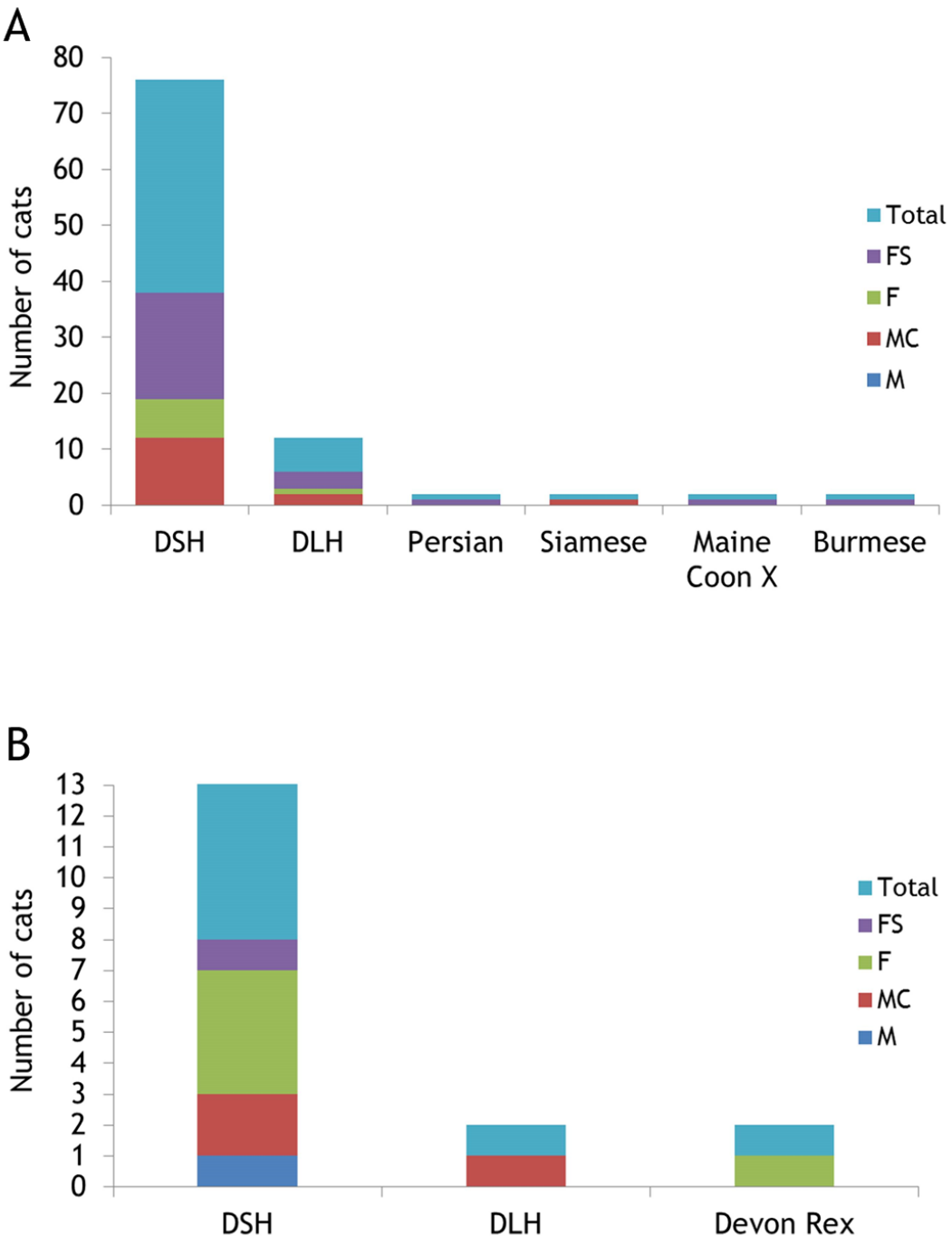

Figure 6.2: Breed and gender distribution of Hip-path OA (A) and no Hip-path OA/normal (B) cats.

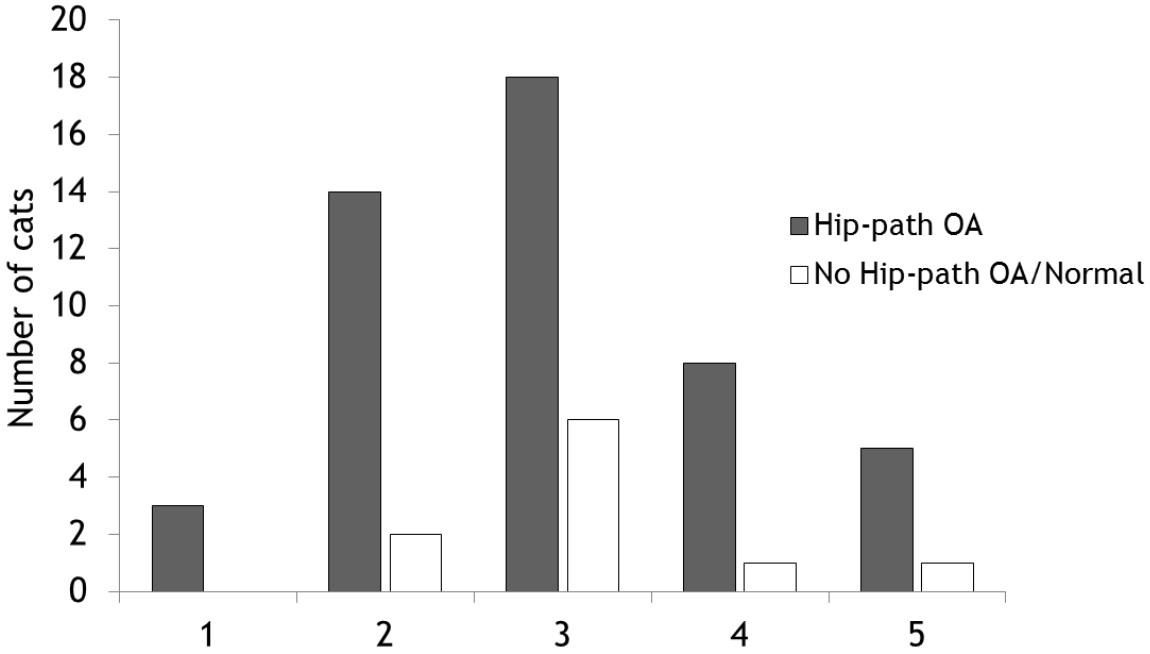

Figure 6.3: Distribution of body condition scores (BCS) of Hip-path OA and no Hip-path OA/normal cats.

6.3.3 Radiographic findings

The overall prevalence of Hip-rOA was 79.3% (46 of 58 cats). Of 46 cats with radiographic changes, 36 cats had bilateral and 10 had unilateral hip involvement (5 on the left and 5 on the right) giving a total number of 82 Hip-rOA joints (Table 6.2). The mean total radiographic score of left and right hip joints was 2.3 and 2.4 respectively. The median total radiographic score of left and right hip joints was 2 with a range from 1 to 6 for each joint. Of 82 hip joints, 80 were given a Global score of 1 and two a Global score of 2 (Tables 6.3 and 6.4).

Osteophytes were identified in 69 (84.1%) of 82 Hip-rOA joints, bilaterally in 28 cats and unilaterally in 13 cats (6 on the left and 7 on the right). Osteophytes were commonly observed at the cranial effective acetabular rim (63/69) (Figures 6.4.B-D) and femoral head/neck (5/69) (Figures 6.4.E-F). In one joint, osteophytes were seen at the cranial effective acetabular rim, femoral head/neck and the caudal acetabular rim (Figure 6.6). Severity was graded mild in 51/82 joints (62.2%) (26 on the left and 25 on the right), moderate in 17/82 joints (20.7%) (7 on the left and 10 on the right) and severe in 1/82 joints (1.2%) (on the left hip joint). The mean osteophyte size in mm ± SD for mildly affected joints was 1.2 ± 0.4, for moderately affected joints it was 2.6 ± 0.3 and for severely affected joints it was 5.2 ± 0.0 (Table 6.5).

Of 82 Hip-rOA joints, 80 (97.6%) had an increase in radio-opacity of the femoral head/neck (Figures 6.5.B-E). Ninety-six joints had both an increased radio-opacity of the femoral head/neck and osteophyte formation. Nine joints had an increase in radio-opacity of the femoral head/neck only and two joints had osteophyte formation only. Physeal scars were present in some cases and should not be confused with a pathologic increase of radio-opacity (Figure 6.5.F).

Joint remodelling was observed in 3/82 (3.7%) hip joints (2 on the left and 1 on the right), identified as changes in anatomical shape of the femoral head and acetabulum (Figure 6.6.B).

Decrease in joint space was seen in 11/82 (13.4%) hip joints (bilaterally in 4 cats and unilaterally in 3 cats) particularly at the cranial joint space (Figures 6.7.B-D).

Enthesiophytes, abnormal mineralisation and synovial effusion were not observed in any hip joint.

	Radiographic findings			
	No Hip-rOA		Hip-rOA	
	Number of Joints	Percentage (%)	Number of joints	Percentage (%)
Left hip	17	29.3	41	70.7
Right hip	17	29.3	41	70.7
Total	34	29.3	82	70.7

Table 6.2: Showing numbers of hip joints with normal and abnormal radiographic findings. Total number of joints 116.

	Radiographic OA Global score			
	Score 0	Score 1	Score 2	Score 3
Left hip	17	40	1	0
Right hip	17	40	1	0
Total	34	80	2	0
Percentage (%)	29.3	69	1.7	0

Table 6.3: The number and percentage of hip joints with different radiographic OA Global scores.

Cat ID	Osteophytes		Enthesiophytes		Abnormal mineralisation		Increase radio-opacity of the femoral head/neck		Synovial effusion		Joint remodelling		Joint space		Total score		Global score	
	L	R	L	R	L	R	L	R	L	R	L	R	L	R	L	R	L	R
X1	0	0	0	0	0	0	0	0	0	0	0	0	0	0	0	0	0	0
X2	0	0	0	0	0	0	0	0	0	0	0	0	0	0	0	0	0	0
X3	0	0	0	0	0	0	0	0	0	0	0	0	0	0	0	0	0	0
X4	0	0	0	0	0	0	0	0	0	0	0	0	0	0	0	0	0	0
X5	0	0	0	0	0	0	0	0	0	0	0	0	0	0	0	0	0	0
X6	1	1	0	0	0	0	1	1	0	0	0	0	0	0	2	2	1	1
X7	0	0	0	0	0	0	1	1	0	0	0	0	0	0	1	1	1	1
X8	1	1	0	0	0	0	1	1	0	0	0	0	0	0	2	2	1	1
X9	0	1	0	0	0	0	0	1	0	0	0	0	0	0	0	2	0	1
X10	2	2	0	0	0	0	1	1	0	0	0	0	0	0	3	3	1	1
X11	1	0	0	0	0	0	1	1	0	0	0	0	0	0	2	1	1	1
X12	1	2	0	0	0	0	1	1	0	0	0	0	2	2	4	5	1	1
X13	0	1	0	0	0	0	0	1	0	0	0	0	0	0	0	2	0	1
X14	0	0	0	0	0	0	0	0	0	0	0	0	0	0	0	0	0	0
X15	0	0	0	0	0	0	0	0	0	0	0	0	0	0	0	0	0	0
X16	1	0	0	0	0	0	1	0	0	0	0	0	0	0	2	0	1	0
X17	1	1	0	0	0	0	0	0	0	0	0	0	0	0	1	1	1	1
X18	0	0	0	0	0	0	1	1	0	0	0	0	0	0	1	1	1	1
X19	0	0	0	0	0	0	0	0	0	0	0	0	0	0	0	0	0	0

Table 6.4: Radiographic and Global scores of the left (L) and right (R) hip joints in 58 cats. Scoring: 0: absent, 1: mild, 2: moderate, 3: severe. For joint space: 0: no abnormality, 1: increase joint space, 2: decrease joint space. Global score: 0: no abnormality, 1: mild, 2: moderate, 3: severe.

Cat ID	Osteophytes		Enthesiophytes		Abnormal mineralisation		Increase radio-opacity of the femoral head/neck		Synovial effusion		Joint remodelling		Joint space		Total score		Global score	
	L	R	L	R	L	R	L	R	L	R	L	R	L	R	L	R	L	R
X20	1	1	0	0	0	0	1	1	0	0	0	0	0	0	2	2	1	1
X21	0	1	0	0	0	0	0	1	0	0	0	0	0	0	0	2	0	1
X22	1	2	0	0	0	0	1	1	0	0	0	0	0	0	2	5	1	1
X23	1	2	0	0	0	0	1	1	0	0	0	0	0	0	2	3	1	1
X24	1	1	0	0	0	0	1	1	0	0	0	0	0	0	2	2	1	1
X25	1	0	0	0	0	0	1	0	0	0	0	0	0	0	2	0	1	0
X26	1	1	0	0	0	0	1	1	0	0	0	0	2	2	4	4	1	1
X27	1	1	0	0	0	0	1	1	0	0	0	0	0	0	2	2	1	1
X28	1	1	0	0	0	0	1	1	0	0	0	0	0	0	2	2	1	1
X29	1	1	0	0	0	0	1	1	0	0	0	0	0	0	2	2	1	1
X30	1	1	0	0	0	0	1	1	0	0	0	0	0	0	2	2	1	1
X31	2	1	0	0	0	0	1	1	0	0	0	0	0	0	3	2	1	1
X32	0	0	0	0	0	0	1	0	0	0	0	0	0	0	1	0	1	0
X33	0	0	0	0	0	0	1	0	0	0	0	0	0	0	1	0	1	0
X34	1	1	0	0	0	0	1	1	0	0	0	0	0	0	2	2	1	1
X35	1	2	0	0	0	0	1	1	0	0	0	0	0	0	2	3	1	1
X36	2	2	0	0	0	0	1	1	0	0	0	0	0	0	3	3	1	1
X37	1	1	0	0	0	0	1	1	0	0	0	0	0	2	4	1	1	1
X38	2	2	0	0	0	0	1	1	0	0	0	0	0	0	3	3	1	1
X39	0	1	0	0	0	0	0	1	0	0	0	0	0	0	0	2	0	1

Table 6.4 continued.

Cat ID	Osteophytes		Enthesiophytes		Abnormal mineralisation		Increase radio-opacity of the femoral head/neck		Synovial effusion		Joint remodelling		Joint space		Total score		Global score	
	L	R	L	R	L	R	L	R	L	R	L	R	L	R	L	R	L	R
X40	1	2	0	0	0	0	1	1	0	0	0	0	0	0	2	3	1	1
X41	1	0	0	0	0	0	1	1	0	0	0	0	0	0	1	1	1	1
X42	0	0	0	0	0	0	1	1	0	0	0	0	0	0	1	1	1	1
X43	0	1	0	0	0	0	1	1	0	0	0	0	0	0	1	2	1	1
X44	0	0	0	0	0	0	0	0	0	0	0	0	0	0	0	0	0	0
X45	2	2	0	0	0	0	1	1	0	0	0	0	0	0	3	3	1	1
X46	1	0	0	0	0	0	1	1	0	0	0	0	0	0	2	1	1	1
X47	3	1	0	0	0	0	1	1	0	0	1	0	0	0	5	2	1	1
X48	1	1	0	0	0	0	1	1	0	0	0	0	0	0	2	2	1	1
X49	2	2	0	0	0	0	1	1	0	0	1	1	2	2	6	6	2	2
X50	0	1	0	0	0	0	0	1	0	0	0	0	0	0	0	2	0	1
X51	0	0	0	0	0	0	0	0	0	0	0	0	0	0	0	0	0	0
X52	0	0	0	0	0	0	0	0	0	0	0	0	0	0	0	0	0	0
X53	0	0	0	0	0	0	0	0	0	0	0	0	0	0	0	0	0	0
X54	1	1	0	0	0	0	1	1	0	0	0	0	0	0	2	2	1	1
X55	2	1	0	0	0	0	1	1	0	0	0	0	0	0	3	2	1	1
X56	1	1	0	0	0	0	1	1	0	0	0	0	2	2	4	4	1	1
X57	1	0	0	0	0	0	1	0	0	0	0	0	2	0	4	0	1	0
X58	0	1	0	0	0	0	1	1	0	0	0	0	0	0	1	2	1	1

Table 6.4 continued.

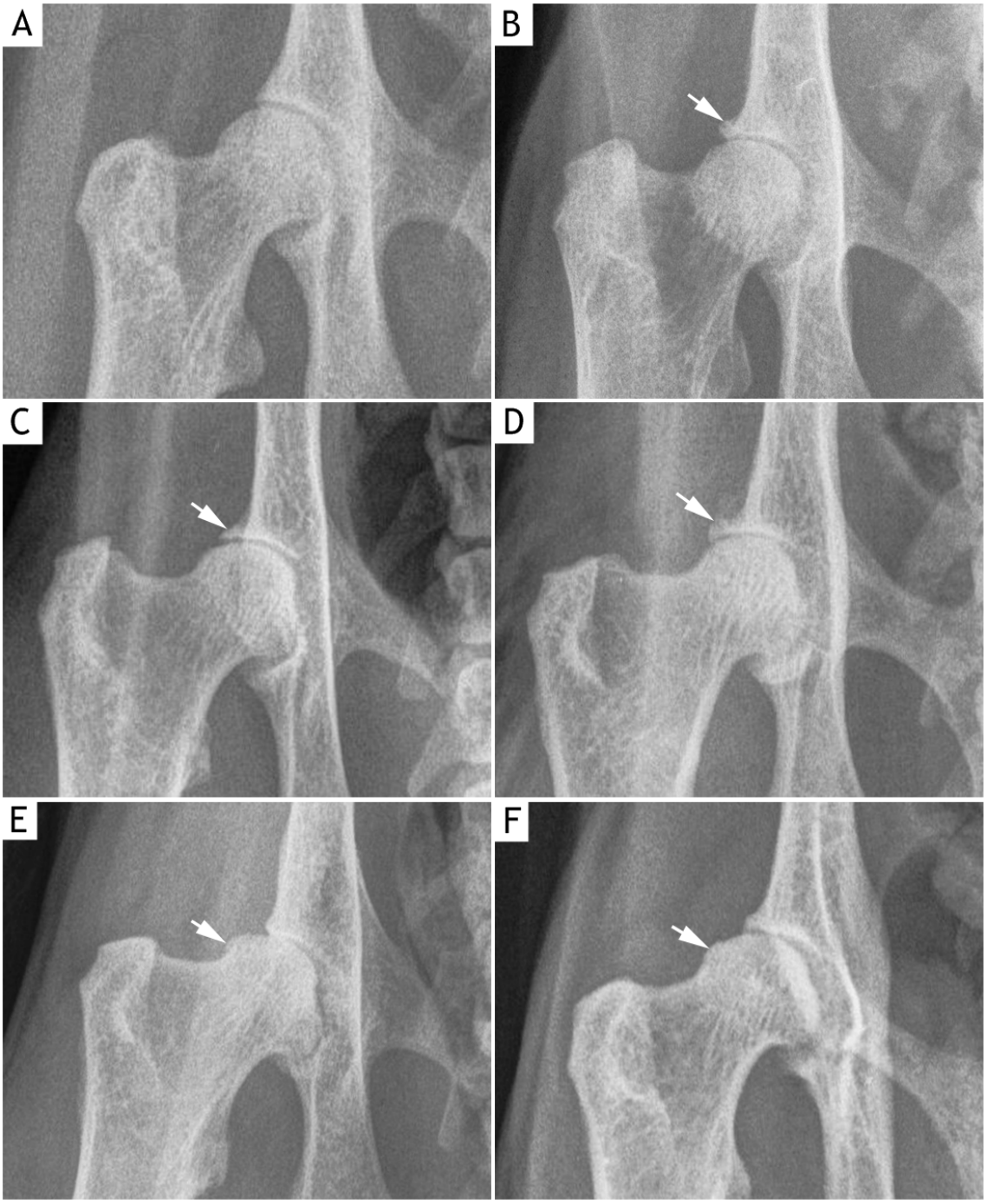

Figure 6.4: Ventrodorsal radiographs of hip joints showing osteophytes.

(A) Normal hip joint. Cat ID: X51, right hip. Mild (B), moderate (C) and severe (D) osteophyte formation is seen at the cranial effective acetabular rim (white arrow). Cat ID: B: X30, right hip, C: X45, right hip, D: X47, right hip. (E & F) Osteophyte formation is seen on the femoral head (white arrow). E: Cat ID: X49, right hip, F: Cat ID: X10, right hip.

Cat ID	Left hip		Right hip	
	Score	Osteophyte size (mm)	Score	Osteophyte size (mm)
X6	1	1.4	1	0.8
X8	1	1.0	1	0.7
X9	0	-	1	0.9
X10	2	2.2	2	2.4
X11	1	0.8	0	-
X12	1	1.2	2	2.4
X13	0	-	1	0.7
X16	1	1.4	0	-
X17	1	0.8	1	1.6
X20	1	0.7	1	1.8
X21	0	-	1	1.4
X22	1	1.2	2	2.0
X23	1	1.3	2	2.5
X24	1	1.4	1	0.8
X25	1	1.6	0	-
X26	1	1.4	1	0.7
X27	1	1.3	1	1.2
X28	1	0.9	1	0.7
X29	1	0.7	1	1.6
X30	1	1.6	1	1.8
X31	2	2.8	1	1.1
X34	1	1.8	1	1.6
X35	1	1.1	2	2.6
X36	2	3.0	2	2.7
X37	1	1.7	1	1.1
X38	2	2.6	2	2.1
X39	0	-	1	0.6
X40	1	1.1	2	2.1
X41	1	0.6	0	-
X43	0	-	1	0.9
X45	2	2.9	2	3.1
X46	1	0.9	0	-
X47	3	5.7	1	1.5
X48	1	1.5	1	1.6
X49	2	3.0	2	2.4
X50	0	-	1	0.5
X54	1	1.6	1	1.4
X55	2	2.6	1	1.2
X56	1	0.8	1	1.1
X57	1	0.8	0	-
X58	0	-	1	1.4

Table 6.5: Osteophytes when present were graded according to their size (mm) and whether a single site or multiple sites were involved.

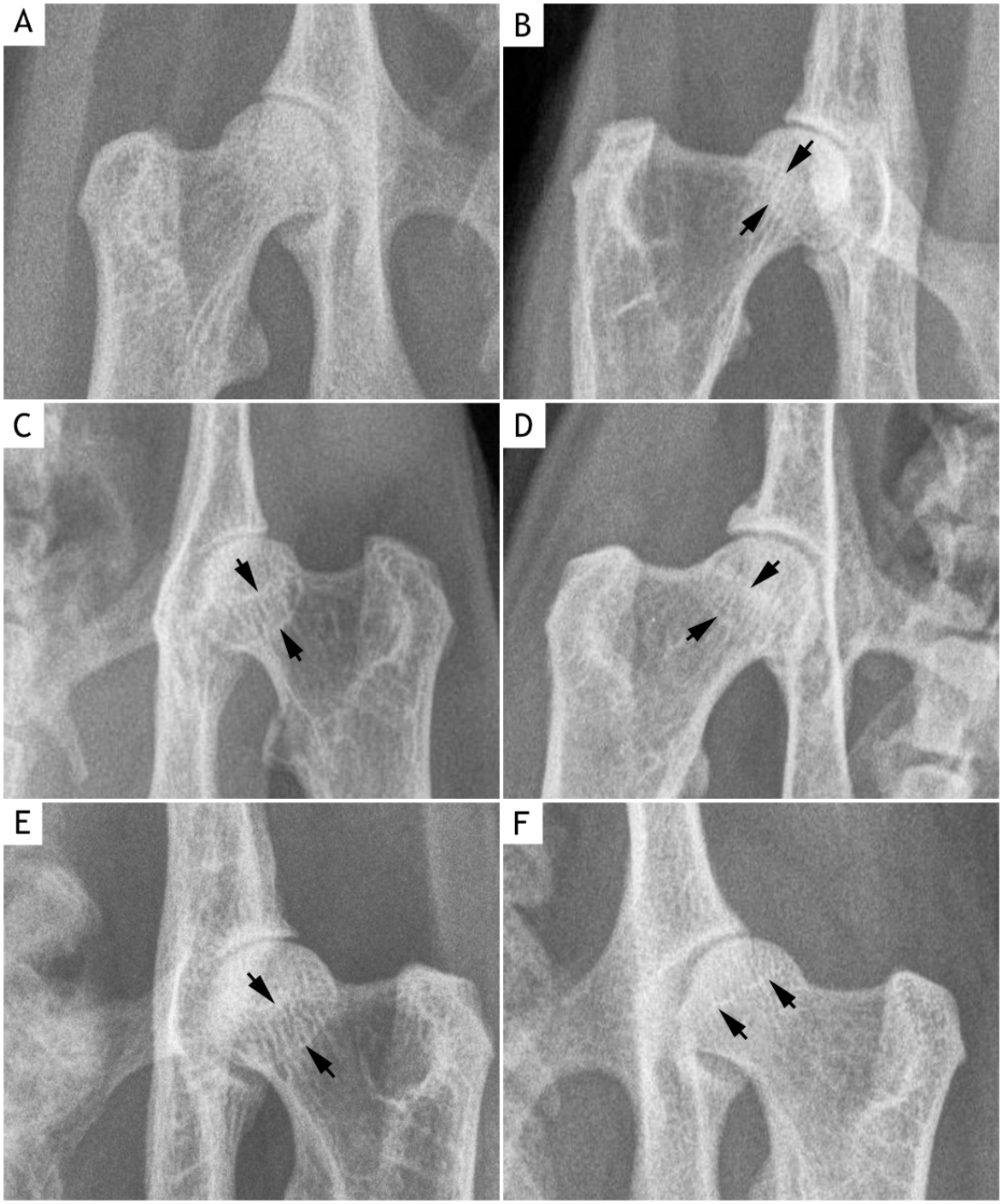

Figure 6.5: Ventrodorsal radiographs of hip joints with and without increased radio-opacity of the femoral head/neck.

(A) Normal hip joint with normal bone opacity of the femoral head/neck. Cat ID: X51, right hip. (B, C, D & E) Increased radio-opacity of the femoral head/neck (black arrows) is observed. This increased radio-opacity represents osteophytes at the articular margin (see Figures 6.11.A-D and 6.12.A for gross pathology). F: The physeal scar separating the epiphysis from the metaphysis is seen (black arrows) and should not be confused with a pathological increase of radio-opacity of the femoral head/neck. It appears as a single fine white line and in generally more proximal. No osteophytes were identified in this cat on gross examination. B: Cat ID: X27, right hip; C: Cat ID: X43, left hip; D: Cat ID: X10, right hip; E: Cat ID: X31, left hip; F: Cat ID: X51, left hip.

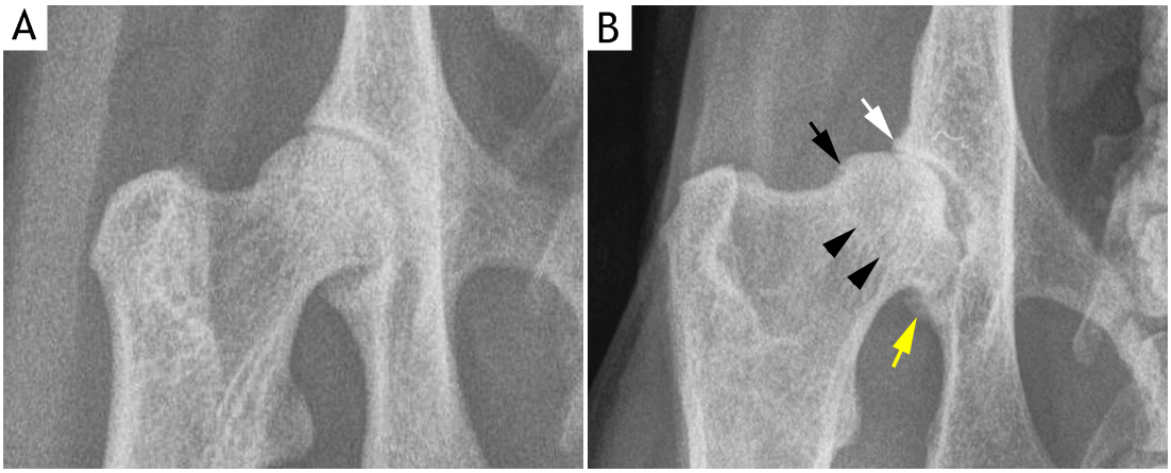

Figure 6.6: Ventrodorsal radiographs of hip joints showing remodelling and hip dysplasia.

(A) Normal hip joint with normal anatomical shape of the femoral head and acetabulum. Cat ID: X51, right hip. (B) A change in anatomical shape of the femoral head/neck and acetabulum is observed. This joint has HD, the acetabulum is shallow and the coverage of the femoral by the dorsal acetabular rim is less than 50%. There are also osteophytes at the cranial effective acetabular rim (white arrow), femoral head/neck (black arrow) and the caudal acetabular edge (yellow arrow). Increased radio-opacity of the femoral head/neck is also observed (black arrowheads). Cat ID: X49, right hip.

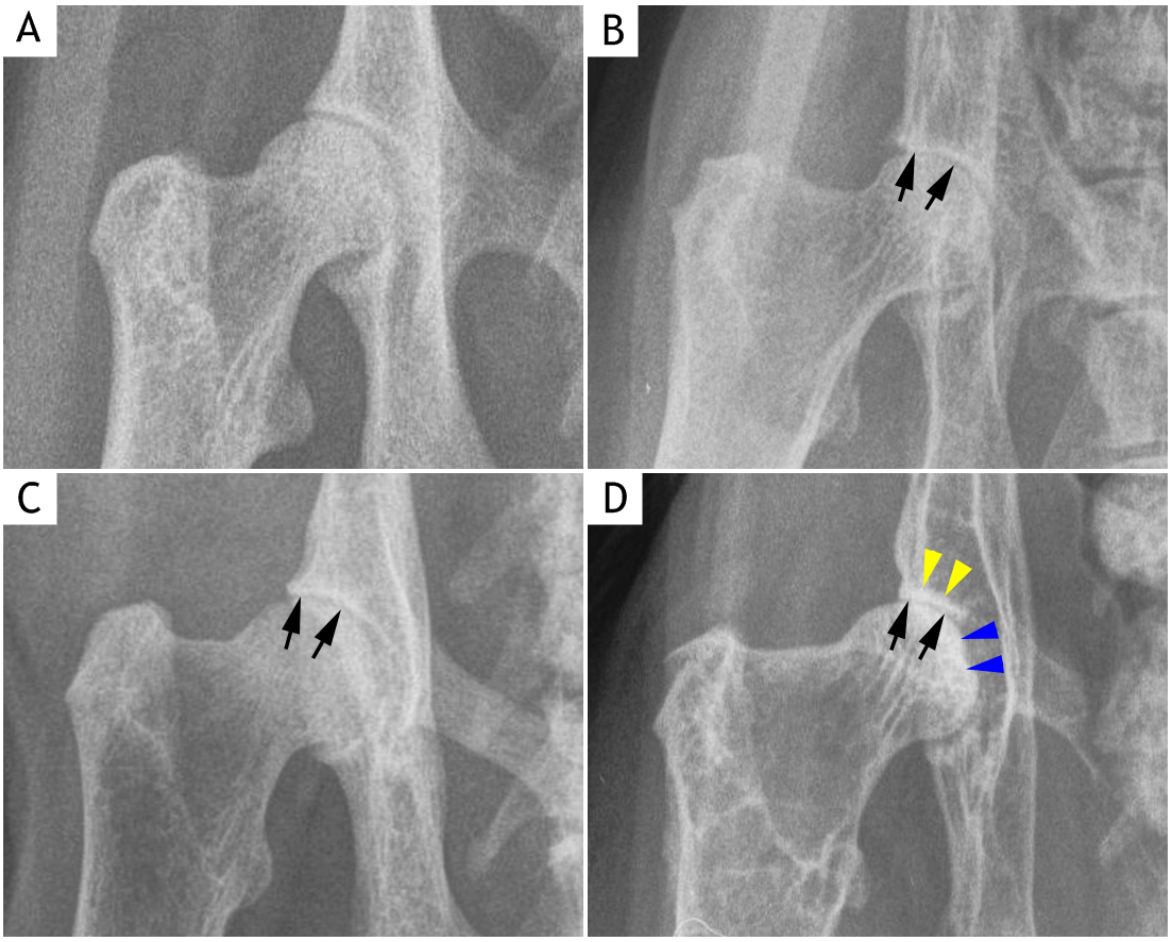

Figure 6.7: Ventrodorsal radiographs of hip joints illustrating changes in joint space.

(A) Normal hip joint with normal joint space. Cat ID: X51, right hip. (B, C, & D): Decreased joint space particularly at the cranial part (black arrows) is seen. There does appear to be an increased bone opacity at the articular margin of the femoral head (blue arrowheads) and acetabulum (yellow arrowheads) but this was not assessed (scored) in this study. B: Cat ID: X22, right hip. C: cat ID: X56, right hip. D: Cat ID: X26, right hip.

Fifty-seven hip joints were assessed for HD. Of 57 joints, 45 (78.9%) had ≥50% of the femoral head covered by the acetabulum and 12 (21.1%) had <50% of the femoral head covered by the acetabulum and were thus considered to have HD (bilaterally in 3 cats and unilaterally in 6 cats) (Figure 6.6.B). The mean percentage of the ≥50% and <50% of the femoral head covered by the acetabulum was 55% and 38% respectively. The mean ± SD NA of the hip with ≥50% and <50% coverage was 99.1° ± 2.9 and 93.2° ± 9.0 respectively, a difference which was significantly different (P<0.05).

Of 12 joints with HD (<50% coverage), 11 were Hip-rOA (91.7%) and one was no Hip-rOA (8.3%). The mean ± SD NA for dysplastic hip joints with and without secondary OA was 92.7° ± 9.3 and 90.8° ± 0.0 respectively. Of 11 Hip-rOA joints with HD, 9 were given a Global score 1 and two a Global score 2.

Of 45 joints with ≥50% coverage, 34 were Hip-rOA and 11 were no Hip-rOA. The Hip-rOA joints had a significantly lower NA with a mean ± SD of 97.3°± 3.0 compared to the no Hip-rOA joints with a mean ± SD of 99.9°± 2.8 (P<0.05).

Irrespective of the HD status, the mean ± SD NA of the Hip-rOA joints (96.8°± 5.5) was significantly lower compared to the no Hip-rOA joints (99.8° ± 3.5) (P<0.05). The results are summarised in Table 6.6 and Figure 6.8.

	Total number of joints		Joints with<50% coverage (HD)		Joints with ≥50% coverage		Total number of joints with and without rOA			
	≥50% coverage	<50% coverage (HD)	No hip-rOA	Hip-rOA	No hip-rOA	Hip-rOA	Hip-rOA NA°(96.8°± 5.5)		No Hip-rOA NA °(99.8° ± 3.5)	
							+HD	-HD	+HD	-HD
Number of joints	45	12	1	11	11	34	11	34	1	11
Mean percentage of femoral head (%)	55	38	33	39	54	55	39	55	33	54
Mean ± SD Norberg angle (NA°)	99.1° ± 2.3	93.2° ± 9.0	90.8° ± 0.0	92.7° ± 9.3	99.9°± 2.8	97.3°± 3.0	92.7° ± 9.3	97.3°± 3.0	90.8° ± 0.0	99.9°± 2.8

Table 6.6: Details of NA in different populations of cat. Those joints with <50% of the femoral head covered by the acetabulum were considered to indicate hip dysplasia (HD).

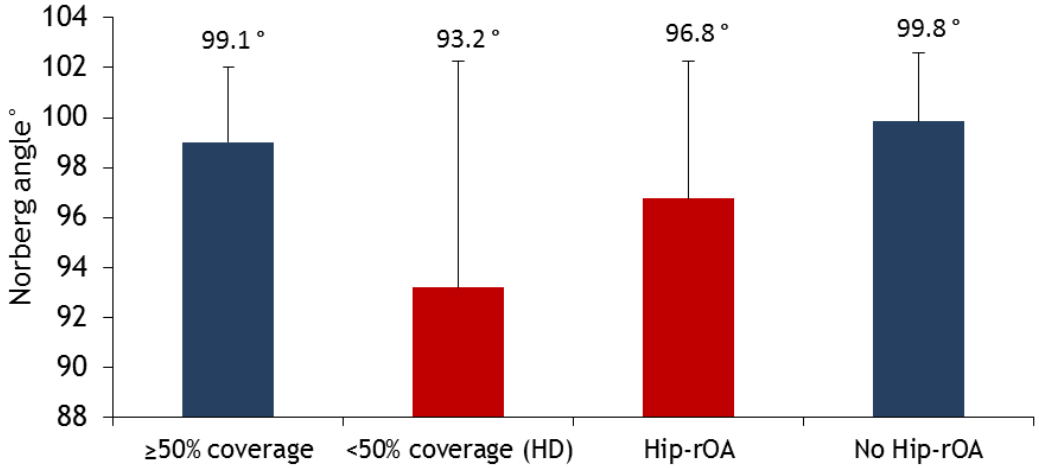

Figure 6.8: Showing mean Norberg angle for hip joints with and without HD and OA. A joint with less than 50% of the femoral head covered by the acetabulum was considered to be dysplastic.

6.3.4 Gross pathologic findings

Gross pathologic examinations were performed on 116 hip joints from 58 cats. The overall prevalence of Hip-path OA was 82.8% (48 of 58 cats). Of 48 cats with cartilage abnormalities, 45 cats had bilateral and 3 cats had unilateral hip involvement (1 on the left and 2 on the right) (Table 6.7), thus giving a total of 93 Hip-path OA joints. Of 93 Hip-path OA joints, 70 (75.3%) had cartilage changes on the femoral head and acetabulum, 18 (19.4%) had cartilage changes on the femoral head only and 5 (5.4%) had cartilage changes on the acetabulum only. Of 93 Hip-path OA joints, 91 were given a Global score of one and 2 a Global score of 3 (Table 6.8). The total possible gross pathologic score was 22; the highest score recorded was 16 (Table 6.9). The median total gross pathologic score for left and right Hip-path OA joints was 3.5 and 4 respectively. The total gross pathologic scores were not significantly different between left and right Hip-path OA joints (P=0.64). Of 34 no Hip-rOA joints, 23 (67.6%) were normal (no Hip-path OA/normal) on the gross pathologic examinations. Ten cats (39.7%) had grossly normal articular cartilage on both left and right hip joints. Three cats (5.2%) had unilateral grossly normal articular cartilage (2 on the left and 1 on the right side) (Table 6.7).

A normal femoral head and acetabulum had a smooth, white and shining articular surface (Figure 6.9.A). All hip-path OA joints had cartilage fibrillation, 75 were scored as mild, 16 were scored as moderate and 2 as severe. With mild OA (Global score 1), the fibrillation was seen as a focal dullness and roughening of the articular surface particularly at the caudal aspect of the femoral head (Figure 6.9.B) and dorsal periphery of the acetabulum (Figure 6.10.A). The lesions were generalised in moderate to severe OA (Global scores 2 and 3) (Figures 6.9.C-D, 6.10.B, 6.12.B). Yellow discolouration of the articular surface was seen in 91/93 (97.8%) hip joints (45 on the left and 46 on the right). Cartilage erosion was identified in 5/93 (5.4%) hip joints (3 on the left and 2 on the right) particularly on the cranial and caudal aspects of the femoral head and dorsal periphery of the acetabulum (Figure 6.10.B). Of these, 3 were scored as mild and 2 were scored as moderate. Six (6.6%) hip joints had cartilage ulceration (4 on the left and 2 on the right). The ulceration was scored mild in 4 and moderate in 2 joints (Figures 6.9.C-D). The lesions were seen at the caudal aspects of the femoral head. Cartilage erosion and ulceration were seen in all joints with a radiographic decreased joint space.

Osteophyte formation was observed in all Hip-path OA joints. The osteophytes were commonly identified at the femoral head-neck junction (Figures 6.11.A-D) and around the acetabular margin (Figures 6.11.E-F). In 71 hip joints osteophyte development was mild, in 21 it was moderate and in one hip joint it was severe. All Hip-rOA joints with increased radio-opacity on the femoral head/neck had osteophyte formation at the femoral head-neck junction.

Joint remodelling (changes in shape of the femoral head and acetabulum) was seen in 4/93 (4.3%) hip joints (Figure 6.12). All these joints also had moderate to severe osteophyte formation at the femoral head-neck junction and acetabulum.

Thickening of the joint capsule (Figures 6.10.A and 6.10.D) and discolouration of the synovium were observed in 25 (26.9%) and 24 (25.8%) joints respectively.

Of 12 joints with hip dysplasia, 11 had gross cartilage changes and 1 had normal articular cartilage on both femoral head and acetabulum. Of 11 Hip-path OA joints with HD, 9 were given a Global score of 1 and two a Global score of 3. Those two joints (the left and right joints from the same cat) with a Global score 3 had severe cartilage abnormalities including discolouration, fibrillation, erosion and ulceration of the femoral head and acetabulum, together with osteophyte formation and remodelling (Figure 6.12).

	Gross pathologic findings			
	No Hip-path OA		Hip-path OA	
	Number of Joints	Percentage (%)	Number of joints	Percentage (%)
Left shoulder	12	20.7	46	79.3
Right shoulder	11	19.0	47	81.0
Total	23	19.8	93	80.2

Table 6.7: Showing numbers of hip joints with normal and abnormal gross pathologic findings. Total number of joints 116.

	Gross pathologic OA Global scores			
	Score 0	Score 1	Score 2	Score 3
Left shoulder	12	45	0	1
Right shoulder	11	46	0	1
Total	23	91	0	2

Table 6.8: Showing the number of hip joints with different gross pathologic OA Global Scores.

Cat ID	Cartilage surface discolouration		Cartilage fibrillation		Cartilage erosion		Cartilage ulceration		Osteophytes		Joint remodelling		Thickening of joint capsule		Synovium discolouration		Total score		Global Score		Sample for histopathologic examination
	L	R	L	R	L	R	L	R	L	R	L	R	L	R	L	R	L	R	L	R	
X1	0	0	0	0	0	0	0	0	0	0	0	0	0	0	0	0	0	0	0	0	
X2	0	0	0	0	0	0	0	0	0	0	0	0	0	0	0	0	0	0	0	0	
X3	0	0	0	0	0	0	0	0	0	0	0	0	0	0	0	0	0	0	0	0	CBS-L&R
X4	0	0	0	0	0	0	0	0	0	0	0	0	0	0	0	0	0	0	0	0	CBS-L
X5	0	0	0	0	0	0	0	0	0	0	0	0	0	0	0	0	0	0	0	0	
X6	1	1	1	1	0	0	0	0	1	1	0	0	0	0	1	0	4	3	1	1	CBS-L
X7	1	1	1	1	0	0	0	0	1	2	0	0	0	0	0	0	3	4	1	1	
X8	1	1	1	1	0	0	0	0	2	2	0	0	0	0	0	0	4	4	1	1	CBS-R
X9	1	1	1	2	0	0	0	0	1	2	0	0	0	0	0	0	3	5	1	1	CBS-L
X10	1	1	2	1	0	0	0	0	1	2	0	0	0	1	0	0	4	5	1	1	
X11	1	1	1	1	0	0	0	0	1	1	0	0	0	0	0	1	3	4	1	1	
X12	1	1	1	1	0	0	0	0	1	1	0	0	0	0	0	0	3	3	1	1	
X13	0	1	0	1	0	0	0	0	0	1	0	0	0	0	0	0	0	3	0	1	
X14	0	0	0	0	0	0	0	0	0	0	0	0	0	0	0	0	0	0	0	0	CBS-R
X15	1	1	1	2	0	0	0	0	1	1	0	0	0	0	1	1	4	5	1	1	CBS-L
X16	1	1	1	1	0	0	0	0	1	2	0	0	0	0	0	0	3	4	1	1	
X17	1	1	1	1	0	0	0	0	1	1	0	0	0	0	0	0	3	3	1	1	CBS-R
X18	1	1	1	1	0	0	0	0	1	1	0	0	0	0	0	0	3	3	1	1	
X19	0	0	0	0	0	0	0	0	0	0	0	0	0	0	0	0	0	0	0	0	CBS-L&R
X20	1	1	1	1	0	0	0	0	1	1	0	0	0	0	0	0	3	3	1	1	

Table 6.9: Gross pathologic scores and Global scores of the left (L) and right (R) hip joints of 58 cats. Global score: 0: normal, 1: mild, 2: moderate, 3: severe. Sample selected for histopathologic examination:- CBS-L: Cartilage Bone Synovium-Left; CBS-R: Cartilage Bone Synovium-Right, CBS-L&R: Cartilage Bone Synovium-Left and right.

Cat ID	Cartilage surface discolouration		Cartilage fibrillation		Cartilage erosion		Cartilage ulceration		Osteophytes		Joint remodelling		Thickening of joint capsule		Synovium discolouration		Total score		Global Score		Sample for histopathologic examination
	L	R	L	R	L	R	L	R	L	R	L	R	L	R	L	R	L	R	L	R	
X21	0	1	0	1	0	0	0	0	0	1	0	0	0	0	0	0	0	3	0	1	CBS-L
X22	1	1	1	1	0	0	0	0	1	1	0	0	0	0	0	0	3	3	1	1	
X23	1	1	1	1	0	0	0	0	2	2	0	0	0	0	0	1	4	5	1	1	CBS-R
X24	1	1	1	2	0	0	0	0	1	2	0	0	0	0	1	0	4	5	1	1	CBS-R
X25	1	1	1	1	0	0	0	0	1	1	0	0	0	0	0	0	3	3	1	1	
X26	1	1	2	2	0	0	1	1	2	2	1	1	0	0	0	0	7	7	1	1	CBS-L
X27	1	1	2	2	0	0	0	0	2	2	0	0	0	0	0	0	5	5	1	1	
X28	1	1	1	1	0	0	0	0	1	1	0	0	0	0	0	0	3	3	1	1	
X29	1	1	1	1	0	0	0	0	1	1	0	0	0	0	0	0	3	3	1	1	
X30	1	1	1	1	0	0	0	0	1	1	0	0	0	0	0	0	3	3	1	1	
X31	1	1	1	1	0	0	0	0	1	1	0	0	0	0	0	0	3	3	1	1	CBS-R
X32	1	1	1	2	0	0	0	0	1	1	0	0	0	0	0	0	3	4	1	1	
X33	1	0	1	0	0	0	0	0	1	0	0	0	0	0	0	0	3	0	1	0	
X34	1	1	1	1	0	0	0	0	1	1	0	0	1	0	0	0	4	3	1	1	
X35	1	1	1	1	0	0	0	0	2	1	0	0	1	0	0	0	5	3	1	1	
X36	1	1	1	1	0	0	0	0	1	1	0	0	1	0	1	0	5	3	1	1	CBS-R
X37	1	1	2	1	0	0	0	0	1	1	0	0	1	1	1	1	6	5	1	1	
X38	1	1	1	1	0	0	0	0	1	1	0	0	0	1	0	0	3	4	1	1	
X39	1	1	1	1	0	0	0	0	1	1	0	0	1	1	0	0	4	4	1	1	
X40	1	1	1	1	0	0	0	0	2	2	0	0	1	1	0	0	5	5	1	1	
X41	1	1	1	1	0	0	0	0	1	1	0	0	1	1	1	1	5	5	1	1	CBS-R
X42	1	1	1	1	0	0	0	0	1	2	0	0	0	1	0	1	3	6	1	1	CBS-L&R
X43	1	1	2	1	1	0	0	0	1	1	0	0	1	1	1	1	7	5	1	1	

Table 6.9 continued.

Cat ID	Cartilage surface discolouration		Cartilage fibrillation		Cartilage erosion		Cartilage ulceration		Osteophytes		Joint remodelling		Thickening of joint capsule		Synovium discolouration		Total score		Global score		Sample for histopathologic examination
	L	R	L	R	L	R	L	R	L	R	L	R	L	R	L	R	L	R	L	R	
X44	1	1	1	1	0	0	0	0	1	1	0	0	0	0	0	1	3	4	1	1	
X45	1	1	2	1	0	0	0	0	2	2	0	0	1	1	1	1	7	6	1	1	CBS-L
X46	0	0	1	1	0	0	0	0	1	1	0	0	0	1	0	0	2	3	1	1	
X47	1	1	1	1	0	0	0	0	1	2	0	0	0	1	0	1	3	6	1	1	
X48	1	1	1	1	0	0	0	0	1	1	0	0	1	0	0	0	4	3	1	1	
X49	1	1	3	3	2	2	1	2	2	3	1	1	2	2	2	2	14	16	3	3	CBS-L&R
X50	1	1	1	1	0	0	0	0	1	1	0	0	0	0	0	0	3	3	1	1	
X51	0	0	0	0	0	0	0	0	0	0	0	0	0	0	0	0	0	0	0	0	CBS-L&R
X52	0	0	0	0	0	0	0	0	0	0	0	0	0	0	0	0	0	0	0	0	
X53	0	0	0	0	0	0	0	0	0	0	0	0	0	0	0	0	0	0	0	0	CBS-L&R
X54	1	1	1	1	0	0	0	0	1	1	0	0	0	0	0	0	3	3	1	1	
X55	1	1	2	1	0	0	1	0	1	1	0	0	0	1	0	0	5	4	1	1	CBS-L
X56	1	1	2	2	0	1	1	0	1	1	0	0	0	1	1	1	6	7	1	1	CBS-L&R
X57	1	1	2	1	1	0	0	0	1	1	0	0	0	0	0	0	5	3	1	1	
X58	1	1	1	1	0	0	0	0	1	1	0	0	0	0	1	1	4	4	1	1	

Table 6.9 continued.

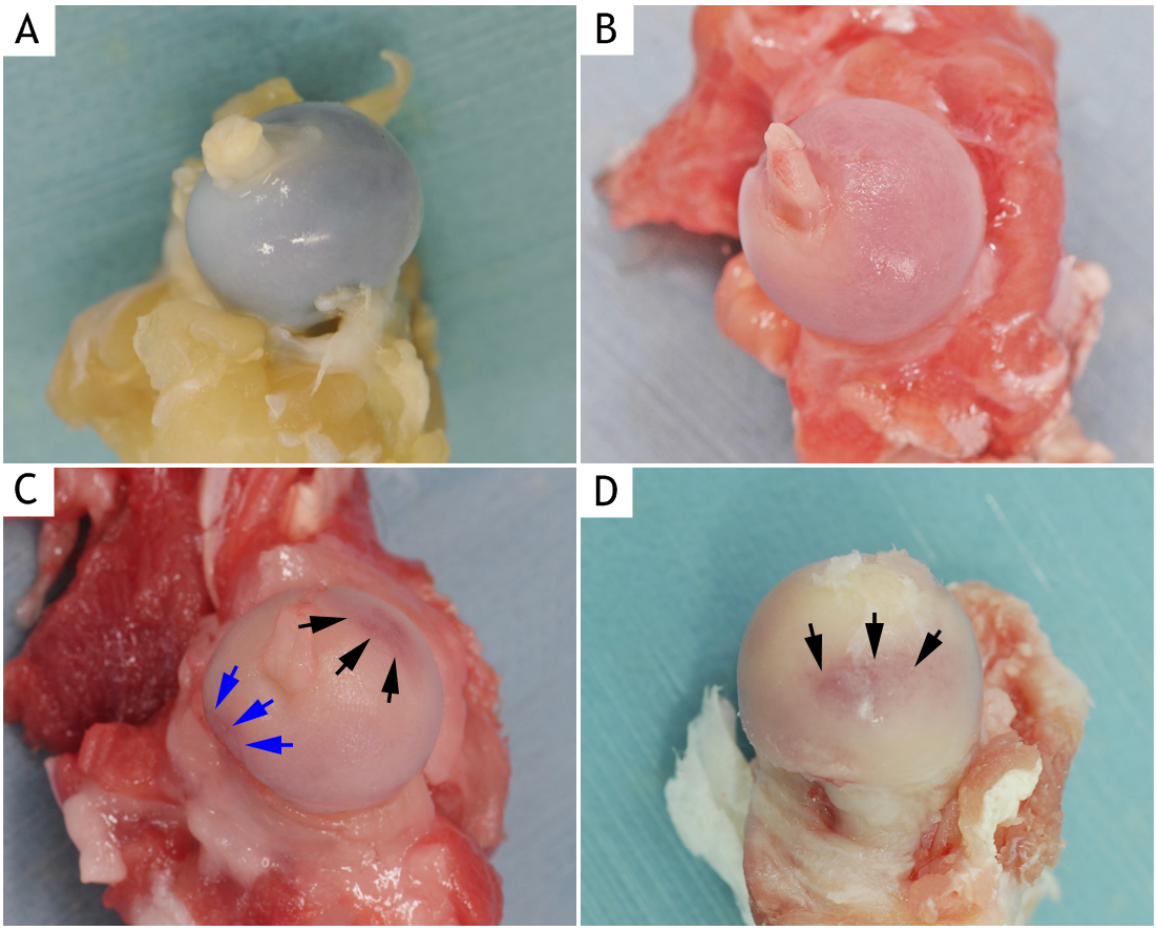

Figure 6.9: Photographs of femoral articular surface showing gross pathologic features.

(A) Normal femoral cartilage has a smooth and shining appearance. Cat ID: X51, right hip. (B) Generalised surface dullness and fibrillation is seen. Cat ID: X30, right hip. (C) Close to the cranial (blue arrows) and caudal (black arrows) aspects of the femoral head, localised cartilage ulceration is seen. Cat ID: X43, left hip. (D) Diffuse yellow discolouration of the articular cartilage is observed. There is also cartilage ulceration at the caudal aspect of the femoral head (black arrows). Cat ID: X26, right hip.

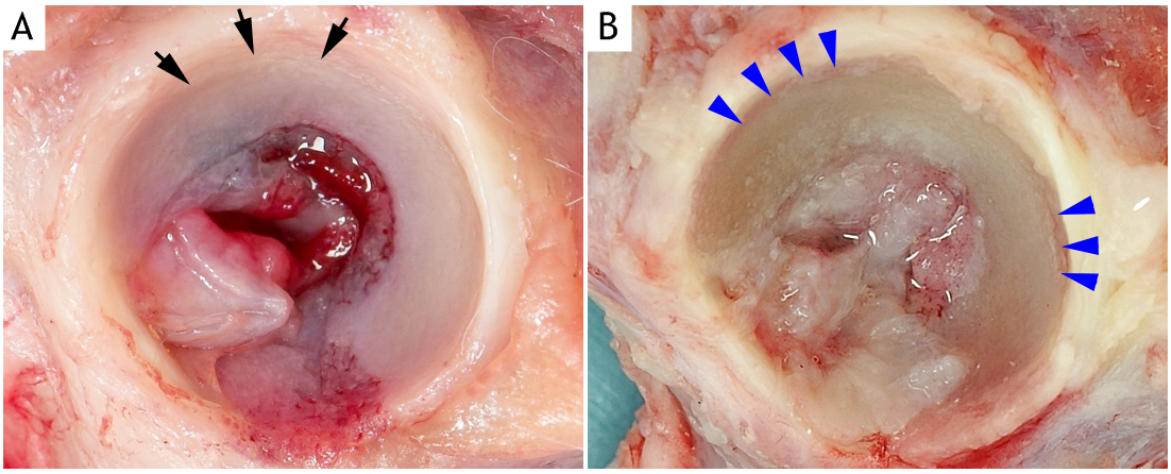

Figure 6.10: Photographs of acetabular surface showing gross pathologic changes.

(A) Cartilage roughening and fibrillation (black arrows) is seen particularly at the dorsal periphery of the acetabulum. Cat ID: X30, right hip. (B) Severe cartilage fibrillation with yellow discolouration is observed on the entire surface of the acetabulum. There is also cartilage erosion (blue arrowheads) at the dorsal periphery of the acetabulum. A moderately thickened joint capsule is also present. Cat ID: X26, right hip.

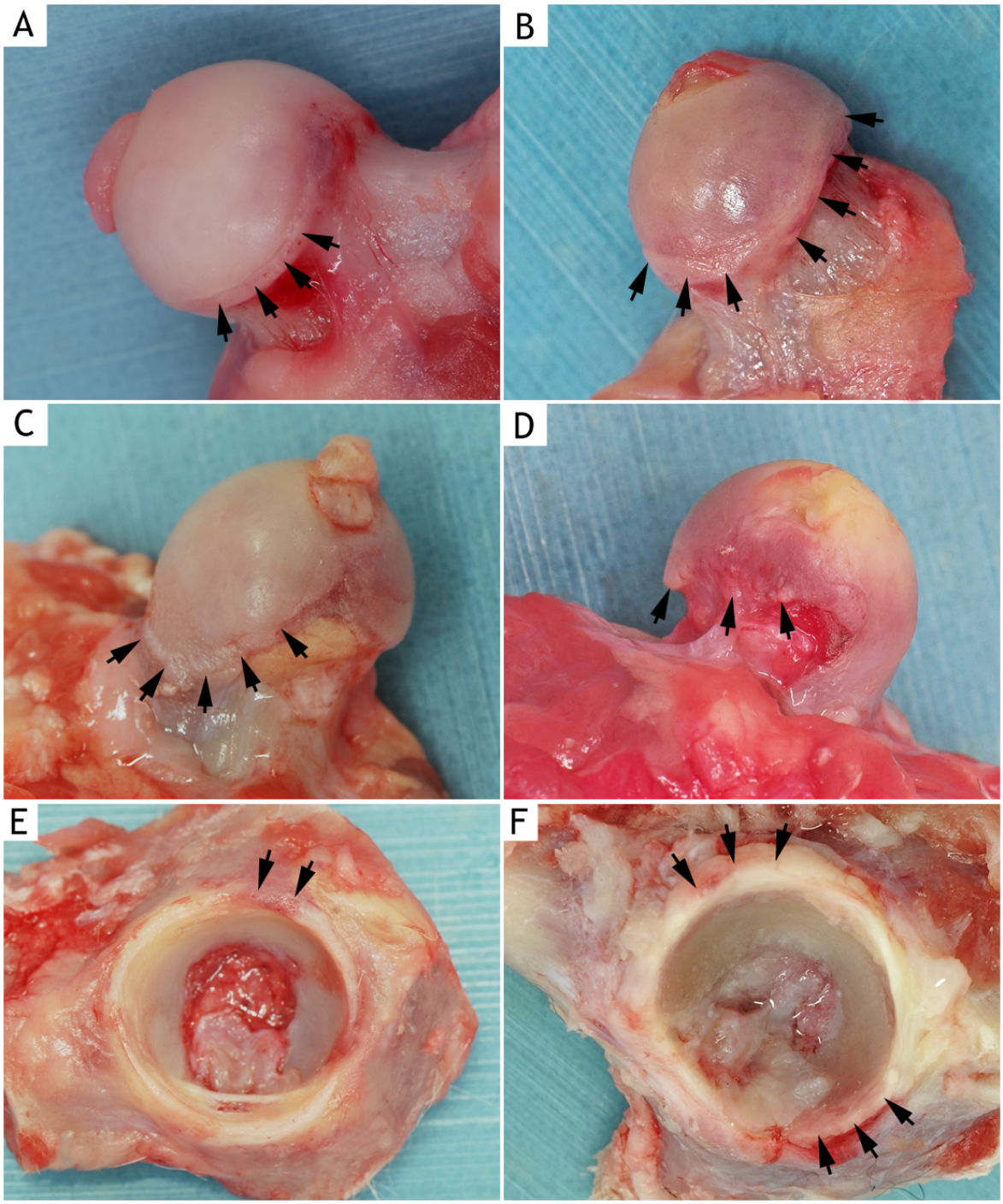

Figure 6.11: Examples of osteophyte formation at the femoral head-neck junction and acetabulum of the hip joint.

(A & B) There is osteophyte formation (black arrows) along the femoral head-neck junction. Cat ID: X 41, right hip, B: Cat ID: X10, right hip. (C & D) Osteophyte formation (black arrows) at the femoral head-neck junction is seen. C: Cat ID: X26, right hip, D: Cat ID: X43, left hip. Osteophyte formation at the femoral head-neck junction appears as an increase in radio-opacity of the femoral head/neck on the radiograph (see Figures 6.5.B-E for radiographs). (E & F) Acetabular osteophyte (black arrows) formation is observed (see Figures 6.4.C-D for radiographs). E: Cat ID: X45, right hip, F: Cat ID: X47, right hip.

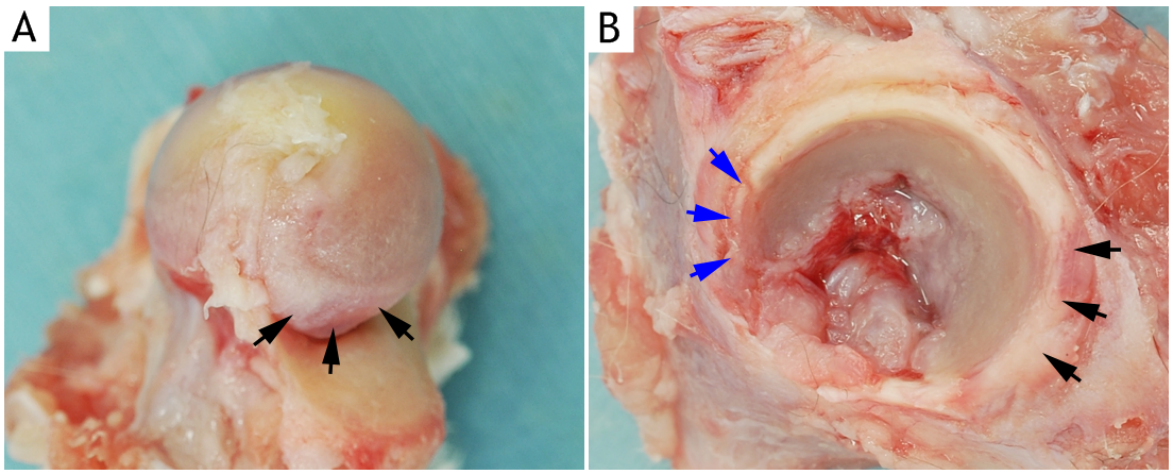

Figure 6.12: Showing examples of severe secondary OA that occurs with hip dysplasia.

(A) Yellow discolouration with severe cartilage damage is seen on the femoral head. Femoral head remodelling with severe osteophyte formation (black arrows) is also identified. (B) Surface dullness with fibrillation is noted affecting the entire acetabular cartilage. Osteophyte formation is also present at the cranial effective acetabular rim (black arrows) and caudal acetabular edge (blue arrows). See Figure 6.4.E for the radiograph. A & B: Cat ID: X49, right hip.

6.3.5 Correlation studies

6.3.5.1 Correlation between total radiographic and gross pathologic OA scores

All Hip-rOA joints (82) had gross cartilage changes. Of 34 no Hip-rOA joints, 11 (32.4%) had gross cartilage lesions on the femoral head or acetabulum or both. There was a significant moderate positive correlation between the radiographic and gross pathologic total scores in both left (r_s=0.65, P<0.0001) and right (r_s=0.54, P<0.0001) hip joints (Figures 6.13.A and 6.13.B).

6.3.5.2 Correlation between total radiographic score and age, BW and BCS

There was a significant fair positive correlation between the radiographic total score of the left (r_s=0.29, P<0.05) and right (r_s=0.27, P<0.05) hip joints and age (Figures 6.14.A and 6.14.B). There was a slight, negative relationship between the radiographic total score of the left (r_s=-0.19, P=0.15) and right (r_s=-0.15, P=0.26) hip joints and BW, which was not statistically significant (Figures 6.14.C and 6.14.D). A similar finding was also observed between the radiographic total score of the left (r_s=-0.20, P=0.12) and right (r_s=-0.13, P=0.32) hip joints and BCS (Figures 6.14.E and 6.14.F).

6.3.5.3 Correlation between total gross pathologic score and age, BW, and BCS

Correlation analysis revealed a significant moderate positive relationship between the total gross pathologic score of the left (r_s=0.46, P<0.001) and right (r_s=0.55, P<0.0001) hip joints and age (Figures 6.15.A and 6.15.B). Correlation analysis revealed a fair and slight negative relationship between the total gross pathologic score of the left (r_s=-0.31, P=0.19) and right (r_s=-0.27, P=0.10) hip joints and BW respectively (Figures 6.15.C and 6.15.D). However, the relationships were not statistically significant. A similar finding was also observed between the total gross pathologic score of the left (r_s=-0.28, P=0.36) and right (r_s=-0.26, P=0.10) hip joints and BCS (Figures 6.15.E and 6.15.F).

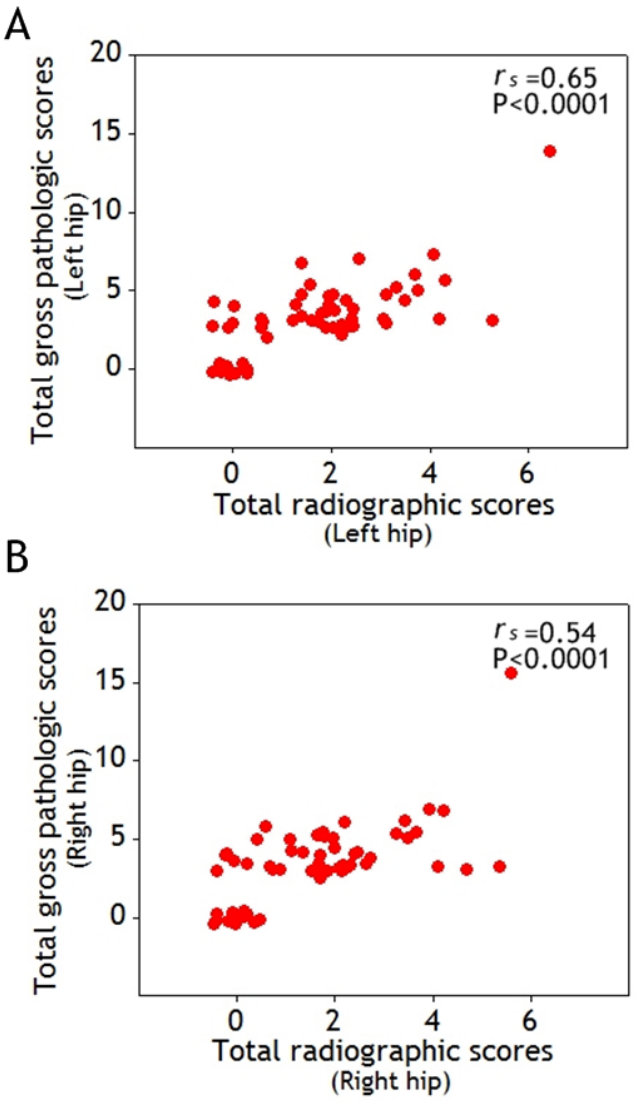

Figure 6.13: Graph showing correlation between radiographic and gross pathologic OA scores in left (A) and right (B) hip joints. There is a moderate significant relationship between the radiographic and gross pathologic scores in both left and right hip joints.

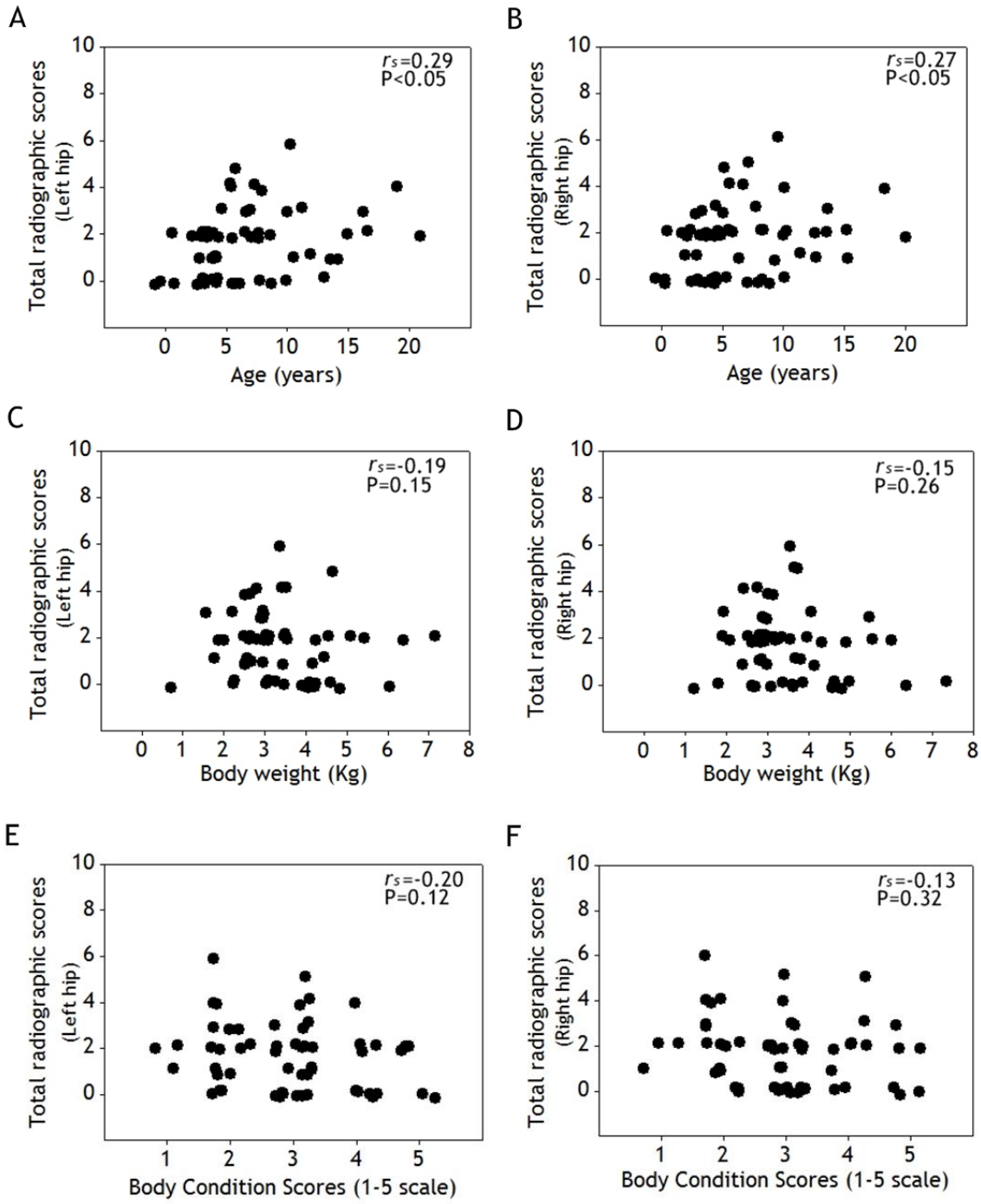

Figure 6.14: Correlation analysis of total radiographic scores of the left (A, C and E) and right (B, D and F) hip joints with age, BW and BCS. (A & B) There is a significant fair positive relationship between total radiographic scores of the left and right hip joints and age. There are no significant relationships between the total radiographic scores of the left and right hip joint with BW (C & D) and BCS (E & F).

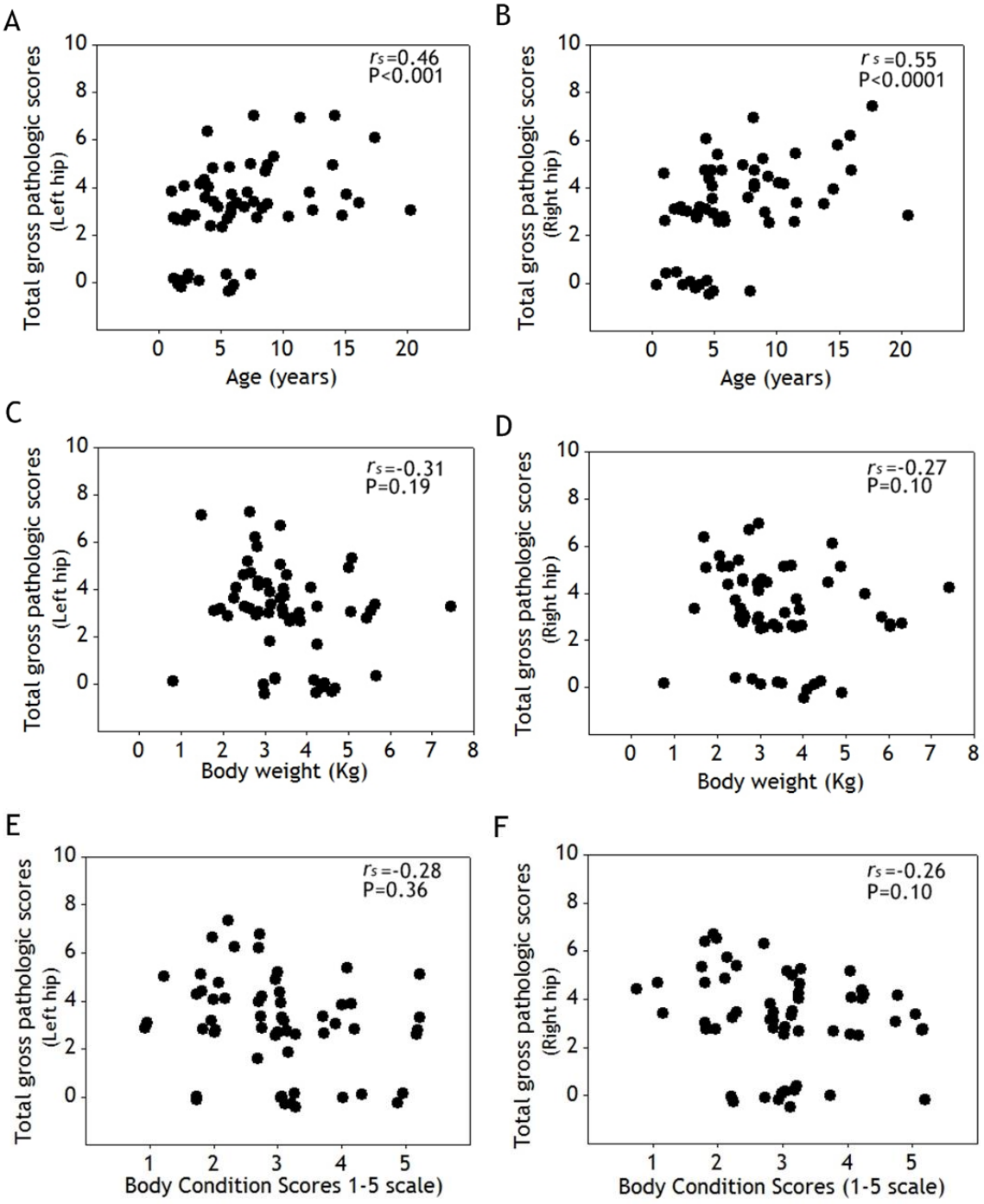

Figure 6.15: Correlation analysis of total gross pathologic scores of the left (A, C and E) and right (B, D and F) hip joints with age, BW and BCS. (A & B) There is a significant moderate positive relationship between total gross pathologic scores of the left and right hip joints and age. There are no significant relationships between the total gross pathologic scores of the left and right hip joint with BW (C & D) and BCS (E & F).

6.4 Discussion

The prevalence of Hip-rOA and Hip-path OA was 79.3% (46 of 58 cats) and 82.8% (48 of 58 cats) respectively. The retrospective study by Hardie et al. (2002) reported a lack of hip OA cases in 100 geriatric cats aged over 12 years. However, the actual number and prevalence of hip OA were not clearly defined. In another retrospective study, Clarke et al. (2005) reported hip OA in 25/113 (22.0%) hip joints from 218 cats. The low prevalence of hip OA in these retrospective studies might reflect a bias of the sample population, where hip radiographs were less consistently available and assessed. Clarke and Bennett (2006) prospectively reported hip OA in 27 joints (48.0%) from 28 cats. In a recent prospective study by Lascelles et al. (2010), 131/200 (65.0%) hip joints had radiographic OA. Freire et al. (2011) and Slingerland et al. (2011) reported hip OA in 29/59 (49.0%) and 49/200 (24.5%) hip joints respectively. Differences in the study design and size probably explain the variation in the prevalence. In addition, differences between the geographic location and genetic make-up of the study populations may be a factor (Lascelles et al., 2010).

The mean age of cats with Hip-path OA was significantly greater than that of no Hip-path OA/normal cats. A fair to moderate positive correlation was found between the radiographic and gross pathologic total scores and age in both hip joints. It is possible, as with other joints, that age plays a significant factor in hip OA. Aging is associated with alterations in the cartilage matrix such as reduced proteoglycan content and glycosaminoglycan composition, which can contribute to the development of OA (Hardingham and Bayliss 1990).

The mean BW of cats with Hip-path OA was slightly lower than no Hip-path OA cats but this was not significantly different. No difference in BCS was observed between the Hip-path OA and no Hip-path OA cats. A non-significant negative correlation was found between the radiographic and gross pathologic total scores and BW and BCS in both hip joints. This might suggest that BW and BCS are not risk factors for OA of the hip. However, these should be interpreted cautiously since excess body weight with high BCS when the cat was younger could be a factor (Lund et al., 2005).

The common radiographic features of hip OA were osteophytes, increased radio-opacity of the femoral head/neck and decreased joint space. Joint remodelling was seen but less commonly. Ninety-one percent of osteophytes were identified at the cranial effective acetabular rim with only 7.0% at the femoral head/neck and 2.0% at multiple

sites. However the increased linear radio-opacity on the femoral head/neck also represents osteophyte formation (Figures 6.11.A-D), but was scored separately.

The study confirmed that an increased radio-opacity of the femoral head/neck was an important radiographic feature in evaluating hip OA. An increase in radio-opacity of the femoral head/neck was seen in 80/89 (97.6%) Hip-rOA joints. This increased radio-opacity represents osteophytes at the articular margin of the femoral head/neck (Figures 6.11.A-D). Considerable caution however, must be made when interpreting this feature since the physeal scar may leave a line of increased radio-opacity between the femoral head and neck which mimics osteophyte formation (Hammond and McConnell, 2013; Muhlbauer and Kneller, 2013). The physeal scar is usually seen as a single fine white line and generally more proximal in its portion. Pathologically increased radio-opacity is more irregular and often appears as two separate lines (Figures 6.5.B-D). An increased radio-opacity at the articular margin of the acetabulum and femoral head was observed (Figure 6.7) in some cases; however no attempt was made to score this because of its very subjective nature.

Decreased joint space was common particularly at the cranial aspect, being found in 11/82 (13.4%) Hip-rOA joints. A loss of joint space reflects a loss of articular cartilage (Owens, 1982). All Hip-rOA joints with a decreased joint space had cartilage erosion and ulceration either of the femoral head or acetabulum or both. Interestingly, cartilage damage was usually more severe and more commonly found on the caudal part of the femoral head and acetabulum despite reductions in joint space being more obvious radiographically at the cranial joint space. This probably reflects that evaluation of joint space on the standard hip ventrodorsal leg extended view is not reliable. Accurate radiographic assessment of joint space requires weight bearing views (Morgan, 1969; Leach et al., 1970) which are difficult to take in small animal patients. In addition, the more advanced pathology on the caudal part of the joint probably reflects an increased load bearing of this part of the joint. According to a kinematic study by Beck et al. (2005), the major load bearing areas of the feline acetabulum are the central and caudal thirds rather than the cranial third.

Remodelling was relatively uncommon, affecting 3/82 (3.7%) Hip-rOA joints and two of these joints had hip dysplasia. Godfrey (2007) reported remodelling in 19/72 (26.0%) of hip joints, much greater than the present study; however a definition of remodelling was not clearly made. The current study defined remodelling as a definite alteration in anatomical bone shape and not just the presence of osteophytes.

Enthesiophytes, abnormal mineralisation and synovial effusion were not seen in any hip joint, which is consistent with other studies (Clarke et al., 2005; Godfrey, 2007; Freire et al., 2011).

Hip dysplasia was defined as less than 50.0% coverage of the femoral head by the dorsal edge of the acetabulum and was seen in 12/57 (21.1%) Hip-rOA joints. Only 57 joints could be assessed for HD because of suboptimal positioning. In a previous study, the mean NA was significantly lower in joints with HD (87.5 °) than in normal hip joints (100.1 °) (Clarke and Bennett, 2006) and a similar finding was found in the present study, the mean being 92.5 °and 99.1 ° respectively. The normal NA is much less than that reported for the dog (105.0°) (Olsson, 1961) indicating a shallower acetabulum in the cat. The mean NA of Hip-rOA joints (96.8 °) was significantly lower compared to the no Hip-rOA joints (99.8 °) even after excluding the HD joints. This suggests that the definition of HD used in this study (<50.0% coverage of femoral head by dorsal acetabulum) may not be sensitive enough in diagnosing all cases of feline HD. Further studies are required, including the assessment of hip joint laxity (Langenbach et al., 1998).

Osteoarthritis secondary to HD is said to be common in cats (Langenbach et al., 1998, Keller et al., 1999; Clarke and Bennett 2006; Godfrey, 2007). Some large breed cats such as the Maine Coon appears predisposed to HD. Mills (1995) reported that approximately 18.0% of Maine Coon cats suffer from this condition. Only one Maine Coon cross was seen in the current study and the hip joints were not dysplastic. Langenbach et al. (1998) reported the prevalence of HD as 32.0%, based on the OFA-like scoring system which was developed to diagnose canine HD. The prevalence of HD in another study was 6.6% based on a radiographic survey of 684 cats (Keller et al., 1999). However, a definition of HD was not clearly stated. HD was subjectively diagnosed based on the radiographic findings including subluxation, shallow acetabulum, remodelling of the femoral head/neck, changes on the acetabular rim and OA.

Cartilage changes were more commonly found on the femoral head (88/93; 94.6%) than the acetabulum (75/93; 80.6%). The exact reason for this is not clear. Farese et al. (1998) stated that in dogs with HD, the load-bearing area shifts to the perifoveal region of the femoral head and to the dorsolateral edge of the acetabular rim. Similar changes could occur in cats with subluxated hip joints. A subluxating femoral head could be more susceptible to “wear and tear” since the acetabular rim will rub against the femoral articular surface.

Apart from HD, there was no identifiable underlying cause to explain a secondary OA, suggesting that hip OA is mainly idiopathic or primary in nature.

Chapter 7 Radiographic and pathologic features of osteoarthritis of the feline carpal and tarsal joints

7.1 Introduction and aims

The carpal joint consists of four articulations including the antebrachiocarpal joint, the midcarpal joint, the carpometacarpal joint and the distal radioulnar joint. The antebrachiocarpal and the radioulnar joints share a common joint cavity. The midcarpal and carpometacarpal joint cavities are interconnected (Dyce et al., 2010). The carpus comprises of two rows of bones: the proximal row and the distal row. The proximal row consists of four carpal bones: the radial carpal bone, the ulnar carpal bone, the intermediate carpal bone and the accessory carpal bone. The radial and intermediate carpal bones fuse in cats (Dyce et al., 2010). The distal row consists of the first, the second, the third and the fourth carpal bones. The antebrachiocarpal joint is located between the distal radius and ulna and the proximal row of the carpal bones. The midcarpal joint consists of the articulation between the proximal and distal row of the carpal bones. The carpometacarpal joint is formed between the distal row of the carpal bones and the metacarpal bones (Liebich et al., 2007). The main movement of the carpus occurs at the antebrachiocarpal joint with relative minimal movement of the midcarpal and the carpometacarpal joints. The antebrachiocarpal joint is supported by the medial and lateral collateral ligaments. On the dorsal aspect, the short ligaments join the carpal bones in the same row and those of the distal row to the metacarpus. The deep ligament covers the entire palmar surface of the skeleton. A second superficial transverse ligament passes from the accessory carpal bone to the medial aspect pf the carpus. The accessory carpal bones are joining to the adjacent carpal and metacarpal bones by the small ligaments (Dyce et al., 2010).

Osteoarthritis of the carpal joint is an uncommon radiographic abnormality in cats. Radiographic signs of carpal OA include osteophyte formation, most often seen on the cranial aspect of the distal radius and the carpal bones (Bennett et al., 2012a).

Similarly, the tarsal joint comprises four articulations consisting of the tarsocrural joint, the proximal intertarsal joint, distal intertarsal joint and the tarsometatarsal joint (Liebich et al., 2007). The tarsus is a hinge joint with its primary motion being flexion and extension. The majority of tarsal range of motion occurs at the tarsocrural joint. The tarsus consists of three rows of bones: the proximal, the middle and the distal row. The proximal row is comprised of the talus and the calcaneus. The middle row is composed of a single central tarsal bone. The distal row consists of the first, the

second, the third and the fourth tarsal bones. The tarsocrural joint is located the distal tibia and fibula and the proximal row of the tarsal bones. The proximal intertarsal joint formed by the articulation between the talus and central tarsal bone. The distal intertarsal joint is located between the central tarsal bone and the distal row of the tarsal bones. The tarsometatarsal joint is formed between the distal row of the carpal bones and the metacarpal bones. Stability to the tarsal joint is provided primarily by the medial and lateral collateral ligaments. The medial and lateral collateral ligaments arise from the tibia (and fibula) and insert to the proximal extremity of the metatarsus (Dyce et al., 2010).

Godfrey (2007) reported radiographic OA in 18/129 (14.0%) tarsal joints. Osteoarthritis of the tarsus is predominantly characterised by osteophyte formation on the distal tibia and on the tarsal bones, together with soft tissue mineralisation (Bennett et al., 2012a).

The aim of this study was to define the radiographic features of carpal and tarsal OA and to relate the radiographic findings to the gross pathologic features. In particular the following questions were to be addressed:

a) Can the radiographic features be a good indicator of the severity of cartilage pathology?

b) Are there any underlying causes of carpal and tarsal OA in the cat?

7.2 Materials and methods

7.2.1 Determination of carpal and tarsal OA populations

Determination of the carpal and tarsal OA population was done as described in Section 2.2, page 58 and Figure 2.1, page 59.

7.2.2 Comparative analyses of signalment, body weight and body condition score between Carp/Tars-path OA and no Carp/Tars-path/normal cats

Median of age, BW and BCS of Carp/Tars-path OA and no Carp/Tars-path OA/normal cats were shown with a scatter plot graph and statistically analysed by using Mann-Whitney *U* test. The distribution of breed and gender of Carp/Tars-path OA and no Carp/Tars-path OA/normal cats was visualised using a stacked bar graph. The distribution of BCS of Carp/Tars-path OA and no Carp/Tars-path OA/normal cats was shown by a column bar graph.

7.2.3 Radiographic assessment of carpal and tarsal joints

Radiographic changes associated with carpal and tarsal OA were assessed using a radiographic scoring system (see Section 2.3.3, page 60 and Table 2.1, page 62). The radiographic features assessed were osteophytes, enthesiophytes, areas of abnormal mineralisation, synovial effusion and joint remodelling. The prevalence of Carp/Tars-rOA and no Carp/Tars-rOA was calculated as the percentage of cats which had or had no radiographic changes. The prevalence of each radiographic feature was determined as the percentage of affected carpal and tarsal joints which had the feature. The mean and SD of osteophyte size was calculated.

7.2.4 Gross pathologic assessment of carpal and tarsal joints

Gross pathologic changes associated with OA were assessed and scored using a gross pathologic scoring system (see Section 2.4.1, page 66 and Table 2.3, page 67). For the carpal joint, the gross pathologic changes of the distal radius, distal ulna and the proximal carpal bones were not scored individually but given a single overall score-only the antebrachiocarpal joint was assessed. For the tarsal joint, the distal tibia and the trochlea of the talus were also given a single overall score- only the tarsocrural joint was assessed. The total gross pathologic scores and the global scores were recorded. The prevalence of Carp/Tars-path OA and no Carp/Tars-path OA/normal were determined as the percentage of cats which had or had no gross changes in the articular

cartilage. The prevalence of each gross pathologic feature was calculated as the percentage of affected carpal and tarsal joints which had the feature. The Mann-Whitney *U* test was used to analyse the difference between total gross pathologic scores of the left and right carpal and tarsal joints. The results were illustrated with a scatter plot graph.

7.2.5 Correlation studies

7.2.5.1 Correlation between total radiographic and gross pathologic OA scores

A correlation analysis between total radiographic and gross pathologic scores for the left and right carpal and tarsal joints was performed using a nonparametric, Spearman's rank correlation. Correlation coefficient results were interpreted as described in Table 2.9, page 80. The correlation was illustrated by scatter plot graphs.

7.2.5.2 Correlation between total radiographic OA scores and age, BW and BCS

A correlation analysis between total radiographic OA scores for the left and right carpal and tarsal joints and age, BW and BCS was carried out using Spearman's rank correlation. The coefficient results were interpreted as described in Table 2.9, page 80. The correlation for left and right carpal and tarsal joints was illustrated by scatter plot graphs.

7.2.5.3 Correlation between total gross pathologic OA scores and age, BW and BCS

A correlation analysis between total gross pathologic OA scores for the left and right carpal and tarsal joints and age, BW and BCS was done using a nonparametric, Spearman's rank correlation. The coefficient results were interpreted as described in Table 2.9, page 80. The correlation for left and right carpal and tarsal joints was illustrated by scatter plot graphs.

7.3 Results

7.3.1 Carpal and tarsal OA population

A total of 116 carpal and tarsal joints from 58 cats were evaluated for the radiographic signs of OA. Of 58 cats, 16 had radiographic changes associated with carpal OA (Carp-rOA). All Carp-rOA joints had cartilage changes. Of 42 cats with radiographically normal carpal joints (no Carp-rOA), 13 had cartilage changes, thus giving a total population of 29 cats with carpal OA (Carp-path OA) (Table 7.1).

Of 58 cats, 41 had radiographic changes associated with tarsal OA (Tars-rOA). All Tars-rOA had cartilage changes. Of 17 cats with radiographically normal tarsal joint (no Tars-rOA), two had cartilage changes, thus giving a total population of 43 cats with Tarsal OA (Tars-path OA) (Table 7.2).

Population	Number of cats	Percentage (%)
Carp-rOA	16	27.6
No Carp-rOA	42	72.4
Carp-path OA	29	50.0
No Carp-path OA/normal	29	50.0

Table 7.1: Showing the number and percentage of the Carp-rOA, no Carp-rOA, Carp-path OA and no Carp-path OA/normal populations. Total number of cats is 58.

Population	Number of cats	Percentage (%)
Tars-rOA	41	70.7
No Tars-rOA	17	29.3
Tars-path OA	43	74.1
No Tars-path OA/normal	15	25.9

Table 7.2: Showing the number and percentage of the Tars-rOA, no Tars-rOA, Tars-path OA and no Tars-path OA/normal populations. Total number of cats is 58.

7.3.2 Comparative analyses of signalment, body weight and body condition score between Carp/Tars-path OA and no Carp/Tars-path OA.

7.3.2.1 Signalment

Carpal OA

The mean age of the Carp-path OA was 7.9 years (SD 3.9) with a minimum age of 2 years and a maximum of 15 years. The median age was 8 years. The mean age of the no Carp-path OA/normal cats was 5.6 years (SD 4.8) with a minimum age of 3 months and a maximum of 20 years. The median age was 5 years. The age difference between the Carp-path OA and no Carp-path OA/normal cats was significant ($P<0.01$) (Figure 7.1.A). Eleven Carp-path OA cats were MC, 4 cats were F and 14 cats were FS. One of the no Carp-path OA/normal cats was M, 7 cats were MC, 9 cats were F and 12 cats were FS. In the Carp-path OA group 72.4% were DSH, 20.7% were DLH and 6.8% were pedigree cats. In the no Carp-path OA/normal group 82.8% were DSH, 6.9% were DLH and 10.2% were pedigree cats (Figures 7.2.A and 7.2.B).

Tarsal OA

The mean age of the Tars-path OA was 7.7 years (SD 4.5) with a minimum age of 2 years and a maximum of 20 years. The median age was 8 years. The mean age of the no Tars-path OA/normal cats was 4.1 years (SD 2.6) with a minimum age of 3 months and a maximum of 10 years. The median age was 5 years. The age difference between the Tars-path OA and no Tars-path OA/normal cats was significant ($P<0.01$) (Figure 7.3.A). Thirteen Tars-path OA cats were MC, 7 cats were F and 23 cats were FS. One of the no Tars-path OA/normal cats was M, 5 cats were MC, 6 cats were F and 3 cats were FS. In the Tars-path OA group 74.4% were DSH, 16.3% were DLH and 9.3% were pedigree cats. In the no Tars-path OA/normal group 86.7% were DSH, 6.7% were DLH and 6.7% were pedigree cats (Figures 7.4.A and 7.4.B).

7.3.2.2 Body weight

Carpal OA

The mean BW of the Carp-path OA cats was 3.5 kg (SD 1.3) with a minimum weight of 1.9 kg and a maximum of 7.0 kg. The median BW was 3.3 kg. The mean BW of the no Carp-path OA/normal cats was 3.3 kg (SD 1.0) with a minimum weight of 0.8 kg and a maximum of 5.6 kg. The median was 3.1 kg. The difference between the Carp-path OA and no Carp-path OA/normal cats for BW was not significant ($P=0.52$) (Figure 7.1.B).

Tarsal OA

The mean BW of the Tars-path OA cats was 3.4 kg (SD 1.2) with a minimum weight of 1.9 kg and a maximum of 7.0 kg. The median BW was 3.1 kg. The mean BW of the no Tars-path OA/normal cats was 3.5 kg (SD 1.2) with a minimum weight of 0.8 kg and a maximum of 5.9 kg. The median was 3.2 kg. The difference between the Tars-path OA and no Tars-path OA/normal cats for BW was not significant (P=0.40) (Figure 7.3.B).

7.3.2.3 Body condition score

Carpal OA

The Carp-path OA cats had a median BCS of 3with a minimum BCS of 1 and a maximum of 5. The no Carp-path OA/normal cats had a median 3 with a minimum BCS of 2 and a maximum of 4. There was no significant difference between BCS of the Carp-path OA and no Carp-path OA/normal cats (P=0.59) (Figure 7.1.C). The distribution of BCS of the Carp-path OA and no Carp-path OA/normal cats is shown in Figure 7.5.A.

Tarsal OA

The Tars-path OA cats had a median BCS of 3 with a minimum BCS of 1 and a maximum of 5. The no Tars-path OA/normal cats had a median 3 with a minimum BCS of 2 and a maximum of 5. There was no significant difference between BCS of the Tars-path OA and no Tars-path OA/normal cats (P=0.52) (Figure 7.3.C). The distribution of BCS of the Tars-path OA and no Tars-path OA/normal cats is shown in Figure 7.5.B.

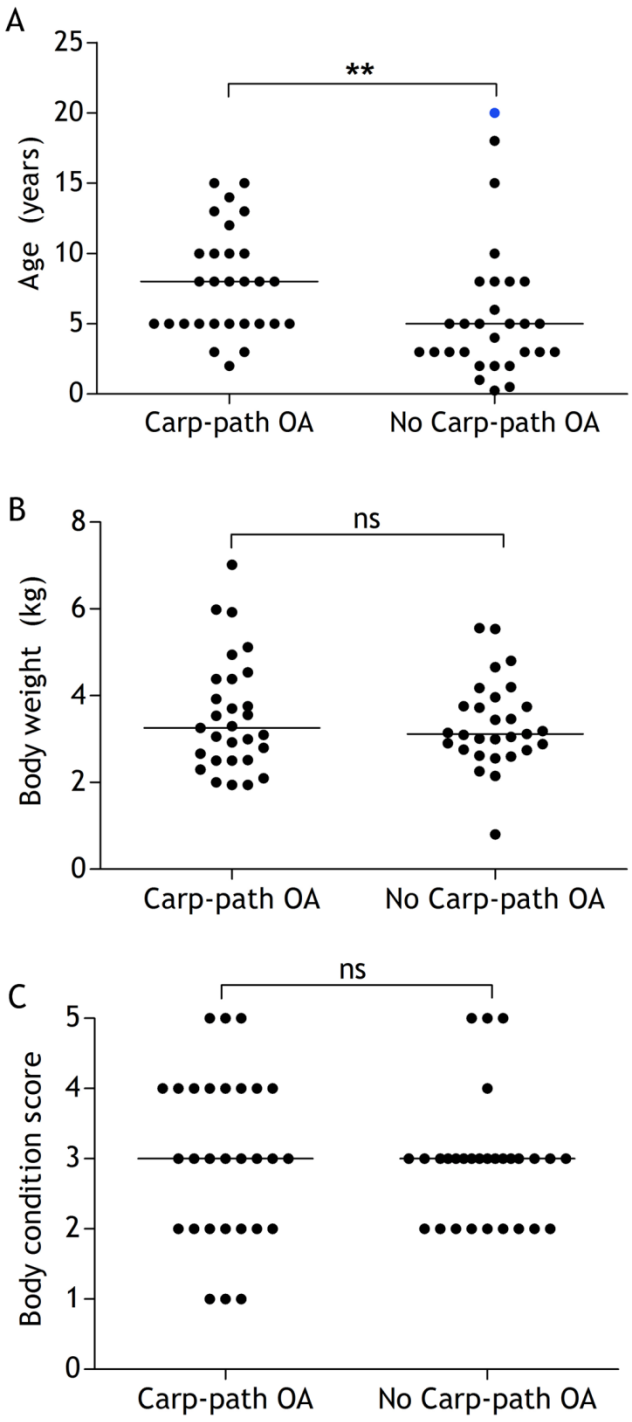

Figure 7.1: The comparative analysis of age, BW and BCS between Carp-path OA (*N*=29) and no Carp-path OA/normal (*N*=29) cats.

(A) The age difference between the Carp-path OA and no Carp-path OA/normal cats is significant. There is no significant difference in BW (B) and BCS (C) of cats with and without Carp-path OA. Data presented as median and plotted in vertical scatter plot. (Mann Whitney *U* test, ** represents P<0.01; ns: not significant P>0.05).

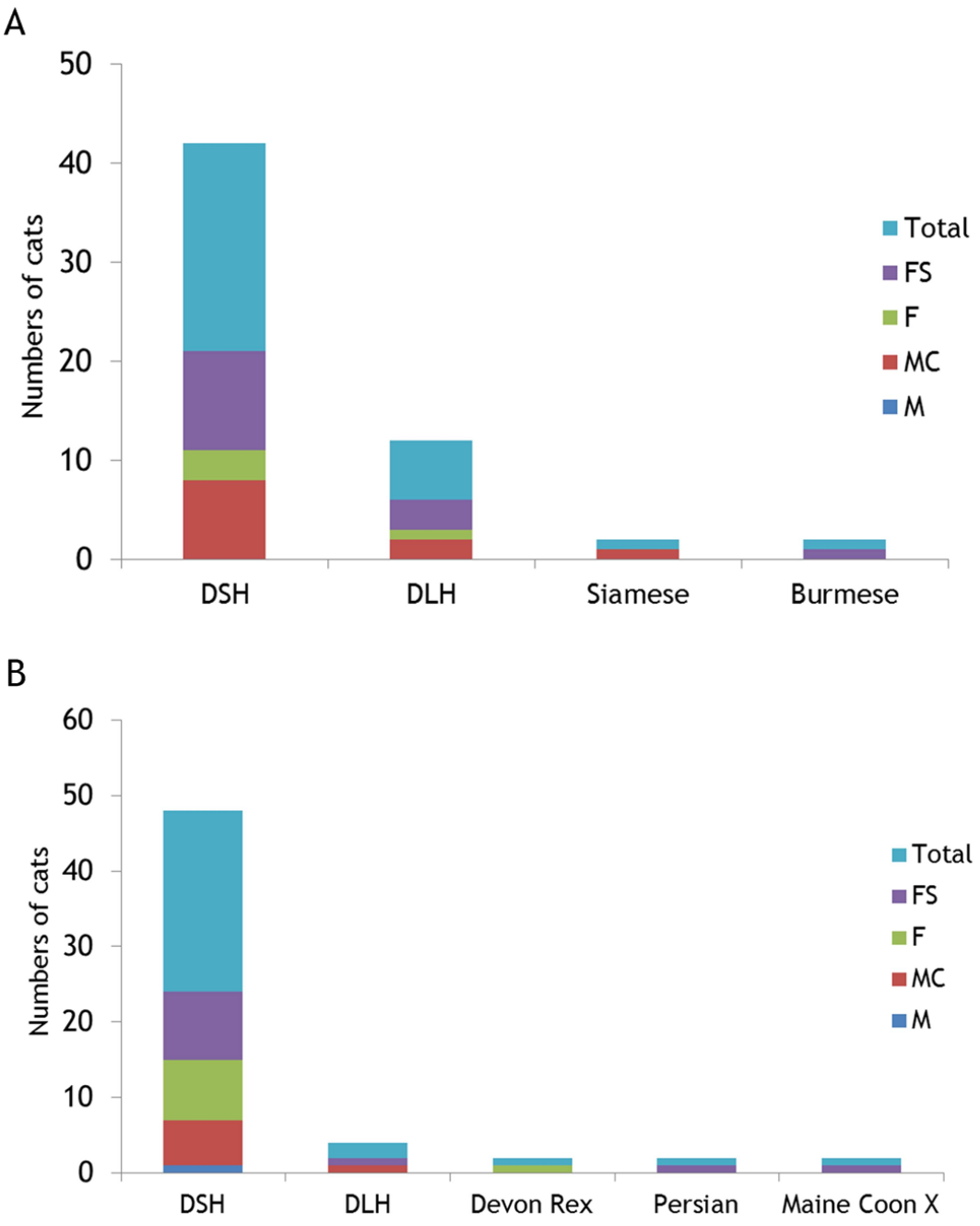

Figure 7.2: Breed and gender distribution of Carp-path OA (A) and no Carp-path OA/normal (B) cats.

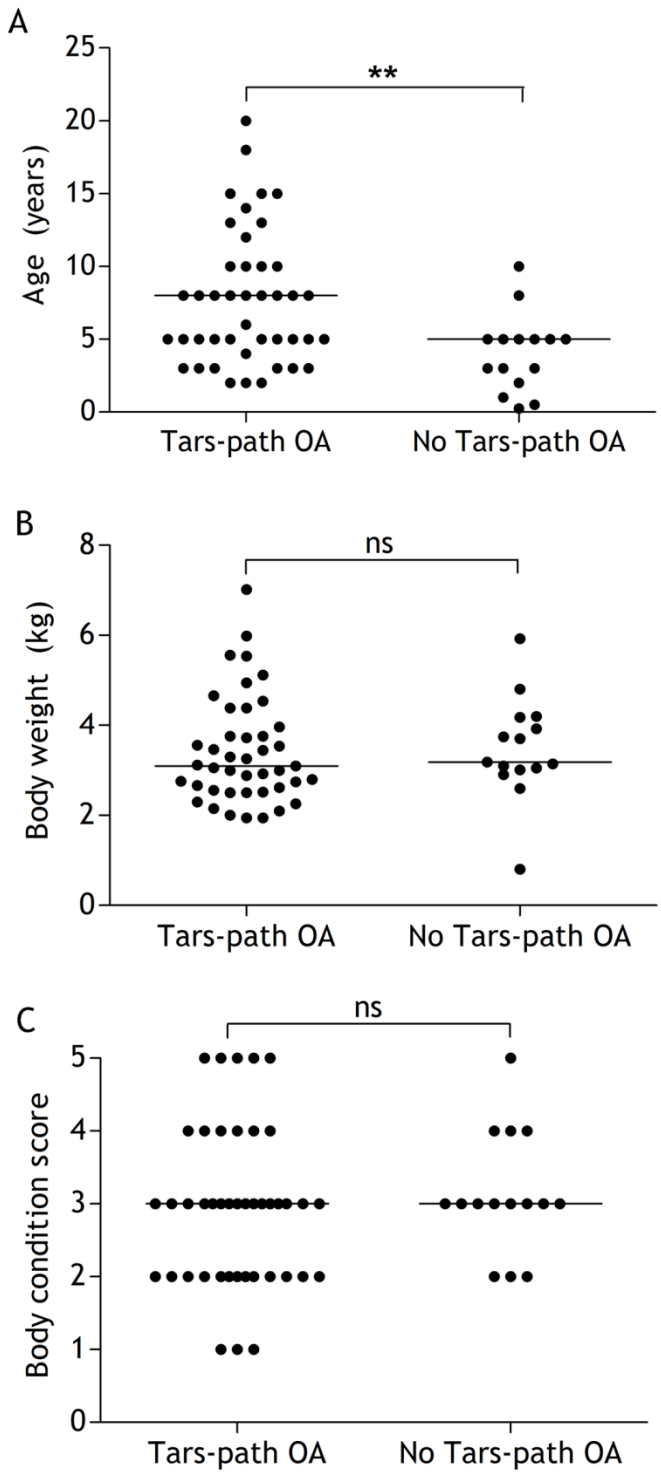

Figure 7.3: The comparative analysis of age, BW and BCS between Tars-path OA (*N*=43) and no Tars-path OA/normal (*N*=15) cats.

(A) The age difference between the Tars-path OA and no Tars-path OA/normal cats is significant. There is no significant difference in BW (B) and BCS (C) of cats with and without Tars-path OA. Data presented as median and plotted in vertical scatter plot. (Mann Whitney *U* test, ** represents P<0.01; ns: not significant P>0.05).

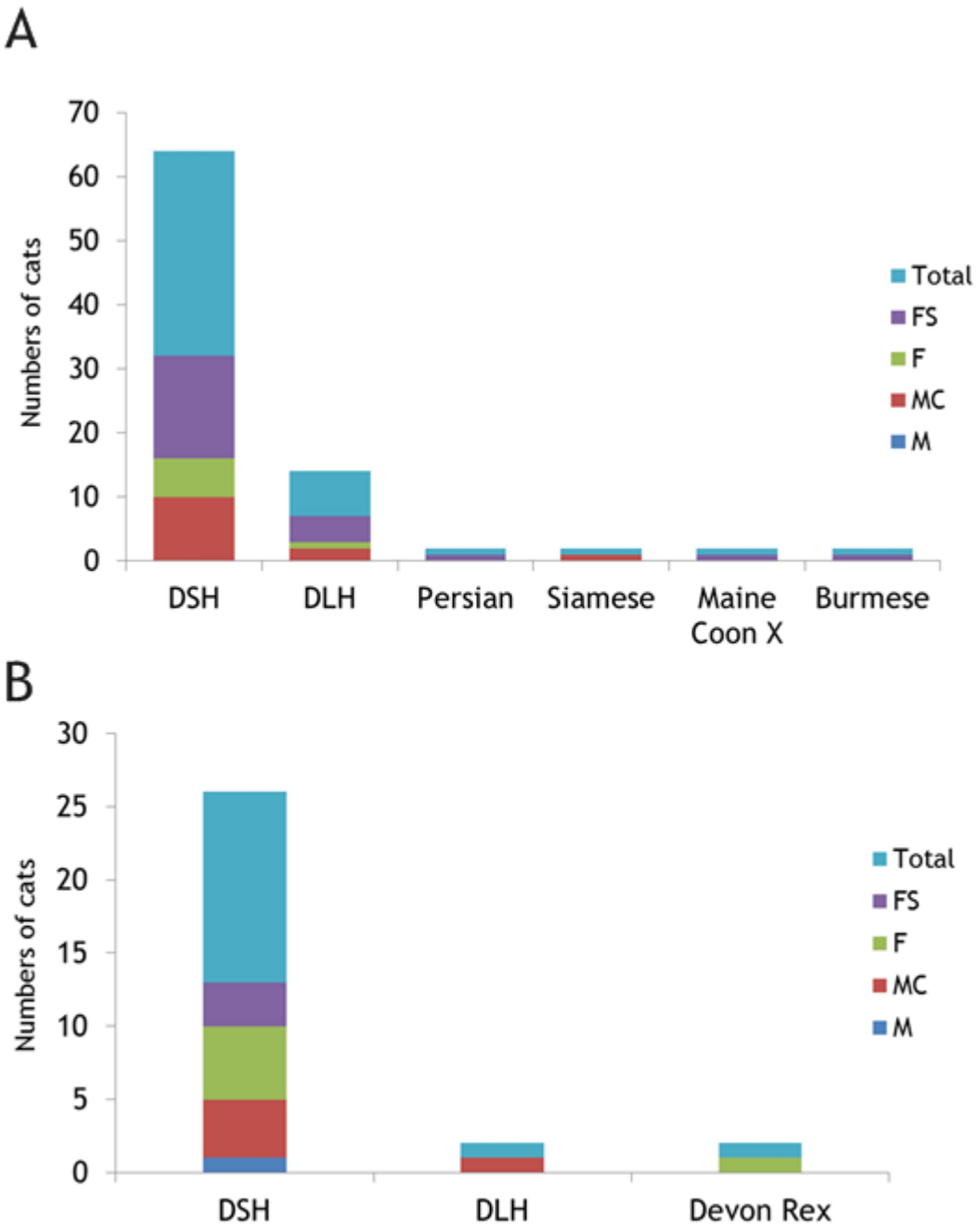

Figure 7.4: Breed and gender distribution of Tars-path OA (A) and no Tars-path OA/normal (B) cats.

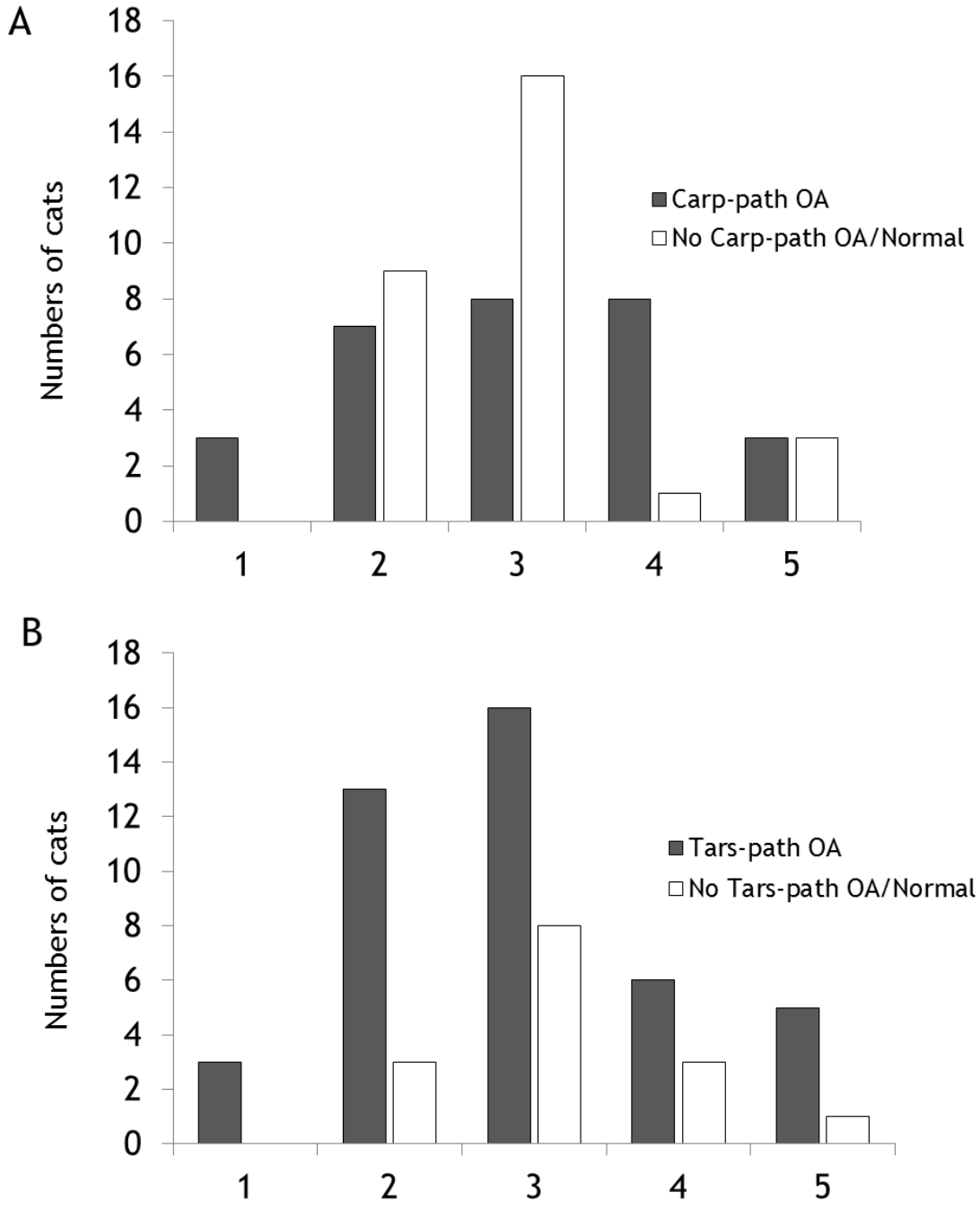

Figure 7.5: Distribution of body condition scores (BCS) of carpal (A) and tarsal (B) OA cats.

7.3.3 Radiographic findings

7.3.3.1 Carpal OA

The overall prevalence of Carp-rOA was 27.6% (16 of 58 cats). Of 16 cats with radiographic changes, 9 cats had bilateral and 7 had unilateral carpal involvement (5 on the left and 2 on the right) giving a total number of 25 Carp-rOA joints (Table 7.3). The mean total radiographic score of left and right carpal joints was 1.4 and 1.8 respectively. The median total radiographic score of left and right carpal joints was 1 with a range from 1 to 6 for each joint. Of 25 Carp-rOA joints, 23 were given a Global score of 1 and two a Global score of 2 (Tables 7.4 and 7.5).

All Carp-rOA joints had osteophyte formation, bilaterally in 9 cats and unilaterally in 7 cats (5 on the left and 2 on the right). Osteophytes were seen on the distal radius and radial carpal bones (Figures 7.6.B-D). Severity was graded mild in 20/25 (80.0%) joints (13 on the left and 7 on the right), moderate in 3/25 (12.0%) joints (all on the right) and severe in 2/25 (8.0%) joints (1 on the left and 1 on the right). The mean osteophyte size in mm ± SD for mildly affected joints was 1.1 ± 0.4, for moderately affected joints was 3.1 ± 0.4 and for severely affected joints was 5.1 ± 0.1 (Table 7.6).

Areas of abnormal mineralisation were present in 3/25 (12.0%) joints bilaterally in one cat and unilaterally in one cat (both on the right). In all carpal joints this was graded moderate (Figures 7.6.C-D). Areas of abnormal mineralisation were commonly seen on the cranial aspect of the carpus.

Joint remodelling was identified in 2/25 (8.0%) carpal joints (1 on the left and 1 on the right), defined as changes in anatomical shape of the distal radius/ulna and radial carpal bone (Figures 7.6.C-D).

Enthesiophytes and synovial effusion were not identified in any carpal joint.

	Radiographic findings			
	No Carp-rOA		Carp-rOA	
	Number of joints	Percentage (%)	Number of joints	Percentage (%)
Left carpus	44	75.9	14	24.1
Right carpus	47	81.0	11	19.0
Total	91	78.4	25	21.6

Table 7.3: Showing numbers of carpal joints with normal and abnormal radiographic findings. Total number of joints 116.

	Radiographic findings			
	Score 0	Score 1	Score 2	Score 3
Left carpus	44	13	1	0
Right carpus	47	10	1	0
Total	91	23	2	0
Percentage (%)	78.4	19.8	1.7	0

Table 7.4: The number and percentage of carpal joints with different radiographic OA Global scores.

Cat ID	Osteophytes		Enthesiophytes		Area of abnormal mineralisation		Synovial effusion		Joint remodelling		Total score		Global score	
	L	R	L	R	L	R	L	R	L	R	L	R	L	R
X1	0	0	0	0	0	0	0	0	0	0	0	0	0	0
X2	0	0	0	0	0	0	0	0	0	0	0	0	0	0
X3	1	2	0	0	0	0	0	0	0	0	1	2	1	1
X4	0	0	0	0	0	0	0	0	0	0	0	0	0	0
X5	0	0	0	0	0	0	0	0	0	0	0	0	0	0
X6	0	1	0	0	0	0	0	0	0	0	1	0	1	0
X7	1	0	0	0	0	0	0	0	0	0	1	0	1	0
X8	1	2	0	0	0	0	0	0	0	0	1	1	1	1
X9	0	0	0	0	0	0	0	0	0	0	0	0	0	0
X10	1	1	0	0	0	0	0	0	0	0	1	1	1	1
X11	0	0	0	0	0	0	0	0	0	0	0	0	0	0
X12	0	0	0	0	0	0	0	0	0	0	0	0	0	0
X13	0	0	0	0	0	0	0	0	0	0	0	0	0	0
X14	0	0	0	0	0	0	0	0	0	0	0	0	0	0
X15	0	0	0	0	0	0	0	0	0	0	0	0	0	0
X16	0	1	0	0	0	0	0	0	0	0	0	1	0	1
X17	0	0	0	0	0	0	0	0	0	0	0	0	0	0
X18	0	0	0	0	0	0	0	0	0	0	0	0	0	0
X19	0	0	0	0	0	0	0	0	0	0	0	0	0	0
X20	0	0	0	0	0	0	0	0	0	0	0	0	0	0

Table 7.5: Radiographic features and Global scores of the left (L) and right (R) carpal joints in 58 cats. Scoring: 0: absent, 1: mild/present, 2: moderate, 3: severe. Global score: 0: no abnormality, 1: mild, 2: moderate, 3: severe.

Cat ID	Osteophytes		Enthesiophytes		Area of abnormal mineralisation		Synovial effusion		Joint remodelling		Total score		Global score	
	L	R	L	R	L	R	L	R	L	R	L	R	L	R
X21	1	0	0	0	0	0	0	0	0	0	1	0	1	0
X22	0	0	0	0	0	0	0	0	0	0	0	0	0	0
X23	0	0	0	0	0	0	0	0	0	0	0	0	0	0
X24	0	0	0	0	0	0	0	0	0	0	0	0	0	0
X25	1	1	0	0	0	0	0	0	0	0	1	1	1	1
X26	1	0	0	0	0	0	0	0	0	0	1	0	1	0
X27	1	0	0	0	0	0	0	0	0	0	1	0	1	0
X28	0	0	0	0	0	0	0	0	0	0	0	0	0	0
X29	1	0	0	0	0	0	0	0	0	0	1	0	1	0
X30	1	1	0	0	0	0	0	0	0	0	1	1	1	1
X31	3	3	0	0	2	2	0	0	1	1	6	6	2	2
X32	1	1	0	0	0	0	0	0	0	0	1	1	1	1
X33	0	0	0	0	0	0	0	0	0	0	0	0	0	0
X34	0	0	0	0	0	0	0	0	0	0	0	0	0	0
X35	0	0	0	0	0	0	0	0	0	0	0	0	0	0
X36	0	0	0	0	0	0	0	0	0	0	0	0	0	0
X37	0	0	0	0	0	0	0	0	0	0	0	0	0	0
X38	0	0	0	0	0	0	0	0	0	0	0	0	0	0

Table 7.5 continued.

Cat ID	Osteophytes		Enthesiophytes		Area of abnormal mineralisation		Synovial effusion		Joint remodelling		Total score		Global score	
	L	R	L	R	L	R	L	R	L	R	L	R	L	R
X39	0	0	0	0	0	0	0	0	0	0	0	0	0	0
X40	0	0	0	0	0	0	0	0	0	0	0	0	0	0
X41	1	2	0	0	0	2	0	0	0	0	1	4	1	1
X42	1	1	0	0	0	0	0	0	0	0	1	1	1	1
X43	0	0	0	0	0	0	0	0	0	0	0	0	0	0
X44	0	0	0	0	0	0	0	0	0	0	0	0	0	0
X45	0	0	0	0	0	0	0	0	0	0	0	0	0	0
X46	0	0	0	0	0	0	0	0	0	0	0	0	0	0
X47	0	0	0	0	0	0	0	0	0	0	0	0	0	0
X48	0	0	0	0	0	0	0	0	0	0	0	0	0	0
X49	0	0	0	0	0	0	0	0	0	0	0	0	0	0
X50	0	0	0	0	0	0	0	0	0	0	0	0	0	0
X51	0	0	0	0	0	0	0	0	0	0	0	0	0	0
X52	0	0	0	0	0	0	0	0	0	0	0	0	0	0
X53	0	0	0	0	0	0	0	0	0	0	0	0	0	0
X54	0	0	0	0	0	0	0	0	0	0	0	0	0	0

Table 7.5 continued.

Cat ID	Osteophytes		Enthesiophytes		Area of abnormal mineralisation		Synovial effusion		Joint remodelling		Total score		Global score	
	L	R	L	R	L	R	L	R	L	R	L	R	L	R
X55	0	0	0	0	0	0	0	0	0	0	0	0	0	0
X56	0	0	0	0	0	0	0	0	0	0	0	0	0	0
X57	0	0	0	0	0	0	0	0	0	0	0	0	0	0
X58	0	0	0	0	0	0	0	0	0	0	0	0	0	0

Table 7.5 continued.

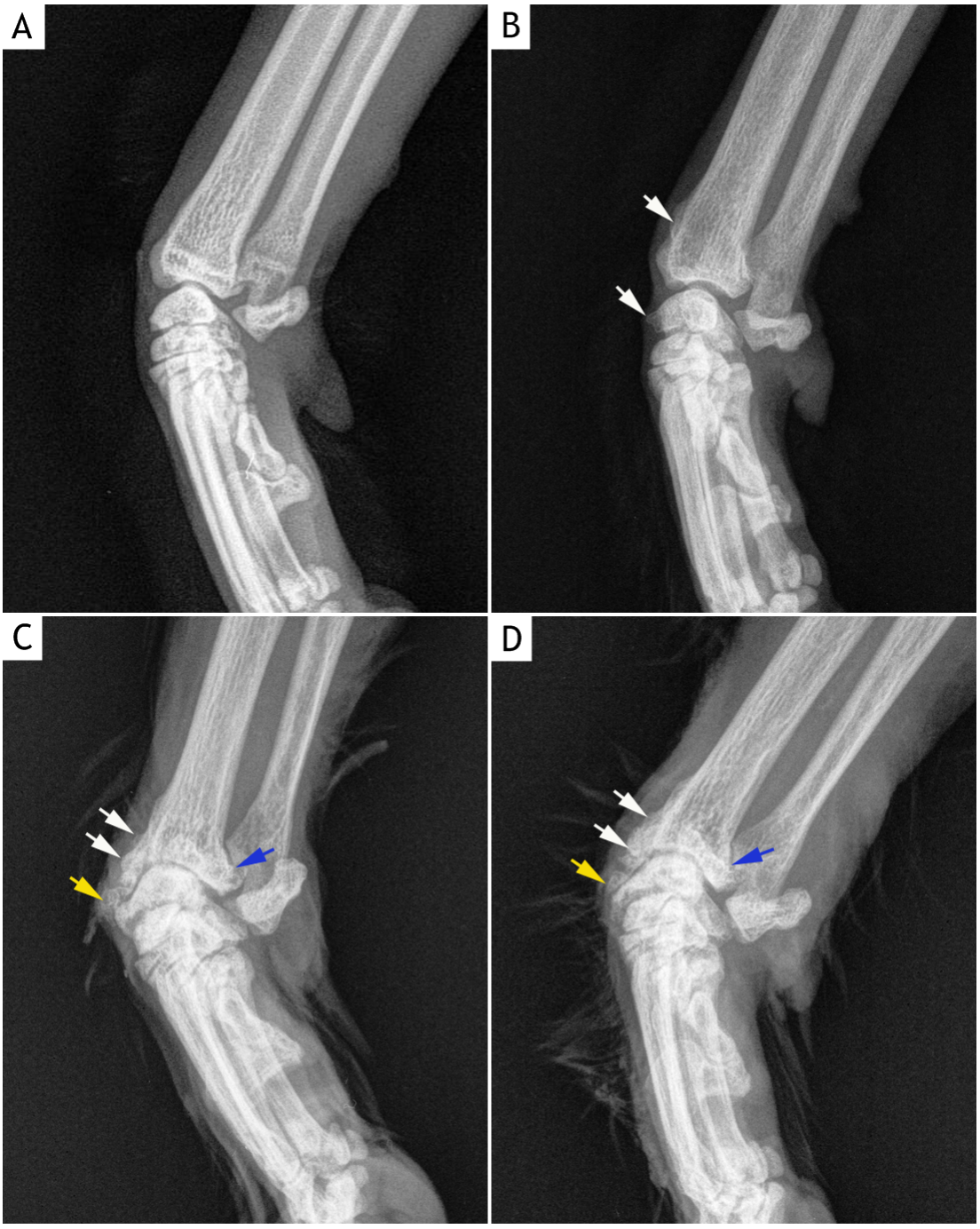

Figure 7.6: Mediolateral radiographs of carpal joints with radiographic changes associated with OA.

(A) Normal carpal joint. Cat ID: X34, left carpus. (B) Mild osteophyte formation is identified on the distal radius (white arrow) and radial carpal bone (white arrow). Cat ID: X32, right carpus. (C & D) Severe osteophyte formation is seen at the cranial (white arrows) and caudal (blue arrow) aspect of the distal radius. Areas of abnormal mineralisation are also observed (yellow arrow). A change in anatomical shape of the distal radius and radial carpal bone (remodelling) is identified. C: Cat ID: X31, left carpus; D: Cat ID: X31, right carpus.

Cat ID	Left carpus		Right carpus	
	Score	Osteophyte size (mm)	Score	Osteophyte size (mm)
X3	1	0.7	2	2.8
X6	0	-	1	1.0
X7	1	0.9	0	-
X8	1	0.9	2	2.9
X10	1	1.2	1	1.3
X16	0	-	1	1.1
X21	1	0.5	0	-
X25	1	1.8	1	1.4
X26	1	1.0	0	-
X27	1	0.9	0	-
X29	1	0.8	0	-
X30	1	0.9	1	0.8
X31	3	5.1	3	5.0
X32	1	1.1	1	1.8
X41	1	1.8	2	3.6
X42	1	1.4	1	1.2

Table 7.6: Osteophytes when present were graded according to their size (mm) and whether a single site or multiple sites were involved.

7.3.3.2 Tarsal OA

The overall prevalence of Tars-rOA was 70.7% (41 of 58 cats). Of 41 cats with radiographic changes, 28 cats had bilateral and 13 had unilateral tarsal involvement (10 on the left and 3 on the right) giving a total number of 69 Tars-rOA joints (Table 7.7). The mean total radiographic score for the left and right tarsus was 1.3. The median total radiographic score of the left tarsus was 1 with a range from 1 to 3. The median total radiographic score of the right tarsal joint was 1 with a range from 1 to 4. Of 69 Tars-rOA joints, 65 were given a Global score 1, two a Global score 2 and two a Global score 3 (Tables 7.8 and 7.9).

All Tars-rOA joints had osteophyte formation. In 28 cats this was bilateral and in 13 cats unilateral (10 on the left and 3 on the right). Osteophytes were commonly identified at the distal tibia, tibial tarsal bone and central tarsal bone (Figures 7.7.B-D). Severity was graded mild in 52/69 (75.4%) joints (28 on the left and 24 on the right), moderate in 15/69 (21.7%) joints (10 on the left and 5 on the right) and severe in 2/69 (2.9%) joints (both on the right). The mean osteophyte size in mm ± SD for mildly affected joints was 0.9 ± 0.3, for moderately affected joints was 2.6 ± 0.3 and for severely affected joints was 5.3 ± 0.3 (Table 7.10).

Joint remodelling was identified in 4/69 (5.8%) tarsal joints (1 on the left and 3 on the right) identified as changes in anatomical shape of the distal tibia, fibula and tarsal bones (Figure 7.7).

Enthesiophytes, areas of abnormal mineralisation and synovial effusion were not identified in any tarsal joint.

	Radiographic findings			
	No Tars-rOA		Tars-rOA	
	Number of joints	Percentage (%)	Number of joints	Percentage (%)
Left tarsus	20	34.5	38	65.5
Right tarsus	27	46.6	31	53.4
Total	47	40.5	69	59.5

Table 7.7: Showing numbers of tarsal joints with normal and abnormal radiographic findings. Total number of joints 116.

	Radiographic OA Global score			
	Score 0	Score 1	Score 2	Score 3
Left tarsus	20	37	1	0
Right tarsus	27	28	1	2
Total	47	65	2	2
Percentage (%)	40.5	56.0	1.7	1.7

Table 7.8: The number and percentage of tarsal joints with different radiographic OA Global scores.

Cat ID	Osteophytes		Enthesiophytes		Area of abnormal mineralisation		Synovial effusion		Joint remodelling		Total score		Global score	
	L	R	L	R	L	R	L	R	L	R	L	R	L	R
X1	2	1	0	0	0	0	0	0	0	0	1	1	1	1
X2	0	0	0	0	0	0	0	0	0	0	0	0	0	0
X3	1	0	0	0	0	0	0	0	0	0	1	0	1	0
X4	0	0	0	0	0	0	0	0	0	0	0	0	0	0
X5	0	0	0	0	0	0	0	0	0	0	0	0	0	0
X6	1	0	0	0	0	0	0	0	0	0	1	0	1	0
X7	1	1	0	0	0	0	0	0	0	0	1	1	1	1
X8	1	1	0	0	0	0	0	0	0	0	1	1	1	1
X9	1	0	0	0	0	0	0	0	0	0	1	0	1	0
X10	2	0	0	0	0	0	0	0	0	0	2	0	1	0
X11	2	2	0	0	0	0	0	0	0	0	2	2	1	1
X12	0	0	0	0	0	0	0	0	0	0	0	0	0	0
X13	0	0	0	0	0	0	0	0	0	0	0	0	0	0
X14	0	0	0	0	0	0	0	0	0	0	0	0	0	0
X15	2	1	0	0	0	0	0	0	0	0	2	1	1	1
X16	1	1	0	0	0	0	0	0	0	0	1	1	1	1
X17	1	1	0	0	0	0	0	0	0	0	1	1	1	1
X18	2	1	0	0	0	0	0	0	0	0	2	1	1	1
X19	0	0	0	0	0	0	0	0	0	0	0	0	0	0
X20	1	1	0	0	0	0	0	0	0	0	1	1	1	1

Table 7.9: Radiographic features and Global scores of the left (L) and right (R) tarsal joints in 58 cats. Scoring: 0: absent, 1: mild/present, 2: moderate, 3: severe. Global score: 0: no abnormality, 1: mild, 2: moderate, 3: severe.

Cat ID	Osteophytes		Enthesiophytes		Area of abnormal mineralisation		Synovial effusion		Joint remodelling		Total score		Global score	
	L	R	L	R	L	R	L	R	L	R	L	R	L	R
X21	0	0	0	0	0	0	0	0	0	0	0	0	0	0
X22	1	1	0	0	0	0	0	0	0	0	1	1	1	1
X23	1	1	0	0	0	0	0	0	0	0	1	1	1	1
X24	1	1	0	0	0	0	0	0	0	0	1	1	1	1
X25	0	1	0	0	0	0	0	0	0	0	0	1	0	1
X26	1	1	0	0	0	0	0	0	0	0	1	1	1	1
X27	1	0	0	0	0	0	0	0	0	0	1	0	1	0
X28	2	1	0	0	0	0	0	0	0	0	2	1	1	1
X29	1	0	0	0	0	0	0	0	0	0	1	0	1	0
X30	2	2	0	0	0	0	0	0	1	1	3	3	2	2
X31	1	3	0	0	0	0	0	0	0	1	1	4	1	3
X32	1	1	0	0	0	0	0	0	0	0	1	1	1	1
X33	0	1	0	0	0	0	0	0	0	0	0	1	0	1
X34	0	0	0	0	0	0	0	0	0	0	0	0	0	0
X35	1	0	0	0	0	0	0	0	0	0	1	0	1	0
X36	0	0	0	0	0	0	0	0	0	0	0	0	0	0
X37	1	1	0	0	0	0	0	0	0	0	1	1	1	1
X38	1	0	0	0	0	0	0	0	0	0	1	0	1	0
X39	1	2	0	0	0	0	0	0	0	0	1	2	1	1
X40	1	0	0	0	0	0	0	0	0	0	1	0	1	0
X41	1	2	0	0	0	0	0	0	0	0	1	2	1	1

Table 7.9 continued.

Cat ID	Osteophytes		Enthesiophytes		Area of abnormal mineralisation		Synovial effusion		Joint remodelling		Total score		Global score	
	L	R	L	R	L	R	L	R	L	R	L	R	L	R
X42	2	1	0	0	0	0	0	0	0	0	2	1	1	1
X43	2	2	0	0	0	0	0	0	0	0	2	2	1	1
X44	1	1	0	0	0	0	0	0	0	0	1	1	1	1
X45	1	1	0	0	0	0	0	0	0	0	1	1	1	1
X46	0	0	0	0	0	0	0	0	0	0	0	0	0	0
X47	2	3	0	0	0	0	0	0	0	1	2	4	1	3
X48	0	1	0	0	0	0	0	0	0	0	0	1	0	1
X49	1	0	0	0	0	0	0	0	0	0	1	0	1	0
X50	0	0	0	0	0	0	0	0	0	0	0	0	0	0
X51	0	0	0	0	0	0	0	0	0	0	0	0	0	0
X52	0	0	0	0	0	0	0	0	0	0	0	0	0	0
X53	0	0	0	0	0	0	0	0	0	0	0	0	0	0
X54	1	1	0	0	0	0	0	0	0	0	1	1	1	1
X55	1	1	0	0	0	0	0	0	0	0	1	1	1	1
X56	1	1	0	0	0	0	0	0	0	0	1	1	1	1
X57	0	0	0	0	0	0	0	0	0	0	0	0	0	0
X58	0	0	0	0	0	0	0	0	0	0	0	0	0	0

Table 7.9 continued.

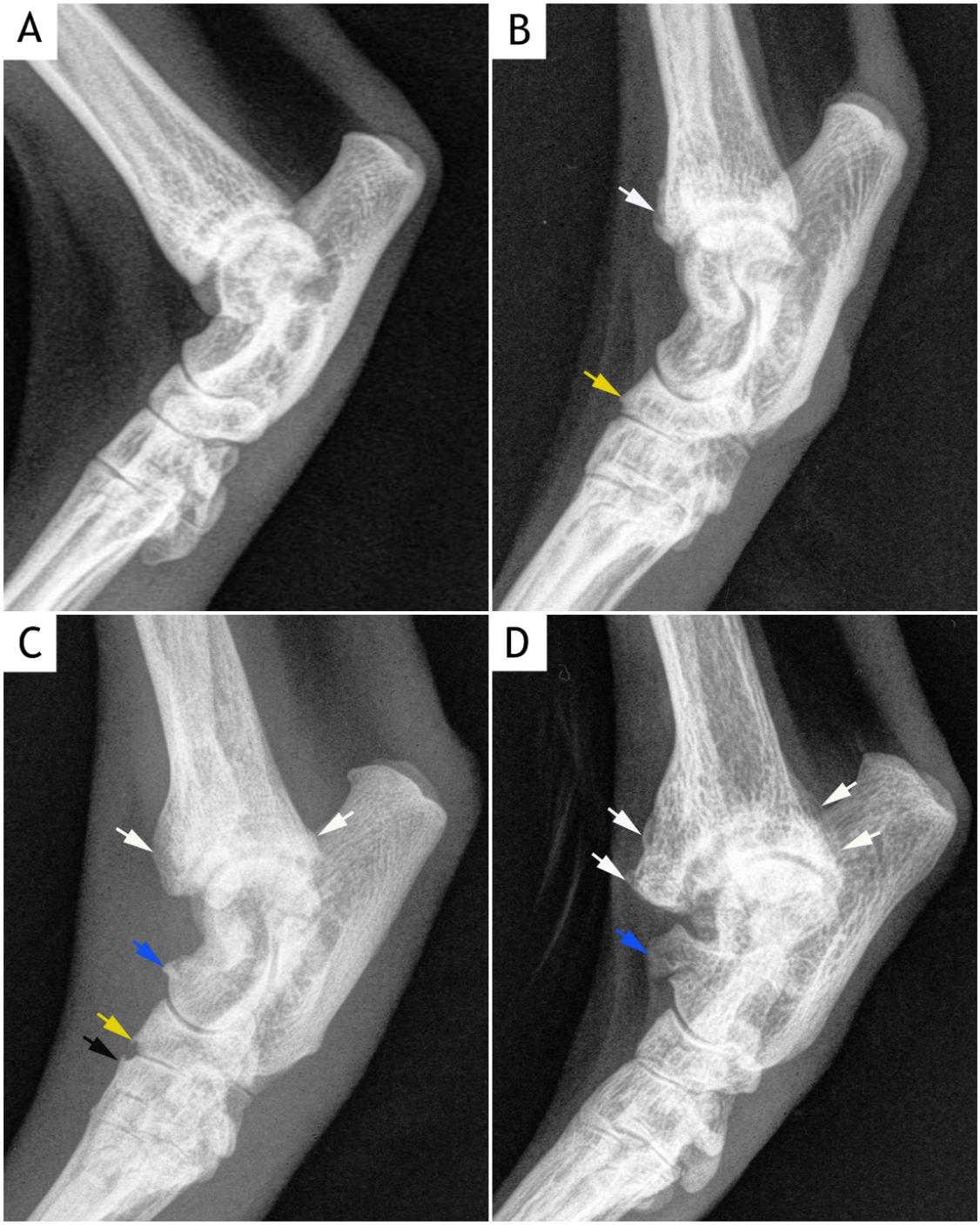

Figure 7.7: Mediolateral radiographs of tarsal joints showing radiographic changes associated with OA.

(A) Normal tarsal joint. Cat ID: X19, right tarsal. (B, C & D) Osteophyte formation is observed at the distal tibia (white arrows), tibial tarsal bone (blue arrow), central tarsal bone (yellow arrow), and the third tarsal bone (black arrow). Joint remodelling is obvious in (C) and (D) characterised by change in anatomical shape of the distal tibia and tibial tarsal bone. B: Cat ID: X43, right tarsus; C: Cat ID: X30, right tarsus; D: Cat ID: X31, right tarsus.

Cat ID	Left tarsus		Right tarsus	
	Score	Osteophyte size (mm)	Score	Osteophyte size (mm)
X1	2	2.1	1	1.4
X3	1	1.8	0	-
X6	1	1.0	0	-
X7	1	0.6	1	0.4
X8	1	0.9	1	0.9
X9	1	0.5	0	-
X10	2	2.5	0	-
X11	2	3.5	2	2.6
X15	2	2.4	1	1.9
X16	1	0.8	1	1.0
X17	1	1.0	1	0.8
X18	2	2.8	1	0.7
X20	1	0.8	1	0.7
X22	1	0.6	1	0.8
X23	1	1.1	1	1.0
X24	1	0.8	1	1.0
X25	0	-	1	0.8
X26	1	0.7	1	0.7
X27	1	1.2	0	-
X28	2	2.5	1	1.2
X29	1	1.2	0	-
X30	2	3.1	2	2.6
X31	1	1.4	3	5.1
X32	1	0.8	1	0.7
X33	0	-	1	0.7
X35	1	0.8	0	-
X37	1	1.1	1	0.8
X38	1	0.7	0	-
X39	1	1.2	2	2.4
X40	1	1.2	0	-
X41	1	1.1	2	2.6
X42	2	2.1	1	1.1
X43	2	2.2	2	2.4
X44	1	1.0	1	0.7
X45	1	0.5	1	0.6
X47	2	2.5	3	5.4
X48	0	-	1	0.8
X49	1	0.5	0	-
X54	1	0.7	1	0.5
X55	1	1.0	1	1.1
X56	1	1.4	1	0.8

Table 7.10: Osteophytes when present were graded according to their size (mm) and whether a single site or multiple sites were involved (see Table 2.1, page 37).

7.3.4 Gross pathologic findings

7.3.4.1 Carpal OA

Gross pathologic examinations were performed on 116 carpal joints from 58 cats. The overall prevalence of Carp-path OA was 50.0% (29 of 58 cats). Of 29 cats with cartilage abnormalities, 17 cats had bilateral and 12 cats had unilateral carpus involvement (10 on the left and 2 on the right) (Table 7.11). All Carp-rOA joints (25) had gross cartilage abnormalities. Of 91 no Carp-rOA joints, 21 (23.1%) had gross cartilage lesions on the distal radius or proximal row of carpal bones or both thus giving a total of 46 Carp-path OA joints. Of 46 Carp-path OA joints, 44 were given a Global score 1 and two a Global score 3 (Table 7.12). The total possible gross pathologic score was 22; the highest score observed was 8 (Table 7.13). The median total gross pathologic score for left and right carpal joints was 2. The difference between total gross pathologic scores of left and right Carp-path OA joints was not statistically significant (P=0.93). Of 91 no Carp-rOA joints, 70 (no Carp-path OA/normal) were normal on the gross pathologic examinations and were given a Global score 0. Twenty-nine cats (50.0%) had grossly normal articular cartilage on both left and right carpal joints. Twelve cats had unilateral grossly normal articular cartilage (2 on the left and 10 on the right side) (Table 7.11).

Of 46 Carp-path OA joints, 26 (56.5%) had cartilage changes on the distal radius, radial carpal and ulnar carpal bones, 15 (32.6%) had cartilage changes on the radial carpal bones only and 5 (10.9%) had cartilage changes on the distal radius only. Yellow discolouration of the articular surface was seen in 31/46 (67.4%) carpal joints. All Carp-path OA joints had cartilage fibrillation. Cartilage fibrillation was scored as mild in 41 joints and moderate in 5 joints. Cartilage erosion and ulceration were identified in 2/46 (4.3%) and 2/46 (4.3%) carpal joints respectively (Figures 7.8.C-D).

All Carp-rOA joints (25) had osteophyte formation on gross inspection. Of 91 no Carp-rOA joints, 4 had osteophytes on gross pathologic examination, thus giving a total number of 29 (63.0%) joints. The osteophytes were often seen at the articular margin of the distal radius and radial carpal bone (Figures 7.8.C-D). Osteophytes were scored mild in 24 joints, moderate in 3 and severe in two.

Joint remodelling was identified in 2/46 (4.3%) carpal joints (Figures 7.8.C-D). Both these joints also had severe osteophyte formation affecting the distal radius and proximal carpal bones.

Thickening of the joint capsule and discolouration of the synovium were not observed in any joint.

	Gross pathologic findings			
	No Carp-path OA		Carp-path OA	
	Number of Joints	Percentage (%)	Number of joints	Percentage (%)
Left carpus	31	53.4	27	46.6
Right carpus	39	67.2	19	32.8
Total	70	60.3	46	39.7

Table 7.11: Showing numbers of carpal joints with normal and abnormal gross pathologic findings. Total number of joints 116.

	Gross pathologic OA Global scores			
	Score 0	Score 1	Score 2	Score 3
Left carpus	31	26	0	1
Right carpus	39	18	0	1
Total	70	44	0	2

Table 7.12: Showing the number of carpal joints with different gross pathologic OA Global Scores.

Cat ID	Cartilage surface discolouration		Cartilage fibrillation		Cartilage erosion		Cartilage ulceration		Osteophytes		Joint remodelling		Thickening of joint capsule		Synovium discolouration		Total score		Global Score		Sample for histopathologic examination
	L	R	L	R	L	R	L	R	L	R	L	R	L	R	L	R	L	R	L	R	
X1	0	0	0	0	0	0	0	0	0	0	0	0	0	0	0	0	0	0	0	0	
X2	0	0	0	0	0	0	0	0	0	0	0	0	0	0	0	0	0	0	0	0	CBS-L
X3	0	1	1	1	0	0	0	0	1	1	0	0	0	0	0	0	2	3	1	1	CBS-R
X4	0	0	0	0	0	0	0	0	0	0	0	0	0	0	0	0	0	0	0	0	CBS-R
X5	0	0	0	0	0	0	0	0	0	0	0	0	0	0	0	0	0	0	0	0	CBS-L
X6	0	1	0	1	0	0	0	0	0	1	0	0	0	0	0	0	0	3	0	1	
X7	1	0	1	0	0	0	0	0	1	0	0	0	0	0	0	0	3	0	1	0	
X8	0	0	1	1	0	0	0	0	1	2	0	0	0	0	0	0	2	3	1	1	CBS-L
X9	0	0	0	0	0	0	0	0	0	0	0	0	0	0	0	0	0	0	0	0	
X10	0	0	1	1	0	0	0	0	1	1	0	0	0	0	0	0	2	2	1	1	
X11	1	0	1	1	0	0	0	0	1	1	0	0	0	0	0	0	3	2	1	1	
X12	0	0	1	1	0	0	0	0	1	1	0	0	0	0	0	0	2	2	1	1	
X13	0	0	0	0	0	0	0	0	0	0	0	0	0	0	0	0	0	0	0	0	CBS-R
X14	0	0	0	0	0	0	0	0	0	0	0	0	0	0	0	0	0	0	0	0	CBS-L
X15	0	0	0	0	0	0	0	0	0	0	0	0	0	0	0	0	0	0	0	0	CBS-R
X16	0	1	0	1	0	0	0	0	0	0	0	0	0	0	0	0	0	2	0	1	
X17	0	0	0	0	0	0	0	0	0	0	0	0	0	0	0	0	0	0	0	0	
X18	0	0	0	0	0	0	0	0	0	0	0	0	0	0	0	0	0	0	0	0	
X19	0	0	0	0	0	0	0	0	0	0	0	0	0	0	0	0	0	0	0	0	
X20	0	0	0	0	0	0	0	0	0	0	0	0	0	0	0	0	0	0	0	0	

Table 7.13: Gross pathologic scores and Global scores of the left (L) and right (R) carpal joints of 58 cats. Global score: 0: normal, 1: mild, 2: moderate, 3: severe. Samples selected for histopathologic examination. CBS-L: Cartilage Bone Synovium-Left; CBS-R: Cartilage Bone Synovium-Right, CBS-L&R: Cartilage Bone Synovium-Left and right.

Cat ID	Cartilage surface discolouration		Cartilage fibrillation		Cartilage erosion		Cartilage ulceration		Osteophytes		Joint remodelling		Thickening of joint capsule		Synovium discolouration		Total score		Global Score		Sample for histopathologic examination
	L	R	L	R	L	R	L	R	L	R	L	R	L	R	L	R	L	R	L	R	
X21	1	0	1	0	0	0	0	0	0	0	0	0	0	0	0	0	2	0	1	0	
X22	0	0	0	0	0	0	0	0	0	0	0	0	0	0	0	0	0	0	0	0	CBS-R
X23	0	0	0	0	0	0	0	0	0	0	0	0	0	0	0	0	0	0	0	0	CBS-R
X24	0	0	0	0	0	0	0	0	0	0	0	0	0	0	0	0	0	0	0	0	
X25	1	0	1	1	0	0	0	0	0	0	0	0	0	0	0	0	2	1	1	1	CBS-L
X26	1	0	1	0	0	0	0	0	1	0	0	0	0	0	0	0	3	0	1	0	
X27	1	0	1	0	0	0	0	0	1	0	0	0	0	0	0	0	3	0	1	0	
X28	0	0	0	0	0	0	0	0	0	0	0	0	0	0	0	0	0	0	0	0	
X29	0	0	1	0	0	0	0	0	1	0	0	0	0	0	0	0	2	0	1	0	
X30	1	1	2	2	0	0	0	0	2	2	0	0	0	0	0	0	5	5	1	1	CBS-L
X31	1	1	3	3	2	2	2	2	3	3	1	1	0	0	0	0	12	12	3	3	CBS-L&R
X32	1	1	1	1	0	0	0	0	1	1	0	0	0	0	0	0	3	3	1	1	
X33	0	0	0	0	0	0	0	0	0	0	0	0	0	0	0	0	0	0	0	0	
X34	0	0	0	0	0	0	0	0	0	0	0	0	0	0	0	0	0	0	0	0	
X35	0	0	0	0	0	0	0	0	0	0	0	0	0	0	0	0	0	0	0	0	CBS-L
X36	0	0	0	0	0	0	0	0	0	0	0	0	0	0	0	0	0	0	0	0	
X37	0	0	1	0	0	0	0	0	1	0	0	0	0	0	0	0	2	0	1	0	
X38	1	0	1	0	0	0	0	0	0	0	0	0	0	0	0	0	2	0	1	0	
X39	0	0	1	1	0	0	0	0	0	1	0	0	0	0	0	0	1	2	1	1	CBS-L
X40	1	1	1	1	0	0	0	0	0	1	0	0	0	0	0	0	2	3	1	1	
X41	1	1	1	1	0	0	0	0	0	0	0	0	0	0	0	0	2	2	1	1	

Table 7.13 continued.

Cat ID	Cartilage surface discolouration		Cartilage fibrillation		Cartilage erosion		Cartilage ulceration		Osteophytes		Joint remodelling		Thickening of joint capsule		Synovium discolouration		Total score		Global Score		Sample for histopathologic examination
	L	R	L	R	L	R	L	R	L	R	L	R	L	R	L	R	L	R	L	R	
X42	1	1	1	1	0	0	0	0	1	1	0	0	0	0	0	0	3	3	1	1	CBS-L
X43	1	0	1	1	0	0	0	0	0	0	0	0	0	0	0	0	2	1	1	1	CBS-R
X44	0	0	1	0	0	0	0	0	0	0	0	0	0	0	0	0	1	0	1	0	
X45	1	1	1	1	0	0	0	0	0	0	0	0	0	0	0	0	2	2	1	1	CBS-R
X46	0	0	0	0	0	0	0	0	0	0	0	0	0	0	0	0	0	0	0	0	
X47	1	0	1	0	0	0	0	0	1	0	0	0	0	0	0	0	3	0	1	0	
X48	1	1	1	1	0	0	0	0	0	0	0	0	0	0	0	0	2	2	1	1	
X49	1	1	2	1	0	0	0	0	1	1	0	0	0	0	0	0	4	3	1	1	CBS-R
X50	1	0	1	0	0	0	0	0	0	0	0	0	0	0	0	0	2	0	1	0	CBS-L
X51	0	0	0	0	0	0	0	0	0	0	0	0	0	0	0	0	0	0	0	0	
X52	0	0	0	0	0	0	0	0	0	0	0	0	0	0	0	0	0	0	0	0	CBS-L
X53	0	0	0	0	0	0	0	0	0	0	0	0	0	0	0	0	0	0	0	0	CBS-L
X54	0	0	0	0	0	0	0	0	0	0	0	0	0	0	0	0	0	0	0	0	CBS-R
X55	0	0	0	0	0	0	0	0	0	0	0	0	0	0	0	0	0	0	0	0	
X56	0	0	0	0	0	0	0	0	0	0	0	0	0	0	0	0	0	0	0	0	
X57	0	0	0	0	0	0	0	0	0	0	0	0	0	0	0	0	0	0	0	0	
X58	0	0	0	0	0	0	0	0	0	0	0	0	0	0	0	0	0	0	0	0	

Table 7.13 continued.

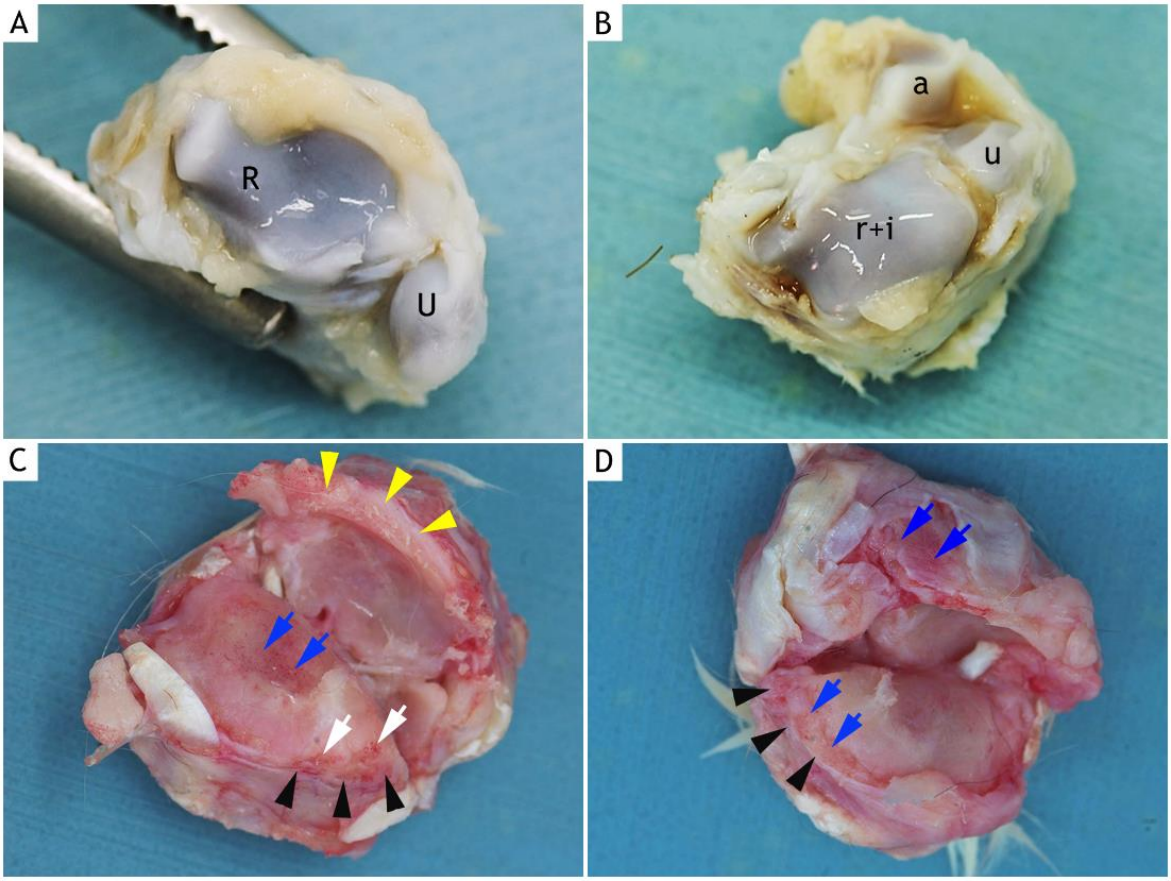

Figure 7.8: Examples of gross cartilage changes of the distal radius and proximal carpal bones of the carpal joint.

(A) Normal distal radius (R) and ulna (U). (B) Normal proximal carpal bones; r: radial carpal bone, i: intermediate carpal bone, u: ulnar carpal bone, a: accessory carpal bone. Note the radial and intermediate carpal bones fuse in the cat. The articular cartilage of the normal carpal joint is smooth and shining. (C & D) Severe articular lesions with diffuse cartilage fibrillation, erosion (white arrows) and ulceration (blue arrows) are seen. The articular cartilage is dull and discoloured. Osteophyte formation is identified at the distal radius (yellow arrowheads) and at the articular margin of the radial carpal bone (black arrowheads), together with remodelling (See Figures 7.6.C-D). A: Cat ID: X53, left carpus; B: Cat ID: X53, left carpus; C: Cat ID: X31, left carpus; D: Cat ID: X31, right carpus.

7.3.4.2 Tarsal OA

Gross pathologic examinations were performed on 116 tarsal joints from 58 cats. The overall prevalence of Tars-path OA was 74.1% (43 of 58 cats). Of 43 cats with cartilage abnormalities, 33 cats had bilateral and 10 cats had unilateral tarsus involvement (7 on the left and 3 on the right) (Table 7.14). All Tars-rOA joints (69) had gross cartilage changes. Of 47 no Tars-rOA joints, 7 (14.9%) had gross cartilage abnormalities on the distal tibia or trochlea of the talus or both thus giving a total of 76 Tars-path OA joints. Of 76 Tars-path OA joints, 70 were given a Global score 1, two a Global score 2 and four a Global score 3 (Table 7.15). The total possible gross pathologic score was 22; the highest score observed was 12 (Table 7.16). The median total gross pathologic score for left and right tarsal joints was 2.0 and 3.0 respectively. The difference between total gross pathologic scores of left and right Tars-path OA joints was not statistically significant (P=0.79). Of 47 no Tars-rOA joints, 40 were normal on the gross pathologic examinations (no Tars-path OA/normal) and were given a Global score 0. Fifteen cats (25.9%) had grossly normal articular cartilage on both left and right tarsal joints. Ten cats had unilateral grossly normal articular cartilage (3 on the left and 7 on the right side) (Table 7.14).

Of 76 Tars-path OA joints, 50 (65.8%) had cartilage changes on the distal tibia and trochlea of the talus, 19 (25.0%) had cartilage changes on the trochlea of the talus only and 7 (9.2%) had cartilage changes on the distal tibia only. All Tars-path OA joints had cartilage fibrillation. It was scored mild in 71 joints and moderate in 5 joints. Mild cartilage fibrillation was seen as a focal roughening of the articular surface (Figure 7.9.B), while in the moderate and severely affected joints, diffuse cartilage roughness was commonly seen. Thirty-seven Tars-paths OA joints (48.7%) had cartilage discolouration, characterised by a dull yellow surface. Cartilage erosion was identified in 4/76 (5.3%) Tars-path OA joints, it was moderate in 3 and severe in one tarsal joint (Figures 7.9.D and 7.10.B). Cartilage ulceration was seen in 4/76 (5.3%) Tars-path OA joints. It was scored mild in 3 joints and moderate in one joint. Ulceration with marked "wear-lines" was more often seen at the lateral part of the trochlea and distal tibia (Figures 7.9.C-D and 7.10.D).

Osteophyte formation was seen in 74/76 (97.4%) Tars-path OA joints. All Tars-rOA joints (69) had osteophyte formation. Of 47 no Tars-rOA joints, 5 had osteophytes on gross pathologic examination. The osteophytes were commonly identified at the articular margin of the distal tibia and tibial tarsal bone (Figures 7.9.C and 7.10.B-D). In 71

joints, osteophytes were scored as mild, moderate in one joint and severe in two tarsal joints.

Joint remodelling (changes in the shape of the distal tibia and tibial tarsal bone) was identified in 7/76 (9.2%) tarsal joints. Four of these joints also had obvious osteophyte formation affecting the distal tibia and tibial tarsal bone.

Thickening of the joint capsule and discolouration of the synovium were observed in 8/76 (10.5%) and 11/76 (14.5%) tarsal joints respectively.

	Gross pathologic findings			
	No Tars-path OA		Tars-path OA	
	Number of Joints	Percentage (%)	Number of joints	Percentage (%)
Left tarsus	18	31.0	40	69.0
Right tarsus	22	38.0	36	62.0
Total	40	34.5	76	65.5

Table 7.14: Showing numbers of tarsal joints with normal and abnormal gross pathologic findings. Total number of joints 116.

	Gross pathologic OA Global scores			
	Score 0	Score 1	Score 2	Score 3
Left tarsus	18	37	0	2
Right tarsus	22	33	2	2
Total	40	70	2	4

Table 7.15: Showing the number of tarsal joints with different gross pathologic OA Global Scores.

Cat ID	Cartilage surface discolouration		Cartilage fibrillation		Cartilage erosion		Cartilage ulceration		Osteophytes		Joint remodelling		Thickening of joint capsule		Synovium discolouration		Total score		Global Score		Sample for histopathologic examination
	L	R	L	R	L	R	L	R	L	R	L	R	L	R	L	R	L	R	L	R	
X1	0	0	1	1	0	0	0	0	1	1	0	0	0	0	0	0	2	1	1	1	
X2	0	0	0	0	0	0	0	0	0	0	0	0	0	0	0	0	0	0	0	0	
X3	0	0	1	0	0	0	0	0	1	1	0	0	0	0	0	0	2	0	1	0	
X4	0	0	0	0	0	0	0	0	0	0	0	0	0	0	0	0	0	0	0	0	CBS-R
X5	0	0	0	0	0	0	0	0	0	0	0	0	0	0	0	0	0	0	0	0	CBS-L
X6	0	0	1	1	0	0	0	0	1	1	0	0	0	0	0	0	2	2	1	1	
X7	1	1	1	1	0	0	0	0	1	1	0	0	0	0	0	0	3	3	1	1	
X8	0	0	1	1	0	0	0	0	1	1	0	0	0	0	0	0	2	2	1	1	CBS-L
X9	0	0	1	0	0	0	0	0	1	0	0	0	0	0	0	0	2	0	1	0	
X10	0	0	1	0	0	0	0	0	1	0	0	0	0	0	0	0	2	0	1	0	
X11	0	1	1	1	0	0	0	0	1	1	0	0	0	0	0	0	2	3	1	1	
X12	0	0	0	0	0	0	0	0	0	0	0	0	0	0	0	0	0	0	0	0	
X13	0	0	0	0	0	0	0	0	0	0	0	0	0	0	0	0	0	0	0	0	
X14	0	0	0	0	0	0	0	0	0	0	0	0	0	0	0	0	0	0	0	0	
X15	0	1	1	1	0	0	0	0	1	1	0	0	0	0	0	0	2	3	1	1	
X16	0	0	1	1	0	0	0	0	1	1	0	0	0	0	0	0	2	2	1	1	CBS-R
X17	0	1	1	1	0	0	0	0	1	1	0	0	0	0	0	0	2	3	1	1	CBS-L
X18	0	0	1	1	0	0	0	0	1	1	0	0	0	0	0	0	2	2	1	1	
X19	0	0	0	0	0	0	0	0	0	0	0	0	0	0	0	0	0	0	0	0	CBS-R
X20	0	0	1	1	0	0	0	0	1	1	0	0	0	0	0	0	2	2	1	1	
X21	0	0	0	0	0	0	0	0	0	0	0	0	0	0	0	0	0	0	0	0	CBS-R

Table 7.16: Gross pathologic scores and Global scores of the left (L) and right (R) tarsal joints of 58 cats. Global score: 0: normal, 1: mild, 2: moderate, 3: severe. Sample selected for histopathologic examination: CBS-L: Cartilage Bone Synovium-Left; CBS-R: Cartilage Bone Synovium-Right, CBS-L&R: Cartilage Bone Synovium-Left and right.

Cat ID	Cartilage surface discolouration		Cartilage fibrillation		Cartilage erosion		Cartilage ulceration		Osteophytes		Joint remodelling		Thickening of joint capsule		Synovium discolouration		Total score		Global Score		Sample for histopathologic examination
	L	R	L	R	L	R	L	R	L	R	L	R	L	R	L	R	L	R	L	R	
X22	0	0	1	1	0	0	0	0	1	1	0	0	0	0	0	0	2	2	1	1	
X23	0	0	1	1	0	0	0	0	1	1	0	0	0	0	0	0	2	2	1	1	
X24	0	0	1	1	0	0	0	0	1	1	0	0	0	0	0	0	2	2	1	1	
X25	0	0	0	1	0	0	0	0	0	1	0	0	0	0	0	0	0	2	0	1	
X26	0	0	1	1	0	0	0	0	1	1	0	0	0	0	0	0	2	2	1	1	
X27	0	0	1	0	0	0	0	0	1	0	0	0	0	0	0	0	2	0	1	0	
X28	0	0	1	1	0	0	0	0	1	1	0	0	0	0	0	0	2	2	1	1	
X29	1	0	1	1	0	0	0	0	1	0	0	0	0	0	0	0	3	1	1	1	CBS-R
X30	1	1	2	2	1	1	1	1	3	3	1	1	1	1	0	0	10	10	3	3	CBS-L&R
X31	1	1	3	1	2	1	1	2	3	3	1	1	0	0	0	0	10	12	3	3	CBS-L&R
X32	0	0	1	1	0	0	0	0	1	1	0	0	0	0	0	0	2	2	1	1	CBS-L
X33	0	0	0	1	0	0	0	0	0	1	0	0	0	0	0	0	0	1	0	1	
X34	0	1	0	1	0	0	0	0	0	1	0	0	0	0	0	0	0	3	0	1	
X35	0	0	1	0	0	0	0	0	1	0	0	0	0	0	0	0	2	0	1	0	
X36	0	0	0	0	0	0	0	0	0	0	0	0	0	0	0	0	0	0	0	0	CBS-L&R
X37	1	1	1	1	0	0	0	0	1	1	0	0	0	0	0	0	3	3	1	1	CBS-L
X38	1	1	1	1	0	0	0	0	1	1	0	0	0	0	0	0	3	3	1	1	
X39	1	1	1	1	0	0	0	0	1	1	0	0	0	0	0	0	3	3	1	1	
X40	1	1	1	1	0	0	0	0	1	1	0	0	0	0	0	0	3	3	1	1	
X41	1	1	1	1	0	0	0	0	1	1	0	0	0	0	0	0	3	3	1	1	
X42	1	1	1	1	0	0	0	0	1	1	1	0	0	0	0	0	4	3	1	1	

Table 7.16 continued.

Cat ID	Cartilage surface discolouration		Cartilage fibrillation		Cartilage erosion		Cartilage ulceration		osteophytes		Joint remodelling		Thickening of joint capsule		Synovium discolouration		Total score		Global Score		Sample for histopathologic examination
	L	R	L	R	L	R	L	R	L	R	L	R	L	R	L	R	L	R	L	R	
X43	1	0	2	1	0	0	0	0	1	1	1	0	0	0	1	0	5	2	1	1	
X44	1	1	1	1	0	0	0	0	1	1	0	0	0	0	0	0	3	3	1	1	CBS-R
X45	1	1	2	1	0	0	0	0	1	1	0	0	0	0	1	0	5	3	1	1	
X46	0	0	0	0	0	0	0	0	0	0	0	0	0	0	0	0	0	0	0	0	CBS-R
X47	1	1	1	2	0	0	0	0	1	2	0	0	0	1	2	2	5	8	1	2	CBS-R
X48	0	1	1	1	0	0	0	0	1	1	0	0	0	1	0	1	3	5	1	1	CBS-L
X49	0	0	1	0	0	0	0	0	1	0	0	0	0	0	0	0	2	0	1	0	
X50	0	0	0	0	0	0	0	0	0	0	0	0	0	0	0	0	0	0	0	0	CBS-R
X51	0	0	0	0	0	0	0	0	0	0	0	0	0	0	0	0	0	0	0	0	CBS-L
X52	0	0	0	0	0	0	0	0	0	0	0	0	0	0	0	0	0	0	0	0	
X53	0	0	0	0	0	0	0	0	0	0	0	0	0	0	0	0	0	0	0	0	
X54	1	1	1	1	0	0	0	0	1	1	0	0	0	0	1	1	4	4	1	1	CBS-L
X55	1	1	1	1	0	0	0	0	0	1	1	0	2	2	1	2	6	7	1	2	CBS-L&R
X56	1	1	1	1	0	0	0	0	1	1	0	0	1	1	1	1	5	5	1	1	
X57	0	0	0	0	0	0	0	0	0	0	0	0	0	0	0	0	0	0	0	0	CBS-R
X58	0	0	1	0	0	0	0	0	0	0	0	0	0	0	0	0	1	0	1	0	

Table 7.16 continued.

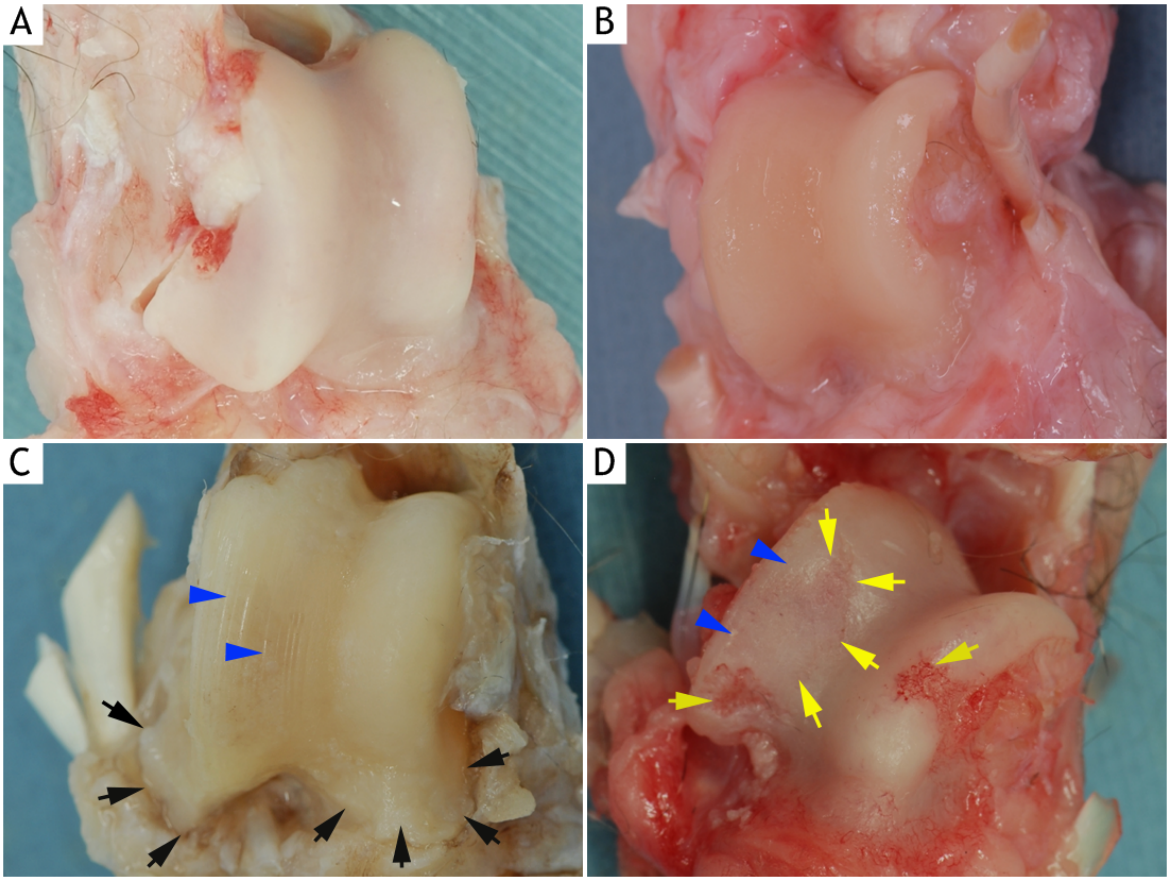

Figure 7.9: Examples of gross cartilage changes of the trochlea of the talus (tarsal joint).

(A) Normal trochlea of the talus. Cat ID: X19, right tarsus. (B) Mild fibrillation with dullness and roughening of the articular cartilage. Cat ID: X43, right tarsus. (C & D) Cartilage ulceration with marked ridges and grooves ("wear lines") (blue arrowheads) particularly affecting the lateral aspect of the bone. Focal cartilage erosion is also seen (yellow arrows). Large osteophytes are observed at the distal part of the tibial tarsal bone (black arrows). C: Cat ID: X30, right tarsus: D: Cat ID: X31, right tarsus.

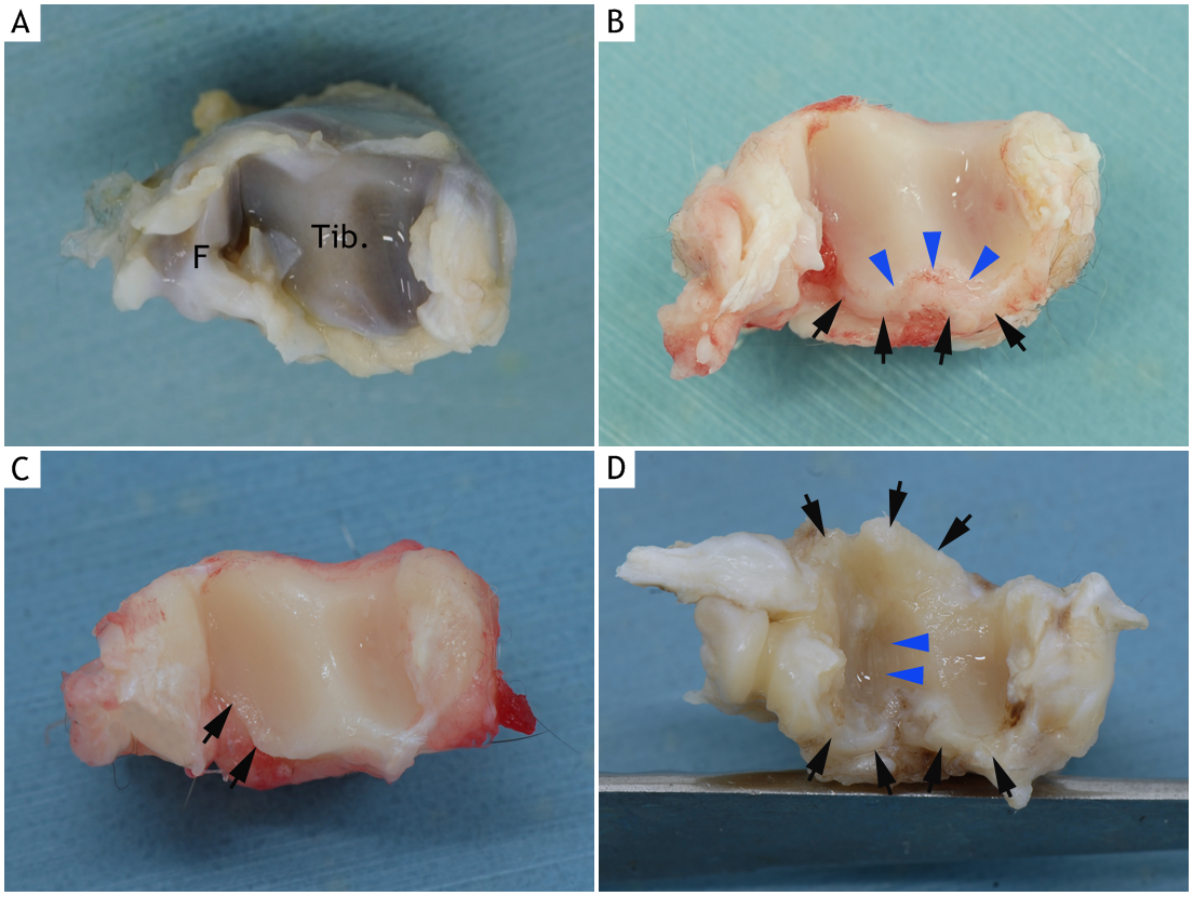

Figure 7.10: Examples of gross cartilage changes of the distal tibia and fibula (tarsal joint).

(A) Normal distal tibia (Tib.) and fibula (F). Cat ID: X53, right tarsus. (B) Cartilage erosion is seen at the distal tibia (blue arrowheads). There is also osteophyte formation (black arrows) at the margin of the articular cartilage. Cat ID: X31, right tarsus. (C) Mild cartilage lesions with osteophyte formation (black arrows) at the distal tibia. Cat ID: X43, right tarsus. (D) Cartilage lesions with ridges and grooves ("wear lines") (blue arrowheads) are seen on the lateral part of the distal tibia. Osteophyte formation (black arrows) is also identified at the articular margin of the distal tibia. Cat ID: X30, right tarsus.

7.3.5 Correlation studies

7.3.5.1 Correlation between total radiographic and gross pathologic OA scores

Carpal OA

All Carp-rOA joints (25) had gross lesions. Of 91 no Carp-rOA joints, 21 (23.1%) had gross lesions. There was a significant moderate and good positive correlation between the radiographic and gross pathologic total scores in left (r_s=0.67, P<0.0001) and right (r_s=0.72, P<0.0001) carpal joints respectively (Figures 7.11.A and 7.11.B).

Tarsal OA

All Tars-rOA joints (69) had gross lesions. Of 47 no Tars-rOA joints, 7 (14.9%) had gross lesions. A good positive correlation was observed between the radiographic and gross pathologic total scores of the left (r_s=0.76, P<0.0001) and right (r_s=0.78, P<0.0001) tarsal joints. The correlations were significant (Figures 7.11.C and 7.11.D).

7.3.5.2 Correlation between total radiographic score and age, BW and BCS

Carpal OA

There was a significant slight positive correlation between the radiographic total score of the left (r_s =0.20, P=0.13) and right (r_s=0.10, P=0.50) carpal joints and age (Figures 7.12.A and 7.12.B). A slight negative relationship between the radiographic total score of the left (r_s=-0.21, P=0.12) and right (r_s=-0.15, P=0.91) carpal joint and BW was observed, which was not statistically significant (Figures 7.12.C and 7.12.D). A similar finding was also observed between the total radiographic score of the left (r_s=-0.15, P=0.27) and right (r_s=-0.10, P=0.46) carpal joint and BCS (Figures 7.12.E and 7.12.F).

Tarsal OA

There was a significant fair positive correlation between the radiographic total score of the left (r_s=0.40, P<0.01) and right (r_s=0.30, P<0.05) tarsal joints and age (Figures 7.13.A and 7.13.B). A non-significant slight and fair negative relationship between the radiographic total score of the left (r_s=-0.28, P=0.10) and right (r_s=-0.12, P=0.35) tarsal joint and BW was observed (Figures 7.13.C and 7.13.D). A similar finding was also

observed between the radiographic total score of the right (r_s=-0.20, P=0.14) and left (r_s=-0.12, P=0.36) tarsal joint and BCS (Figures 7.13.E and 7.13.F).

7.3.5.3 Correlation between total gross pathologic score and age, BW and BCS

Carpal OA

Correlation analysis revealed a significant slight and fair positive relationship between the total gross pathologic score of the left (r_s=0.32, P<0.05) and right (r_s=0.20, P<0.05) carpal joints and age (Figures 7.14.A and 7.14.B). Correlation analysis revealed a slight negative relationship between the total gross pathologic score of the left (r_s=-0.15, P=0.25) and right (r_s=-0.10, P=0.88) carpal joints and BW (Figures 7.14.C and 7.14.D). However, the relationships were not statistically significant. A similar finding was also observed between the gross pathologic total score of the left (r_s=-0.12, P=0.42) and right (r_s=-0.10, P=0.42) carpal joints and BCS (Figures 7.14.E and 7.14.F).

Tarsal OA

There was a significant moderate and fair positive correlation between the total gross pathologic score of the left (r_s=0.54, P<0.0001) and right (r_s=0.35, P<0.01) tarsal joints and age respectively (Figures 7.15.A and 7.15.B). Correlation analysis revealed a fair negative relationship between the total gross pathologic score of the left (r_s=-0.26, P=0.10) and right (r_s=-0.21, P=0.14) tarsal joints and BW (Figures 7.15.C and 7.15.D). However, the relationships were not statistically significant. A non-significant slight negative relationship was observed between the gross pathologic total score of the left (r_s=-0.19, P=0.15) and right (r_s=-0.15, P=0.26) tarsal joints and BCS (Figures 7.15.E and 7.15.F).

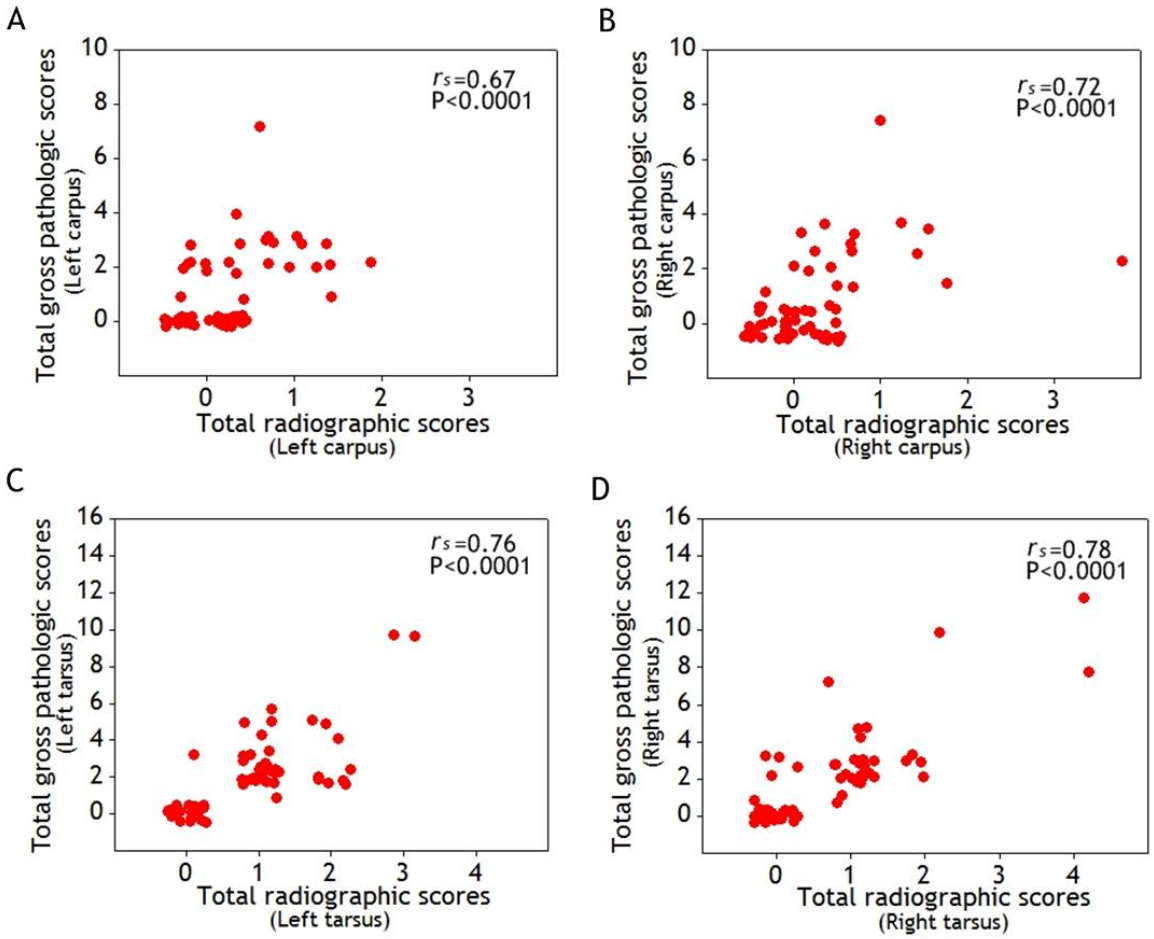

Figure 7.11: Graph showing correlation between radiographic and gross pathologic OA scores in carpal and tarsal joints. There is a significant moderate and good relationship between the radiographic and gross pathologic scores in left (A) and right (B) carpal joints. A good positive relationship was seen between the radiographic and gross pathologic scores in left (C) and right (D) tarsal joints.

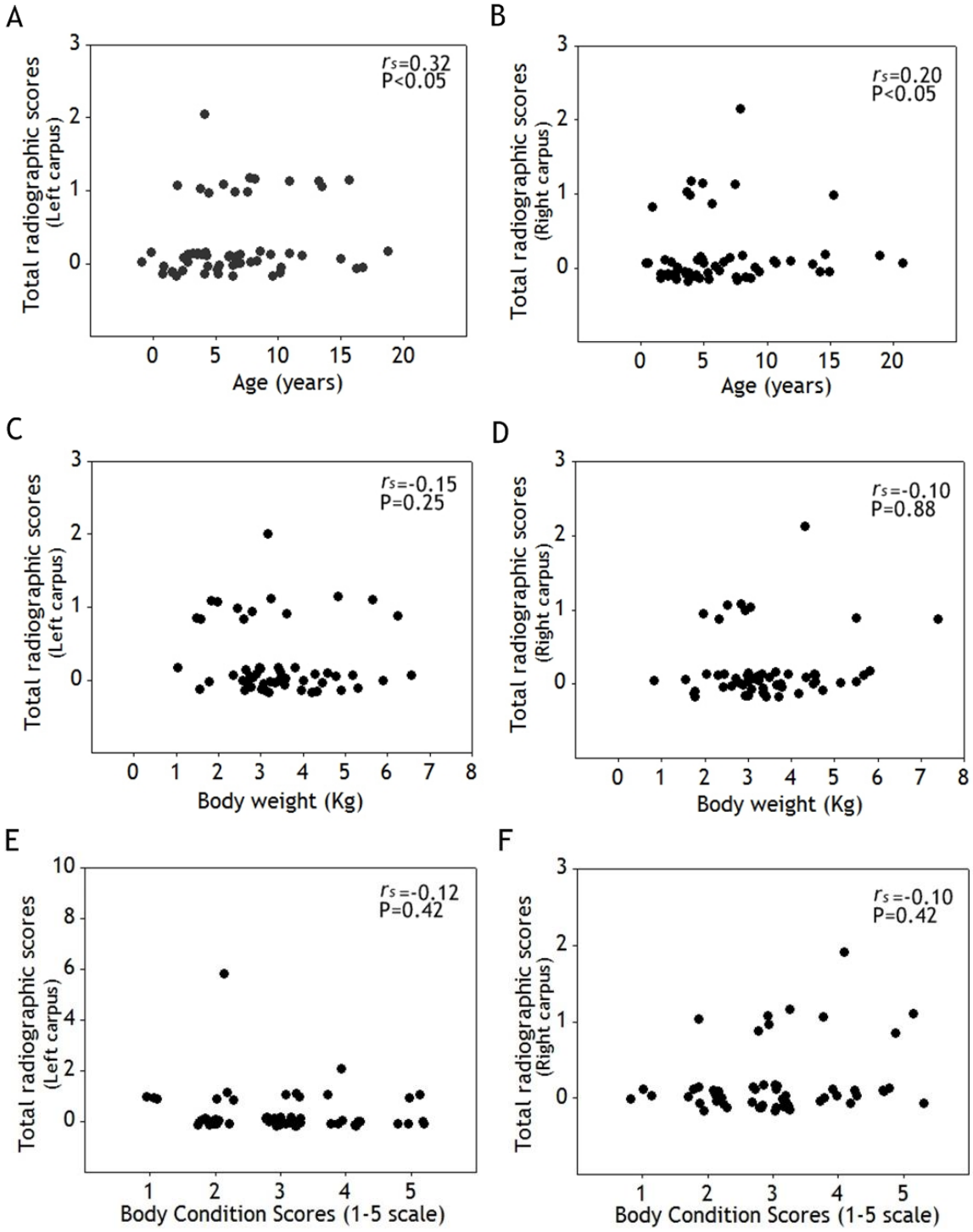

Figure 7.12: Correlation analysis of total radiographic scores of the left (A, C and E) and right (B, D and F) carpal joints with age, BW and BCS. (A & B) There is a significant slight positive relationship between total radiographic scores of the left and right carpal joints and age. There are no significant relationships between the total radiographic scores of the left and right carpal joint with BW (C & D) and BCS (E & F).

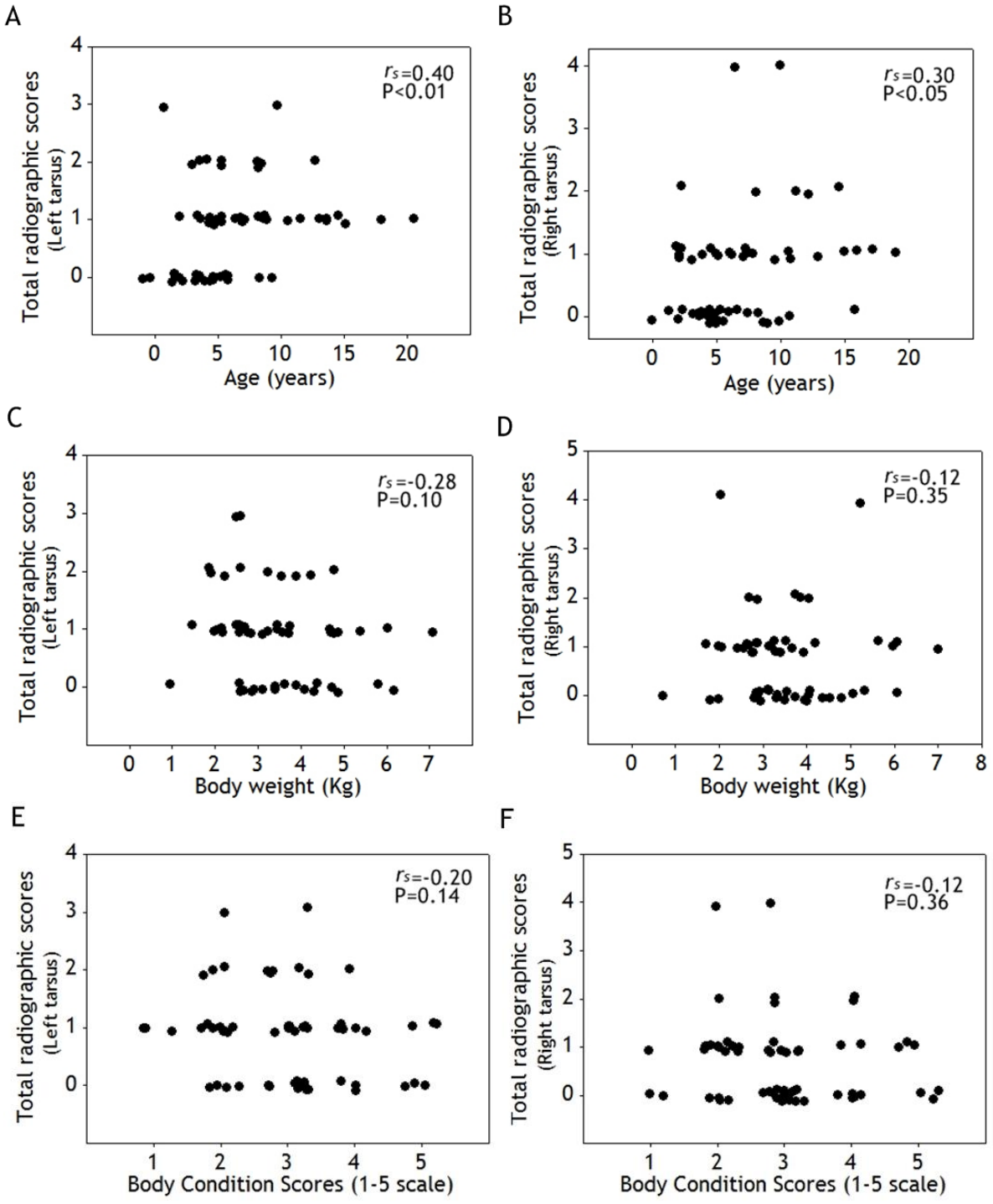

Figure 7.13: Correlation analysis of total radiographic scores of the left (A, C and E) and right (B, D and F) tarsal joints with age, BW and BCS. (A & B) There is a significant fair positive relationship between total radiographic scores of the left and right tarsal joints and age. There are no significant relationships between the total radiographic scores of the left and right tarsal joint with BW (C & D) and BCS (E & F).

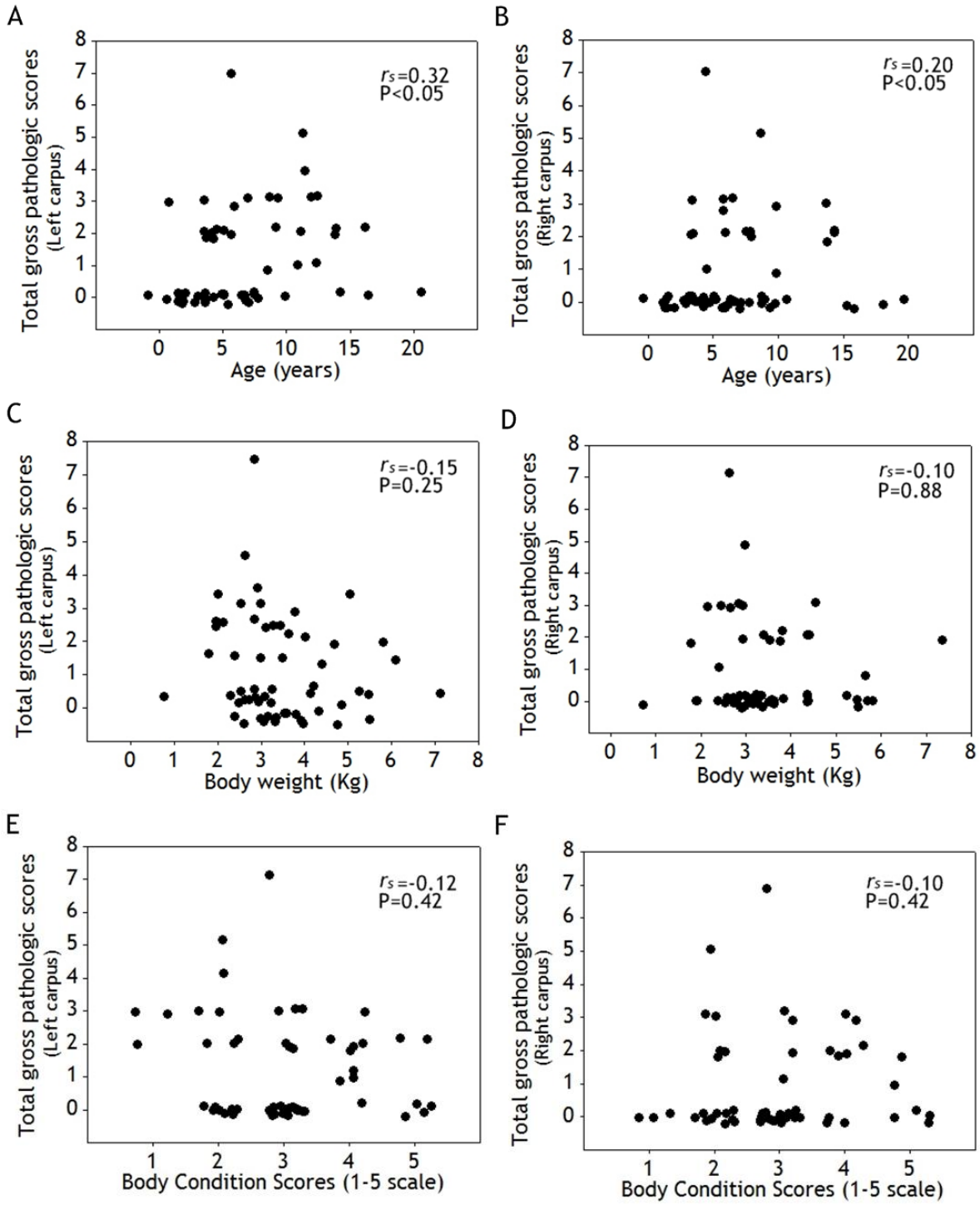

Figure 7.14: Correlation analysis of total gross pathologic scores of the left (A, C and E) and right (B, D and F) carpal joints with age, BW and BCS. (A & B) There is a significant slight and fair positive relationship between total gross pathologic scores of the left and right carpal joints and age. There are no significant relationships between the total gross pathologic scores of the left and right carpal joint with BW (C & D) and BCS (E & F).

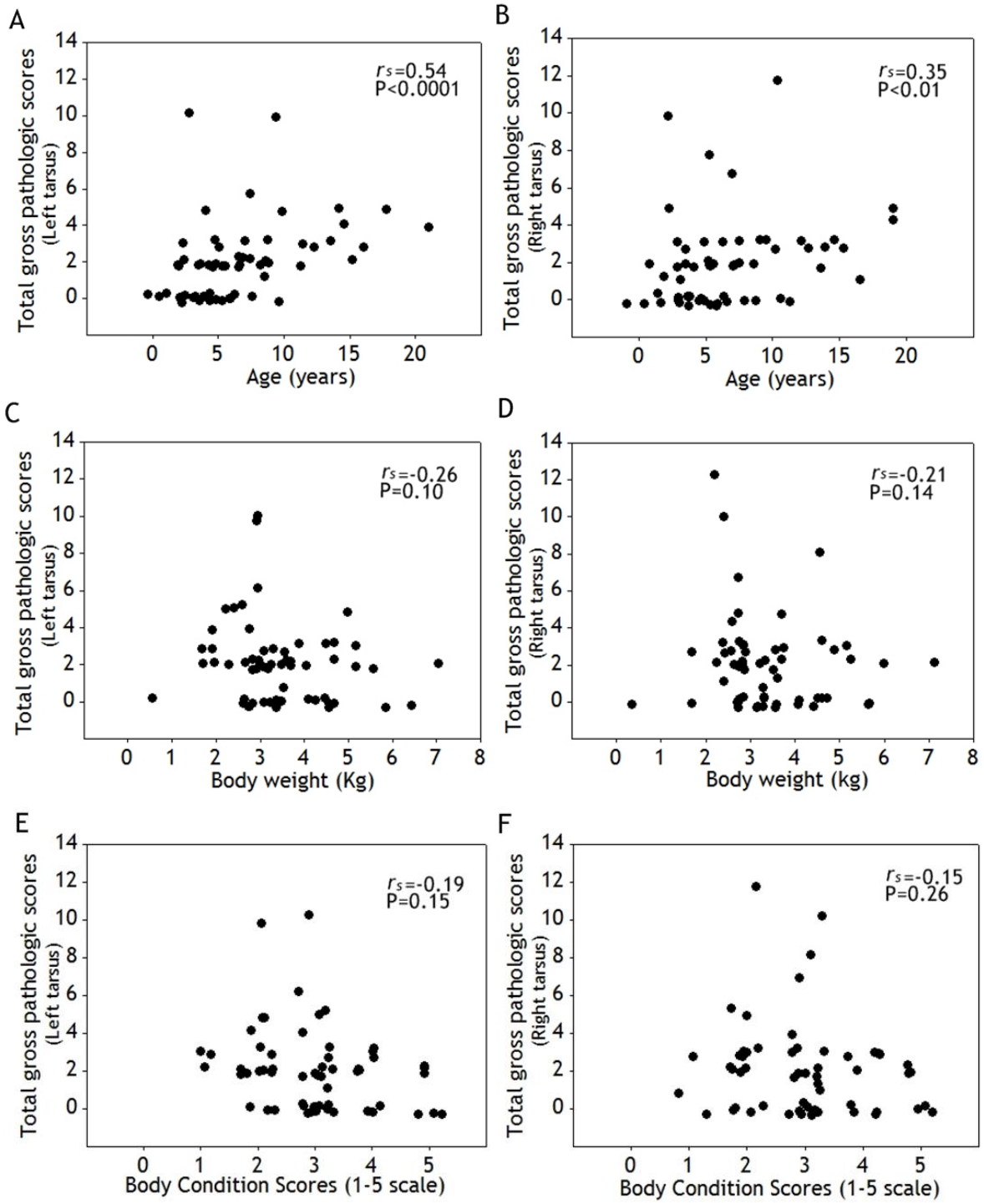

Figure 7.15: Correlation analysis of total gross pathologic scores of the left (A, C and E) and right (B, D and F) tarsal joints with age, BW and BCS. (A & B) There is a significant moderate and fair positive relationship between total gross pathologic scores of the left and right tarsal joints and age. There are no significant relationships between the total gross pathologic scores of the left and right tarsal joint with BW (C & D) and BCS (E & F).

7.4 Discussion

The prevalence of Carp-rOA and Carp-path OA was 27.6% (16 of 58 cats) and 50.0% (29 of 58 cats) respectively. The present study showed a large number of cats had carpal OA, particularly when assessed by gross examination. The marked difference between the prevalence as assessed by radiography and by gross pathologic examination reflects the difficulty in identifying radiographic changes which in many cases are minimal. Other studies which relied on radiographic assessment have reported low prevalence figures (Godfrey, 2005; Clarke et al., 2005; Clarke and Bennett, 2006; Lascelles et al., 2010; Slingerland et al., 2011). The retrospective study by Godfrey (2005) did not detect any cats with carpal OA. In another retrospective study, Clarke et al. (2005) reported carpal OA in only one of 26 joints from 218 cats. The low prevalence of carpal OA in these retrospective studies might reflect a bias of the sample population. Both studies evaluated any radiographs that were available and on which one or more joints could be evaluated (often thorax or abdomen films). This meant that only a restricted number of joints could be assessed in any one animal. In a recent prospective study by Lascelles et al. (2010), 19/100 (19%) cats with a mean age of 9.4 years had carpal radiographic OA. However, Clarke and Bennett (2006) prospectively examined 28 cats for clinical OA, and none of the carpal joints were affected. Also, OA was not detected in any carpal joint of 100 cats in a cross sectional study by Slingerland et al. (2011). As well as differences in the study design explaining a variation in the prevalence, environmental or genetic differences between the study populations may also be a factor (Lascelles et al., 2010). The pathologic assessment carried out in this study gives a more accurate prevalence figure of carpal OA (50.0%), at least in the older cat.

The main radiographic feature of Carp-rOA was osteophyte formation. Areas of abnormal mineralisation and remodelling were less frequently seen. All the Carp-rOA joints (25) with radiographic osteophytes had gross cartilage abnormalities. However, there were 21 carpal joints with no radiographic changes which also had cartilage lesions. Of these 21, 4 had osteophyte formation evident on gross pathologic examination. Failure to identify osteophytes with computed radiography may be explained by the size and location of the osteophytes. The presence of radiographic changes normally indicates that cartilage changes are present but almost a quarter (23.0%) of radiographically normal joints may have pathological changes indicating OA, much greater than found with other joints. These joint could also have clinical disease despite appearing normal on radiographic examination.

A moderate and good correlation between total radiographic scores and total gross pathologic scores was found with the left and right carpal joints indicating that the high radiographic scores correlated with high gross pathologic scores. Although the mean age of cats with Carp-path OA was high (7.9 years), only a slight to fair positive correlation was observed between the gross pathologic total scores and age in both carpal joints. This suggests that the severity of gross pathologic changes is only slightly influenced by age in this study group. A similar finding was observed between the radiographic scores and age in both carpal joints. Body weight and BCS were found to be negatively associated with the severity of radiographic and gross pathologic OA in both carpal joints. The finding of a negative association is likely explained by the effect of age on body weight and BCS, where cats tend to lose weight and BCS as they become older (Kronfeld et al., 1994; Laflamme, 2005).

The overall prevalence of Tars-rOA and Tars-path OA was 70.7 % (41 of 58 cats) and 74.1% (43 of 58 cats) respectively. Tars-rOA and Tars-path OA was detected in 69/116 (59.5%) and 79/116 (65.5%) tarsal joints respectively. Lascelles et al. (2010) reported radiographic OA in 85/200 (42.5%) tarsal joints. In a later study by Freire et al. (2011), radiographic and gross pathologic OA was found in 17/60 (28.3%) and 32/60 (53.3%) tarsal joints. As discussed above, a variation in prevalence may exist which different geographical populations and inter-rater differences in examining appendicular radiographs may also be a factor.

Tars-rOA joints were characterised by osteophyte formation particularly on the distal tibia, tibial tarsal bone and central tarsal bone. Joint remodelling was less frequently identified. Gross pathologic studies of the articular cartilage showed degenerative changes which predominantly involved the tarsocrural joint. Articular changes with marked ridges and grooves (“wear lines”) were found mainly on the lateral side of the tibial tarsal bone and distal tibia although changes on the medial side were also identified. This findings support previous studies reported by Bennett et al. (2012a). The more advanced pathology in the lateral part of the joint probably reflects an increased load bearing of this part of the joint. Dyce et al. (2010) described the tarsus as an “atypical” hinge joint since the obliquity of the interlocking ridges and grooves of the tibia and talus imposes a lateral deviation of the foot when it is carried forward on flexion. It is thus reasonable to assume that the tarsal joint is loaded more on the lateral side during normal physiological movements.

A good correlation between total radiographic scores and total gross pathologic scores was found in both tarsal joints indicating that the high radiographic scores correlated

with high gross pathologic scores. A fair positive correlation was observed between the total radiographic scores and age in both tarsal joints. As discussed above, this suggests that the severity of radiographic changes is only slightly influenced by age in this study group. Similarly, body weight and BCS were seen to be negatively associated with the severity of radiographic and gross pathologic OA in both tarsal joints. Although the correlation was not significant, the finding of a negative association is likely to be explained by changes in body weight and BCS which are often attributed to aging (Kronfeld et al., 1994; Laflamme, 2005).

There was no identifiable underlying cause seen in either the carpal or tarsal joints to explain the OA, suggesting that carpal and tarsal OA are mainly idiopathic or primary in nature.

Chapter 8 Histopathologic features of joint tissues from cats with and without Osteoarthritis

8.1 Introduction and aims

The histopathologic features of the articular cartilage, synovial membrane and menisci in feline OA have recently published by a number of authors (Kamishina, 2003; Freire et al., 2010; Ryan et al., 2013; Freire et al., 2014). Kamishina (2003) reported on the histopathologic features of hip OA. Hypocellularity, reduced intensity of Safranin O staining and irregularity of the articular surface are often identified. However, this work did not evaluate other joint tissues such as the synovial membrane. Freire et al. (2010) reported on the presence of meniscal mineralisation and its relationship to the articular cartilage abnormalities in the stifle joint. The presence of meniscal mineralisation was associated with articular cartilage degeneration within the medial compartment of the joint. Ryan et al. (2013) studied the histomorphometry of the humeral condyle in elbow OA and suggested a concentration of lesions on the medial part of the condyle. Common histomorphometric findings were reduction in the articular chondrocyte density and subchondral bone porosity. Freire et al. (2014) described the histopathologic characteristics of the articular cartilage and synovial membrane in normal and OA elbow joints. Differing degrees of cartilage fibrillation, erosion and ulceration, decreased number and size of chondrocytes, reduced intensity of Safranin O staining and fibrosis in the subchondral bone were the common findings. In addition, a mild lymphoplasmacytic infiltration with chondroid metaplasia of the synovial membrane was reported. Osteochondromas were also identified in ten elbow joints from six different cats with OA.

The purpose of the present study was to characterise the histopathologic features of the articular tissues of cats with and without OA.

8.2 Materials and Methods

8.2.1 Samples

Details of the articular tissue samples used in the histopathology study are given in Table 3.8 (page 98 - 100) for the shoulder joints, Table 4.12 (page 140 - 143) for the elbow joints, Table 5.11 (page 196 - 198) for the stifle joints, Table 6.9 (page 241 - 243) for the hip joints, Table 7.13 (page 285 -287) for the carpal joints and Table 7.16 (page 292 - 294) for the tarsal joints. The total number of samples evaluated are summarised in Table 8.1.

Articular tissues	Joints						
	Shoulder	Elbow	Stifle	Hip	Carpal	Tarsal	Total
Cartilage Bone Synovium (CBS)	25	50	37	30	24	26	192
Osteochondromas	1	25	2	-	-	-	28
Tendon of origin of supinator muscle	-	116	-	-	-	-	116
Menisci	-	-	116	-	-	-	116
Cranial cruciate ligaments	-	-	30	-	-	-	30
Total	26	191	185	30	24	26	482

Table 8.1: Showing numbers of articular tissues selected for histopathologic examination.

8.2.2 Processing of tissue for paraffin wax sections and staining

All the articular tissues samples collected were prepared and processed as described in section 2.5.1 (page 68). All the articular tissues sections were routinely stained with H&E (for details see section 2.5.2.1, page 68). In addition, section of articular cartilage, bone, tendon of origin of supinator muscle, cranial cruciate ligament, osteochondromas and menisci were stained with Safranin O (for details see section 2.5.2.2, page 69) and sections of synovium were stained with von Kossa Stain (for details see section 2.5.2.3, page 69). Additional sections of articular cartilage were stained with DAPI (for details see section 2.5.2.4, page 69). Localisation of collagen types I and II was performed for the articular cartilage, osteochondromas, tendon of origin of supinator muscle and meniscal sections as described in section 2.5.2.5 (page 70).

8.3 Results

8.3.1 Histopathologic features of articular cartilage in cats with and without OA

Histopathologic features of the articular cartilage included changes in structure, chondrocytes, tidemark integrity and intensity of Safranin O staining.

Structural changes

The normal articular cartilage (Gross pathologic Global score 0) showed a smooth surface with all layers intact (Figure 8.1.A). In mildly affected joints (Gross pathologic Global score 1), articular cartilage fibrillation with fissures in the superficial layer were often seen (Figures 8.2.A-B). In moderate to severely affected joints (Gross pathologic Global score 2 and 3), the fissures extended to the middle and deep layers of the articular cartilage (Figures 8.2.C-D). Erosion of the superficial layer was also identified. Full thickness loss of cartilage was observed in all elbow and tarsal joints where "wear lines" were seen grossly, particularly evident on the medial part of the humeral condyle and lateral part of the tibial tarsal bone (Figure 8.7).

Chondrocyte changes

In normal joints, the superficial layer contained elongated chondrocytes with their long axis parallel to the surface. The chondrocytes were rounded and evenly scattered within the middle layer and were organised into columns in the deep layer (Figures 8.1.A-B). In mildly affected joints, loss of chondrocytic cellularity at the superficial layer was often seen (Figures 8.3.A and 8.3.C). In moderate to severely affected joints, chondrocyte clusters were observed, mainly in the middle and deep layers (Figure 8.3). Some of the chondrocyte clusters revealed areas of weak haematoxylin and Safranin O staining and others were characterized by cell clusters with intense pericellular haematoxylin and Safranin O staining (Figures 8.3.B and 8.3.D). Total loss of chondrocytes was not seen in any joint.

Tidemark integrity

Normal articular cartilage was characterised by an intact and distinct tidemark. A similar appearance was also observed in mildly affected joints (Figures 8.2.A-B). An increased number of tidemarks up to maximum 6 lines were observed in moderate to

severely affected joints (Figures 8.4.A-C). Increased number of tidemarks was more obvious in the elbow OA samples. The tidemarks, both in normal and OA cartilage showed positive fluorescence signals for DAPI (Figure 8.4.C). Loss of the tidemark where it was crossed by blood vessels was seen in severely affected joints (Figure 8.4.D).

Safranin O staining

There was intense and uniform Safranin O staining throughout the normal articular cartilage (Figure 8.1.B). Reduced Safranin O staining was observed in the superficial layer of all mildly affected joints (Figure 8.2.B). Reduction of Safranin O staining was prominent into the middle and deep layers in moderate to severely affected joints (Figures 8.2.D and 8.3.C-D).

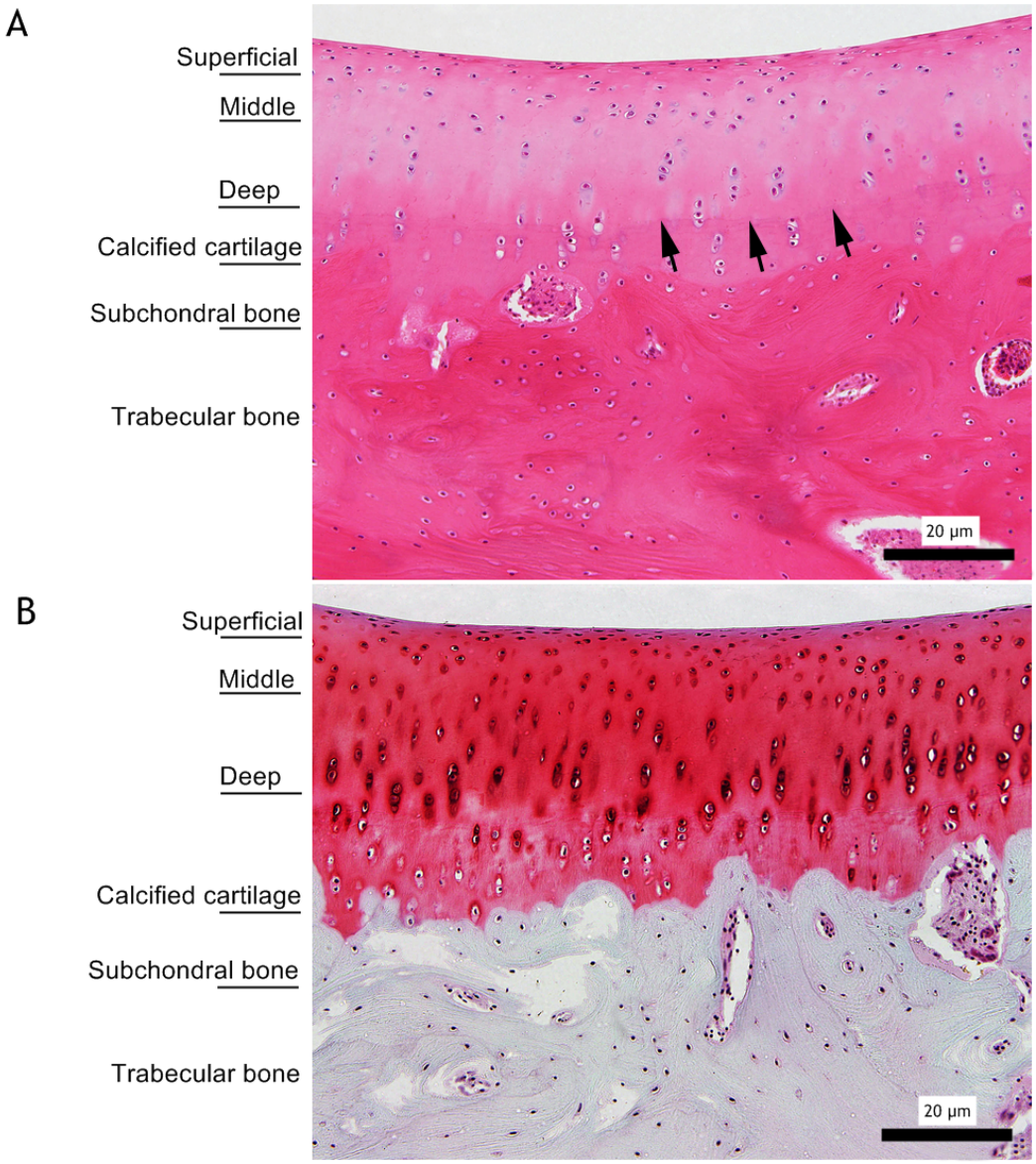

Figure 8.1: Normal articular cartilage from the distal humeral condyle stained with H&E (A) and Safranin O (B). A & B: 100x magnification.

(A) Normal articular cartilage structure has an intact surface, normal chondrocyte orientation, an intact and single tidemark (black arrows) and a normal thickening of subchondral and trabecular bone. (B) Safranin O staining is evenly distributed throughout the articular cartilage. A & B: Cat ID: X19, left elbow.

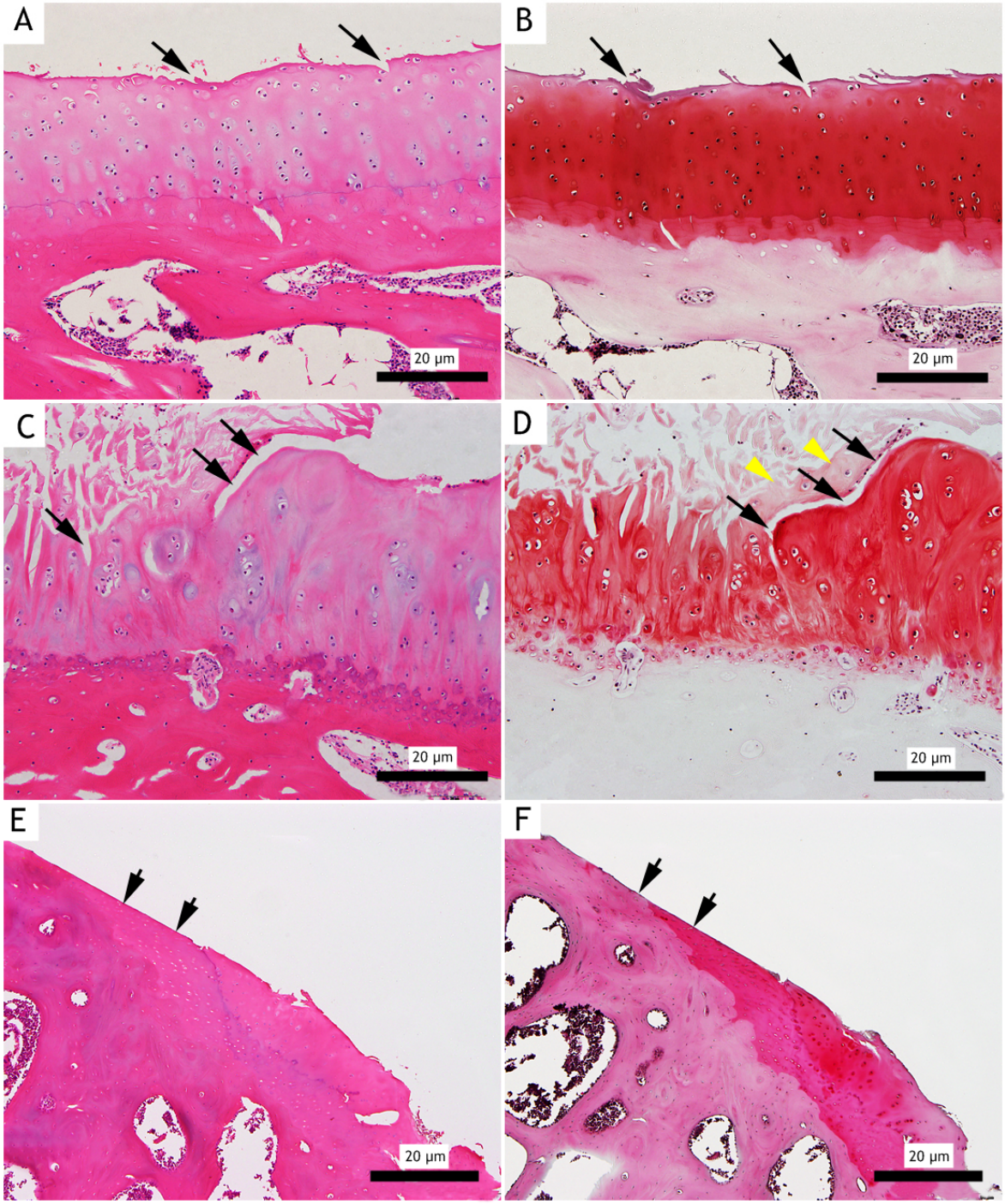

Figure 8.2: Showing OA articular cartilage stained with H&E (A, C & E) and Safranin O (B, D & F). A - F: 100x magnification.

(A & B) Mild structural changes of the articular cartilage. Articular fibrillation with fissures in the superficial layer is seen (arrows). Tidemark is intact and distinct. (B) Slight reduction of Safranin O staining in the superficial layer is also observed (see Figure 3.6.B for gross pathology). Cat ID: X31, left shoulder (C & D) Moderate to severe structural changes of the articular cartilage. The fissures have generally extended to the middle and deep layers of the articular cartilage (black arrows). Erosion of the superficial and middle layers is seen (see Figure 4.13.A for gross pathology). Moderate reduction of Safranin O staining into the middle layer can be observed (yellow arrowheads). Cat ID: X36, right elbow. (E & F) Full thickness cartilage defects (black arrows) with exposed subchondral bone are identified. Cat ID: X49, right hip.

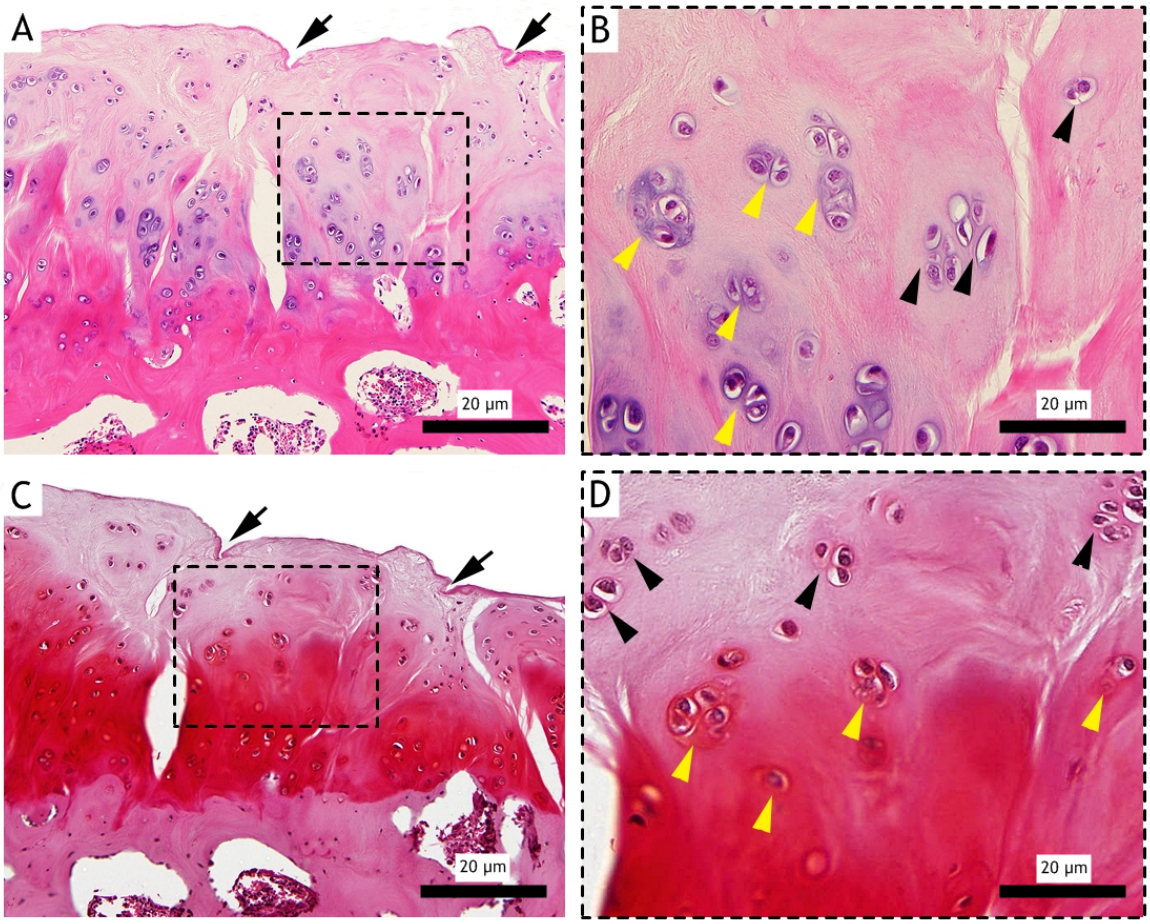

Figure 8.3: Showing chondrocyte changes associated with OA. A & B: H&E; C & D: Safranin O. A & C: 100x magnification; B & D: 200x magnification.

(A) OA cartilage shows several characteristic pathological changes such as chondrocyte loss at the superficial layer, chondrocyte clustering in the middle and deep layers and fissuring of the cartilage (black arrows). The boxed area in the low magnification is shown at a higher magnification in B. (B) Note that some of the chondrocyte clusters show areas of intense pericellular haematoxylin staining (yellow arrowheads) and others are characterized by weak pericellular haematoxylin staining (black arrowheads). (C) Reduced Safranin O staining into the middle layer is observed. Fissuring of the articular cartilage also can be identified (black arrows). The boxed area in the low magnification is shown at a higher magnification in D. (D) Intense (yellow arrowheads) and weak (black arrowheads) Safranin O staining is observed in the pericellular area of the chondrocyte clusters. A - D: Cat ID: X42, right stifle (see Figure 5.13.D for gross pathology).

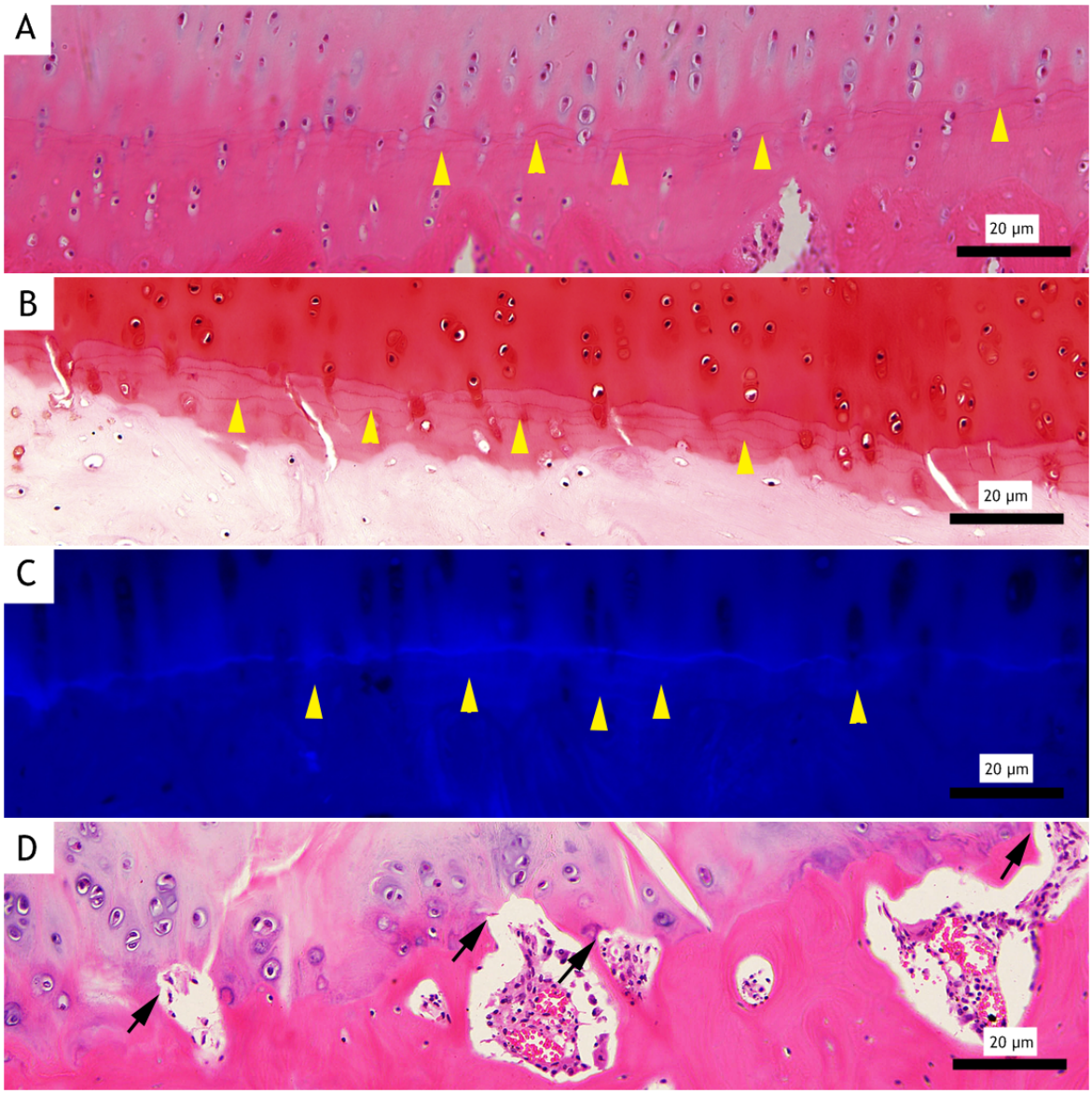

Figure 8.4: Showing tidemark changes associated with OA. A & D: H&E; B: Safranin O; C: 4',6-diamidino-2-phenylindole (DAPI). A - D: 100x magnification.

(A & B) Multiples tidemarks in the calcified cartilage are seen (yellow arrowheads). Cat ID: X37, right elbow. (C) Multiple tidemarks show blue fluorescence signals for DAPI (yellow arrowheads). The main tidemark shows obvious blue fluorescence signals for DAPI (white arrows). Cat ID: X37, right elbow. (D) Blood vessels cross the tide mark (black arrows) (see Figure 4.12.D for gross pathology). Cat ID: X42, left elbow.

8.3.2 Histopathologic features of bone in cats with and without OA

Histopathologic changes of the bone included presence of osteophytes, thickening of the subchondral bone plate and trabeculae, subchondral bone "cysts" and subchondral bone fibrosis.

Osteophytes

Osteophytes appeared as an osteo-cartilaginous protrusion at the margins of the joint (Figure 8.5). Occasionally, there was a line of separation between the osteophyte and epiphysis indicating that the osteophyte had not completely been integrated into the bone (Figure 8.5.C).

Thickening of the subchondral bone plate and trabeculae

Generally, thickening of the subchondral bone plate and trabeculae was seen in areas underlying fibrillated and eroded articular cartilage (Figures 8.6.A-B). A marked increase in subchondral plate and trabecular thickness was seen in severely affected joints which had full thickness loss of the articular cartilage (Figure 8.6.A).

Subchondral bone "cyst"

Subchondral bone "cysts" were identified in 18/192 (9.4%) samples (2 in the shoulder joints and 16 in the elbow joints). These "cysts" were filled with fibrous material, communicated with the joint space and were situated beneath cartilage defects (Figures 8.6.C-F). The average number of "cysts" observed in each joint was one. The "cysts" were not observed in other joints.

Subchondral bone fibrosis

Lesions were sometimes seen within the subchondral bone immediately below full thickness loss of the articular cartilage, characterised by fibrosis within the bone marrow spaces with single foci of cartilage "islands" (Figure 8.7). These cartilage "islands" consisted of a proliferation of chondrocytes with an extracellular matrix stainable with Haematoxylin (Figure 8.7.B) and Safranin O (Figure 8.7.D) and located in close proximity to the exposed subchondral bone surface. The lesions were only identified in 8/192 (4.2%) samples particularly in the distal humeral condyle and semilunar notch of the elbow where marked "wear lines" were seen grossly.

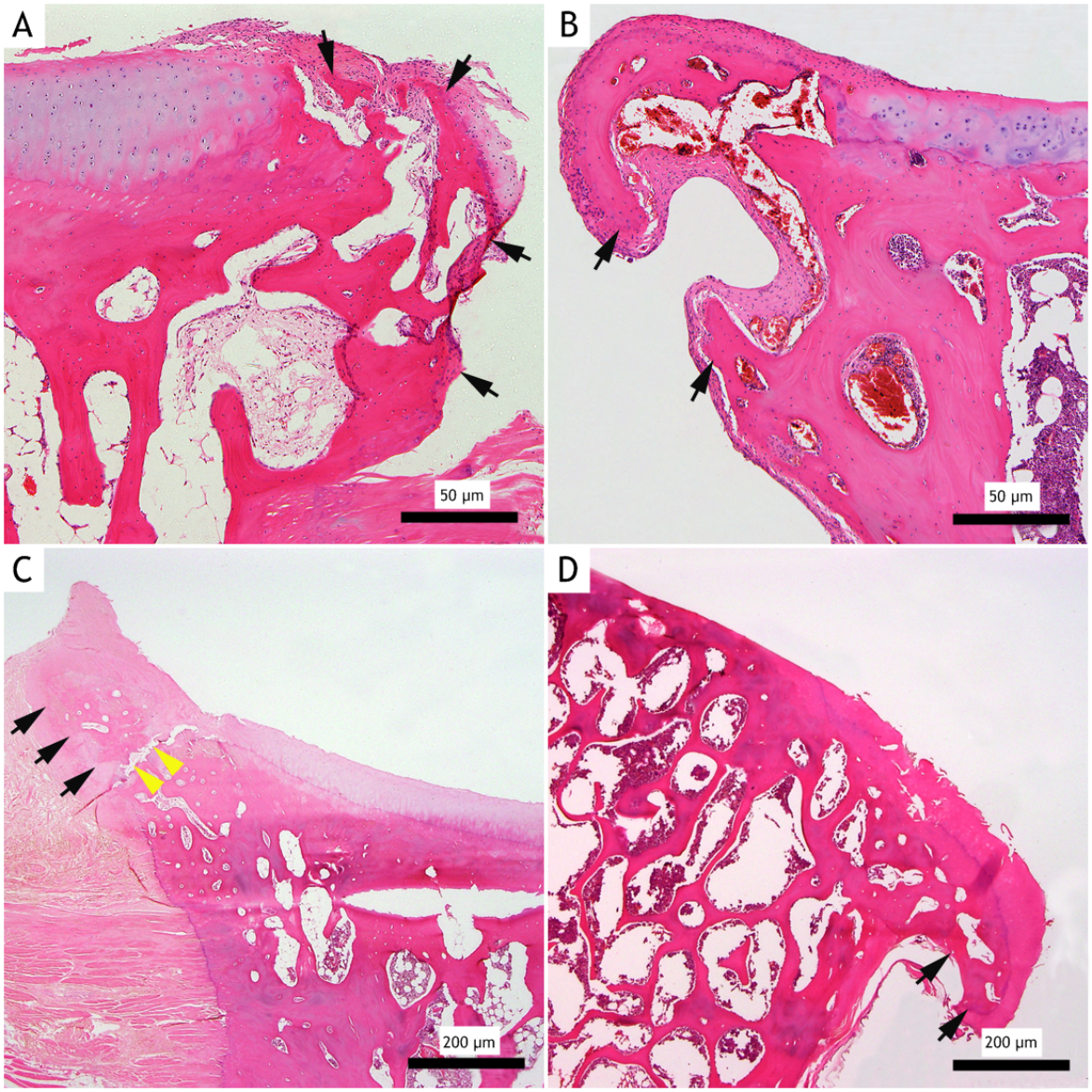

Figure 8.5: Showing osteophyte formation at the joint margin. A – D: H&E. A & B: 40x magnification. C & D: 12.5x magnification.

(A) Osteophyte formation at the joint margin of the radial carpal bone (black arrows) (see Figure 7.8.C for gross pathology). Cat ID: X31, left carpus. (B) Osteophyte formation at the joint margin of the radial head (black arrows) (see Figure 4.13.B for gross pathology). Cat ID: X30, left elbow. (C) An osteophyte at the margin the glenoid (black arrows). Line of separation between osteophyte and glenoid is seen (yellow arrows) indicating that the osteophyte has not completely integrated with the glenoid. Cat ID: X6, left shoulder. (D) An osteophyte is present at the margin of the humeral head (black arrows) (see Figure 3.5.C for gross pathology). Cat ID: X24, right shoulder.

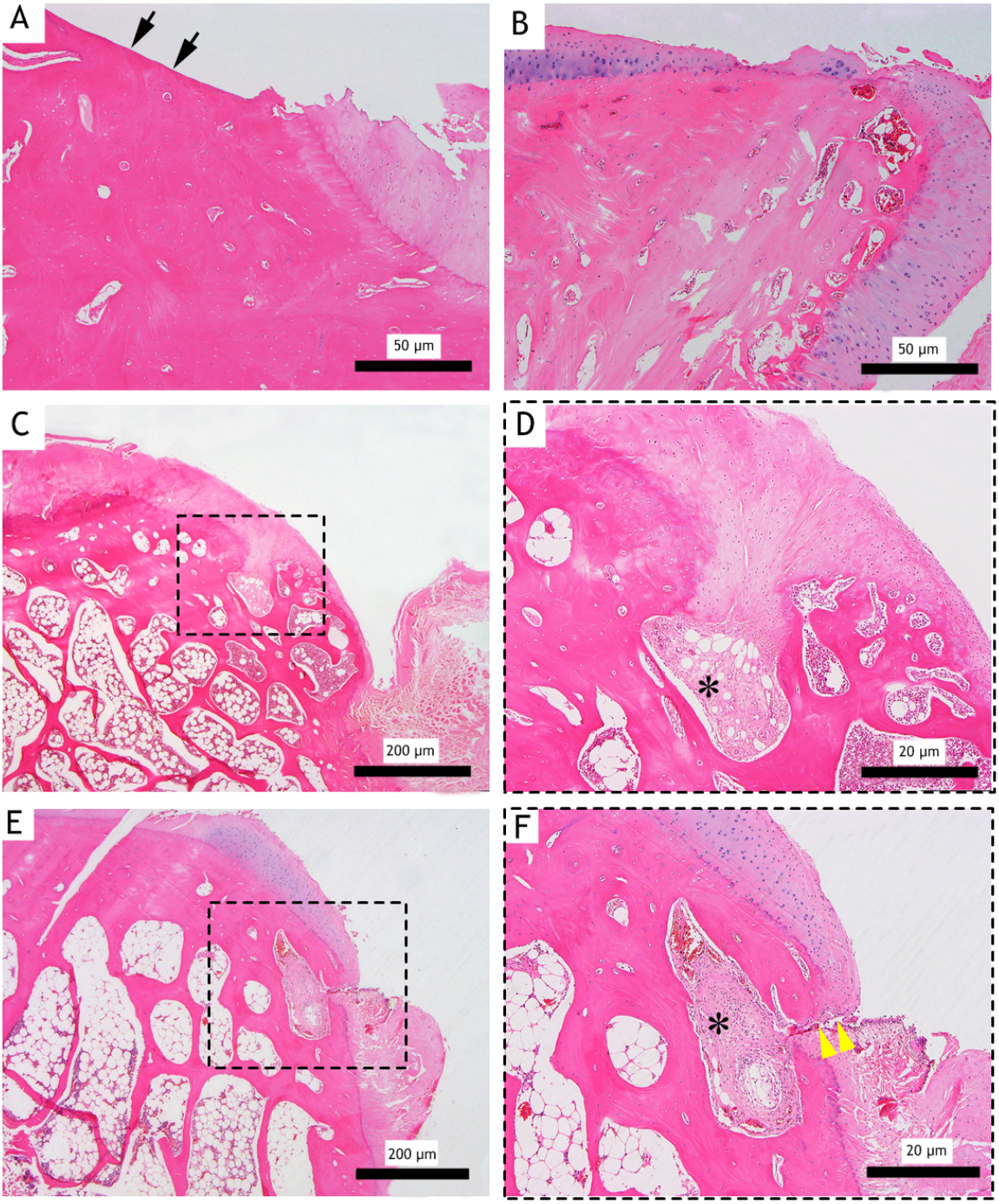

Figure 8. 6: Bone structural changes in OA. A - D: H&E. A & B: 40x magnification; C & E: 12.5x magnification; D & F: 100x magnification.

(A) Full thickness loss of cartilage (black arrows) with marked increase in the subchondral bone plate and trabeculae thickness is present (see Figure 4.12.D for gross pathology). Cat ID: X42, left elbow. (B) Partial loss of cartilage with increase in the subchondral bone plate and trabeculae is observed (see Figure 7.9.B for gross pathology). Cat ID: X31, right tarsus. (C) Cartilage fibrillation, erosion and a subchondral cyst are seen. Cat ID: X21, right shoulder. (D) 100x magnification of the cyst showing it is filled with fibrous material (asterisk) and the opening is covered with cartilage contiguous with the articular cartilage. Cat ID: X21, right shoulder. (E&F) Subchondral cyst is filled with fibrous material (asterisk). It is communicating with the joint space through a small opening (yellow arrowheads). Cat ID: X16, left elbow.

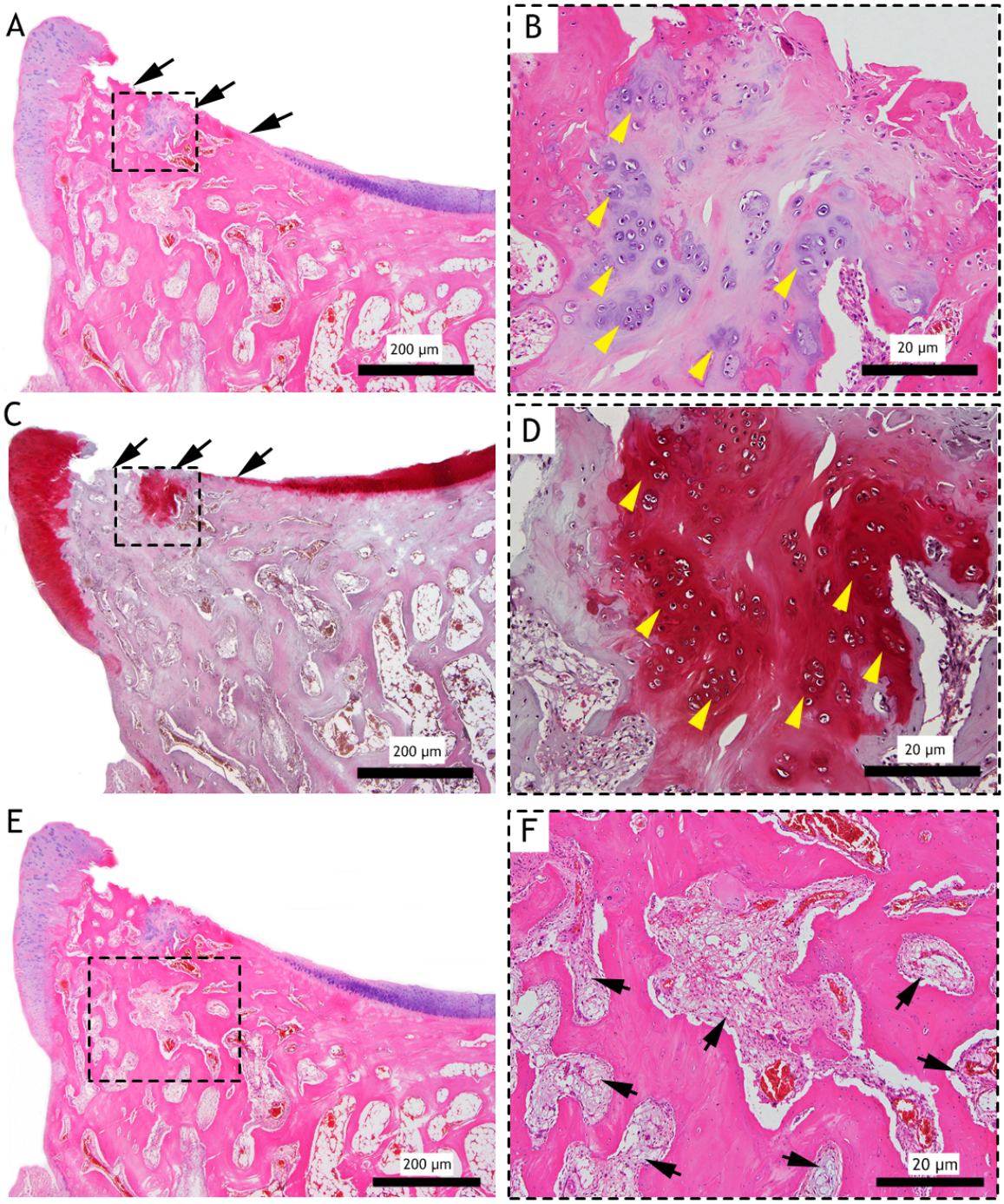

Figure 8.7: OA cartilage from the distal humeral condyle stained with H&E (A,B, E & F) and Safranin O (C & D). A, C & E: 12.5x magnification; B, D & F: 100x magnification.

(A & B) Full thickness loss of articular cartilage (black arrows) is identified; grossly the sample showed "wear lines" (see Figure 4.12.C) particularly on the medial part of the humeral condyle. The remaining articular cartilage shows intense Safranin O staining in all layers. The boxed areas in the low magnification are shown at a higher magnifications in B and D. (B & D) An area of chondrocyte "islands" with extracellular matrix stainable with Haematoxylin and Safranin O is seen beneath the area of cartilage loss (yellow arrowheads). (E & F) The bone marrow spaces underneath the cartilage loss are filled with fibrotic granulation tissue (black arrows). A - F: Cat ID: X26, left elbow.

8.3.3 Histopathologic features of intra-articular structures in cats with and without OA

Osteochondromas

Osteochondromas consisted of trabecular bone with marrow spaces (Figures 8.8.A-B, E-F) covered by a hyaline cartilage cap which stained with Safranin O (Figures 8.8.C-D). Generally there was evidence of a synovial attachment (Figures 8.8.A-B).

Tendon of origin of supinator muscle

The supinator sesamoid bone was seen in 55/116 tendons. In 45 (81.8%) tendons, it appeared as a round or oval shaped bone. Its structure comprised trabecular bone with marrow spaces (Figures 8.9.A & C). The sesamoid bone was seen embedded within the tendon of origin of the supinator muscle and the surface facing the joint space had a cartilage cap (Figure 8.9.B). The cartilage cap was evenly stained with Safranin O (Figure 8.9.D). Ten (18.2%) tendons showed areas of chondro-osseous metaplasia of fibrocartilage (Figure 8.9.E). In cases where the supinator sesamoid bone was not visible radiographically (61/116), only dense regular connective tissue was seen in the tendon (Figure 8.9.F).

Menisci

In cases where the mineralisation was not radiographically identified, only fibrocartilaginous tissue typical of a normal meniscus was observed (Figure 8.10.A). Mineralisation was identified histologically in all the medial menisci (49) in which mineralisation were visible on radiography. The areas of mineralisation were located in the cranial horn of the medial meniscus. Of these 49 menisci, 26 (53.1%) had intrameniscal ossification consisting of trabecular bone with marrow spaces (Figure 8.10.C). Twenty (40.8%) menisci showed intrameniscal mineralisation with areas of chondro-osseous metaplasia (Figure 8.10.E). Three (6.1%) menisci showed intrameniscal ossification consisting of trabecular bone with marrow spaces but also with an obvious articular cartilage cap on the proximal (femoral) surface which stained with Safranin O (Figure 8.11). No mineralisation was detected in any of the lateral menisci.

Stifle joints with gross cartilage pathology (Gross Pathology Global Score 2 and 3) contained degenerated menisci, characterised mainly by disorganisation of fibrocartilage with fibrillation at the femoral side, tibial side and/or the inner border. There was

variable pattern of Safranin O staining. Normal menisci showed Safranin O staining confined to the inner border (Figure 8.10.B). Menisci from OA joints had an extensive Safranin O staining (Figures 8.10.D & F).

Cranial cruciate ligaments

Longitudinal sections of the cranial cruciate ligaments from 10 normal (Gross pathologic Global score 0) stifle joints had well organised collagen bundles with fibrocytes aligned between the bundles (Figure 8.12.A). A similar normal appearance was seen in 18 ligaments from OA joints. Pathological changes were seen in only 2 cranial cruciate ligaments from OA stifle joints of a single cat (Cat X42) (Gross pathologic Global score 3) characterised by disorganisation of the collagen bundles and fibrocytes. The affected ligaments were relatively hypocellular (Figure 8.12.B) and stained faintly with Safranin O (Figure 8.12.D).

Attempts to localise collagen types I and II in articular cartilage, osteochondromas, SSB and menisci were not successful.

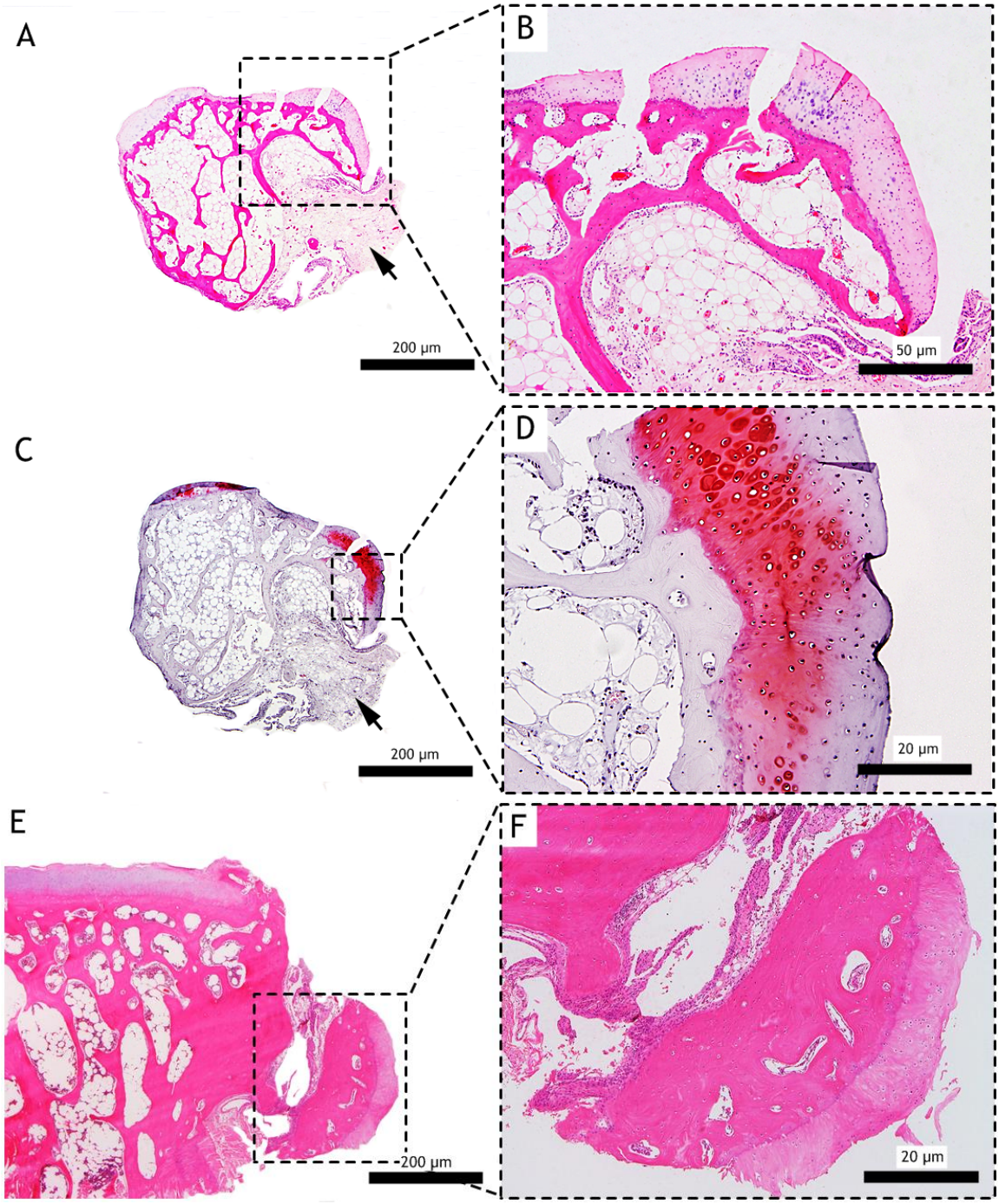

Figure 8.8: Histologic characteristics of osteochondromas using H&E (A, B, E & F) and Safranin O (C & D). A, C and E: 12.5x magnification; B: 40x magnification; D and F: 100x magnification.

(A & B) Histologic features of an osteochondroma originally attached to the synovial membrane of the distal humeral condyle (see Figure 4.17.A for gross pathology). It is composed of trabecular bone between which is bone marrow. The remnants of the synovial membrane attachment are seen (black arrow). (B) At higher magnification, the structure is seen covered with a cartilage "cap". (C & D) The cartilage cap is strongly positive for Safranin O staining especially in the middle and deep layers of the cartilage. An intense Safranin O staining is also observed in the pericellular area of many chondrocytes. (E & F) An osteochondroma attached to the synovial membrane at the articular margin of the ulna. The bony lesion is covered with a cartilaginous "cap". A - D: Cat ID: X28, right elbow. E - F: Cat ID: X29, left elbow.

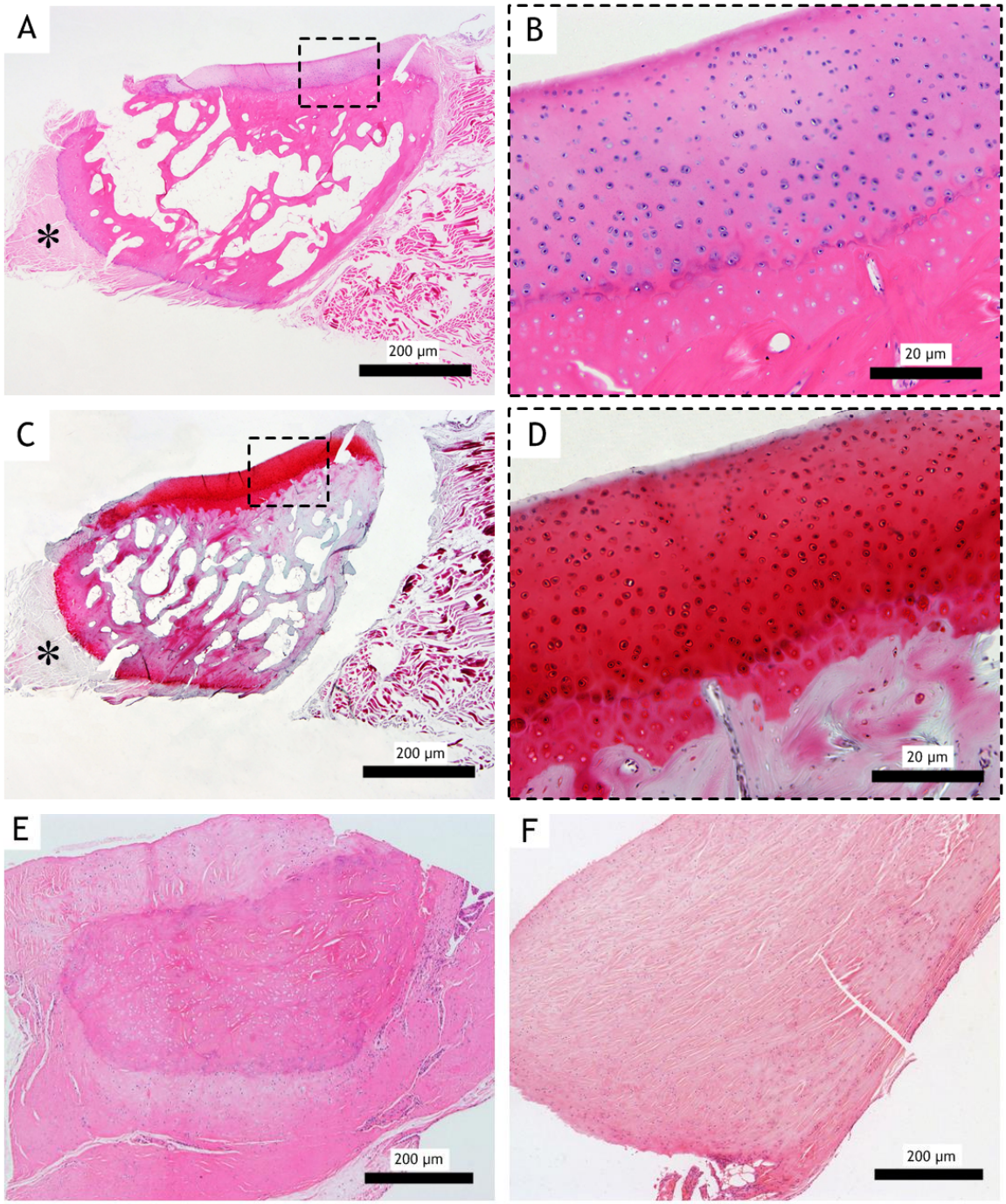

Figure 8.9: A cross section of the supinator sesamoid bone. A, B, E & F: H&E; C & D: Safranin O. A, C, E & F: 12.5x magnification; B & D: 100x magnification.

(A & C) The SSB consists of trabecular bone and bone marrow. The SSB has a round to oval shape and is seen embedded within the tendon of origin of the supinator muscle (asterisk). The "articular" surface of the sesamoid bone is covered with a cartilage cap. The boxed area in the low magnification is shown at a higher magnification in B. (B) At higher magnifications; the sesamoid bone is seen covered with articular cartilage. (D) Safranin O staining is intense and evenly positive throughout the cartilage layer. (E) Tendon of origin of supinator muscle shows mineralisation with areas of chondro-osseous metaplasia of fibrocartilage. (F) Tendon of origin of supinator muscle consists of dense regular connective tissue. A - D: Cat ID: X37, left elbow; (E) Cat ID: X38, right elbow; (F) Cat ID: X19, left elbow.

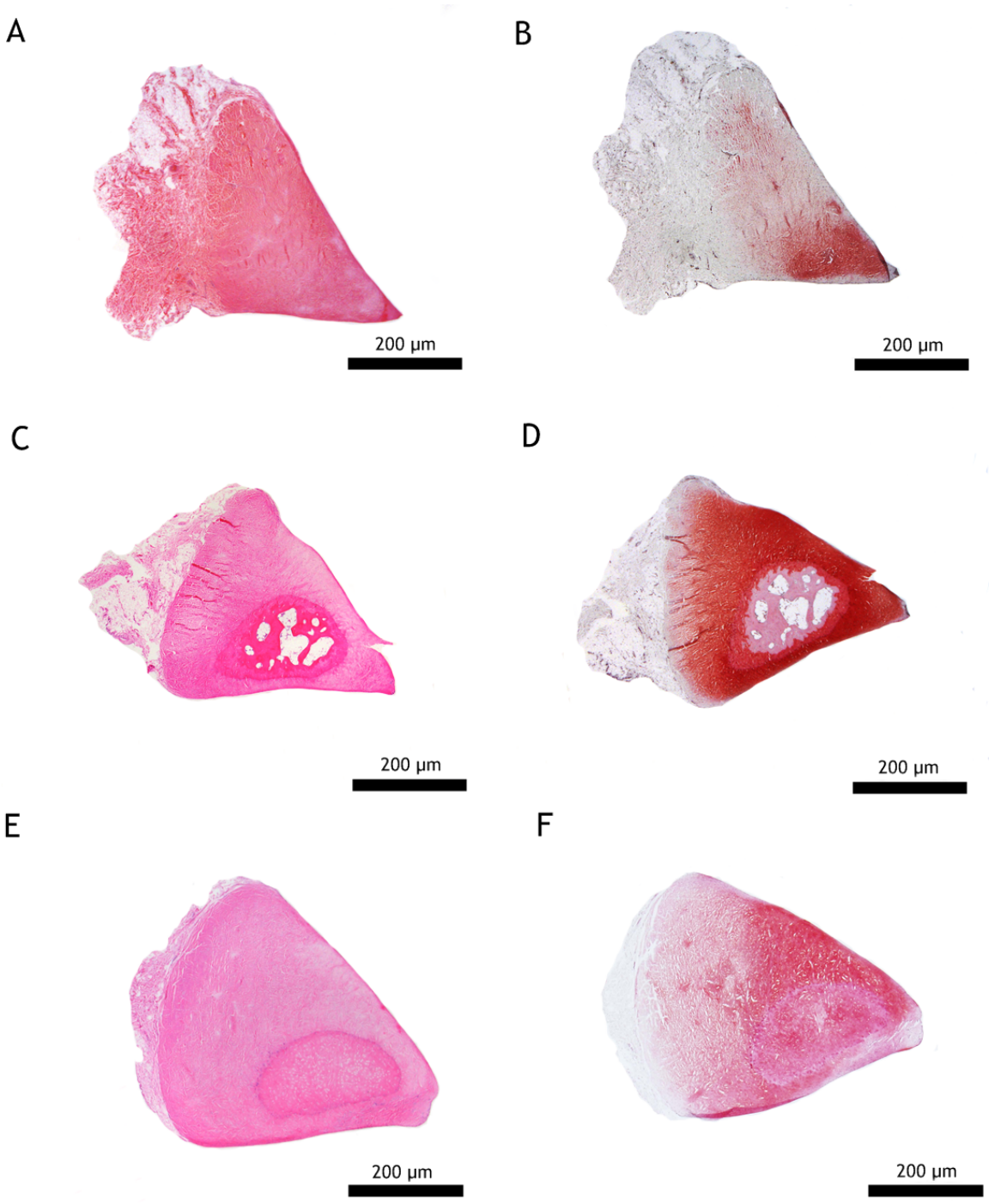

Figure 8.10: A cross section of the cranial horn of medial meniscus. A, C & E: H&E; B, D & F: Safranin O. A – F: 12.5x maginification.

(A) Normal meniscus, consisting of normal fibrocartilage with no evidence of mineralisation of its matrix. (B) Safranin O staining is seen at the inner border of the normal meniscus. (C) Intrameniscal ossification appears as an organised structure with trabecular bone and marrow spaces. (D) Strong Safranin O staining is observed of the entire body of the meniscus. (E) Meniscus shows intrameniscal mineralisation with areas of chondro-osseous metaplasia of the fibrocartilage but no trabecular bone. (F) There is an uneven staining of Safranin O of the body of the meniscus. A & B: Cat ID: X51, left stifle. C & D: Cat ID X42, left stifle. E & F: Cat ID: X36, right stifle.

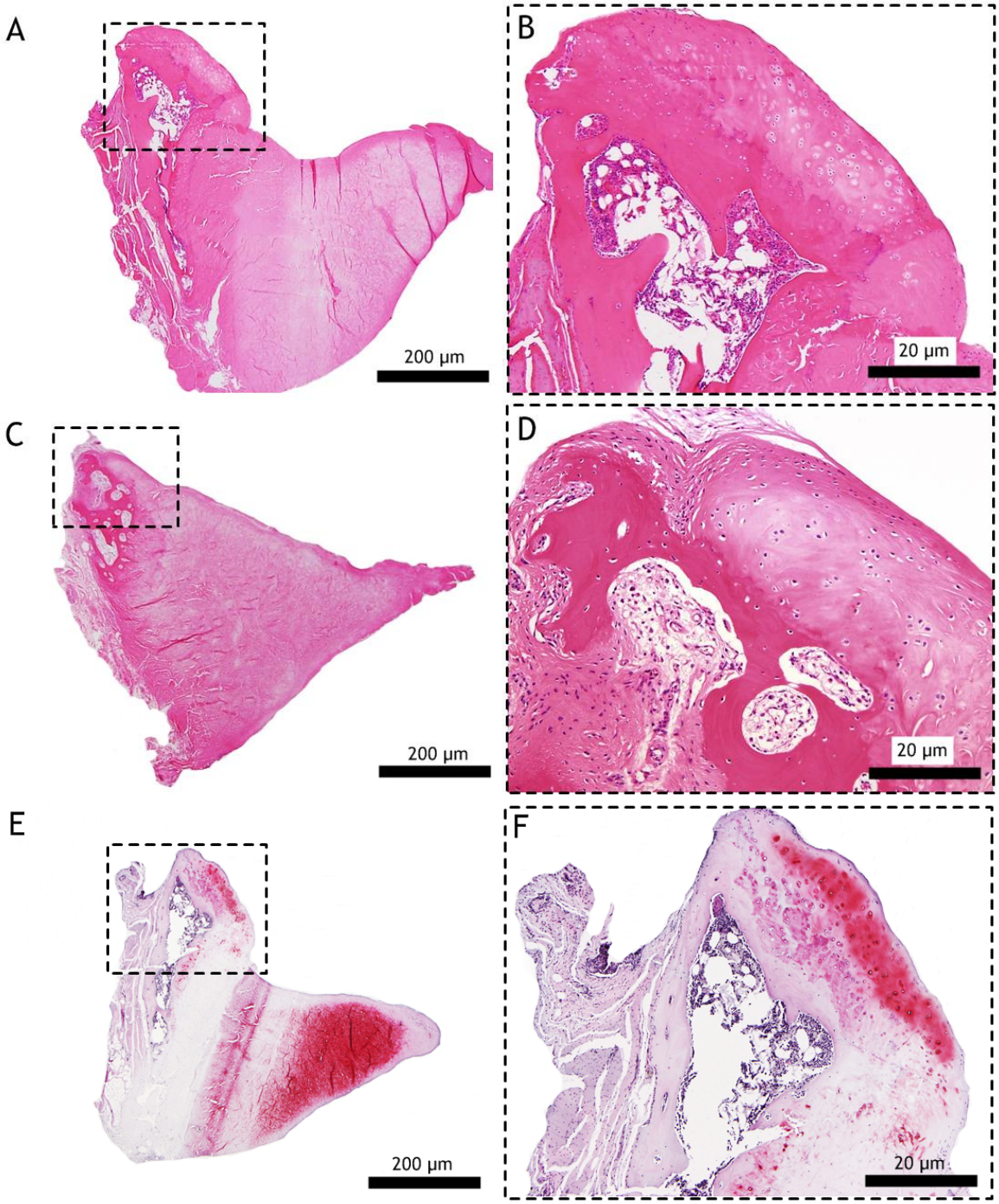

Figure 8.11: A cross section of the cranial horn of medial meniscus. A - D: H&E; E - F: Safranin O. A, C & E: 12.5x maginification; B, D & F: 100x magnification.

(A, C & E) Intrameniscal ossification consisting of trabecular bone with marrow spaces is seen. The boxed areas in the low magnification are shown at a higher magnification in B, D and F. (B, D & F) At higher magnifications; the proximal (femoral) surface of the ossification is seen covered with an articular cartilage "cap". Safranin O staining is intense and evenly positive throughout the cartilage layer. A, B, E & F: Cat ID: X22, left stifle; C – D: Cat ID: X32, left stifle.

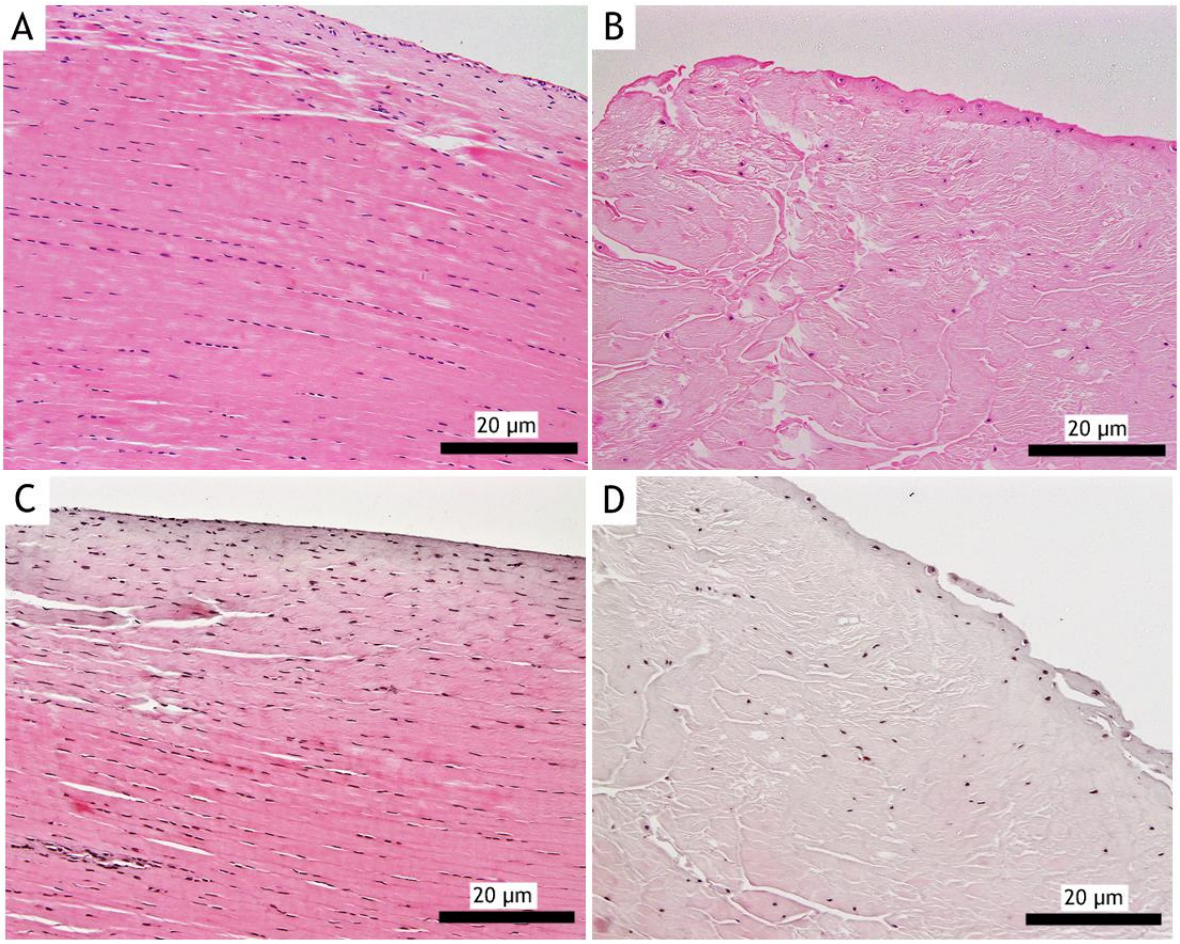

Figure 8.12: A longitudinal section of the cranial cruciate ligament of the stifle joint. A & B: H&E; C & D: Safranin O. A - D: 100x magnification.

(A) Normal cranial cruciate ligament consisting of well organised collagen bundles with fibrocytes longitudinally aligned between the bundles. (B) Disorganisation of the cranial cruciate ligament collagen networks and fibrocytes is seen in the OA stifle joint. The collagen fibres and fibrocytes are not longitudinally orientated and the number of fibrocytes is reduced. (C) There is even staining of Safranin O of the normal cruciate ligament. (D) The affected cruciate ligament is stained faintly with Safranin O. A & C: Cat ID: X51, right stifle; B & D: Cat ID: X42, left stifle.

8.3.4 Histopathologic features of the synovial membrane in cats with and without OA

A total of 192 (62 no OA/normal and 130 OA) synovium were examined. Normal synovial membrane was seen in all no OA/normal joints and in 78/130 OA joints (Gross pathologic Global score 1). Normal synovial membrane had a lining layer of 1 to 2 cells, no villous hyperplasia, no inflammatory infiltrate and no calcification present (Figure 8.13.A). Pathologic changes in the synovial membrane from 52/130 OA joints (Gross pathologic Global score 2 & 3) included lining layer hyperplasia, typically 3 to 6 cell layers thick (Figure 8.13.B). Villous hyperplasia and hypertrophy was also identified, characterised by short to finger-like villi, seen in 30/130 OA joints (Figure 8.13.C).

For the 192 synovial samples that were assessed from no OA/normal and OA joints, the inflammation was graded. Inflammatory cell infiltration was identified in 16 (8.3%) joints (7/50 elbow joints, 5/37 stifle joints, 2/25 shoulder joints and 2/26 tarsal joints). Severity was graded mild in all joints. The inflammatory cells infiltrating the synovial tissue were mainly lymphocytes and macrophages (Figure 8.13.D), and were present in the supporting layer, often around blood vessels. Inflammation was not seen in any hip and carpal synovial membranes.

Von Kossa staining demonstrated calcification particularly in the supporting layer in 15/130 OA samples (Figures 8.14.B-D). Calcification was not seen in any normal synovial membrane. Bone formation was present in 50/130 OA samples examined (Figure 8.13.C).

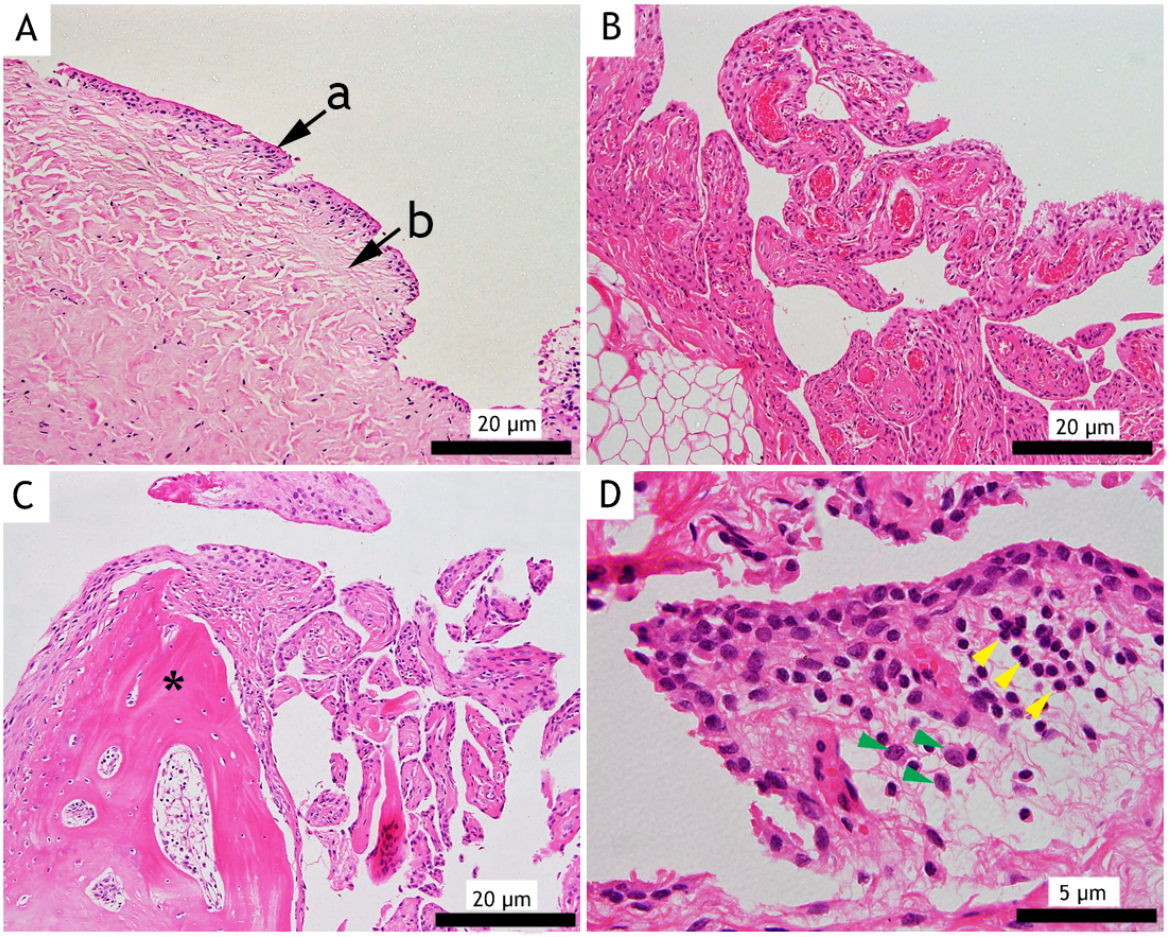

Figure 8.13: Synovium stained with H&E. A - C: 100x magnification, D: 400x magnification.

(A) Histologic appearance of normal synovial membrane, (a) lining layer (b) supporting layer. (B) OA synovium with marked lining layer hyperplasia and finger like hypertrophy. (C) There is bone formation (asterisk) within the joint capsule. There is extensive hyperplasia of the lining layer and marked villous hypertrophy of the synovium. (D) Showing OA synovium with infiltration of predominantly lymphocytes (yellow arrowheads) and macrophages (green arrowheads) in the supporting layer. A: Cat ID: X19, left elbow; B: Cat ID: X49, right hip; C: Cat ID X18, left elbow; D: Cat ID: X42, right stifle.

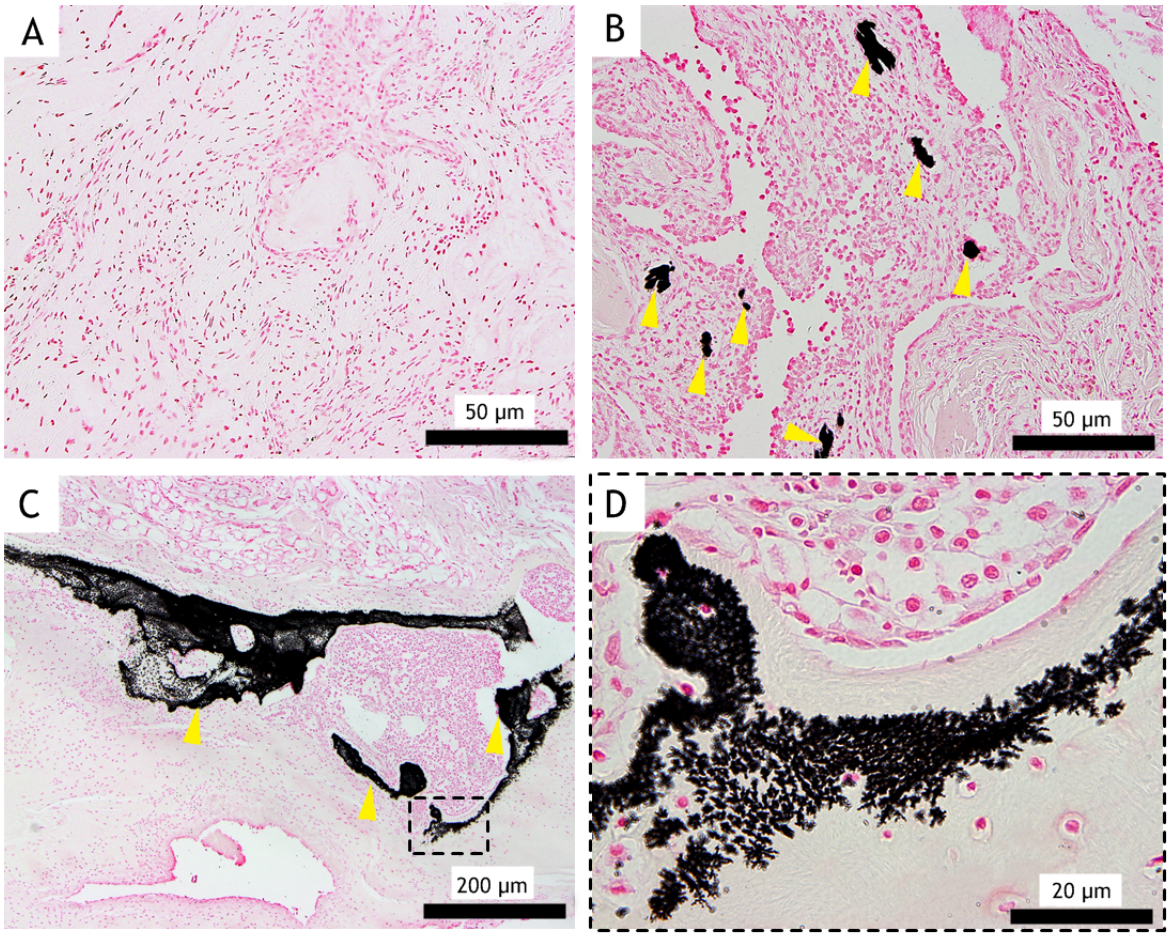

Figure 8.14: Synovial membrane stained with von Kossa. A - B: 40x magnification, C: 12.5x magnification, D: 100x magnification.

(A) Synovial membrane with negative von Kossa staining. (B) There are multiple foci of calcification (yellow arrowheads) observed in the supporting layer of the synovial membrane. The positive staining is noted by the black colouration. (C) Large areas of calcification (yellow arrowheads). The boxed area in the low magnification is shown at a higher magnification in D. (D) At higher magnifications, the boxed area in (C) shows black-stained crystalline deposits with the von Kossa stain indicating the presence of calcium within an area of osseochondral metaplasia. A: Cat ID: X51, right shoulder; B: Cat ID: X42, right stifle; C & D: Cat ID: X12, right elbow.

8.4 Discussion

Generally, most of the histopathologic changes seen in cats with OA are the same as those described in other mammalian species- human (Pritzker et al., 2006), dog (Cook et al., 2010), rabbit (Laverty et al., 2010) and horse (McIlwraith et al., 2010). The histopathologic changes of the articular cartilage, bone and synovium showed a considerable variation in the severity of the pathology.

Structural changes of the articular cartilage varied from fibrillation in the superficial layer to full thickness loss of the cartilage with exposure of the subchondral bone. The most severe histopathologic lesions of the articular surfaces were observed in those elbow and tarsal joints where "wear lines" were seen grossly, specifically on the medial part of the humeral condyle and the lateral part of the tibial tarsal bone. The presence of more severe histopathologic lesions in the medial compartment of the feline elbow joint has been documented (Bennett et al., 2012a; Ryan et al., 2013; Freire et al., 2014).

Chondrocyte proliferation which appeared as "clusters" of cells was considered as an attempt to repair and counteract cartilage degeneration by producing more matrix proteins (van Der Kraan and van Den Berg, 2012). Haematoxylin and Safranin O are basic dyes that stain acidic proteoglycan present in cartilage tissue (Schmitz et al., 2010). This was seen as an intense pericellular haematoxylin and Safranin O staining in some of the clusters particularly in the severely affected joints (Figures 8.3 and 8.7.A-B). An overall reduction of cartilage safranin O staining was noted in the early stages of OA and became more marked in the later stages suggesting that a progressive loss of proteoglycans occurs in feline OA. In a recent publication, Freire et al. (2014) reported that chondrocyte "clusters" were not present in feline articular cartilage with OA; however in the present study these "clusters" were common particularly in the moderate to severely affected joints.

Changes in the tidemark particularly vascular invasion and the presence of multiple tidemarks were consistently seen in the moderate to severely (Gross pathologic Global score 2 and 3) affected joints. These findings were again contrary to what was reported by Freire et al. (2014) where multiple tidemarks and blood vessels crossing the tidemark were not identified in any feline elbow joint. The DAPI fluorescence studies demonstrated the presence of DNA in the tidemark of normal joints and in all of the multiple tidemarks of OA joints. DAPI is a fluorescent stain which binds strongly and selectively to the minor groove of adenine-thymine regions in DNA. A previous study

reported that the number of tidemarks correlated with the severity of human OA (Roudier et al., 2013). The tidemark may contain hyaluronan, collagen, phospholipids, alkaline phosphatase and adenosine triphosphatase (Dmitrovsky et al., 1978; Havelka et al., 1984; Oettmeier et al., 1989; Lyons et al., 2005). DNA and phospholipids are large anionic compounds of chondrocytes that cannot directly enter the dense and negatively charged matrix of cartilage (van Den Berg and van De Putte, 1985; Zatarain-Rios and Mannik, 1987). However they will be released when chondrocytes die and enter the matrix (Simkin, 2008). Simkin (2008) suggested that multiple tidemarks seen in OA occur as a result of the deposition of chondrocyte apoptotic nuclei and debris. Since there are no macrophages in the articular cartilage, any debris from apoptotic chondrocyte will simply diffuse into the surrounding interterritorial matrix and gradually diffuse towards the underlying bone as a result of cyclic loading of the cartilage during normal joint usage. This movement is stopped by the underlying calcified cartilage which acts as a semipermeable membrane, allowing only water and smaller molecules to pass into the subchondral bone but retaining larger chondrocytic molecules such as DNA which form the tidemark. Calcification of the articular cartilage increases in OA which causes the calcified cartilage to increase in thickness (Hashimoto et al., 1998) thus allowing additional tidemarks to be created at the new calcified and uncalcified cartilage boundary. The increased chondrocyte necrosis in OA will result in additional cellular debris being released and subsequently died at the tidemark.

Changes in the bone such as thickening of the subchondral bone plate and trabeculae were seen in those joints with moderate to severe gross cartilage lesions which is similar to that reported in the dog (Brandt et al. 1991), human (Bobinac et al., 2003) and in guinea pig models (Pastoureau et al., 2003). However, it appears to contradict a previous study that found subchondral bone plate thinning in feline stifle OA using an experimental model (Boyd et al., 2005). During the early-stages of OA, it is thought the subchondral plate becomes thinner due to increases in remodelling rates and turn over (Burr and Gallant, 2012). As a result, much of the bone has not had an opportunity to become fully mineralised and thus becomes more porous with reduced stiffness. At the same time, subchondral bone trabeculae become thinner. A decrease in the subchondral bone porosity has been reported in cat and was thought to be part of the OA process (Ryan et al., 2013). In late-stage OA, in response to the reduced mineralisation, it is thought the bone increases its volume by a thickening of the subchondral bone plate providing increased stiffness (Burr and Gallant, 2012). In addition, the calcified cartilage becomes thicker thus creating a thicker mineralised plate which is apparent radiographically as an area of increased radio-opacity (Burr and Gallant, 2012). In the current study, the assessment of the bone changes was done subjectively. To

understand the role of bone remodelling in the initiation and progression of OA, a longitudinal study needs to be done and monitored carefully from the very early stages to the very late stages of OA.

The present study has shown the presence of subchondral bone "cysts" in feline OA. They were relatively rare and only found in 18/192 samples. These "cysts" have been described in humans and horses, and their association with OA is well-known (Plewes, 1940; Petterson and Sevelius, 1968; Tanamas et al., 2010). However, these lesions are not commonly found in the dog (Biery et al., 1976). The origin of the subchondral bone "cyst" still remains uncertain. Durr et al. (2004) hypothesised that these lesions develop as a result of integrity of the cartilage and subchondral bone which allows intrusion of the synovial fluid into the bone. When no further fluid can be forced in, a granulation tissue develops which may later ossify (Landells, 1953). The present findings seem to be consistent with this theory which found the "cyst" was communicating with the joint space through a small opening (Figure 4.27.D) and was filled with fibrous material rather than fluid. The small opening may develops as a result of an abnormal load bearing which causes a defect in the articular cartilage and subchondral bone. However, Ondrouch (1963) believed that the subchondral bone "cyst" originates from necrotic lesions in the subchondral bone, which are induced by abnormal mechanical stress and lead to microfractures and focal bone resorption. The present study could not detect these "cysts" radiographically. This might be due to the small size of the "cysts" and the fine trabecular appearance of feline bone on radiographs which would make identification of a small radiolucent "cyst" very difficult. CT scanning is better able to help define the dimension of a subchondral bone "cyst" than MRI and plain radiography (Allan, 2013).

Histopathologic examination of the subchondral bone marrow mainly showed a normal appearance although fibrovascular changes, in which the bone marrow was replaced with fibrous tissue was seen in 8/192 sections examined. These changes were only seen in the elbow joint, particularly in the distal humeral condyle and semilunar notch of the ulna where marked "wear lines" were seen grossly. Subchondral bone fibrosis was also reported by Freire et al. (2014) in the feline elbow joint.

Osteochondromas have been described as either primary or secondary (Smith et al., 2012). Primary osteochondromas usually occur without any existing cause and are described histologically as having metaplastic cartilage containing atypical chondrocytes with patchy calcification and they lack articular cartilage and subchondral bone. Secondary osteochondromas are often seen with coexistent joint trauma, OA or

inflammatory joint disease (Flo et al., 1987; Edinger and Manley, 1998). Histologically, they are described as an osteochondral fragment with metaplastic cartilage and normal evenly distributed chondrocytes and regular calcification (Flo et al., 1987; Freire et al., 2014). In this study, osteochondromas consisted of trabecular bone covered by a cartilage cap, which stained with Safranin O and generally with evidence of a synovial attachment (Figure 8.8), and were thus considered secondary. The evidence for a synovial attachment suggest these osteochondromas do arise from metaplasia of the synovium although it is possible that fragment of degenerate cartilage could separate from the articular surface, become embedded within the synovium and vascularised. These fragments could then grow and undergo metaplasia.

The SSB consisted mainly of trabecular bone and bone marrow, embedded within the tendon of origin of the supinator muscle and were covered with a cartilage cap. Safranin O stained sections showed intense and even staining of the cartilage cap, consistent with the proteoglycan-rich matrix of hyaline cartilage (Engiles, 2013). The tendon of the supinator muscle often includes areas of chondro-osseous metaplasia. Meyer et al. (1964) suggested that sesamoid bones forms in response to excessive mechanical friction occurring in a tendon. It has been known that mechanical stress is able to induce expression of growth factors such as BMPs (BMP-2) which can stimulate formation of bone and cartilage (Sato et al., 1999). Under stimulation of BMPs, mesenchymal stem cells which are present in tendon tissues (De Mos et al., 2007) are capable of initiating metaplasia of tendon cells into osteogenic cells via a chondro-osseous differentiation pathway (Zhang and Wang, 2012). Supinator sesamoid bone was present in 55/93 OA joints. It is possible that an abnormal gait due to painful OA increases the mechanical stress on the tendon of the supinator muscle causing fibrocartilaginous metaplasia and formation of the sesamoid bone to allow the tendon to function more effectively (Wood et al., 1995).

The present study found three different types of mineralisation within the feline medial meniscus: intrameniscal ossification consisting of trabecular bone with marrow spaces totally embedded within the meniscus, intrameniscal ossification consisting of trabecular bone with marrow spaces but also with an obvious articular surface covered by a cartilage cap and intrameniscal mineralisation with areas of chondro-osseous metaplasia. Two explanations have been proposed for the origin of meniscal mineralisation. The first is that meniscal mineralisation is caused by chondro-osseous transdifferentiation from fibrocartilage tissue with mineral deposition which later forms trabecular bone and bone marrow (Freire et al., 2010) presumably as a result of mechanical stress due to gait abnormality or abnormal hind limb conformation both at

which could be caused by the pain of OA. The second explanation is that the mineralisation represents a meniscal sesamoid bone, the lunula which has been reported in several species including the cat (Pearson and Davin, 1921; Pedersen, 1949; Greene, 1955; Shaw and Martin, 1962; Cooper and Schiller, 1975; Hebel and Stromberg, 1976; Whiting and Pool, 1985; Araujo et al., 2010). The histopathologic findings of the present study suggest that most cases of meniscal mineralisation were due to chondro-osseous transdifferentiation. However in 3/116 cases (Figure 8.12) the mineralised structure contained an articular surface consistent with a lunula (Whiting and Pool, 1985).

Unlike the articular cartilage, degeneration of menisci occurs within the fibrocartilage itself rather than at its surface. Fibrillation of the meniscal surface was sometimes seen at the inner body of the meniscus and sometimes on the femoral and tibial surfaces as well. Safranin O staining showed that the proteoglycan content increased in OA menisci when compared to normal menisci. This suggests an attempt of the OA menisci to adapt and regenerate by producing more cartilage matrix. In studies of human meniscal tissue, Sun et al. (2012) reported similar findings.

Efforts to localise collagen types I and II in sections of the articular cartilage, osteochondromas, SSB and menisci by immunohistochemistry were unsuccessful. The antibodies used in this study were monoclonal antibodies raised in mice against collagen types I (Abcam 90395) and II (Abcam 3092). However, although they were thought to be specific against types I and II collagen, the antibodies failed to react with feline tissues. It was unlikely that further manipulation of the experimental conditions such as using more concentrated antibodies or increasing antibody incubation time would improve the result by very much. It was concluded that these antibodies did not cross-react with feline articular tissues. Other collagen antibodies are commercially available against dog, chicken, human and rabbit, but time restraints did not allow these to be assessed in this study.

Degenerative changes of the CCL were identified histologically in 2/30 samples, this cat had radiographic and gross pathologic evidence of bilateral OA of the stifle joints. Feline CCL disease is reported but is far less common than in the dog. Harasen (2005) reported the presence of cruciate disease in 8/17 cats. Of these 8 cats, one had radiographic evidence of bilateral stifle OA. These cats were relatively old (mean age 8.5 years) and overweight (6.5 kg). Degenerative changes in the canine CCL also have been reported to be more prevalent in heavier animals (Vasseur et al., 1985). The histopathologic characteristics of the degenerative CCLs included disorganisation of

collagen fibres and fibrocytes. Areas of hypocellular were also seen. Similar findings have also been reported in feline (Harasen, 2005) and canine (Vasseur et al., 1985) CCLs by other workers. The presence of chondroid metaplasia, fibrocyte proliferation and focal mineralisation are also reported in cats and dogs (Vasseur et al., 1985; Harasen, 2005); however, these features were not seen in the current study. Degeneration, weakening and subsequent rupture is an important caused of secondary OA in the dog (Bennett et al., 1988). The present study has provided some evidence that CCL disease might be a rare cause of stifle OA in cats but further studies are needed.

In 140/192 samples examined, synovial membrane was normal. When changes were present they were mainly lining layer hyperplasia, villous hyperplasia and hypertrophy, mild inflammatory infiltration and synovial calcification. The presence of a moderate or severe synovial inflammatory infiltrate was not observed in any of the samples evaluated. The inflammatory infiltrate was scored as mild in all cases (16/130 samples) suggesting that synovitis is not a marked feature of feline OA unlike the dog (Brandt et al., 1991; Hewicker-Trautwein et al., 1999). In human and equine OA, the synovial membrane often exhibits mononuclear cell infiltration, increase in lining layer thickness, vascular proliferation and supporting layer oedema (Frisbie et al., 2002, Benito et al., 2005).

Generally, only a limited number of histologic sections per sample could be assessed for the evaluation of the histopathologic features of OA and only certain areas of each joint were examined. Thus, lesions might have been missed, and false negative results were possible. However, the tissues collected for the histopathologic study were selected to be representative of lesions present on gross pathologic examination.

Chapter 9 Histopathologic features of non-articular tissues from cats with and without Osteoarthritis.

9.1 Introduction and aims

Chronic hypersecretion of growth hormone (GH) by pituitary adenomas leads to acromegaly (Killinger et al., 2012). Excessive production of GH consequently stimulates the liver to produce and release IGF-1. Both GH and IGF-1 play an important role in the regulation of bone metabolism (Killinger et al., 2012). Elevation of GH and IGF-1 levels promotes growth of the articular cartilage and periarticular ligaments, subsequently leading to mechanical changes (Lugo et al., 2012). Arthropathy due to acromegaly has been documented in the cat. Peterson et al. (1990) diagnosed acromegaly in 14 cats (mean age 10.2 years) based on clinical history, routine haematology, serum biochemical tests, urinalysis and CT of the brain and pituitary gland. The diagnosis was further confirmed by *post-mortem* and histopathologic examinations which revealed an acidophilic adenoma of the pituitary gland. Of the 14 cats, 6 had articular degenerative changes associated with OA, affecting the shoulder, elbow, stifle, carpus and metacarpus. Radiographic changes included osteophyte formation, soft tissue swelling, decrease in joint space and periarticular periosteal reaction. Gross pathologic examination showed articular cartilage dullness and significant fibrillation consistent with OA.

Osteoarthritis and chronic kidney disease (CKD) are both common in older cats. In a retrospective study, Hardie et al. (2002) reported the prevalence of OA in 84/100 (84.0%) geriatric cats (mean age 15.2 years). Lascelles et al. (2010) prospectively reported OA in 92/100 (92.0%) cats with a mean age of 9.9 years. The study also showed that the radiographic OA score changes with age; with a 1 year increase in age, the OA score increased by approximately 13.6%. Similarly, CKD was reported in 39/74 (53.0%) cats, age greater than 7 years (DiBartola et al., 1987). In a retrospective study, 22/34 (64.7%) older cats (median age 15.5 years) affected with OA had concurrent CKD (Gowan et al., 2011). Lascelles et al. (2010) found a strong association between lipase and feline OA which may be due to a decreased renal function leading to reduced excretion of lipase. It is not clear if lipase has any role in the development of OA.

Another reason why CKD in cats with OA is important relates to the treatment of feline OA which can be challenging. Marino et al. (2013) found a significant concurrence between CKD and OA in cats of all ages, thus suggesting the need for screening for CKD when selecting OA treatment. A multimodal approach to therapy is probably most

beneficial, but NSAIDs are likely to be the basis of therapy in the majority of cases. NSAIDs have been shown to be effective for the control of pain associated with OA in cats (Clarke and Bennett, 2006; Gunew et al., 2008; Bennett and Morton, 2009; Gowan et al., 2011) but such drugs can be toxic for the kidneys and should be used with care in animals with pre-existing renal disease (Bennett et al., 2012b).

The aim of this study was to histologically examine the pituitary glands and kidneys of cats with and without OA for possible signs of GH-secreting pituitary adenomas and chronic kidney disease respectively.

9.2 Materials and methods

9.2.1 Samples

The total number of samples evaluated are summarised in Table 9.1.

Population	Pituitary glands	Kidneys
[†] OA population	47	52
[§] No OA/normal population	6	6
Unable to assess	5	0
Total	53	58

Table 9.1: Showing numbers of pituitary glands and kidneys for histopathologic examination. [†] These cats have OA in at least one joint. [§] These cats had no OA in any joint.

9.2.2 Processing of tissue for paraffin wax sections and staining

All the pituitary glands and kidney samples collected were prepared and processed as described in section 2.5.1 (page 68) and were routinely stained with H&E (for details see section 2.5.2.1, page 68). Pituitary glands with histopathologic changes consistent with adenoma were stained with GH and Prolactin antibodies as described in section 2.5.2.5 (page 70) (Growth hormone and Prolactin).

9.2.3 Evaluation of pituitary glands and scoring for kidneys

The pituitary glands were examined as described in section 2.5.3.3 (page 73) and kidneys were scored as described in section 2.5.3.4 (page 73) and Table 2.6 (page 74). The sections were also examined by a single veterinary pathologist to confirm the findings. Mean and SD of age of cats with normal kidney, mild and CKD was calculated and statistically analysed by using 2 sample t-test.

9.3 Results

9.3.1 Pituitary glands

Of the 58 pituitary glands examined, interpretation was not possible in 5 cases due to *post-mortem* autolysis. Of the remaining 53, 48 were normal (42 from the OA population and 6 from the no OA/normal population) and 5 had histopathologic changes (all from the OA population).

One cat (Cat ID: X49) had a non-functioning pituitary adenoma (NFPA). Histologically, the pars distalis was replaced by groups of neoplastic cells supported by a fine fibrovascular stroma (Figures 9.1.C-D). Neoplastic cells were round to polygonal with variable amounts of acidophilic cytoplasm with H&E and a round hyperchromatic nucleus (Figure 9.2.A). There was also anisokaryosis. The neoplastic cells were negative for GH and Prolactin (Figures 9.2.B-D). The remaining parenchymal cells demonstrated occasional positivity for GH (score 1) (Figure 9.2.C) and Prolactin (score 1) (Figure 9.2.D).

Two cats (Cat ID: X27 and X31) had degenerative changes in the pars distalis. Most of the cells were distended with abundant clear cytoplasm. Nuclei were displaced from the centre of the cells (Figure 9.3.A).

Two cats (Cat ID: X28 and X43) had cystic dilatation of the pars intermedia and infundibulum. The cysts were characterised by variably sized, colloid filled follicles and lined by attenuated epithelium (Figure 9.3.B).

A GH-secreting pituitary adenoma was not seen in any cat. The histopathologic findings are summarised in Table 9.2.

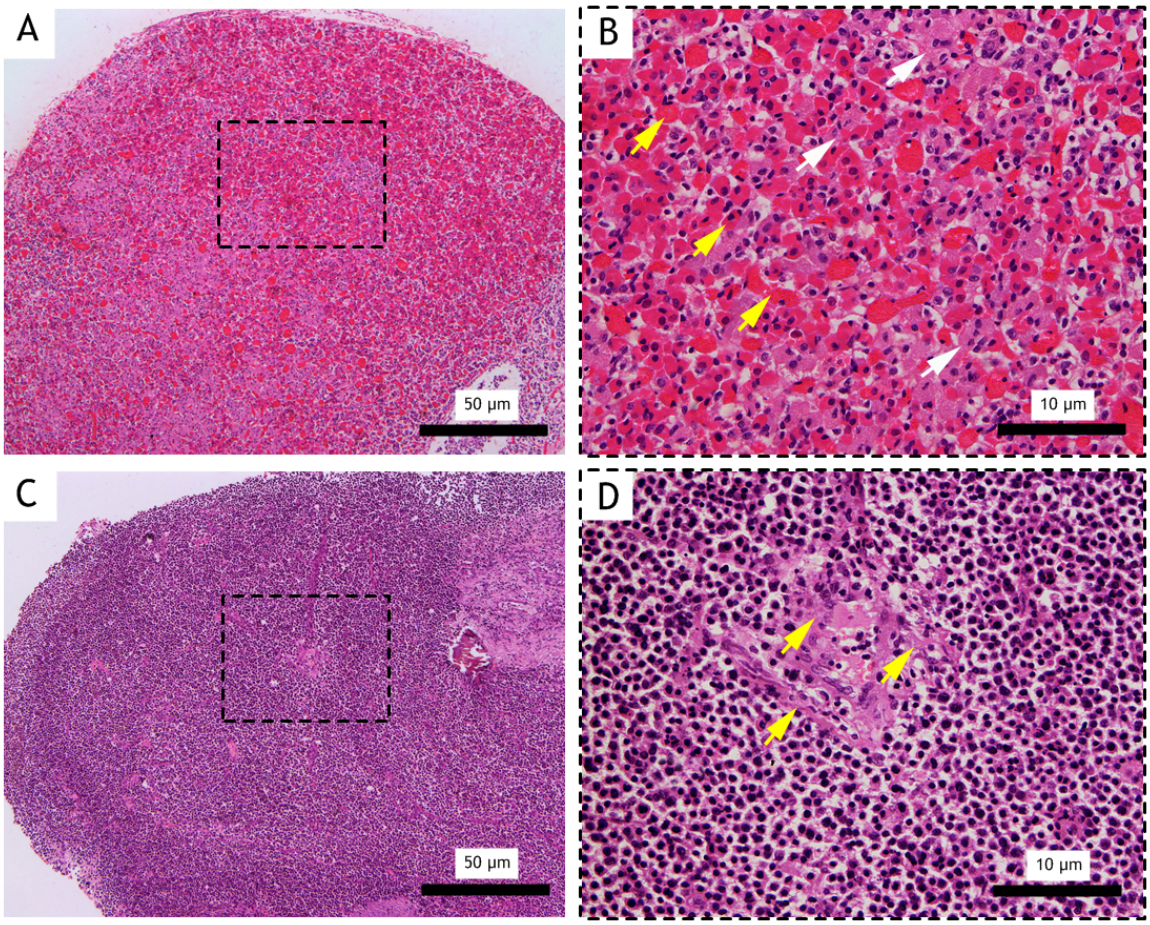

Figure 9.1: Showing pars distalis of the anterior pituitary gland stained with H & E. A & C: 40x magnification; B & D: 200x magnification.

(A) Pars distalis of normal anterior pituitary gland. Cat ID: X19. (B) This is a higher magnification view of the pars distalis showing two types of chromophil cells; acidophils (yellow arrows) and basophils (white arrows). The acidophils secrete GH and Prolactin while the basophils secrete TSH, LH, FSH and ACTH. Cat ID: X19. (C) Non-functioning pituitary adenoma. Pars distalis is replaced by groups of neoplastic cells. Cat ID: X49. (D) The neoplastic cells are supported by a fine fibrovascular stroma (yellow arrows). Cat ID: X49.

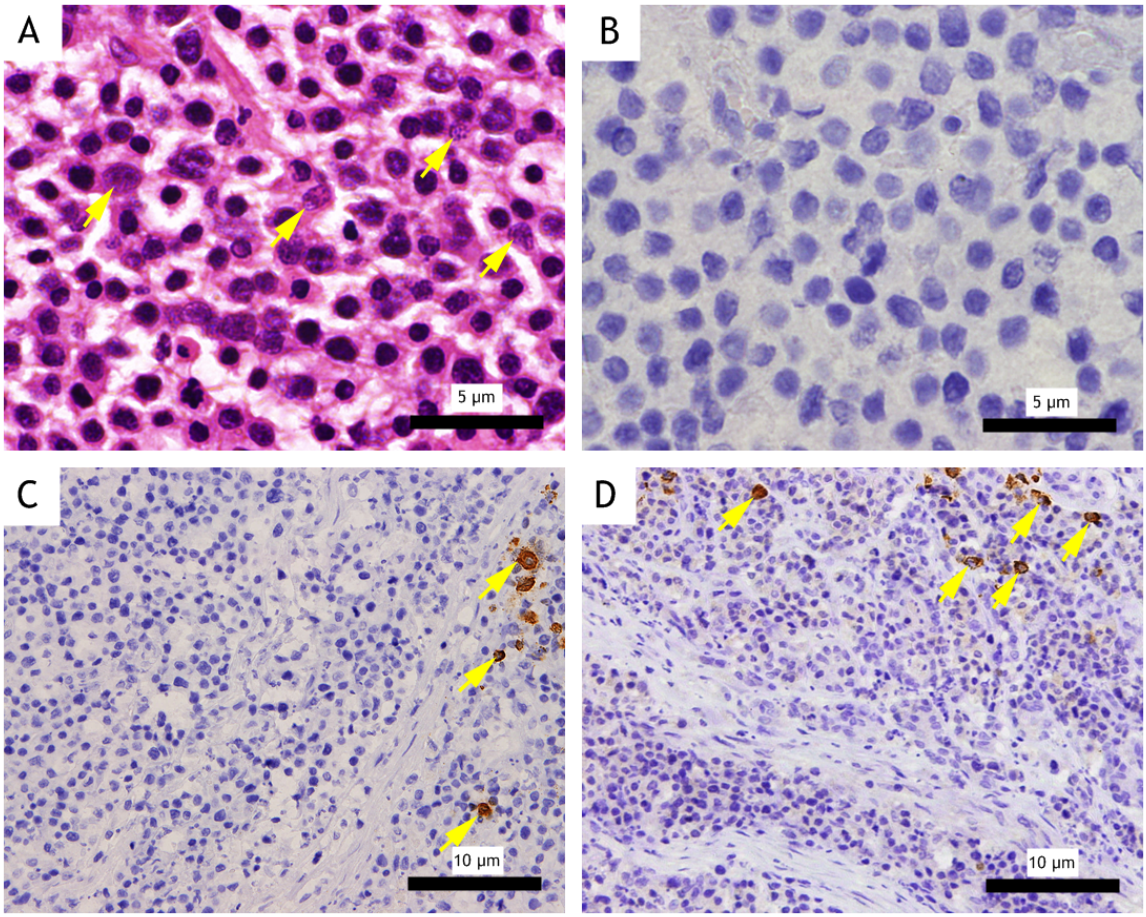

Figure 9.2: Histopathologic and immunohistochemical (IHC) features of non-functioning pars distalis adenoma. A: H & E; B & C: GH; D: Prolactin. A – B: 400x magnification; C – D: 200x magnification.

(A) Neoplastic cells are round to polygonal with variable amounts of eosinophilic cytoplasm and a round hyperchromatic nucleus (yellow arrows). Anisokaryosis is also present within the neoplastic cells. (B) The neoplastic cells are completely immunonegative for GH. A similar result was seen for Prolactin. (C) Remaining parenchymal cells demonstrate occasional positivity for GH (yellow arrows). (D) Occasional positivity for Prolactin (yellow arrows) is identified in the remaining parenchymal cells. A – D: Cat ID: X49.

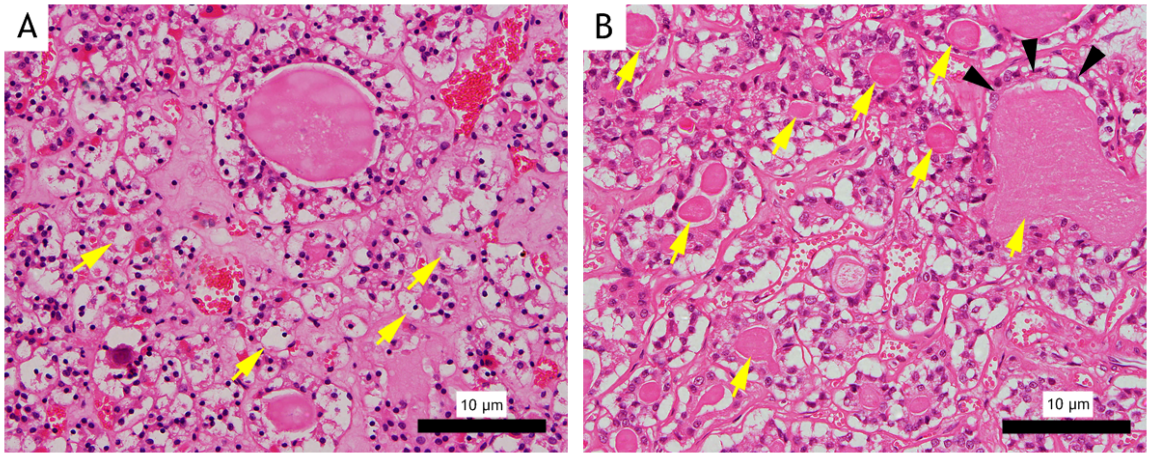

Figure 9.3: Histopathologic features of degenerate pars distalis and cystic dilatation of the pars intermedia and infundibulum. A – B: H & E. A – B: 200x magnification.

(A) Most of the cells are distended with abundant clear cytoplasm. Nuclei are displaced from the centre of the cells (yellow arrows). Cat ID: X27. (B) Variably sized colloid filled follicles (yellow arrows) are seen within the pars intermedia. The cysts are lined by attenuated epithelium (black arrowheads). Cat ID: X28.

Cat ID	Age (years)	Population	Histopathologic diagnosis of pituitary gland
X1	3	OA	Normal
X2	0.5	No OA/normal	Normal
X3	8	OA	Normal
X4	5	OA	Normal
X5	5	OA	Normal
X6	5	OA	Normal
X7	12	OA	Normal
X8	5	OA	Normal
X9	6	OA	Normal
X10	5	OA	Normal
X11	8	OA	Not assessed due to autolysis
X12	5	OA	Normal
X13	2	No OA/normal	Normal
X14	3	OA	Normal
X15	8	OA	Normal
X16	8	OA	Not assessed due to autolysis
X17	3	OA	Normal
X18	5	OA	Normal
X19	3	No OA/normal	Normal
X20	3	OA	Not assessed due to autolysis
X21	5	OA	Normal
X22	8	OA	Normal
X23	2	OA	Normal
X24	15	OA	Normal
X25	3	OA	Not assessed due to autolysis
X26	8	OA	Normal
X27	8	OA	Pituitary pars distalis degeneration
X28	5	OA	Cystic dilatation of the infundibular recess of the third ventricle
X29	15	OA	Not assessed due to autolysis
X30	2	OA	Normal
X31	10	OA	Pituitary pars distalis degeneration
X32	5	OA	Normal
X33	3	OA	Normal
X34	2	OA	Normal
X35	4	OA	Normal
X36	10	OA	Normal
X37	5	OA	Normal
X38	8	OA	Normal
X39	13	OA	Normal
X40	5	OA	Normal
X41	13	OA	Normal
X42	14	OA	Normal
X43	10	OA	Cystic dilatation of the infundibular recess of the third ventricle
X44	10	OA	Normal
X45	15	OA	Normal
X46	3	OA	Normal
X47	5	OA	Normal
X48	3	OA	Normal
X49	10	OA	Non-functioning pituitary adenoma
X50	5	OA	Normal

Table 9.2: Summarising histopathologic features of pituitary glands taken from cats with and without OA.

Cat ID	Age (years)	Population	Histopathologic diagnosis of pituitary gland
X51	5	No OA/normal	Normal
X52	1	No OA/normal	Normal
X53	0.25	No OA/normal	Normal
X54	20	OA	Normal
X55	8	OA	Normal
X56	18	OA	Normal
X57	8	OA	Normal
X58	5	OA	Normal

Table 9.2 continued.

9.3.2 Kidney

General

A total of 58 kidneys were examined. Of the 58, 11 (18.9%) were normal; 6 from the OA population and 5 from the no OA/normal population. Twenty-seven (46.6%) had mild changes (27/52 of the OA population) and 20 (34.5%) had CKD (19/52 of the OA population and 1/6 of the no OA/normal population). The mean and median total histopathologic score of the kidneys was 3.5. The minimum and maximum scores recorded were 0.5 and 7.5 respectively. Of the 58 kidneys, 11 were given a Global score of zero, 27 were given a Global score of one, 15 a Global score of two and 5 a Global score of three. The histopathologic findings are summarised in Table 9.3.

Normal kidney (Total score 0, Global score 0)

The mean age of OA cats with a normal kidney was 3.3 years (SD 0.9) with a minimum age of 2 years and a maximum age of 5 years. The median age was 3 years. Three cats were DSH, 1 cat was DLH, 1 cat was a Maine Coon cross and 1 cat was Persian. Two cats were MC, 1 cat was F and 3 cats were FS. The mean age of no OA/normal cats with a normal kidney was 1.8 years (SD 1.7) with a minimum age of 3 months and a maximum age of 5 years. The median age was 1 year. Four cats were DSH and 1 cat was Devon Rex. Two cats were MC and 3 cats were FS. The normal kidney cortex consisted of tubules, interstitium, glomeruli and blood vessels. The capsule was thin (Figure 9.4.A). There was only a small amount of interstitial tissue within the cortex. The tubular basement membrane was close to other tubules adjacent to it (Figure 9.5.A). The glomerular capillaries were thin and the nuclei were evenly scattered (Figure 9.5.A). The mesangial matrix was encircled with one nucleus (Figure 9.5.A). There were no tubular abnormalities observed.

Mild changes (total score < 4 and global score of 1)

All cats (27) with mild kidney changes had OA. The mean age of these cats was kidney was 7.6 years (SD 4.1) with a minimum age of 2 years and a maximum age of 18 years. The median age was 8 years. Five cats were MC, 7 cats were F and 15 cats were FS. Twenty-two cats were DSH and 5 cats were DLH. Of the 27 kidneys, 16 (59.3%) had interstitial fibrosis which was minimal. The mean interstitial fibrosis score was 0.5. Interstitial inflammation was observed in 21/27 (89.4%) kidneys. The inflammatory cells infiltrating the interstitial tissue were mainly lymphocytes. The mean interstitial

inflammation score was 0.5. Thickening of the glomerular basement membrane and mesangial matrix were identified in 12/27 (44.4%) and 9/27 (33.3%) kidneys respectively and the mean score for both changes was 0.5. Tubular protein and mineralisation were present in 4/27 (14.8%) and 3/27 (11.1%) kidneys respectively. An undulating capsule was not seen in any kidney.

CKD (total score ≥ 4 and global scores of 2 and 3)

Chronic kidney disease was observed in 20/58 (34.5%) cats, particularly, amongst the OA population where the prevalence of CKD was 19/52 (36.5%) cats. The mean age of the OA cats with CKD was 8.1 years (SD 4.5) with a minimum age of 3 years and a maximum age of 20 years. The median age was 8 years. The age difference between cats with CKD and normal kidney was significantly different ($P<0.001$), however the age differencce between cats with CKD and mildly affected kidney was not significant ($P=0.96$). Nine OA cats with CKD were MC, 2 cats were F and 8 cats were FS. Fourteen OA cats with CKD were DSH, 3 cats were DLH, 1 was Siamese and 1 was Burmese. The mean BW of OA cats with CKD was 3.2 kg. The OA cats with CKD had a mean BCS of 3, median 3 with a minimum BCS of 1 and a maximum of 5. The prevalence of CKD in no OA/normal population was 1/6 (16.7%) cats. The affected cat was 3 years old, DSH with BW and BCS of 4.8 kg and 3 respectively.

An undulating capsule was identified in 4/20 (20.0%) affected kidneys. The undulated capsule was seen as a wavy thick stranded bundle of fibres (Figure 9.4.B). Of the 20, 19 (95.0%) had cortical interstitial fibrosis. The severity was scored mild and moderate in 16 and 3 kidneys respectively. Interstitial fibrosis was a very prominent feature of CKD. In the mild stages of fibrosis, it was minimal and consisted of a thin layer of dense fibrous tissue surrounding the tubule and glomerulus. In moderate stages of fibrosis, it was diffuse and often replaced small areas of renal cortical parenchyma (Figures 9.4.C-D). The mean interstitial fibrosis score was 1.

Interstitial inflammation was identified in all CKD kidneys. Lymphocytes were the predominant cells, but plasma cells were also present. The severity was scored mild in 10/20 kidneys, moderate in 9/20 kidneys and severe in 1/20 kidneys. In the mild cases, only occasional inflammatory cells were identified in the interstitial tissue. In the moderately severe cases, multiple patches of inflammatory cell infiltration were often seen (Figures 9.4.E-F). Inflammation became more widely distributed and diffuse in the severely affected kidneys. The mean interstitial inflammation score was 2.

All kidneys with CKD had thickening of the glomerular basement membrane (Figure 9.5.B). The severity was scored mild in 13/20 kidneys and moderate in 7/20 kidneys. The mean glomerular basement membrane score was 1. Thickening of the mesangial matrix was also seen in all CKD kidneys (Figure 9.5.B). The severity was scored mild in 12 kidneys and moderate in 8. The mean thickening of the mesangial matrix score was 1. Tubular protein (Figure 9.5.C) and mineralisation (Figure 9.5.D) were present in 11/20 (55.0%) and 5/20 (25%) kidneys respectively.

Cat ID	Age (years)	Population	Histopathologic features of the cortex									
			Interstitium		Glomerulus		Tubule		Capsule	Total score	Global score	Kidney status
			Interstitial fibrosis	Interstitial inflammation	Thickening of basement membrane	Thickening of mesangial matrix	Leaking of protein	Mineralisation	Undulating capsule			
X1	3	OA	1	1.5	0	1	+	-	-	3.5	1	Mild
X2	0.5	No OA/normal	0	0	0	0	-	-	-	0	0	normal
X3	8	OA	1	1	0	0	-	-	-	2	1	Mild
X4	5	OA	0	0.5	0	0	-	-	-	0.5	1	Mild
X5	5	OA	0	0	0	0	-	-	-	0	0	Normal
X6	5	OA	1	0.5	1	1	+	+	+	3.5	1	Mild
X7	12	OA	1	1	2	1	+	-	-	5	2	CKD
X8	5	OA	0.5	1	1	0	-	-	-	2.5	1	Mild
X9	6	OA	1	0.5	0	0	-	-	-	1.5	1	Mild
X10	5	OA	1	0	0	0	-	-	-	1	1	Mild
X11	8	OA	1	0.5	0	0	-	-	-	1.5	1	Mild
X12	5	OA	0	0	2	0	-	-	-	2	1	Mild
X13	2	No OA/normal	0	0	0	0	-	-	-	0	0	Normal
X14	3	OA	1	0.5	0	0	-	-	-	1.5	1	Mild
X15	8	OA	1.5	1.5	2	2	+	-	+	7	3	CKD
X16	8	OA	1	0.5	0	0	-	-	-	1.5	1	Mild
X17	3	OA	0.5	0.5	1	1	-	-	-	3	1	Mild
X18	5	OA	1.5	2	2	2	+	-	-	7.5	3	CKD
X19	3	No OA/normal	0	0	0	0	-	-	-	0	0	Normal
X20	3	OA	0	0	0	0	-	-	-	0	0	Normal
X21	5	OA	0.5	1.5	1	1	-	-	-	4.5	2	CKD
X22	8	OA	0.5	1.5	1	1	-	-	-	4.5	2	CKD
X23	2	OA	0	0	0	0	-	-	-	0	0	Normal

Table 9.3: Histopathologic scores of the kidneys of 58 cats with and without OA.

Cat ID	Age (years)	Population	Histopathologic features of the cortex									
			Interstitium		Glomerulus		Tubule		Capsule	Total score	Global score	Kidney status
			Interstitial fibrosis	Interstitial inflammation	Thickening of basement membrane	Thickening of mesangial matrix	Leaking of protein	Mineralisation	Undulating capsule			
X24	15	OA	1.5	2	1	1	+	-	-	5.5	2	CKD
X25	3	OA	0	0	0	0	-	-	-	0	0	Normal
X26	8	OA	1.5	2	2	2	+	-	-	7.5	3	CKD
X27	8	OA	0	0.5	1	0	-	-	-	1.5	1	Mild
X28	5	OA	0.5	1	2	2	-	-	-	5.5	2	CKD
X29	15	OA	0	0.5	0	0	-	-	-	0.5	1	Mild
X30	2	OA	0.5	1.5	1	2	-	-	-	5	2	CKD
X31	10	OA	0	0.5	1	1	-	+	-	2.5	1	Mild
X32	5	OA	1.5	2	1	1	-	+	+	5.5	2	CKD
X33	3	OA	0	0	0	0	-	-	-	0	0	Normal
X34	2	OA	0	1	0	1	-	-	-	2	1	Mild
X35	4	OA	0	0	0	0	-	-	-	0	0	Normal
X36	10	OA	1.5	1.5	1	1	-	-	-	5	2	CKD
X37	5	OA	2	2	1	2	+	+	+	7	3	CKD
X38	8	OA	0	2	1	1	+	-	-	4.5	2	CKD
X39	13	OA	0.5	1	1	1	-	-	-	3.5	1	Mild
X40	5	OA	1	1.5	2	1	+	+	+	5.5	2	CKD
X41	13	OA	0	1	1	0	-	-	-	2	1	Mild
X42	14	OA	0.5	1	0	1	+	-	-	2.5	1	Mild
X43	10	OA	0.5	1	1	1	-	-	-	3.5	1	Mild
X44	10	OA	0.5	1	1	0	-	+	-	2.5	1	Mild
X45	15	OA	2	2	1	1	-	-	-	6	2	CKD
X46	3	OA	0.5	1	0	1	+	-	-	2.5	1	Mild
X47	5	OA	1.5	2	1	1	+	-	-	5.5	2	CKD
X48	3	OA	2.5	3	1	1	+	-	-	7.5	3	CKD
X49	10	OA	1.5	2	2	2	+	+	-	7.5	3	CKD

Table 9.3 continued.

Cat ID	Age (years)	Population	Histopathologic features of the cortex									
			Interstitium		Glomerulus		Tubule		Capsule	Total score	Global score	Kidney status
			Interstitial fibrosis	Interstitial inflammation	Thickening of basement membrane	Thickening of mesangial matrix	Leaking of protein	Mineralisation	Undulating capsule			
X50	5	OA	0	0	1	0	-	-	-	1	1	Mild
X51	5	No OA/normal	0	0	0	0	-	-	-	0	0	Normal
X52	1	No OA/normal	1	1.5	1	2	-	-	-	5.5	2	CKD
X53	0.25	No OA/normal	0	0	0	0	-	-	-	0	0	Normal
X54	20	OA	1	1.5	1	1	-	-	-	4.5	2	CKD
X55	8	OA	0	0.5	0	0	-	-	-	0.5	1	Mild
X56	18	OA	0	0	1	0	-	-	-	1	1	Mild
X57	8	OA	0	0.5	0	0	-	-	-	0.5	1	Mild
X58	5	OA	1	0	0	0	-	-	-	1	1	Mild

Table 9.3 continued. Cats with total and global scores of 0 were assigned as "Normal", cats with a total score less than 4 and global score of 1 were assigned as a "Mild" and cats with a total score of 4 and above and global scores of 2 and 3 were diagnosed as having "CKD (chronic kidney disease)". "+": present; "-": absent.

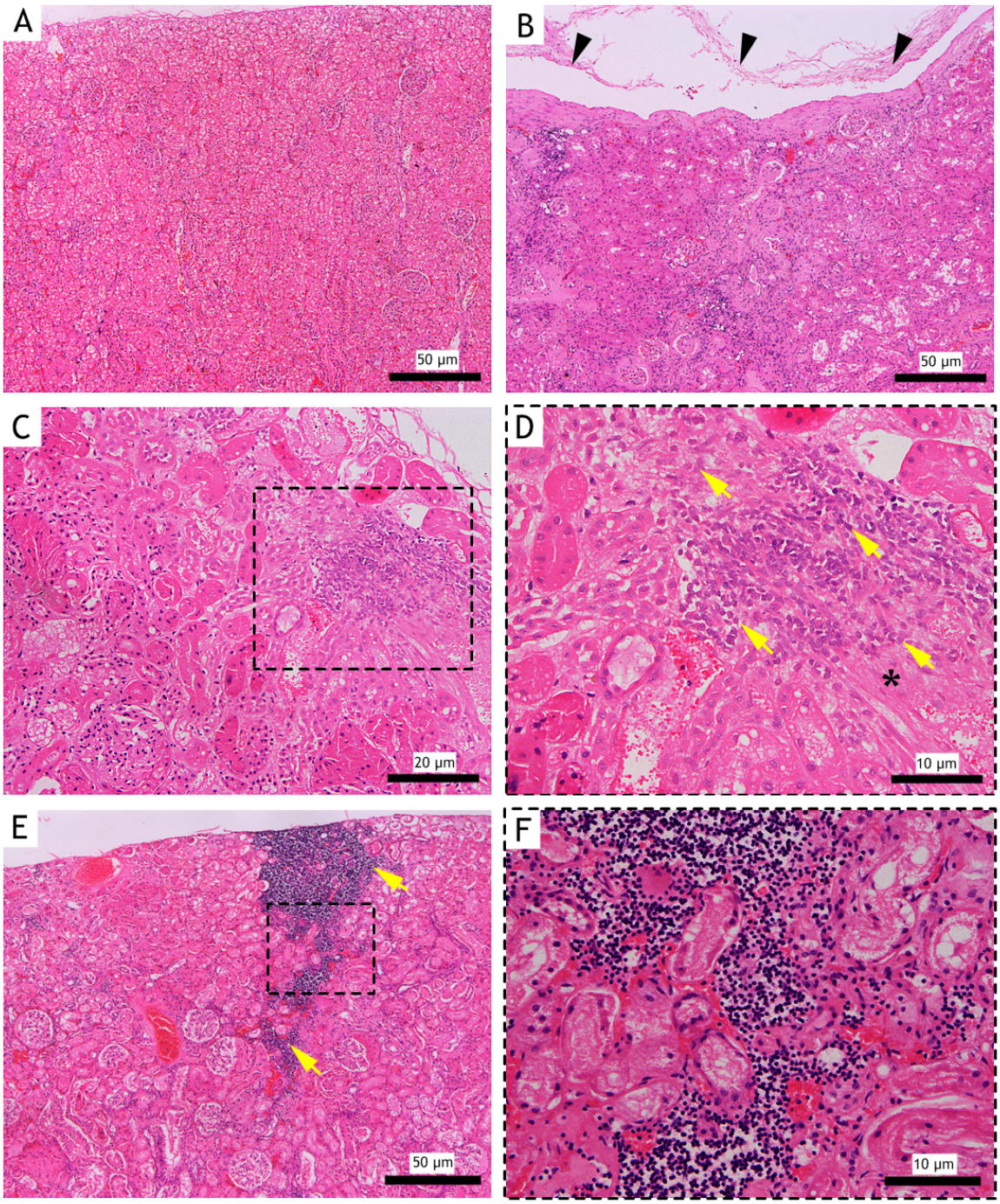

Figure 9.4: Showing cortical kidney histology of normal (A) and CKD (B – F) cats. A – F: H&E. A, B & E: 40x magnification; C: 100x magnification; D & F: 200x magnification.

(A) Normal histology of kidney cortex. Note a thin capsule and the even appearance of the glomeruli and tubules. Cat ID: X51. (B) The capsule of the CKD kidney appears undulated and thick (black arrowheads). Cat ID: X15. (C) Moderate interstitial fibrosis is seen within the cortical parenchyma. Cat ID: X45. (D) On higher magnification, myofibroblasts (yellow arrows) are seen surrounded by fibrous tissues (asterisk). Cat ID: X45. (E) Interstitial inflammation (yellow arrows) extends across the cortical parenchyma. Cat ID: Cat X37. (F) Higher magnification shows the interstitial inflammation composed mainly of lymphocytes. Cat ID: X37.

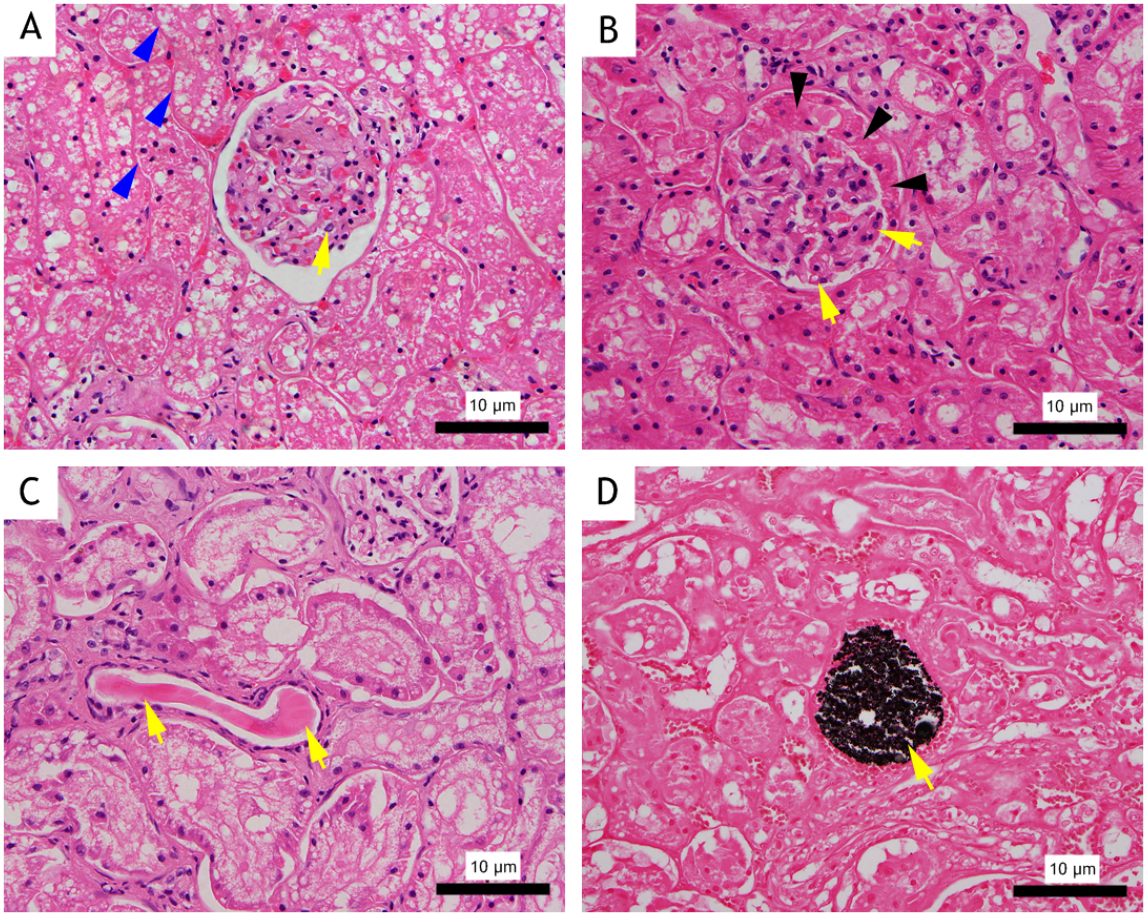

Figure 9.5: Showing histopathologic changes of glomerulus and renal tubules. A – C: H&E; D: Von Kossa stain. A – D: 200x magnification.

(A) Showing a normal glomerulus. There is only one mesangial cell (yellow arrow) per capillary tuft and the glomerular basement membrane is thin. The tubular basement membrane (blue arrowheads) is close to the other tubules adjacent to it. Cat ID: X51. (B) The glomerulus of the CKD kidney shows a thickening of the glomerular basement membrane (yellow arrows) and mesangial matrix (black arrowheads). There is also mild interstitial fibrosis. Cat ID: X30. (C) Showing example of protein casts (yellow arrows) in the renal tubules. Cat ID: X48. (D) Note the brown to black foci (yellow arrow) which represent mineralised tubules. Cat ID: X28.

9.4 Discussion

GH- secreting pituitary adenoma was not seen in any cats with or without OA. GH-secreting pituitary adenomas are thought to cause clinical acromegaly in cats (Peterson et al., 1990) and acromegaly is a risk factor for secondary OA in cats (Peterson et al., 1990). However the mean age of cats in Peterson et al.'s study was 10.2 year and it is possible these cats could have been suffering pre-existing idiopathic/primary OA. Wassenaar et al. (2010) reported that human patients with secondary OA due to acromegaly had more severe osteophyte formation compared to patients with primary OA. This consistent with the fact that GH and IGF-1 promote bone formation and osteophytosis.

A NFPA was identified in one cat. The affected cat was old and had OA in all joints except the tarsi. These adenomas are benign and grow slowly. No link between arthropathy and NFPA has been reported. The effects of the mass itself may lead to serious clinical signs such as visual impairments and pituitary insufficiency (Greenman and Stern, 2009). Since a complete clinical history was not available for this cat it is not possible to relate the histopathologic findings with the clinical signs experienced when the cat was still alive.

The histopathologic prevalence of CKD in cats with and without OA was 36.5% (19 of 52 cats) and 16.7% (1 of 6 cats) respectively. A retrospective study by Marino et al. (2013) reported that 88/128 (68.8%) cats with OA had CKD. The diagnosis of CKD was based on laboratory testing of renal function, complete blood count, serum biochemistry and radiographic size of the kidney. In contrast, a recent retrospective study by Greene et al. (2014) reported that only 38/1230 (3.1%) of cats with CKD had a previous diagnosis of OA. The lower prevalence of CKD in this study could be due to several factors. The study was not specifically designed to provide an estimate of the prevalence of CKD in cats with OA and failure to identify cats with OA might have underestimated the actual prevalence of OA in cats with CKD.

The present study showed that cats with CKD were significantly older than cats with normal kidney support earlier findings that older cats are more likely to present with CKD (Dibartola et al., 1987; Lawler et al., 2006; Marino et al., 2013). The demographic data for cats with CKD was comparable to a previous study (Elliott and Barber, 1998). More females than males had CKD in the OA cats, although Chakrabarti et al. (2012) reported more males than females were affected. This difference in gender balance might be related to the sample size of the population studied. Most of the OA cats with

CKD were DSH and DLH. Increased risks for CKD in purebred cats such as Siamese, Maine Coon, Burmese, Abyssinian and Russian Blue have been reported (Lulich et al., 1992). However, the small number of purebred cats in the present study precluded the ability to identify any breed predispositions for CKD in cats with OA.

In the current study, most of the CKD kidneys showed chronic tubulointerstitial and glomerular disease. Interstitial inflammation was the most severe feature observed. Chronic inflammation is often associated with the development of fibrosis. Lymphocyte activation induces the production of profibrotic cytokines which initiate fibroblast to myofibroblast transformation and the excessive deposition of ECM in the interstitial tissue, mainly comprising collagen type I (Ueha et al., 2012). Treating OA in cats with CKD is challenging since NSAIDs can have detrimental effects on the damaged kidneys (Weir, 2002). However, this was not supported by a retrospective study by Gowan et al. (2011) into the effects of long-term treatment with meloxicam on the kidney function in aged cats with OA. The group of cats with kidney disease that received meloxicam showed less of an increase in blood creatinine levels over time compared to cats with kidney disease that did not receive meloxicam. The current study has shown an inflammatory component to CKD and it is interesting to speculate that NSAIDs such as meloxicam may have a direct anti-inflammatory effect on the kidney, leading to a reduction in ongoing interstitial inflammation and fibrosis that would otherwise cause further deterioration in renal function, and thus actually have a “protective” effect on the diseased kidney (Bennett et al. 2012b).

Chapter 10 The Presence of Protease activated receptor-2 (PAR-2) and Matriptase in cats with and without Osteoarthritis

10.1 Introduction and aims

Protease activated receptor-2 (PAR-2) is a second member of the G protein-coupled receptors. They are activated through proteolytic cleavage by serine proteases. Proteases cleave PAR-2 at the extracellular N-terminal domain to expose the tethered peptide that binds and activates the receptor itself on its second extracellular loop, to initiate an intracellular signal. This activation is an irreversible process (Vu et al., 1991; Coughlin et al., 1992).

Studies in human OA and murine models of OA have demonstrated a key role of PAR-2 in mediating arthritic inflammation (Kawabata et al., 1998; Ferrell et al., 2003; Xiang et al., 2006; Boileau et al. 2007; Amiable et al., 2011). Increased expression of PAR-2 mRNA and increased PAR-2 protein levels have been observed in chondrocytes and synovial fibroblasts from OA patients compared to normal (Xiang et al., 2006; Boileau et al., 2007; Tsai et al., 2009; Chen et al., 2011). It is known that PAR-2 activation can promote the release of pro-inflammatory cytokines such as IL-1, TNF-α and IL-6 (Asokanathan et al., 2002; Hirota et al., 2005; Ramachandran et al., 2006). The secreted pro-inflammatory cytokines up-regulate the expression of PAR-2, stimulating more secretion of pro-inflammatory cytokines and metalloproteinases to enhance inflammatory responses and initiate cartilage degradation.

Matriptase is type II transmembrane serine proteases and has been recognised as an activator of PAR-2. In an OA model study, Milner et al. (2010) studied wild type and PAR-2 deficient mice and reported the ability of matriptase to act as an activator of PAR-2, causing inflammatory changes within the stifle joint as evidenced by vascular perfusion and vasodilatation. Immunohistochemical analysis of the articular cartilage also confirmed the presence of chondrocyte PAR-2 and matriptase expression in chondrocytes from the OA model but not in sham-operated mice.

With the demonstration that PAR-2 and matriptase have pro-inflammatory effect in human OA and murine arthritis, the author believed that PAR-2 could also play an important role in the pathogenesis of feline OA.

The purpose of this study was to determine the presence of PAR-2 and matriptase protein and to quantify PAR-2 and matriptase mRNA expression in the articular cartilage and synovial membrane of cats with and without OA. In addition, the study needed to determine the most suitable reference genes for feline articular cartilage and synovial membrane gene expression assays.

10.2 Materials and methods

Details of the samples used in this study are given in Appendices (ib). A total number of 10 cats (5 OA and 5 no OA/normal) were used for PAR-2 and matriptase immunoreactivity studies. Articular cartilage and synovial membrane samples from the elbow joint were collected, prepared and processed as described in section 2.5.1 (page 68). Sections were stained with PAR-2 and matriptase antibodies as described in section 2.5.2.5 (Protease activated receptor-2 (PAR-2) and matriptase) (page 71).

A total of 28 articular cartilage samples from adult cats (14 OA and 14 no OA/normal), 10 synovial membranes from adult cats (5 OA and 5 no OA/normal) and 3 cartilage samples from 9 week old foetal cats were included in the PAR-2 and matriptase gene expression analysis. Total RNA from elbow OA and no OA/normal cartilage and synovial membrane samples was prepared as described in section 2.6.2 - 2.6.4 (page 75 and 76) and cDNA was prepared as described in section 2.6.5 (page 76). Analysis of qPCR data was performed as described in section 2.6.7.4 (page 79).

The selection of reference genes for normalisation in articular tissue was carried out as described in section 2.6.6 (page 77) and comparative assessment of PAR-2 and matriptase mRNA levels was done as described in section 2.6.7 (page 78).

10.3 Results

10.3.1 PAR-2 and matriptase immunoreactivity

10.3.1.1 PAR-2

PAR-2 was detected in all OA and no OA/normal articular cartilage samples. In no OA/normal articular cartilage, a positive cytoplasmic immunoreactivity of the chondrocytes was seen only in the superficial layer of the cartilage (Figure 10.1.A). In OA articular cartilage, a positive PAR-2 staining was observed in the superficial, middle and deep layers (Figure 10.1.C). PAR-2 immunoreactivity was also variable in different areas of the OA cartilage. In the areas where PAR-2 was present, extracellular matrix was only faintly stained with haematoxylin (Figure 10.1.C). Nonspecific stained sections showed only background staining (Figure 10.1.E).

Positive immunostaining for PAR-2 was observed in the synovial lining layer and the supporting layer in all OA and no OA/normal synovial samples (Figure 10.2). Immunoreactivity was present in the cytoplasm of the synovial cells.

10.3.1.2 Matriptase

Matriptase immunoreactivity was not detected in any of the no OA/normal samples (Figures 10.1.B and 10.2.B). Matriptase expression was detected in all OA articular cartilage samples. However, the chondrocyte distribution of matriptase immunoreactivity was variable: in three cats the expression was intense particularly at the superficial and middle layers (Figure 10.1.D); in another two, virtually all the chondrocytes exhibited faint matriptase immunoreactivity in all layers. Despite the variability in the immunoreactivity, matriptase was seen only in locations where PAR-2 was also present. In the areas where matriptase was present, extracellular matrix was only faintly stained with haematoxylin (Figure 10.1.D).

Matriptase immunoreactivity was also detected in all OA synovial membrane samples, mainly in the cytoplasm of the synovial lining cells (Figures 10.2.E-F). The immunoreactivity was not detected in any of the no OA/normal synovial samples (Figure 10.2.B).

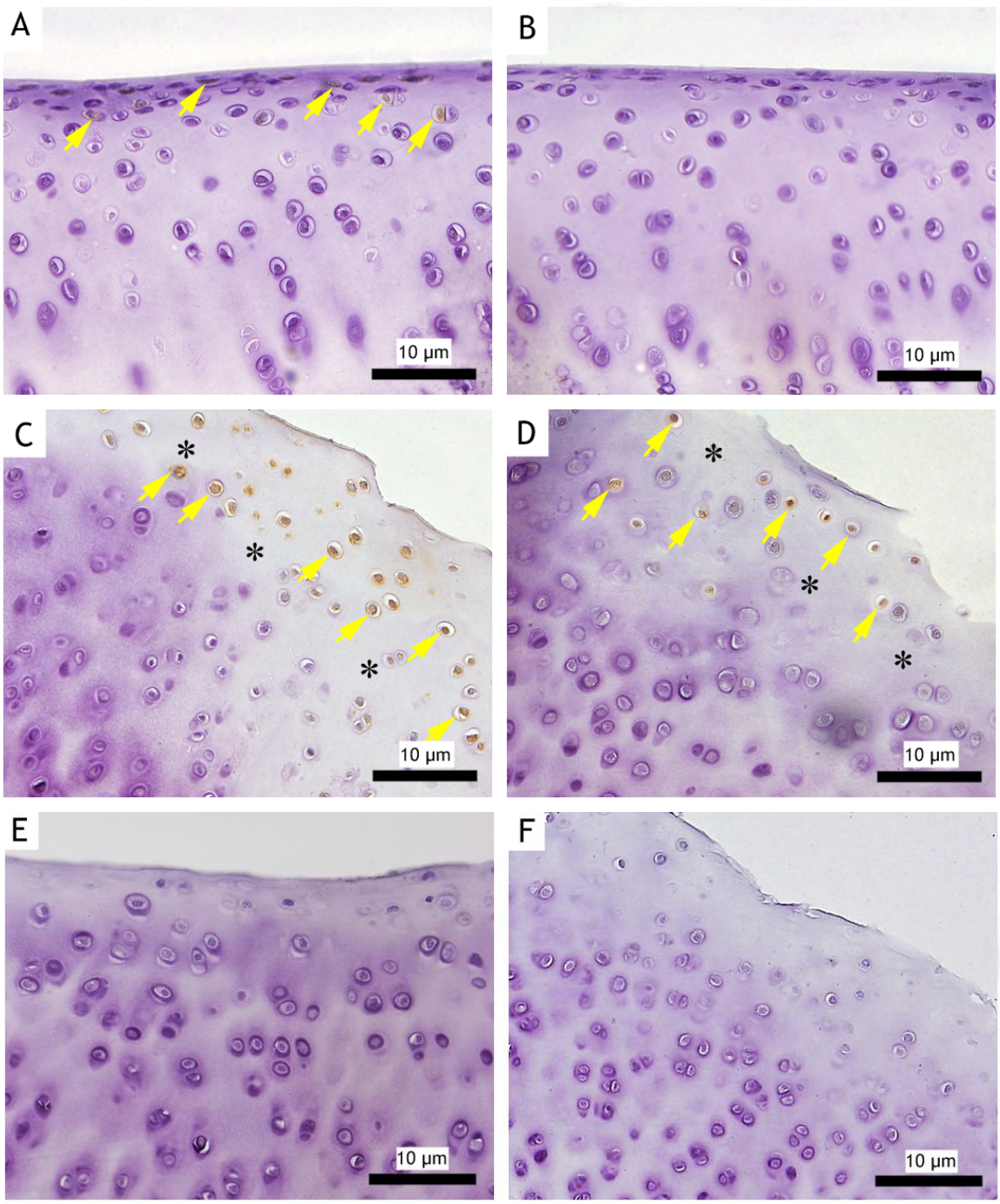

Figure 10.1: Representative sections showing PAR-2 (A & C) and matriptase (B & D) immunostaining in healthy (A & B) and OA (C & D) articular cartilage. A – F: 200x magnification.

(A) In no OA/normal articular cartilage, PAR-2 expression is seen in a few superficial chondrocytes (yellow arrows). (B) Matriptase immunoreactivity is not detected in no OA/normal articular cartilage. (C) PAR-2 (yellow arrows) is diffuse from the superficial layer to the middle and deep layers of the OA articular cartilage. Only faint haematoxylin staining is seen in the extracellular matrix (asterisks). (D) Matriptase is present only in locations where PAR-2 is also present. The extracellular matrix is only faintly stained with haematoxylin (asterisks). (E & F) There is no staining in articular cartilage when a primary antibody of irrelevant specificity was used.

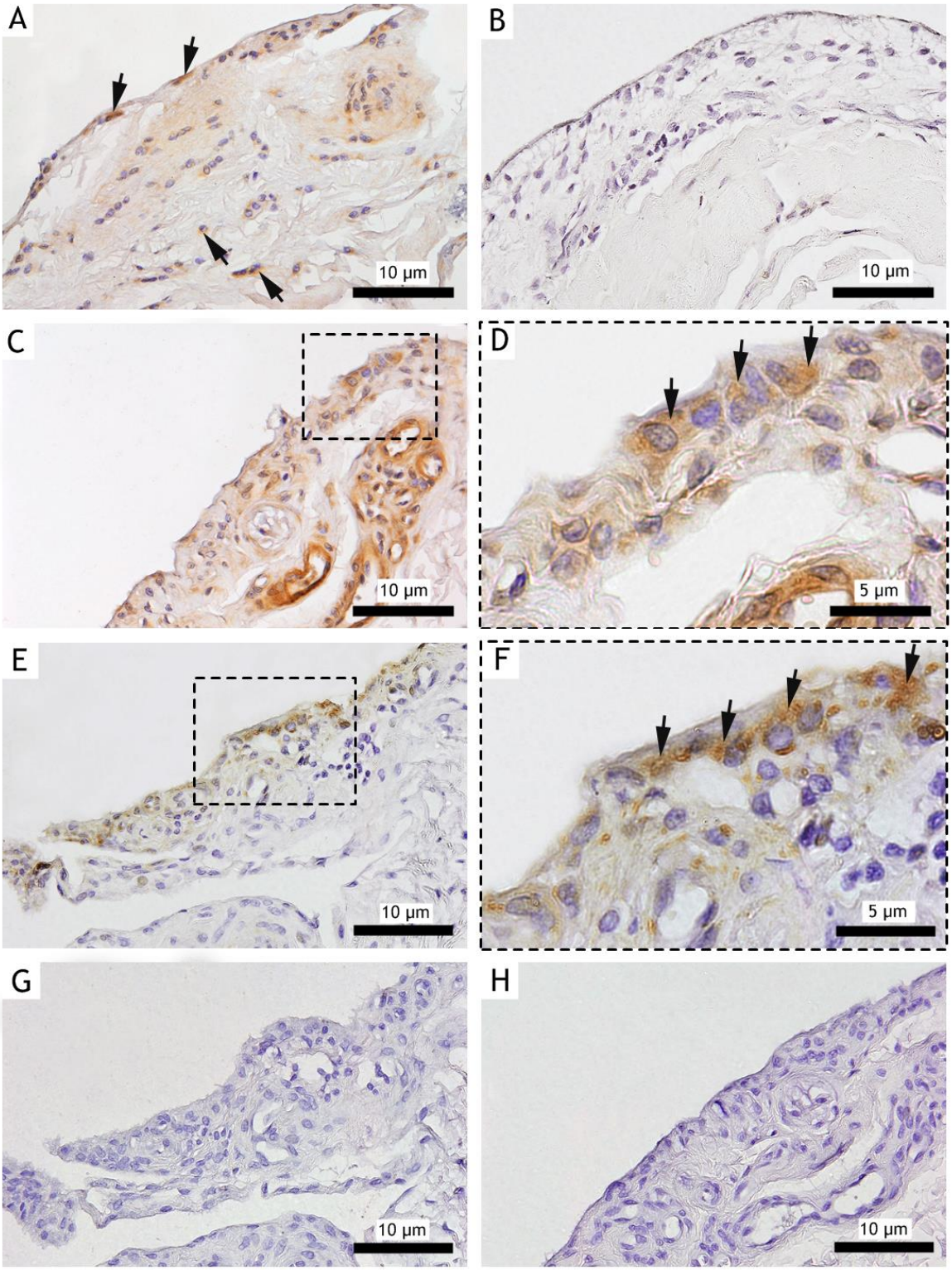

Figure 10.2: Presence of proteinase-activated receptor 2 (PAR-2) (A, C & D) and matriptase (B, E & F) in no OA/normal (A & B) and OA (C, D, E & F) synovial tissues. A, B, C, E, G & H: 200x magnification, D & F: 400x magnification.

(A) PAR-2 immunoreactivity (black arrows) is seen in the no OA/normal synovial membrane. (B) Matriptase immunoreactivity is not identified in no OA/normal synovial membrane. (C) PAR-2 is expressed in the synovial lining layer from OA joints. (D) Higher magnification shows PAR-2 is expressed in the cytoplasm of synovial lining cells (black arrows). (E) Matriptase protein is present in the synovial lining layer. (F) Higher magnification shows matriptase expression in the cytoplasm of the synovial lining cells (black arrows). (G & H) There is no staining in the synovium when a primary antibody of irrelevant specificity was used.

10.3.2 Selection of reference genes for normalisation in articular cartilage and synovial membrane

The six reference genes demonstrated a wide range of expression levels in the articular cartilage samples (Figure 10.3.A) from the lowest Ct of 23.68 for the RPL18 gene to the highest Ct of 34.75 for the ACTB gene. The reference genes expression level showed a different pattern in the synovial membrane (Figure 10.3.B) with the lowest Ct of 17.53 for the GAPDH gene and the highest Ct of 30.89 for the GUSB gene.

The program geNorm calculates the gene expression stability (*M*) of a list of selected reference genes in all samples, and ranks them according to gene stability measurement (*M)*. Basically *M* is defined as the mean pairwise variation of a gene with all the other reference genes in a given set of samples, so that a low *M* value is indicative of more stable expression. The *M* values for the genes (from the least stable to the most stable) for both articular cartilage and synovial membrane are shown in Figure 10.4. The ideal reference genes for comparing no OA/normal and OA cartilage were HPRT, SDHA and GUSB. The best reference genes for comparing gene expression data between no OA/normal and OA synovial membrane were RPL18, ACTB and HPRT.

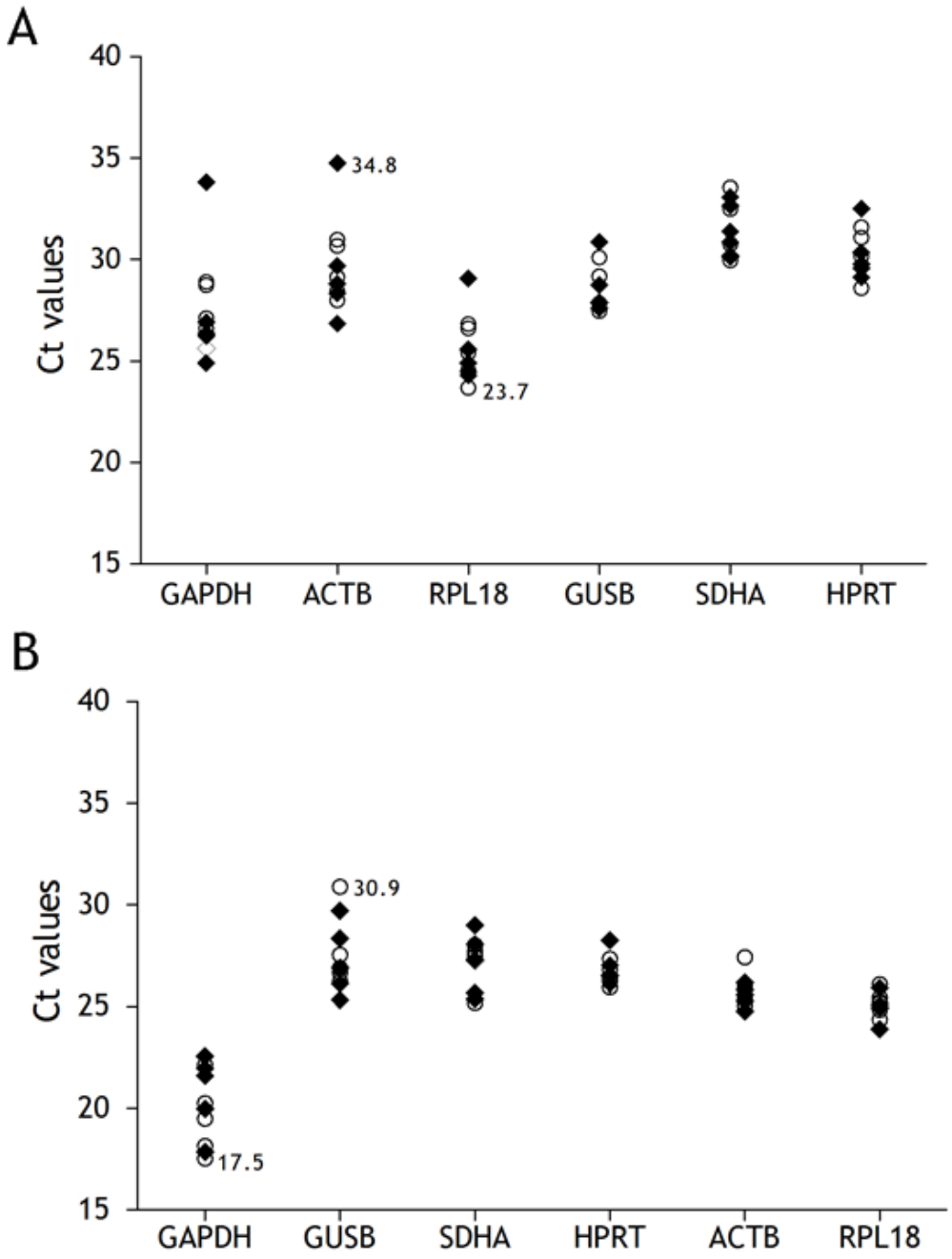

Figure 10.3: Distribution of 6 candidate reference gene Ct values for the OA and no OA/normal groups.

Values are given as quantitative real-time PCR cycle threshold (Ct) values for the reference genes in the feline articular cartilage (A) and synovial membrane (B). HPRT was equally expressed in the OA and no OA/normal articular cartilage (A), while the RPL18 was equally expressed in the OA and no OA/normal synovial membrane (B). o: OA; ♦: no OA/normal.

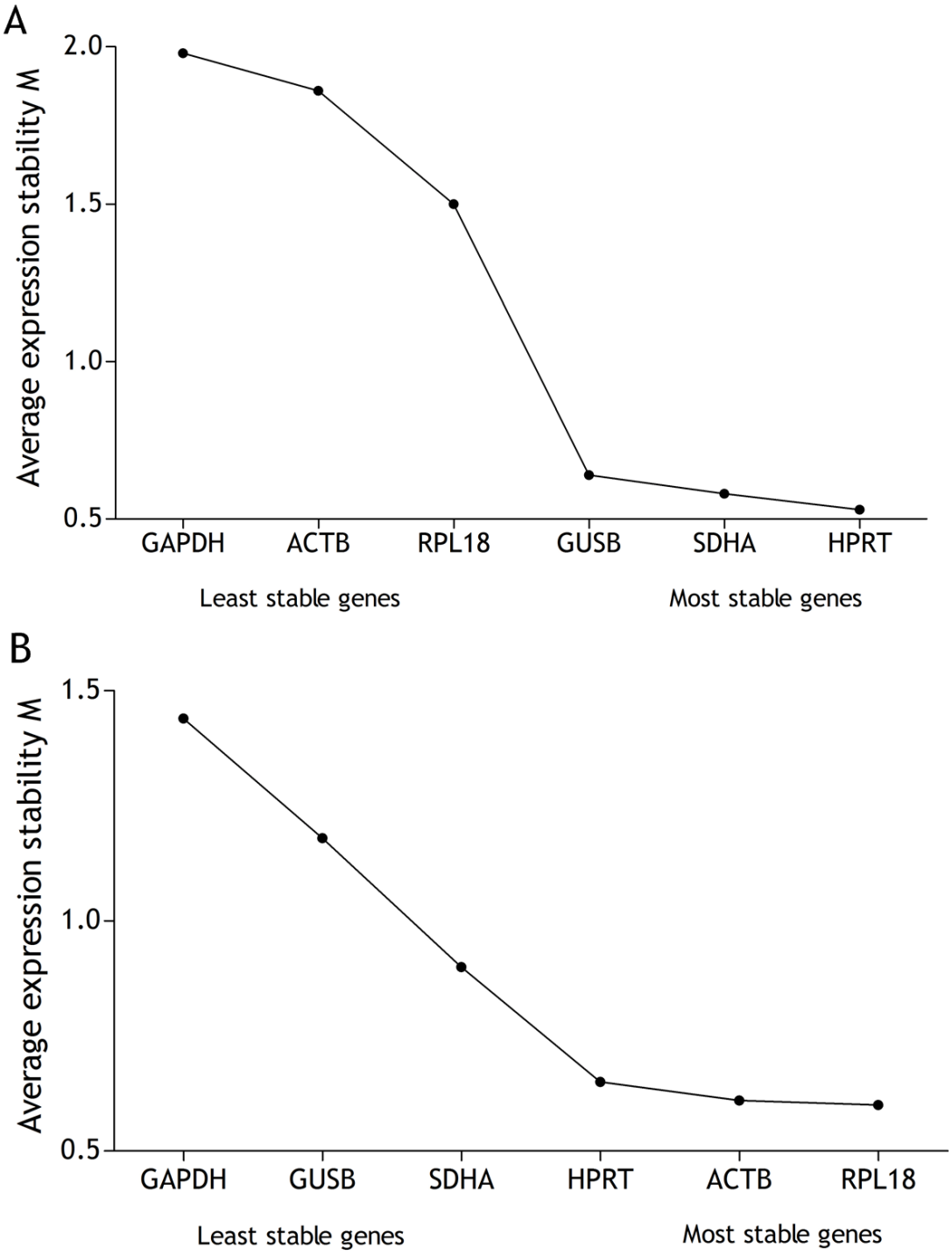

Figure 10.4: Average expression stability values of 6 candidate reference genes in feline articular cartilage (A) and synovial membrane (B). Calculations based on the geNorm program.

10.3.3 The comparative assessment of PAR-2 and matriptase mRNA levels in cats with and without OA

10.3.3.1 PAR-2 mRNA gene expression

PAR-2 mRNA expression was detected in all the articular tissues. The PAR-2 mRNA expression levels in OA and foetal articular cartilage were 5 and 3 times higher than the healthy group respectively (Figure 10.5.A). The PAR-2 mRNA expression level in OA synovium was 1.5 times higher than in healthy synovium (Figure 10.5.B). A significantly higher expression of PAR-2 mRNA ($P<0.001$) was seen in the OA articular cartilage group (Figure 10.5.C). Synovial membrane samples did not show significantly different levels of expression between no OA/normal and OA samples (Figure 10.5.D). Because of the small sample size, statistical analysis for the foetal samples was not carried out.

10.3.3.2 Matriptase gene expression

Matriptase mRNA expression was identified in all the articular tissues. The matriptase mRNA expression levels in OA and foetal articular cartilage were 3.3 and 1.4 times higher than the no OA/normal group respectively (Figure 10.6.A). Matriptase mRNA expression level in OA synovium was 1.1 times higher than the no OA/normal group (Figure 10.6.B). The matriptase mRNA expression of the OA articular cartilage was significantly higher than the no OA/normal group ($P<0.001$) (Figure 10.6.C). There was no significant difference in the OA synovium matriptase mRNA expression compared to the OA/normal samples (Figure 10.6.D).

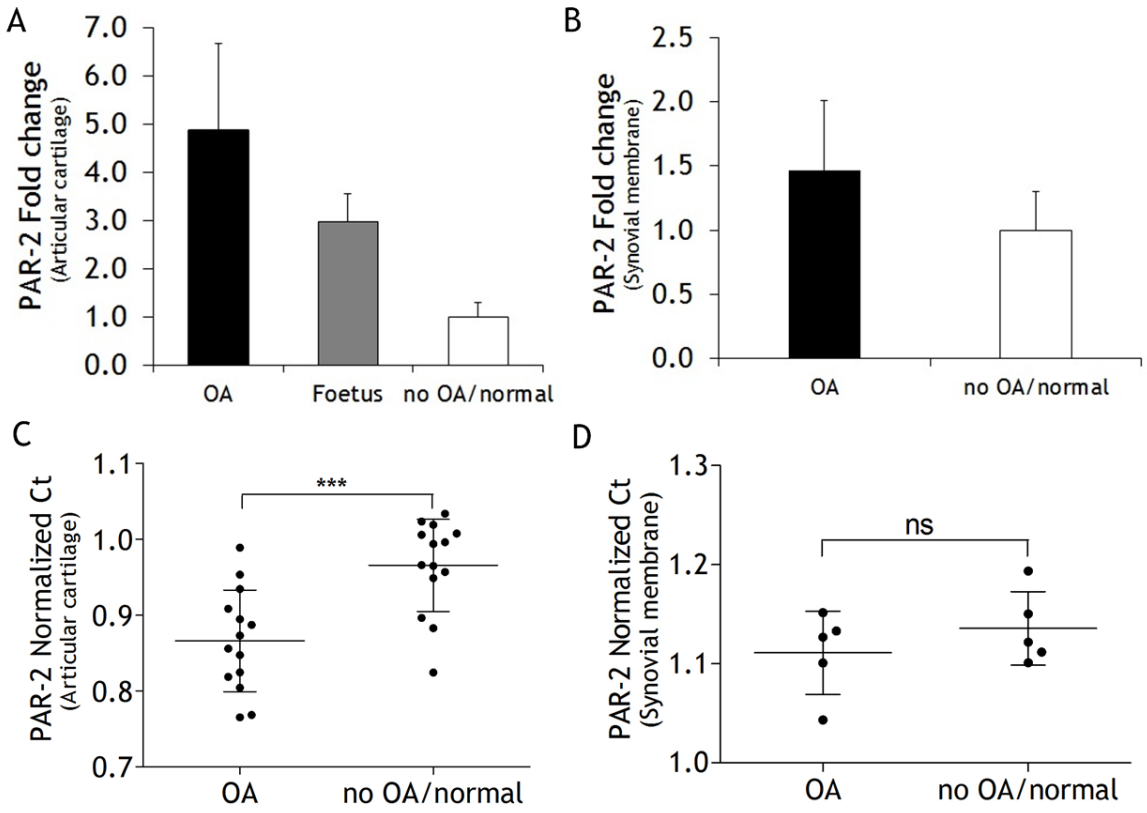

Figure 10.5: Protease activated receptor-2 (PAR-2) mRNA expression as determined by qPCR in articular cartilage and synovium.

(A) Bar graph shows the fold-change in PAR-2 mRNA expression in OA (*N*=14) and foetal (*N*=3) articular cartilage compared to no OA/normal (*N*=14). The PAR-2 mRNA expression levels in OA and foetal articular cartilage were 5 and 3 times higher than the no OA/normal group respectively. (B) Bar graph depicts the fold-change in PAR-2 mRNA expression in OA synovium (*N*=5). The PAR-2 mRNA expression level in synovium was 1.5 times higher than the no OA/normal group. (C) The PAR-2 mRNA expression of the OA articular cartilage was significantly higher than the no OA/normal group. (D) There is no significant difference in synovium PAR-2 mRNA expression between the OA and no OA/normal group. (C & D) Data presented as mean ± standard deviation, (2-sample t-test,*** represents P<0.001 and "ns" = not significant)

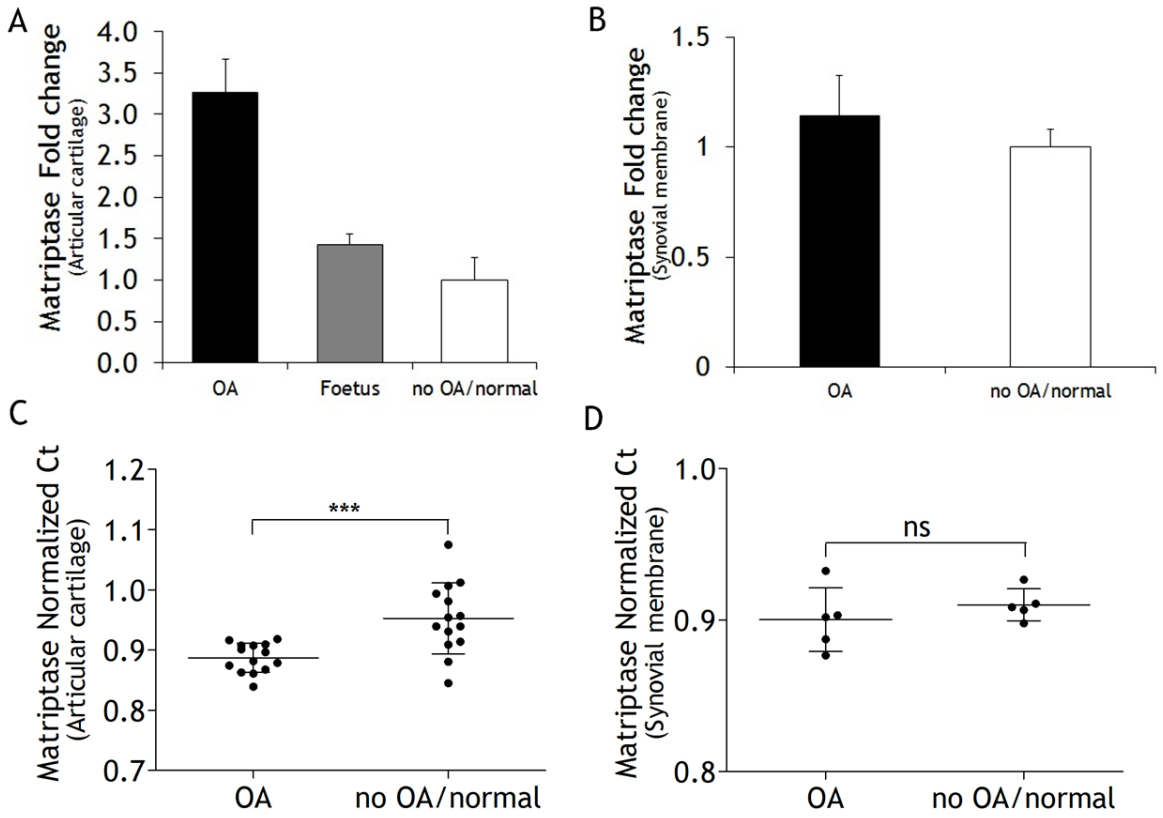

Figure 10.6: Matriptase mRNA expression as determined by qPCR in articular cartilage and synovium.

(A) Bar graph shows the fold-change in matriptase mRNA expression in OA (*N*=14) and foetal (*N*=3) articular cartilages compared to no OA/normal (*N*=14). The PAR-2 mRNA expression levels in OA and foetal articular cartilage were 3.3 and 1.4 times higher than the no OA/normal group respectively. (B) Bar graph depicts the fold-change in matriptase mRNA expression in OA synovium (*N*=5). The matriptase mRNA expression level in OA synovium was 1.1 times higher than the no OA/normal group. (C) The matriptase mRNA expression of the OA articular cartilage was significantly higher than the no OA/normal group. (D) There is no significant difference between the OA synovium matriptase mRNA expression and the no OA/normal group. (C & D) Data presented as mean ± standard deviation, (2-sample t-test, *** represents $P<0.001$; "ns" = not significant).

10.4 Discussion

The present study has shown that PAR-2 is present in feline articular cartilage and synovial membrane from no OA/normal and OA cats. In the no OA/normal articular cartilage, PAR-2 protein was found mainly in the superficial layers, while in the OA articular cartilage, PAR-2 protein was present in the superficial, middle and deep layers of the cartilage. These results demonstrated that in OA, PAR-2 protein is present throughout all layers of the cartilage matrix, and upon activation, it is very likely to be involved in cartilage degradation. The presence of PAR-2 protein was also variable in different areas of the OA cartilage. This may reflect differences in the severity of cartilage pathology in different areas. Ideally, a morphometric analysis needs to be done to quantify and estimate the number of chondrocytes staining positive in the entire thickness of cartilage.

Matriptase protein was consistently identified in feline articular cartilage and synovial membrane of OA cats. Matriptase protein was seen in locations where PAR-2 was also identified. None of the no OA/normal cats showed immunoreactivity for matriptase. Matriptase is reported not to be present in normal human articular cartilage (Oberst et al., 2003). Moreover, matriptase is also not detected in the chondrocytes of the normal articular cartilage of laboratory mice but is consistently seen in OA articular cartilage (Milner et al., 2010). The similarities in matriptase distribution in cat, human and mouse chondrocytes may reflect genuine physiological similarities between rodents, felidae and primates.

PAR-2 and matriptase are important mediators of collagenolytic activity in OA cartilage (Boileau et al., 2007; Milner et al., 2010). Collagenolysis initially occurs in the pericellular area of the chondrocytes (Hollander et al., 1995); suggesting proteases are associated with the chondrocyte cell surface. Collagen breakdown allowing proteoglycans to “escape” from the matrix is supported by the faint staining with haematoxylin in the areas where PAR-2 and matriptase were present (Figures 10.1.C-D).

Quantitative real-time PCR is a sensitive and widely used technique for the quantitative analysis of gene expression levels. To make an accurate comparative study of changes in gene expression, it is important to select the best reference gene(s) for normalizing data (Vandesompele et al., 2002). To determine the optimal reference genes for gene expression analyses in feline articular tissues, the author used an established and standardized tool, geNorm, which was specifically designed for this purpose. geNorm software is a bioinformatics tool designed to rank candidate reference genes by using a

normalisation factor calculated on the basis of the geometric mean of the expression level of the candidate reference genes in an array of representative samples.

The candidate reference genes that were evaluated in this study were selected from various studies that had examined gene expression in articular tissues (Ayers et al., 2007; Maccoux et al., 2007; Pombo-Suarez et al., 2008; McCulloch et al., 2012; Peng et al., 2012) and from published work defining their stability as reference genes with feline tissues (Penning et al., 2007; Kessler et al., 2009). Evaluation of appropriate reference genes in human cartilage with advanced OA has been reported by Pombo-Suarez and colleagues (2008) who reported that TBP, RPL13a and B2M should be used in such studies. RPL13a (which is similar in function to RPL18) did not perform so well as the other candidate genes in the present study. HPRT was the most stable gene although Pombo-Suarez et al. (2008) found that HPRT1 (another name for HPRT) was the most unstable in human articular cartilage. SDHA was reported to be amongst the best reference genes in porcine and canine articular cartilage (Ayers et al., 2007; McCulloch et al., 2012).

In the present study, GAPDH was not amongst the best reference genes for feline articular tissue even though it had been reported to be suitable for feline peripheral blood mononuclear cells (Leutenegger et al., 1999), palatoglossal mucosa (Dolieslager et al., 2013), intestinal tissues (Nguyen Van et al., 2006) and skin samples (Taglinger et al., 2008). Previous studies have reported that GAPDH is less stably expressed in human, canine and rabbit articular cartilage (Pombo-Suarez et al., 2008; Ayers et al., 2007; Maccoux et al., 2007; Peng et al., 2012). Another study by Ryan et al. (2013) excluded GAPDH as one of the reference genes used in the transcriptomic studies of articular cartilage and subchondral bone of the humeral condyle of cats with and without OA. Thus reference genes suitable for a specific organism or tissue may not be suitable for a different organism and/or tissue (Dundas and Ling, 2012). The reference gene selection has to be performed on a tissue and disease specific basis, even when evaluating tissues with the same or similar diseases.

Quantitative real-time PCR showed that PAR-2 and matriptase mRNA was detected in feline no OA/normal and OA articular tissues. PAR-2 and matriptase expression levels were significantly increased in OA compared with no OA/normal feline articular cartilage. Specific mechanisms that trigger the activation of matriptase are incompletely understood (Benaud at al., 2002). However, PAR-2 has been identified as one of the natural substrates for matriptase (Takeuchi et al., 2000). Matriptase activates PAR-2 via the proteolytic release of a tethered ligand (Wang et al., 2008).

Previously, Milner et al. (2010) reported that matriptase has several functions as an inducer and activator of procollagenases which lead to cartilage breakdown. PAR-2 activation has been associated with an increase in the production of MMP-1 and MMP-13, as well as COX-2, which are key mediators of OA pathophysiology (Boileau et al., 2007). Thus in OA cartilage a high matriptase and PAR-2 level of gene expression would be expected. The findings suggest that matriptase and PAR-2 have a role in OA pathogenesis. However, further studies need to be done in order to characterise and explore the pathobiological activities of matriptase and PAR-2 in feline articular tissues with and without OA. The importance of matriptase and PAR-2 in OA pathology is summarised in Figure 10.7.

It has been reported that PAR-2 expression is strongly correlated with synovitis in human OA (Tindell et al., 2012). PAR-2 regulates the synovial release of proinflammatory cytokines including IL-1β (Kelso et al., 2007) which in turn up-regulates PAR-2 expression in OA chondrocytes (Xiang et al., 2006; Boileau et al., 2007). The present study showed that the fold-change expression level of PAR-2 and matriptase mRNA in OA synovium was higher than in no OA/normal synovium. However, there was no significant difference between the transcription levels of PAR-2 and matriptase mRNA in the synovium samples from the no OA/normal and OA cats. This finding maybe related to the degree of inflammatory cell infiltration in the feline synovium. PAR-2 expression has been shown in fibroblast-like synoviocytes (Xiang et al., 2006) and macrophages and lymphocytes derived from OA synovia (Tindell et al., 2012). The present study has shown that synovial inflammation is minimal in feline OA (see Chapter 8, section 8.3.4). Another explanation may be the limited sample quantity. A larger number of synovium tissue samples need to be studied to identify gene expression.

Jenkins et al. (2000) reported the expression of PAR-2 during embryonic development in murine tissues. In the developing chondrocyte, PAR-2 expression was detectable at 17 days of gestation but was absent in adult cartilage. However the study did not specifically state the age of the adult mice. They suggested that the chondrocytic expression of PAR-2 appears to be associated with metabolically active cartilage. The present study showed increase fold-change in PAR-2 expression in foetal cartilage (9 weeks of age) which supports the conclusions of Jenkins et al. (2000). Presumably there is a rapid growth of cartilage in the foetus with increased turnover of cartilage matrix which would involve PAR-2 and matriptase. Similarly in OA cartilage there is an attempt at repair with matrix breakdown and replacement. There is no study reported on matriptase expression in foetal articular tissue.

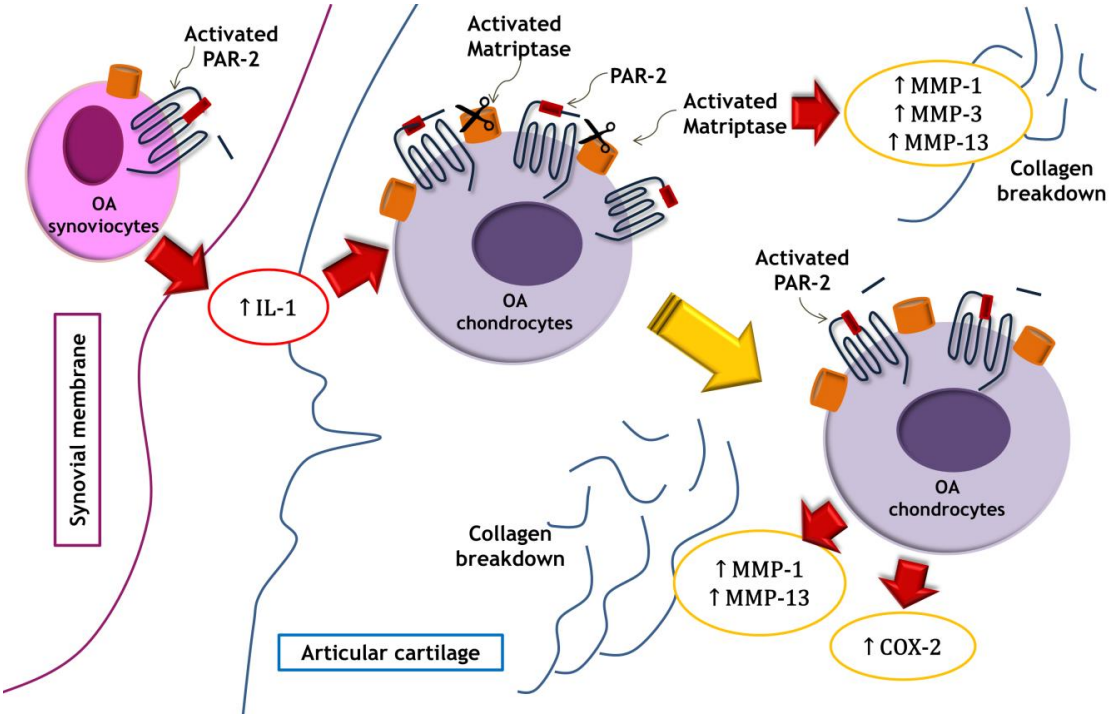

Figure 10.7: Diagram summarising the importance of matriptase and PAR-2 in OA pathology.

In conclusion, PAR-2 protein and mRNA expression has been shown in adult and foetal articular cartilage and synovial membrane of cats with and without OA. Matriptase protein was only present in the OA articular cartilage and synovial membrane; however the matriptase mRNA expression was detected in all articular tissues irrespective of the disease condition. This discrepancy may reflect the fact that gene expression does not always equate to protein secretion (Vogel and Marcotte, 2012). Translation of mRNA to protein is presumably under the control of inflammatory cytokines (Palanisamy et al., 2012), although the exact mechanism for matriptase secretion is unknown (Benaud at al., 2002). Increased levels of PAR-2 and matriptase protein and mRNA expression in OA articular cartilage suggests that PAR-2 and matriptase may play an important pathological role in OA. The identification of appropriate reference genes defined in this study will facilitate accurate gene expression studies of feline articular tissues in the future.

Chapter 11 General discussion

11.1 Risk factors for feline OA

- **Age.** Cats with OA are significantly older than cats without OA. This finding is expected in a chronic progressive age-related disease and has been reported previously in cats (Godfrey, 2005; Clarke et al., 2005; Clarke and Bennett, 2006; Lascelles et al., 2010, Slingerland et al., 2011). Age records were not available for all cats and, thus the approximate age had to be determined, in some cases by examination of the teeth. This might have under-estimated the age in some cats since cats who had received dental care during their life will have had better looking teeth than those who did not.

- **Sex.** Relatively more females (10 F and 26 FS) than males (16 MC) had OA. The current study supports previous findings by Godfrey (2007) who reported being female is a risk factor for feline OA. It is known that postmenopausal women are predisposed to OA due to oestrogen deficiency which can influence the molecular activity of joint tissues (Roman-Blas et al., 2009). Considering the high number of spayed female cats in this population, a similar hormonal association might be worthy of further consideration.

- **Breed predisposition.** It has been suggested that the Burmese breed is predisposed to OA. Godfrey (2007) reported that nine of 86 cats with elbow OA were Burmese. Only 5 pedigree cats, including one Burmese were included in the present study; 4 had OA in at least one joint. Some large breed cats such as the Maine coon have a genetic predisposition for HD-a prevalence of 18% is reported in this breed (Mills, 1995). Most cats with OA in this study were domestic shorthaired, which reflects the majority of cats in the general population.

- **Body weight and body condition score.** No significant differences between 6 no OA/normal and 52 OA cats were shown for BW and BCS. The mean values of BW and BCS were 3.5 kg and 3.0 respectively, which are generally ideal values for adult cats. Furthermore, the age and BCS were observed to be negatively correlated with the severity of radiographic and gross pathologic changes in all joints. In the present study, no previous records of BW and BCS were available. The BW and BCS were only determined at the time of the *post-mortem* examination, and thus it is not possible to exclude obesity earlier in life as a predisposing factor for OA. Obesity is known to be a risk factor in humans (Carman et al., 1994) and dogs (Kealy et al., 2002).

11.2 Secondary OA

Radiographic assessment in conjunction with gross pathologic and histopathologic examination has successfully identified four underlying diseases that lead to secondary OA in the cat.

Radioulnar incongruity characterised by elevation of the radial head above the level of the ulnar coronoid process has been recognised as a possible cause of elbow OA. This can be regarded as a form of feline elbow dysplasia. In no cases was a primary pathology of the coronoid process identified. Fragmented medial coronoid process has been reported as the most common cause of secondary OA in the canine elbow joint, and most commonly develops in fast-growing and large breed dogs such as the Bernese mountain dog (Boulay, 1998; Hartmann et al., 2012). Fragmented medial coronoid process has also been described in cats (Staiger and Beale, 2005).

The current study has also identified HD as a cause of hip OA. Of 12 cats with HD, 11 (91.7%) had OA. Joints with HD showed more severe radiographic and gross pathologic changes of OA than those without. Most degenerative changes appeared on the caudal part of the femoral head and acetabular margins, with a high incidence of osteophyte formation and remodelling on the femoral head and neck. Clarke and Bennett (2006) reported 22.0% of cats with HD eventually develop secondary OA. Using criteria similar to the present study, Godfrey (2007) identified hip dysplasia in 16/152 (11.0%) and ten of these had hip OA. An attempt was made to measure the NA. The present study recorded a NA for the dysplastic hip of 93.2 ° compared with 99.1 ° for the non-dysplastic hip.

A complete rupture of the cranial cruciate ligament was not seen in any stifle joint although this condition is regularly diagnosed in primary practice and has previously been reported in cats as a cause of secondary OA (Harasen, 2005; Ruthrauff et al., 2011). Gross pathologic and histopathologic examinations showed that degenerative changes were present in two CCLs from OA stifle joints. It is possible that CCL disease might be a cause of stifle OA. The histopathologic changes were similar to those observed in dogs with cruciate disease, including hypocellular, disorganised collagen fibres and fibrocytes (Vasseur et al., 1985). It is unclear whether the pathogenesis of cruciate disease in felines and canines is similar.

Meniscal mineralisation was radiographically visible in two stifle joints (one cat) where the articular cartilage was normal and which could have a represented a primary intrameniscal calcification which can lead to secondary OA.

GH- secreting pituitary adenoma was not seen in any cats with or without OA. Thus it appears that acromegaly is not an important cause of OA in the cat.

Severe or repetitive trauma to joints is a well-recognised cause of secondary OA. There were no pathological findings in this study to directly support this hypothesis, although clinical data would be more useful to evaluate this. More severe pathologic changes in the medial compartments of the elbow and stifle joints and the lateral compartment of the tarsocrural joint were observed in this study. These more severe changes may be related to increased mechanical loading and trauma to these parts of the joint.

This study supports the view that most cases of OA in cats are primary or idiopathic in nature.

11.3 Radiographic features and prevalence of feline OA

In Chapters 3, 4, 5, 6 and 7 of this thesis, the author has defined the radiographic features of OA for each appendicular joint. Of 696 joints examined, 389 (55.9%) had radiographic OA. The radiographic prevalence was highest in both the elbow (23.9%, 93/389) and stifle (23.9%, 93/389) joints, followed by the hip (21.1%, 82/389), tarsal (17.7%, 69/389), shoulder (6.7%, 27/389) and carpal (6.4%, 25/389) joints. Bilateral disease was invariably a feature, particularly in the elbow, stifle, hip, tarsal and carpal joints. The radiographic findings are summarised in Table 11.1.

The radiographic features of OA rely predominantly on identifying the presence of osteophytes and enthesiophytes (Hardie et al., 2002; Clarke et al., 2005; Godfrey, 2005; Godfrey, 2007). In more recent studies, Lascelles et al. (2010) and Freire et al. (2011) included articular soft tissue mineralisation as a feature of OA. In this thesis, five important radiographic features of OA were used to assess each of the appendicular joints; osteophytes, enthesiophytes, areas of abnormal mineralisation, synovial effusion and joint remodelling.

- **Osteophytes.** Prevalence rates for osteophytes were 96.3% for the shoulder joints (26/27), 83.9% for the elbow joints (78/93), 61.3% for the stifle joints (57/93), 84.1% for the hip joints (69/82) and 100% for both carpal (25/25) and

tarsal (69/69) joints. Osteophytes were the most common radiographic feature seen in the study. They were measured and scored according to their size. In mild, moderate and severely affected joints, osteophytes had a mean size of 1.1 ± 0.1 mm, 2.8 ± 0.2 mm and 5.2 ± 0.1 mm respectively.

- **Enthesiophytes.** They were only seen in the stifle (35.5%, 33/93) and elbow (9.7%, 9/93) joints. Enthesiophyte formation is not necessarily associated with OA. They can form in response to inflammation, repetitive strain or in the absence of any specific cause (Smillie, 1970; Resnick and Niwayama, 1983). In this study, enthesiophytes were never seen without gross cartilage changes which suggest that they are a genuine feature of feline OA particularly in the stifle and elbow joints.

- **Areas of abnormal mineralisation.** Prevalence rates for abnormal mineralisation were 25.8% for the elbow joints (24/93), 18.3% for the stifle joints (17/93), 12.0% for the carpal joints (3/25) and 3.7% for the shoulder joints (1/27). The findings support the previous studies by Clarke et al. (2005) and Godfrey (2007) who reported that abnormal mineralisation was found predominantly in the elbow and stifle joints.

- **Synovial effusion.** Synovial effusions were only seen in the stifle (44.1%, 41/93) and elbow (4.3%, 4/93) joints. The findings contradicted the previous study by Godfrey (2007) who reported effusion was confined to the carpal and tarsal joints. The variations may due to experimental design where most of the radiographs in the Godfrey study were not taken for joint evaluation and effusion may thus have been under-diagnosed. Morgan (1999) suggested joint effusion in small animals is most easily seen radiographically on a lateral view of the stifle. However, in the current study computed radiography often gave a false positive assessment for the stifle joint. In 41 cats where effusion was present radiographically, it was only confirmed at gross pathologic examination in 20 cats.

- **Joint remodelling**. Remodelling was observed in the elbow (16.1%), carpal (8.0%), stifle (7.5%), tarsal (5.8%) and hip (3.7%) joints but was not recognised in the shoulder joints.

Other radiographic features were also assessed in specific joints:

- **Increase in radio-opacity of bone.** The current study has suggested that an increased radio-opacity beneath the semilunar notch, along the femoral trochlea, beneath the tibial plateau and on the femoral head/neck is an important radiographic feature. The feature was confirmed on gross pathologic examination as being the result of marginal osteophytes on the bone surface, areas of mineralised joint capsule superimposed on the articular bone or superimposed osteochondromas. Increased radio-opacity possibly due to thickening of the subchondral bone was also confirmed by histopathologic assessment in some joints. Although the assessment was subjectively done, the intra- and inter- observer study for the elbow joint demonstrated that it appears to be a useful feature to assess at least for this joint. Inter- and intra-observer assessment of the increased radio-opacity of the ulnar trochlear notch has been reported in the dog. However, Burton et al. (2008) identified that the inter-observer agreement was only fair and the agreements were observer dependent.

- **Changes in joint space.** An attempt was made to assess changes in joint space in the elbow and hip joints. A decreased joint space was commonly seen in the humero-ulnar joint. A decrease in the joint space indicates articular cartilage loss (Owens, 1982). The present study confirmed that a decrease in the humero-ulnar joint space correlated with cartilage loss, particularly on the medial humeral condyle. With the hip joint, a decreased joint space was more commonly seen at the cranial aspect despite there being more cartilage damage at the caudal part of the femoral head and acetabulum. This probably reflects the fact that joint space is more difficult to assess on the standard ventrodorsal extended view of the hip.

			Radiographic features										
Joint	**rOA (%)**	**Number of joint affected (%)**	**Osteophytes**	**Enthesiophytes**	**Areas of abnormal mineralisation**	**Increase radio-opacity**	**Synovial effusion**	**Joint space**	**Joint remodelling**	**SSB**	**MM**	**New bone formation on the fabellae**	**Joint incongruity**
Shoulder 6 bilateral, 15 unilateral	21/58 (36.2%)	27/116 (23.3%)	26/27 (96.3%)	0/27 (0%)	1/27 (3.7%)	-	0/27 (0%)	-	0/27 (0%)	-	-	-	-
Elbow 43 bilateral, 7 unilateral	50/58 (86.2%)	93/116 (80.2%)	78/93 (83.9%)	9/93 (9.7%)	24/93 (25.8%)	86/93 (92.5%)	4/93 (4.3%)	(48.4%) 45/93	15/93 (16.1%)	55/93 (59.1%)	-	-	9/93 (9.7%)
Stifle 43 bilateral, 7 unilateral	50/58 (86.2%)	93/116 (80.2%)	57/93 (61.3%)	33/93 (35.5%)	17/93 (18.3%)	89/93 (95.7%)	41/93 (44.1%)	-	7/93 (7.5%)	-	49/93 (52.7%)	24/93 (36.4%)	-
Hip 36 bilateral, 10 unilateral	46/58 (79.3%)	82/116 (70.7%)	69/82 (84.1%)	0/82 (0%)	0/82 (0%)	80/82 (97.6%)	0/82 (0%)	(13.4%) 11/82	3/82 (3.7%)	-	-	-	-
Carpus 9 bilateral, 7 unilateral	16/58 (27.6%)	25/116 (21.6%)	25/25 (100%)	0/25 (0%)	3/25 (12.0%)	-	0/25 (0%)	-	2/25 (8.0%)	-	-	-	-
Tarsus 28 bilateral, 13 unilateral	41/58 (70.7%)	69/116 (59.5%)	69/69 (100%)	0/69 (0%)	0/69 (0%)	-	0/69 (0%)	-	4/69 (5.8%)	-	-	-	-

Table 11.1: Showing the number and percentage of radiographic findings for each joint. Total number of cats is 58.

11.4 Supinator sesamoid bone

The presence of a radiographically apparent SSB is an indicator of OA in the elbow joint although some OA joints do not have a radiographically evident SSB. Most of the SSB consists of trabecular bone and bone marrow. It has a round or oval shape and is embedded within the tendon of origin of the supinator muscle and is covered with a cartilage cap which has the histological appearance of hyaline cartilage. The tendon of the supinator muscle often includes areas of chondro-osseous metaplasia suggesting that SSB development may be an adaptation in response to excessive mechanical friction occurring in a tendon (Meyer et al., 1964) in order to maintain the anatomical function of the humeroradial articulations especially during flexion, extension, supination and pronation (Wood et al., 1995). In joints which are arthritic, the SSB may become a focus of new bone deposition and thus more likely to be radiographically visible. Alternatively, altered gait or conformation due to painful OA may increase the mechanical friction on the supinator tendon promoting development of the SSB. The presence of a SSB is associated with advancing age and the presence of articular cartilage damage (Ariffin et al., 2012). Cats with radiographically visible SSB are older than those without and the joints tend to have more severe changes in the articular cartilage.

11.5 Meniscal mineralisation

The overall prevalence of radiographic MM was 42.2% (49/116). The prevalence of radiographic MM in radiographic and pathologic OA stifle joints was 52.7% (49/93) and 49.5% (49/99) respectively. The present study demonstrated that radiographically apparent MM is associated with cartilage pathology, and can be used to diagnose OA of the feline stifle joint. Meniscal mineralisation was always present in the cranial horn of the medial meniscus and is associated with advancing age and articular cartilage damage. Those cats where the MM was radiographically visible were significantly older than those without and the joints tended to have more severe changes in the articular cartilage particularly in the medial compartment of the joint. The current study supports previous findings by Freire et al. (2010) and Ariffin et al. (2013) who reported mineralisation of the menisci related to severe cartilage pathology. MM may reflect degeneration of the medial meniscus as part of the OA process affecting the stifle joint. However it is also feasible that it could represent a primary degeneration of the meniscus possibly as a result of repetitive trauma. The meniscus would then lose much of its “shock-absorption” properties causing an increased load on the femorotibial joint

(particularly the medial compartment) will resultant secondary OA. Even if the MM is part of secondary OA, the changes in meniscal resilience and function could be expended to promote or increase the progression of the disease. MM was radiographically visible in two stifle joints of a single cat where there was normal articular cartilage. In 3/116 menisci, the histologic feature of the MM were more consistent with a sesamoid bone (the lunula) rather than degenerative change (these did not include the single cat with MM and normal articular cartilage). Intrameniscal ossification consisting of trabecular bone with marrow spaces and with an obvious articular cartilage cap (similar in appearance to hyaline cartilage) on the proximal (femoral) surface was typical of these cases.

11.6 Fabellae

The overall prevalence of two radiographically apparent fabellae was 65.5% (76/116). The presence of two fabellae is also related to cartilage pathology, and again can help to diagnose OA of the feline stifle joint. It is rare to see both fabellae in the normal cat stifle joint; generally only the lateral one is visible. The medial fabella is present but is generally not sufficiently mineralised to show on a routine radiograph and this lack of mineralisation is thought to be common in cats (Arnbjerg and Heje, 1993). The current studies have shown that a radiographically apparent medial fabella is commonly seen in stifle joints with gross cartilage changes. In this study 70/116 had two fabellae. As part of the arthritic process, active new bone deposition occurs (Gupta et al., 2004), and this may involve the fabellae, which then become more radiopaque. The radiographic presence of lateral fabellae and its relationship with OA has also been reported in human (Pritchett, 1984).

11.7 Gross pathology

Gross pathologic changes were identified in 506/696 (72.7%) joints. The gross pathologic prevalence was highest in the elbow (20.2%, 102/506) joints, followed by the stifle (19.6%, 99/506), hip (18.4%, 93/506), shoulder (17.8%, 90/506), tarsal (15.0%, 76/506), and carpal (9.1%, 46/506) joints. Bilateral involvement was common particularly in the elbow, stifle, hip, shoulder, tarsus and carpal joints. The gross pathologic findings are summarised in Table 11.2.

			Gross pathologic features							
Joint	**Path OA (%)**	**Number of joint affected (%)**	**Thickening of joint capsule**	**Synovium discolouration**	**Cartilage discolouration**	**Cartilage fibrillation**	**Cartilage erosion**	**Cartilage ulceration**	**Osteophytes**	**Joint remodelling**
Shoulder 42 bilateral, 6 unilateral	48/58 (82.8%)	90/116 (77.6%)	9/90 (10.0%)	10/90 (11.2%)	73/90 (81.1%)	90/90 (100.0%)	5/90 (5.6%)	4/90 (4.4%)	78/90 (86.7%)	0/90 (0%)
Elbow 50 bilateral, 2 unilateral	52/58 (89.7%)	102/116 (87.9%)	41/102 (40.2%)	55/102 (53.9%)	97/102 (95.1%)	102/102 (100.0%)	55/102 (53.9%)	41/102 (40.2%)	93/102 (91.1%)	19/102 (18.6%)
Stifle 48 bilateral, 3 unilateral	51/58 (87.9%)	99/116 (85.3%)	9/99 (9.1%)	30/99 (30.3%)	97/99 (98.0%)	99/99 (100.0%)	37/99 (37.4%)	14/99 (14.1%)	81/99 (81.8%)	13/99 (13.1%)
Hip 45 bilateral 3 unilateral	48/58 (82.8%)	93/116 (80.2%)	25/93 (26.9%)	24/93 (25.8%)	91/93 (97.8%)	93/93 (100.0%)	5/93 (5.4%)	6/93 (6.6%)	93/93 (100.0%)	4/93 (4.3%)
Carpus 17 bilateral 12 unilateral	29/58 (50.0%)	46/116 (39.7%)	0/46 (0%)	0/46 (0%)	31/46 (67.4%)	46/46 (100.0%)	2/46 (4.3%)	2/46 (4.3%)	29/46 (63.0%)	2/46 (4.3%)
Tarsus 33 bilateral 10 unilateral	43/58 (74.1%)	76/116 (65.5%)	8/76 (10.5%)	11/76 (14.5%)	37/76 (48.7%)	76/76 (100.0%)	4/76 (5.3%)	4/76(5.3%)	74/76 (97.4%)	7/76 (9.2%)

Table 11.2: Showing the number and percentage of gross pathologic findings for each joint. Total number of cats is 58.

Eight important gross pathologic changes were used to assess each of the appendicular joints- cartilage discolouration, cartilage fibrillation, cartilage ulceration, cartilage erosion, osteophytes, thickening of joint capsule, synovium discolouration and joint remodelling.

- **Cartilage discolouration.** A yellow discolouration was common in all OA joints. Prevalence rates for cartilage discolouration were 81.1% for the shoulder joints (73/90), 95.1% for the elbow joints (97/102), 98.0% for the stifle joints (97/99), 97.8% for the hip joints (91/93) 67.4% for the carpal joints (31/46) and 48.7% for the tarsal joints (37/76).

- **Cartilage fibrillation.** All joints affected with OA had fibrillation. Fibrillation was seen as a focal or diffuse area of dullness and roughness of the articular cartilage. In the elbow and stifle joints, the medial part of the joint demonstrated greater fibrillation than the lateral.

- **Cartilage erosion.** Prevalence rates for cartilage erosion were highest in the elbow (53.9%, 55/102) joints, followed by the stifle (37.4%, 37/99), shoulder (5.6%, 5/90), hip (5.4%, 5/93), tarsal (5.3%, 4/76) and carpal (4.3%, 2/46) joints. This reflects the fact that the elbow joints showed more advanced stages of cartilage damage.

- **Cartilage ulceration.** Complete loss of the articular cartilage with exposure of the subchondral bone was commonly seen in the elbow (40.2%, 41/102) and stifle (14.1%, 14/99) joints. The prevalence rates for cartilage erosion were low in the hip (6.6%, 6/93), tarsal (5.3%, 4/76), shoulder (4.4%, 4/90) and carpal (4.3%, 2/46) joints. Cartilage ulceration with marked "wear-lines" was commonly seen particularly on the medial humeral condyle, the semilunar notch of the ulna, the lateral parts of the trochlea of the tibial tarsal bone and the distal tibia.

- **Osteophytes.** The prevalence of osteophytes was highest in the hip (100%, 93/93) and tarsal (97.4%, 74/76) joints. However, osteophytes were also common in the elbow (91.1%, 93/102), shoulder (86.7%, 78/90), stifle (81.8%, 81/99) and carpal (63.0%, 29/46) joints.

- **Thickening of joint capsule.** Thickening of the joint capsule was common in the elbow (40.2%, 41/102), hip (26.9%, 25/93), tarsal (10.5%, 8/76), shoulder (10.0%, 9/90) and stifle (9.1%, 9/99) joints. It was not seen in any carpal joint.

- **Synovium discolouration.** Prevalence rates for synovium discolouration were 53.9% for the elbow joints (55/102), 30.3% for the stifle joints (30/99), 25.8% for the hip joints (24/93), 14.5% for the tarsal joints (11/76) and 11.2% for the shoulder joints (10/90). Synovium discolouration was not identified in any carpal joint.

- **Joint remodelling.** Remodelling was most common in the elbow (18.6%, 19/102), but was present in all joints except the shoulder.

The presence of osteochondromas was identified in the elbow (11.8%, 12/102) and stifle (2.0%, 2/99) joints with OA. In all cases, the osteochondromas were attached to the synovium and protruded into the articular cavity.

11.8 Correlation between radiographic and gross pathologic findings

There was a positive correlation between radiographic and gross pathologic total scores in feline appendicular joints. However, the correlation coefficient was variable in each joint, ranging from fair to good (left elbow: r_s=0.77; right elbow: r_s=0.79; left tarsal: r_s=0.76; right tarsal: 0.78; left stifle: r_s=0.71; right stifle: r_s=0.71; left carpal: r_s=0.67; right carpal: r_s=0.72; left shoulder: r_s=0.46; right shoulder: r_s=0.31). The joint that is most likely to have cartilage damage without radiographic evidence of OA is the shoulder (71.1%, 64/90) followed by the elbow (39.1%, 9/23), hip (32.4%, 11/34), stifle (26.1%, 6/23), carpal (23.1%, 21/91) and tarsal (14.9%, 7/47) joints. This finding is in contrast with a previous study by Freire et al. (2011) who reported the stifle joint as being the most likely to have cartilage damage without radiographically apparent OA (71.0% , 15/21 of radiographically normal stifle joints had cartilage changes).

11.9 Articular histopathology

The characterisation of the histopathologic features of the articular tissues has proven that OA is a disease of the whole joint. Cartilage changes in OA ranged from fibrillation to complete ulceration and exposure of the subchondral bone. Chondrocyte clustering, multiple tidemarks, blood vessels crossing the tidemark and loss of safranin O staining

from the cartilage matrix were all apparent. Most of the histopathologic changes seen in the present study are the same as those reported in humans (Pritzker et al., 2006), dogs (Cooke et al., 2010), rabbits (Laverty et al., 2010) and horses (McIlwraith et al., 2010). These findings challenge a recent publication by Freire et al. (2014) where chondrocyte clustering, multiple tidemarks and blood vessels crossing the tidemark were not observed. DAPI fluorescence studies demonstrated that DNA is present in the tidemark of normal joints and in all of the multiple tidemarks of OA joints. These findings support the hypothesis that multiple tidemarks seen in OA occur as a result of the disintegration of chondrocyte apoptotic nuclei and debris which diffuses through the matrix until it reaches the junction between calcified and non-calcified cartilage (Simkin 2008), the position of which changes with advancing calcification of the deeper layer of articular cartilage.

The present study also identified osteophytes, thickening of the subchondral bone plate and trabeculae, subchondral bone "cysts" and fibrosis. Intra-articular osteochondral fragments or osteochondromas were found in the elbow and stifle joints and in all cases changes were present in the articular cartilage as well. On histopathologic examination, osteochondromas consisted of trabecular bone with marrow spaces, covered by a hyaline cartilage cap and generally there was evidence of a synovial attachment. It seems likely that osteochondromas arise from the synovial membrane as a result of chronic inflammation as suggested by Freire et al. (2014). The term (secondary) "osteochondroma" as used in this study was the appropriate one to use when describing a calcified body which is clearly delineated, lying free or partly adhered to the synovium.

Lining layer hyperplasia, villous hyperplasia and hypertrophy, an inflammatory infiltrate and synovial calcification are the common features seen in the OA synovium although 78/130 (60.0%) of OA synovium had a normal histological appearance. The inflammatory infiltrate was generally minimal, suggesting that synovial inflammation is not a marked feature of feline OA. In the dog, the synovium is prone to developing changes such as hyperplasia and hypertrophy which is usually accompanied by a marked infiltration of the supporting layer with foci of lymphocytes (Brandt et al., 1991; Hewicker-Trautwein et al., 1999).

11.10 Renal histopathology

The histopathologic assessment of kidney tissue revealed that 36.5% of cats with OA had CKD. Because OA and CKD are age-related disorders, cats with OA can be expected to

have concurrent CKD. NSAIDs have proven to be very effective for treating chronic pain in arthritic cats (Clarke and Bennett, 2006; Bennett and Morton, 2009; Gunew et al., 2008; Gowan et al., 2011). However treating OA in cats with concurrent CKD is a challenging task since inhibition of prostaglandin production by NSAIDs may reduce renal blood flow and glomerular filtration rate and increase the possibility of precipitating acute renal failure (Weir, 2002). The current study found that interstitial inflammation is common in CKD, a feature reported elsewhere (Chakrabarti et al., 2012) and it is interesting to speculate that NSAIDs such as meloxicam might have a beneficial effect on kidney function by reducing inflammatory activity, which would support the clinical observations of Gowan et al. (2011).

11.11 PAR-2 and matriptase

The identification of PAR-2 and matriptase proteins and gene expression in feline articular tissues is a novel and important finding given the hypothesis that serine proteases are involved in feline OA. The consistent presence of PAR-2 and matriptase protein in the cytoplasm of OA chondrocytes suggests a possible contribution of proteases in cartilage degradation in the pathogenesis of OA (Boileau et al., 2007; Milner et al., 2010). A significantly higher gene expression in OA articular cartilage was seen for PAR-2 (5-fold change, $P<0.001$) and matriptase (3.3-fold change, $P<0.001$). This suggests that cartilage degradation in feline OA may be stimulated by an activation of matriptase and PAR-2 at the cellular level, which then facilitates pericellular collagenolysis of the matrix. Further investigations into the PAR-2 and matriptase pathobiology could thus improve our understanding of the proteolytic cascades in feline OA which could lead to the development of novel therapeutic strategies in the future.

11.12 Conclusion

The work in this thesis adds valuable information to the current knowledge on feline OA. It provides information on the radiographic features for each individual appendicular joint and how they relate to the gross pathologic and histopathologic features. Furthermore, the current study also provides information on possible predisposing factors that may be important and contribute to the development of feline OA. This thesis is an important step towards a better understanding of the molecular pathobiology of feline OA by identifying the presence of PAR-2 and matriptase in feline

articular cartilage and providing a basis for future studies on this important chronic feline disease.

Appendices

(i) List of cases included in this project

(ia) Radiographic and pathologic study

No.	Pathology No.	Radiography No.	Cat ID	Weight (kg)	Age (years)	Breed	Sex	BCS	Healthy/OA
1	282339	227374	CAT X1	3.44	3	DLH	CM	3	OA
2	282338	227374	CAT X2	2.6	0.5	DSH	F	3	Healthy
3	282340	227374	CAT X3	4.38	8	DSH	SF	4	OA
4	282337	227374	CAT X4	4.66	5	DSH	F	5	OA
5	282336	227374	CAT X5	4.2	5	DSH	CM	3	OA
6	282335	227374	CAT X6	3.06	5	DLH	CM	3	OA
7	286751	227374	CAT X7	2.3	12	DLH	F	1	OA
8	286774	227374	CAT X8	3.26	5	DSH	F	4	OA
9	286856	227374	CAT X9	3.46	6	DSH	CM	3	OA
10	286857	227374	CAT X10	2.92	5	DSH	F	3	OA
11	286854	227374	CAT X11	3.76	8	DSH	SF	4	OA
12	286855	-70	CAT X12	3.92	5	DSH	F	4	OA
13	286858	227374	CAT X13	4.18	2	DSH	CM	4	Healthy
14	294680	227374	CAT X14	3.1	3	DSH	F	2	OA
15	294696	227374	CAT X15	2.15	8	DSH	F	2	OA
16	294697	227374	CAT X16	7.02	8	DLH	SF	5	OA

17	294705	227374	CAT X17	2.56	3	DSH	F	2	OA
18	294704	227374	CAT X18	3.96	5	DSH	SF	3	OA
19	294706	227374	CAT X19	3.05	3	DSH	F	3	Healthy
20	294723	227374	CAT X20	5.56	3	DSH	F	5	OA
21	294724	227374	CAT X21	5.92	5	DLH	CM	5	OA
22	294732	227374	CAT X22	3.76	8	DSH	CM	3	OA
23	294753	227374	CAT X23	3	2	Persian	SF	2	OA
24	294761	227374	CAT X24	2.74	15	DSH	CM	2	OA
25	294763	227374	CAT X25	5.98	3	DSH	CM	5	OA
26	294786	227374	CAT X26	3	8	Siamese	CM	2	OA
27	294772	227374	CAT X27	2.1	8	DSH	SF	1	OA
28	294785	227374	CAT X28	2.62	5	DSH	SF	2	OA
29	294802	227374	CAT X29	1.94	15	DLH	SF	1	OA
30	294869	227374	CAT X30	2.5	2	DSH	SF	3	OA
31	294880	227374	CAT X31	2.52	10	DSH	SF	2	OA
32	294886	227374	CAT X32	2.66	5	DSH	CM	3	OA
33	296926	227374	CAT X33	3.72	3	Maine Coon X	SF	3	OA
34	296870	227374	CAT X34	3.12	2	DSH	SF	3	OA
35	296890	227374	CAT X35	5.54	4	DSH	SF	5	OA
36	296927	227374	CAT X36	2.9	10	DSH	SF	2	OA
37	296931	227374	CAT X37	2.8	5	DSH	SF	3	OA
38	296947	227374	CAT X38	3.3	8	DSH	CM	3	OA
39	296948	227374	CAT X39	4.38	13	DSH	SF	4	OA
40	296963	227374	CAT X40	4.54	5	DSH	SF	4	OA

41	296993	227374	CAT X41	3.56	13	DLH	SF	2	OA
42	296994	227374	CAT X42	2	14	DSH	SF	2	OA
43	301474	227374	CAT X43	2.5	10	DSH	SF	3	OA
44	301475	227374	CAT X44	5.12	10	DSH	CM	4	OA
45	301563	227374	CAT X45	1.94	15	DSH	CM	2	OA
46	301626	227374	CAT X46	3.18	3	DSH	SF	3	OA
47	301627	227374	CAT X47	4.94	5	Burmese	SF	3	OA
48	301628	227374	CAT X48	3.54	3	DSH	CM	2	OA
49	301685	227374	CAT X49	3.1	10	DSH	CM	2	OA
50	301686	227374	CAT X50	3.7	5	DSH	CM	4	OA
51	308920	227374	CAT X51	3.74	5	DSH	CM	3	Healthy
52	308987	227374	CAT X52	4.8	1	DSH	M	3	Healthy
53	309036	227374	CAT X53	0.8	0.25	Devon Rex	F	2	Healthy
54	314558	227374	CAT X54	2.88	20	DSH	SF	3	OA
55	315601	227374	CAT X55	2.76	8	DSH	SF	3	OA
56	317158	227374	CAT X56	2.26	18	DSH	SF	2	OA
57	317190	227374	CAT X57	3.14	8	DSH	SF	3	OA
58	317233	227374	CAT X58	3.01	5	DSH	F	3	OA

Signalment for all cats included in radiographic and pathologic study. Following abbreviations are used: Identity (ID), kilograms (kg), body condition score (BCS), osteoarthritis-at least one joint affected (OA), domestic long hair (DLH), domestic short hair (DSH), Maine coon cross (Maine coon X), castrated male (CM), male (M), spayed female (SF), female (F).

(ib) mRNA and IHC studies

No.	Cat ID	Weight (kg)	Age (years)	Breed	Sex	BCS	Healthy/OA	Sample
1	F1	2.75	1	DSH	F	2	Healthy	♦, ●,Δ,□
2	F2	2.50	5	DSH	SF	2	Healthy	♦, ●,Δ,□
3	F3	3.58	3	Burmese	SF	3	Healthy	♦, ●,Δ,□
4	F4	2.75	1	DSH	F	2	Healthy	♦, ●,Δ,□
5	F5	2.50	2	DSH	SF	2	Healthy	♦, ●,Δ,□
6	F6	2.08	7	DSH	CM	2	OA-(B)	♦, ●,Δ,□
7	F7	4.10	15	DSH	CM	4	OA-(B)	♦, ●,Δ,□
8	F8	3.72	15	DSH	SF	3	OA-(B)	♦, ●,Δ,□
9	F9	4.68	10	DSH	M	4	OA-(B)	♦, ●,Δ,□
10	F10	2.30	15	DSH	SF	2	OA-(B)	♦, ●,Δ,□
11	F11	2.25	2	DSH	F	3	Healthy	§,◊
12	F12	5.50	6	DSH	M	5	Healthy	§,◊
13	F13	5.00	2	DSH	M	4	Healthy	§,◊
14	F14	2.70	0.1	DSH	F	3	Healthy	§,◊
15	F15	4.00	4	DSH	M	3	Healthy	§,◊
16	F16	4.40	2	DLH	M	4	Healthy	§,◊
17	F17	3.60	2	DSH	F	5	Healthy	§,◊
18	F18	2.40	1	DLH	F	3	Healthy	§
19	F19	3.20	12	DLH	M	5	Healthy	§
20	F20	10.00	10	DSH	M	8	OA-(B)	§
21	F21	3.50	9	DSH	SF	4	OA-(B)	§,◊

22	F22	6.44	12	DSH	SF	7	OA-(B)	§,◊
23	F23	4.80	6	DSH	CM	4	OA-(B)	§,◊
24	F24	8.00	11	DSH	CM	8	OA-(B)	§,◊
25	F25	8.00	7	DSH	SF	8	OA-(B)	§,◊
26	F26	4.50	13	DLH	CM	5	OA-(B)	§,◊
27	F27	3.50	19	DLH	CM	4	OA-(B)	§,◊
28	F28	5.60	6	DLH	CM	6	OA-(B)	§,◊
29	Foetus 1	0.11	9 week old	DSH	F	-	Healthy	♦
30	Foetus 2	0.10	9 week old	DSH	F	-	Healthy	♦
31	Foetus 3	0.12	9 week old	DSH	CM	-	Healthy	♦

Signalment for all cats included in mRNA and immunohistochemical (IHC) study. Only elbow joints were included in the study.
Following abbreviations are used; osteoarthritis-bilateral (OA-(B)), osteoarthritis-left elbow (OA-(L)).
Following symbols are used; articular cartilage (♦) and synovial (●) samples for mRNA analysis, epiphyses consisting of articular cartilage and bone (Δ) and synovial (□) tissue for IHC. For F1-F10, both left and right elbow joints were collected.
F11-F28 RNA samples were received from the Royal (Dick) School of Veterinary Studies, University of Edinburgh. Right elbow articular cartilage RNA (§), left elbow articular cartilage RNA (◇) for for mRNA analysis.

(ii) Radiography study

(iia) Pre-set and programmable exposure settings for cat

	kV	mA	Sec	mAs
Extremities	50	100	0.035	3.50
Ventro-dorsal view (pelvis)	53	200	0.015	3.00

(iii) Pathology study

(iiia) General solutions and buffers

10% buffered neutral formaldehyde	162.5 g disodium hydrogen orthophosphate and 87.5 g sodium dihydrogen phosphate dissolved in 2.5 L of 37% formaldehyde. dH_2O added to give final volume of 25 L. pH 7.2-7.4
14% EDTA	137.5 g of 5.5% EDTA and 250 ml of 10% formaldehyde dissolved in 2250 ml water. pH 8.0
1% acid alcohol	1% HCl in methylated spirit.
0.001% Fast Green	0.01 g Fast Green dissolved in 1000 ml dH_2O.
1% acetic acid	2 ml acetic acid in 198 ml dH_2O.
0.1% Safranin O	0.1 g Safranin O dissolved in 100 ml dH_2O.
1% silver nitrate	1 g silver nitrate dissolved in 100 ml dH_2O.
5% sodium thiosulphate	5 g sodium thiosulphate dissolved in 100 ml dH_2O.
1% neutral red	1 g neutral red dissolved in 100 ml dH_2O and 1 ml glacial acetic acid.
1X PBS	100 ml of 10X concentrated PBS in 900 ml dH_2O.
0.01M sodium citrate buffer	2.94 g sodium citrate dehydrate, 0.5 ml polyoxyethylene sorbitan monolaurate dissolved in 1000 ml dH_2O. Adjust pH to 6.0 with 1 M HCl.
1X TBS	12.2 g Tris base and 8.76 g NaCl dissolved in 800 ml dH_2O. Adjust pH to 7.5 with 1 M HCl and make volume up to 1 L with ddH_2O.

(iiib) Processing Schedule

Duration: 17 hours

Station	Content	Duration
1	70% alcohol	1 hour
2	90% alcohol	1 hour
3	Absolute alcohol	1 hour
4	Absolute alcohol	1 hour
5	Absolute alcohol	2 hours
6	Absolute alcohol	2 hours 30 minutes
7	Xylene	30 minutes
8	Xylene	1 hour
9	Xylene	2 hours
10	Wax	2 hours
11	Wax	2 hours
12	Wax	2 hours

(iiic) Deparaffinising, rehydrating and dehydrating sections

Step	Reagent	Duration
Deparaffinising	Histo-clear	2 minutes
Rehydrating	70% alcohol	2 minutes
	70% methylated spirit	2 minutes
	Tap water	5 minutes
Dehydrating	70% methylated spirit	2 minutes
	70% alcohol	2 minutes

(iiid) Deparaffinising, rehydrating and dehydrating sections for DAPI and IHC

Step	Reagent	Duration
Deparaffinising	Xylene	5 minutes
Rehydrating	100% alcohol	2 minutes
	90% alcohol	2 minutes
	80% alcohol	2 minutes
	70% alcohol	2 minutes
Dehydrating	70% alcohol	2 minutes
	80% alcohol	2 minutes
	90% alcohol	2 minutes
	100% alcohol	2 minutes

(iiie) Scott's tap water substitute

Amount	Chemical
8.25 g	Sodium bicarbonate
50 g	Magnesium sulphate
2500 ml	Tap water
2 crystals	Thymol

Total volume for 2.5 L.

(iiif) DAPI solution

DAPI stock (14.3 mM)	10 mg DAPI dissolved in 2 ml dH_2O. Store away from light.
DAPI working solution (300 nM)	Dilute 10 µl DAPI stock solutions in 5 ml 1X PBS.

(iiig) Diluents for PAR-2 and matriptase IHC

PBS/BSA diluent	0.05g of 0.5% BSA dissolved in 10 ml 1X PBS.
PBS/BSA-serum diluent	200 µl horse serum in 1 ml PBS/BSA diluent. Total volume for 1 ml.
Supplemented blocking serum	4 drops of Avidin D in 1 ml PBS/BSA-serum diluent. Total volume for 1 ml.
Primary antibody diluent	4 drops of Biotin solution in 20 µl PBS/BSA-serum diluent.980 µl of 1X PBS were added to give final volume of 1 ml.
Secondary antibody diluent	18.75 µl horse serum in 1.25 ml 1X PBS.

(iv) mRNA analyses

(iva) General solutions

70% alcohol	140 ml absolute alcohol was added to 60 ml dH_2O to give final volume of 200 ml.

(ivb) DNase I preparation

DNase I stock	Add 500 µl RNase-free water to DNAse I lyophilized powder and mix gently. Aliquot and store at -20°C.
DNase I incubation mixture	10 µl DNase I stock solution in 70 µl RDD buffer (supplied with DNase I by manufacturer).

(v) Owner's consent form

UNIVERSITY OF GLASGOW SCHOOL OF VETERINARY MEDICINE

POSTMORTEM SUBMISSION FORM

Pathology No.: **Date of Submission:**

Species: **Breed:** **Gender:** **Age:**

Number in Group: **Number Sick:** **Number Dead:**

Veterinary Surgeon: **Owner's Name:**

Veterinary Surgeon's Address & Postcode:

Hospital Case Number or Animal Identification:

Euthanased ☐ **Died** ☐ *(Please tick)* **Private Cremation: Yes** ☐ **No** ☐ *(Please tick)*

Type of Case: Diagnostic (report and charged) ☐ **Teaching (no report, no charge)** ☐ *(Please tick)*

Legal or Insurance Case: Yes ☐ **No** ☐ *(Please tick)*

*** Please note that legal and insurance cases will incur an extra charge***

Neurological Examination Requested: Yes ☐ **No** ☐ *(Please tick)*

History: (include clinical signs, duration, significant lab results, vaccinations, treatments, etc.)

Clinical Diagnosis:

I certify that I have the legal right to authorise a post mortem examination on this animal.
I understand that this animal may be used for teaching or investigative purposes.

Signature: **Date:**

Print Name:

AUG 2010

References

Abe,K., Aslam,A., Walls,A.F., Sato, T., and Inoue, H. (2006). Up-regulation of protease-activated receptor-2 by bFGF in cultured human syovial fibroblasts. *Life Sciences*. **79**, 898–904.

Adams,C.S. and Horton,W.E. (1998). Chondrocyte apoptosis increases with age in the articular cartilage of adult animals. *The Anatomical Record*. **250**, 418–425.

Adams,M. and Billingham,M. (1982). Animal models for degenerative joint disease. In: Berry,C.L. (Ed.) *Current Topics in Pathology, Bone and Joint Disease*. 1st edn. pp. 521–534.

Adams,M.E., Billingham,M.E. and Muir,H. (1983). The glycosaminoglycans in menisci in experimental and natural osteoarthritis. *Arthritis & Rheumatology*. **26**, 69–76.

Afonso,V., Champy,R., Mitrovic,D., Collin,P. and Lomri,A. (2007). Reactive oxygen species and superoxide dismutases: role in joint diseases. *Joint Bone Spine*. **74**, 324–329.

Aigner,T. and Dudhia,J. (1997). Phenotypic modulation of chondrocytes as a potential therapeutic target in osteoarthritis: a hypothesis. *Annals of the Rheumatic Diseases*. **56**, 287–291.

Allan,G. (2013). Radiographic signs of joint disease in dogs and cats. In: Thrall,D.E. (Ed.), Textbook of Veterinary Diagnostic Radiology, 6th edn. pp. 319-348.

Allan,G.S. (2000). Radiographic features of feline joint diseases. *The Veterinary Clinics of North America: Small Animal Practice*. **30**, 281–302.

Allen,A.A., Caldwell,G.L. and Freddie,H.F.U. (1995). Anatomy and biomechanics of the meniscus. *Operative Techniques in Orthopaedics*. **5**, 2–9.

Alsalameh,S., Mollenhauer,J., Hain,N., Stock,K.P., Kalden,J.R. and Burmester,G.R. (1990) Cellular immune response toward human articular chondrocytes. T cell reactivities against chondrocyte and fibroblast membranes in destructive joint diseases. Arthritis and Rheumatology. **33**, 1477-1486.

Altman, R.D. and Gold, G.E. (2007). Atlas of individual radiographic features in osteoarthritis, revised. *Osteoarthritis and Cartilage*. **15**, A1–A56.

Amiable,N., Martel-Pelletier,J., Lussier, B., Kwan Tat,S., Pelletier,J.-P. and Boileau,C. (2011). Proteinase-activated receptor-2 gene disruption limits the effect of osteoarthritis on cartilage in mice: a novel target in joint degradation. The *Journal of Rheumatology*. **38**, 911–920.

Araujo,F.A., Rahal,F.C., Doiche,D.P., Machado,M.R., Vulcano,L.C., Teixeira,C.R. and El-Warrak,A.O. (2010). Imaging studies of the hindlimbs of pacas (*Cuniculus paca*) bred in captivity. *Veterinary and Comparative Orthopaedics and Traumatology*. **23**, 439–443.

Ariffin,S.M.Z., Johnston,P and Bennett,D. (2012). Radiographic and pathologic features of osteoarthritis (OA) of the feline elbow joint. In: *16th International Veterinary*

Radiology Association (IVRA) and European Veterinary Diagnostic Imaging (EVDI) Meeting. pp. 13.

Ariffin,S.M.Z., Johnston,P. and Bennett,D. (2013). Radiographic and pathologic features of osteoarthritis (OA) of the feline stifle joint. In: *British Small Animal Veterinary Association Congress 2013 Scientific Proceedings: Veterinary Programme*. pp. 537-538.

Arnbjerg,J. and Heje,N.I. (1993). Fabellae and popliteal sesamoid bones in cats. *Journal of Small Animal Practice*. **34**, 95–98.

Ashraf,S. and Walsh,D.A. (2008). Angiogenesis in osteoarthritis. *Current Opinion in Rheumatology*. **20**, 573–580.

Asokananthan,N., Graham,P.T., Stewart,D.J., Bakker,A.J., Eidne,K.A., Thompson,P.J. and Stewart,G.A. (2002). House dust mite allergens induce proinflammatory cytokines from respiratory epithelial cells: the cysteine protease allergen, Der p 1, activates Protease-Activated Receptor (PAR)-2 and inactivates PAR-1. *Journal of Immunology*. **169**, 4572–4578.

Attur,M., Al-Mussawir,H.E., Patel,J., Kitay,A., Dave,M., Palmer,G., Pillinger,M.H. and Abramson,S.B. (2008). Prostaglandin E2 exerts catabolic effects in osteoarthritis cartilage: evidence for signaling via the EP4 receptor. *Journal of Immunology*. **181**, 5082–5088.

Ayers,D., Clements,D.N., Salway,F. and Day,P.J.R. (2007). Expression stability of commonly used reference genes in canine articular connective tissues. *BMC Veterinary Research*. **3**, 7.

Baird,D.K., Hathcock,J.T., Kincaid,S.A., Rumph,P.F., Kammermann,J., Widmer,W.R., Visco,D. and Sweet,D. (1998). Low-field magnetic resonance imaging of early subchondral cyst-like lesions in induced cranial cruciate ligament deficient dogs. *Veterinary Radiology and Ultrasound*. **39**, 167–173.

Barck,K.H., Lee,W.P., Diehl,L.J., Ross,J., Gribling,P., Zhang,Y., Nguyen,K., van Bruggen,N., Hurst,S. and Carano,R.A.D. (2004). Quantification of cortical bone loss and repair for therapeutic evaluation in collagen-induced arthritis, by micro-computed tomography and automated image analysis. *Arthritis and Rheumatology*. **50**, 3377–3386.

Bardet,J. (1998). Diagnosis of shoulder instability in dogs and cats: a retrospective study. *Journal of American Animal Hospital Association*. **34**, 42–54.

Beale,B.S., Hulse,D., Schulz,K. and Whitney,W. (2003). Arthroscopically assisted surgery of the elbow joint. In: *Small Animal Arthroscopy*, 1st edn. pp. 51-79.

Beck,A.L., Pead,M.J. and Draper,E. (2005). Regional load bearing of the feline acetabulum. *Journal of Biomechanics*. **38**, 427–432.

Benaud,C.M., Oberst,M., Dickson,R.B. and Lin,C.-Y. (2002). Deregulated activation of matriptase in breast cancer cells. *Clinical and Experimental Metastasis*. **19**, 639–649.

Benito,M.J., Veale,D.J., FitzGerald,O., van den Berg,W.B. and Bresnihan,B. (2005). Synovial tissue inflammation in early and late osteoarthritis. *Annals of the Rheumatic Diseases*. **64**, 1263–1267.

Bennett,D. (1990). Diagnosis of joint disease. In: Whittick,W.G., (Ed.), *Canine Orthopedics*, 2nd edn. pp. 761–833.

Bennett,D. (2010). Canine and feline osteoarthritis. In: Ettinger,S.J. and Feldman, E.C., (Eds.), *Textbook of Veterinary Internal Medicine*, 7th edn. pp. 750–761.

Bennett,D., Ariffin,S.M.Z. and Johnston,P. (2012a). Osteoarthritis in the cat: 1. how common is it and how easy to recognise? *Journal of Feline Medicine and Surgery*. **14**, 65–75.

Bennett,D., Ariffin,S.M.Z. and Johnston,P. (2012b). Osteoarthritis in the cat: 2. how should it be managed and treated ? *Journal of Feline Medicine and Surgery*. **14**, 76-84.

Bennett,D. and Clarke,S. (2004). Feline osteoarthritis. In: *12th European Society of Veterinary Orthopaedics and Traumatology Congress Munich*. pp. 14.

Bennett,D. and May,C. (1995). Joint diseases of dogs and cats. In: Ettinger, S.J., and Feldman,E.C., (Eds.), *Textbook of Veterinary Internal Medicine,* 3rd edn. pp. 2053.

Bennett,D. and Morton,C. (2009). A study of owner observed behavioural and lifestyle changes in cats with musculoskeletal disease before and after analgesic therapy. *Journal of Feline Medicine and Surgery*. **11**, 997–1004.

Bennett,D., Tennant,B., Lewis,D.G., Baughan,J., May,C. and Carter,S. (1988). A reappraisal of anterior cruciate ligament disease in the dog. *Journal of Small Animal Practice*. **29**, 275–297.

Bennett,G.A., Waine,H. and Bauer,W. (1942). Changes in the knee joint at various ages. *The American Journal of Medicine*. **205**, 136–137.

Biery,D.N., Goldschmidt,M., Riser,W.H. and Rhodes,W.H. (1976). Bone cysts in the dog. *Veterinary Radiology*. **17**, 202–212.

Blanco,F.J., Guitian,R., Vazquez-Martul,E.J., de Toro,F.J., and Galdo,F. (1998). Osteoarthritis chondrocytes die by apoptosis. A possible pathway for osteoarthritis pathology. *Arthritis and Rheumatology*. **41**, 284–289.

Blom,A.B., and van den Berg,W.B. (2007). The synovium and its role in osteoarthritis. In: Bronner, F. and Farach-Carson, M.C., (Eds.), *Bone and Osteoarthritis*, 1st edn. pp. 65–79.

Blom,A.B., van Lent,P.L.E.M., Holthuysen,A.E.M., van der Kraan,P.M., Roth,J., van Rooijen,N., and van den Berg,W.B. (2004). Synovial lining macrophages mediate osteophyte formation during experimental osteoarthritis. *Osteoarthritis and Cartilage*. **12**, 627–635.

Bobinac,D., Spanjol,J., Zoricic,S. and Maric,I. (2003). Changes in articular cartilage and subchondral bone histomorphometry in osteoarthritic knee joints in humans. *Bone*. **32**, 284–290.

Boczek-Funcke,A., Kuhtz-Buschbeck,J., Paschmeyer,B. and Illert,M. (2000). X-ray kinematic analysis of forelimb movements during target reaching and food taking in the cat. *European Journal of Neuroscience*. **12**, 1817–1826.

Boileau,C., Amiable,N., Martel-Pelletier,J., Fahmi,H., Duval,N. and Pelletier, J.P. (2007). Activation of proteinase-activated receptor-2 in human osteoarthritic cartilage upregulates catabolic and proinflammatory pathways capable of inducing cartilage degradation: a basic science study. *Arthritis Research and Therapy*. **9**, R121.

Boileau,C., Martel-Pelletier,J., Caron,J., Paré,F., Troncy,E., Moreau,M. and Pelletier,J.-P. (2009). Oral treatment with a *Brachystemma calycinum D* don plant extract reduces disease symptoms and the development of cartilage lesions in experimental dog osteoarthritis: inhibition of protease-activated receptor-2. *Annals of Rheumatology Disease*. **69**, 1179–1184.

Bonaventure,J., Kadhom,N., Cohen-Solal,L., Ng,K.H., Bourguignon,J., Lasselin,C. and Freisinger,P. (1994). Reexpression of cartilage-specific genes by dedifferentiated human articular chondrocytes cultured in alginate beads. *Experimental Cell Research*. **212**, 97–104.

Bonnett,C.S. and Walsh,D.A. (2005). Osteoarthritis, angiogenesis and inflammation. *Rheumatology (Oxford)*. **44**, 7–16.

Botter,S.M., van Osch,G.J.V.M., Waarsing,J.H., Day,J.S., Verhaar,J.A.N., Pols,H.A.P., van Leeuwen,J.P.T.M. and Weinans,H. (2006). Quantification of subchondral bone changes in a murine osteoarthritis model using micro-CT. *Biorheology*. **43**, 379–388.

Boulay,J.P. (1998). Fragmented medial coronoid process of the ulna in the dog. *Veterinary Clinics of North America: Small Animal Practice*. **28**, 51–74.

Boulocher,C.B., Viguier,E.R., Cararo,R.D.R., Fau,D.J., Arnault,F., Collard,F., Maitre,P.A., Roualdes,O., Duclos,M.E., Vignon,E.P. and Roger,T.W. (2010). Radiographic assessment of the femorotibial joint of the CCLT rabbit experimental model of osteoarthritis. *BMC Medical Imaging*. **10**:3.

Boyd,S.K., Muller,R., Leonard,T. and Herzog,W. (2005). Long-term periarticular bone adaptation in a feline knee injury model for post-traumatic experimental osteoarthritis. *Osteoarthritis Cartilage*. **13**, 235–242.

Boyd,S.K., Muller,R. and Zernicke,R.F. (2002). Mechanical and architectural bone adaptation in early stage experimental osteoarthritis. Journal of Bone and Mineral Research. **17**, 687–694.

Brandt,K.D., Braunstein,E.M., Visco,D.M., O'Connor,B.L., Heck,D. and Albrecht,M. (1991). Anterior (cranial) cruciate ligament transection in the dog: a bona fide

model of osteoarthritis, not merely of cartilage injury and repair. *Journal of Rheumatology*. **18**, 436–446.

Bredella,M., Tirman,P., Peterfy,C.G., Zarlingo,M., Feller,J.F., Bost,F.W., Belzer,J.P., Wischer,T.K. and Genant,H.K. (1999). Accuracy of T2-weighted fast spin-echo MR imaging with fat saturation in detecting cartilage defects in the knee: comparison with arthroscopy in 130 patients. *American Journal of Roentgenology*. **172**, 1073–1080.

Buckland-Wright,C. (2003). Imaging osteoarthritis and related disorders. In: Hochberg, M., Silman, A., Smolen, J., Weinblatt, M. and Weisman, M., (Eds.), *Rheumatology*, 3rd edn. pp. 1823–1833.

Buckwalter,J.A., Mankin,H.J. and Grodzinsky,A.J. (2005). Articular cartilage and osteoarthritis. *Instructional course lectures*. **54**, 465–480.

Bullough,P.G. and Jagannath,A. (1983). The morphology of the calcification front in articular cartilage. *Journal of Bone and Joint Surgery*. **65-B**, 72–78.

Burr, D.B. and Gallant,M.A. (2012). Bone remodelling in osteoarthritis. *Nature Reviews Rheumatology*. **8**, 665–673.

Burr,D.B. and Radin, E.L. (1990). Trauma as a factor in the initiation of osteoarthritis. In: Brandt,K.D. (Ed.), *Cartilage Changes in Osteoarthritis*, 1st edn. pp. 73–80.

Burr,D.B. and Schaffler,M.B. (1997). The involvement of subchondral mineralized tissue in osteoarthrosis: quantitative microscopic evidence. *Microscopy Research and Technique*. **37**, 343–357.

Burton,N.J., Dobney,J.A., Owen,M.R. and Colborne,G.R. (2008). Joint angle, moment and power compensations in dogs with fragmented medial coronoid process. *Veterinary Comparative Orthopaedic and Traumatology*. **21**, 110–118.

Buschmann,M.D., Gluzband,Y.A., Grodzinsky,A.J., Kimura,J.H., and Hunziker,E.B. (1992). Chondrocytes in agarose culture synthesize a mechanically functional extracellular matrix. *Journal of Orthopaedic Research*. **10**, 745–758.

Carlson,C.S., Loeser,R.F., Jayo,M.J., Weaver,D.S., Adams,M.R. and Jerome,C.P. (1994). Osteoarthritis in cynomolgus macaques: a primate model of naturally occurring disease. *Journal of Orthopaedic Research*. **12**, 331–339.

Carman,W.J., Sowers,M., Hawthorne,V.M. and Weissfeld,L.A. (1994). Obesity as a risk factor for osteoarthritis of the hand and wrist: a prospective study. *The American Journal of Epidemiology*. **139**, 119–129.

Carrig,C.B. (1997). Diagnostic imaging of osteoarthritis. *Veterinary Clinics of North America: Small Animal Practice*. **27**, 777–814.

Castor,C.W. (1960). The microscopic structure of normal human synovial tissue. *Arthritis and Rheumatology*. **3**, 140–151.

Cerveny,C. and Paral,V. (1995). Sesamoid bones of the knee joint of the Puma Concolor. *Acta Veterinaria Brno*. **64**, 79–82.

Chaisson,C.E., Gale,D.R., Gale,E., Kazis,L., Skinner,K. and Felson,D.T. (2000). Detecting radiographic knee osteoarthritis: what combination of views is optimal? *Rheumatology (Oxford)*. **39**, 1218–1221.

Chakrabarti,S., Syme,H.M., Brown,C.A, and Elliott,J. (2012). Histomorphometry of feline chronic kidney disease and correlation with markers of renal dysfunction. *Veterinary Pathology*. **50**, 147–155.

Champagne,C.M., Takebe,J., Offenbacher,S. and Cooper,L.F. (2002). Macrophage cell lines produce osteoinductive signals that include bone morphogenetic protein-2. *Bone*. **30**, 26–31.

Chen,T.-L., Lin,Y.-F., Cheng,C.-W., Chen,S.-Y., Sheu,M.-T., Leung,T.-K., Qin,C.-H. and Chen,C.-H. (2011). Anti-Inflammatory mechanisms of the proteinase-activated receptor 2-inhibiting peptide in human synovial cells. *Journal of Biomedical Sciences*. **18**, 43.

Chhem,R.K., Kaplan,P.A. and Dussault,R.G. (1994). Ultrasonography of the musculoskeletal system. *Radiologic Clinics of North America*. **32**, 275–289.

Chubinskaya,S., Kuettner,K.E. and Cole,A.A. (1999). Expression of matrix metalloproteinases in normal and damaged articular cartilage from human knee and ankle joints. *Laboratory Investigation*. **79**, 1669–1677.

Clarke,S.P. and Bennett,D. (2005). Feline osteoarthritis: provisional results of a prospective study. In: *British Small Animal Veterinary Association Congress 2005 Scientific Proceedings: Veterinary Programme*. pp. 620.

Clarke,S.P. and Bennett,D. (2006). Feline osteoarthritis: a prospective study of 28 cases. Journal of Small Animal Practice. **47**, 439–445.

Clarke,S.P., Mellor,D., Clements,D.N., Gemmil,T., Farrell,M., Carmichael,S. and Bennett,D. (2005). Prevalence of radiographic signs of degenerative joint disease in a hospital population of cats. *Veterinary Record*. **157**, 793–799.

Cook,J.L., Kuroki,K., Visco,D., Pelletier,J.-P., Schulz,L. and Lafeber,F.P.J.G. (2010). The OARSI histopathology initiative-recommendations for histological assessments of osteoarthritis in the dog. *Osteoarthritis and Cartilage*. **18**, S66–S79.

Cooper,G. and Schiller,A.L. (1975). The skeletal system. In: *Anatomy of the Guinea Pig*, 1st edn. pp. 17–79.

Coughlan,A.R., Robertson,D.H., Burke,R., Beynon,R.J. and Carter,S.D. (1998). Isolation and identification of canine matrix metalloproteinase-2 (MMP-2). *Veterinary Journal*. **155**, 231–237.

Coughlin,S.R., Vu,T.K., Hung,D.T. and Wheaton,V.I. (1992). Characterization of a functional thrombin receptor. Issues and opportunities. *Journal of Clinical Investigation*. **89**, 351–355.

Craig,E., Hohn,R.B. and Anderson,W.D. (1980). Surgical stabilization of traumatic medial shoulder dislocation. *Journal of the American Animal Hospital Association*. **16**, 93–102.

Craig,L.E. and Reed,A. (2012). Age-associated cartilage degeneration of the canine humeral head. *Veterinary Pathology*. **50**, 264–268.

Cutolo,M., Sulli,A., Barone,A., Seriolo,B. and Accardo,S. (1993). Macrophages, synovial tissue and rheumatoid arthritis. *Clinical and Experimental Rheumatology*. **11**, 331–339.

D'Anjou,M.-A., Troncy E., Moreau,M., Abram,F., Raynauld,J.-P., Martel-Pelletier,J., and Pelletier,J.-P. (2008). Temporal assessment of bone marrow lesions on magnetic resonance imaging in a canine model of knee osteoarthritis: impact of sequence selection. *Osteoarthritis Cartilage*. **16**, 1307–1311.

Dancey,C. and Reidy,J. (2004). *Statistics without maths for psychology*, 5th Edn. pp. 191-206.

De Bakker,E., Saunders,J., Gielen,I., van Bree,H., Coppieters,E. and Van Ryssen,B. (2012). Radiographic findings of the medial humeral epicondyle in 200 canine elbow joints. *Veterinary and Comparative Orthopaedics and Traumatology*. **25**, 359–365.

De Mos,M., Koevoet,W.J.L.M., Jahr,H., Verstegen,M.M.A., Heijboer,M.P., Kops,N., van Leeuwen,J.P.T.M., Weinans,H., Verhaar,J.A.N. and van Osch,G.J.V.M. (2007). Intrinsic differentiation potential of adolescent human tendon tissue: an in-vitro cell differentiation study. *BMC Musculoskeletal Disorder*. **8**:16.

Dedrick,D.K., Goldstein,S.A., Brandt,K.D., O'Connor,B.L., Goulet,R.W. and Albrecht,M. (1993). A longitudinal study of subchondral plate and trabecular bone in cruciate-deficient dogs with osteoarthritis followed up for 54 months. *Arthritis and Rheumatology*. **36**, 1460–1467.

Dennis,R., Kiberger,R.M., Wrigley,R.H. and Barr,F.J. (2001). Joints. In: *Hand Book of Small Animal Radiological Differential Diagnosis*, 1st edn. pp. 31–38.

Denny,H.R. and Butterworth,S.J. (2000). The stifle. In: Denny, H.R. (Ed.), *A Guide to Canine and Feline Orthopaedis Surgery*, 4th edn. pp. 512–553.

Dery,O., Corvera,C.U., Steinhoff,M. and Bunnett,N.W. (1998). Proteinase-activated receptors: novel mechanisms of signaling by serine proteases. *American Journal of Physiology*. **274**, C1429–1452.

Dewire,P. and Simkin,P.A. (1996). Subchondral plate thickness reflects tensile stress in the primate acetabulum. *Journal of Orthopeadic Research*. **14**, 838–841.

DiBartola,S.P., Rutgers,H.C., Zack,P.M. and Tarr,M.J. (1987). Clinicopathologic findings associated with chronic renal disease in cats: 74 cases (1973-1984). *Journal of the American Veterinary Medical Association*. **190**, 1196–202.

Disler,D. (1997). Fat-suppressed three-dimensional spoiled gradient-recalled MR imaging: assessment of articular and physeal hyaline cartilage. *American Journal of Roentgenology*. **169**, 1117–1123.

Djurasovic,M., Aldridge,J.W., Grumbles,R., Rosenwasser,M.P., Howell,D. and Ratcliffe,A. (1998). Knee joint immobilization decreases aggrecan gene expression in the meniscus. *The American journal of sports medicine*. **26**, 460–466.

Dmitrovsky,E., Lane,L.B., and Bullough,P.G. (1978). The characterization of the tidemark in human articular cartilage. *Metabolic Bone Disease and Related Research*. **1**, 115–118.

Dolieslager,S.M.J., Lappin, D.F., Bennett, D., Graham, L., Johnston, N. and Riggio, M.P. (2013). The influence of oral bacteria on tissue levels of Toll-like receptor and cytokine mRNAs in feline chronic gingivostomatitis and oral health. *Veterinary Immunology and Immunopathology*. **151**, 263–274.

Draffan,D., Carrera,I., Carmichael,S., Heller,J. and Hammond,G. (2009). Radiographic analysis of trochlear notch sclerosis in the diagnosis of osteoarthritis secondary to medial coronoid disease. *Veterinary Comparative Orthopaedic and Traumatology*. **22**, 7–15.

Duncan,H., Jundt,J.W., Riddle,J.M., Pitchford,W. and Christopherson,T. (1987). The tibial subchondral plate. A scanning electron microscopic study. *Journal of Bone and Joint Surgery*. **69**, 1212–1220.

Dundas,J. and Ling,M. (2012). Reference genes for measuring mRNA expression. *Theory in Biosciences*. **131**, 215–223.

Durr,H.D., Martin,H., Pellengahr,C., Schlemmer,M., Maier,M. and Jansson,V. (2004). The cause of subchondral bone cysts in osteoarthrosis: a finite element analysis. *Acta Orthopaedica Scandinavica*. **75**, 554–558.

Dyce,K.M., Sack,W.O. and Wensing,C.J.G. (2002). Chapter 1: Some basic facts and concepts. In: Dyce,K.M., Sack,W.O. and Wensing,C.J.G., (Eds.), *Textbook of Veterinary Anatomy*, 3rd edn. pp. 1–34.

Dyce,K.M., Sack,W.O. and Wensing,C.J.G. (2010). Chapter 2: The locomotor apparatus. In: Dyce,K.M., Sack,W.O. and Wensing,C.J.G., (Eds.), *Textbook of Veterinary Anatomy*, 4th edn. pp. 32-99.

Edinger,D.T. and Manley,P.A. (1998). Arthrodesis of the shoulder for synovial osteochondromatosis. *The Journal of Small Animal Practice*. **39**, 397-400.

Edwards,J.C.W. and Willoughby,D.A. (1982). Demonstration of bone marrow-derived cells in synovial lining by means of giant intracellular granules as genetic markers. *Annals of the Rheumatic Diseases*. **41**, 177–182.

Elliott,J. and Barber,P.J. (1998). Feline chronic renal failure: clinical findings in 80 cases diagnosed between 1992 and 1995. Journal of Small Animal Practice. **39**, 78–85.

Engelke,E., Pfarrer,C. and Waibl,H. (2011). Anatomy of the collateral ligaments of the feline elbow joint: functional implications. *Anatomia, Histologia, Embryologia*. **40**, 80–88.

Engiles,J.B. (2013). Disease of the skeletal system. In: Buergelt,C.D. and Piero,F.D., (Eds), *Color atlas of equine pathology*, 1st edn. pp. 301-343.

Farese,J.P., Todhunter,R.J., Lust,G., Williams,A.J. and Dykes,N.L. (1998). Dorsolateral subluxation of hip joints in dogs measured in a weight-bearing position with radiography and computed tomography. *Veterinary Surgery*. **27**, 393–405.

Ferrell,W.R., Kelso,E.B., Lockhart,J.C., Plevin,R. and McInnes,I.B. (2010). Protease-activated receptor 2: a novel pathogenic pathway in a murine model of osteoarthritis. *Annals of the Rheumatic Diseases*. **69**, 2051–2054.

Ferrell,W.R., Lockhart,J.C., Kelso,E.B., Dunning,L., Plevin,R., Meek,S.E., Smith,A.J.H., Hunter,G.D., McLean,J.S., McGarry,F., Ramage,R., Jiang,L., Kanke,T. and Kawagoe,J. (2003). Essential role for proteinase-activated receptor-2 in arthritis. *The Journal of Clinical Investigation*. **111**, 35–41.

Fife,R.S., Brandt,K.D., Braunstein,E.M., Katz,B.P., Shelbourne,K.D., Kalasinski,L.A. and Ryan,S. (1991). Relationship between arthroscopic evidence of cartilage damage and radiographic evidence of joint space narrowing in early osteoarthritis of the knee. *Arthritis and Rheumatology*. **34**, 377–382.

Flo,G.L., Stickle,R.L. and Dunstan,R.W. (1987). Synovial chondrometaplasia in five dogs. *Journal of the American Veterinary Medical Association*. **11,** 1417-1422.

Franssen,M.J., Boerbooms,A.M., Karthaus,R.P., Buijs,W.C. and van de Putte,L.B. (1989). Treatment of pigmented villonodular synovitis of the knee with yttrium-90 silicate: prospective evaluations by arthroscopy, histology, and 99mTc pertechnetate uptake measurements. *Annals of Rheumatic Diseases*. **48**, 1007–1013.

Freire,M., Brown,J., Robertson,I.D., Pease,A.P., Hash,J., Hunter,S., Simpson,W., Sumrell,A.T. and Lascelles,B.D.X. (2010). Meniscal mineralization in domestic cats. *Veterinary Surgery*. **39**, 545–552.

Freire,M., Meuten,D. and Lascelles,D. (2014). Pathology of articular cartilage and synovial membrane from elbow joints with and without degenerative joint disease in domestic cats. *Veterinary Pathology*. **51,** 968-978.

Freire,M., Robertson,I., Bondell,H.D., Brown,J., Hash,J., Pease,A.P. and Lascelles,B.D.X. (2011). Radiographic evaluation of feline appendicular degenerative joint disease vs. macroscopic appearance of articular cartilage. *Veterinary Radiology and Ultrasound*. **52**, 239–247.

Frisbie,D.D., Ghivizzani,S.C., Robbins,P.D., Evans,C.H. and McIlwraith,C.W. (2002). Treatment of experimental equine osteoarthritis by in vivo delivery of the equine interleukin-1 receptor antagonist gene. *Gene Therapy*. **9**, 12–20.

Gabriel,N., Innes,J.F., Caterson,B. and Vaughan-Thomas,A. (2010). Development of an in vitro model of feline cartilage degradation. *Journal of Feline Medicine and Surgery*. **12**, 614–620.

Gahunia,H.K., Babyn,P., Lemaire,C., Kessler,M.J. and Pritzker,K.P.H. (1995). Osteoarthritis staging: comparison between mahnetic resonance imaging, gross

pathology and histopathology in the rhesus macaque. *Osteoarthritis and Cartilage*. **3**, 169–180.

Ganey,T.M., Ogden,J.A., Abou-Madi,N., Colville,B., Zdyziarski,J.M. and Olsen,J.H. (1994). Meniscal ossification. II. The normal pattern in the tiger knee. *Skeletal Radiology*. **23**, 173–179.

Gilbertson,E.M.M. (1975). Development of periarticular osteophytes in experimentally induced osteoarthritis in the dog. A study using microradiographic, microangiographic, and fluorescent bone-labelling techniques. *Annals of Rheumatic Diseases*. **34**, 12–25.

Godfrey,D.R. (2000). Preliminary retrospective study of osteoarthritis in the legs of cats. In: *British Small Animal Veterinary Association Congress 2000 Scientific Proceedings: Veterinary Programme*. pp. 289.

Godfrey,D.R. (2002). Osteoarthritis in cats: a retrospective series of 31 cases. *Journal of Small Animal Practice*. **43**, 260.

Godfrey,D.R. (2003). Osteoarthritis in cats: a prospective series of 40 cases. *Journal of Small Animal Practice*. **44**, 418.

Godfrey,D.R. (2005). Osteoarthritis in cats: a retrospective radiological study. *Journal of Small Animal Practice*. **46**, 425 –429.

Godfrey,D.R. (2007). Studies of osteoarthritis in domestic cats (*felis catus*). Diploma Fellowship Thesis, Royal College of Veterinary Surgeons.

Godfrey,D.R. (2011). Diagnosis and management of osteoarthritis in cats. *In Practice*. **33**, 380-385.

Goggs,R., Carter,S.D., Schulze-Tanzil,G., Shakibaei,M. and Mobasheri,A. (2003). Apoptosis and the loss of chondrocyte survival signals contribute to articular cartilage degradation in osteoarthritis. *Veterinary Journal*. **166**, 140–158.

Gowan,R.A., Lingard,A.E., Johnston,L., Stansen,W., Brown,S.A. and Malik,R. (2011). Retrospective case-control study of the effects of long-term dosing with meloxicam on renal function in aged cats with degenerative joint disease. *Journal of Feline Medicine and Surgery*. **13**, 752–761.

Greene,E.C. (1955). Skeleton. In: Greene,E.C. (Ed.), *Anatomy of the Rat*. No.27, pp. 5–30.

Greene,J.P., Lefebvre,S.L., Wang,M., Yang,M., Lund,E.M. and Polzin,D.J. (2014). Risk factors associated with the development of chronic kidney disease in cats evaluated at primary care veterinary hospitals. *Journal of American Veterinary Medical Association*. **244**, 320–327.

Greenman,Y. and Stern,N. (2009). Non-functioning pituitary adenomas. *Best Practice and Research Clinical Endocrinology and Metabolism*. **23**, 625–638.

Grynpas,M.D., Alpert,B., Katz,I., Lieberman,I. and Pritzker,K.P. (1991). Subchondral bone in osteoarthritis. *Calcified Tissue International*. **49**, 20–26.

Guillot,M., Moreau,M., Marc-Andre,D., Pelletier,J.-P., Pelletier,J.M., and Troncy,E. (2012). Evaluation of osteoarthritis in cats: novel information from a pilot study. *Veterinary Surgery*. **41**, 328–335.

Gunew,M.N., Menrath,V.H., Marshall,R.D. (2008). Long-term safety, efficacy and palatability of oral meloxicam at 0.01-0.03 mg/kg for treatment of osteoarthritic pain in cats. Journal of Feline Medicine and Surgery. **10**, 235–241.

Gupta,K.B., Duryea,J. and Weissman,B.N. (2004). Radiographic evaluation of osteoarthritis. *Radiologic Clinics of North America*. **42**, 11-41.

Guthrie,S. (1989). Use of a radiographic scoring technique for the assessment of dogs with elbow osteochondrosis. *Journal of Small Animal Practice*. **30**, 639–644.

Hammond,G. and McConnell,F. (2013). Radiology of the appendicular skeleton. In: Holloway,A. and McConnell,F. (Eds.), *BSAVA Manual of Canine and Feline Radiography and Radiology. A Foundation Manual*, 1st edn. pp. 240-246.

Harasen,G.L.G. (2005). Feline cranial cruciate ligament rupture. 17 cases and review of the literature. *Veterinary and Comparative Orthopaedics and Traumatology*. **4**, 254–257.

Hardie,E.M., Roe,S.C. and Martin,F.R. (2002). Radiographic evidence of degenerative joint disease in geriatric cats: 100 cases (1994-1997). *Journal of the American Veterinary Medical Association*. **220**, 628–632.

Hardingham,T.,and Bayliss,M. (1990). Proteoglycans of articular cartilage: changes in aging and in joint disease. *Arthritis and Rheumatology*. **20**, 12–33.

Hartmann,P., Stock,K.-F. and Distl,O. (2012). Multivariate prediction of breeding values for canine hip and elbow dysplasia as well as humeral osteochondrosis in the Bernese mountain dog. *Berliner und Münchener tierärztliche Wochenschrift*. **125**, 432–440.

Hashimoto,S., Ochs,R.L., Rosen,F., Quach,J., McCabe,G., Solan,J., Seegmiller,J.E., Terkeltaub,R. and Lotz,M. (1998). Chondrocyte-derived apoptotic bodies and calcification of articular cartilage. *Proceedings of the National Academy of Sciences of the United States of America*. **95**, 3094–3099.

Havelka,S., Horn,V., Spohrová,D. and Valouch,P. (1984). The calcified-noncalcified cartilage interface: the tidemark. *Acta Biologica Hungarica*. **35**, 271–279.

Hayami,T., Pickarski,M., Zhuo,Y., Wesolowski,G.A., Rodan,G.A. and Duong,L.T. (2006). Characterization of articular cartilage and subchondral bone changes in the rat anterior cruciate ligament transection and meniscectomized models of osteoarthritis. *Bone*. **38**, 234–243.

Hayes,C.W. and Conray,W.F. (1992). Evaluation of articular cartilage: radiographic and cross-sectional imaging techniques. *Radiographics*. **12**, 409–428.

Hayes,H.M., Wilson,G.P. and Burt,J.K. (1979). Feline hip dysplasia. *Journal of the American Veterinary Medical Association*. **5**, 447–448.

Haywood,L., McWilliams,D.F., Pearson,C.I., Gill,S.E., Ganesan,A., Wilson,D. and Walsh, D. (2003). Inflammation and angiogenesis in osteoarthritis. *Arthritis and Rheumatology*. **48**, 2173–2177.

Hebel,R. and Stromberg,M.W. (1976). Osteology. In: *Anatomy of the Laboratory Rat*, 6th Edn. pp. 1–17.

Hellio Le Graverand,M.P., Sciore,P., Eggerer,J., Rattner,J.P., Vignon,E., Barclay,L., Hart,D.A. and Rattner,J.B. (2001). Formation and phenotype of cell clusters in osteoarthritic meniscus. *Arthritis and Rheumatology*. **44**, 1808–1818.

Henrotin,Y., Pesesse,L. and Sanchez,C. (2012). Subchondral bone and osteoarthritis: biological and cellular aspects. *Osteoporosis International*. **23**, S847–S851.

Hewicker-Trautwein,M., Carter,S.D., Bennett,D. and Kelly,D.F. (1999). Immunocytochemical demonstration of lymphocyte subsets and MHC class II antigen expression in synovial membranes from dogs with rheumatoid arthritis and degenerative joint disease. *Veterinary Immunology and Immunopathology*. **67**, 341–357.

Hirota,Y., Osuga,Y., Hirata,T., Harada,M., Morimoto,C., Yoshino,O., Koga,K., Yano,T., Tsutsumi,O. and Taketani,Y. (2005). Activation of protease-activated receptor 2 stimulates proliferation and interleukin (IL)-6 and IL-8 secretion of endometriotic stromal cells. *Human Reproduction*. **20**, 3547–3553.

Hoch,B.L., Klein,M.J. and Schiller,A.L. (2008). Bones and joints. In: Rubin,R., and Strayer,D.S., (Eds.), *Rubin's Pathology Clinicopathologic Foundations of Medicine*, 5th edn. pp. 1083–1170.

Hoffmann,A.H. and Grigg,P. (1989). Measurements of joint capsule tissue loading in the cat knee using calibrated mechanoreceptors. *Journal of Biomechanics*. **22**, 787–791.

Hollander,A.P., Pidoux,I., Reiner,A., Rorabeck,C., Bourne,R. and Poole,A.R. (1995). Damage to type II collagen in aging and osteoarthritis starts at the articular surface, originates around chondrocytes, and extends into the cartilage with progressive degeneration. *The Journal of Clinical Investigation*. **96**, 2859–2869.

Holt,P. (1978). Hip dysplasia in a cat. *Journal of Small Animal Practice*. **19**, 273–276.

Hough,A.J. (1993). Pathology of osteoarthritis. In: McCarty,D.J. and Cooman,W.J. (Eds.*), Arthritis and Allied Conditions: A Text Book of Rheumatology*, 12th edn. pp. 1699–1721.

Houlton,J. (1994). Ancillary aids to the diagnosis of joint disease. In: Houlton,J. and Collinson,R.W. (Eds.), *Manual of Small Animal Arthrology. British Small Animal Veterinary Association*. pp. 22–38.

Hunziker,E.B., Kapfinger,E. and Geiss,J. (2007). The structural architecture of adult mammalian articular cartilage evolves by a synchronized process of tissue resorption and neoformation during postnatal development. *Osteoarthritis and Cartilage*. **15**, 403–413.

Ingman,A.M., Ghosh,P. and Taylor,T.K.F. (1974). Variation of collagenous and non-collagenous proteins of human knee joint menisci with age and degeneration. *Gerontologia*. **20**, 212–233.

Innes,J.F., Costello,M., Barr,F.J., Rudorf,H. and Barr,A.R.S. (2004). Radiographic progression of osteoarthritis of the canine stifle joint: a prospective study. *Veterinary Radiology and Ultrasound*. **45**, 143–148.

Jeffreys,T.E. (1967). Synovial chondromatosis. *Journal of Bone and Joint Surgery* (British). **49**, 530–534.

Jenkins,A.L., Chinni,C., De Niese,M.R., Blackhart,B. and Mackie,E.J. (2000). Expression of protease-activated receptor-2 during embryonic development. Developmental Dynamics. **218**, 465–471.

Jewell,F.M., Watt,I. and Doherty,M. (1998). Plain radiographic features of osteoarthritis. In: Jewell,F.M., Watt,I. and Doherty,M. (Eds), *Osteoarthritis*, pp. 217-237.

Jorgensen,B. and Jensen,H.E. (2002). Periarticular ossification at the elbow joint and meniscal ossification in the stifle joint of pigs occurrence, pathomorphology, breed differences and correlations with osteochondrosis, leg weakness and production parameters. *Journal of Veterinary Medicine. A, Physiology, Pathology, Clinical Medicine*. **49**, 353–357.

Kamishina,H. (2003). Degenerative joint disease of the hip in cats: imaging, pathology, and in vitro studies. PhD thesis, University of Florida.

Kamishina,H. and Miyabayashi,T. (2002). Degenerative joint disease in feline hip joints. A retrospective radiographic survey. In: *Annual Scientific Meeting of American College of Veterinary Radiology 2002*.

Kamishina,H., Miyabayashi,T., Clemmons,R.M., Farese,J.P., Uhl E.W. and Silver,X. (2006). High field (4.7 T) magnetic resonance imaging of feline hip joints. *The Journal of Veterinary Medical Science*. **68**, 285–288.

Kawabata,A., Kuroda,R., Minami,T., Kataoka,K. and Taneda,M. (1998). Increased vascular permeability by a specific agonist of protease-activated receptor-2 in rat hindpaw. *British Journal of Pharmacology*. **125**, 419–422.

Kealy,R.D., Lawler,D.F., Ballam,J.M., Mantz,S.L., Biery,D.N., Greeley,E.H., Lust,G., Segre,M., Smith,G.K. and Stowe,H.D. (2002). Effects of diet restriction on life span and age-related changes in dogs. *Journal of the American Veterinary Medical Association*. **220**, 1315–1320.

Keller,G.G., Reed,A.L., Lattimer,J.C. and Corley,E.A. (1999). Hip dysplasia: a feline population study. *Veterinary Radiology and Ultrasound*. **40**, 460–464.

Kellgren,J.H. and Lawrence,J.S. (1957). Radiological assessment of osteoarthrosis. Annals of Rheumatic Diseases. **16**, 494–502.

Kellgren,J.H. and Moore,R. (1952). Generalized osteoarthritis and Heberden's nodes. *British Journal of Medicine*. **1**, 181–187.

Kelso,E.B., Ferrell,W.R., Lockhart,J.C., Elias-Jones,I., Hembrough,T., Dunning,L., Gracie,J.A. and McInnes,I.B. (2007). Expression and proinflammatory role of proteinase-activated receptor 2 in rheumatoid synovium: ex vivo studies using a novel proteinase-activated receptor 2 antagonist. *Arthritis and Rheumatology*. **56**, 765–771.

Kessler,Y., Helfer-Hungerbuehler,A.K., Cattori,V., Meli,M.L., Zellweger,B., Ossent,P., Riond,B., Reusch,C.E., Lutz,H. and Hofmann-Lehmann,R. (2009). Quantitative TaqMan real-time PCR assays for gene expression normalisation in feline tissues. *BMC Molecular Biology*. **10**:106.

Killinger,Z., Kužma,M., Sterančáková,L. and Payer,J. (2012). Osteoarticular changes in acromegaly. *International Journal of Endocrinology*. **2012**, 839282.

Killinger,Z., Payer J., Lazurova,I., Imrich,R., Homerova,Z., Kuzma,M. and Rovensky,J. (2010). Arthropathy in acromegaly. *Rheumatic Disease Clinics of North America*. **36**, 713–720.

Kim,H.A., Lee,Y.J., Seong,S.C., Choe,K.W. and Song,Y.W. (2000). Apoptotic chondrocyte death in human osteoarthritis. *Journal of Rheumatology*. **27**, 455–462.

Kiviranta,I., Jurvelin,J., Tammi,M., Saamanen,A.M. and Helminen,H.J. (1987). Weight bearing controls glycosaminoglycan concentration and articular cartilage thickness in the knee joints of young beagle dogs. *Arthritis and Rheumatology*. **30**, 801–809.

Knight,A.D. and Levick,J.R. (1983). The density and distribution of capillaries around a synovial cavity. *Quarterly Journal of Experimental Physiology and Cognate Medical Sciences*. **68**, 629–644.

Konde,L.J., Thrall,M.A., Gasper,P., Dial,S.M., McBiles,K., Colgan,S. and Haskins,M. (1987). Radiographically visualised skeletal changes associated with mucopolysaccharidosis VI in cats. *Veterinary Radiology and Ultrasound*. **28**, 223–228.

Konig,H.C. and Liebich,H.G. (2007). Locomotor apparatus (apparatus locomotorius). In: Konig,H.C. and Liebich,H.G. (Eds.), *Veterinary Anatomy of Domestic Mammals*, 3rd edn. pp. 8–33.

Kramer,M., Gerwing,M., Hach,V. and Schimke,E. (1997). Sonography of the musculoskeletal system in dogs and cats. *Veterinary Radiology and Ultrasound*. **38**, 139–149.

Krey,P.R. and Cohen,A.S. (1973). Fine structural analysis of rabbit synovial cells. I. The normal synovium and changes in organ culture. *Arthritis and Rheumatology*. **16**, 324–340.

Kronfeld,D.S., Donoghue,S. and Glickman,L.T. (1994). Body condition of cats. *Journal of Nutrition*. **124**, 2683S–2684S.

Kwan Tat,S., Lajeunesse,D., Pelletier,J.-P. and Pelletier,J.M. (2010). Targeting subchondral bone for treating osteoarthritis: what is the evidence? *Best Practice and Research Clinical Rheumatology*. **24**, 51–70.

Laflamme,D.P. (2005). Nutrition for aging cats and dogs and the importance of body condition. *Veterinary Clinics of North America: Small Animal Practice*. **35**, 713–742.

Landells,J.W. (1953). The bone cysts of osteoarthritis. *Journal of Bone and Joint Surgery (British)*. **35-B**, 643–649.

Landis,J.R., Koch,G.G., Freeman,J.L., Freeman Jr,D.H. and Lehnen,R.C. (1977). A general methodology for the analysis of experiments with repeated measurement of categorical data. *Biometrics*. **33**, 138–158.

Langenbach,A., Green,P., Giger,U., Rhodes,H., Gregor,T.P., LaFond,E. and Smith,G. (1998). Relationship between degenerative joint disease and hip joint laxity by use of distraction index and Norberg angle measurement in a group of cats. *Journal of the American Veterinary Medical Association*. **213**, 1439–1443.

Lascelles,B.D.X. (2010). Feline degenerative joint disease. *Veterinary Surgery*. **39**, 2–13.

Lascelles,B.D.X., Hansen,B.D., Roe,S.C., DePuy,V., Thomson,A., Pierce,C.C., Smith,E.S. and Rowinski,E. (2007). Evaluation of client-specific outcome measures and activity monitoring to measure pain relief in cats with osteoarthritis. *Journal of Veterinary Internal Medicine*. **21**, 410–416.

Lascelles,B.D.X., Henry,J.B., Brown,J., Robertson,I., Sumrell,A.T., Simpson,W., Hansen,B.D., Zamprogno,H., Freire,M. and Pease,A.P. (2010). Cross-sectional study of the prevalence of radiographic degenerative joint disease in domesticated cats. *Veterinary Surgery*. **39**, 535–544.

Laverty,S., Girard,C.A., Williams,J.M., Hunziker,E.B. and Pritzker,K.P.H. (2010). The OARSI histopathology initiative, recommendations for histological assessments of osteoarthritis in the rabbit. *Osteoarthritis and Cartilage*. **18**,S53–S65.

Lawler,D.F., Evans,R.H., Chase,K., Ellersieck,M., Li,Q., Larson,B.T. and Satyaraj,E., Heininger,K. (2006). The aging feline kidney: a model mortality antagonist? *Journal of Feline Medicine and Surgery*. **8**, 363–371.

Le Minor,J.M. (1987). Comparative anatomy and significance of the sesamoid bone of the peroneus longus muscle (os peroneum). *Journal of Anatomy*.**151**, 85–99.

Leach,R.E., Gregg,T. and Siber,F.J. (1970). Weight-bearing radiography in osteoarthritis of the knee. *Radiology*. **97**, 265–268.

Leutenegger,C.M., Mislin,C.N., Sigrist,B., Ehrengruber,M.U., Hofmann-Lehmann,R. and Lutz,H. (1999). Quantitative real-time PCR for the measurement of feline cytokine mRNA. *Veterinary Immunology and Immunopathology*. **71**, 291–305.

Liebich,H.G., Konig,H.E. and Maierl,J. (2007). Chapter 3: forelimb or thoracic limb. In: Konig,H.E. and Liebich,H.G. (Eds.), *Veterinary Anatomy of Domestic Mammals*, 3rd edn. pp. 167–214.

Loeuille,D., Chary-Valckenaere,I., Champigneulle,J., Rat A.C., Toussaint,F. and Pinzano-Watrin,A. (2005). Macroscopic and microscopic features of synovial membrane inflammation in the osteoarthritic knee: correlating magnetic resonance imaging findings with disease severity. *Arthritis and Rheumatology*. **52**, 3492–3501.

Lotz, M. (1997). Cytokines and their receptors. In: Koopman,W.J. (Ed.), *Arthritis and Allied Condition*, 13th edn. pp. 439–478.

Loughin,C.A., Kerwin,S.C., Hosgood,G., Ringwood,P.B., Williams,J. and Stefanacci,J.D., McCarthy,R.J. (2006). Clinical signs and results of treatment in cats with patellar luxation: 42 cases (1992-2002). *Journal of the American Veterinary Medical Association*. **228**, 1370–1375.

Lugo,G., Pena,L. and Cordido,F. (2012). Clinical manisfestations and diagnosis of acromegaly. *International Journal of Endocrinology*. **2012**, 540398.

Lulich,J.P., Osborne,C.A., O'Brien,R.D. and Polzin,D.J. (1992). Feline renal failure: questions, answers, questions. *Compendium on Continuing Education for the Practising Veterinarian*. **67**, 127–153.

Lund,E.M., Armstrong,P.J., Kirk,C.A. and Klausner,J.S. (2005). Prevalence and risk factors for obesity in adult cats from private US veterinary practices. *International Journal of Applied Research in Veterinary Medicine*. **3**, 4–6.

Lyons,T.J., Stoddart,R.W., McClure,S.F. and McClure,J. (2005). The tidemark of the chondro-osseous junction of the normal human knee joint. *The Journal of Molecular Histology*. **36**, 207–215.

Ma, W. (2010). Chronic prostaglandin E2 treatment induces the synthesis of the pain-related peptide substance P and calcitonin gene-related peptide in cultured sensory ganglion explants. *Journal of Neurochemistry*. **115**, 363–372.

Maccoux,L.J., Salway,F., Day,P.J. and Clements D.M. (2007). Expression profiling of select cytokines in canine osteoarthritis tissues. Veterinary Immunology and Immunopathology. **118**, 59–67.

MacPhail,C.M. (2000). Treatment of canine osteoarthritis. *Waltham Focus*. **10**, 25–31.

Madry,H., Dijk,N. V. and Mueller-Gerbl,M. (2010). The basic science of the subchondral bone. *Knee Surgery, Sports Traumatology, Arthroscopy*. **18**, 419–433.

Malik,R., Allan,G.S., Howlett,C.R., Thompson,D.E., James,G., McWhirter,C. and Kendall,K. (1999). Osteochondrodysplasia in scottish fold cats. *The Australian Veterinary Journal*. **77**, 85–92.

Mankin,H.J. (1985). Normal articular cartilage and the alterations in osteoarthritis. In: Lombardino,J.G. (Ed.), *Nonsteroidal Antiinflammatory Drugs*, 1st edn. p. 28-29.

Mankin,H.J. and Brandt,K.D. (1997). Pathogenesis of osteoarthritis. In: Kelly,W.N., Harris,E.D., Ruddy,S. and Sledge,C.B. (Eds.), *Textbook of Rheumatology*, 5th edn. pp. 1369–1382.

Mankin,H.J., Dorfman,H., Lippiello,L. and Zarins,A. (1971). Biochemical and metabolic abnormalities in articular cartilage from osteoarthritic human hips. II. Correlation of morphology with biochemical and metabolic data. *Journal of Bone and Joint Surgery*. **53**, 523–537.

Marino,C.L., Lascelles,B.D.X., Vaden,S.L., Gruen,M.E. and Marks,S.L. (2013). Prevalence and classification of chronic kidney disease in cats randomly selected from four age groups and in cats recruited for degenerative joint disease studies. *Journal of Feline Medicine and Surgery*. **16**, 465–472.

Maroudas,A., Evans,H. and Almeida,L. (1973). Cartilage of the hip joint: topographical variation of glycosaminoglycan content in normal and fibrillated tissue. *Annals of Rheumatic Diseases*. **32**, 1–9.

Marshall,J.L. (1969). Periarticular osteophytes. Initiation and formation in the knee of the dog. *Clinical Orthopaedics and Related Research*. **62**, 37–47.

Marshall,J.L. and Olsson,S.-E. (1971). Instability of the knee: a long-term experimental study in dogs. *Journal of Bone and Joint Surgery*. **53**, 1561.

Martel-Pelletier,J. (2004). Pathophysiology of osteoarthritis. *Osteoarthritis and Cartilage*. **12**, 31–33.

Martel-Pelletier,J., Alaaeddine,N. and Pelletier,J.P. (1999). Cytokines and their role in the pathophysiology of osteoarthritis. *Frontiers in Bioscience*. **4**, D694–703.

McCulloch,R.S., Ashwell,M.S., O'Nan,A.T. and Mente,P.L. (2012). Identification of stable normalization genes for quantitative real-time PCR in porcine articular cartilage. *Journal of Animal Science and Biotechnology*. **3**, 36.

McDevitt,C.A. and Muir,H. (1976). Biochemical changes in the cartilage of the knee in experimental and natural osteoarthritis in the dog. Journal of Bone and Joint Surgery. **58**, 94–101.

McIlwraith,C.W., Frisbie,D.D., Kawcak,C.E., Fuller,C.J., Hurtig,M. and Cruz,A. (2010). The OARSI histopathology initiative - recommendations for histological assessments of osteoarthritis in the horse. *Osteoarthritis Cartilage*. **18**, S93–105.

McNicol,D. and Roughley,P.J. (1980). Extraction and characterization of proteoglycan from human meniscus. *The Biochemical Journal*. **185**, 705–713.

Meyer,P., Sick,H. and Grosshans,E. (1964). Adaptation fonctionnelle au glissement et a la reflexion des tendons, des poulies de reflexion des tendons et des ligaments articulaires. *ACTA Biologica Hungarica*. **75**, 745–770.

Michele,U., Gerwing,M., Kramer,M. and Schimke,E. (1998). Ultrasonographic possibilities in the elbow of the dog: anatomical structures and pathological findings. In: *Annual Conference on the DVG-FG on Small Animal Illnesses 1998*. pp. 385–388.

Mills,D.L. (1995). Feline joint problems. In: *Proceedings of the 5th American College of Veterinary Surgeons*. pp. 533–535.

Milner,J.M., Patel,A., Davidson,R.K., Swingler,T.E., Desilets,A., Young,D.A., Kelso,E.B., Donell,S.T., Cawston,T.E., Clark,I.M., Ferrell,W.R., Plevin,R., Lockhart,J.C., Leduc,R. and Rowan,A.D. (2010). Matriptase is a novel initiator of cartilage matrix degradation in osteoarthritis. *Arthritis and Rheumatology*. **62**, 1955–1966.

Mirza,H., Schmidt,V.A., Derian,C.K., Jesty,J. and Bahou,W.F. (1997). Mitogenic responses mediated through the proteinase-activated receptor-2 are induced by expressed forms of mast cell alpha- or beta-tryptases. *Blood*. **90**, 3914–3922.

Mistry,D., Oue,Y., Chambers,M.G., Kayser,M. V and Mason,R.M. (2004). Chondrocyte death during murine osteoarthritis. *Osteoarthritis and Cartilage*. **12**, 131–141.

Molino,M., Barnathan,E.S., Numerof,R., Clark,J., Dreyer,M., Cumashi,A., Hoxie,J.A., Schechter,N., Woolkalis,M. and Brass, L.F. (1997). Interactions of mast cell tryptase with thrombin receptors and PAR-2. *The Journal of Biological Chemistry*. **272**, 4043–4049.

Morgan,J.P. (1969). Radiological pathology and diagnosis of degenerative joint disease in the stifle joint of the dog. *Journal of Small Animal Practice*. **10**, 541–544.

Morgan,J.P. (1972). Chapter 3: the joints, osteoarthrosis. In: Morgan,J.P. (Ed.) *Radiology in Veterinary Orthopedics*, 1st edn. pp. 183-193.

Morgan,J.P. (1999). Radiographic diagnosis of joint disease. In: Morgan,J.P. (Ed.), *Radiology of Veterinary Orthopedics: Features of Diagnosis*, 2nd edn. pp. 169-236.

Mow,V. (1990). Structure-function relationships of articular cartilage and the effects of joint instability and trauma on cartilage function. In: Brandt,K. (Ed.), *Cartilage Changes in Osteoarthritis*. pp. 22–42.

Muhlbauer,M.C. and Kneller,S.K. (2013). Chapter 4: Musculoskeleton. In: Muhlbauer,M.C. and Kneller,S.K (Eds.), *Radiography of the dog and cat: guide to making and interpreting radiographs*, 1st edn. pp. 189-191.

Muir,H. (1986). Current and future trends in articular cartilage research and osteoarthritis. In: Kuettner,K.E., Schleyerbach,R. and Hascall,V.C. (Eds.), *Articular Cartilage Biochemistry*. 1st edn. pp. 423–440.

Murphy,S.T., Lewis,D.D., Shiroma,J.T., Neuwirth,L.A., Parker,R.B. and Kubilis,P.S. (1998). Effect of radiographic positioning on interpretation of cubital joint congruity in dogs. *American Journal of Veterinary Research*. **59**, 1351–1357.

Myers,S.L., Brandt,K.D., O'Connor,B.L., Visco,D.M. and Albrecht,M.E. (1990). Synovitis and osteoarthritic changes in canine articular cartilage after anterior cruciate ligament transection. Effect of surgical hemostasis. *Arthritis and Rheumatology*. **33**, 1406–1415.

Myers,S.L., Dines,K., Brandt,D.A., Brandt,K.D. and Albrecht,K.D. (1995). Experimental assessment by high frequency ultrasound of articular cartilage thickness and osteoarthritic changes. *Journal of Rheumatology*. **22**, 109–116.

Neogi,T. (2012). Clinical significance of bone changes in osteoarthritis. *Therapeutic Advances in Musculoskeletal Disease*. **4**, 259–267.

Nguyen Van,N., Taglinger,K., Helps,C.R., Tasker,S., Gruffydd-Jones,T.J. and Day,M.J. (2006). Measurement of cytokine mRNA expression in intestinal biopsies of cats with inflammatory enteropathy using quantitative real-time RT-PCR. *Veterinary Immunology and Immunopathology*. **113**, 404–414.

Nikahva,B., Nazhvani,S.D., Bagheri,M.H. and Tanideh,N. (2011). Radiographic follow up of early phases of osteoarthritis. *Global Veterinary*. **6**, 190–194.

Nolte-Ernsting,C.C.A., Adam,G., Buhne,M., Prescher,A. and Gunther,R.W. (1996). MRI of degenerative bone marrow lessions in experimental osteoarthritis of canine knee joints. *Skeletal Radiology*. **25**, 413–420.

Nystedt,S., Emilsson,K., Wahlestedt,C. and Sundelin,J. (1994). Molecular cloning of a potential proteinase activated receptor. *Proceedings of the National Academy of Sciences of the United States of America*. **91**, 9208–9212.

O'Connor,B.L. and McConnaughey,J.S. (1978). The structure and innervation of cat knee menisci, and their relation to a "sensory hypothesis" of mensical function. *American Journal of Anatomy*. **153**, 431–442.

Oberst,M.D., Singh,B., Ozdemirli,M., Dickson,R.B., Johnson,M.D. and Lin,C.-Y. (2003). Characterization of matriptase expression in normal human tissues. *Journal of Histochemistry and Cytochemistry*. **51**, 1017–1025.

Oehler,S., Neureiter,D., Meyer-Scholten,C. and Aigner,T. (2002). Subtyping of osteoarthritic synoviopathy. *Clinical and Experimental Rheumatology*. **20**, 633–640.

Oettmeier,R., Abendroth,K. and Oettmeier,S. (1989). Analyses of the tidemark on human femoral heads. II. Tidemark changes in osteoarthrosis--a histological and histomorphometric study in non-decalcified preparations. *Acta Morphologica Hungarica*. **37**, 169–180.

Okada,Y., Nakanishi,I. and Kajikawa,K. (1981). Secretory granules of B-cells in the synovial membrane. An ultra-structural and cytochemical study. *Cell and Tissue Research*. **216**, 131–141.

Olsson,S.-E. (1961). Roentgen examination of the hip joints of German Shepherd dogs. *Advances in Small Animal Practice*. **3**, 117–120.

Ondrouch,A.S. (1963). Cyst formation in osteoarthritis. *Journal of Bone and Joint Surgery (British)*. **45**, 755–760.

Owens,J.M. (1982). Chapter 3: the joints. In: Cann,C.C. (Ed.), *Radiographic Interpretation for the Small Animal Clinician*. 1st Edn. pp. 25–51.

Pacchiana,P.D., Gilley,R.S., Wallace,L.J., Hayden,D.W., Feeney,D.A., Jessen,C.R. and Aird,B. (2004). Absolute and relative cell counts for synovial fluid from clinically normal shoulder and stifle joints in cats. *Journal of the American Veterinary Medical Association*. **225**, 1866–1870.

Palanisamy,V., Jakymiw,A., Van Tubergen,E.A., D'Silva,N.J., Kirkwood,K.L. (2012). Control of cytokine mRNA expression by RNA-binding proteins and microRNAs. *Journal of Dental Research*. **91**, 651–658.

Pastoureau,P., Leduc,S., Chomel,A. and Ceuninck,F.D. (2003). Quantitative assessment of articular cartilage and subchondral bone histology in the meniscectomized guinea pig model of osteoarthritis. *Osteoarthritis and Cartilage*. **11**, 412–423.

Patsikas,M.N., Papazoglou,L.G., Komninou,A., Dessiris,A.K. and Tsimopoulos,G. (1998). Hip dysplasia in the cat: a report of three cases. *Journal of Small Animal Practice*. **39**, 290–294.

Pauli,C., Grogan,S.P., Patil,S., Otsuki,S., Hasegawa,A., Koziol,J., Lotz,M.K. and D'Lima,D.D. (2011). Macroscopic and histologic analysis of human knee menisci in aging and osteoarthritis. *Osteoarthritis and Cartilage*. *19*, 1132–1141.

Pearle,A.D., Warren,R.F. and Rodeo,S.A. (2005). Basic science of articular cartilage and osteoarthritis. *Clinical Journal of Sport Medicine*. **24**, 1–12.

Pearson,K. and Davin,A.G. (1921). On the sesamoids of the knee joint. Biometrika. **13**, 350–400.

Pedersen,H.E. (1949). The ossicles of the semilunar cartilages of rodents. *The Anatomical Record*. **95**, 1–9.

Peiffer,R.L., Young,W.O. and Blevins,W.E. (1974). Hip dysplasia and pectineus resection in the cat. *Feline Practice*. **4**, 40-43.

Pelletier,J.-P., Caron,J.P., Evans,C., Robbins,P.D., Georgescu,H.I., Jovanovic,D., Fernandes,J.C. and Martel-Pelletier,J. (1997). In vivo suppression of early experimental osteoarthritis by interleukin-1 receptor antagonist using gene therapy. *Arthritis and Rheumatology*. **40**, 1012–1019.

Pelletier,J.-P., Roughley,P., DiBattista,J., McCollum,R. and Martel-Pelletier,J. (1991). Are cytokines involved in osteoarthritic pathophysiology? *Seminars in Arthritis and Rheumatism*. **20**, 12–25.

Peng,X.-X., Zhao,R.-L., Song,W., Chu,H.-R., Li, M.,Song, S.-Y., Li,G.-Z. and Liang,D.-C. (2012). Selection of suitable reference genes for normalization of quantitative real-time PCR in cartilage tissue injury and repair in rabbits. *International Journal of Molecular Sciences*. **13**, 14344–14355.

Penning,L.C., Vrieling,H.E., Brinkhof,B., Riemers,F.M., Rothuizen,J., Rutteman,G.R. and Hazewinkel,H.A.W. (2007). A validation of 10 feline reference genes for gene expression measurements in snap-frozen tissues. *Veterinary Immunology and Immunopathology*. **120**, 212–222.

Pesesse,L., Sanchez,C. and Henrotin,Y. (2011). Osteochondral plate angiogenesis: a new treatment target in osteoarthritis. *Joint Bone Spine*. **78**, 144–149.

Peterfy,C.G. (2002). Imaging of the disease process. *Current Opinion in Rheumatology*. **14**, 590–596.

Peterson,M.E., Taylor,S., Greco,D.S., Nelson,R.W., Randolp,J.F., Foodman,M.S., Moroff,S.D., Morisson,S.A. and Lothrop,C.D. (1990). Acromegaly in 14 cats. *Journal of Veterinary Internal Medicine*. **4**, 192–201.

Petterson,H. and Sevelius,F. (1968). Subchondral bone cysts in the horse: a clinical study. *Equine Veterinary Journal*. **1**, 75–82.

Piscaer,T.M., van Osch,G.J.V.M., Verhaar,J.A.N. and Weinans,H. (2008a). Imaging of experimental osteoarthritis in small animal models. *Biorheology*. **45**, 355–364.

Piscaer,T.M., Waarsing,J.H., Kops,N., Pavljasevic,P., Verhaar,J.A.N., van Osch,G.J.V.M. and Weinans, H. (2008b). In vivo imaging of cartilage degeneration using microCT-arthrography. *Osteoarthritis and Cartilage*. **16**, 1011–1017.

Plewes,L.W. (1940). Osteo-arthritis of the hip. *British Journal of Surgery*. **27**, 682–695.

Pombo-Suarez,M., Calaza,M., Gomez-Reino,J.J. and Gonzalez,A. (2008). Reference genes for normalization of gene expression studies in human osteoarthritic articular cartilage. *BMC Molecular Biology*. **9**:17.

Poole,A.R. (1999). An introduction to the pathophysiology of osteoarthritis. *Frontiers in Bioscience*. **4**, 662–670.

Pritchett,J.W. (1984). The incidence of fabellae in osteoarthrosis of the knee. *The Journal of Bone & Joint Surgery (American)*. **66**, 1379-1380.

Pritzker,K.P.H., Gay,S., Jimenez,S.A., Ostergaard,K., Pelletier,J.-P., Revell,P.A., Salter,D., Path,F.R.C. and van den Berg,W.B. (2006). Osteoarthritis cartilage histopathology: grading and staging. *Osteoarthritis and Cartilage*. **14**, 13–29.

Prose,L.P. (1984). Anatomy of the knee joint of the cat. Acta Anatomica. **119**, 40-48.

Pujol,J.P., Galera,P., Redini,F., Mauviel,A. and Loyau. (1991). Role of cytokines in osteoarthritis: comparative effects of interleukin-1 and transforming growth factor-beta on cultured rabbit articular chondrocytes. *Journal of Rheumatology Supplement*. **27**, 76–79.

Quasnichka,H.L., Anderson-MacKenzie,J.M. and Bailey,A.J. (2006). Subchondral bone and ligament changes precede cartilage degradation in guinea pig osteoarthritis. *Biorheology*. **43**, 389–397.

Quintavalla,J., Kumar,C., Daouti,S., Slosberg,S. and Uziel-Fusi,S. (2005). Chondrocyte cluster formation in agarose cultures as a funtional assay to identify genes expressed in osteoarthritis. *The Journal of Cellular Physiology*. **204**, 560–566.

Raatikainen,T., Väänänen,K. and Tamelander,G. (1990). Effect of glycosaminoglycan polysulfate on chondromalacia patellae. A placebo-controlled 1-year study. *Acta Orthopaedica Scandinavica*. **61**, 443–448.

Rader,C.P., Baumann,B., Rolf, O., Radke,S., Hendrich,C., Schütze,N., Seufert,J. and Jakob,F. (2002). Detection of differentially expressed genes in particle disease using array-filter analysis. *Biomedizinische Technik. Biomedical engineering*. **47**, 111–116.

Radin,E.L., Paul I.L. and Lowry,M. (1970). A comparison of the dynamic force transmitting properties of subchondral bone and articular cartilage. *Journal of Bone and Joint Surgery*. **52-A**, 444–456.

Radin,E.L. and Rose,R.M. (1986). Role of subchondral bone in the initiation and progression of cartilage damage. *Clinical Orthopaedics and Related Research*. **213**, 34–40.

Radin,E.L., Schaffler,M.B., Gibson,G. and Tashman,S. (1995). Osteoarthrosis as the result of repetitive trauma. *Journal of the American Academy of Orthopaedic Surgeons*. **13**, 197–203.

Rahal,S.C., Filipi,M.G., Mamprim,M.J., Oliveira,H.S., Teixeira,C.R., Teixeira,R.H.F. and Monteiro,F.O.B. (2013). Meniscal mineralisation in little spotted cats. *BMC Veterinary Research*. **9**:50.

Ralphs,J.R. and Benjamin,M. (1994). The joint capsule: structure, composition, ageing and disease. *Journal of Anatomy*. **184**, 503–509.

Ramachandran,R., Morice,A.H. and Compton,S.J. (2006). Proteinase-activated receptor2 agonists upregulate granulocyte colony-stimulating factor, IL-8, and VCAM-1 expression in human bronchial fibroblasts. *American Journal of Respiratory Cell and Molecular Biology*. **35**, 133–141.

Rayward,R.M., Thomson,D.G., Davie,J.V., Innes,J.F. and Whitelock,R.G. (2004). Progression of osteoarthritis following TPLO surgery: a prospective radiographic study of 40 dogs. *Journal of Small Animal Practice*. **45**, 92–97.

Reboul,P., Pelletier,J.P., Tardif,J.M., Cloutier,J.-M. and Martell-Pelletier,J. (1996). The new collagenase, collagenase-3, is expressed and synthesized by human chondrocytes but not by synoviocytes. A role in osteoarthritis. *The Journal of Clinical Investigation*. **97**, 2011–2019.

Rech,M.P., Pirraino,D.W., Paletta,G.A., Schils,J.P. and Belhobek,G.P. (1996). Accuracy of fat-supressed three-dimensional spoiled gradient-echo FLASH MR imaging in the detection of patellofemoral articular cartilage abnormalities. *Radiology*. **198**, 209–212.

Reed,A.L., Payne,J.T. and Constantinescu,G.M. (1995). Ultrasonographic anatomy of the normal canine stifle. *Veterinary Radiology and Ultrasound*. **6**, 315–321.

Renberg,W.C. (2005). Pathophysiology and management of arthritis. *Veterinary Clinics of North America: Small Animal Practice*. **35**, 1073–1091.

Resnick,D. (1996). Degenerative disease of extraspinal locations. In: Resnick,D. and Kransdorf,M.J. (Eds.), Bone and Joint Imaging, 2nd edn. pp. 321-354.

Resnick,D. and Niwayama,G. (1983). Entheses and enthesopathy. Anatomical, pathological, and radiological correlation. *Radiology*. **146**, 1–9.

Riser,W.H. (1964). In: Catcott,E.J. (Ed.), *Feline medicine and surgery*, 1st edn. pp. 296.

Rochat,M.C. (2012). Chapter 51: Scapulohumeral Joint. In: Tobias.K. and Johnston,S. (Eds.) Veterinary Surgery: Small Animal (Volume 2), 1st edn. pp. 692-708.

Rogers,J., Shepstone,L. and Dieppe,P. (1997). Bone formers: osteophyte and enthesophyte formation are positively associated. *Annals of Rheumatic Diseases*. **56**, 85–90.

Roman-Blas,J.A., Castañeda,S., Largo R. and Herrero-Beaumont,G. (2009). Osteoarthritis associated with estrogen deficiency. *Arthritis Research and Therapy*. **11:** 241.

Roudier,M., Li,X., Niu,Q.-T., Pacheco,E., Pretorius,J.K., Graham,K., Yoon,B.-R.P., Gong J., Warmington,K., Ke,H.Z., Black,R.A., Hulme,J. and Babij,P. (2013). Sclerostin is expressed in articular cartilage but loss or inhibition does not affect cartilage remodeling during aging or following mechanical injury. *Arthritis and Rheumatology*. **65**, 721–31.

Ruthrauff,C.M., Glerum,L.E. and Gottfried,S.D. (2011). Incidence of meniscal injury in cats with cranial cruciate ligament ruptures. *The Canadian Veterinary Journal*. **52**, 1106–1110.

Ryan,J.M., Lascelles,B.D.X., Benito,J., Hash,J., Smith,S.H., Bennett,D., Argyle,D.J. and Clements,D.N. (2013). Histological and molecular characterisation of feline humeral condylar osteoarthritis. *BMC Veterinary Research*. **9**:110.

Rychel,J.K. (2010). Diagnosis and treatment of osteoarthritis. *Topics in Companion Animal Medicine*. **25**, 20–25.

Samii,V.F. and Long,C.D. (2002). Musculoskeletal system. In: Nyland,T.G. and Mattoon,J.S. (Eds.), *Small Animal Diagnostic Ultrasound*, 2nd edn. pp. 267–284.

Samoy,Y., Van Ryssen,B., Gielen,I., Walschot,N. and van Bree,H. (2006). Review of the literature: elbow incongruity in the dog. *Veterinary Orthopaedics and Traumatology*. **19**, 1–8.

Sandell,L.J. and Aigner,T. (2001). Articular cartilage and changes in arthritis. An introduction: cell biology of osteoarthritis. *Arthritis Research*. **3**, 107–113.

Sandell,L.J. (1995). Molecular biology of collagens in normal and osteoarthritic cartilage. In: Kuettner,K.E. and Goldberg,V.M. (Eds.), *Osteoarthritic Disorders*. pp. 131–146.

Sarin,V.K. and Carter,D.R. (2000). Mechanobiology and joint conformity regulate endochondral ossification of sesamoids. *Journal of Orthopaedic Research*. **18**, 706–712.

Sato,M., Ochi,T., Nakase,T., Hirota,S., Kitamura,Y., Nomura,S. and Yasui,N. (1999). Mechanical tension-stress induces expression of bone morphogenetic protein (BMP)-2 and BMP-4, but not BMP-6, BMP-7, and GDF-5 mRNA, during distraction osteogenesis. *Journal of Bone and Mineral Research*. **14**, 1084–95.

Schaefer,H. (1932). Die ossificationsvorgange im glied massen skelett der hauskatze. Morphol. *Jahrbuch*. **70**, 548–600.

Schmitz,N., Laverty,S., Kraus,V.B. and Aigner,T. (2010). Basic methods in histopathology of joint tissues. *Osteoarthritis and Cartilage*. **18**, S113–116.

Schrader,S.C. and Sherding,R.G. (1994). Disorders of the skeletal system. In: Sherding,R.G. (Ed.), *The Cat: Diseases and Clinical Management*, 2nd edn. pp. 1599–1645.

Schumacher,H.R. (1969). The microvasculature of the synovial membrane of the monkey: ultrastructural studies. *Arthritis and Rheumatology*. **12**, 387–404.

Shaw,N.E. and Martin,B.F. (1962). Histological and histochemical studies on mammalian knee joint tissues. *Journal of Anatomy (London)*. **96**, 359–373.

Siemering,G.H. (1978). Arthroscopy of dogs. *Journal of the American Veterinary Medical Association*. **172**, 575–577.

Simkin,P.A. (2008). A biography of the chondrocyte. *Annals of Rheumatic Diseases*. **67**, 1064–1068.

Simkin,P.A., Graney,D.O. and Fiechtner,J.J. (1980). Roman arches, human joints, and disease. *Arthritis and Rheumatology*. **23**, 1308–1311.

Simkin,P.A., Heston,T.F., Downey,D.J., Benedict,R.S. and Choi,H.S. (1991). Suchondral architecture in bones of the canine shoulder. *Journal of Anatomy*. **175**, 213–227.

Slingerland,L.I., Hazewinkel,H.A.W., Meij,B.P., Picavet,P. and Voorhout,G. (2011). Cross-sectional study of the prevalence and clinical features of osteoarthritis in 100 cats. *Veterinary Journal*. **187**, 304–309.

Smillie,I.S. (1970). In: Smillie,I.S. (Ed.), *Injuries of the knee joint*, 4th edn.

Smith,G.K., Biery,D.N., Gregor,T.P. (1990). New concepts of coxofemoral joint stability and the development of a clinical stress-radiographic method for quantitating hip joint laxity in the dog. *Journal of the American Veterinary Medical Association*. **196**, 56–70.

Smith, M.D. (2011). The normal synovium. *Open Rheumatology*. **5**, 100–116.

Smith,M.D., Triantafillou,S., Parker,A., Youssef,P.P. and Coleman,M. (1997). Synovial membrane inflammation and cytokine production in patients with early osteoarthritis. *Journal of Rheumatology*. **24**, 365–371.

Smith,M.M. (2002). Pathobiology of the synovium in osteoarthritis. *Asia Pacific League of Associations for Rheumatology*. **5**, A5.

Smith,T.J., Baltzer,W.I., Löhr,C. and Stieger-Vanegas,S.M. (2012). Primary synovial osteochondromatosis of the stifle in an English Mastiff. *Veterinary Orthopaedics and Traumatology*. **25**, 160–166.

Sniekers,Y.H., Intema,F., Lafeber,F.P.J.G., van Osch,G.J.V.M., van Leeuwen,J.P.T.M., Weinans,H. and Mastbergen,S.C. (2008). A role for subchondral bone changes in the process of osteoarthritis; a micro-CT study of two canine models. *BMC Musculoskeletal Disorder*. **9**:20.

Sokoloff,L. (1980). The pathology of osteoarthritis and the role of ageing. In: Nuki,J. (Ed.), *The Aetiopathogenesis of Osteoarthritis*. pp. 1–15.

Soler,M., Murciano,J., Latorre,R., Belda,E., Rodriguez,M.J. and Agut,A. (2007). Ultrasonographic, computed tomographic and magnetic resonance imaging anatomy of the normal canine stifle joint. *Veterinary Journal*. **174**, 351–361.

Sowers,M.F., Hayes,C., Jamadar,D., Capul,D., Lachance L., Jannausch,M. and Welch,G. (2003). Magnetic resonance-detected subchondral bone marrow and cartilage defect characteristics associated with pain and X-ray-defined knee osteoarthritis. *Osteoarthritis and Cartilage*. **11**, 387–393.

Staiger,B.A. and Beale,B.S. (2005). Use of arthroscopy for debridement of the elbow joint in cats. *Journal of the American Veterinary Medical Association*. **226**, 401-403.

Streubel,R., Geyer,H. and Montavon,P.M. (2012). Medial humeral epicondylitis in cats. *Veterinary Surgery*. **41**, 795–802.

Sun,Y., Mauerhan,D.R., Honeycutt P.C., Kneisl,J.S., Norton,H.J., Zinchenko,N.L., Jr,E.N.H. and Gruber,H.E. (2010). Calcium deposition in osteoarthritic meniscus and meniscal cell culture. Arthritis Research and Therapy. **12**:R56.

Sun,Y., Mauerhan,D.R., Kneisl,J.S., James Norton,H., Zinchenko,N., Ingram,J., Hanley,E.N. and Gruber,H.E. (2012). Histological examination of collagen and proteoglycan changes in osteoarthritic menisci. *The Open Rheumatology Jou*rnal. **6**, 24–32.

Suter,E.R. and Majno,G. (1964). Ultrastructure of the joint capsule in the rat: presence of two kinds of capillaries. *Nature*. **202**, 920–921.

Taglinger,K., Van Nguyen,N., Helps,C.R., Day,M.J. and Foster,A.P. (2008). Quantitative real-time RT-PCR measurement of cytokine mRNA expression in the skin of normal cats and cats with allergic skin disease. *Veterinary Immunology and Immunopathology*. **122**, 216–230.

Takeuchi,T., Harris,J.L., Huang,W., Yan,K.W., Coughlin,S.R. and Craik C.S. (2000). Cellular localization of membrane-type serine protease 1 and identification of protease-activated receptor-2 and single-chain urokinase-type plasminogen activator as substrates. *Journal of Biological Chemistry*. **275**, 26333–26342.

Taljanovic,M.S., Graham,A.R., Benjamin,J.B., Gmitro,A.F., Krupinski,E.A., Schwartz,S.A., Hunter,T.B. and Resnick,D.L. (2008). Bone marrow edema pattern in advanced hip osteoarthritis: quantitative assessment with magnetic resonance imaging and correlation with clinical examinatio, radiographic findings and histopathology. *Skeletal Radiology*. **37**, 423–431.

Tanamas,S.K., Wluka,A.E., Pelletier,J.-P., Martel-Pelletier,J., Abram,F., Wang,Y. and Cicuttini,F.M. (2010). The association between subchondral bone cysts and tibial cartilage volume and risk of joint replacement in people with knee osteoarthritis: a longitudinal study. *Arthritis Research and Therapy*. **12**:R58.

Teitelbaum,S. and Bullough,P. (1979). The pathophysiology of bone and joint disease. *The American Journal of Pathology*. **96**, 283–354.

Thomas,C.M., Fuller,C.J., Whittles,C.E. and Sharif,M. (2007). Chondrocyte death by apoptosis is associated with cartilage matrix degradation. *Osteoarthritis and Cartilage*. **15**, 27–34.

Thrall,D.E. (2005). Editorial opacity and density. *Veterinary Radiology*. **27**, 162–163.

Thrall,D.E. (2007). Radiographic signs of joint disease in dogs and cats. In: Thrall,D.E. (Ed.), *Textbook of Veterinary Diagnostic Radiology*, 5th edn. pp. 330–332.

Tindell,A.G., Kelso,E.B., Ferrell,W.R., Lockhart,J.C., Walsh,D.A., Dunning,L. and McInnes,I.B. (2012). Correlation of protease-activated receptor-2 expression and synovitis in rheumatoid and osteoarthritis. *Rheumatology International*. **32**, 3077–3086.

Tirgari,M. and Vaughan,L.C. (1973). Clinico-pathological aspects of osteoarthritis of the shoulder in dogs. *Journal of Small Animal Practice*. **14**, 353–360.

Tirgari, M. and Vaughan, L.C. (1975). Arthritis of the canine stifle joint. *Veterinary Record*. **96**, 394–399.

Todhunter,R.J. (1992). Synovial joint anatomy, biology and pathobiology. In: Auer,J.A. (Ed.), *Equine Surgery*, 1st edn. pp. 844–866.

Tortorella,M.D., Malfait,A.M., Deccico,D. and Arner,E. (2001). The role of ADAM-TS4 (aggrecanase-1) and ADAM-TS5 (aggrecanase-2) in a model of cartilage degradation. *Osteoarthritis and Cartilage*. **9**, 539–552.

Tremoleda,J.L., Khalil,M., Gompels,L.L., Wylezinska-Arridge,M., Vincent,T. and Gsell,W. (2011). Imaging technologies for preclinical models of bone and joint disorders. *The European Journal of Nuclear Medicine and Molecular Imaging Research*.**1**, 11.

Tsai,S.-H., Sheu,M.-T., Liang,Y.-C., Cheng,H.-T., Fang,S.-S. and Chen,C.-H. (2009). TGF-beta inhibits IL-1beta-activated PAR-2 expression through multiple pathways in human primary synovial cells. *Journal of Biomedical Science*. **16**, 97.

Tuddenham,W.J. (1984). Glossary of terms for thoracic radiology: recommendations of the Nomenclature Committee of the Fleischner Society. *American Journal of Roentgenology*. **143**, 509–517.

Ueha,S., Shand,F.H.W. and Matsushima,K. (2012). Cellular and molecular mechanisms of chronic inflammation-associated organ fibrosis. *Frontiers in Immunology*. **3**, 71.

Van Beuningen,H.M., Glansbeek,H.L., van der Kraan,P.M. and van den Berg,W.B. (1998). Differential effects of local application of BMP-2 or TGF-beta 1 on both articular cartilage composition and osteophyte formation. *Osteoarthritis and Cartilage*. **6**, 306–317.

van Bree,H.J. and Van Ryssen,B. (1998). Diagnostic and surgical arthroscopy in osteochondrosis lesions. *Veterinary Clinics of North America: Small Animal Practice*. **28**, 161–189.

van Bree,H.J., Dingemanse,W. and Gielen,I. (2011). MRI and arthroscopy for evaluation of shoulder joint pathology. In: *European College of Veterinary Surgeons Proceedings 2011: Small Animal Orthopaedic Session*. pp. 101-103.

van Den Berg,W.B. and van De Putte,L.B. (1985). Electrical charge of the antigen determines its localization in the mouse knee joint. Deep penetration of cationic BSA in hyaline articular cartilage. *The American Journal of Pathology*. **121**, 224–234.

van Der Kraan,P.M. and van Den Berg,W.B. (2012). Chondrocyte hypertrophy and osteoarthritis: role in initiation and progression of cartilage degeneration? *Osteoarthritis and Cartilage*. **20**, 223–232.

Van Lent,P.L.E.M., Blom,A.B., van der Kraan,P., Holthuysen,A.E.M., Vitters,E., van Rooijen,N., Smeets,R.L., Nabbe,K.C.A.M. and van den Berg,W.B. (2004). Crucial role of synovial lining macrophages in the promotion of transforming growth factor beta-mediated osteophyte formation. *Arthritis and Rheumatology*. **50**, 103–111.

Vandesompele,J., De Preter,K., Pattyn,F., Poppe,B., Van Roy,N., De Paepe,A. and Speleman,F. (2002). Accurate normalization of real-time quantitative RT-PCR data by geometric averaging of multiple internal control genes. *Genome Biology*. **3**, research 0034.1–research 0034.11.

Vasseur,P.B., Pool,R.R., Arnoczky,S.P. and Lau,R.E. (1985). Correlative biomechanical and histologic study of the cranial cruciate ligament in dogs. *American Journal of Veterinary Research*. **46**, 1842–1854.

Veihelmann,A., Szczesny,G., Nolte,D., Krombach,F., Refior,H.J. and Messmer,K. (1998). A novel model for the study of synovial microcirculation in the mouse knee joint in vivo. *Research in Experimental Medicine*. **198**, 43–54.

Vermote, K.A.G., Bergenhuyzen, A.L.R., Gielen,I., van Bree,H., Duchateau,L. and Van Ryssen, B. (2010). Elbow lameness in dogs of six years and older: arthroscopic and imaging findings of medial coronoid disease in 51 dogs. *Veterinary and Comparative Orthopaedics and Traumatology*. **23**, 43–50.

Videman,T., Eronen,I., Friman,C. and Langenskiöld,A. (1979). Glycosaminoglycan metabolism of the medial meniscus, the medial collateral ligament and the hip joint capsule in experimental osteoarthritis caused by immobilization of the rabbit knee. *Acta Orthopaedica Scandinavica*. **50**, 465–470.

Vigorita,V.J. (2008). Synovium. In: Vigorita,V.J. (Ed.), *Orthopaedic Pathology*, 2nd edn. pp. 574–625.

Vogel,C. and Marcotte,E.M. (2012). Insights into the regulation of protein abundance from proteomic and transcriptomic analyses. *Nature Reviews Genetics*. **13**, 227–232.

Von der Mark,K., Gauss,V., von der Mark,H. and Muller,P. (1977). Relationship between cell shape and type of collagen synthesised as chondrocytes lose their cartilage phenotype in culture. *Nature*. **267**, 531–532.

Von Lindern,J.J., Theuerkauf,I., Niederhagen,B., Bergé,S., Appel,T. and Reich,R.H. (2002). Synovial chondromatosis of the temporomandibular joint: clinical, diagnostic, and histomorphologic findings. *Oral Surgery, Oral Medicine, Oral Pathology, Oral Radiology, and Endodontology*. **94**, 31–38.

Vu,T.-K.H., Hung,D.T., Wheaton,V.I. and Coughlin,S.R. (1991). Molecular cloning of a functional thrombin receptor reveals a novel proteolytic mechanism of receptor activation. *Cell*. **64**, 1057–1068.

Walker,M., Phalan,D., Jensen,J., Johnson,J., Drew,M., Samii,V., Henry,G. and McCauley,J. (2002). Meniscal ossicles in large non-domestic cats. Veterinary Radiology and Ultrasound. **43**, 249–254.

Walker,P.S. and Erkman,M.J. (1975). The role of the menisci in force transmission across the knee. *Clinical Orthopaedics and Related Research*. **109**, 184–192.

Wang,H., Wen,S., Bunnett,N.W., Leduc,R., Hollenberg,M.D. and MacNaughton,W.K. (2008). Proteinase-activated receptor-2 induces cyclooxygenase-2 expression through beta-catenin and cyclic AMP-response element-binding protein. *Journal of Biological Chemistry*. **283**, 809–815.

Wassenaar,M.J.E., Biermasz,N.R., Bijsterbosch,J., Pereira,A.M., Meulenbelt,I., Smit,J.W.A., Roelfsema,F., Kroon,H.M., Romijn,J.A., Kloppenburg,M. (2010). Arthropathy in long-term cured acromegaly is characterised by osteophytes without joint space narrowing: a comparison with generalised osteoarthritis. *Annals of Rheumatic Diseases*. **70**, 320–325.

Weber,N.A. (1998). Apparent primary ossification of the menisci in a dog. *Journal of the American Veterinary Medical Association*. **212**, 1892–1894.

Weir,M.R. (2002). Renal effects of nonselective NSAIDs and coxibs. *Cleveland Clinic Journal of Medicine*. **69,** 53–58.

Weisbrode,.E. and Doige,C.E. (2001). Bone and joints. In: McGavin,M.D., Carlton,W.W., Zachary,J.F. (Eds.), *Thomson's Special Veterinary Pathology*, 3rd edn. pp. 499–536.

Wenham,C.Y. and Conaghan,P.G. (2009). Imaging the painful osteoarthritic knee joint: what have we learned? *Nature Clinical Practice Rheumatology*. **5**, 149–158.

Whiting,P.G. and Pool,R.R. (1985). Intrameniscal calcification and ossification in the stifle joints of three domestic cats. *Journal of the American Animal Hospital Association*. **21**, 579–584.

Wind, A. (1986). Elbow incongruity and developmental elbow diseases in the dog. *Journal of the American Animal Hospital Association*. **22**, 711–724.

Wind,A.P. and Packard,M.E. (1986). Elbow incongruity and developmental elbow diseases in the dog: part I. *Journal of the American Animal Hospital Association*. **22**, 711–724.

Wood,A.K., McCarthy,P.H. and Howlett,C.R. (1985). Anatomic and radiographic appearance of a sesamoid bone in the tendon of origin of the supinator muscle of dogs. *American Journal of Veterinary Research*. **46**, 2043–2047.

Wood,A.K., McCarthy,P.H. and Martin,I.C. (1995). Anatomic and radiographic appearance of a sesamoid bone in the tendon of origin of the supinator muscle of the cat. *American Journal of Veterinary Research*. **56**, 736–738.

Wu,H., Du,J. and Zheng,Q. (2008). Expression of MMP-1 in cartilage and synovium of experimentally induced rabbit ACLT traumatic osteoarthritis: immunohistochemical study. *Rheumatology International*. **29**, 31–36.

Xiang,Y., Masuko-Hongo,K., Sekine,T., Nakamura,H., Yudoh,K., Nishioka,K. and Kato,T. (2006). Expression of proteinase-activated receptors (PAR)-2 in articular chondrocytes is modulated by IL-1B, TNF-α and TGF-B. *Osteoarthritis and Cartilage*. **14**, 1163–1173.

Yoshihara,Y., Nakamura,H., Obata,K., Yamada,H., Hayakawa,T., Fujikawa,K. and Okada,Y. (2000). Matrix metalloproteinases and tissue inhibitors of metalloproteinases in synovial fluids from patients with rheumatoid arthritis or osteoarthritis. *Annals of Rheumatic Diseases*. **59**, 455–461.

Yuan,J.S., Reed,A., Chen,F. and Jr,C.N.S. (2006). Statistical analysis of real-time PCR data. *BMC Bioinformatics*. **7**:85.

Zambrano,N.Z., Montes,G.S., Shigihara,K.M., Sanchez,E.M. and Junqueira,L.C. (1982). Collagen arrangements in cartilages. *Acta Anatomica*. **113**, 26–38.

Zamli,Z., Adams,M.A., Tarlton,J.F. and Sharif,M. (2013). Increased chondrocyte apoptosis is associated with progression of osteoarthritis in spontaneous Guinea pig models of the disease. *International Journal of Molecular Sciences*. **14**, 17729–17743.

Zatarain-Rios,E. and Mannik,M. (1987). Charge-charge interactions between articular cartilage and cationic antibodies, antigens, and immune complexes. *Arthritis and Rheumatology*. **30**, 1265–1273.

Zhang,J. and Wang,J.H.-C. (2012). BMP-2 mediates PGE(2) -induced reduction of proliferation and osteogenic differentiation of human tendon stem cells. *Journal of Orthopaedic Research*. **30**, 47–52.

Zrimsek,P., Kadunc KosV., Mrkun,J. and Kosec,M. (2007). Diagnostic value of matrix metalloproteinases MMP-2 and MMP-9 in synovial fluid for identifying osteoarthritis in the distal interphalangeal joint in horses. *Acta Veterinaria Brno*. **76**, 87–95.